RHEOLOGICAL METHODS IN FOOD PROCESS ENGINEERING

Second Edition

James F. Steffe, Ph.D., P.E.

Professor of Food Process Engineering
Dept. of Food Science and Human Nutrition
Dept. of Agricultural Engineering
Michigan State University

Freeman Press

2807 Still Valley Dr.
East Lansing, MI 48823
USA

Prof. James F. Steffe
209 Farrall Hall
Michigan State University
East Lansing, MI 48824-1323
USA

Phone: 517-353-4544
FAX: 517-432-2892
E-mail: steffe@msu.edu
URL: www.egr.msu.edu/~steffe/

Printed on acid-free paper in the United States of America

Second Printing

Library of Congress Catalog Card Number: 96-83538

International Standard Book Number: 0-9632036-1-4

Freeman Press
2807 Still Valley Dr.
East Lansing, MI 48823
USA

Table of Contents

Preface

Growth and development of this work sprang from the need to provide educational material for food engineers and food scientists. The first edition was conceived as a textbook and the work continues to be used in graduate level courses at various universities. Its greatest appeal, however, was to individuals solving practical day-to-day problems. Hence, the second edition, a significantly expanded and revised version of the original work, is aimed primarily at the rheological practitioner (particularly the industrial practitioner) seeking a broad understanding of the subject matter. The overall goal of the text is to present the information needed to answer three questions when facing problems in food rheology: 1. What properties should be measured? 2. What type and degree of deformation should be induced in the measurement? 3. How should experimental data be analyzed to generate practical information? Although the main focus of the book is food, scientists and engineers in other fields will find the work a convenient reference for standard rheological methods and typical data.

Overall, the work presents the theory of rheological testing and provides the analytical tools needed to determine rheological properties from experimental data. Methods appropriate for common food industry applications are presented. All standard measurement techniques for fluid and semi-solid foods are included. Selected methods for solids are also presented. Results from numerous fields, particularly polymer rheology, are used to address the flow behavior of food. Mathematical relationships, derived from simple force balances, provide a fundamental view of rheological testing. Only a background in basic calculus and elementary statistics (mainly regression analysis) is needed to understand the material. The text contains numerous practical example problems, involving actual experimental data, to enhance comprehension and the execution of concepts presented. This feature makes the work convenient for self-study.

Specific explanations of key topics in rheology are presented in Chapter 1: basic concepts of stress and strain; elastic solids showing Hookean and non-Hookean behavior; viscometric functions including normal stress differences; modeling fluid behavior as a function of shear rate, temperature, and composition; yield stress phenomena, extensional flow; and viscoelastic behavior. Efficient methods of attacking problems and typical instruments used to measure fluid properties are discussed along with an examination of problems involving interfacial

rheology, electrorheology, and on-line viscometry for control and monitoring of food processing operations. Common methods and empirical instruments utilized in the food industry are also introduced: Texture Profile Analysis, Compression-Extrusion Cell, Warner-Bratzler Shear Cell, Bostwick Consistometer, Adams Consistometer, Amylograph, Farinograph, Mixograph, Extensigraph, Alveograph, Kramer Shear Cell, Brookfield disks and T-bars, Cone Penetrometer, Hoeppler Viscometer, Zhan Viscometer, Brabender-FMC Consistometer.

The basic equations of tube (or capillary) viscometry, such as the Rabinowitsch-Mooney equation, are derived and applied in Chapter 2. Laminar flow criteria and velocity profiles are evaluated along with data correction methods for many sources of error: kinetic energy losses, end effects, slip (wall effects), viscous heating, and hole pressure. Techniques for glass capillary and slit viscometers are considered in detail. A section on pipeline design calculations has been included to facilitate the construction of large scale tube viscometers and the design of fluid pumping systems.

A general format, analogous to that used in Chapter 2, is continued in Chapter 3 to provide continuity in subject matter development. The main foci of the chapter center around the theoretical principles and experimental procedures related to three traditional types of rotational viscometers: concentric cylinder, cone and plate, and parallel plate. Mathematical analyses of data are discussed in detail. Errors due to end effects, viscous heating, slip, Taylor vortices, cavitation, and cone truncations are investigated. Numerous methods in mixer viscometry, techniques having significant potential to solve many food rheology problems, are also presented: slope and matching viscosity methods to evaluate average shear rate, determination of power law and Bingham plastic fluid properties. The vane method of yield stress evaluation, using both the slope and single point methods, along with a consideration of vane rotation during testing, is explored in detail.

The experimental methods to determine extensional viscosity are explained in Chapter 4. Techniques presented involve uniaxial extension between rotating clamps, biaxial extensional flow achieved by squeezing material between lubricated parallel plates, opposing jets, spinning, and tubeless siphon (Fano) flow. Related procedures, involving lubricated and nonlubricated squeezing, to determine shear flow behavior are also presented. Calculating extensional viscosity from flows through tapered convergences and flat entry dies is given a thorough examination.

Essential concepts in viscoelasticity and standard methods of investigating the phenomenon are investigated in Chapter 5. The full scope of viscoelastic material functions determined in transient and oscillatory testing are discussed. Mechanical analogues of rheological behavior are given as a means of analyzing creep and stress relaxation data. Theoretical aspects of oscillatory testing, typical data, and a discussion of the various modes of operating commercial instruments -strain, frequency, time, and temperature sweep modes- are presented. The Deborah number concept, and how it can be used to distinguish liquid from solid-like behavior, is introduced. Start-up flow (stress overshoot) and the relationship between steady shear and oscillatory properties are also discussed. Conversion factors, mathematical relationships, linear regression analysis, and typical rheological data for food as well as cosmetics and polymers are provided in the Appendices. Nomenclature is conveniently summarized at the end of the text and a large bibliography is furnished to direct readers to additional information.

J.F. Steffe
June, 1996

Dedication

To Susan, Justinn, and Dana.

Chapter 1. Introduction to Rheology

1.1. Overview

The first use of the word "rheology" is credited to Eugene C. Bingham (circa 1928) who also described the motto of the subject as παντα ρει ("panta rhei," from the works of Heraclitus, a pre-Socratic Greek philosopher active about 500 B.C.) meaning "everything flows" (Reiner, 1964). Rheology is now well established as the science of the deformation and flow of matter: It is the study of the manner in which materials respond to applied stress or strain. All materials have rheological properties and the area is relevant in many fields of study: geology and mining (Cristescu, 1989), concrete technology (Tattersall and Banfill, 1983), soil mechanics (Haghighi et al., 1987; Vyalov, 1986), plastics processing (Dealy and Wissburn, 1990), polymers and composites (Neilsen and Landel, 1994; Yanovsky, 1993), tribology (study of lubrication, friction and wear), paint flow and pigment dispersion (Patton, 1964), blood (Dintenfass, 1985), bioengineering (Skalak and Chien, 1987), interfacial rheology (Edwards et al., 1991), structural materials (Callister, 1991), electrorheology (Block and Kelly, 1988), psychorheology (Drake, 1987), cosmetics and toiletries (Laba, 1993b), and pressure sensitive adhesion (Saunders et al., 1992). The focus of this work is food where understanding rheology is critical in optimizing product development efforts, processing methodology and final product quality. To the extent possible, standard nomenclature (Dealy, 1994) has been used in the text.

One can think of food rheology as the material science of food. There are numerous areas where rheological data are needed in the food industry:

a. Process engineering calculations involving a wide range of equipment such as pipelines, pumps, extruders, mixers, coaters, heat exchangers, homogenizers, calenders, and on-line viscometers;
b. Determining ingredient functionality in product development;
c. Intermediate or final product quality control;
d. Shelf life testing;
e. Evaluation of food texture by correlation to sensory data;
f. Analysis of rheological equations of state or constitutive equations.

Many of the unique rheological properties of various foods have been summarized in books by Rao and Steffe (1992), and Weipert et al. (1993).

Fundamental rheological properties are independent of the instrument on which they are measured so different instruments will yield the same results. This is an ideal concept and different instruments rarely yield identical results; however, the idea is one which distinguishes true rheological material properties from subjective (empirical and generally instrument dependent, though frequently useful) material characterizations. Examples of instruments giving subjective results include the following (Bourne, 1982): Farinograph, Mixograph, Extensograph, Viscoamlyograph, and the Bostwick Consistometer. Empirical testing devices and methods, including Texture Profile Analysis, are considered in more detail in Sec. 1.13.

1.2. Rheological Instruments for Fluids

Common instruments, capable of measuring fundamental rheological properties of fluid and semi-solid foods, may be placed into two general categories (Fig. 1.1): rotational type and tube type. Most are commercially available, others (mixer and pipe viscometers) are easily fabricated. Costs vary tremendously from the inexpensive glass capillary viscometer to a very expensive rotational instrument capable of measuring dynamic properties and normal stress differences. Solid foods are often tested in compression (between parallel plates), tension, or torsion. Instruments which measure rheological properties are called rheometers. Viscometer is a more limiting term referring to devices that only measure viscosity.

Rotational instruments may be operated in the steady shear (constant angular velocity) or oscillatory (dynamic) mode. Some rotational instruments function in the controlled stress mode facilitating the collection of creep data, the analysis of materials at very low shear rates, and the investigation of yield stresses. This information is needed to understand the internal structure of materials. The controlled rate mode is most useful in obtaining data required in process engineering calculations. Mechanical differences between controlled rate and controlled stress instruments are discussed in Sec. 3.7.3. Rotational systems are generally used to investigate time-dependent behavior because tube systems only allow one pass of the material through the apparatus. A detailed discussion of oscillatory testing, the primary method of determining the viscoelastic behavior of food, is provided in Chapter 5.

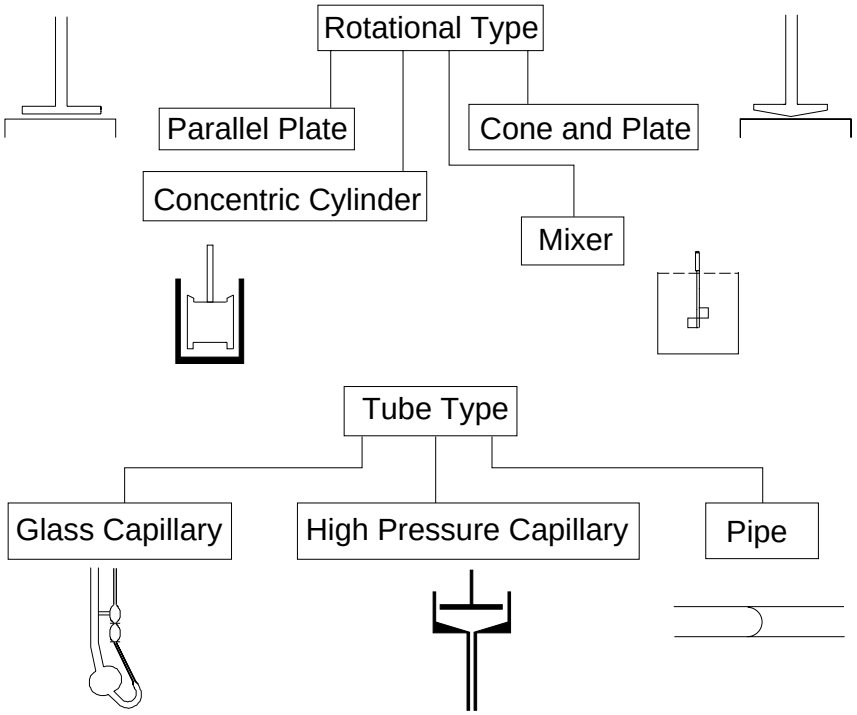

Figure 1.1. Common rheological instruments divided into two major categories: rotational and tube type.

There are advantages and disadvantages associated with each instrument. Gravity operated glass capillaries, such as the Cannon-Fenske type shown in Fig. 1.1, are only suitable for Newtonian fluids because the shear rate varies during discharge. Cone and plate systems are limited to moderate shear rates but calculations (for small cone angles) are simple. Pipe and mixer viscometers can handle much larger particles than cone and plate, or parallel plate, devices. Problems associated with slip and degradation in structurally sensitive materials are minimized with mixer viscometers. High pressure capillaries operate at high shear rates but generally involve a significant end pressure correction. Pipe viscometers can be constructed to withstand the rigors of the production or pilot plant environment.

All the instruments presented in Fig. 1.1 are "volume loaded" devices with container dimensions that are critical in the determination of rheological properties. Another common type of instrument, known as a vibrational viscometer, uses the principle of "surface loading" where the surface of an immersed probe (usually a sphere or a rod) generates a shear wave which dissipates in the surrounding medium. A large enough container is used so shear forces do not reach the wall and reflect back to the probe. Measurements depend only on ability of the surrounding fluid to damp probe vibration. The damping characteristic of a fluid is a function of the product of the fluid viscosity (of Newtonian fluids) and the density. Vibrational viscometers are popular as in-line instruments for process control systems (see Sec. 1.12). It is difficult to use these units to evaluate fundamental rheological properties of non-Newtonian fluids (Ferry, 1977), but the subjective results obtained often correlate well with important food quality attributes. The coagulation time and curd firmness of renneted milk, for example, have been successfully investigated using a vibrational viscometer (Sharma et al., 1989).

Instruments used to evaluate the extensional viscosity of materials are discussed in Chapter 4. Pulling or stretching a sample between toothed gears, sucking material into opposing jets, spinning, or exploiting the open siphon phenomenon can generate data for calculating tensile extensional viscosity. Information to determine biaxial extensional viscosity is provided by compressing samples between lubricated parallel plates. Shear viscosity can also be evaluated from unlubricated squeezing flow between parallel plates. A number of methods are available to calculate an average extensional viscosity from data describing flow through a convergence into a capillary die or slit.

1.3. Stress and Strain

Since rheology is the study of the deformation of matter, it is essential to have a good understanding of stress and strain. Consider a rectangular bar that, due to a tensile force, is slightly elongated (Fig. 1.2). The initial length of the bar is L_o and the elongated length is L where $L = L_o + \delta L$ with δL representing the increase in length. This deformation may be thought of in terms of Cauchy strain (also called engineering strain):

$$\varepsilon_c = \frac{\delta L}{L_o} = \frac{L - L_o}{L_o} = \frac{L}{L_o} - 1 \qquad [1.1]$$

or Hencky strain (also called true strain) which is determined by evaluating an integral from L_o to L:

$$\varepsilon_h = \int_{L_o}^{L} \frac{dL}{L} = \ln(L/L_o) \qquad [1.2]$$

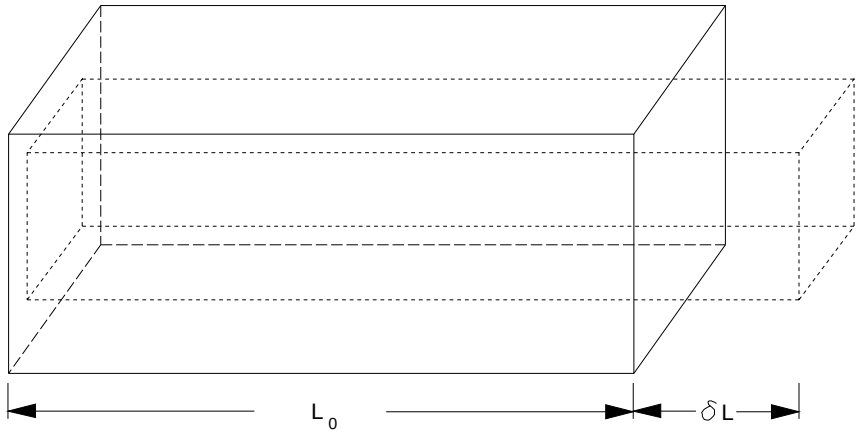

Figure 1.2. Linear extension of a rectangular bar.

Cauchy and Hencky strains are both zero when the material is unstrained and approximately equal at small strains. The choice of which strain measure to use is largely a matter of convenience and one can be calculated from the other:

$$\varepsilon_h = \ln(1 + \varepsilon_c) \qquad [1.3]$$

ε_h is preferred for calculating strain resulting from a large deformation.

Another type of deformation commonly found in rheology is simple shear. The idea can be illustrated with a rectangular bar (Fig. 1.3) of height h. The lower surface is stationary and the upper plate is linearly displaced by an amount equal to δL. Each element is subject to the same level of deformation so the size of the element is not relevant. The angle of shear, γ, may be calculated as

$$\tan(\gamma) = \frac{\delta L}{h} \qquad [1.4]$$

With small deformations, the angle of shear (in radians) is equal to the shear strain (also symbolized by γ), $\tan\gamma = \gamma$.

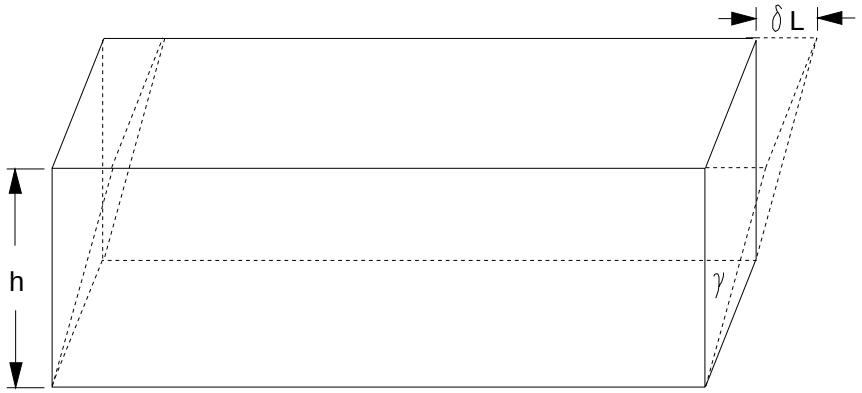

Figure 1.3. Shear deformation of a rectangular bar.

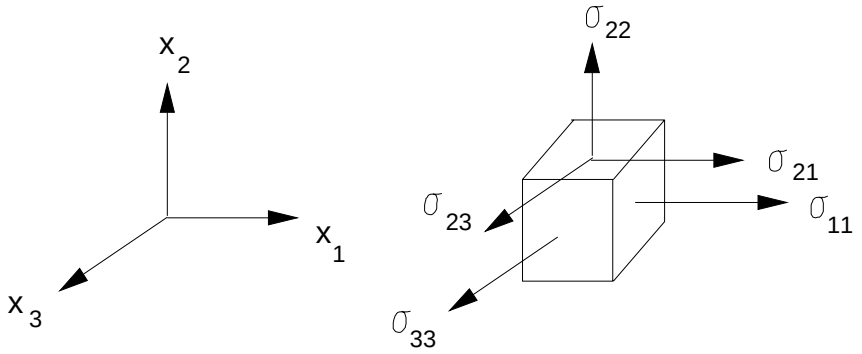

Figure 1.4. Typical stresses on a material element.

Stress, defined as a force per unit area and usually expressed in Pascal (N/m^2), may be tensile, compressive, or shear. Nine separate quantities are required to completely describe the state of stress in a material. A small element (Fig. 1.4) may be considered in terms of

Cartesian coordinates (x_1, x_2, x_3). Stress is indicated as σ_{ij} where the first subscript refers to the orientation of the face upon which the force acts and the second subscript refers to the direction of the force. Therefore, σ_{11} is a normal stress acting in the plane perpendicular to x_1 in the direction of x_1 and σ_{23} is a shear stress acting in the plane perpendicular to x_2 in the direction of x_3. Normal stresses are considered positive when they act outward (acting to create a tensile stress) and negative when they act inward (acting to create a compressive stress).

Stress components may be summarized as a stress tensor written in the form of a matrix:

$$\sigma_{ij} = \begin{bmatrix} \sigma_{11} & \sigma_{12} & \sigma_{13} \\ \sigma_{21} & \sigma_{22} & \sigma_{23} \\ \sigma_{31} & \sigma_{32} & \sigma_{33} \end{bmatrix} \qquad [1.5]$$

A related tensor for strain can also be expressed in matrix form. Basic laws of mechanics, considering the moment about the axis under equilibrium conditions, can be used to prove that the stress matrix is symmetrical:

$$\sigma_{ij} = \sigma_{ji} \qquad [1.6]$$

so

$$\sigma_{12} = \sigma_{21} \qquad [1.7]$$

$$\sigma_{31} = \sigma_{13} \qquad [1.8]$$

$$\sigma_{32} = \sigma_{23} \qquad [1.9]$$

meaning there are only six independent components in the stress tensor represented by Eq. [1.5].

Equations that show the relationship between stress and strain are either called rheological equations of state or constitutive equations. In complex materials these equations may include other variables such as time, temperature, and pressure. A modulus is defined as the ratio of stress to strain while a compliance is defined as the ratio of strain to stress. The word rheogram refers to a graph of a rheological relationship.

1.4. Solid Behavior

When force is applied to a solid material and the resulting stress versus strain curve is a straight line through the origin, the material is obeying Hooke's law. The relationship may be stated for shear stress and shear strain as

$$\sigma_{12} = G\gamma \qquad [1.10]$$

where G is the shear modulus. Hookean materials do not flow and are linearly elastic. Stress remains constant until the strain is removed and the material returns to its original shape. Sometimes shape recovery, though complete, is delayed by some atomistic process. This time-dependent, or delayed, elastic behavior is known as anelasticity. Hooke's law can be used to describe the behavior of many solids (steel, egg shell, dry pasta, hard candy, etc.) when subjected to small strains, typically less than 0.01. Large strains often produce brittle fracture or non-linear behavior.

The behavior of a Hookean solid may be investigated by studying the uniaxial compression of a cylindrical sample (Fig. 1.5). If a material is compressed so that it experiences a change in length and radius, then the normal stress and strain may be calculated:

$$\sigma_{22} = \frac{F}{A} = \frac{F}{\pi(R_o)^2} \qquad [1.11]$$

$$\varepsilon_c = \frac{\delta h}{h_o} \qquad [1.12]$$

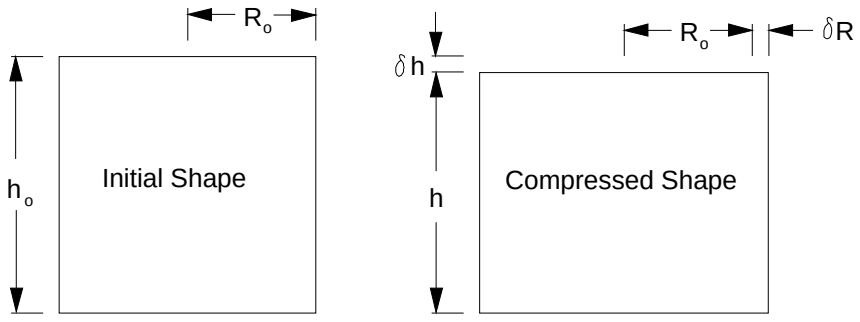

Figure 1.5 Uniaxial compression of a cylindrical sample.

This information can be used to determine Young's modulus (E), also called the modulus of elasticity, of the sample:

$$E = \frac{\sigma_{22}}{\varepsilon_c} \qquad [1.13]$$

If the deformations are large, Hencky strain (ε_h) should be used to calculate strain and the area term needed in the stress calculation should be adjusted for the change in radius caused by compression:

$$\sigma_{22} = \frac{F}{\pi(R_o + \delta R)^2} \qquad [1.14]$$

A critical assumption in these calculations is that the sample remains cylindrical in shape. For this reason lubricated contact surfaces are often recommended when testing materials such as food gels.

Young's modulus may also be determined by flexural testing of beams. In one such test, a cantilever beam of known length (a) is deflected a distance (d) when a force (F) is applied to the free end of the beam. This information can be used to calculate Young's modulus for materials having a rectangular or circular crossectional area (Fig. 1.6). Similar calculations can be performed in a three-point bending test (Fig. 1.7) where deflection (d) is measured when a material is subjected to a force (F) placed midway between two supports. Calculations are sightly different depending on wether-or-not the test material has a rectangular or circular shape. Other simple beam tests, such as the double cantilever or four-point bending test, yield comparable results. Flexural testing may have application to solid foods having a well defined geometry such as dry pasta or hard candy.

In addition to Young's modulus, Poisson's ratio (ν) can be defined from compression data (Fig. 1.5):

$$\nu = \frac{\text{lateral strain}}{\text{axial strain}} = \frac{\delta R/R_o}{\delta h/h_o} \qquad [1.15]$$

Poisson's ratio may range from 0 to 0.5. Typically, ν varies from 0.0 for rigid like materials containing large amounts of air to near 0.5 for liquid like materials. Values from 0.2 to 0.5 are common for biological materials with 0.5 representing an incompressible substance like potato

flesh. Tissues with a high level of cellular gas, such as apple flesh, would have values closer to 0.2. Metals usually have Poisson ratios between 0.25 and 0.35.

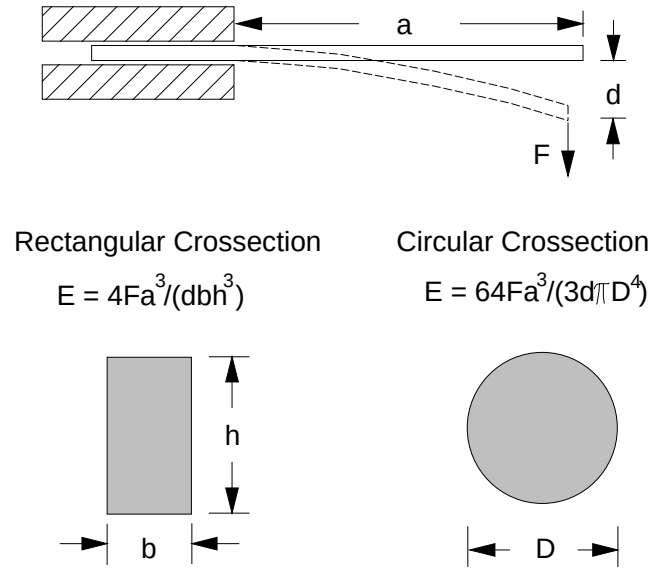

Figure 1.6 Deflection of a cantilever beam to determine Young's modulus.

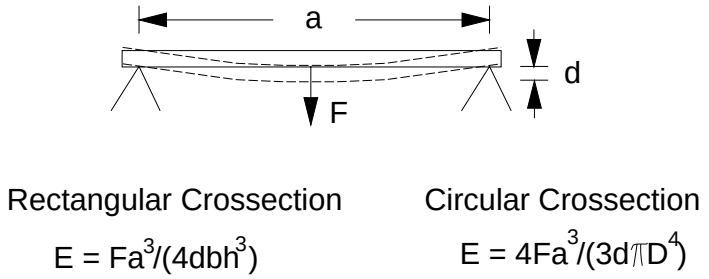

Figure 1.7 Three-point beam bending test to determine Young's modulus (b, h, and D are defined on Fig. 1.6).

If a material is subjected to a uniform change in external pressure, it may experience a volumetric change. These quantities are used to define the bulk modulus (K):

$$K = \frac{\text{change in pressure}}{\text{volumetric strain}} = \frac{\text{change in pressure}}{\text{(change in volume/original volume)}} \qquad [1.16]$$

The bulk modulus of dough is approximately 10^6 Pa while the value for steel is 10^{11} Pa. Another common property, bulk compressibility, is defined as the reciprocal of bulk modulus.

When two material constants describing the behavior of a Hookean solid are known, the other two can be calculated using any of the following theoretical relationships:

$$\frac{1}{E} = \frac{1}{3G} + \frac{1}{9K} \qquad [1.17]$$

$$E = 3K(1-2\nu) = 2G(1+\nu) \qquad [1.18]$$

$$\nu = \frac{3K-E}{6K} = \frac{E-2G}{2G} \qquad [1.19]$$

Numerous experimental techniques, applicable to food materials, may be used to determine Hookean material constants. Methods include testing in tension, compression and torsion (Mohsenin, 1986; Polakowski and Ripling, 1966; Dally and Ripley, 1965). Hookean properties of typical materials are presented in the Appendix [6.5].

Linear-elastic and non-linear elastic materials (like rubber) both return to their original shape when the strain is removed. Food may be solid in nature but not Hookean. A comparison of curves for linear elastic (Hookean), elastoplastic and non-linear elastic materials (Fig. 1.8) shows a number of similarities and differences. The elastoplastic material has Hookean type behavior below the yield stress (σ_o) but flows to produce permanent deformation above that value. Margarine and butter, at room temperature, may behave as elastoplastic substances. Investigation of this type of material, as a solid or a fluid, depends on the shear stress being above or below σ_o (see Sec. 1.6 for a more detailed discussion of the yield stress concept and Appendix [6.7] for typical yield stress values). Furthermore, to fully distinguish fluid from solid like behavior, the characteristic time of the material and the characteristic time of the deformation process involved must be considered simulta-

neously. The Deborah number has been defined to address this issue. A detailed discussion of the concept, including an example involving silly putty (the "real solid-liquid") is presented in Sec. 5.5.

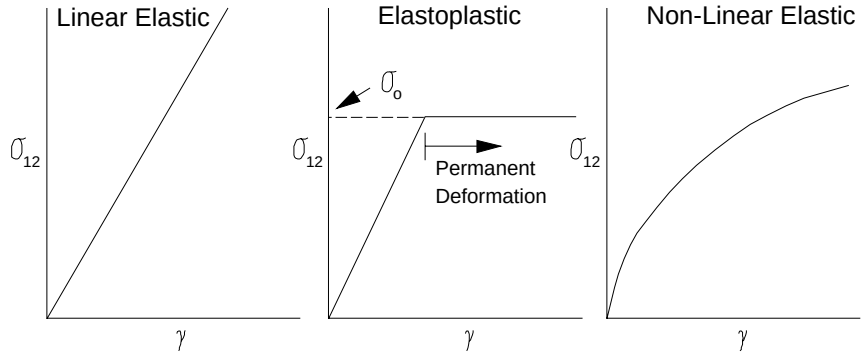

Figure 1.8. Deformation curves for linear elastic (Hookean), elastoplastic and non-linear elastic materials.

Food rheologists also find the failure behavior of solid food (particularly, brittle materials and firm gels) to be very useful because these data sometimes correlate well with the conclusions of human sensory panels (Hamann, 1983; Montejano et al., 1985; Kawanari et al., 1981). The following terminology (taken from American Society for Testing and Materials, Standard E-6) is useful in describing the large deformation behavior involved in the mechanical failure of food:

elastic limit - the greatest stress which a material is capable of sustaining without any permanent strain remaining upon complete release of stress;

proportional limit - the greatest stress which a material is capable of sustaining without any deviation from Hooke's Law;

compressive strength - the maximum compressive stress a material is capable of sustaining;

shear strength - the maximum shear stress a material is capable of sustaining;

tensile strength - the maximum tensile stress a material is capable of sustaining;

yield point - the first stress in a test where the increase in strain occurs without an increase in stress;

yield strength - the engineering stress at which a material exhibits a specified limiting deviation from the proportionality of stress to strain.

A typical characteristic of brittle solids is that they break when given a small deformation. Failure testing and fracture mechanics in structural solids are well developed areas of material science (Callister, 1991) which offer much to the food rheologist. Evaluating the structural failure of solid foods in compression, torsion, and sandwich shear modes were summarized by Hamann (1983). Jagged force-deformation relationships of crunchy materials may offer alternative texture classification criteria for brittle or crunchy foods (Ulbricht et al., 1995; Peleg and Normand, 1995).

1.5. Fluid Behavior in Steady Shear Flow

1.5.1. Time-Independent Material Functions

Viscometric Functions. Fluids may be studied by subjecting them to continuous shearing at a constant rate. Ideally, this can be accomplished using two parallel plates with a fluid in the gap between them (Fig. 1.9). The lower plate is fixed and the upper plate moves at a constant velocity (u) which can be thought of as an incremental change in position divided by a small time period, $\delta L/\delta t$. A force per unit area on the plate is required for motion resulting in a shear stress (σ_{21}) on the upper plate which, conceptually, could also be considered to be a layer of fluid.

The flow described above is steady simple shear and the shear rate (also called the strain rate) is defined as the rate of change of strain:

$$\dot{\gamma} = \frac{d\gamma}{dt} = \frac{d}{dt}\left(\frac{\delta L}{h}\right) = \frac{u}{h} \qquad [1.20]$$

This definition only applies to streamline (laminar) flow between parallel plates. It is directly applicable to sliding plate viscometer described by Dealy and Giacomin (1988). The definition must be adjusted to account for curved lines such as those found in tube and rotational viscometers; however, the idea of "maximum speed divided by gap size" can be useful in estimating shear rates found in particular applications like brush coating. This idea is explored in more detail in Sec. 1.9.

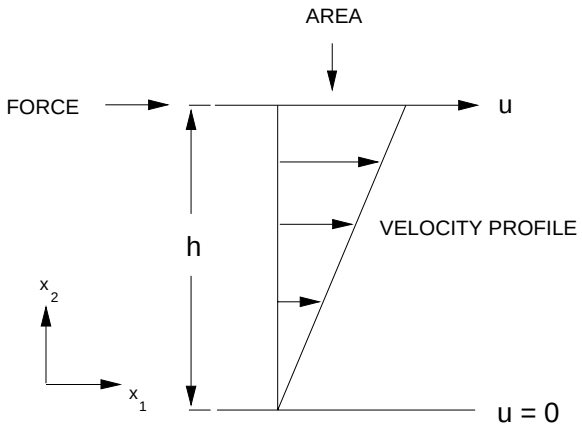

Figure 1.9. Velocity profile between parallel plates.

Rheological testing to determine steady shear behavior is conducted under laminar flow conditions. In turbulent flow, little information is generated that can be used to determine material properties. Also, to be meaningful, data must be collected over the shear rate range appropriate for the problem in question which may vary widely in industrial processes (Table 1.1): Sedimentation of particles may involve very low shear rates, spray drying will involve high shear rates, and pipe flow of food will usually occur over a moderate shear rate range. Extrapolating experimental data over a broad range of shear rates is not recommended because it may introduce significant errors when evaluating rheological behavior.

Material flow must be considered in three dimensions to completely describe the state of stress or strain. In steady, simple shear flow the coordinate system may be oriented with the direction of flow so the stress tensor given by Eq. [1.5] reduces to

$$\sigma_{ij} = \begin{bmatrix} \sigma_{11} & \sigma_{12} & 0 \\ \sigma_{21} & \sigma_{22} & 0 \\ 0 & 0 & \sigma_{33} \end{bmatrix} \qquad [1.21]$$

Table 1.1. Shear Rates Typical of Familiar Materials and Processes

Situation	$\dot{\gamma}(1/s)$	Application
Sedimentation of particles in a suspending liquid	10^{-6} - 10^{-3}	Medicines, paints, spices in salad dressing
Leveling due to surface tension	10^{-2} - 10^{-1}	Frosting, paints, printing inks
Draining under gravity	10^{-1} - 10^{1}	Vats, small food containers, painting and coating
Extrusion	10^{0} - 10^{3}	Snack and pet foods, toothpaste, cereals, pasta, polymers
Calendering	10^{1} - 10^{2}	Dough Sheeting
Pouring from a bottle	10^{1} - 10^{2}	Foods, cosmetics, toiletries
Chewing and swallowing	10^{1} - 10^{2}	Foods
Dip coating	10^{1} - 10^{2}	Paints, confectionery
Mixing and stirring	10^{1} - 10^{3}	Food processing
Pipe flow	10^{0} - 10^{3}	Food processing, blood flow
Rubbing	10^{2} - 10^{4}	Topical application of creams and lotions
Brushing	10^{3} - 10^{4}	Brush painting, lipstick, nail polish
Spraying	10^{3} - 10^{5}	Spray drying, spray painting, fuel atomization
High speed coating	10^{4} - 10^{6}	Paper
Lubrication	10^{3} - 10^{7}	Bearings, gasoline engines

Simple shear flow is also called viscometric flow. It includes axial flow in a tube, rotational flow between concentric cylinders, rotational flow between a cone and a plate, and torsional flow (also rotational) between parallel plates. In viscometric flow, three shear-rate-dependent material functions, collectively called viscometric functions, are needed to completely establish the state of stress in a fluid. These may be described as the viscosity function, $\eta(\dot{\gamma})$, and the first and second normal stress coefficients, $\Psi_1(\dot{\gamma})$ and $\Psi_2(\dot{\gamma})$, defined mathematically as

$$\eta = f(\dot{\gamma}) = \frac{\sigma_{21}}{\dot{\gamma}} \qquad [1.22]$$

$$\Psi_1 = f(\dot{\gamma}) = \frac{\sigma_{11} - \sigma_{22}}{(\dot{\gamma})^2} = \frac{N_1}{(\dot{\gamma})^2} \qquad [1.23]$$

$$\Psi_2 = f(\dot{\gamma}) = \frac{\sigma_{22} - \sigma_{33}}{(\dot{\gamma})^2} = \frac{N_2}{(\dot{\gamma})^2} \qquad [1.24]$$

The first ($\sigma_{11} - \sigma_{22}$) and second ($\sigma_{22} - \sigma_{33}$) normal stress differences are often symbolically represented as N_1 and N_2, respectively. N_1 is always positive and considered to be approximately 10 times greater than N_2. Measurement of N_2 is difficult; fortunately, the assumption that $N_2 = 0$ is usually satisfactory. The ratio of N_1/σ_{12}, known as the recoverable shear (or the recoverable elastic strain), has proven to be a useful parameter in modeling die swell phenomena in polymers (Tanner, 1988). Some data on the N_1 values of fluid foods have been published (see Appendix [6.6]).

If a fluid is Newtonian, $\eta(\dot{\gamma})$ is a constant (equal to the Newtonian viscosity) and the first and second normal stress differences are zero. As $\dot{\gamma}$ approaches zero, elastic fluids tend to display Newtonian behavior. Viscoelastic fluids simultaneously exhibit obvious fluid-like (viscous) and solid-like (elastic) behavior. Manifestations of this behavior, due to a high elastic component, can be very strong and create difficult problems in process engineering design. These problems are particularly prevalent in the plastic processing industries but also present in processing foods such as dough, particularly those containing large quantities of wheat protein.

Fig. 1.10 illustrates several phenomena. During mixing or agitation, a viscoelastic fluid may climb the impeller shaft in a phenomenon known as the Weissenberg effect (Fig. 1.10). This can be observed in home mixing of cake or chocolate brownie batter. When a Newtonian fluid emerges from a long, round tube into the air, the emerging jet will normally contract; at low Reynolds numbers it may expand to a diameter which is 10 to 15% larger than the tube diameter. Normal stress differences present in a viscoelastic fluid, however, may cause jet expansions (called die swell) which are two or more times the diameter of the tube (Fig. 1.10). This behavior contributes to the challenge of designing extruder dies to produce the desired shape of many pet, snack, and cereal foods. Melt fracture, a flow instability causing distorted extrudates, is also a problem related to fluid viscoelasticity. In addition, highly elastic fluids may exhibit a tubeless siphon effect (Fig. 1.10).

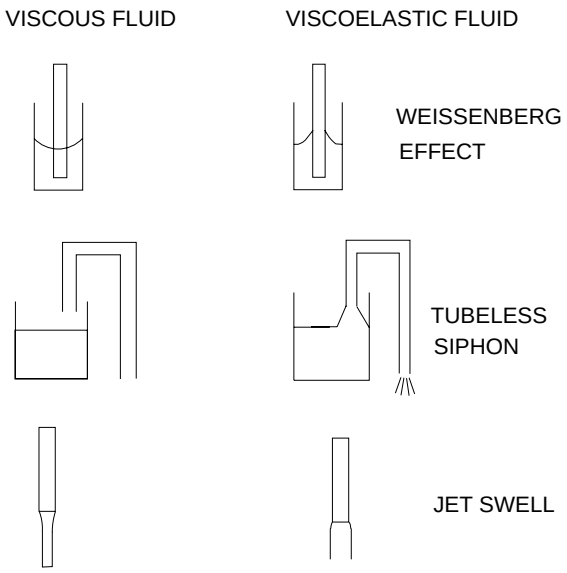

Figure 1.10. Weissenberg effect (fluid climbing a rotating rod), tubeless siphon and jet swell of viscous (Newtonian) and viscoelastic fluids.

The recoil phenomena (Fig. 1.11), where tensile forces in the fluid cause particles to move backward (snap back) when flow is stopped, may also be observed in viscoelastic fluids. Other important effects include drag reduction, extrudate instability, and vortex inhibition. An excellent pictorial summary of the behavior of viscoelastic polymer solutions in various flow situations has been prepared by Boger and Walters (1993).

Normal stress data can be collected in steady shear flow using a number of different techniques (Dealy, 1982): exit pressure differences in capillary and slit flow, axial flow in an annulus, wall pressure in concentric cylinder flow, axial thrust in cone and plate as well as parallel plate flow. In general, these methods have been developed for plastic melts (and related polymeric materials) with the problems of the plastic industries providing the main driving force for change.

Cone and plate systems are most commonly used for obtaining primary normal stress data and a number of commercial instruments are available to make these measurements. Obtaining accurate data for food materials is complicated by various factors such as the presence of a yield stress, time-dependent behavior and chemical reactions occurring during processing (e.g., hydration, protein denaturation, and starch gelatinization). Rheogoniometer is a term sometimes used to describe an instrument capable of measuring both normal and shear stresses. Detailed information on testing viscoelastic polymers can be found in numerous books: Bird et al. (1987), Barnes et al. (1989), Bogue and White (1970), Darby (1976), Macosko (1994), and Walters (1975).

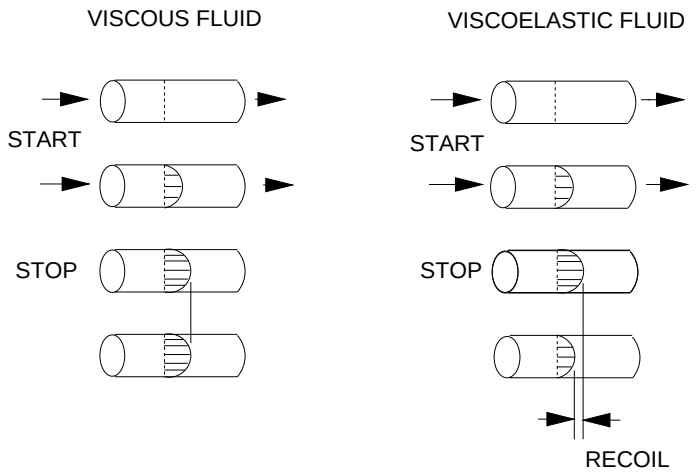

Figure 1.11. Recoil phenomenon in viscous (Newtonian) and viscoelastic fluids.

Viscometric functions have been very useful in understanding the behavior of synthetic polymer solutions and melts (polyethylene, polypropylene, polystyrene, etc.). From an industrial standpoint, the viscosity function is most important in studying fluid foods and much of the current work is applied to that area. To date, normal stress data for foods have not been widely used in food process engineering. This is partly due to the fact that other factors often complicate the evaluation of the fluid dynamics present in various problems. In food extrusion, for example, flashing (vaporization) of water when the product exits the

die makes it difficult to predict the influence of normal stress differences on extrudate expansion. Future research may create significant advances in the use of normal stress data by the food industry.

Mathematical Models for Inelastic Fluids. The elastic behavior of many fluid foods is small or can be neglected (materials such as dough are the exception) leaving the viscosity function as the main area of interest. This function involves shear stress and shear rate: the relationship between the two is established from experimental data. Behavior is visualized as a plot of shear stress versus shear rate, and the resulting curve is mathematically modeled using various functional relationships. The simplest type of substance to consider is the Newtonian fluid where shear stress is directly proportional to shear rate [for convenience the subscript on σ_{21} will be dropped in the remainder of the text when dealing exclusively with one dimensional flow]:

$$\sigma = \mu\dot{\gamma} \qquad [1.25]$$

with μ being the constant of proportionality appropriate for a Newtonian fluid. Using units of N, m^2, m, m/s for force, area, length and velocity gives viscosity as Pa s which is 1 poiseuille or 1000 centipoise (note: 1 Pa s = 1000 cP = 1000 mPa s; 1 P = 100 cP). Dynamic viscosity and coefficient of viscosity are synonyms for the term "viscosity" in referring to Newtonian fluids. The reciprocal of viscosity is called fluidity. Coefficient of viscosity and fluidity are infrequently used terms. Newtonian fluids may also be described in terms of their kinematic viscosity (ν) which is equal to the dynamic viscosity divided by density (μ/ρ). This is a common practice for non-food materials, particularly lubricating oils. Viscosity conversion factors are available in Appendix [6.1].

Newtonian fluids, by definition, have a straight line relationship between the shear stress and the shear rate with a zero intercept. All fluids which do not exhibit this behavior may be called non-Newtonian. Looking at typical Newtonian fluids on a rheogram (Fig. 1.12) reveals that the slope of the line increases with increasing viscosity.

Van Wazer et al. (1963) discussed the sensitivity of the eye in judging viscosity of Newtonian liquids. It is difficult for the eye to distinguish differences in the range of 0.1 to 10 cP. Small differences in viscosity are clearly seen from approximately 100 to 10,000 cP: something at 800 cP may look twice as thick as something at 400 cP. Above 100,000 cP it is difficult to make visual distinctions because the materials do not

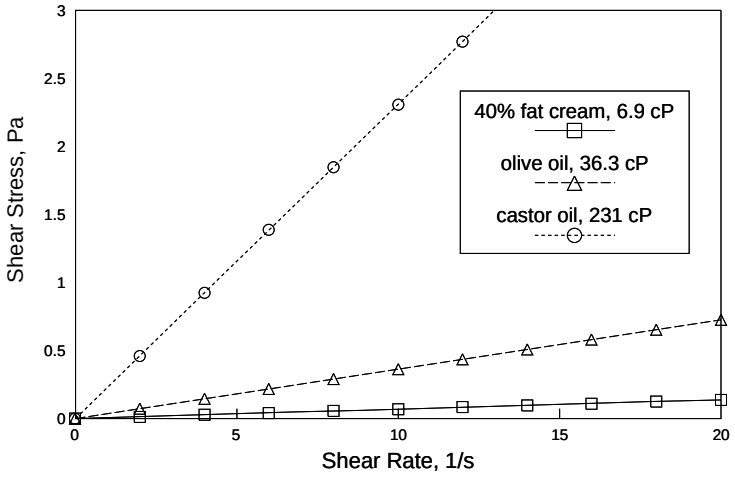

Figure 1.12. Rheograms for typical Newtonian fluids.

pour and appear, to the casual observer, as solids. As points of reference the following represent typical Newtonian viscosities at room temperature: air, 0.01 cP; gasoline (petrol), 0.7 cP; water, 1 cP; mercury, 1.5 cP; coffee cream or bicycle oil, 10 cP; vegetable oil, 100 cP; glycerol, 1000 cP; glycerine, 1500 cP; honey, 10,000 cP; tar, 1,000,000 cP. Data for many Newtonian fluids at different temperatures are presented in Appendices [6.8], [6.9], and [6.10].

A general relationship to describe the behavior of non-Newtonian fluids is the Herschel-Bulkley model:

$$\sigma = K(\dot{\gamma})^n + \sigma_o \qquad [1.26]$$

where K is the consistency coefficient, n is the flow behavior index, and σ_o is the yield stress. This model is appropriate for many fluid foods. Eq. [1.26] is very convenient because Newtonian, power law (shear-thinning when $0 < n < 1$ or shear-thickening when $1 < n < \infty$) and Bingham plastic behavior may be considered as special cases (Table 1.2, Fig. 1.13). With the Newtonian and Bingham plastic models, K is commonly called the viscosity (μ) and plastic viscosity (μ_{pl}), respectively. Shear-thinning and shear-thickening are also referred to as pseudoplastic and dilatent behavior, respectively; however, shear-thinning and

shear-thickening are the preferred terms. A typical example of a shear-thinning material is found in the flow behavior of a 1% aqueous solution of carrageenan gum as demonstrated in Example Problem 1.14.1. Shear-thickening is considered with a concentrated corn starch solution in Example Problem 1.14.2.

Table 1.2. Newtonian, Power Law and Bingham Plastic Fluids as Special Cases of the Herschel-Bulkley Model (Eq. [1.26])

Fluid	K	n	σ_o	Typical Examples
Herschel-Bulkley	> 0	$0 < n < \infty$	> 0	minced fish paste, raisin paste
Newtonian	> 0	1	0	water, fruit juice, milk, honey, vegetable oil
shear-thinning (pseudoplastic)	> 0	$0 < n < 1$	0	applesauce, banana puree, orange juice concentrate
shear-thickening (dilatent)	> 0	$1 < n < \infty$	0	some types of honey, 40% raw corn starch solution
Bingham plastic	> 0	1	> 0	tooth paste, tomato paste

An important characteristic of the Herschel-Bulkley and Bingham plastic materials is the presence of a yield stress (σ_o) which represents a finite stress required to achieve flow. Below the yield stress a material exhibits solid like characteristics: It stores energy at small strains and does not level out under the influence of gravity to form a flat surface. This characteristic is very important in process design and quality assessment for materials such as butter, yogurt and cheese spread. The yield stress is a practical, but idealized, concept that will receive additional discussion in a later section (Sec. 1.6). Typical yield stress values may be found in Appendix [6.7].

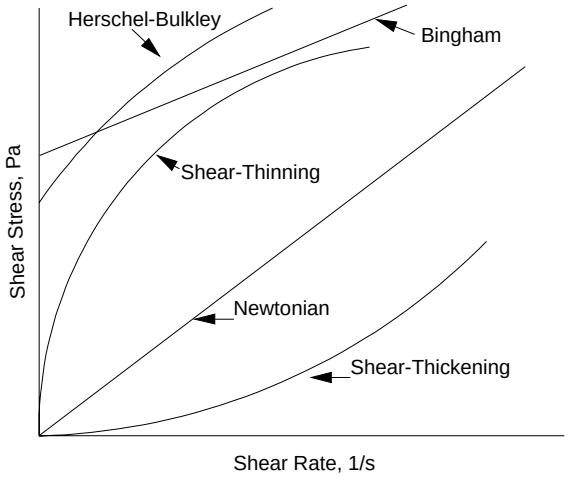

Figure 1.13. Curves for typical time-independent fluids.

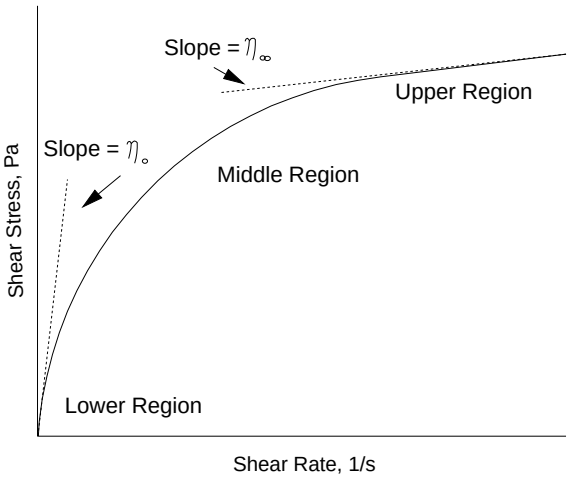

Figure 1.14. Rheogram of idealized shear-thinning (pseudoplastic) behavior.

Shear-thinning behavior is very common in fruit and vegetable products, polymer melts, as well as cosmetic and toiletry products (Appendices [6.11], [6.12], [6.13]). During flow, these materials may exhibit three distinct regions (Fig. 1.14): a lower Newtonian region where the apparent viscosity (η_o), called the limiting viscosity at zero shear rate, is constant with changing shear rates; a middle region where the apparent viscosity (η) is changing (decreasing for shear-thinning fluids) with shear rate and the power law equation is a suitable model for the phenomenon; and an upper Newtonian region where the slope of the curve (η_∞), called the limiting viscosity at infinite shear rate, is constant with changing shear rates. The middle region is most often examined when considering the performance of food processing equipment. The lower Newtonian region may be relevant in problems involving low shear rates such as those related to the sedimentation of fine particles in fluids. Values of η_o for some viscoelastic fluids are given in Table 5.4.

Numerous factors influence the selection of the rheological model used to describe flow behavior of a particular fluid. Many models, in addition to the power law, Bingham plastic and Herschel-Bulkley models, have been used to represent the flow behavior of non-Newtonian fluids. Some of them are summarized in Table 1.3. The Cross, Reiner-Philippoff, Van Wazer and Powell-Eyring models are useful in modeling pseudoplastic behavior over low, middle and high shear rate ranges. Some of the equations, such as the Modified Casson and the Generalized Herschel-Bulkley, have proven useful in developing mathematical models to solve food process engineering problems (Ofoli et al., 1987) involving wide shear rate ranges. Additional rheological models have been summarized by Holdsworth (1993).

The Casson equation has been adopted by the International Office of Cocoa and Chocolate for interpreting chocolate flow behavior. The Casson and Bingham plastic models are similar because they both have a yield stress. Each, however, will give different values of the fluid parameters depending on the data range used in the mathematical analysis. The most reliable value of a yield stress, when determined from a mathematical intercept, is found using data taken at the lowest shear rates. This concept is demonstrated in Example Problem 1.14.3 for milk chocolate.

Apparent Viscosity. Apparent viscosity has a precise definition. It is, as noted in Eq. [1.22], shear stress divided by shear rate:

$$\eta = f(\dot{\gamma}) = \frac{\sigma}{\dot{\gamma}} \qquad [1.27]$$

With Newtonian fluids, the apparent viscosity and the Newtonian viscosity (μ) are identical but η for a power law fluid is

$$\eta = f(\dot{\gamma}) = \frac{K(\dot{\gamma})^n}{\dot{\gamma}} = K(\dot{\gamma})^{n-1} \qquad [1.28]$$

Table 1.3. Rheological Models to Describe the Behavior of Time-independent Fluids

Model (Source)	Equation*
Casson (Casson, 1959)	$\sigma^{0.5} = (\sigma_o)^{0.5} + K_1(\dot{\gamma})^{0.5}$
Modified Casson (Mizrahi and Berk, 1972)	$\sigma^{0.5} = (\sigma_o)^{0.5} + K_1(\dot{\gamma})^{n_1}$
Ellis (Ellis, 1927)	$\dot{\gamma} = K_1\sigma + K_2(\sigma)^{n_1}$
Generalized Herschel-Bulkley (Ofoli et al., 1987)	$\sigma^{n_1} = (\sigma_o)^{n_1} + K_1(\dot{\gamma})^{n_2}$
Vocadlo (Parzonka and Vocadlo, 1968)	$\sigma = \left((\sigma_o)^{1/n_1} + K_1\dot{\gamma}\right)^{n_1}$
Power Series (Whorlow, 1992)	$\dot{\gamma} = K_1\sigma + K_2(\sigma)^3 + K_3(\sigma)^5 \ldots$
	$\sigma = K_1\dot{\gamma} + K_2(\dot{\gamma})^3 + K_3(\dot{\gamma})^5 \ldots$
Carreau (Carreau, 1968)	$\eta = \eta_\infty + (\eta_o - \eta_\infty)\left[1 + (K_1\dot{\gamma})^2\right]^{(n-1)/2}$
Cross (Cross, 1965)	$\eta = \eta_\infty + \frac{\eta_o - \eta_\infty}{1 + K_1(\dot{\gamma})^n}$
Van Wazer (Van Wazer, 1963)	$\eta = \frac{\eta_o - \eta_\infty}{1 + K_1\dot{\gamma} + K_2(\dot{\gamma})^{n_1}} + \eta_\infty$
Powell-Eyring (Powell and Eyring, 1944)	$\sigma = K_1\dot{\gamma} + \left(\frac{1}{K_2}\right)\sinh^{-1}(K_3\dot{\gamma})$
Reiner-Philippoff (Philippoff, 1935)	$\sigma = \left(\eta_\infty + \frac{\eta_o - \eta_\infty}{1 + ((\sigma)^2/K_1)}\right)\dot{\gamma}$

*K_1, K_2, K_3 and n_1, n_2 are arbitrary constants and power indices, respectively, determined from experimental data.

Apparent viscosities for Bingham plastic and Herschel-Bulkley fluids are determined in a like manner:

$$\eta = f(\dot{\gamma}) = \frac{K(\dot{\gamma}) + \sigma_o}{\dot{\gamma}} = K + \frac{\sigma_o}{\dot{\gamma}} \qquad [1.29]$$

$$\eta = f(\dot{\gamma}) = \frac{K(\dot{\gamma})^n + \sigma_o}{\dot{\gamma}} = K(\dot{\gamma})^{n-1} + \frac{\sigma_o}{\dot{\gamma}} \qquad [1.30]$$

η decreases with increasing shear rate in shear-thinning and Bingham plastic substances. In Herschel-Bulkley fluids, apparent viscosity will decrease with higher shear rates when $0<n<1.0$, but behave in the opposite manner when $n>1.0$. Apparent viscosity is constant with Newtonian materials and increases with increasing shear rate in shear-thickening fluids (Fig. 1.15).

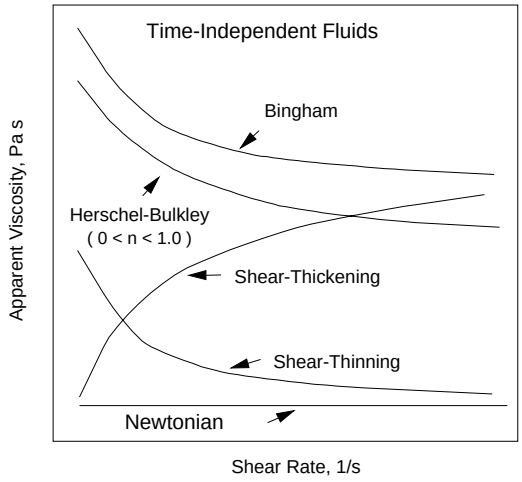

Figure 1.15. Apparent viscosity of time-independent fluids.

A single point apparent viscosity value is sometimes used as a measure of mouthfeel of fluid foods: The human perception of thickness is correlated to the apparent viscosity at approximately 60 s^{-1}. Apparent viscosity can also be used to illustrate the axiom that taking single point tests for determining the general behavior of non-Newtonian materials may cause serious problems. Some quality control instruments designed for single point tests may produce confusing results. Consider, for

example, the two Bingham plastic materials shown in Fig. 1.16. The two curves intersect at 19.89 1/s and an instrument measuring the apparent viscosity at that shear rate, for each fluid, would give identical results: η = 1.65 Pa s. However, a simple examination of the material with the hands and eyes would show them to be quite different because the yield stress of one material is more than 4 times that of the other material. Clearly, numerous data points (minimum of two for the power law or Bingham plastic models) are required to evaluate the flow behavior of non-Newtonian fluids.

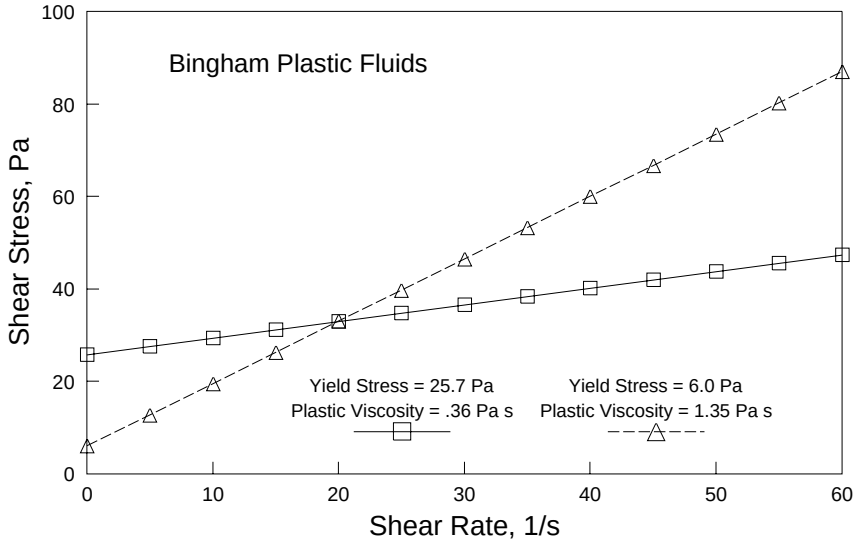

Figure 1.16. Rheograms for two Bingham plastic fluids.

Solution Viscosities. It is sometimes useful to determine the viscosities of dilute synthetic or biopolymer solutions. When a polymer is dissolved in a solvent, there is a noticeable increase in the viscosity of the resulting solution. The viscosities of pure solvents and solutions can be measured and various values calculated from the resulting data:

$$\text{relative viscosity} = \eta_{\text{rel}} = \frac{\eta_{solution}}{\eta_{solvent}} \qquad [1.31]$$

$$\text{specific viscosity} = \eta_{sp} = \eta_{\text{rel}} - 1 \qquad [1.32]$$

$$\text{reduced viscosity} = \eta_{red} = \frac{\eta_{sp}}{C} \qquad [1.33]$$

$$\text{inherent viscosity} = \eta_{inh} = \frac{\ln \eta_{\text{rel}}}{C} \qquad [1.34]$$

$$\text{intrinsic viscosity} = \eta_{\text{int}} = \left[\frac{\eta_{sp}}{C} \right]_{C \to 0} \qquad [1.35]$$

where C is the mass concentration of the solution in units of g/dl or g/100ml. Note that units of reduced, inherent, and intrinsic viscosity are reciprocal concentration (usually deciliters of solution per grams of polymer). The intrinsic viscosity has great practical value in molecular weight determinations of high polymers (Severs, 1962; Morton-Jones, 1989; Grulke, 1994). This concept is based on the Mark-Houwink relation suggesting that the intrinsic viscosity of a dilute polymer solution is proportional to the average molecular weight of the solute raised to a power in the range of 0.5 to 0.9. Values of the proportionality constant and the exponent are well known for many polymer-solvent combinations (Progelf and Throne, 1993; Rodriquez, 1982). Solution viscosities are useful in understanding the behavior of some biopolymers including aqueous solutions of locust bean gum, guar gum, and carboxymethylcellulose (Rao, 1986). The intrinsic viscosities of numerous protein solutions have been summarized by Rha and Pradipasena (1986).

1.5.2. Time-Dependent Material Functions

Ideally, time-dependent materials are considered to be inelastic with a viscosity function which depends on time. The response of the substance to stress is instantaneous and the time-dependent behavior is due to changes in the structure of the material itself. In contrast, time effects found in viscoelastic materials arise because the response of stress to applied strain is not instantaneous and not associated with a structural change in the material. Also, the time scale of thixotropy may be quite different than the time scale associated with viscoelasticity: The most dramatic effects are usually observed in situations involving short process times. Note too, that real materials may be both time-dependent and viscoelastic!

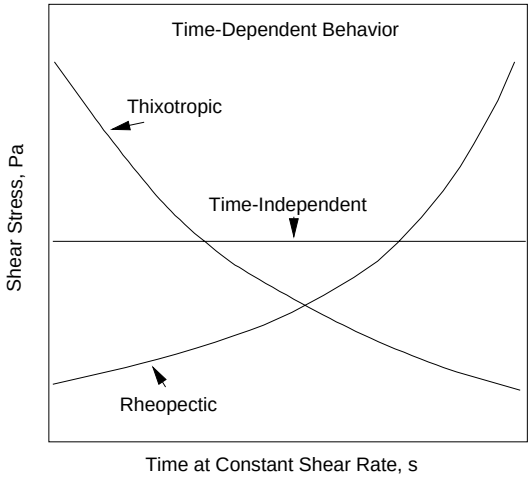

Figure 1.17. Time-dependent behavior of fluids.

Separate terminology has been developed to describe fluids with time-dependent characteristics. Thixotropic and rheopectic materials exhibit, respectively, decreasing and increasing shear stress (and apparent viscosity) over time at a fixed rate of shear (Fig. 1.17). In other words, thixotropy is time-dependent thinning and rheopexy is time-dependent thickening. Both phenomena may be irreversible, reversible or partially reversible. There is general agreement that the term "thixotropy" refers to the time-dependent decrease in viscosity, due to shearing, and the subsequent recovery of viscosity when shearing is removed (Mewis, 1979). Irreversible thixotropy, called rheomalaxis or rheodestruction, is common in food products and may be a factor in evaluating yield stress as well as the general flow behavior of a material. Anti-thixotropy and negative thixotropy are synonyms for rheopexy.

Thixotropy in many fluid foods may be described in terms of the sol-gel transition phenomenon. This terminology could apply, for example, to starch-thickened baby food or yogurt. After being manufactured, and placed in a container, these foods slowly develop a three dimensional network and may be described as gels. When subjected to shear (by standard rheological testing or mixing with a spoon), structure is broken down and the materials reach a minimum thickness where

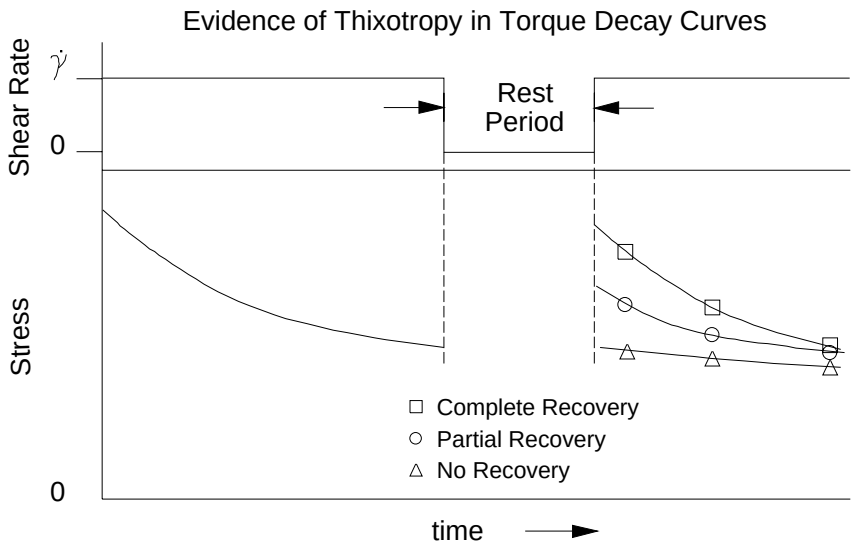

Figure 1.18. Thixotropic behavior observed in torque decay curves.

they exist in the sol state. In foods that show reversibility, the network is rebuilt and the gel state reobtained. Irreversible materials remain in the sol state.

The range of thixotropic behavior is illustrated in Fig. 1.18. Subjected to a constant shear rate, the shear stress will decay over time. During the rest period the material may completely recover, partially recover or not recover any of its original structure leading to a high, medium, or low torque response in the sample. Rotational viscometers have proven to be very useful in evaluating time-dependent fluid behavior because (unlike tube viscometers) they easily allow materials to be subjected to alternate periods of shear and rest.

Step (or linear) changes in shear rate may also be carried out sequentially with the resulting shear stress observed between steps. Typical results are depicted in Fig. 1.19. Actual curve segments (such as 1-2 and 3-4) depend on the relative contribution of structural breakdown and buildup in the substance. Plotting shear stress versus shear rate for the increasing and decreasing shear rate values can be used to generate hysteresis loops (a difference in the up and down curves) for the material. The area between the curves depends on the time-dependent nature of the substance: it is zero for a time-independent

fluid. This information may be valuable in comparing different materials, but it is somewhat subjective because different step change periods may lead to different hysteresis loops. Similar information can be generated by subjecting materials to step (or linear) changes in shear stress and observing the resulting changes in shear rates.

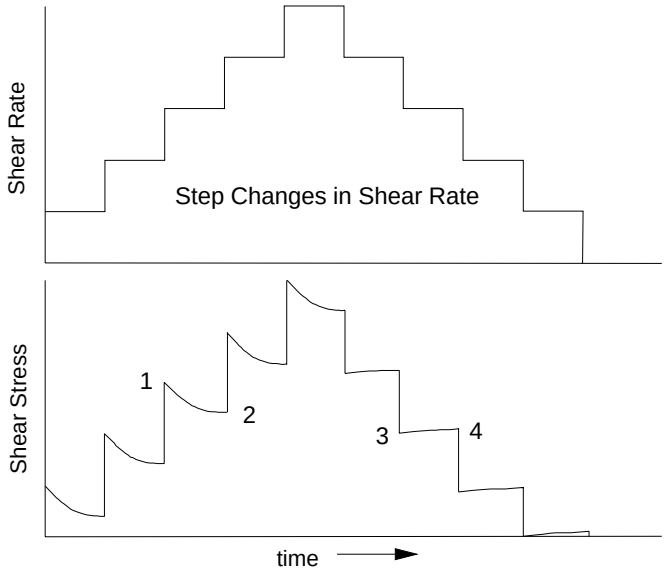

Figure 1.19. Thixotropic behavior observed from step changes in shear rate.

Torque decay data (like that given for a problem in mixer viscometry described in Example Problem 3.8.22) may be used to model irreversible thixotropy by adding a structural decay parameter to the Herschel-Bulkley model to account for breakdown (Tiu and Boger, 1974):

$$\sigma = f(\lambda, \dot{\gamma}) = \lambda(\sigma_o + K(\dot{\gamma})^n) \qquad [1.36]$$

where λ, the structural parameter, is a function of time. $\lambda = 1$ before the onset of shearing and λ equals an equilibrium value (λ_e) obtained after complete breakdown from shearing. The decay of the structural parameter with time may be assumed to obey a second order equation:

$$\frac{d\lambda}{dt} = -k_1(\lambda - \lambda_e)^2 \quad \text{for} \quad \lambda > \lambda_e \qquad [1.37]$$

where k_1 is a rate constant that is a function of shear rate. Then, the entire model is completely determined by five parameters: $\sigma_o, K, n, k_1(\dot{\gamma})$, and λ_e. K, n and σ_o are determined under initial shearing conditions when $\lambda = 1$ and $t = 0$. In other words, they are determined from the initial shear stress in the material, observed at the beginning of a test, for each shear rate considered.

λ and λ_e are expressed in terms of the apparent viscosity ($\eta = \sigma/\dot{\gamma}$) to find k_1. Equating the rheological model (Eq. [1.36]) to the definition of apparent viscosity (which in this case is a function of both shear rate and the time-dependent apparent viscosity) yields an expression for λ:

$$\lambda = \frac{\eta\dot{\gamma}}{\sigma_o + K(\dot{\gamma})^n} \qquad [1.38]$$

Eq. [1.38] is valid for all values of λ including λ_e at η_e, the equilibrium value of the apparent viscosity. Differentiating λ with respect to time, at a constant shear rate, gives

$$\frac{d\lambda}{dt} = \frac{d\eta}{dt}\left(\frac{\dot{\gamma}}{\sigma_o + K(\dot{\gamma})^n}\right) \qquad [1.39]$$

Using the definition of $d\lambda/dt$, Eq. [1.37] and [1.39] may be combined yielding

$$-k_1(\lambda - \lambda_e)^2 = \frac{d\eta}{dt}\left(\frac{\dot{\gamma}}{\sigma_o + K(\dot{\gamma})^n}\right) \qquad [1.40]$$

Considering the definition of λ given by Eq. [1.38], this may be rewritten as

$$-k_1\left[\left(\frac{\eta\dot{\gamma}}{\sigma_o + K(\dot{\gamma})^n}\right) - \left(\frac{\eta_e\dot{\gamma}}{\sigma_o + K(\dot{\gamma})^n}\right)\right]^2 = \frac{d\eta}{dt}\left(\frac{\dot{\gamma}}{\sigma_o + K(\dot{\gamma})^n}\right) \qquad [1.41]$$

Simplification yields

$$\frac{d\eta}{dt} = -k_1\left(\frac{\dot{\gamma}}{\sigma_o + K(\dot{\gamma})^n}\right)(\eta - \eta_e)^2 \qquad [1.42]$$

or

$$\frac{d\eta}{dt} = -a_1(\eta - \eta_e)^2 \qquad [1.43]$$

where

$$a_1 = \frac{k_1\dot{\gamma}}{\sigma_o + K(\dot{\gamma})^n} \qquad [1.44]$$

Integrating Eq. [1.43] gives

$$\int_{\eta_o}^{\eta} (\eta - \eta_e)^{-2} d\eta = \int_0^t -a_1 dt \qquad [1.45]$$

so

$$\frac{1}{\eta - \eta_e} = \frac{1}{\eta_o - \eta_e} + a_1 t \qquad [1.46]$$

where η_o is the initial value of the apparent viscosity calculated from the initial ($t = 0$ and $\lambda = 1$) shear stress and shear rate.

Using Eq. [1.46], a plot $1/(\eta - \eta_e)$ versus t, at a particular shear rate, is made to obtain a_1. This is done at numerous shear rates and the resulting information is used to determine the relation between a_1 and $\dot{\gamma}$ and, from that, the relation between k_1 and $\dot{\gamma}$. This is the final information required to completely specify the mathematical model given by Eq. [1.36] and [1.37].

The above approach has been used to describe the behavior of mayonnaise (Tiu and Boger, 1974), baby food (Ford and Steffe, 1986), and buttermilk (Butler and McNulty, 1995). More complex models which include terms for the recovery of structure are also available (Cheng, 1973; Ferguson and Kemblowski, 1991). Numerous rheological models to describe time-dependent behavior have been summarized by Holdsworth (1993).

1.5.3. Modeling Rheological Behavior of Fluids

Modeling provides a means of representing a large quantity of rheological data in terms of a simple mathematical expression. Rheograms, summarized in terms of the Herschel-Bulkley equation (Eq. [1.26]), represent one example of modeling. In this section we will expand the idea to include temperature and concentration (or moisture content) effects into single empirical expressions. Many forms of the equations are possible and one master model, suitable for all situations,

does not exist. The equations covered here are acceptable for a large number of practical problems involving homogeneous materials which do not experience a phase change over the range of conditions under consideration.

The influence of temperature on the viscosity for Newtonian fluids can be expressed in terms of an Arrhenius type equation involving the absolute temperature (T), the universal gas constant (R), and the energy of activation for viscosity (E_a):

$$\mu = f(T) = A \exp\left(\frac{E_a}{RT}\right) \qquad [1.47]$$

E_a and A are determined from experimental data. Higher E_a values indicate a more rapid change in viscosity with temperature. The energy of activation for honey is evaluated in Example Problem 1.14.4.

Considering an unknown viscosity (μ) at any temperature (T) and a reference viscosity (μ_r) at a reference temperature (T_r), the constant (A) may be eliminated from Eq. [1.47] and the resulting equation written in logarithmic form:

$$\ln\left(\frac{\mu}{\mu_r}\right) = \left(\frac{E_a}{R}\right)\left(\frac{1}{T} - \frac{1}{T_r}\right) \qquad [1.48]$$

In addition to modeling the viscosity of Newtonian fluids, an Arrhenius relationship can be used to model the influence of temperature on apparent viscosity in power law fluids. Considering a constant shear rate, with the assumption that temperature has a negligible influence on the flow behavior index, yields

$$\ln\left(\frac{\eta}{\eta_r}\right) = \frac{E_a}{R}\left(\frac{1}{T} - \frac{1}{T_r}\right) \qquad [1.49]$$

or

$$\frac{\eta}{\eta_r} = \exp\left(\frac{E_a}{R}\left(\frac{1}{T} - \frac{1}{T_r}\right)\right) \qquad [1.50]$$

Eq. [1.50] can be used to find η at any temperature (T) from appropriate reference values (η_r, T_r). Activation energies and reference viscosities for a number of fluid foods are summarized in Appendix [6.14].

The effect of temperature on viscosity can also be modeled using a relationship known as the Williams-Landel-Ferry (WLF) equation proposed by Williams et al. (1955). A reference viscosity at a reference temperature, and the numerical value of two constants are needed to specify the relationship. The WLF equation is very useful in modeling the viscosity of amorphous foods above the glass transition temperature (Roos, 1992; Roos, 1995).

The effect of shear rate and temperature can be combined into a single expression (Harper and El Sahrigi, 1965):

$$\eta = f(T,\dot{\gamma}) = K_T \exp\left(\frac{E_a}{RT}\right)(\dot{\gamma})^{\bar{n}-1} \qquad [1.51]$$

where $\bar{n}$ is an average value of the flow behavior index based on all temperatures. Eq. [1.51] can also be expressed in terms of shear stress:

$$\sigma = f(T,\dot{\gamma}) = K_T \exp\left(\frac{E_a}{RT}\right)(\dot{\gamma})^{\bar{n}} \qquad [1.52]$$

The practical value of Eq. [1.52] is demonstrated for concentrated orange juice in Example Problem 1.14.5. Parameters in the model ($K_T, \bar{n}, E_a$) were determined using a limited number of data sets taken at a few specific temperatures. The final model (Eq. [1.52]), however, can generate a rheogram at any temperature in the range. This is useful in solving many food engineering problems such as those requiring a prediction of the fluid velocity profile or pressure drop during tube flow.

Effects of temperature and concentration (C) on apparent viscosity, at a constant shear rate, can also be combined into a single relationship (Vitali and Rao, 1984; Castaldo et al. 1990):

$$\eta = f(T,C) = K_{T,C} \exp\left(\frac{E_a}{RT}\right)C^B \qquad [1.53]$$

The three constants ($K_{T,C}, E_a, B$) must be determined from experimental data. Shear rate, temperature, and concentration (or moisture content) can also be combined into a single expression (Mackey et al., 1989):

$$\eta = f(T,\dot{\gamma},C) = K_{\dot{\gamma},T,C}(\dot{\gamma})^{\bar{n}-1} \exp\left[\left(\frac{E_a}{RT}\right) + B(C)\right] \qquad [1.54]$$

where the influence of shear rate is given in terms of a power law function. The parameters ($K_{\dot{\gamma},T,C}$, n, E_a and B) cannot be given an exact physical interpretation because the sequence of steps used in determining them influences the magnitude of the constants. Equation

parameters, for example, may be determined using stepwise regression analysis with the assumption that interaction effects (such as temperature dependence of n and b) can be neglected. $K_{\dot{\gamma},T,C}$ is a constant which combines the effects of shear rate, temperature and concentration.

Rheological behavior of fluid foods is complex and influenced by numerous factors. Eq. [1.54] allows prediction of apparent viscosity on the basis of shear rate, temperature, and moisture content. Time-temperature history and strain history may be added to form a more comprehensive equation (Dolan et al., 1989; Dolan and Steffe, 1990; Mackey et al., 1989; Morgan et al., 1989) applicable to protein and starch based dough or slurry systems.

The influence of temperature on the behavior of polymeric materials may be modeled by determining a shift factor using the principle of time-temperature superposition (Bird et al., 1987). This technique is one example of the method of reduced variables (outlined in detail by Ferry, 1980) which can be expanded to include the effect of concentration and pressure on rheological behavior. Time-temperature superposition equates the effect of time and temperature on rheological properties. The useful consequence of the method is that material behavior can be investigated in time domains (usually very long or very short) that are otherwise unavailable due to the experimental limitations. Time-temperature superposition has proven to be a valuable method in studying creep and stress relaxation of synthetic polymers (Neilsen and Landel, 1994); but the technique, which is sometimes applicable to biological materials, has not been widely applied to foods. Da Silva et al. (1994) found the time-temperature superposition principle was inappropriate for modeling the temperature dependence of storage and loss moduli of pectin dispersions. The idea, however, can provide a useful empirical method for developing master-curves of rheological data for many fluid foods. The technique is illustrated in Example Problem 1.14.5 where a shift factor is calculated for concentrated orange juice.

1.6. Yield Stress Phenomena

A yield stress (σ_o) may be defined as the minimum shear stress required to initiate flow. The existence of a yield stress has been challenged (Barnes and Walters, 1985) using the argument that everything flows given sufficient time or very sensitive measuring equipment. This concept is explored in more detail in Sec. 5.6. From a practical stand-

point, there is little doubt that σ_o is an engineering reality (Hartnett and Hu, 1989) which may strongly influence process engineering calculations.

Table 1.4. Methods of Determining Yield Stress

Method	Description or Parameter Measured	Reference
Extrapolation	Shear stress versus shear rate curve extrapolated to zero shear rate.	Ofoli et al. (1987) Keentok (1982) Yoshimura et al. (1987)
Extrapolation	Apparent viscosity versus shear stress curve extrapolated to infinite apparent viscosity.	Van Wazer et al. (1963) Kaletunc-Gencer and Peleg (1984)
Stress Decay	Residual stress on a bob.	Lang and Rha (1981)
Stress Decay	Residual stress in a back extruder (annular pump).	Steffe and Osorio (1987)
Stress to Initiate Flow	Controlled stress rheometers measure the minimum stress required for flow in traditional geometries: cone and plate, etc.	James et al. (1987)
Stress to Initiate Flow	Stress on a smooth, rough or grooved bob.	Lang and Rha (1981); Vocadlo and Charles (1971)
Stress to Initiate Flow	Stress to move an immersed vertical plate.	DeKee et al. (1980)
Stress to Initiate Flow	Stress to cause motion in a tube viscometer.	Cheng (1986)
Stress to Initiate Flow	Stress to create vane motion.	Nguyen and Boger (1985) Qiu and Rao (1988) Yoo et al. (1995)
Stress to Initiate Flow	Size of the plug flow radius in an annulus.	Lang and Rha (1981)
Stress to Initiate Flow	Force to move material through a finned, cylindrical cell.	Goodrich et al. (1989)
Dynamic Testing	Flat response of an oscillatory input.	Cheng (1986)
Vertical Plate Coating	Amount of fluid remaining on a plate after withdrawal from sample.	Lang and Rha (1981) Charm (1962)
Squeezing Flow	Deformation between parallel circular disks.	Campanella and Peleg (1987a)
Cone Penetrometer	Depth of penetration.	Tanaka et al. (1971)

There are many ways to evaluate the yield stress for fluid like substances (Table 1.4) and no single, "best" technique can be identified. Different applications require different methods. One common method of obtaining a yield stress value is to extrapolate the shear stress versus shear rate curve back to the shear stress intercept at zero shear rate. Values obtained using this method will be strongly influenced by the rheological model (Bingham, Herschel-Bulkley, etc.) and shear rate range selected to represent the data (Ofoli et al., 1987). This difficulty is demonstrated for milk chocolate in Example Problem 1.14.3. An alternative numerical procedure is to plot apparent viscosity versus shear stress and determine σ_o from the point (related to zero shear rate) where η becomes infinite.

Reported yield stress values are actually defined by the rheological techniques and assumptions used in the measurement. An absolute yield stress is an elusive property: It is not unusual for a yield stress obtained by one technique to be very different from one found using a different method. Cheng (1986) has written an excellent review of the yield stress problem and shown that the magnitudes of measured values are closely associated with creep, stress growth, thixotropy, and the characteristic times of these transient responses. He described a concept of static and dynamic yield stresses that has great practical value in rheological testing of fluid foods.

Many foods, such as starch-thickened baby food (Steffe and Ford, 1985), thicken during storage and exhibit irreversible thixotropic behavior when stirred before consumption. Chemical changes (e.g., starch retrogradation) cause a weak gel structure to form in the material during storage. This structure is sensitive and easily disrupted by fluid movement. The yield stress, measured in an undisturbed sample, is the static yield stress. The yield stress of a completely broken down sample, often determined from extrapolation of the equilibrium flow curve, is the dynamic yield stress (Fig. 1.20). A static yield stress may be significantly higher than the dynamic yield stress. If the material recovers its structure during a short period of time (uncommon in food products), then a rate parameter may be utilized to fully describe rheological behavior.

The idea of a static and a dynamic yield stress can be explained by assuming there are two types of structure in a thixotropic fluid (Cheng, 1986). One structure is insensitive to shear rate and serves to define the dynamic yield stress associated with the equilibrium flow curve. A

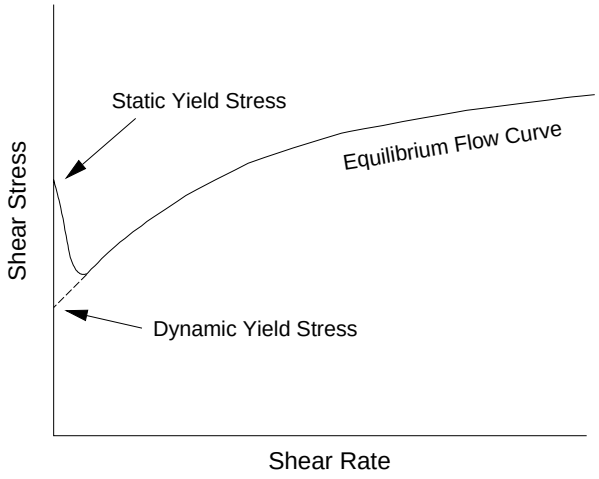

Figure 1.20. Static and dynamic yield stresses.

second structure, the weak structure, forms over a certain period of time when the sample is at rest. Combined, the two structures cause a resistance to flow which determines the static yield stress. Behavior discussed above has been observed, though not mentioned in terms of the static and dynamic yield stress, for many food products: apple sauce, banana and peach baby food, mustard, tomato ketchup (Barbosa Canovas and Peleg, 1983); and meat and yeast extracts (Halomos and Tiu, 1981). Also, the same terminology (and essentially the same meaning) was used by Pokorny et al. (1985) to interpret rheological data for margarine. Yoo et al. (1995) defined a new dimensionless number, the yield number defined as the static yield stress divided by the dynamic yield stress, to differentiate yield stresses.

An important issue in yield stress measurement, particularly from a quality control standpoint, is reproducibility of the experimental data. This is critical when comparing the overall characteristics of products made on different production lines or in different plants. In this situation the measurement is closely tied to the application and the absolute value of the yield stress may be unimportant. A "true value (most likely the dynamic value)," of the yield stress may be essential to properly design food processing systems like those required in tubular thermal processing equipment where fluid velocity profiles are critical. Typical

yield stresses, including data showing differences between the static and dynamic yield values, are summarized in Appendix [6.7]. The vane method, a simple and practical means of measuring the yield stress, is presented in detail in Sec. 3.7.3 and Example Problems 3.8.19, 3.8.20, and 3.8.21. Evaluating yield stresses using controlled stress rheometers is discussed in Sec. 3.7.3 and the role of the yield stress in determining the thickness of a food coating is examined in Example Problem 1.14.6.

1.7. Extensional Flow

Viscometric flow may be defined as that which is indistinguishable from steady simple shear flow. Additional information may be obtained from a different type of flow: extensional flow that yields an extensional viscosity. Pure extensional flow does not involve shearing and is sometimes referred to as "shear free" flow. In published literature, elongational viscosity and Trouton viscosity are frequently used synonyms for extensional viscosity. Similarly, elongational flow is a synonym for extensional flow.

Many food processing operations involve extensional deformation and the molecular orientation caused by extension, versus shear, can produce unique food products and behavior. The reason shear and extensional flow have a different influence on material behavior may be explained by the way in which flow fields orient long molecules of high molecular weight. In shear flow, the preferred orientation corresponds to the direction of flow; however, the presence of a differential velocity across the flow field encourages molecules to rotate thereby reducing the degree of stretching induced in molecular chains. The tendency of molecules to rotate, versus elongate, depends on the magnitude of the shear field: There is relatively more elongation, less rotation, at high shear rates. In extensional flow, the situation is very different. The preferred molecular orientation is in the direction of the flow field because there are no competing forces to cause rotation. Hence, extensional flow will induce the maximum stretching of the molecules producing a chain tension that may result in a large (compared to shear flow) resistance to deformation.

The nature of the molecule, branched versus linear, may significantly influence flow behavior in extension. In comparable fluid systems (i.e., high-density polyethylene, a linear molecule, versus low-density polyethylene, a branched molecule) branched molecules will cause a fluid to be less tension-thinning then linear molecules. A similar

argument can be made in comparing the relative stiffness of biopolymer molecules: Stiffer molecules are more quickly oriented in an extensional flow field. This phenomenon may be a factor in the choice of a thickening agent for pancake syrup: Stringiness can be reduced, while maintaining thickness, when stiffer molecules are selected as additives. Reduced stringiness leads to what can be called a clean "cut-off" after pouring syrup from a bottle. An example of a stiff molecule would be the rod-like biopolymer xanthan compared to sodium alginate or carboxymethyl-cellulose which exhibit a randon-coil-type conformation in solution (Padmanabhan, 1995).

Extensional flow is an important aspect of food process engineering and prevalent in many operations such as dough processing. Sheet stretching, as well as extrudate drawing, provides a good example of extensional flow (Fig. 1.21). Converging flow into dies, such as those found in single and twin screw extruders, involves a combination of shear and extensional flow; the extensional component of deformation is illustrated in Fig. 1.21. The analysis of flow in a converging die (see Sec. 4.4) allows one to separate the pressure drop over the die into the shear and extensional components. Converging flow may also be observed when fluid is sucked into a pipe or a straw, or when applying a food spread with a knife.

One of the most common examples of extensional flow is seen when stretching warm mozzarella cheese while pulling a slice of pizza away from the serving pan. Sometimes this behavior is subjectively referred to as stringiness. A similar observation can be made when pulling apart a caramel filled candy bar or a pastry with fruit filling. Extensional deformation is also present in calendering (Fig. 1.22), a standard operation found in dough sheeting. Gravity induced sagging (Fig. 1.22) also embodies extensional deformation. This may be observed in a cut-off apparatus associated with fruit filling systems for pastry products. Extensional flow in this situation is undesirable because it may contribute to inconsistent levels of fill or an unsightly product appearance due to smeared filling. Bubble growth from the production of carbon dioxide gas occurring during dough fermentation, extrudate expansion from the vaporization of water, and squeezing to achieve product spreading involve extensional deformation (Fig. 1.23). Extensional flow is also a factor in die swell and mixing, particularly dough mixing with ribbon blenders.

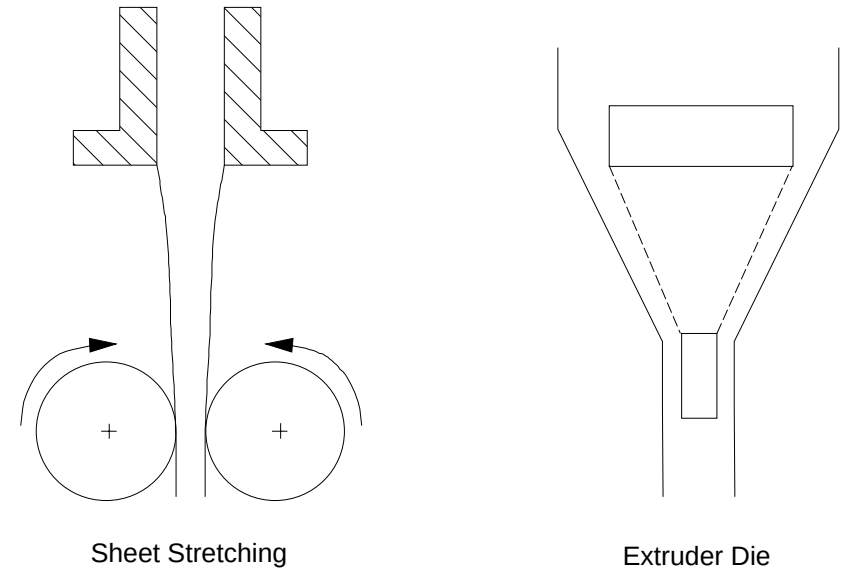

Figure 1.21. Extensional flow found in sheet stretching (or extrudate drawing) and convergence into an extruder die.

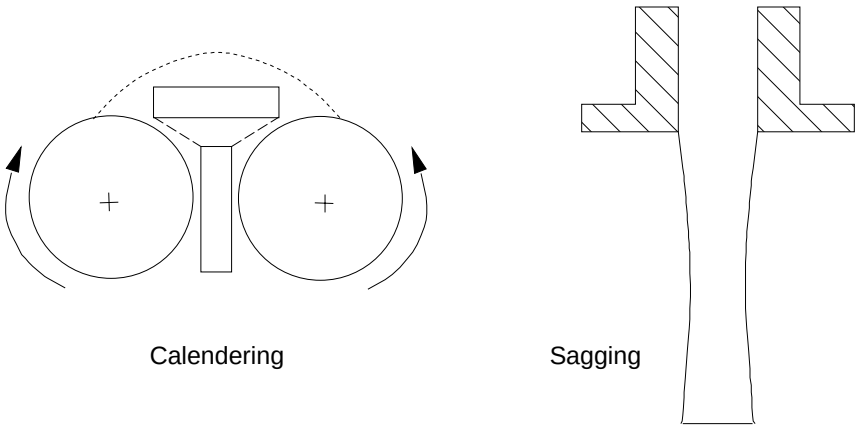

Figure 1.22. Extensional flow in calendering and gravity induced sagging.

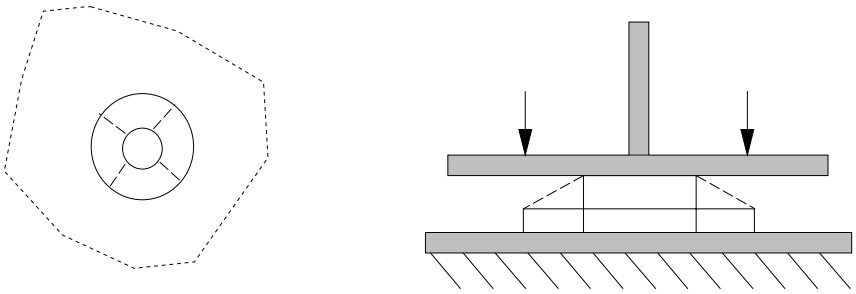

Figure 1.23. Extensional flow found in bubble growth and squeezing flow between lubricated plates.

Although extensional viscosity is clearly a factor in food processing, our use of this rheological property in engineering design of processes and equipment is still at an early stage of development. Extensional flow is also an important factor in the human perception of texture with regard to the mouthfeel and swallowing of fluid foods and fluid drugs. In addition, many plastic manufacturing operations involve extensional flow: compression moulding, thermoforming, blow moulding, fiber spinning, film blowing, injection moulding, and extrusion.

Extensional viscosity has been measured for various food products. Leighton et al. (1934) used the sagging beam method developed by Trouton (1906) to measure the extensional viscosity of ice cream. Results were presented in terms of apparent viscosity by using the well known Trouton ratio showing that extensional viscosity is equal to three times the shear viscosity (see Eq. [1.78]). This appears to be the first reported measurement of the extensional flow of a food product. Mozzarella cheese has been tested in uniaxial tension by Ak and Gunasekaran (1995). Biaxial extensional flow, produced by squeezing material between parallel plates, has been used in evaluating cheese (Campanella et al., 1987; Casiraghi et al., 1985), wheat flour doughs (Huang and Kokini, 1993; Wikström et al., 1994), gels (Bagley et al. 1985; Christianson et al. 1985), and butter (Rohn, 1993; Shuka et al., 1995). Data from the Chopin Alveograph, a common dough testing device where a spherical bubble of material is formed by inflating a sheet, can be interpreted in terms of biaxial extensional viscosity (Faridi

and Rasper, 1987; Launay and Buré, 1977). This technique requires an accurate determination of the sample geometry before and during inflation. Doughs have also been evaluated by subjecting them to uniaxial extension (de Bruijne et al., 1990).

The spinning test (also called extrudate drawing) was applied to measure the stretchability of melted Mozzarella cheese (Cavella et al., 1992). Entrance pressure drop from converging flow into a die has been used to evaluate an extensional viscosity for corn meal dough (Bhattacharya et al., 1994; Padmanabhan and Bhattacharya, 1993; Seethamraju and Bhattacharya, 1994) and bread dough (Bhattacharya, 1993). Additional methods have been proposed for evaluating the extensional behavior of polymeric materials (Ferguson and Kemblowski, 1991; James and Walters, 1993; Jones et al., 1987; Macosko, 1994; Petrie, 1979; Tirtaamadja and Sridhar, 1993; Walters, 1975): bubble collapse, stagnation flow in lubricated and unlubricated dies, open siphon (Fano flow), filament stretching, spinning drop tensiometer, and converging jets. Extensional viscosities for some Newtonian and non-Newtonian fluids are presented in Appendices [6.15] and [6.16], respectively. Measurement methods, and example problems, are discussed in Chapter 4.

Types of Extensional Flow. There are three basic types of extensional flow (Fig. 1.24): uniaxial, planar, and biaxial. During uniaxial extension material is stretched in one direction with a corresponding size reduction in the other two directions. In planar extension, a flat sheet of material is stretched in the x_1 direction with a corresponding decrease in thickness (x_2 decreases) while the width (x_3 direction) remains unchanged. Biaxial extension looks like uniaxial compression, but it is usually thought of as flow which produces a radial tensile stress.

Uniaxial Extension. With a constant density material in uniaxial extension (Fig. 1.24), the velocity distribution in Cartesian coordinates, described with the Hencky strain rate, is

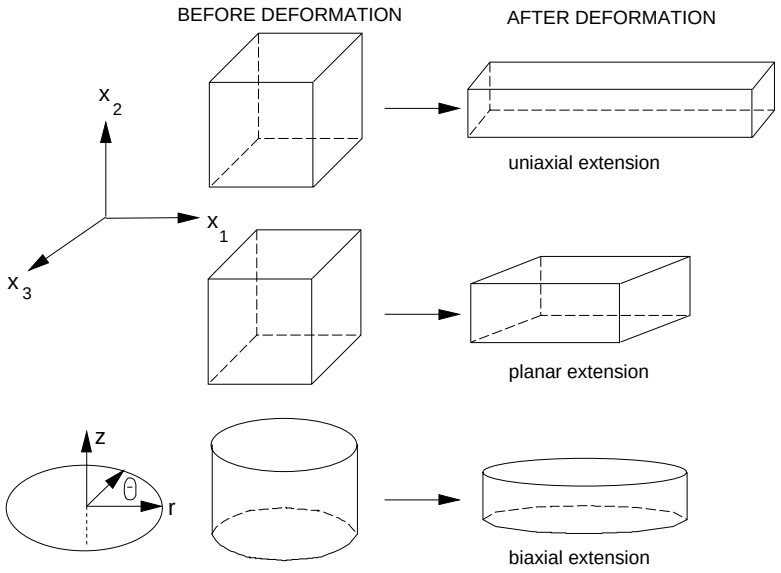

Figure 1.24. Uniaxial, planar, and biaxial extension.

$$u_1 = \dot{\varepsilon}_h x_1 \qquad [1.55]$$

$$u_2 = \frac{-\dot{\varepsilon}_h x_2}{2} \qquad [1.56]$$

$$u_3 = \frac{-\dot{\varepsilon}_h x_3}{2} \qquad [1.57]$$

where $\dot{\varepsilon}_h > 0$. Since this flow is axisymmetric, it may also be described in cylindrical coordinates (it may be helpful to visualize this situation with the positive z axis aligned with the x_1 axis, Fig. 1.24):

$$u_z = \dot{\varepsilon}_h z \qquad [1.58]$$

$$u_r = \frac{-\dot{\varepsilon}_h r}{2} \qquad [1.59]$$

$$u_\theta = 0 \qquad [1.60]$$

Pure extensional flow does not involve shear deformation; therefore, all the shear stress terms are zero:

$$\sigma_{12} = \sigma_{13} = \sigma_{23} = \sigma_{r\theta} = \sigma_{rz} = \sigma_{z\theta} = 0 \qquad [1.61]$$

Stress is also axisymmetric:

$$\sigma_{rr} = \sigma_{22} = \sigma_{33} \qquad [1.62]$$

resulting in one normal stress difference that can be used to define the tensile extensional viscosity:

$$\eta_E = f(\dot{\varepsilon}_h) = \frac{\sigma_{11} - \sigma_{22}}{\dot{\varepsilon}_h} = \frac{\sigma_{11} - \sigma_{33}}{\dot{\varepsilon}_h} = \frac{\sigma_{zz} - \sigma_{rr}}{\dot{\varepsilon}_h} \qquad [1.63]$$

Materials are considered tension-thinning (or extensional-thinning) if η_E decreases with increasing values of $\dot{\varepsilon}_h$. They are tension-thickening (extensional-thickening) if η_E increases with increasing values of $\dot{\varepsilon}_h$. These terms are analogous to shear-thinning and shear-thickening used previously (Sec. 1.5.1) to describe changes in apparent viscosity with shear rate.

Biaxial Extension. The velocity distribution produced by uniaxial compression causing a biaxial extensional flow (Fig. 1.24) can be expressed in Cartesian coordinates as

$$u_1 = \dot{\varepsilon}_B x_1 \qquad [1.64]$$

$$u_2 = -2\,\dot{\varepsilon}_B x_2 \qquad [1.65]$$

$$u_3 = \dot{\varepsilon}_B x_3 \qquad [1.66]$$

where $\dot{\varepsilon}_B > 0$. Since $\dot{\varepsilon}_h = 2\dot{\varepsilon}_B$, biaxial extension can actually be viewed as a form of tensile deformation. Uniaxial compression, however, should not be viewed as being simply the opposite of uniaxial tension because the tendency of molecules to orient themselves is stronger in tension than compression. Axial symmetry allows the above equations to be rewritten in cylindrical coordinates (Fig. 1.24) as

$$u_z = -2\dot{\varepsilon}_B z \qquad [1.67]$$

$$u_r = \dot{\varepsilon}_B r \qquad [1.68]$$

$$u_\theta = 0 \qquad [1.69]$$

Biaxial extensional viscosity is defined in terms of the normal stress difference and the strain rate:

$$\eta_B = f(\dot{\varepsilon}_B) = \frac{\sigma_{11} - \sigma_{22}}{\dot{\varepsilon}_B} = \frac{\sigma_{33} - \sigma_{22}}{\dot{\varepsilon}_B} = \frac{\sigma_{rr} - \sigma_{zz}}{\dot{\varepsilon}_B} = \frac{2(\sigma_{rr} - \sigma_{zz})}{\dot{\varepsilon}_h} \qquad [1.70]$$

Planar Extension. In planar extension (Fig. 1.24), the velocity distribution is

$$u_1 = \dot{\varepsilon}_h x_1 \quad [1.71]$$

$$u_2 = -\dot{\varepsilon}_h x_2 \quad [1.72]$$

$$u_3 = 0 \quad [1.73]$$

This type of flow produces two distinct stress differences: $\sigma_{11} - \sigma_{22}$ and $\sigma_{11} - \sigma_{33}$. Planar extensional viscosity is defined in terms of the most easily measured stress difference, $\sigma_{11} - \sigma_{22}$:

$$\eta_P = f(\dot{\varepsilon}_h) = \frac{\sigma_{11} - \sigma_{22}}{\dot{\varepsilon}_h} \quad [1.74]$$

It is difficult to generate planar extensional flow and experimental tests of this type are less common than those involving tensile or biaxial flow.

Relation Between Extensional and Shear Viscosities. The following limiting relationships between extensional and shear viscosities can be expected for non-Newtonian fluids at small strains (Dealy, 1994; Walters, 1975; Petrie, 1979):

$$\lim_{\dot{\varepsilon}_h \to 0} \eta_E(\dot{\varepsilon}_h) = 3 \lim_{\dot{\gamma} \to 0} \eta(\dot{\gamma}) \quad [1.75]$$

$$\lim_{\dot{\varepsilon}_B \to 0} \eta_B(\dot{\varepsilon}_B) = 6 \lim_{\dot{\gamma} \to 0} \eta(\dot{\gamma}) \quad [1.76]$$

$$\lim_{\dot{\varepsilon}_h \to 0} \eta_P(\dot{\varepsilon}_h) = 4 \lim_{\dot{\gamma} \to 0} \eta(\dot{\gamma}) \quad [1.77]$$

Reliable relationships for non-Newtonian fluids at large strains have not been developed. The above equations may be precisely defined for the special case of Newtonian fluids:

$$\eta_E = 3\mu \quad [1.78]$$

$$\eta_B = 6\mu \quad [1.79]$$

$$\eta_P = 4\mu \quad [1.80]$$

Eq. [1.78], [1.79], and [1.80] can be used to verify the operation of extensional viscometers. Clearly, however, a Newtonian fluid must be extremely viscous to maintain its shape and give the solid-like appearance required in many extensional flow tests. Extensional behavior of low viscosity fluids can be evaluated with the method of opposing jets (Sec. 4.5), by spinning (Sec. 4.6), or by investigating tubeless siphon behavior (Sec. 4.7).

Trouton established a mathematical relationship between tensile extensional viscosity (he called it the coefficient of viscous traction) and shear viscosity (Trouton, 1906). Presently, data for extensional and shear viscosities are often compared using a dimensionless ratio known as the Trouton number (N_{Tr}):

$$N_{Tr} = \frac{\text{extensional viscosity}}{\text{shear viscosity}} \qquad [1.81]$$

Since extensional and shear viscosities are functions of different strain rates, a conventional method of comparison is needed to remove ambiguity. Based on a consideration of viscoelastic and inelastic fluid behavior, Jones et al. (1987) advocated the following conventions in computing the Trouton numbers for uniaxial and planar extensional flow:

$$(N_{Tr})_{uniaxial} = \frac{\eta_E(\dot{\varepsilon}_h)}{\eta(\sqrt{3}\,\dot{\varepsilon}_h)} \qquad [1.82]$$

$$(N_{Tr})_{planar} = \frac{\eta_P(\dot{\varepsilon}_h)}{\eta(2\,\dot{\varepsilon}_h)} \qquad [1.83]$$

meaning that shear viscosities are calculated at shear rates equal to $\sqrt{3}\,\dot{\varepsilon}_h$ or $2\,\dot{\varepsilon}_h$ for uniaxial or planar extension, respectively. Using the similar considerations, Huang and Kokini (1993) showed that the Trouton number for case of biaxial extension should be calculated as

$$(N_{Tr})_{biaxial} = \frac{\eta_B(\dot{\varepsilon}_B)}{\eta(\sqrt{12}\,\dot{\varepsilon}_B)} \qquad [1.84]$$

The Trouton ratio for a Newtonian fluid may be determined from Eq. [1.78], [1.79], and [1.80]: in tensile extension it is equal to 3; it is 6 and 4, respectively, in biaxial and planar flow. Departure from these numbers are due to viscoelastic material behavior. Experimental results may produce considerably higher values.

1.8. Viscoelastic Material Functions

Fluids that have a significant elastic component may exhibit unusual behavior (Fig. 1.10; Fig. 1.11): Weissenberg effect (rod climbing), tubeless siphon, jet expansion, and recoil. Elastic behavior may be evaluated using viscometric methods to determine the normal stress differences found in steady shear flow. Alternatively, viscoelastic

material functions may be determined from experiments involving the application of unsteady state deformations. Generally, these dynamic testing techniques may be divided into two major categories: transient and oscillatory. Transient methods include tests of start-up flow, cessation of steady shear flow, step strain, creep, and recoil. In oscillatory testing, samples are deformed by the application of harmonically varying strain which is usually applied over a simple shear field. A comprehensive review of linear and nonlinear viscoelastic material functions is summarized in Chapter 5. Steady shear and linear viscoelastic material functions can be related (see Sec. 5.7) using various empirical relationships such as the Cox-Merz rule, the Gleissele's mirror relation, and Laun's rule (Bird et al., 1987).

Creep and Step-Strain (Stress Relaxation). In a creep test, material is subjected to a constant stress and the corresponding strain is measured as a function of time, $\gamma(t)$. The data are often plotted in terms of the shear creep compliance,

$$J = f(t) = \frac{\gamma}{\sigma_{constant}} \qquad [1.85]$$

versus time. In a step-strain test, commonly called a stress relaxation test, a constant strain is applied to the test sample and the changing stress over time is measured, $\sigma(t)$. The data are commonly presented in terms of a shear stress relaxation modulus,

$$G = f(t) = \frac{\sigma}{\gamma_{constant}} \qquad [1.86]$$

versus time. Data from creep and stress relaxation tests can also be described in terms of mechanical (spring and dashpot) analogs (Mohsenin, 1986; Sherman, 1970; Barnes et al., 1989; Polakowski and Ripling (1966)) which will be considered in more detail in Chapter 5. Creep and stress relaxation experiments can be conducted in shear, compression, or tension. Shear creep parameters for various creamy style salad dressings are given in Appendix [6.19].

Oscillatory Testing. The viscoelastic behavior of fluids can be determined from dynamic testing where samples are subjected to oscillatory motion when held in various containment systems, usually a cone and plate or a parallel plate apparatus. Typically, a sinusoidal strain is applied to the sample causing some level of stress to be transmitted through the material. The magnitude and the time lag of the transmission depend on the viscoelastic nature of the test substance.

In viscous (more liquid like) materials, much of the stress is dissipated in frictional losses; it is mostly transmitted in highly elastic materials. Likewise, the time lag (also called the phase lag) is large for highly viscous substances but small for materials exhibiting a high degree of elasticity. Investigating this type of phenomena leads to the definition of various material functions: complex viscosity (η^*), dynamic viscosity (η'), complex modulus (G^*), loss modulus (G''), and storage modulus (G'). These functions are discussed in detail in Chapter 5. Sometimes, oscillatory testing is referred to as "small amplitude oscillatory testing" because small deformations must be employed to maintain linear viscoelastic behavior. Typical oscillatory data for various food products are summarized in Appendices [6.20], [6.21], and [6.22].

1.9. Attacking Problems in Rheological Testing

Attacking rheological problems involves a critical judgement regarding the type of flow behavior involved and a careful determination of the appropriate instruments and techniques to use in finding a solution. A simple classification of material behavior (Fig. 1.25) provides a useful framework to approach rheological testing of an unknown fluid. Behavioral extremes would be that of pure Hookean behavior (ideally elastic material) and pure Newtonian behavior (ideally viscous material); hence, these categories have been placed on the upper right and left extremity of the figure. This symbolizes the fact that all real materials exhibit both viscous and elastic behavior although one type of behavior is frequently dominant. Water, for instance, is considered Newtonian but will show some degree of elasticity under conditions involving a very short process time, e.g., when a high velocity object impacts a body of water. In evaluating solids, one is typically looking at a stress-strain relationship as opposed to a fluid where a shear stress-shear rate relationship is studied.

When investigating the behavior of a new fluid, one must first determine if the material can be considered inelastic (purely viscous) meaning that behavior associated with elasticity (die swell, rod climbing, etc.) is not important in the application. If purely viscous, the next question deals with time-dependency and involves issues of structural stability or breakdown when subjected to a shear force. With materials that are time-independent, a rheogram may be developed and different mathematical equations (power law, Bingham, Herschel-Bulkley, or any of those presented in Table 1.3) considered to find a model that accurately describes flow behavior. Viscoelastic fluids, those showing

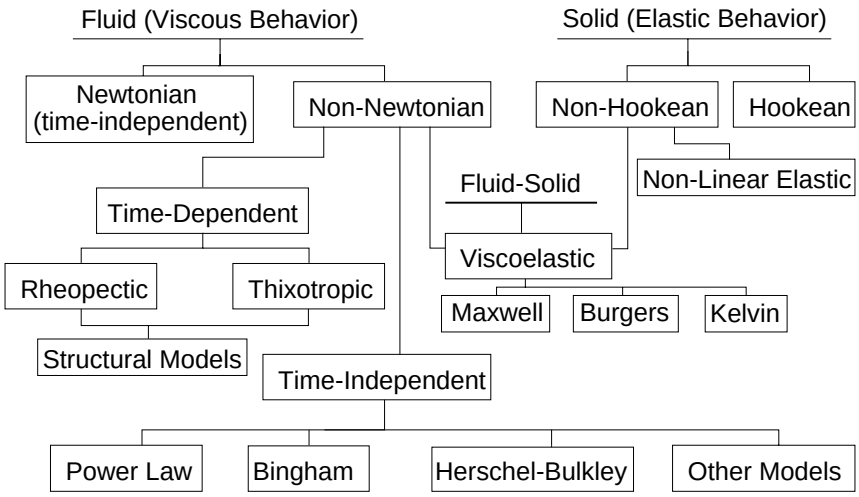

Figure 1.25. Simple classification of rheological behavior.

significant levels of both viscous and elastic behavior, may be tested using dynamic methods or static techniques (creep or stress relaxation) with various mechanical models (discussed in Sec. 5.2) being used to interpret results: Kelvin, Maxwell or Burgers models. Normal stress differences can be determined from viscometric flow. Extensional deformation may be used to determine additional material functions associated with stretching.

Classifying fluids is a valuable way to conceptualize fluid behavior; however, it is not meant to imply that the types of behavior noted in Fig. 1.25 are mutually exclusive. A material showing elastic behavior (such as dough) may simultaneously be shear-thinning and time-dependent! Other factors, like aging, may also influence rheological behavior. Tomato ketchup, for example, may be properly described as a time-independent, shear-thinning, fluid immediately after manufacture but aging often gives the material a weak gel like structure causing the product to exhibit thixotropic behavior when used by the consumer. This explains why agitating the ketchup, by stirring or shaking in the bottle, makes the condiment more pourable. Clearly, the ability to

conceptualize different types of rheological behavior is very important in the development, or improvement, of many new food products and processes.

Estimating Shear Rates in Practical Applications. It is very important that steady shear data be collected over the appropriate shear rate range. The minimum shear rate is often zero due to the presence of stationary equipment surfaces. Estimates of the maximum shear rate found in many processing systems can be obtained from a critical evaluation of the equipment.

In systems where fluid is closely contained between moving machinery parts, the maximum shear rate can be estimated from the velocity difference divided by the separation distance. An example of this can be found with an anchor impeller turning in a mixing vessel (Fig. 1.26) where the maximum shear rate is calculated as the tip speed of the impeller divided by the gap between the impeller and the mixing tank:

$$\dot{\gamma}_{max} = \frac{d\Omega}{D-d} \qquad [1.87]$$

Spreading (butter or margarine) or brushing (frosting or paint) operations are frequently found in the food industry. In this case (Fig. 1.26), the maximum shear rate can be estimated from the velocity of the brush (or knife) divided by the thickness of the coating:

$$\dot{\gamma}_{max} = u/z \qquad [1.88]$$

Estimating maximum shear rates in systems with widely spaced moving parts presents a different problem. Consider, for example, a paddle mixer in a vessel where $D \gg d$ so the influence of the wall is negligible (Fig. 1.27). Experimental data, taken a small distance from the impeller, can be used to obtain the velocity profile perpendicular to the axis of rotation. If these data are available, the maximum shear rate can be estimated from the differential velocity and the height of the blade (Fig. 1.27):

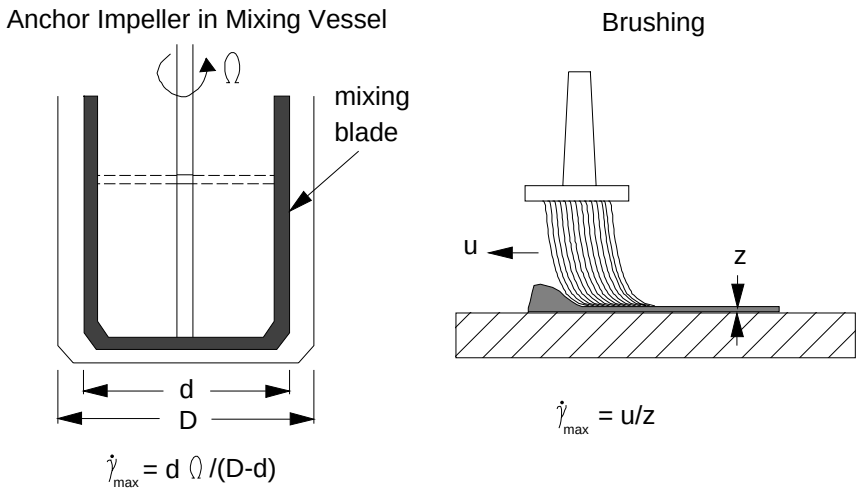

Figure 1.26. Maximum shear rates found in mixing with an anchor impeller and brushing.

$$\dot{\gamma}_{max} = (u_{b/2} - u_b)/(b/2) \qquad [1.89]$$

In the absence of experimental data, the tip speed of the impeller ($d\Omega/2$) can be used in place of ($u_{b/2}-u_b$) but this procedure will give an over estimate of the maximum shear rate because ($u_{b/2}-u_b$) < ($d\Omega/2$) due to the fact that fluid momentum is rapidly dissipated in the mixing vessel. Data of fluid velocity in the vicinity of mixing blades have been collected for a radial flat-blade turbine type mixer (Oldshue, 1983; Koutsakos and Nienow, 1990).

The maximum shear rate for fluid flow in a tubular geometry (Fig. 1.27) can be determined from the volumetric flow rate (Q) and the inside radius of the tube:

$$\dot{\gamma}_{max} = \frac{4Q}{\pi R^3} \qquad [1.90]$$

This calculation is exact for Newtonian fluids but must be modified for power law materials to include the flow behavior index:

$$\dot{\gamma}_{max} = \left(\frac{3n+1}{4n}\right)\frac{4Q}{\pi R^3} \qquad [1.91]$$

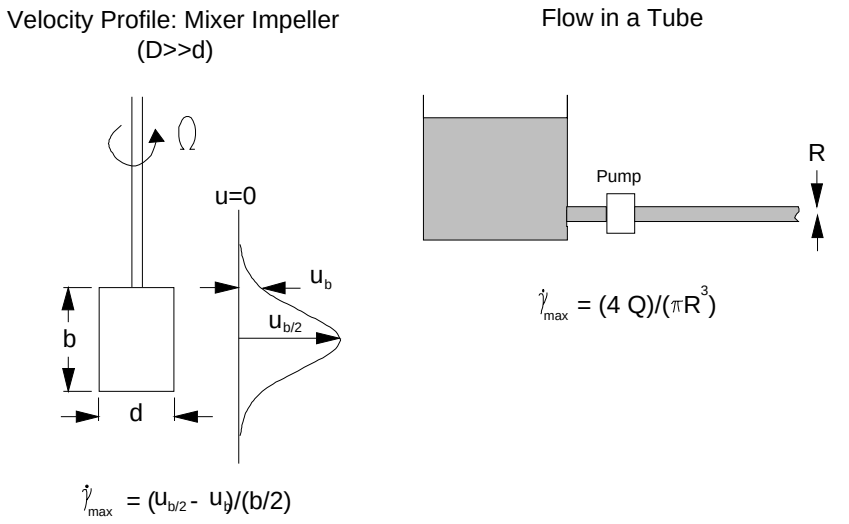

Figure 1.27. Maximum shear rate in a mixer when $D \gg d$ (where D is the vessel diameter), and flow of a Newtonian fluid in a tube.

Eq. [1.91] is very helpful in estimating the shear rate range needed to determine rheological data for pipeline design calculations because many fluid foods exhibit shear-thinning behavior, $0 < n < 1$. These relationships can also be used in considering flow through tube type systems such as ointment and tooth paste containers, frosting tubes, and spray nozzels. The origins of Eq. [1.90] and [1.91] will be clarified in a later discussion of tube viscometry given in see Sec. 2.2.

1.10. Interfacial Rheology

Both the shear and extensional viscosities discussed in preceding sections of this chapter are bulk material properties. Flow behavior at material interfaces, however, can be very different than bulk flow behavior. Interfacial rheology is a field of study that investigates deformations occurring at fluid interfaces. Many practical problems may involve interfacial rheological phenomena: formation, stability and processing of foams and emulsions; spraying and atomization; selection of surfactants; and film formation. Bulk and interfacial viscosities can be related using the Boussinesq number:

$$N_{Bo} = \frac{\text{interfacial viscosity}}{\text{bulk viscosity (length scale)}} \qquad [1.92]$$

Interfacial viscosity (usually reported in units of surface poise, sp, equivalent to 1 g s^{-1}) strongly affects bulk flow behavior at fluid interfaces when $N_{Bo} > 1$ (Edwards et al., 1991).

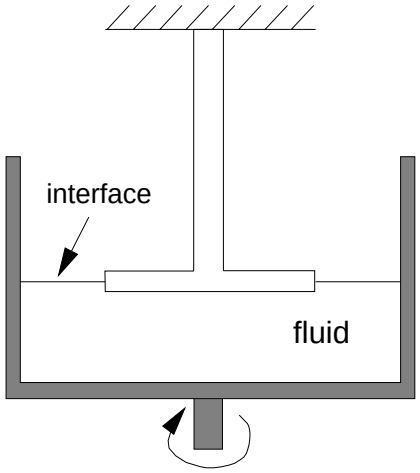

Figure 1.28. Disk surface viscometer to measure interfacial shear viscosity.

Various techniques are available to measure interfacial rheological behavior. These can be divided into indirect methods involving the examination of velocity profiles or direct methods involving the measurement of interfacial torsion. The disk surface viscometer is a classical (direct) method of measuring interfacial shear viscosity (Fig. 1.28). In this system the cup is turned and the resulting torque is measured on the fixed plate. To determine the interfacial viscosity, the torque contribution is considered in two parts: 1) one part, related to the bulk viscosity, due to fluid contact under the plate; 2) one part, related to the interfacial shear viscosity, due to the film induced traction along the rim of the plate. Interfacial shear viscosity may exhibit Newtonian or non-Newtonian behavior. Additional instruments to study interfacial rheology include the deep-channel surface viscometer, biconical interfacial viscometer, and various types of knife edge viscometers. Edwards et al. (1991) gives a detailed summary of numerous measurement

techniques for the determination of interfacial shear viscosity. Future research in interfacial rheology will lead to many improved products and processes in the food industry.

1.11. Electrorheology

The phenomenon of electrorheology refers to changes in the rheological behavior due to the imposition an electric field on a material. It is sometimes called the Winslow effect after W.M. Winslow who discovered it in 1947 (Winslow, W.M. 1947. U.S. Patent Specification 2417850). There has been a great deal of interest in electrorheological (ER) fluids for use in various mechanical devices (Block and Kelly, 1988): clutches, brakes, hydraulic valves, active or tunable damper systems, wide-band-high-power vibrators, chucks, exercise equipment, and robotic control systems. In the future, ER fluids will have a strong impact on the automotive industry and may eventually lead to improved designs for food manufacturing machinery. It may also be possible to develop unique processing schemes and new products for foods that exhibit an ER effect. The search for industrially viable electrorheological fluids has been hindered by the abrasiveness and chemical instability of candidate materials. Similar possibilities, and problems, are found with magnetorheological fluids where flow behavior may be changed with the imposition of a magnetic field.

ER fluids are dispersions of solid particulates, typically 0.1 to 100μm in diameter, in an insulating (non-conducting) oil. At low shear rates, in the absence of an electric field, particles are randomly distributed (Fig. 1.29) and many ER fluids will show nearly Newtonian behavior. With the application of an electric field, particles become polarized, causing particle alignment across the electrode gap creating an enhanced fiber-like structure. This alignment, associated with inherent electrical charges on the particles, causes ER substances to thicken dramatically. Application of a voltage causes some materials to develop high yield stresses characteristic of Bingham plastic behavior. In fact, the yield stresses can be so high that flow ceases, effectively transforming the material from a liquid to a solid. Results are influenced by many factors: nature (alternating or direct current) and strength of the electric field, temperature, composition and volume fraction of particles, shear rate, rheological and dielectric properties of the dispersing oil. Extensive experimental work is needed to evaluate the flow behavior of a particular ER fluid. To fully understand this problem involves a

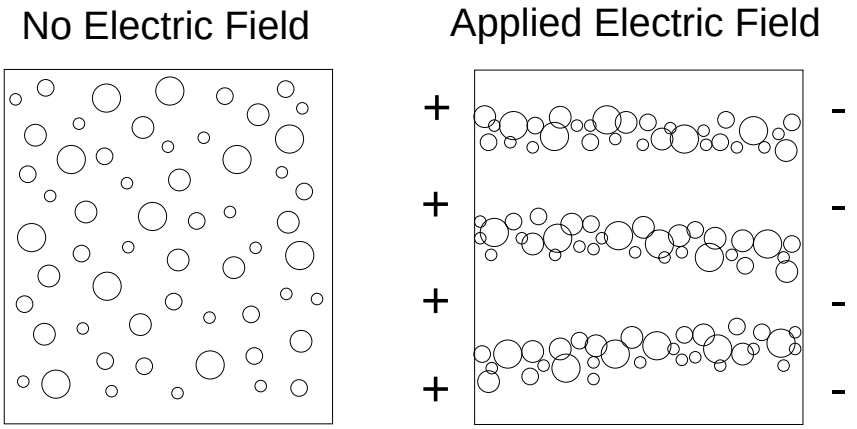

Figure 1.29. Particle alignment with and without an electric field (voltage per unit length) applied across a narrow gap.

careful study of the interplay between viscous, thermal, and polarization forces (Zukoski, 1993). Comments similar to the above may be made for magnetorheological fluids where the magnetic domains of the particles rotate until they line up with the applied magnetic field.

There are a number of food related ER fluids such as cellulose or sodium carboxymethyl cellulose in liquid paraffin, and starch or gelatine in olive oil. Milk chocolate is also known to be an ER fluid. Daubert and Steffe (1996) observed an ER response in this material: milk chocolate rheograms were shifted upward with an increase in electric field strength. A typical example of this is illustrated in Fig. 1.30. The yield stress, defined by the Casson equation, also increased with voltage. Temperature changes had a very interesting effect on ER behavior. In the presence of a voltage, increasing the temperature caused milk chocolate to thicken producing an upward shift in the rheogram. It appears that particle polarity was enhanced at higher temperatures. In the absence of a voltage the usual trend, a decrease in apparent viscosity with temperature increases, was observed.

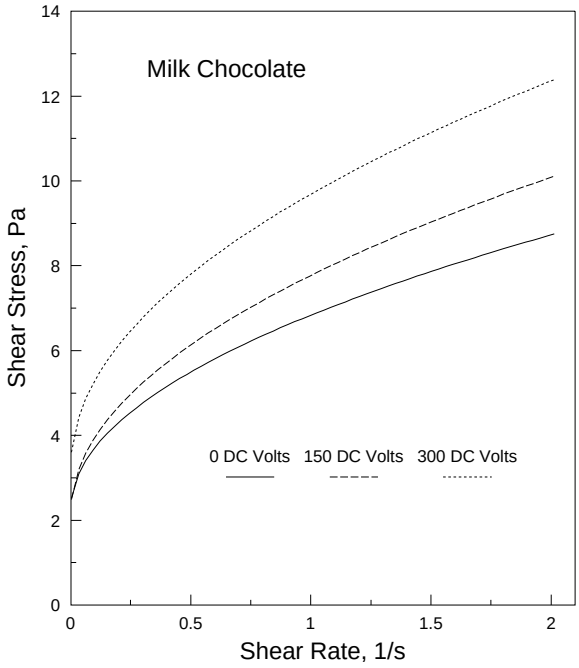

Figure 1.30 Typical influence of electric field strength (DC Volts/mm) on the flow behavior of molten milk chocolate.

1.12. Viscometers for Process Control and Monitoring

The goal of this section is to provide an overview of the primary measurement concepts and issues involved in the use of viscometers for continuous process control or monitoring. All process viscometers used for food products must conform to appropriate sanitary standards and accepted practices such as the 3-A and Egg 3-A standards published by the International Association of Milk, Food and Environmental Sanitarians (Des Moines, IA). Many process control viscometers were not designed for food applications and cannot be modified for acceptable sanitary operation. Viscometers discussed here are typical of industrially available units which are generally acceptable for use in the food industry. The current focus is on units that evaluate a steady shear viscosity. An industrial system to determine extensional viscosity, based on flow through an orifice (see Sec. 4.4.3), is also available.

In-line or On-line Installation. Viscometers for process control or monitoring may be installed using various measurement schemes. "In-line" systems are installed directly in the process line, usually in a pipe. These systems are subject to process variations, such as changes in sample temperature, which may significantly influence sensor output. "On-line" units make measurements on a product side stream, also called a by-pass loop, taken from the main process flow line. One advantage of this type of system is that sample variables (including flow rate, temperature, and pressure) may be controlled during testing. A third type of process control viscometer is the immersion system designed for use in process vessels, particularly mixing tanks. The above units provide alternatives to "off-line" measurements where a small sample is removed from the process line and evaluated in a standard laboratory instrument.

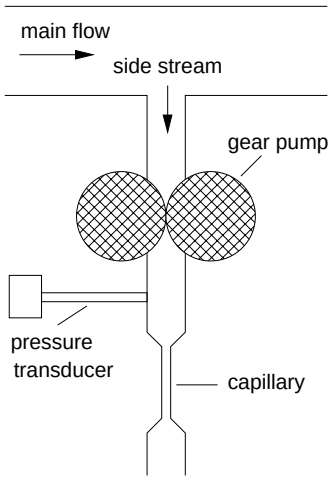

Figure 1.31. Capillary, on-line viscometer using side stream flow.

Measurement Concepts. A side stream capillary viscometer is illustrated in Fig. 1.31. Sample flow rate is determined by the speed of the gear pump. The system may be operated in two modes: constant flow rate or constant pressure. In the constant pressure mode, the gear pump is driven at the speed required to maintain a set pressure at the entrance to the capillary. In the constant flow rate mode, the pump

speed is fixed and the pressure drop required to force material through the capillary is measured. Regardless of the mode of operation, viscosity is directly proportional to the pressure drop across the capillary divided by the flow rate through the system. A commercial version of the side stream capillary viscometer, designed primarily for polymer melts, is produced by Goettfert, Inc. (Rock Hill, SC).

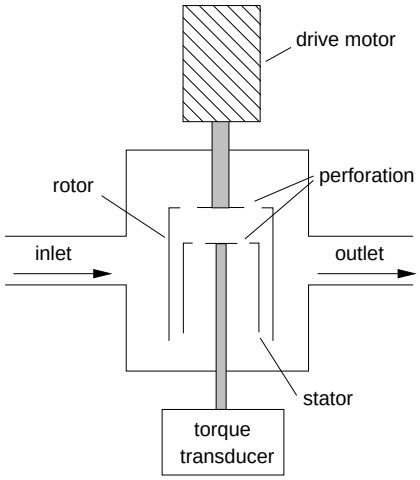

Figure 1.32. Concentric cylinder type in-line viscometer.

An in-line concentric cylinder viscometer measures the torque, on the inner cylinder, generated by the outer cylinder moving at a fixed speed (Fig. 1.32). Viscosity is proportional to the torque divided by the speed of the outer cylinder. The viscometer relies on perforations in the bob and cup to achieve continuous flow throughout the annular gap where fluid properties are measured. An alternative rotational viscometer is illustrated in Fig. 1.33. In this case, an off-set cylindrical element is attached to a rotating shaft causing a gyratory motion of the sensor. A continuous flow of test fluid moves through a perforated sheath during testing. Torque required to maintain a fixed speed of rotation is measured. Viscosity is proportional to the torque required to maintain a constant speed of rotation. Brookfield Engineering Laboratories (Stoughton, MA), and C.W. Brabender Instruments (S. Hackensack, NJ), respectively, produce instruments like those illustrated in Fig. 1.32 and 1.33.

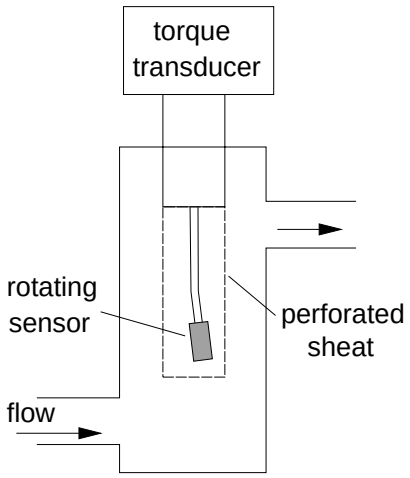

Figure 1.33. In-line viscometer using an off-set rotating element.

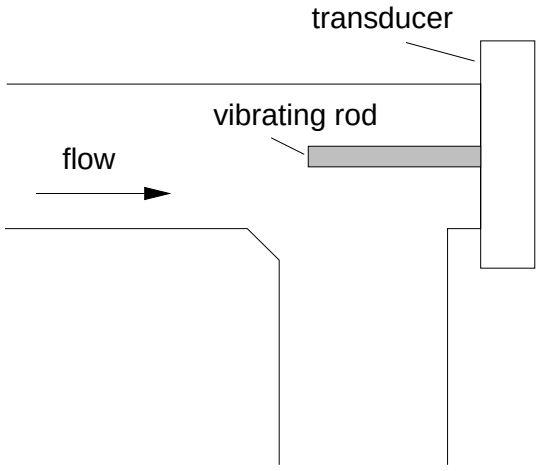

Figure 1.34. In-line viscometer using a vibrating rod.

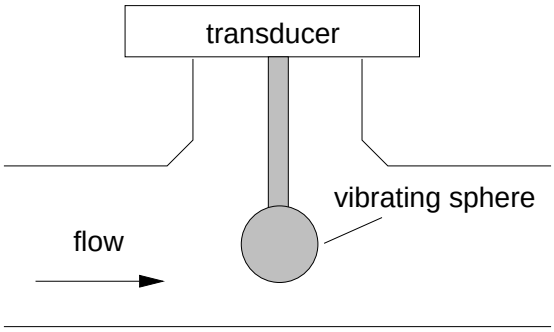

Figure 1.35. In-line viscometer using a vibrating sphere.

Vibrational viscometers are considered surface loaded systems because they respond to a thin layer of fluid at the surface of the sensor. In-line units may involve rod (Fig. 1.34) or spherical (Fig. 1.35) sensors. In each case, the sensor is driven at a fixed frequency and the power required to maintain a precise amplitude is measured. Since the vibrating probe accelerates the fluid, power input is proportional to product of viscosity and density. Density compensation can be incorporated allowing a direct computation of Newtonian viscosity. Spherical type vibrational viscometers are manufactured by Nameter (Metuchen, NJ).

An immersion type, falling body viscometer is illustrated in Fig. 1.36. A piston is periodically raised allowing sample to fill the cylindrical container. During testing, sample is expelled from the cylinder by the piston which is allowed to fall under the influence of gravity. Using reference data for standard Newtonian fluids, the falling time is correlated to sample viscosity. This concept can also be applied to an on-line processing system. Various falling piston viscometers are manufactured by Norcross Corporation (Newton, MA).

Practical Considerations in Selecting a Process Control Viscometer. It is important to have a good understanding of the fluid under consideration before selecting a process control viscometer. The influence of temperature, ingredient formulation, and processing conditions on flow behavior must be ascertained before quality control or set-points can be accurately established. Temperature has such a strong

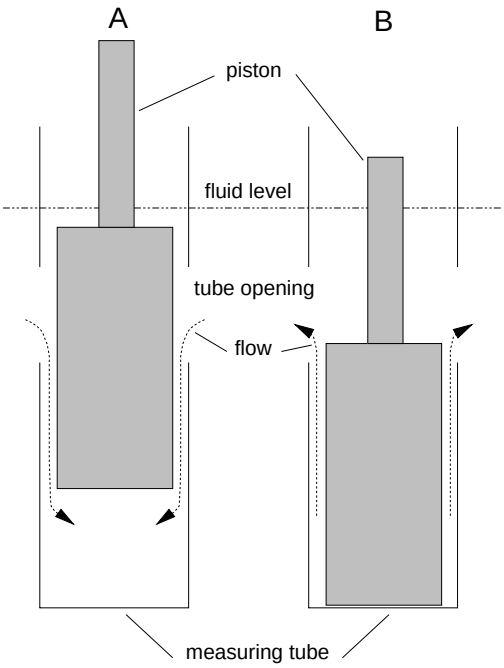

Figure 1.36. Falling piston, immersion type: (A) loading phase, (B) end of measurement.

influence on rheological behavior that it is usually necessary to either carefully control it when conducting measurements or compensate for it when making final calculations.

Process control viscometers are generally designed for Newtonian fluids where the viscosity is not a function of shear rate. To evaluate non-Newtonian fluids, multiple data points, taken at different shear rates are required. Hence, operational shear rates must be established and matched to the capabilities of the process control viscometer. The shear rates can be easily estimated in the capillary viscometers (Fig. 1.31) or concentric cylinder systems (Fig. 1.32), but they are very difficult to calculate in others such as the unit with the offset rotational element illustrated in Fig. 1.33. Determining fundamental rheological properties when shear rates cannot be evaluated is very complex; hence, some

process control viscometers can only generate comparative flow behavior data (not absolute rheological properties) for non-Newtonian fluids.

Process control viscometers may provide a strictly empirical parameter, an apparent viscosity, or a flow curve if samples are deformed at multiple shear rates. This information must be correlated to specific processing factors, such as the amount of cocoa butter in chocolate or the amount of water in tomato paste, before a control scheme can be initiated. If an on-line instrument is used for quality control, then quality must be carefully defined and directly related to the rheological property being measured. Also, the acceptable variation in quality must be known to establish the proper limits (or set-points) required in developing a control strategy. All process control viscometers must be calibrated regularly and carefully observed to ensure satisfactory long term performance.

1.13. Empirical Measurement Methods for Foods

The food industry uses many empirical instruments (Table 1.5) to measure the flow behavior of food products. These devices are not used to determine fundamental rheological properties, but results may find diverse applications: quality control, correlation to sensory data, or even serve as official standards of identity. Food engineers may find it necessary to replace empirical devices, like the Bostwick Consistometer used for pureed foods, with more fundamental instruments to achieve engineering objectives related to process control. With the exception of the melt flow indexer for molten polymers, all the instruments discussed in this section are used for food products.

It is important to recognize the fact that numerous foods are so complex it is not practical, and in many cases not possible, to measure their fundamental rheological properties. Carrots, peanuts, peas, or beans (for example) are non-homogeneous, nonisotropic materials with complex geometries. Only empirical testing devices, capable of measuring composite material behavior, provide a suitable means of characterizing these foods. Empirical instruments are a valuable and well established part of the food industry. Since they do not measure fundamental properties, they may appropriately be called indexers. Some of the most common units are described in this section. Consult Bourne (1982) and Brennan (1980) for additional information on evaluating food texture.

Table 1.5. Typical Empirical Testing Instruments and Applications for Food Products (Summarized from Bourne, 1982)

Device	Common Application
Adams Consistometer	consistency of semifluid food purees
Armour Tenderometer	beef tenderness
Baker Compressimeter	staleness of bread
Ballauf Pressure Tester	puncture testing of fruit and vegetables
BBIRA Biscuit Texture Meter	hardness of cookies and crackers
Bloom Gelometer	puncture test of gelatins and gelatin jellies
Bostwick Consistometer	flow of baby foods and similar purees
Chatillon Pressure Tester	puncture testing of fruit and vegetables
Effi-Gi Pressure Tester	puncture testing of fruit and vegetables
Extensigraph	behavior of wheat dough
Farinograph	baking quality of wheat flour
FMC Pea Tenderometer	quality and maturity of fresh green peas
FTC Texture Test System	attachments for many foods
GF Texturometer	attachments for many foods
Haugh Meter	egg quality
Hilker-Guthrie Plummet	firmness of cultured cream
Instron Universal Testing Machine	attachments for many foods
Kramer Shear Press	tenderness of peas and other particulate foods
Magness-Taylor Pressure Tester	puncture testing of fruit and vegetables
Marine Colloids Gel Tester	puncture test marine extract gels
Mixograph	baking quality of wheat flour
Ottawa Pea Tenderometer	quality and maturity of fresh green peas
Ottawa Texture Measuring System	attachments for many foods
Pabst Texture Tester	firmness of particulate foods
Penetrometer	firmness of butter and margarine
Plint Cheese Curd Torsiometer	setting of cheese curd
Resistograph	baking quality of wheat flour
Ridgelimiter	stiffness of pectin and fruit jellies
Stevens Compression Response Analyzer	attachments for many foods
Succulometer	maturity and quality of fresh sweet corn
SURDD Hardness Tester	hardness of fats and waxes
Torry Brown Homogenizer	toughness of fish
USDA Consistometer	consistency of semifluid food purees
Van Dorran Pressure Tester	puncture testing of butter
Warner-Bratzler Shear	toughness of meat

Dough Testing Equipment (Farinograph, Mixograph, Extensigraph, Alveograph). Dough - a combination of cereal (usually wheat) flour, water, yeast, salt, and other ingredients - is probably the most complex material facing the food rheologist; hence, it is not surprising that many empirical instruments have been developed to evaluate the flow behavior of dough. The instruments may be divided into two major groups: those which measure the power input during dough development caused by a mixing action, and those which subject prepared (developed) dough to an extensional deformation. The following discussion will describe the major instruments found in each group. Standard methods for operating these instruments and interpreting data are published by the American Association of Cereal Chemists (St. Paul, MN), and the International Association for Cereal Chemistry and Technology.

One of the most widely used dough mixers is the **Farinograph** (D'Appolonia and Kunerth, 1984). This instrument combines dough ingredients using two Z-shaped mixing blades that rotate, at different speeds, in opposite directions. Mixing is initiated with dry flour and water is added from a titrating buret during testing. A dynamometer is used to record torque on the drive shaft of the mixing blades. Output is given as a farinogram: a plot of an instrument-dependent parameter proportional to torque, expressed as a Brabender unit (BU, also called consistency), versus time. The shape of the farinogram is interpreted in terms of factors related to flour quality and the behavior of the dough in the bakery: dough development time, stability, mixing tolerance, and degree of softening. The amount of water required to give a consistency of 500 BU to a 14% moisture content (wet basis) flour is also an important flour parameter, known as the farinograph water adsorption, determined using the Farinograph.

An alternative to the Farinograph is the **Mixograph** which involves a planetary rotation of vertical pins (lowered into the dough) about stationary vertical pins attached to the mixing bowl. Torque is recorded while mixing a fixed amount of flour and water. Results are given in terms of a mixogram which is interpreted in a manner analogous to that discussed for the farinogram.

The **Extensigraph** (Rasper and Preston, 1991) generally conducts tests on doughs prepared in the Farinograph. A special molding device shapes the dough into a cylindrical specimen which is placed horizontally into a support system. The ends are clamped firmly in place leaving

the middle section free for testing. A hook contacts the middle of the sample and stretches it while moving downward at a constant speed. The force on the sample, caused by the downward motion of the hook, is recorded. Results are given as an extensogram, a plot of force (in Brabender units) versus time and extension, which provides valuable quality control information for the dough. It is important to note that materials with similar farinograms may have very different extensograms. The effects of oxidizing agents and enzymes on dough behavior, for example, can often be evaluated with extensograms.

The **Alveograph** (Shuey and Tipples, 1980), also called the Chopin Extensigraph, measures dough behavior when subjecting it to an extensional deformation. In this instrument, a circular disk is cut from a sheet of dough and clamped, around its circumference, to the base plate of the test apparatus. Air flowing through the base plate causes the dough to expand into a spherically shaped bubble which eventually ruptures completing the test. The air pressure in the bubble over time is recorded and plotted as an alveogram. In routine testing, the maximum height, overall length, and the area under the curve are the primary parameters taken off the alveogram. Alveograph data have been used to calculate biaxial extensional viscosity (Faridi and Rasper, 1987; Launay and Buré, 1977).

Cone Penetrometer. Stiff materials --like butter, peanut butter, or margarine-- are often assessed for "spreadability" using cone penetration data. This instrument consists of a weighted cone that is positioned vertically over the flat surface of the test sample. Cone angles of 20 or 45 degrees are typical. In standard testing, the cone is released into the sample and the depth of penetration, after a fixed period of time, is measured. Since test materials have a high yield stress, the cone comes to rest quickly. Results may be presented in terms of a yield value which is directly proportional to the weight of the cone assembly and inversely proportional to the depth of penetration (Haighton, 1959; Sone, 1972). Operating cone penetrometers with a constant downward speed, instead of a constant weight, is also an effective method of obtaining experimental data (Tanaka et al., 1971). Standard methods for testing lubricating greases involve double angle cones: one cone, with a small angle, mounted on a second cone with a larger angle.

Warner-Bratzler Shear. The basic part of this instrument is made from a 1 mm thick steel blade with a triangular hole cut from it. Metal bars, one located on each side of the blade, serve two functions: they orient the blade and push the test sample into the V shaped notch of the triangular opening. Maximum force to cut through the sample is recorded. Higher levels of cutting force are associated with increasing sample toughness. The Warner-Bratzler Shear is extensively used to evaluate the texture of raw and cooked meats. In these experiments, careful sample preparation and orientation are essential for obtaining reproducible results. Other foods such as carrots, celery, rhubarb, and asparagus have also been tested in this device.

Bostwick Consistometer. The instrument is a simple device used to evaluate the flow characteristics of pureed foods including applesauce, catsup, and numerous baby-food products. These units are usually made of stainless steel and consist of two abutting compartments connected with a common floor but separated by a spring-loaded gate. The first compartment is 5 X 5 X 3.8 cm when the gate is lowered. This section is loaded with fluid at the beginning of the test which is initiated by pressing a trigger that releases the gate. Fluid flows, under the influence of gravity, into the second compartment consisting of an inclined trough which is 5 cm wide, 24 cm long and approximately 2.5 cm high. The floor of the trough is graduated in 0.5 cm increments and movement down the trough reflects fluid properties. Measurements are taken after a specified time (typically 5 to 30 s) and reported as centimeters of travel from the starting gate. If fluid motion produces a curved surface, the travel distance of the leading edge is reported. The Bostwick Consistometer is still widely used as a quality control tool by the food industry. It is difficult to precisely relate Bostwick readings to fundamental rheological behavior (Vercrusse and Steffe, 1989); however, significant progress has been made for Newtonian and power law fluids using a gravity current analysis (McCarthy and Seymour (1994) which showed Bostwick measurements to be linearly related to apparent viscosity divided by density raised to the -0.2 power: $(\eta/\rho)^{-0.2}$.

Adams Consistometer. This device measures flow, due to gravity, over a horizontal plate made of glass, metal, or steel. The plate has a series of concentric circles, located one-quarter inch apart, radiating out from the geometric center of the plate. A truncated cone is centered on the plate and loaded with sample, then vertically raised by hand allowing material to flow radially outward over the flat surface. After

a fixed period of time (10 to 30 s is typical), the distance traveled in each quadrant is measured and the average value is recorded (in inches) as the "Adams Consistency." The Adams Consistometer is commonly used to evaluate cream style corn and similar products.

Zhan Viscometer. This device is a well known example of an orifice viscometer. It consists of a small cup-shaped vessel with a hole (orifice) in the bottom. The cup is filled with sample which is allowed to discharged through the orifice. Time is measured from the beginning of discharge until the steady stream coming out of the cup begins to drip. Discharge time is correlated to viscosity. Zhan type viscometers are used in many quality control applications.

Visco-Amylograph. The Visco-Amylograph (Shuey and Tipples, 1980) was designed to evaluate the behavior of starch solutions during gelatinization. It consists of a rotating bowl with eight vertical pins and a matching, suspended element, with seven vertical pins. Torque is recorded on the upper element during rotation of the bowl. The system includes a thermoregulator which allows the sample to be heated (the standard rate is 1.5°C per minute) during testing. When an aqueous suspension of starch is heated above the gelatinization temperature, the fluid thickens dramatically. A complete amylograph test usually involves four distinct thermal periods while the bowl is rotated at a constant speed: heating, holding, cooling, and holding. Results are presented as an amylogram which is a plot of torque (given as viscosity in Brabender units) versus time. Amylograms have proven useful in evaluating the quality of starch and its behavior as a thickening agent in many food systems.

Rapid Visco Analyser. This instrument generates data similar to that provided by the Visco-Amylograph. Small samples, typically 3 to 4 grams of starch in water, are heated in a small mixing vessel with a pitched paddle impeller. The aluminum mixing vessel and plastic impeller are both disposable. Samples are subjected to user program changes in temperature (heating, holding, and cooling) intended to match processing conditions found in a particular application. Torque, or instrument viscosity, are measured over time while the sample is agitated and programmed temperature changes are executed. This instrument, originally intended to evaluate the quality of Australian wheat, may be used to examine the quality of a wide variety of food starches.

Brookfield Rotating Disks and T-Bars. Brookfield Engineering Laboratories (Stoughton, MA) manufactures a rotational instrument (called the Brookfield Viscometer) that is extensively used in the food industry. The most common sensors are flat disks (spindles) attached to the instrument with a vertical shaft. Disks are available in various sizes and may be rotated at different speeds. Torque required to maintain constant rotation is measured. This device can read the viscosity of Newtonian fluids directly because it is calibrated with Newtonian materials (silicone oils).

Since a thorough analysis of shear rate on the disk is complex (Williams, 1979), it is difficult to use the Brookfield Viscometer for the determination of non-Newtonian fluid properties. Simplified approaches suggested by Mitschka (1982) and Durgueil (1987) are applicable to some foods. These techniques use numerous constants to convert torque and angular velocity data into shear stress and shear rate values, respectively. Briggs (1995) successfully determined the shear-thinning behavior of banana puree, salad dressing, chocolate syrup, enchilada sauce, and pancake syrup using Brookfield spindles and the Mitschka (1982) method of analysis.

Disk sensors can be very useful in obtaining a relative index of food thickness for the purpose of comparing products or making quality control judgments. In addition to disks, T-shaped bars are made for the same purpose. Instruments, equipped with the T-bars, can also be attached to the Brookfield Helipath Stand which allows the entire instrument to be lowered during testing. This causes the sensor to take a spiral path through the sample while torque data are obtained. The Helipath Stand is typically used for thick pastes and gels where a rotating disk would be difficult to insert or create a channeling effect during measurement.

Falling Ball Viscometer. Equations for the falling ball viscometer are derived in Example Problem 1.14.4. This type of viscometer involves a vertical tube where a ball is allowed to fall, under the influence of gravity, through a Newtonian fluid. Viscosity is calculated on the basis of the time taken to fall a fixed distance. If the vessel diameter is 10 times the ball diameter, wall effects can be neglected.

The rising bubble viscometer represents another application of the falling ball concept. In this case, a bubble of air is allowed to ascend through a column of sample. Rising time over a set distance is correlated to Newtonian viscosity.

Hoeppler Viscometer. The Hoeppler Viscometer is a variation of the falling ball concept. In this case, a ball having a diameter slightly smaller than the cylindrical vessel containing the test fluid, falls through a tube positioned with a 10 degree inclination from the vertical position. Time of fall over a set distance is correlated to the viscosity of Newtonian fluids. Units of this type are sometimes called rolling ball viscometers because descending spheres may roll along the wall of the viscometer.

Brabender-FMC Consistometer. This unit was originally designed to evaluate cream style corn but it has also been used for ketchup, tomato paste, baby food, and similar products. It is designed to lower a thin, rectangular shaped, paddle into a sample held in a stainless steel cup. The cup is rotated at a single speed of 78 rpm. This motion creates a torque on the paddle that is read from a dial located on the top of the instrument. Paddles are available in various sizes: 5.08 cm (2 inch) by 3.56 cm (1.4 inch) is typical.

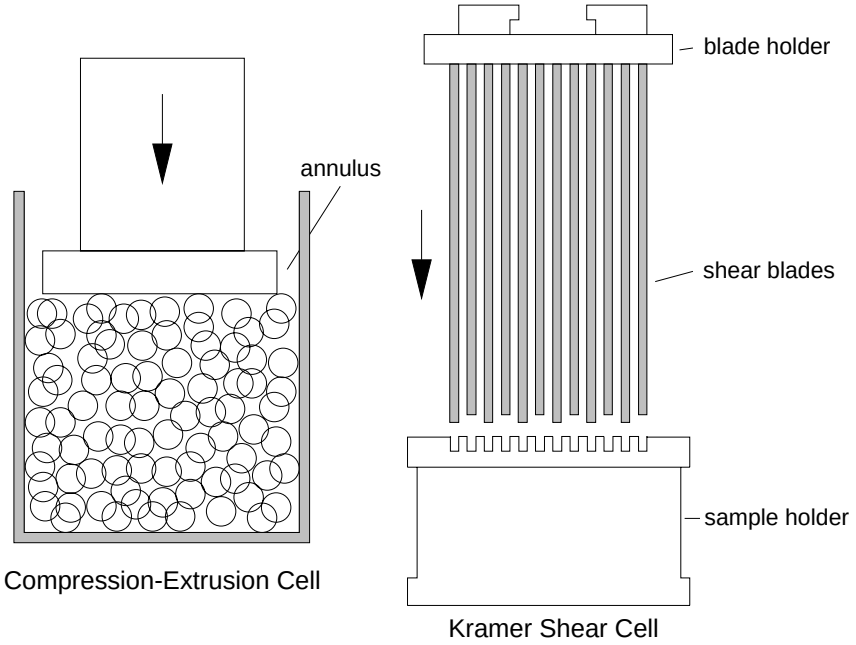

Figure 1.37. Compression-extrusion and Kramer shear cells commonly used to evaluate the behavior of particulate foods.

Compression-Extrusion Cell. This test apparatus (Fig. 1.37) is a common device used to measure the behavior of particulate foods (Bourne, 1982). In the compression-extrusion cell (also called a back extrusion cell), sample compression causes material to flow through the annulus formed between the plunger and the cylindrical container. Sample data consist of a curve relating the force on the plunger versus the distance of plunger travel (or travel time). Curves from different samples, involving different treatments or varieties, are compared to establish differences in product texture.

Kramer Shear Cell. The Kramer shear cell (Fig. 1.37) is a well established tool for evaluating the composite flow behavior of particulate foods. A typical system contains 10 shear blades which are 3.2 mm thick and separated by a distance equal to the thickness (3.2 mm). Bars form matching slits in the top and bottom of the sample holder. The sample box is approximately 65 mm wide, long, and deep. During testing, the sample holder is filled with food and the shear blades (properly aligned with the bars in the top) are forced through the material until they pass through the bars in the bottom of the sample holder. Force on the ram holding the blades is measured over time and correlated to product firmness.

Simple Compression. Biological materials may be evaluated in terms of a bioyield point and a rupture point (Mohsenin, 1984). A curve such as the one illustrated in Fig. 1.38 is typical for solid foods, like fruits and vegetables, when a cylindrical sample is tested in simple compression. The initial portion of the curve (a-b) is a straight line up to the linear limit (b). Young's modulus may be calculated from the stress and strain at that point: $\sigma_b/\varepsilon_b = E$. A secant or a tangent modulus, defined at a particular strain, may be calculated if the line is curved (Mohsenin, 1986). The slope of the initial portion of the curve is often taken as an index of firmness. When stress and strain cannot be calculated, data may be simply plotted in terms of force and deformation.

The bioyield point (c) is related to a failure in the microstructure of the material associated with an initial disruption of cellular structure (Fig. 1.38). It is observed at a stress and strain of σ_c and ε_c, respectively. The rupture point (d) of the material, defined by σ_d and ε_d, correlates to the macroscopic failure in the sample. With more brittle materials the rupture point may be very close to the bioyield point: These points may be widely separated in tough materials. The American Society of

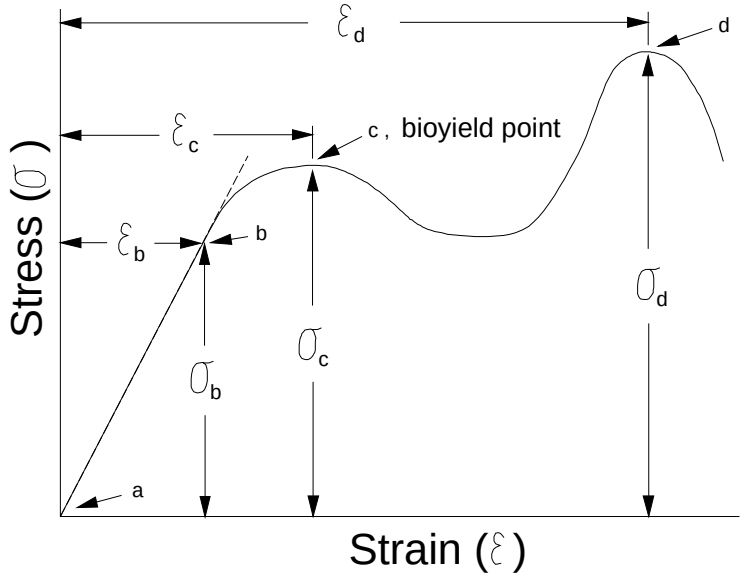

Figure 1.38. Generalized compression curve for a biological solid.

Agricultural Engineers (ASAE, St. Joseph, MI) has established a standard method for the compression testing of food materials of convex shape (ASAE Standard S368.2). It is similar to the simple compression test described here.

Texture Profile Analysis. Texture refers to the human sensation of food derived from its rheological behavior during mastication and swallowing. Obtaining a quantitative description of texture using instrumental data is very complicated because no instrument can duplicate human capabilities. From an engineering perspective, the mouth can be considered an intricate mechanical system and chemical reactor that can crush, wet, enzymatically degrade, pressurize, heat or cool, pump, chemically sample for taste, and sense force and temperature. In addition, this "eating machine" has a sophisticated feedback control system. Initially there is open loop, feed forward control to set primary parameters: size of mouth opening, surface selection for first bite (incisors or molars), etc. Once the food is in the mouth, there is an adaptive feed back control system with a variable gain -high with unfamiliar foods, low with everyday foods- that depends on bolus

development during mastication. This process is influenced by many factors: volume of the oral cavity, rate of addition of saliva, chemical composition of saliva, chemical and physical interaction of saliva and the food, rate of chewing, total number of chews, surface area in contact with the food, movement of the lips and cheeks, dynamic volume of the oral cavity during mastication, residence time of the bolus, initial volume of the bolus, and partial fluid removal (by swallowing) during chewing. Given the above, it is not surprising that little progress has been made in correlating fundamental rheological properties to the human perception of texture. There has been limited success with some fluid (Christensen, 1987; Kokini and Cussler, 1987; Sherman, 1988) and solid foods (Hamann and Lanier, 1987; Montejano et al., 1985).

Overall, there are two methods to evaluate food texture: sensory and instrumental. The sensory method of developing a texture profile (Muñoz et al. 1992) utilizes a human taste panel and provides the ultimate test which, as discussed above, cannot be completely duplicated by any instrumental procedure. Instrumental methods, however, are much less costly and time consuming than sensory tests. Moreover, they often correlate to critical sensory attributes which allow some measure of consumer acceptability. It is, however, rare for them to stand alone as a complete test. In any event, they can certainly be very valuable when used in conjunction with sensory panels. Generating and interpreting texture profile information, with instrumental or sensory means, is called Texture Profile Analysis. A double compression test, the most recognized instrumental means of characterizing the texture of solid and semi-solid foods, is discussed below.

The idea of texture profiling food was proposed in 1963 (Friedman et al., 1963; Szczesnaik et al. 1963) and conducted using an instrument known as the General Foods Texturometer. Bourne (1968 and 1974) adopted, and extended, the technique to the Instron Universal Testing Machine where a food sample (bite size pieces of food, usually a 1 cm cube) is compressed, two times, usually to 80 percent of its original height. Compression is achieved using parallel plates where one plate is fixed and the other plate moves with a reciprocating linear cyclical motion. Since this test is intended to reflect the human perception of texture, the first and second compression cycles are referred to as the first bite and second bite, respectively. A generalized texture profile curve is illustrated in Fig. 1.39. Various textural parameters may be determined from the curve (Bourne, 1978; Szczesnaik et al. 1963):

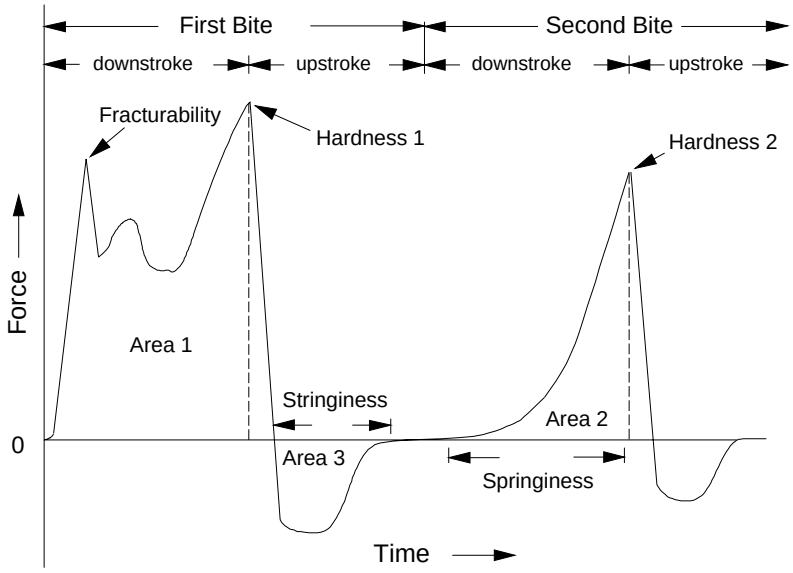

Figure 1.39. Generalized texture profile curve obtained from the Instron Universal Testing Machine (from Bourne et al., 1978).

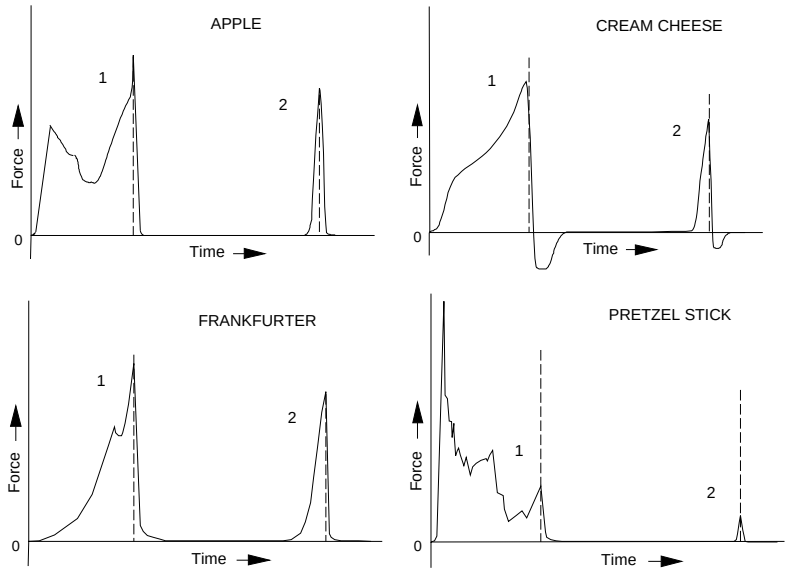

Figure 1.40. Texture profile curves (1 = first bite; 2 = second bite) for four food products (from Bourne, 1978).

- Fracturability: force at the first major drop in force curve. Popular terms describing fracturability are crumbly, crunchy, and brittle.
- Hardness 1: force at maximum compression during first bite. Popular terms describing hardness are soft, firm, and hard.
- Area 1 (area under the solid line up to the dashed line in the first compression cycle): work done on the sample during the first bite.
- Adhesiveness: Area 3 (area under the zero force line) representing the work, caused from a tensile force, needed to pull food apart and separate it from the compression plates. A similar adhesiveness characteristic is present in the second compression cycle. Popular terms describing adhesiveness are sticky, tacky, and gooey.
- Adhesive Force: maximum negative force.
- Stringiness: distance food extends before it breaks away from the compression plates.
- Hardness 2: force at maximum compression during second bite.
- Area 2 (area under the solid line up to the dashed line in the second compression cycle): work done on the sample during the second bite.
- Springiness: distance or length of compression cycle during the second bite. Popular terms describing springiness are plastic and elastic.
- Cohesiveness: the ratio of Area 2 divided by Area 1.
- Gumminess: the product of Hardness (first peak called Hardness 1 in Fig. 1.39) times Cohesiveness. Popular terms describing gumminess are short, mealy, pasty, and gummy.
- Chewiness: the product of Gumminess times Cohesiveness times Springiness which is equivalent to Gumminess times Springiness. Popular terms describing chewiness are tender, chewey, and tough. Though Chewiness and Gumminess are similar, they are mutually exclusive. The same product cannot exhibit both Chewiness and Gumminess: Chewiness refers to solid foods and Gumminess refers to semi-solid foods (Szczesnaik, 1995).

Typical texture profile curves for apple tissue, frankfurter, cream cheese, a pretzel stick are shown in Fig. 1.40. Observing these curves makes it clear that many foods do not exhibit all the textural parameters defined above. Texture Profile Analysis has proved to be a very useful technique for examining food products which fracture; however, texture

profile curves are subject to many variations making the proper interpretation of experimental data challenging. More fundamental analyses can be attempted using the science of fracture mechanics.

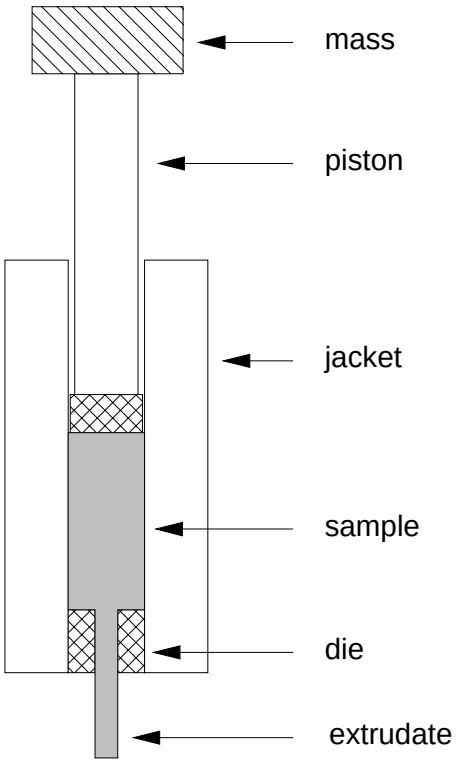

Figure 1.41. Simple melt flow indexer for molten polymers.

Melt Flow Indexer for Polymers. The melt flow indexer is a weight driven capillary instrument used as a quality control device to characterize the behavior of molten polymers. Although the device is not employed for food, use of the instrument in the thermoplastics industry is so widespread that anyone interested in fluid rheology should have a general awareness of how it operates.

A simple melt flow indexer (Fig. 1.41) is contained within a thermal jacket which controls sample temperature. A known mass is placed on the plunger which drives a piston downward causing the sample to be extruded through the die. Exact dimensions and operating procedures

are described by American Society for Testing and Materials (ASTM) standards. Typical dimensions involve a die diameter of 2.1 mm, and a ratio of die length to die diameter equal to 4. In a common testing procedure known as "condition E," a sample (such as polyethylene) is allowed to come to an equilibrium temperature of 190°C. Then, a 2.16 kg mass is placed on the piston and the molten polymer is extruded from the die. The weight, in grams, of the extrudate produced in 10 minutes is the melt flow index, or simply the melt index, of the polymer. Values of the melt flow index reflect the viscosity of the material: Low viscosity materials, corresponding to a low molecular weight, have a high melt flow index. This information is very valuable in the thermoplastics industry because it correlates well to the quality and processing characteristics of numerous polymers.

1.14. Example Problems

1.14.1. Carrageenan Gum Solution

Rheological data for a 1% aqueous solution of carrageenan gum at 25°C are available (Table 1.6). Determine the power law parameters and plot the apparent viscosity curve.

Table 1.6. Steady Shear, Rheological Data for a 1% Aqueous Solution of Carrageenan Gum at 25°C (Data from Prentice and Huber, 1983)

$\dot{\gamma}$ (s^{-1})	σ (Pa)	$\dot{\gamma}$ (s^{-1})	σ (Pa)
9.88	2.61	58.8	8.20
11.4	2.97	75.4	9.08
12.9	2.81	104.1	11.63
14.1	3.44	110.4	10.65
17.6	3.80	120.5	12.75
26.3	4.85	136.5	13.10
42.0	6.61	145.8	14.90
48.6	6.19	187.1	15.85
49.3	5.89	210.2	12.70
55.5	7.22	270.0	20.50

The data were plotted (Fig. 1.42) and an excellent fit was obtained with linear regression analysis using the power law model: K = 0.66 Pa s^n and n = 0.60. Other rheological models could be used to fit the experimental data. Some (like the Newtonian model) would result in

greater statistical variation while others (like the Herschel-Bulkley model) would improve the statistical accuracy with which the equation represents the data.

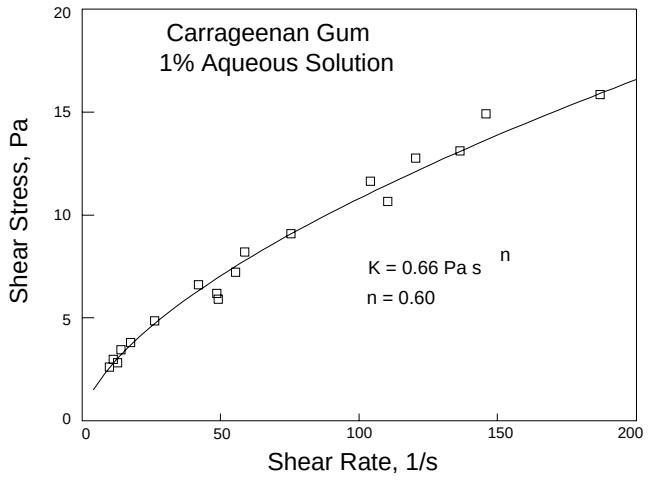

Figure 1.42. Rheogram for a carrageenan gum solution at 25°C.

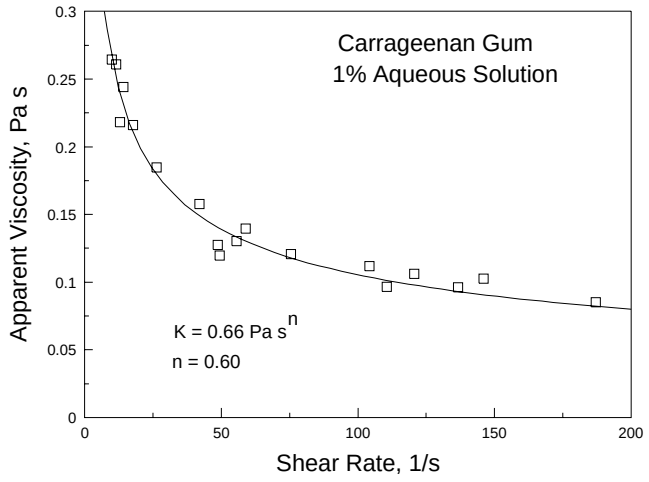

Figure 1.43. Apparent viscosity of a carrageenan gum solution at 25°C.

Apparent viscosity is calculated as $\sigma/\dot{\gamma}$ and plotted as a function of shear rate (Fig. 1.43). Mathematically, the curve can be described in terms of the power law fluid model using K and n values determined from the shear stress versus shear rate data:

$$\eta = K(\dot{\gamma})^{n-1} = .66(\dot{\gamma})^{-.4}$$

The data presented in Table 1.6 have also been evaluated in terms of the Casson, Bingham, and Herschel-Bulkley models in Appendix 6.4 where the method of linear regression analysis is explained.

1.14.2. Concentrated Corn Starch Solution

Examine the rheological information presented (Fig. 1.44) for a concentrated (53% wt/wt) solution of raw corn starch and water. Steady shear data were collected using a conventional cone (4 degree, 60 mm diameter) and plate apparatus.

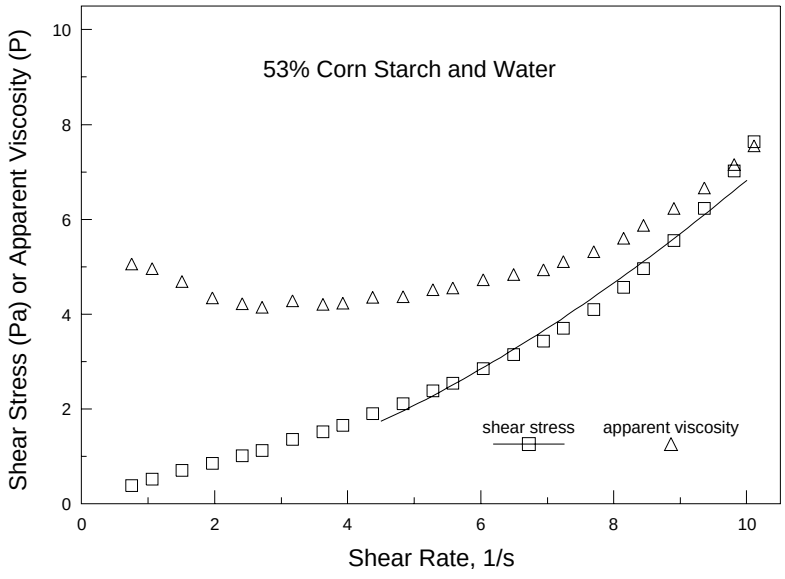

Figure 1.44. Rheogram of a 53% (wt/wt) solution of raw corn starch and water at 25°C.

The corn starch solution is a concentrated suspension of starch particles in water. Examination of the apparent viscosity curve (Fig. 1.44) shows initial shear-thinning followed by strong shear-thickening behavior. At low shear rates ($0 < \dot{\gamma} < 4.5$ s^{-1}), the water has a lubricating effect between the particles and flow is relatively unhindered. With higher shear rates ($\dot{\gamma} \geq 4.5$ s^{-1}), increased resistance from particle to particle interaction causes a significant increase in apparent viscosity. Curve fitting the data, above 4.5 s^{-1}, to the power law model yields:

$$\sigma = K(\dot{\gamma})^n = .131(\dot{\gamma})^{1.72}$$

where K = 0.131 Pa s and n = 1.72. A flow behavior index equal to 1.72, a value significantly greater than 1.0, is a numerical indication of a large shear-thickening effect. The above equation is illustrated as the line plotted in Fig. 1.44.

Table 1.7. Rheological Data for Swedish Commercial Milk Chocolate at 40°C (Data from Prentice and Huber, 1983)

$\dot{\gamma}$ (s^{-1})	σ (Pa)	$\dot{\gamma}$ (s^{-1})	σ (Pa)
0.099	28.6	6.4	123.8
0.140	35.7	7.9	133.3
0.199	42.8	11.5	164.2
0.390	52.4	13.1	178.5
0.790	61.9	15.9	201.1
1.60	71.4	17.9	221.3
2.40	80.9	19.9	235.6
3.90	100.0		

A concentrated corn starch solution can provide an excellent visual and tactile example of shear-thickening behavior. First, a 50 to 55% (wt/wt) solution consisting of raw corn starch (available in most grocery stores) and water is required. Next, one must be willing to examine the material with bare hands. If you slowly move a finger through the material, the solution feels and appears like a liquid. If the finger is moved quickly, however, this substance provides much greater resistance and shows solid-like behavior by fracturing and separating at the higher shear rate! The material quickly reverts to a liquid-like appearance at the cessation of movement.

1.14.3. Milk Chocolate

Rheological data for milk chocolate at 40°C are available (Table 1.7). Determine the Casson and Bingham plastic model parameters for this material.

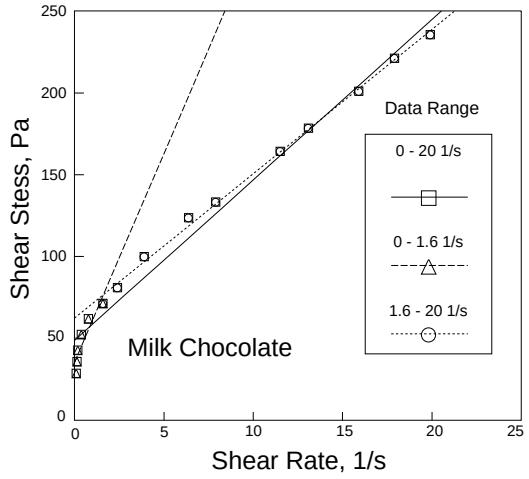

Figure 1.45. Regression analyses of 40°C milk chocolate applying the Bingham plastic model over different shear rate ranges.

Data are present for low shear stresses and a plot (Fig. 1.45) of this information suggests the presence of a yield stress. Casson and Bingham plastic model parameters were calculated over three different shear rate ranges (Table 1.8). The results clearly indicate that the model and shear rate range covered in the analysis have a strong influence on the yield stress (the dynamic yield stress) calculated from the intercept of the regression curve. When data at the lower shear rates are emphasized, the calculated yield stress decreases. This results in Bingham yield values ranging from 35.1 to 52.3 Pa.

Table 1.8. Constants for Bingham Plastic ($\sigma = \sigma_o + \mu_{pl}(\dot{\gamma})^n$) and Casson ($\sigma^{0.5} = (\sigma_o)^{0.5} + K_1(\dot{\gamma})^{0.5}$) Models Used to Describe the Behavior of 40°C Milk Chocolate Over Three Shear Rate Ranges

	Casson Model			Bingham Plastic		
$\dot{\gamma}$ (s^{-1})	K_1 ($Pa^{.5}\ s^{.5}$)	σ_o (Pa)	r^2	μ_{pl} (Pa s)	σ_o (Pa)	r^2
0 - 20	2.21	29.7	.99	8.82	62.3	.99
1.6 - 20	2.14	32.3	.99	9.80	48.7	.98
0 - 1.6	3.04	17.8	.89	25.5	35.1	.84

1.14.4. Falling Ball Viscometer for Honey

The effect of temperature on the viscosity of a Newtonian fluid can be illustrated by considering data from a falling ball viscometer. Derive (**Part a**) the falling ball viscometer equations and use them to evaluate (**Part b**) the viscosity of honey from the data given in Table 1.9. Also, evaluate the influence of temperature on honey viscosity using the Arrhenius equation.

Part a. Consider a sphere (radius=R; density=ρ_s) dropping through a Newtonian fluid (density=ρ_l) otherwise at rest. The sphere, traveling downward at terminal velocity (u_t), is subject to three forces: buoyancy ($(4\pi R^3\rho_l g)/3$), drag ($6\pi R\mu u_t$) and gravity ($(4\pi R^3\rho_s g)/3$). A force balance yields

$$\left(\frac{4}{3}\pi R^3\right)g\rho_l + 6\pi R\mu u_t = \left(\frac{4}{3}\pi R^3\right)g\rho_s \qquad [1.93]$$

where the drag term comes from Stoke's law (Trans. Cambridge Phil. Soc. Vol. 8, 1845 and Vol. 9, 1851). Simplification of Eq. [1.93] gives

$$\frac{\mu}{\rho_s - \rho_l} = \frac{2R^2 g}{9u_t} \qquad [1.94]$$

The time (t) required for the ball to fall a fixed distance (L) is

$$t = \frac{L}{u_t} \qquad [1.95]$$

so the terminal velocity is

Table 1.9. Falling Ball Viscometer Data for Honey at Six Temperatures

		Ball #1	Ball #2	Ball #3
ball diameter (d), m		.00475	.00678	.00792
ball density, kg/m^3		7900	7900	7900
length of fall, m		0.20	0.20	0.20
honey density, kg/m^3		1400	1400	1400
container diameter (D), m		0.036	0.036	0.036
$\alpha = d/D$		0.132	0.188	0.220
Faxen correction factor		0.727	0.617	0.559
t	at 6.5 °C, s	270.0	152.5	122.0
	at 12.5 °C, s	108.3	58.5	46.8
	at 20.0 °C, s	31.7	17.8	14.4
	at 21.5 °C, s	25.7	14.4	11.4
	at 38.0 °C, s	3.0	1.8	1.4
	at 48.0 °C, s	1.5	1.0	0.9
μ	at 6.5 °C, Pa s	107.79	124.04	135.41
	at 12.5 °C, Pa s	43.22	47.58	51.94
	at 20.0 °C, Pa s	12.67	14.51	15.98
	at 21.5 °C, Pa s	10.26	11.67	12.65
	at 38.0 °C, Pa s	1.20	1.46	1.55
	at 48.0 °C, Pa s	0.60	0.81	0.99
μ_c	at 6.5 °C, Pa s	78.38	76.59	75.68
	at 12.5 °C, Pa s	31.43	29.38	29.03
	at 20.0 °C, Pa s	9.21	8.96	8.93
	at 21.5 °C, Pa s	7.46	7.20	7.07
	at 38.0 °C, Pa s	0.87	0.90	0.87
	at 48.0 °C, Pa s	0.44	0.50	0.56
$\dot{\gamma}_{max}$	at 6.5 °C, s^{-1}	0.94	1.16	1.24
	at 12.5 °C, s^{-1}	2.3	3.0	3.2
	at 20.0 °C, s^{-1}	7.9	9.9	10.5
	at 21.5 °C, s^{-1}	9.8	12.3	13.3
	at 38.0 °C, s^{-1}	84.2	98.3	108.2
	at 48.0 °C, s^{-1}	168.9	176.9	168.4

$$u_t = \frac{L}{t} \qquad [1.96]$$

Substituting Eq. [1.96] into Eq. [1.94] yields

$$\frac{\mu}{\rho_s - \rho_l} = \frac{2R^2 g t}{9L} \qquad [1.97]$$

so

$$\frac{\mu}{\rho_s - \rho_l} = kt \qquad [1.98]$$

where k is the falling ball viscometer constant defined as

$$k = \frac{2R^2 g}{9L} \qquad [1.99]$$

Our focus in this section is on the falling ball viscometer. Eq. [1.94], however, can also be used as a basis for calculating settling velocities of particles including pigments in paint, and chocolate in milk.

Using Eq. [1.98] and [1.99] the viscosity of a Newtonian fluid can be calculated directly. It is also possible to calculate the viscosity using a reference liquid, a Newtonian liquid of known viscosity, to eliminate errors caused from inaccurate determination of the ball radius or drop length. k is equal for the unknown and reference liquids, therefore,

$$\frac{\mu_1}{(\rho_s - \rho_1)t_1} = \frac{\mu_2}{(\rho_s - \rho_2)t_2} \qquad [1.100]$$

where the subscripts 1 and 2 refer to the test and reference liquid, respectively. The maximum shear rate, located at the equator of the sphere, is (Sherman, 1970):

$$\dot{\gamma}_{\max} = \frac{3u_t}{R} \qquad [1.101]$$

Eq. [1.100] is acceptable for $N_{Re} = u_t d\rho/\mu < 1.0$ and cases where the sphere diameter is less than 1/10 the vessel diameter. If necessary, one may mathematically account for the presence of the wall when $d/D > 0.1$. Faxen (Arkiv. Mat. Astron. Fyzik. 17(27)1: 1922-1923) showed that the viscosity calculated using Stoke's law could be corrected for wall effects using the following equation:

$$\mu_c = \mu[1 - 2.104(\alpha) + 2.09(\alpha)^3 - .95(\alpha)^5] \qquad [1.102]$$

where α is equal to the sphere diameter (d) divided by the container diameter (D) and μ_c is the corrected viscosity. The term in brackets, the Faxen correction factor, is applicable up to $\alpha = 0.32$. An alternative expression (Chhabra, 1992) can be used when $\alpha<0.97$:

$$\mu_c = \mu\left(\frac{1-\alpha}{1-.475\alpha}\right)^4 \qquad [1.103]$$

Part b. Raw data for a test involving three spheres, one cylindrical container and honey at six different temperatures are presented in Table 1.9. The Faxen correction factor, as well as uncorrected (from Eq. [1.97]) and corrected (from Eq. [1.102]) viscosities were calculated from the experimental data (Table 1.9).

Corrected honey viscosities, taken from Table 1.9, were averaged at each temperature (Table 1.10) and the data fit (r^2=0.99) to the Arrhenius equation (Eq. [1.47]):

$$\mu = f(T) = A\exp\left(\frac{E_a}{RT}\right)$$

yielding

$$\mu = 5.58(10^{-16})\exp\left(\frac{21801}{RT}\right)$$

where: T is the temperature in degrees Kelvin; R = 1.987 cal/(g-mole K); E_a = 21,801 cal/ (g-mole); A = 5.58 (10^{-16}) Pa s. Results may also be expressed in terms of a reference viscosity. Using a value of 3.77 Pa s, calculated at 300 K with the previous relationship, yields

$$\mu = 3.77\exp\left(\frac{21801}{1.987}\left(\frac{1}{T}-\frac{1}{300}\right)\right) = 3.77\exp\left(11,126\left(\frac{1}{T}-\frac{1}{300}\right)\right)$$

Table 1.10. Average of Corrected Viscosities for Honey

T (°C)	T (K)	μ_c (Pa s)
6.5	278.7	76.88
12.5	285.7	29.95
20.0	293.2	9.03
21.5	294.7	7.25
38.0	311.2	0.88
48.0	321.2	0.50

The above equations provide convenient expressions for calculating the viscosity of honey at any temperature from 6.5°C to 48°C.

1.14.5. Orange Juice Concentrate

Rheological data for concentrated orange juice, at four different temperatures, are given in Table 1.11. Describe this data using the rheological model expressed by Eq. [1.52]:

$$\sigma = f(T,\dot{\gamma}) = K_T \exp\left(\frac{E_a}{RT}\right)(\dot{\gamma})^{\bar{n}}$$

Also, make a master-curve of the data using 9.5°C as the reference temperature.

A rheogram (Fig. 1.46), using the power law model, is determined at each temperature generating a flow behavior index and a consistency coefficient for each curve (Table 1.12). Using this data, the average flow behavior index may be calculated:

$$\bar{n} = \frac{.764 + .772 + .762 + .797}{4} = .774$$

Table 1.11. Rheological Data for Concentrated Orange Juice (65° Brix, 5.7% Pulp) Made from Perna Oranges (Data from Vitali and Rao, 1984)

T = -18.8°C		T = -5.4°C		T = 9.5°C		T = 29.2°C	
σ (Pa)	$\dot{\gamma}$ (s^{-1})	σ (Pa)	$\dot{\gamma}$ (s^{-1})	σ (Pa)	$\dot{\gamma}$ (s^{-1})	σ (Pa)	$\dot{\gamma}$ (s^{-1})
14.4	0.5	4.3	0.6	2.6	1.1	3.6	8
24.3	1	6.5	1	10.3	8	7.6	20
141.9	10	38.4	10	17.1	15	13.1	40
240.4	20	65.4	20	29.5	30	17.5	60
327.2	30	88.7	30	50.3	60	31.2	120
408.0	40	111.1	40	69.4	90	54.5	240
483.9	50	131.9	50	103.3	150	94.4	480
555.9	60	151.7	60	153.8	250	141.7	800
635.2	70	171.3	70	199.8	350	170.0	1000
692.5	80	189.4	80	242.8	450	183.2	1100

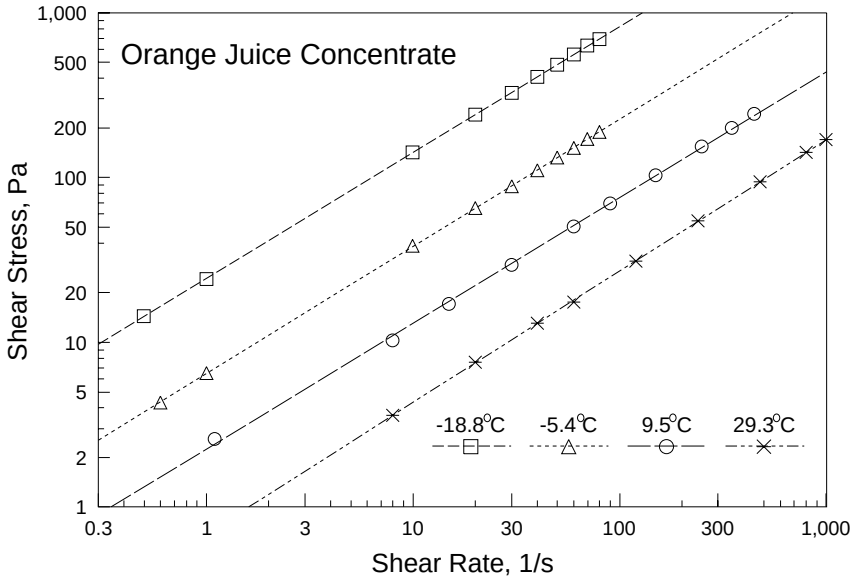

Figure 1.46. Rheograms of orange juice concentrate (Perna oranges: 65 ° Brix, 5.7% pulp) at four different temperatures.

Temperature dependency of the consistency coefficient (data in Table 1.12, plotted in Fig. 1.47) may be determined from regression of

Table 1.12. Power Law Fluid Properties for Concentrated Orange Juice at Four Temperatures

T (°C)	T (K)	1/*T* (1/K)	*K* (Pa s^n)	*n* (-)
-18.8	254.4	0.003931	24.37	0.764
-5.4	267.8	0.003734	6.45	0.772
9.5	282.7	0.003538	2.25	0.762
29.2	302.4	0.003307	0.69	0.797

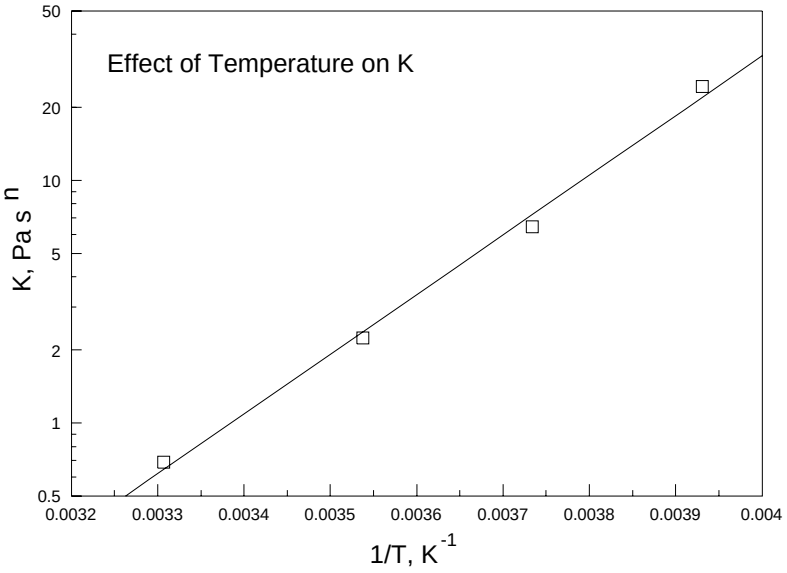

Figure 1.47. Variation of the consistency coefficient of concentrated orange juice with temperature.

$$K = K_T \exp\left(\frac{E_a}{RT}\right) \qquad [1.104]$$

showing that $K_T = 4.65(10^{-9})$ Pa $s^{\bar{n}}$ and $E_a/R = 5668.25$ K. Hence, the complete model, giving shear stress as a function of temperature and shear rate, may be expressed as

$$\sigma = 4.646(10^{-9}) \exp\left(\frac{5668.3}{T}\right)(\dot{\gamma})^{.774}$$

or, in terms of apparent viscosity, as

$$\eta = 4.646(10^{-9}) \exp\left(\frac{5668.3}{T}\right)(\dot{\gamma})^{.774-1.0}$$

Since the shear stress and apparent viscosity equations may be used over the entire temperature and shear rate range, they could be very useful in solving many food process engineering design problems related to the production of orange juice concentrate. A comparison (Fig. 1.48) of the full prediction equation with the original data indicate reasonably

good results when compared to the case where separate rheograms are generated for each data set (Fig. 1.46). This level of accuracy is acceptable in solving most food engineering problems.

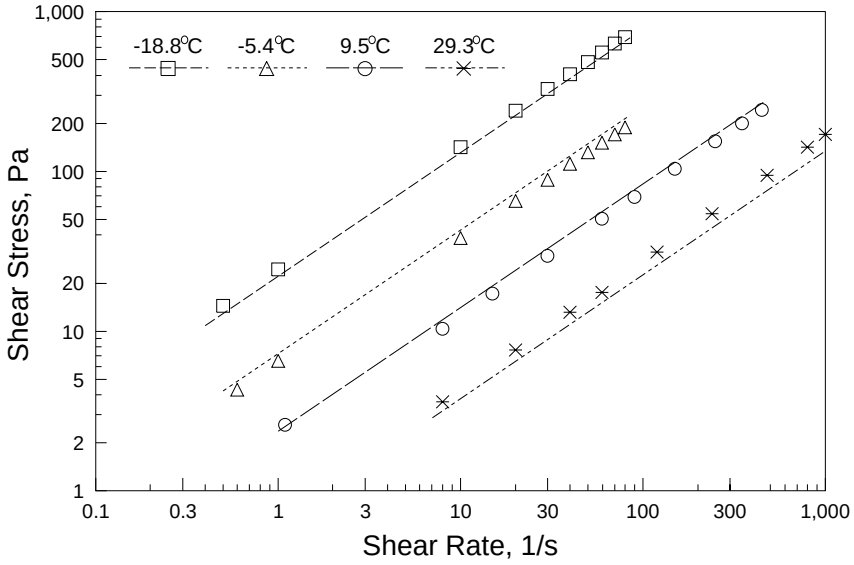

Figure 1.48. Comparison of the raw data and prediction equation for the full shear rate-temperature model of concentrated orange juice.

A reference temperature of 9.5°C will be used in developing a master-curve of the experimental data. Note that any value over the range of temperatures considered could be selected as the reference temperature. Developing a master curve requires a horizontal shifting of the data at -18.8°C, -5.4°C, and 29.3°C to the 9.5°C curve (Fig. 1.46). A dimensionless shift factor (a_T) is numerically found to account for the movement of each curve. Shear stress versus shear rate divided by the shift factor ($\dot{\gamma}/a_T$) are plotted to produce the master-curve.

In this example, a shear stress of 100 Pa will be used as the basis for determining a_T. Shear rates at $\sigma = 100$ Pa are calculated using the constants provided in Table 1.12. At -18.8°C, for instance,

Table 1.13. Shear Rates (at σ = 100 Pa) and Shift Factors

T (°C)	$\dot{\gamma}$ at 100 Pa (1/s)	a_T (-)
-18.8	6.35	6.35 / 145.4 = 0.0437
-5.4	34.83	34.83 / 145.4 = 0.2395
9.5	145.4	145.4 / 145.4 = 1.000
29.3	514.0	514 / 145.4 = 3.536

$$\dot{\gamma} = \left(\frac{\sigma}{K}\right)^{1/.764} = \left(\frac{100}{24.37}\right)^{1/.764} = 6.35\ s^{-1}$$

and at 9.5°C, the shear rate is calculated as

$$\dot{\gamma} = \left(\frac{\sigma}{K}\right)^{1/.762} = \left(\frac{100}{2.25}\right)^{1/.762} = 145.4\ s^{-1}$$

With this information, the shift factor at -18.8°C is found using the shear rate at the reference temperature of 9.5°C:

$$a_T = 6.35/145.4 = 0.0437$$

Calculated shear rates and shift factors for each curve are summarized in Table 1.13.

Table 1.14. Shifted Rheological Data for Concentrated Orange Juice (65 ° Brix, 5.7% Pulp) Used to Produce the Master-Curve

T=-18.8°C		T=-5.4°C		T=9.5°C		T=29.2°C	
σ (Pa)	$\dot{\gamma}/a_T$ (s^{-1})	σ (Pa)	$\dot{\gamma}/a_T$ (s^{-1})	σ (Pa)	$\dot{\gamma}/a_T$ (s^{-1})	σ (Pa)	$\dot{\gamma}/a_T$ (s^{-1})
14.4	11.4	4.3	2.5	2.6	1.1	3.6	2.3
24.3	22.8	6.5	4.2	10.3	8.0	7.6	5.7
141.9	228.8	38.4	41.8	17.1	15.0	13.1	11.3
240.4	457.7	65.4	83.5	29.5	30.0	17.5	17.0
327.2	686.5	88.7	125.3	50.3	60.0	31.2	33.9
408.0	915.3	111.1	167.0	69.4	90.0	54.5	67.9
483.9	1144.2	131.9	208.8	103.3	150.0	94.4	135.7
555.9	1373.0	151.7	250.5	153.8	250.0	141.7	226.2
635.2	1601.8	171.3	292.3	199.8	350.0	170.0	282.8
692.5	1830.7	189.4	334.0	242.8	450.0	183.2	311.1

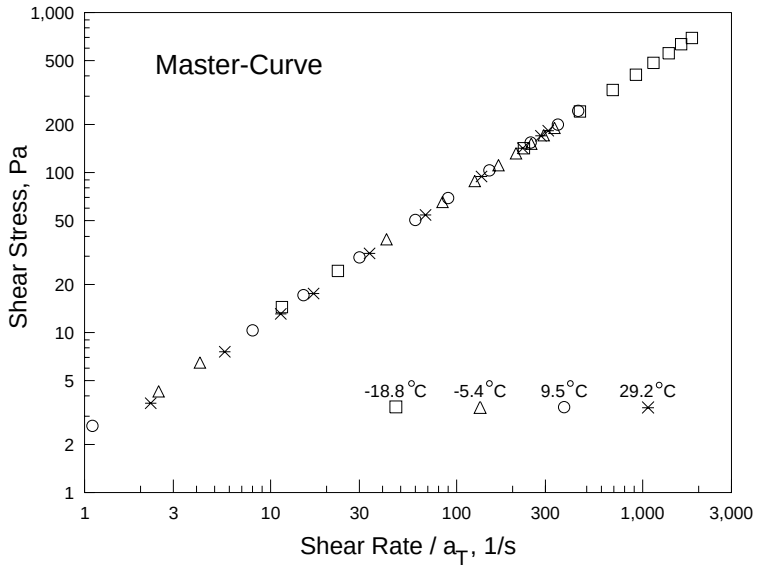

Figure 1.49. Plot of shear stress versus $\dot{\gamma}/a_T$ providing a master-curve of concentrated orange juice having a reference temperature of 9.5°C.

Raw data, shifted using appropriate a_T values, are given in Table 1.14 and plotted to produce a master-curve (Fig. 1.49). Horizontal shifting causes the data to overlap on a single line. Additional analysis could be performed to determine a_T as a function of temperature by plotting the information provided in Table 1.13. Master-curves can be very useful in comparing data from different products such as concentrated orange juice made from different varieties of oranges.

1.14.6. Influence of the Yield Stress in Coating Food

Consider the role of the fluid yield stress (σ_o) in coating food by examining potential flow and coating thickness on an inclined plane.

Assuming the shear stress of the air on the free surface is negligible, a force balance on a fluid on an inclined plane (Fig. 1.50) yields an equation giving shear stress as a function of y (Churchill, 1988):

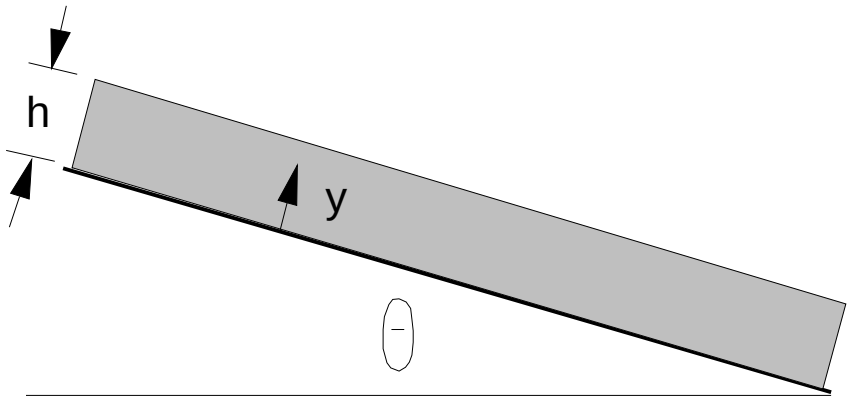

Figure 1.50. Coating material on an inclined plane.

$$\sigma = f(y) = g\rho(h - y)\sin\theta \qquad [1.105]$$

where y is the distance perpendicular to the plane, h is the height or thickness of the coating fluid layer, ρ is the density of the fluid, θ is the angle of inclination, and g is the acceleration due to gravity. This equation shows that the shear stress is a maximum on the surface of the wall (the inclined plane) and decreases in moving toward the free surface of the coating; hence, the maximum shear stress may be expressed as

$$\sigma_{max} = f(0) = g\rho h \sin\theta \qquad [1.106]$$

When the maximum shear stress exceeds the yield stress ($\sigma_{max} > \sigma_o$), gravity alone will cause flow down the wall producing a gross sagging phenomenon known as slumping in the paint industry (Patton, 1964). Similar problems can be observed in food coatings such as milk chocolate, vanilla frosting, and barbecue sauce.

If $\sigma_o \geq \sigma_{max}$, the fluid will remain on the surface of the object being coated. The maximum coating thickness possible, without material flowing off the surface, may be calculated in terms of the yield stress and the angle of inclination:

$$h_{max} = \frac{\sigma_o}{g\rho\sin\theta} \qquad [1.107]$$

The yield stress concept is a very useful tool for examining the thickness of food coatings. Equations given above also apply to a vertical wall where $\sin\theta = \sin 90° = 1$ resulting in

$$h_{\max} = \frac{\sigma_o}{g\rho} \qquad [1.108]$$

Chapter 2. Tube Viscometry

2.1. Introduction

Tube viscometers are very useful in collecting rheological data. These instruments may be placed into three basic categories: glass capillaries (Fig. 2.1), often called U-tube viscometers because of their resemblance to the letter U; high pressure capillaries (Fig. 2.2); and pipe viscometers (Fig. 2.3). All establish a pressure difference to create flow. The major difference between a capillary and a pipe viscometer is the diameter of the tube. Although there is no clearly defined size at which a tube should be called a capillary or a pipe, some guidelines can be offered.

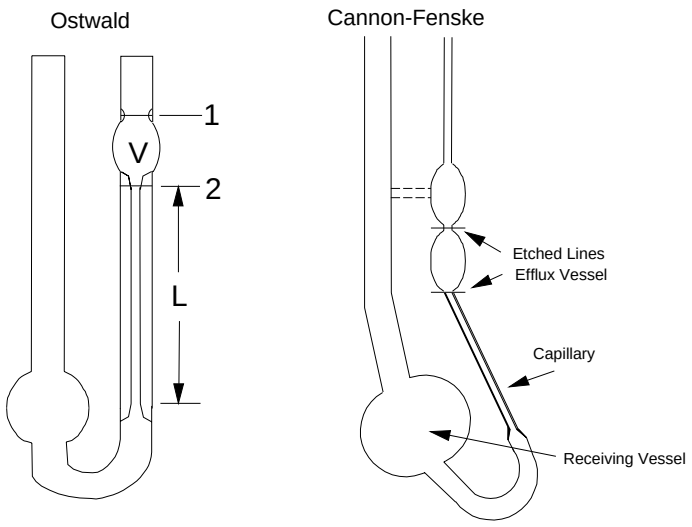

Figure 2.1. Ostwald and Canon-Fenske glass capillary (U-tube) viscometers.

Diameters in commercial capillary instruments typically range from 0.1 to 4 mm with a variation in entrance angles (Fig. 2.2) of 15 to 90 degrees. Pipe viscometers are usually built "on-site" so size varies widely. Some may be as small as 7mm in diameter but values greater

than 12 mm (typically 12 to 32mm) are not uncommon in food applications. *L*/*D* values in tube viscometers range from 2 to 400: The smaller values are found in the capillary units but are seldom seen in pipe systems.

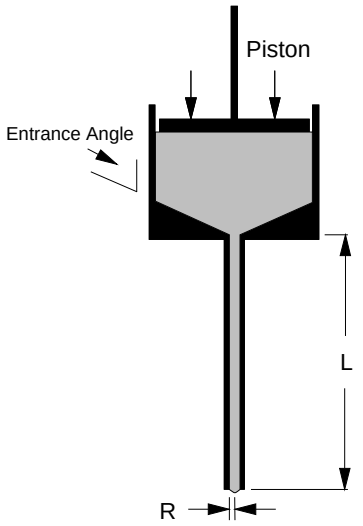

Figure 2.2. High pressure capillary viscometer.

In typical operation, the U-tube viscometer is filled by inverting it into a sample and sucking (into the side with the capillary) fluid into the fixed sample bulb. The viscometer is turned upright, then placed in a temperature controlled bath and allowed to reach thermal equilibrium. After a certain period of time, usually 5 to 10 minutes, the fluid is allowed to flow down through the capillary. A stopwatch is started when fluid passes the upper etched line and stopped when the fluid surface passes the lower etched line. The resulting time is considered the efflux time for fluid discharge from the bulb and fluid viscosity is calculated from this value.

U-tube viscometers are designed as gravity operated instruments. High pressure capillaries, which may also be constructed from glass tubes but are not "U-shaped," are typically piston driven (Fig. 2.2) or gas operated. A pump or gas (Fig. 2.3) system can be used to create a

driving force in pipe viscometers. These units can be operated at elevated pressures such as those found in aseptic food processing equipment (Dail and Steffe, 1990a and 1990b).

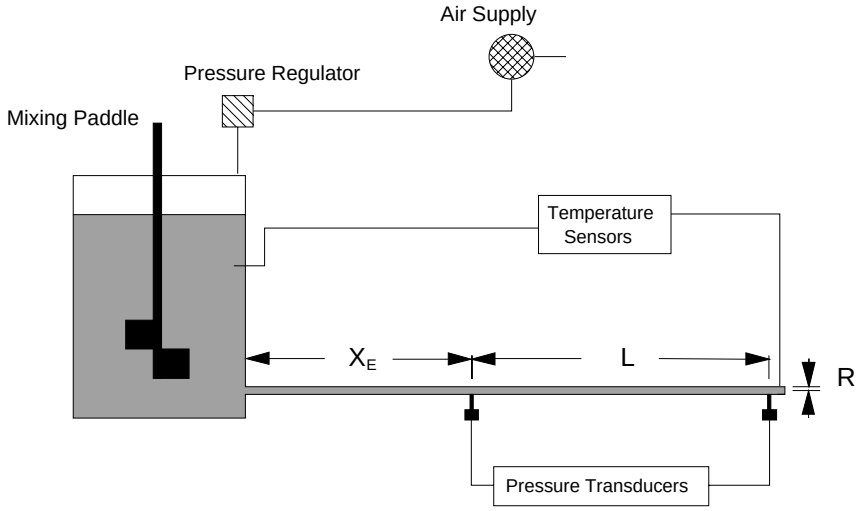

Figure 2.3. Gas driven pipe viscometer.

Raw data for tube viscometers are pressure drop and volumetric flow rate. The pressure drop is determined from pressure transducers or, in the case of U-tube viscometers, the height of fluid above a reference point. In high pressure capillaries, flow rates are calculated from the assumption that volumetric flow in the piston (or barrel) and the capillary are equivalent. Volumetric flow rate may be determined from the mass flow rate measured in pipe systems using a mass flow meter or a weight tank. Density is required for this calculation because the volumetric flow rate equals the mass flow rate divided by the density. The quantity of flow in a glass capillary is fixed by the volume (V) of the efflux vessel (Fig. 2.1).

The main focus of the current chapter is time-independent fluids. Rotational instruments are superior for the investigation of time-dependent materials because the sample can be maintained in the test chamber during periodic evaluation. Little attention is given to evaluating the elastic behavior of fluids from capillary data. Theoretically, it is possible to determine normal stress differences with tube (or

slit) viscometers from data collected using various methods such as axial thrust, residual exit pressure, or jet expansion (Walters, 1975; Whorlow, 1992). Generally, these applications have focused on polymers with minor consideration given to food products. In addition, commercially available tube viscometers require special modifications to make these measurements. Normal stress information can be more easily calculated from axial force data generated on cone and plate viscometers. Tubular systems involving back extrusion (also called annular pumping) have also been developed to evaluate power law fluids (Osorio and Steffe, 1986; Steffe and Osorio, 1987).

2.2. Rabinowitsch-Mooney Equation

Derivation of the Basic Equation. Numerous assumptions are required in developing the Rabinowitch-Mooney equation: flow is laminar and steady, end effects are negligible, fluid is incompressible, properties are not a function of pressure or time, temperature is constant, there is no slip at the wall of the tube meaning that the velocity of the fluid is zero at the wall-fluid interface, and radial and tangential velocity components are zero.

The starting point in the derivation of a tube viscometer equation is a force balance. Consider a fluid flowing through a horizontal tube of length (L) and inside radius (R). A pressure drop (δP) over a fixed length (L) is causing flow. The force balance, equating the shear stress causing flow to the shear stress resisting flow (i.e., the fluid), over a core of fluid (Fig. 2.4) with radius r and length L yields

$$(\delta P)\pi r^2 = \sigma 2\pi rL \qquad [2.1]$$

which can be solved for the shear stress:

$$\sigma = f(r) = \frac{(\delta P)\pi r^2}{2\pi rL} = \frac{(\delta P)r}{2L} \qquad [2.2]$$

Eq. [2.2] can also be obtained by starting from the general conservation of momentum equations (Bird et al., 1960; Brodkey and Hershey, 1988; Darby, 1976; Denn, 1980) as discussed in Example Problem 2.12.1. Eq. [2.2] depicts the shear stress varying over the pipe from zero at the center ($r = 0$) to a maximum at the wall ($r = R$) where the equation may be written as

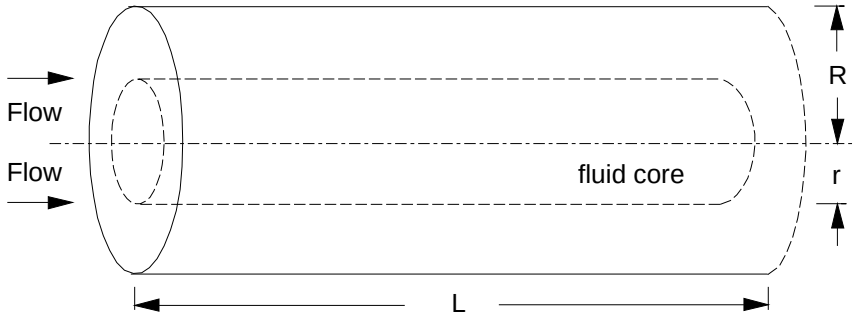

Figure 2.4. Core of fluid in tube flow geometry.

$$\sigma_w = \frac{(\delta P)R}{2L} \qquad [2.3]$$

To develop the shear rate equations, a differential flow element (dQ) must be evaluated. This can be expressed by considering the steady, laminar flow of fluid moving through an annulus located between the core, with radius r, and the position $r + dr$:

$$dQ = u 2\pi r dr \qquad [2.4]$$

where u is the linear velocity at r. The total volumetric flow rate is found by integrating Eq. [2.4] over the radius:

$$Q = \int_0^Q dQ = \pi \int_{r=0}^{r=R} u 2r\, dr \qquad [2.5]$$

Recognizing that $2r dr = dr^2$, so that r^2 becomes the variable of integration, allows Eq. [2.5] to be written as

$$Q = \pi \int_{r^2=0}^{r^2=R^2} (u)\, dr^2 \qquad [2.6]$$

The right hand side of this equation can be integrated by parts:

$$Q = \pi u r^2 \Big|_{r^2=0}^{r^2=R^2} - \pi \int_{r^2=0}^{r^2=R^2} r^2\, du \qquad [2.7]$$

and simplified by applying the no slip boundary condition which stipulates that the fluid velocity is zero at the wall of the pipe or, mathematically, $u = 0$ at $r = R$:

$$Q = \pi[(0)R^2 - u(0)^2] - \pi \int_{r^2=0}^{r^2=R^2} r^2\, du = -\pi \int_{r^2=0}^{r^2=R^2} r^2\, du \qquad [2.8]$$

To further evaluate Eq. [2.8], a number of items must be noted. First, by assuming steady laminar flow, we know the shear rate is some function of the shear stress:

$$-\frac{du}{dr} = f(\sigma) \qquad [2.9]$$

or

$$du = -f(\sigma)\, dr \qquad [2.10]$$

The negative sign is required in Eq. [2.9] because we assume, as indicated in Eq. [2.1], the positive direction of σ to be opposite the direction of flow. Second, Eq. [2.2] and [2.3] can be combined to give

$$r = \frac{\sigma}{\sigma_w} R \qquad [2.11]$$

which, when differentiated, yields

$$dr = \left(\frac{R}{\sigma_w} \right) d\sigma \qquad [2.12]$$

Taking the expression for *du* given by Eq. [2.10], and inserting Eq. [2.12] for *dr*, gives

$$du = -f(\sigma)\, dr = -f(\sigma) \left(\frac{R}{\sigma_w} \right) d\sigma \qquad [2.13]$$

Using Eq. [2.13] and noting, from Eq. [2.11], that $r^2 = (\sigma)^2 R^2/(\sigma_w)^2$ allows Eq. [2.8] to be rewritten as

$$Q = -\pi \int_0^{\sigma_w} \left(\frac{(\sigma)^2}{(\sigma_w)^2} \right) R^2 \left(-f(\sigma) \frac{R}{\sigma_w} \right) d\sigma \qquad [2.14]$$

Observe the change in the limits of integration: σ goes from 0 to σ_w as r goes from 0 to R^2. Simplifying this expression gives the final general equation relating shear stress and shear rate:

$$\frac{Q}{\pi R^3} = \frac{1}{(\sigma_w)^3} \int_0^{\sigma_w} (\sigma)^2 f(\sigma)\, d\sigma \qquad [2.15]$$

Eq. [2.15] may be evaluated by differentiation using Leibnitz' rule, which allows an integral of the form

$$\frac{d}{dz'}\left\{\int_0^{z'} z^2 f(z)\,dz\right\} \qquad [2.16]$$

to be written as

$$(z')^2 f(z') \qquad [2.17]$$

to differentiate the integral. Writing, Eq. [2.15] as

$$\left(\frac{Q}{\pi R^3}\right)(\sigma_w)^3 = \int_0^{\sigma_w} (\sigma)^2 f(\sigma)\,d\sigma \qquad [2.18]$$

then, applying Leibnitz' rule on the right hand side, and differentiating both sides with respect to σ_w (which is z') gives

$$(\sigma_w)^3\left[\frac{d(Q/(\pi R^3))}{d\sigma_w}\right] + \left(\frac{Q}{\pi R^3}\right)3(\sigma_w)^2 = (\sigma_w)^2 f(\sigma_w) \qquad [2.19]$$

Solving Eq. [2.19] for the shear rate at the wall ($\dot{\gamma}_w$) yields the well known Rabinowitsch-Mooney equation:

$$\dot{\gamma}_w = f(\sigma_w) = \left(\frac{3Q}{\pi R^3}\right) + (\sigma_w)\left[\frac{d(Q/(\pi R^3))}{d\sigma_w}\right] \qquad [2.20]$$

where the derivative is evaluated at a particular value of σ_w. Application of this equation is demonstrated for soy dough in Example Problem 2.12.2.

Eq. [2.20] can also be expressed in terms of the apparent wall shear rate, Γ :

$$\dot{\gamma}_w = f(\sigma_w) = \left(\frac{3}{4}\right)\Gamma + \left(\frac{\sigma_w}{4}\right)\left(\frac{d\Gamma}{d\sigma_w}\right) \qquad [2.21]$$

where $\Gamma = 4Q/(\pi R^3)$. Further manipulation gives

$$\dot{\gamma}_w = f(\sigma_w) = \left[\left(\frac{3}{4}\right) + \left(\frac{\sigma_w}{4\Gamma}\right)\left(\frac{d\Gamma}{d\sigma_w}\right)\right]\Gamma \qquad [2.22]$$

or

$$\dot{\gamma}_w = f(\sigma_w) = \left[\left(\frac{3}{4}\right) + \left(\frac{1}{4}\right)\left(\frac{d(\ln\Gamma)}{d(\ln\sigma_w)}\right)\right]\Gamma \qquad [2.23]$$

that can be rewritten in the following simplified format:

$$\dot{\gamma}_w = \left[\frac{3n'+1}{4n'}\right]\Gamma \qquad [2.24]$$

where

$$n' = \frac{d(\ln \sigma_w)}{d(\ln \Gamma)} \qquad [2.25]$$

showing that n' is the point slope of the $\ln(\sigma_w)$ versus $\ln(\Gamma)$. If the fluid behaves as a power law material, the slope of the derivative is a straight line and $n' = n$. Eq. [2.24] is a convenient form of the Rabinowitsch-Mooney equation because power law behavior is frequently observed with fluid foods. Also, slight curvature in the logarithmic plot can often be ignored. Application of Eq. [2.24] and [2.25] is illustrated for a 1.5% solution of sodium carboxymethylcellulose in Example Problem 2.12.3.

Newtonian Fluids. In developing the Rabinowitsch-Mooney equation a general expression relating shear stress to shear rate, Eq. [2.15], was developed:

$$\frac{Q}{\pi R^3} = \frac{1}{(\sigma_w)^3} \int_0^{\sigma_w} (\sigma)^2 f(\sigma)\, d\sigma$$

This can be solved for a Newtonian fluid by inserting the Newtonian definition for shear rate, $\dot{\gamma} = f(\sigma) = \sigma/\mu$:

$$\frac{Q}{\pi R^3} = \frac{1}{(\sigma_w)^3} \int_0^{\sigma_w} (\sigma)^2 (\sigma/\mu)\, d\sigma = \frac{1}{(\sigma_w)^3} \int_0^{\sigma_w} \left(\frac{(\sigma)^3}{\mu} \right) d\sigma \qquad [2.26]$$

Integration of Eq. [2.26] gives

$$\frac{Q}{\pi R^3} = \left(\frac{1}{(\sigma_w)^3} \right) \left(\frac{(\sigma)^4}{4\mu} \right) \Bigg|_0^{\sigma_w} = \frac{\sigma_w}{4\mu} \qquad [2.27]$$

Substituting the shear stress at the wall ($\sigma_w = (\delta P)R/(2L)$) into Eq. [2.27] results in the Poiseuille-Hagen equation:

$$Q = \frac{\pi(\delta P) R^4}{8 L \mu} \qquad [2.28]$$

Eq. [2.28] indicates that the radius has a very strong influence on the behavior of the system since it is raised to the power four. Also, if this equation is written in terms of the definition of a Newtonian fluid ($\sigma_w = \mu \dot{\gamma}_w$), then the formula for the shear rate at the wall may be determined:

$$\dot{\gamma}_w = \frac{4Q}{\pi R^3} \qquad [2.29]$$

This expression is identical to the one given in Eq. [1.90] (and Fig. 1.27) for estimating the maximum shear rate of a Newtonian fluid in tube flow.

Power Law Fluids. Eq. [2.15] can be solved for a power law fluid by inserting $\dot{\gamma} = f(\sigma) = (\sigma/K)^{1/n}$ into the equation:

$$\frac{Q}{\pi R^3} = \left[\frac{1}{(\sigma_w)^3}\right]\int_0^{\sigma_w} (\sigma)^2 \left(\frac{\sigma}{K}\right)^{1/n} d\sigma = \left[\frac{1}{(\sigma_w)^3 K^{1/n}}\right]\int_0^{\sigma_w} (\sigma)^{2+1/n}\, d\sigma \qquad [2.30]$$

Integration and substitution of $\sigma_w = (\delta P)R/(2L)$ gives

$$Q = \pi\left(\frac{(\delta P)}{2LK}\right)^{1/n}\left(\frac{n}{3n+1}\right)R^{(3n+1)/n} \qquad [2.31]$$

If this equation is written in terms of the definition of a power law fluid ($\sigma_w = K(\dot{\gamma}_w)^n$), then the formula for the shear rate at the wall may be determined:

$$\dot{\gamma}_w = \left(\frac{3n+1}{4n}\right)\left(\frac{4Q}{\pi R^3}\right) \qquad [2.32]$$

Eq. [2.32] is an exact solution for a power law fluid and also useful as an estimate of the maximum shear rate in tube flow (as indicated in Eq. [1.91]) for a wide range of fluid foods.

Bingham Plastic Fluids. In a Bingham plastic fluid, the shear rate is defined in terms of the plastic viscosity and the yield stress: $\dot{\gamma} = f(\sigma) = (\sigma - \sigma_o)/\mu_{pl}$. This function is discontinuous because there is no shearing flow at points in the tube near the center where the shear stress is below the yield stress. Mathematically, $f(\sigma) = 0$ for $0 < \sigma < \sigma_o$ in the central plug region and $f(\sigma) = (\sigma - \sigma_o)/\mu_{pl}$ for $\sigma_o \le \sigma < \sigma_w$ in the outer portion of the tube. Given the above, it is clear that Eq. [2.15] must be integrated for each region of the tube to determine the total volumetric flow rate:

$$\frac{Q}{\pi R^3} = \left[\frac{1}{(\sigma_w)^3}\right]\int_0^{\sigma_o} (\sigma)^2 f(\sigma)\, d\sigma + \left[\frac{1}{(\sigma_w)^3}\right]\int_{\sigma_o}^{\sigma_w} (\sigma)^2 \left(\frac{\sigma - \sigma_o}{\mu_{pl}}\right) d\sigma \qquad [2.33]$$

Since shear rate is zero when the shear stress is below the yield stress, Eq. [2.33] can be simplified to

$$\frac{Q}{\pi R^3} = \left[\frac{1}{(\sigma_w)^3}\right]\int_{\sigma_o}^{\sigma_w} (\sigma)^2 \left(\frac{\sigma - \sigma_o}{\mu_{pl}}\right) d\sigma \qquad [2.34]$$

which, when integrated, yields the Buckingham-Reiner equation for flow of a Bingham plastic material in a pipe:

$$Q = \left(\frac{\pi R^4(\delta P)}{8\mu_{pl}L}\right)\left[1 - \left(\frac{4}{3}\right)\left(\frac{\sigma_o}{\sigma_w}\right) + \left(\frac{1}{3}\right)\left(\frac{\sigma_o}{\sigma_w}\right)^4\right] \qquad [2.35]$$

The same technique discussed for Bingham plastics is used to derive the flow rate equation for Casson fluids in Example Problem 2.12.4.

Herschel-Bulkley Fluids. The volumetric flow rate for a Herschel-Bulkley fluid ($\sigma = K(\dot{\gamma})^n + \sigma_o$), is found using the same method discussed for the Bingham plastic material:

$$Q = \left(\frac{\pi R^3}{256}\right)\left(\frac{4n}{3n+1}\right)\left(\frac{\sigma_w}{K}\right)^{1/n}\left(1 - \frac{\sigma_o}{\sigma_w}\right)^{1/n}\left[1 - \frac{(\sigma_o/\sigma_w)}{2n+1}\left[1 + \frac{2n}{n+1}\left(\frac{\sigma_o}{\sigma_w}\right)\left(1 + \frac{n\sigma_o}{\sigma_w}\right)\right]\right] \qquad [2.36]$$

2.3. Laminar Flow Velocity Profiles

Rheological properties have a strong influence on fluid velocity profiles in tube flow. Understanding these profiles is important in developing a clear picture of instrument performance and in making various food process engineering design calculations such as determining the appropriate hold tube length for a thermal processing system. Since tube viscometers operate in the laminar flow regime, only laminar flow velocity profiles are presented here. Equations describing the turbulent velocity of Newtonian and power law fluids are discussed later in Section 2.11.

Combining the shear stress relationship (Eq. [2.2]) and the definition of a Newtonian fluid (Eq. [1.25]) with the shear rate written as $-du/dr$ yields

$$\mu\left(-\frac{du}{dr}\right) = \frac{(\delta P)r}{2L} \qquad [2.37]$$

Integrating this equation, using the no slip boundary condition ($u = 0$ at $r = R$) to determine the unknown constant, gives an expression for the velocity profile of a Newtonian fluid:

$$u = f(r) = \frac{(\delta P)}{4L\mu}(R^2 - r^2) \qquad [2.38]$$

If the definition of a power law fluid is used, Eq. [2.37] becomes

$$K\left(-\frac{du}{dr}\right)^n = \frac{(\delta P)r}{2L} \qquad [2.39]$$

The velocity profile is found after integration and application of the no slip boundary condition:

$$u = f(r) = \left(\frac{(\delta P)}{2LK}\right)^{1/n}\left(\frac{n}{n+1}\right)[R^{(n+1)/n} - r^{(n+1)/n}] \qquad [2.40]$$

By combining Eq. [2.40] with the volumetric flow rate equation (Eq. [2.31]), the relationship between the velocity at r and the volumetric average velocity ($\bar{u} = Q/(\pi R^2)$) may be calculated:

$$u/(\bar{u}) = \left(\frac{3n+1}{n+1}\right)\left[1 - \left(\frac{r}{R}\right)^{(n+1)/n}\right] \qquad [2.41]$$

Lower values of the flow behavior index result in a flatter velocity profile and higher values maximize the difference between the slowest and fastest fluid elements (Fig. 2.5). The extreme case occurs with $n = \infty$ at $r/R = 0$ where $u/\bar{u} = 3.0$. The curve (Fig. 2.5) for a Newtonian fluid is found at $n = 1.0$.

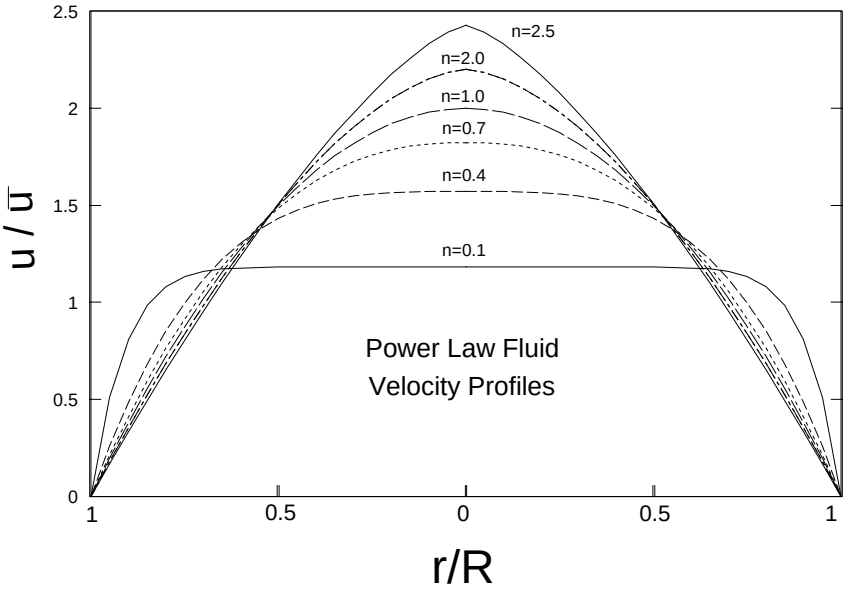

Figure 2.5. Laminar velocity profiles for power law fluids with different values of the flow behavior index.

The maximum velocity, located at the center line where $r = 0$, may be determined from Eq. [2.41] for any value of the flow behavior index:

$$u_{\max}/(\bar{u}) = \frac{3n+1}{n+1} \qquad [2.42]$$

Clearly, the flow behavior index has a very strong influence on the velocity profile. Velocity profiles for power law fluids in turbulent flow are very flat by comparison (see Section 2.11, Table 2.7).

In the case of a Bingham plastic fluid, the force balance equation is

$$\mu_{pl}\left(-\frac{du}{dr}\right) + \sigma_o = \frac{(\delta P)r}{2L} \qquad [2.43]$$

which is valid in the outer regions of the pipe where the fluid is subject to shear. With the no slip boundary condition, Eq. [2.43] may be integrated to give an expression for the velocity profile between the plug and the wall of the tube:

$$u = f(r) = \frac{(\delta P)R^2}{4\mu_{pl}L}\left[1 - \left(\frac{r}{R}\right)^2 - \frac{2R_o}{R}\left(1 - \frac{r}{R}\right)\right] \qquad [2.44]$$

for $R_o \le r \le R$ where $\sigma \ge \sigma_o$. The critical radius (R_o), which defines the outer boundary of the plug, may be calculated from the yield stress:

$$R_o = \frac{\sigma_o 2L}{(\delta P)} \qquad [2.45]$$

The maximum velocity in the pipe, which is the velocity of the plug in the center section of the pipe, is found by substituting $r = R_o$ into Eq. [2.44]:

$$u_{\max} = \frac{(\delta P)R^2}{4\mu_{pl}L}\left[\left(1 - \frac{R_o}{R}\right)^2\right] \qquad [2.46]$$

which is valid for $0 < r \le R_o$ where $\sigma \le \sigma_o$.

Combining Eq. [2.44] or Eq. [2.46] with the volumetric flow rate equation (Eq. [2.35]), the relationship between the velocity at r and the volumetric average velocity ($\bar{u} = Q/(\pi R^2)$) may be calculated as

$$u/(\bar{u}) = \frac{2(1 - 2c + 2cr/R - (r/R)^2)}{1 - 4c/3 + c^4/3} \qquad [2.47]$$

in the sheared portion of the fluid ($1 \ge r/R \ge c$), and

$$u/(\bar{u}) = \frac{2(1-c)^2}{1 - 4c/3 + c^4/3} \qquad [2.48]$$

in the plug ($r/R \le c$). The value of c is defined in terms of the yield stress or the critical radius: $c = \sigma_0/\sigma_w = R_o/R$. Plotting these equations show that increasing the yield stress enlarges the radius of the plug flowing down the center of the pipe (Fig. 2.6). The curve for a Newtonian fluid is illustrated by the line with $c = 0$.

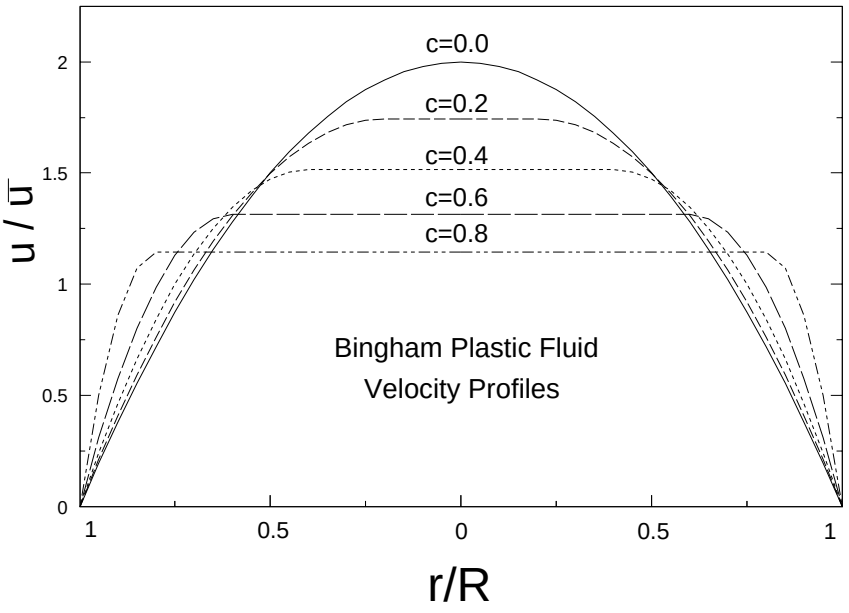

Figure 2.6. Laminar velocity profiles for Bingham plastic fluids with different values of $c = \sigma_o/\sigma_w$.

The same approach described for Bingham plastic fluids can be used to determine the velocity profile for a Herschel-Bulkley fluid:

$$u = f(r) = \frac{2L}{(\delta P)(1+1/n)K^{1/n}}\left[(\sigma_w - \sigma_o)^{1+1/n} - \left(\frac{(\delta P)r}{2L} - \sigma_o\right)^{1+1/n}\right] \qquad [2.49]$$

Velocity of the plug may be determined by using Eq. [2.49] with $r = R_o$, calculated from Eq. [2.45].

2.4. Laminar Flow Criteria

To obtain meaningful rheological data, tube viscometers must operate in the laminar flow regime. Turbulence is rarely involved in high pressure capillaries but may be a problem in pipe viscometers with large diameter tubes or when investigating low viscosity fluids.

The accepted criterion for laminar flow of Newtonian fluids in tube flow is to maintain a Reynolds number less than 2100: $N_{Re} < 2100$ where $N_{Re} = \rho D \bar{u} / \mu$. Transition away from laminar flow, however, has been observed for N_{Re} values between 1225 and 3000. In addition, laminar flow, under ideal conditions, has been observed for N_{Re} numbers as high as 50,000 (Grovier and Aziz, 1972). Similar problems exist for non-Newtonian fluids. Hence, the following discussion can only offer general guidelines to determine if the flow regime is laminar or turbulent.

As noted above, flow is considered laminar for Newtonian fluids when the Reynolds number is below the critical value of 2100:

$$N_{Re} < 2100 = (N_{Re})_{critical} \qquad [2.50]$$

With power law fluids, laminar flow occurs when (Hanks, 1963):

$$N_{Re,PL} < \frac{6464\, n(2+n)^{(2+n)/(1+n)}}{(1+3n)^2} = (N_{Re,PL})_{critical} \qquad [2.51]$$

where the term on the right side of the inequality is the critical power law Reynolds number. The power law Reynolds number is defined as

$$N_{Re,PL} = \left(\frac{D^n (\bar{u})^{2-n} \rho}{8^{n-1} K} \right) \left(\frac{4n}{3n+1} \right)^n \qquad [2.52]$$

Plotting Eq. [2.51] shows the critical Reynolds number increasing sharply to a maximum near $n = 0.4$, then dropping off with greater values of the flow behavior index (Fig. 2.7). Also, for the special case of a Newtonian fluid ($n = 1$) it is equal to the expected value of 2100.

Eq. [2.51] may give a conservative estimate of the critical Reynolds number. Work by Campos et al. (1994) shows that critical Reynolds numbers in the range of 4000 (at $n = 0.46$) to 3000 (at $n = 0.78$) may be determined using a statistical evaluation procedure. Higher numbers are also predicted, particularly for $0 < n < 0.6$, using the equation derived by Mishra and Tripathi (1973):

$$(N_{Re,PL})_{critical} = \frac{2100(4n+2)(5n+3)}{3(1+3n)^2} \qquad [2.53]$$

Eq. [2.53] predicts gradually decreasing values of critical Reynolds numbers from 3480 at $n = 0.1$ to 2357 at $n = 0.60$. Over $0.65 < n < 1.0$, the Mishra and Tripathi (1973) equation predicts values (Fig. 2.7) very similar to those given by Eq. [2.51].

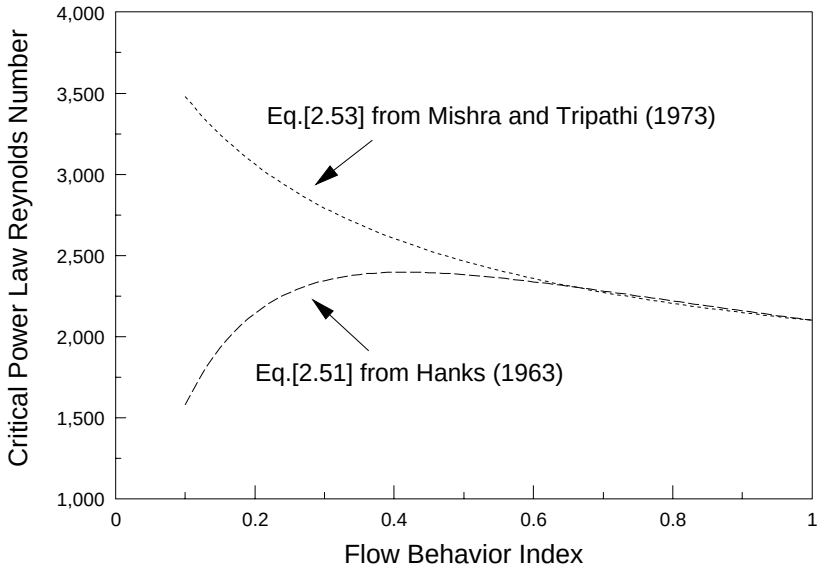

Figure 2.7. Variation of the critical power law Reynolds number with n.

With tube flow of a Bingham plastic fluid, steady-state laminar flow can be expected (Hanks, 1963) when

$$N_{Re,B} \le \frac{N_{He}}{8c_c}(1 - 4c_c/3 + c_c^4/3) = (N_{Re,B})_{critical} \qquad [2.54]$$

The term on the right side of Eq. [2.54] is the critical Bingham Reynolds number and c_c, the critical value of c, is defined as

$$\frac{c_c}{(1-c_c)^3} = \frac{N_{He}}{16,800} \qquad [2.55]$$

The Hedstrom number and the Bingham Reynolds number are defined by the following equations:

$$N_{He} = \frac{D^2 \sigma_o \rho}{(\mu_{pl})^2} \qquad [2.56]$$

$$N_{Re,B} = \frac{D \bar{u} \rho}{\mu_{pl}} \qquad [2.57]$$

Critical values of c versus N_{He} (Eq. [2.55]), and the critical Bingham Reynolds number versus the Hedstrom number (Eq. [2.54]) are plotted in Fig. 2.8 and 2.9, respectively. These illustrations indicate the difficulty in achieving turbulence with materials having a significant yield stress. Note that the Hedstrom number increases with larger values of the yield stress. Laminar flow criterion is also available (but not experimentally verified) for Herschel-Bulkley materials (Garcia and Steffe, 1987).

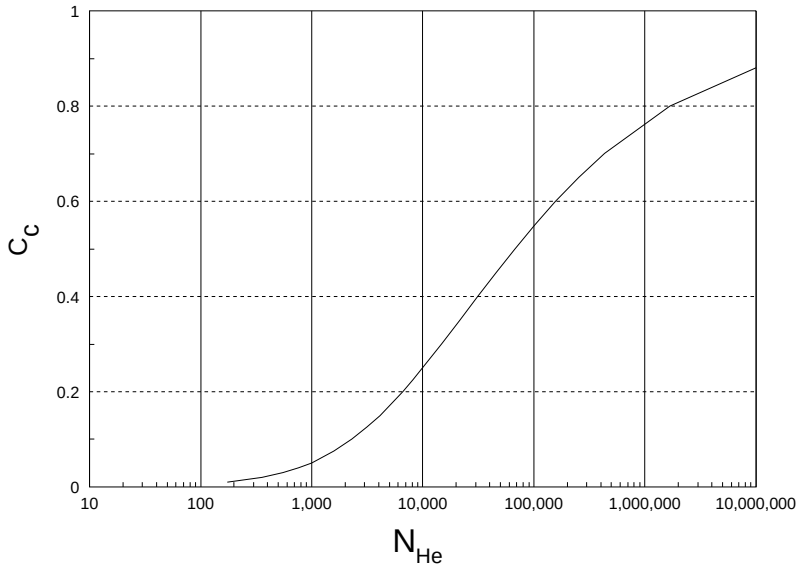

Figure 2.8. Variation of c_c with the Hedstrom number.

2.5. Data Corrections

There are numerous measurement errors which may occur in using tube viscometers (Table 2.1). Some are generally applicable and others only apply to specific systems. Data corrections required for high pressure and pipe viscometers are similar, and constitute the focus of this section. Glass capillaries (gravity operated U-tube viscometers) have special requirements which are discussed in Sec. 2.9.

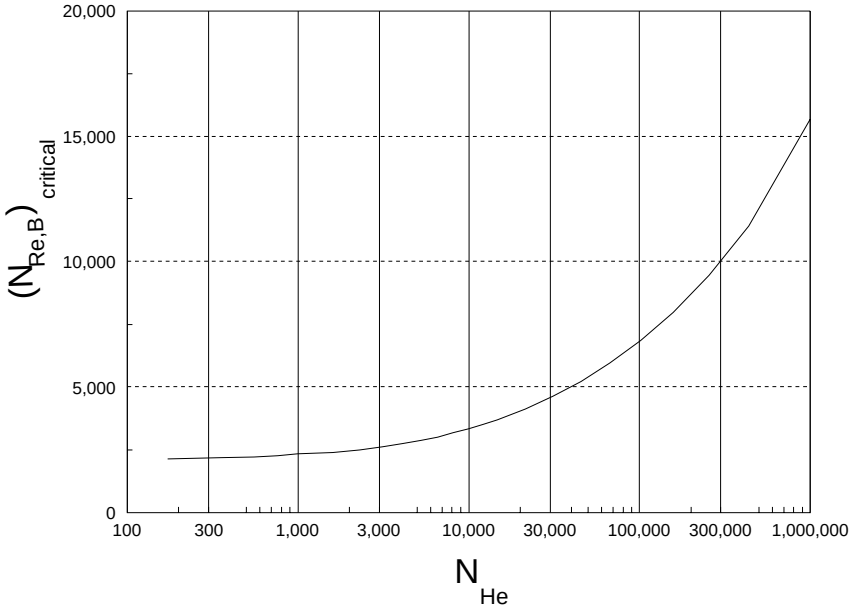

Figure 2.9. Variation of the critical Bingham Reynolds number with the Hedstrom number.

Kinetic Energy Losses. There is a pressure loss, due to a difference in kinetic energy, in high pressure capillaries caused by the acceleration of the fluid from the barrel velocity to the capillary velocity. This pressure loss (δP) may be expressed in terms of the kinetic energy correction factor (α):

$$\delta P = \frac{\rho}{\alpha}((\bar{u}_2)^2 - (\bar{u}_1)^2) \qquad [2.58]$$

where $\bar{u}_2$ and $\bar{u}_1$ are the average capillary and barrel velocities, respectively. Equations for calculating α are available (see Table 2.4 in Sec. 2.10). Losses due to kinetic energy are generally small and very difficult to separate from entrance pressure losses. Hence, it is accepted practice to assume that kinetic energy losses are accounted for in the entrance effect correction.

End Effects: Entrance Correction. Energy losses due to fluid divergence at the end of a capillary are small and usually neglected but entrance losses can be very significant and must be evaluated.

Table 2.1. Sources of Error in Operating Tube Viscometers (from Van Wazer et al., 1963)

Factor	Cause	Applicability
Kinetic energy losses	Loss of effective pressure because of the kinetic energy in the issuing stream.	General
End effects	Energy losses due to viscous or elastic behavior when a fluid converges or diverges at the ends of a capillary	General
Elastic energy	Energy loss by elastic deformation of the fluid not recovered during flow in the capillary	Viscoelastic materials
Turbulence	Departure from laminar flow	General
Pressure losses prior to the capillary	Sticking of the piston or energy dissipated in the flow of the material within the cylinder before entering the capillary.	Cylinder-piston viscometers
Drainage	Liquid adhering to the wall of the viscometer reservoir.	Glass capillary viscometers
Surface-tension effects	Variations in surface tension from one test substance to another.	Glass capillary viscometers
Heat effects	Conversion of pressure energy into heat energy through flow.	High-shear viscometers
Wall effects	Surface phenomena at the fluid-wall interface.	Polyphase fluids
Effect of time-dependent properties	Variations in the residence time in the capillary.	Thixotropic and rheopectic materials

The entrance effect correction accounts for excess pressure loss occurring at the opening of the tube viscometer from sudden changes in geometry caused by a convergence, and losses in kinetic energy. This problem may be experimentally evaluated using a number of tubes

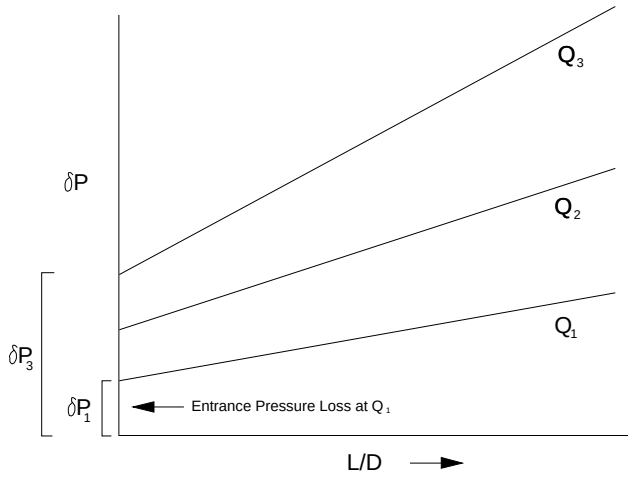

Figure 2.10. Bagley plot illustrating entrance effect pressure corrections determined at three flow rates.

having different L/D ratios (Bagley, 1957). Data of total pressure drop versus flow rate are collected for each tube. Pressure drop versus L/D data are plotted at each flow rate (or apparent wall shear rate, $4Q/(\pi R^3)$) and the lines are extrapolated to L/D equal to zero. These figures (Fig. 2.10) are sometimes called "Bagley plots." The resulting pressure drop is the entrance effect pressure loss at a particular flow rate and pipe diameter. To achieve the greatest level of accuracy, the same procedure must be followed for each diameter under consideration by using a number of tubes (at least three) having the same diameter but different lengths.

Pressure loss at the entrance has also been evaluated by subtracting orifice die data from capillary data. These calculations are made with an orifice and capillary of the same diameter using data taken at an equivalent volumetric flow rate. Results with soy protein isolate show excellent agreement between this method and the Bagley procedure discussed previously (Hyashi et al., 1991).

Entrance pressure loss is used to correct the measured pressure drop values:

$$\delta P = \delta P_m - \delta P_{en} \qquad [2.59]$$

where δP_m is the measured pressure drop, and δP_{en} is the entrance pressure loss. Corrected values of δP are used in calculating the shear stress at the wall, Eq. [2.3]. The above technique is demonstrated for soy dough in Example Problem 2.12.2.

Toms (1958) described an alternative method of eliminating end effects. The concept involves a long and short tube of equivalent diameter and sufficient length so both have an internal section where flow is fully developed. If the volumetric flow rate is the same in both tubes, then the exit pressure loss (δP_{ex}) and the entrance pressure loss (δP_{en}) are equal for the long (subscript L) and short (subscript S) tubes. With this idea, the pressure drop across each tube may be written as

$$\delta P_L = \delta P_{en} + \delta P_{ex} + \delta P_{fd,L} \qquad [2.60]$$

and

$$\delta P_S = \delta P_{en} + \delta P_{ex} + \delta P_{fd,S} \qquad [2.61]$$

where $\delta P_{fd,L}$ and $\delta P_{fd,S}$ are the pressure losses in tube sections where flow is fully developed. At constant flow rate, the pressure gradients in the fully developed sections are equal:

$$\frac{\delta P_{fd,L}}{L_L} = \frac{\delta P_{fd,S}}{L_S} \qquad [2.62]$$

Subtracting Eq. [2.61] from Eq. [2.60], and using Eq. [2.62] yields a pressure gradient term that is free of end effects:

$$\frac{\delta P_{fd,L}}{L_L} = \frac{\delta P_L - \delta P_S}{L_L - L_S} \qquad [2.63]$$

Eq. [2.63] can be used to calculate the gradient term ($\delta P/L$) in calculating the wall shear stress from Eq. [2.3]. In practice, numerous tubes would be used and care taken to be sure $\delta P_L - \delta P_S$ is large enough to avoid significant experimental errors.

Entrance Length. With long tubes, the entrance correction can often be neglected. Pressure transducers can be strategically placed in pipe viscometers so that the entrance region does not influence experimental data. Also, entrance length information may be needed to design, or evaluate the performance of, tube viscometers.

There is some published information for estimating the entrance length (X_E) required to obtain 98% of fully developed flow which should be considered a conservative guideline in the design of tube viscometers. An approximate equation to calculate X_E for Newtonian fluids in laminar flow, based on theoretical and experimental studies (Boger, 1982), is

$$\frac{X_E}{D} = 0.55 + 0.055\,(N_{Re}) \qquad [2.64]$$

The constant, 0.55, accounts for the entrance effect at very low values of the Reynolds number. Entrance length equations given for power law and Bingham plastic fluids discussed subsequently do not have an analogous term.

Collins and Schowalter (1963) presented entrance length data for pseudoplastic fluids in laminar flow. Results were given in terms of a modified power law Reynolds number ($D^n(\bar{u})^{(2-n)}\rho/K$). There was a linear relationship from $0.1 \le n \le 1.0$ that may be expressed as

$$\frac{2X_E}{D} = (-.250n + .350)\left(\frac{D^n(\bar{u})^{(2-n)}\rho}{K}\right) \qquad [2.65]$$

Using Eq. [2.52], the modified power law Reynolds number may be written in terms of $N_{Re,PL}$ as

$$\left(\frac{D^n(\bar{u})^{(2-n)}\rho}{K}\right) = N_{Re,PL}(8^{n-1})\left(\frac{3n+1}{4n}\right)^n \qquad [2.66]$$

which can be substituted into Eq. [2.65] yielding

$$\frac{X_E}{DN_{Re,PL}} = (-.125n + .175)\,(8^{n-1})\left(\frac{3n+1}{4n}\right)^n \qquad [2.67]$$

Plotting Eq. [2.67], assuming constant $N_{Re,PL}$ values, shows X_E/D increasing with increasing values of the flow behavior index (Fig. 2.11) when $0.1 < n < 1.0$.

Entrance length data have also been published for Bingham plastic fluids in laminar flow (Michiyosi et al., 1966). Their data may be summarized with the following equation:

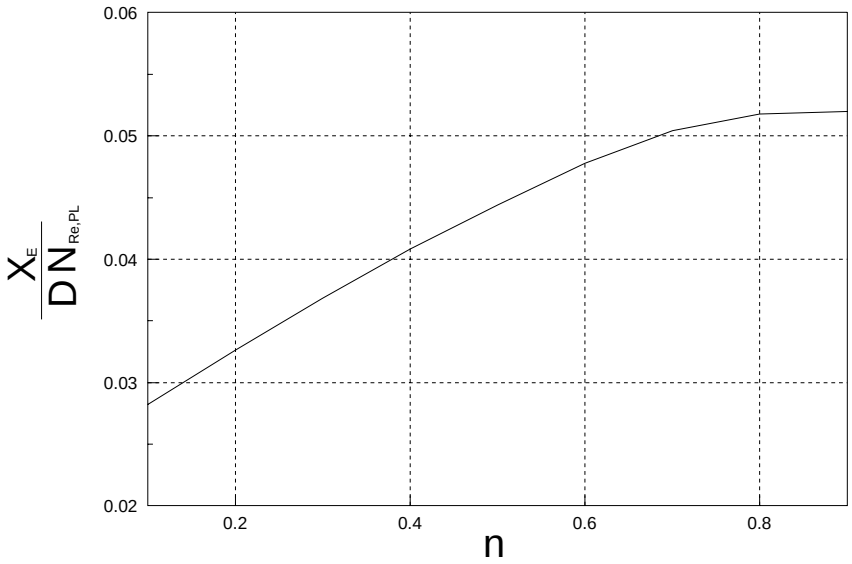

Figure 2.11. Entrance length of power law fluids.

$$\frac{X_E}{DN_{Re,B}} = .0476\exp(-5.125c) \qquad [2.68]$$

where, recall, $c = \sigma_o/\sigma_w$. Plotting Eq. [2.68] illustrates (Fig. 2.12) decreasing entrance length requirements with greater values of the yield stress.

With short or medium length tubes, entrance effects must be experimentally evaluated; however, when tubes are sufficiently long (easily designed this way with pipe viscometers), the entrance correction can be neglected. If X_E/L is in the order of 0.01 problems should be minimal but tubes may be long. Dervisoglu and Kokini (1986) found, through trial and error experimentation, that an entrance length of 90 diameters was sufficient to minimize entrance effect errors in studying various food products including mustard, ketchup, applesauce, and tomato paste. Care should be exercised with elastic fluids because the entrance length may be significantly higher than predicted by equations

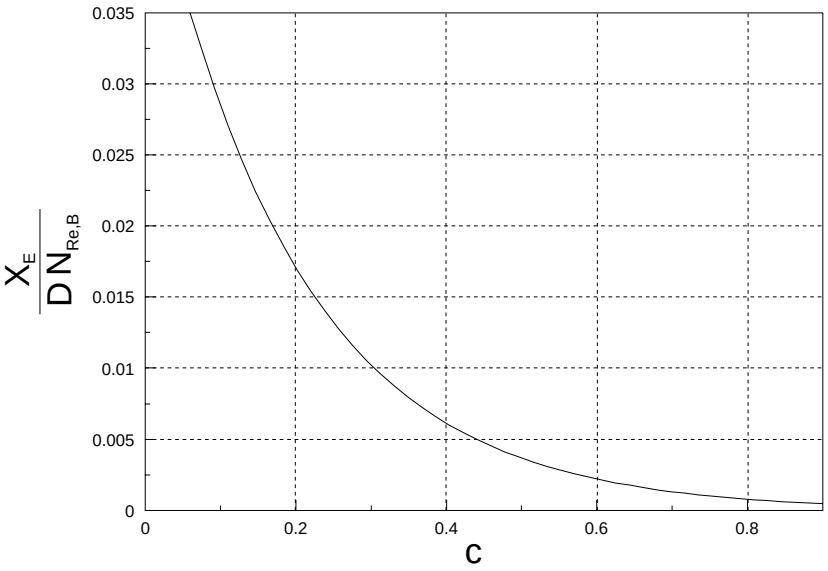

Figure 2.12. Entrance length of Bingham plastic fluids.

such as those presented in this section (Whorlow, 1992). A tube viscometer, where the end effect may be neglected due to high L/D values, is discussed in Example Problem 2.12.3.

Wall Effects - Slip Correction. Slip occurs when a thin layer of fluid, having a viscosity lower than that of the fluid, forms at the wall of the tube (or the wall of any viscometer). This may be a problem in food suspensions like fruit and vegetable purees. Theoretically, the problem may be attacked by adding an additional term, representing added flow, to the overall flow rate term. The expression describing the volumetric flow rate (Eq. [2.15]) may be written as

$$Q_{\text{without slip}} = Q_{ws} = \frac{\pi R^3}{(\sigma_w)^3}\int_0^{\sigma_w} (\sigma)^2 f(\sigma)\, d\sigma \qquad [2.69]$$

At constant values of σ_w, the above integral term is constant so a slip velocity may be introduced to account for variations in the measured values of flow rate:

$$Q_{\text{measured}} = Q_m = Q_{ws} + \pi R^2 u_s \qquad [2.70]$$

where u_s is the effective slip velocity which is assumed to be a function of the shear stress at the wall. In the absence of slip, $u_s = 0$.

Eq. [2.70] can be expanded by defining an effective slip coefficient ($\beta = u_s/\sigma_w$) such that

$$\frac{Q_m}{\sigma_w} = \frac{Q_{ws}}{\sigma_w} + \frac{\pi R^2 u_s}{\sigma_w} \qquad [2.71]$$

or

$$\frac{Q_m}{\sigma_w} = \frac{Q_{ws}}{\sigma_w} + \pi R^2 \beta \qquad [2.72]$$

Simplification yields

$$\frac{Q_m}{\pi R^3 \sigma_w} = \frac{Q_{ws}}{\pi R^3 \sigma_w} + \frac{\beta}{R} \qquad [2.73]$$

which is a form of the equation often seen in the literature. Jastrzebski (1967), however, found that the slip coefficient was a function of the wall shear stress and also varied inversely with tube radius. To account for this finding, a corrected slip coefficient (β_c) was defined to give a better mathematical representation of experimental data:

$$\beta = \frac{\beta_c}{R} \qquad [2.74]$$

Using β_c, the volumetric flow rate expression is written as

$$\frac{Q_m}{\pi R^3 \sigma_w} = \frac{Q_{ws}}{\pi R^3 \sigma_w} + \frac{\beta_c}{R^2} \qquad [2.75]$$

β may be evaluated from capillary tube measurements using various tubes (at least three) having different radii. Experimental data of $Q_m/(\pi R^3 \sigma_w)$ versus σ_w are plotted at different values of R. From this plot, values of $Q_m/(\pi R^3 \sigma_w)$ at different values of R and constant σ_w are obtained. Then, by plotting $Q_m/(\pi R^3 \sigma_w)$ versus $1/R$, at constant σ_w, β can be determined as the slope of the line (Eq. [2.73]) at each value of σ_w. The

resulting information can be used to evaluate β as a function of σ_w. If desired, the same procedure can be followed to find β_c by considering $1/R^2$ in place of $1/R$.

The effective slip coefficient, or the corrected slip coefficient, is used to correct the volumetric flow rate data:

$$Q_{ws} = Q_m - \beta\sigma_w \pi R^2 \qquad [2.76]$$

or

$$Q_{ws} = Q_m - \beta_c\sigma_w \pi R \qquad [2.77]$$

Q_{ws} is used in the Rabinowitsch-Mooney equation (Eq. [2.20]) to determine the shear rate at the wall.

Introducing an effective slip coefficient may be valuable in dealing with suspensions such as fruit and vegetable purees but can give physically meaningless results (those producing negative β values) for dense suspensions where sliding friction may be a significant factor. In these cases it may be more appropriate to model material movements as plug flow instead of viscous flow. This approach was taken by Jasberg et al. (1979) in examining the flow of defatted soy flakes in the screw channel of an extruder.

Kokini and Plutchok (1987) have reported values of the corrected slip coefficient for applesauce (Table 2.2) and slip velocities for potato paste are presented in Halliday and Smith (1995). Corrected slip coefficients were also successfully used by Shukla and Rizvi (1995) to evaluate the flow behavior of butter.

Viscous Heating. Experimental tests should be designed to avoid significant temperature increases due to viscous heat dissipation. Viscous heating occurs when any fluid is sheared. Fortunately, serious experimental errors are generally found only with fluids having a very high viscosity or in instruments operated at very high shear rates.

To determine the temperature rise due to viscous heating, the equations of energy and momentum, coupled by the temperature dependence of viscosity, must be solved. It is not possible to obtain an exact analytical solution to this problem (Warren, 1988). Reasonable estimates are possible using simplifying assumptions and a nomograph outlining a solution of this type is available in Dealy (1982) and Middleman (1968).

Table 2.2. Corrected Slip Coefficients for Applesauce Calculated with Tubes having L/D=65 and Radii of 0.4425 cm, 0.3235 cm and 0.2150 cm (Data from Kokini and Plutchok, 1987)

σ_w Pa	β_c $m^2/(Pa\ s)$
40	.0030
54	.0051
68	.0076
81	.010
95	.013
109	.016
123	.019
136	.022
150	.025

A simple method to evaluate the extent of the problem is discussed by Whorlow (1992). He shows that a pressure drop (δP) causing a volume (V) of material to flow results in work done per second equal to δPV. This energy causes the mean temperature of the volume to increase by δT:

$$\delta T = \frac{\delta P V}{\rho V c_p} = \frac{\delta P}{\rho c_p} \qquad [2.78]$$

where ρ is the density and c_p is the specific heat of the fluid. Many fluid foods are aqueous systems having a density and specific heat of approximately 1000 kg m^{-3} and 4000 J kg^{-1} K^{-1}, respectively. If you assume that a temperature rise of less than 1°C has a negligible effect on rheological testing, then a pressure drop less than 4,000 kPa (approximately 40 atmospheres) will not cause a problem due to viscous heating! It is important to realize that this calculation will overestimate the magnitude of the problem. The effects of viscous heating problems may also be evaluated in terms of the Nahme number defined as the temperature raise due to viscous heating divided by the temperature change necessary to alter viscosity (Macosko, 1994).

Hole Pressure Error. Sometimes the pressure in a tube is measured by a transducer communicating with the fluid in the pipe through a fluid well connected to the pipe. This practice causes curvature in the flow streamlines which may create errors in the pressure measurement. With polymer solutions, in particular, the presence of a normal stress

tends to lift the fluid out of the hole making the measured pressure at the wall less than the true wall pressure (Bird et al. 1987; Barnes et al., 1989). This phenomenon is well established and an instrument, designed to measure normal stress differences, has been developed using the concept (Lodge, 1988). It is difficult to apply the concept to fluids with a significant yield stress because these materials would tend to fill recessed holes hindering the proper transmission of the stress signal.

In designing capillary viscometers, the hole pressure error can be eliminated by using identical pressure transducers at each sensing location. Then, when pressure differences are calculated, the hole pressure errors cancel out. The problem can also be eliminated by using flush mounted (diaphragm type) pressure transducers. Hole pressure errors are minimal for most food materials.

Data Correction Summary. Performing a complete rheological analysis using tube viscometry requires a great deal of data. A typical sequence of the steps is illustrated in Fig. 2.13. To evaluate the entrance effect, tubes having the same radius but different lengths are required. The entrance effect should be evaluated for each tube radius considered before the measured pressure drop can be corrected and the shear stress at the wall calculated. Data from tubes of the same length, having different radii, are needed to evaluate the slip coefficient so the flow rate data can be corrected. Next, the Rabinowitsch-Mooney equation is applied and the rheogram developed. As mentioned previously, viscous heating and hole pressure errors are usually not a problem with food materials.

Accounting for slip adds significantly to the computational requirements. One should note that slip problems will decrease with increasing tube sizes. Also, before correcting for slip, one should see if it is present. This can be done by checking results from data collected using tubes of different radii - at least two tubes with significantly different radii. After correcting for the end effect, rheograms are compared. Allowing for differences in the shear rate range, the rheograms for time-independent fluids should be identical in the absence of slip.

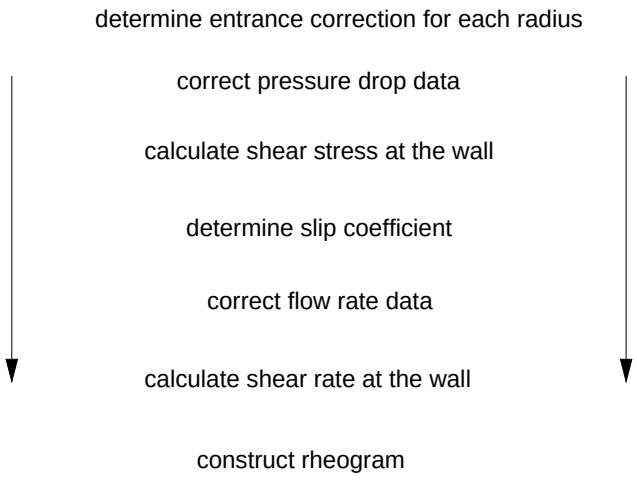

Figure 2.13. Typical sequence of steps required for the analysis of tube viscometer data for time-independent fluids.

2.6. Yield Stress Evaluation

Yield stress may be determined in a tube viscometer from the stress to initiate fluid movement (Cheng, 1986). Using this method, the minimum pressure (δP_{min}) required to cause flow in a horizontal tube viscometer is measured. The yield stress is calculated from a force balance on the fluid (Eq. [2.2]) as

$$\sigma_o = \frac{\delta P_{min} R}{2L} \qquad [2.79]$$

In practice, the pressure drop is slowly increased until flow is observed. If the structure of the material causes the yield stress to exhibit time-dependent characteristics, then the rate of change of the applied pressure may influence results.

2.7. Jet Expansion

Jet expansion (also called die swell or extrudate swell) can be estimated from the primary normal stress difference. Conversely, the normal stress difference can be estimated from the jet expansion. Assuming the phenomenon is caused by elastic recoil, due to the sudden removal of the tube, then swelling can be estimated as (Tanner, 1988)

$$\frac{D_e}{D} = \left[1 + \frac{1}{8} \left(\frac{\sigma_{11} - \sigma_{22}}{\sigma_{12}} \right)^2 \right]^{1/6} \qquad [2.80]$$

where D is the diameter of the capillary and D_e is the final diameter of the extrudate. The first normal stress difference divided by the shear stress ($(\sigma_{11} - \sigma_{22})/\sigma_{12}$), a term called the recoverable shear (Tanner, 1988), is evaluated at the tube wall. Although this equation is adequate for estimation purposes, it excludes some important factors such as extensional viscosity and vaporization (flashing) of moisture, which may strongly influence die swell of extruded foods.

Newtonian fluids may exhibit jet expansion having D_e/D values ranging from 1.12 at low N_{Re} values to 0.87 at high N_{Re} values (Middleman, 1977). Polymer melts may behave similarly at low shear rates but have D_e/D numbers from 2 to 4 at high shear rates (Tadmor and Gogos, 1979).

2.8. Slit Viscometry

The development of equations for slit viscometers is analogous to the methods used in developing tube viscometer equations. Slits can be constructed at food processing facilities with relative ease. Food engineers have successfully used them to determine the rheological properties of various extruded food materials: maize grits and potato flour (Senouci and Smith, 1988a and 1988b); corn meal (Bhattacharya and Padmanabhan, 1992), rice flour dough (Altomare et al., 1992), and wheat flour dough (Gogos and Bhakuni, 1992). This information can be useful in monitoring product quality and is required for various engineering design calculations.

Slit size is described (Fig. 2.14) in terms of the length (L) and aspect ratio (w/h) where w and h are the width and height of the slit, respectively. To neglect edge effects, the aspect ratio should be greater than 10: $w/h > 10$. The velocity profile for a Newtonian fluid in the slit is

$$u = f(x_2) = \left(\frac{3Q}{2hw} \right) \left[1 - 4 \left(\frac{x_2}{h} \right)^2 \right] \qquad [2.81]$$

where $x_2 = 0$ at the center of the slit and $x_2 = h/2$ at the outer edge. The shear rate and shear stress at the wall ($x_2 = h/2$) for a Newtonian fluid are

$$\dot{\gamma}_w = \frac{6Q}{h^2 w} \qquad [2.82]$$

and

$$\sigma_w = \frac{\delta P h}{2L} \qquad [2.83]$$

where δP is the pressure drop across the slit of length L. The shear stress equation, Eq. [2.83], is valid for any time-independent fluid. Newtonian viscosity may be calculated as

$$\mu = \sigma_w / \dot{\gamma}_w = \left(\frac{\delta P}{L} \right) \left(\frac{h^3 w}{12 Q} \right) \qquad [2.84]$$

To calculate the shear rate for non-Newtonian fluids, a general equation relating the volumetric flow rate and the shear rate in the slit is required:

$$Q = \frac{w}{2} \left(\frac{h}{\sigma_w} \right)^2 \int_o^{\sigma_w} \sigma f(\sigma) d\sigma \qquad [2.85]$$

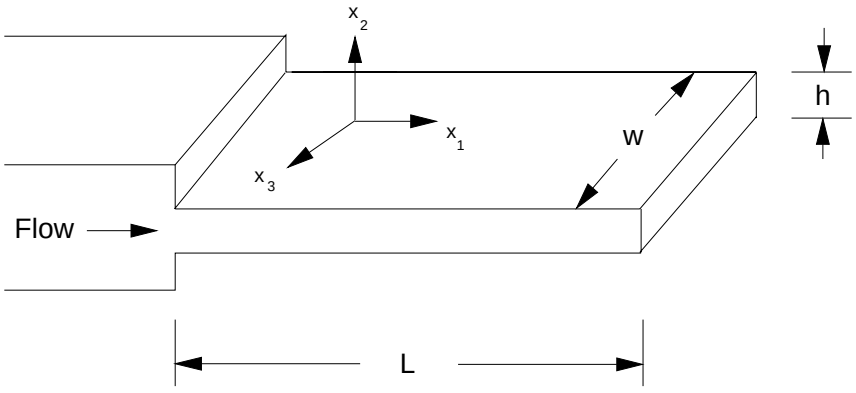

Figure 2.14. Slit viscometer.

Eq. [2.85] is analogous to Eq. [2.15] that was developed in deriving the Rabinowitsch-Mooney equation. It may be solved directly for power law and Bingham plastic fluids:

$$Q = \frac{wh^2}{2(2+1/n)}\left(\frac{\sigma_w}{K}\right)^{1/n} \qquad [2.86]$$

and

$$Q = \frac{h^2 w \sigma_w}{6\mu_{pl}}\left[1 - \frac{3}{2}\left(\frac{\sigma_o}{\sigma_w}\right) + \frac{1}{2}\left(\frac{\sigma_o}{\sigma_w}\right)^3\right] \qquad [2.87]$$

respectively, with the stipulation that $\sigma_w \geq \sigma_o$ for Eq. [2.87].

If an unknown fluid is being tested, a general solution to Eq. [2.85] (comparable to the Rabinowitsch-Mooney solution) is required:

$$\dot{\gamma}_w = f(\sigma_w) = \left(\frac{2n'+1}{3n'}\right)\left(\frac{6Q}{h^2 w}\right) \qquad [2.88]$$

where the correction factor is defined as

$$n' = \frac{d\ln(\delta P h/(2L))}{d\ln(6Q/(wh^2))} = \frac{d\ln(\sigma_w)}{d\ln(6Q/(wh^2))} \qquad [2.89]$$

If the fluid is Newtonian, $n' = 1.0$ and, if power law, $n' = n$. The $6Q/(wh^2)$ term is called the apparent wall shear rate for slit flow. Note, that after accounting for geometrical differences between slits and tubes, Eq. [2.88] and [2.89] are very similar to Eq. [2.24] and [2.25].

The above equations assume fully developed flow in the slit. If corrections to experimental data are needed, the same methods outlined for high pressure capillary viscometers are appropriate. It is very important to evaluate the need for an entrance effect correction when using short slits and taking δP as the pressure drop over the entire slit. A superior method of obtaining experimental data is to use flush mounted pressure transducers installed directly on the slit. The transducers (at least three, preferably four) are placed a sufficient distance from the entrance and exit of the slit so the observed pressure drop per unit length ($\delta P/L$), required in Eq. [2.83], is linear (Han, 1988).

Exit pressure data from a slit have been used to characterize primary normal stress differences in molten polymers (Han, 1988). Bhattacharya (1993) used this method to examine the influence of gluten levels on the rheological behavior of bread dough. This procedure involves

linearly extrapolating pressure profiles through the exit of the slit to determine the exit pressure (P_{ex}). The first normal stress difference is related to the rate of change of the exit pressure with respect to the shear rate at the wall:

$$\sigma_{11} - \sigma_{22} = P_{ex} + \sigma_w \left(\frac{dP_{ex}}{d\sigma_w} \right) = P_{ex} \left(1 + \frac{d(\ln P_{ex})}{d(\ln \sigma_w)} \right) \qquad [2.90]$$

Obtaining good experimental data using the exit pressure method is difficult because small pressure differences are measured. Han (1988) argues that the exit pressure method should produce acceptable results when σ_w is above a critical value of approximately 25 kPa. Unfortunately, the exit pressure method is problematic for many foods because flow does not remain fully developed through the exit of the rheometer violating the assumption that the pressure gradient is constant over the entire instrument (Ofoli and Steffe, 1993). The analysis of slit viscometer data for corn syrup is given in Example Problem 2.12.5.

2.9. Glass Capillary (U-Tube) Viscometers

Glass capillary viscometers (U-tube viscometers) are designed to be gravity operated, and generally limited to use with Newtonian fluids having viscosities in the range of 0.4 to 20,000 mPa s. Simple configurations are seen in Ostwald and Cannon-Fenske type units (Fig. 2.1). Sometimes, they are driven with applied external pressure to increase the viscosity range of the instrument. If the magnitude of the external pressure makes the magnitude of the static pressure head insignificant in comparison, the instruments may be used for non-Newtonian fluids by applying the Rabinowitsch-Mooney equation to the data. This, however, is a laborious procedure and should not be considered "standard practice" for glass capillary viscometers.

The driving force in gravity operated glass capillary viscometers is the hydrostatic head that varies during discharge. This variation in pressure causes a variation in the shear rate during testing which is the main reason gravity operated units are unsuitable for non-Newtonian fluids. With Newtonian fluids the starting point for analysis is the Poiseuille-Hagen equation (Eq. [2.28]) written in terms of the volumetric average velocity, $\bar{u} = Q/\pi R^2$:

$$\bar{u} = \frac{(\delta P) R^2}{8 L \mu} \qquad [2.91]$$

where R and L are the radius and length of the capillary. Pressure drop over the capillary is generated by a height (h) of liquid:

$$\delta P = \rho g h \qquad [2.92]$$

h may be the average or maximum fluid height, but should be the same for all measurements. Substitution of Eq. [2.92] into Eq. [2.91] yields

$$\bar{u} = \frac{\rho g h R^2}{8 L \mu} \qquad [2.93]$$

which can also be written as

$$\frac{\mu}{\rho} = \frac{g h R^2}{8 L \bar{u}} \qquad [2.94]$$

The efflux time, defined as the time to discharge a fixed volume of liquid (V) from the capillary bulb (Fig. 2.1), is

$$t = \frac{V}{\bar{u}(\pi R^2)} \qquad [2.95]$$

so the average velocity may be expressed in terms of the discharge time:

$$\bar{u} = \frac{V}{\pi R^2 t} \qquad [2.96]$$

Substitution of Eq. [2.96] into Eq. [2.94] yields

$$\frac{\mu}{\rho} = \frac{g h \pi R^4 t}{8 L V} \qquad [2.97]$$

which can be expressed in terms of a constant as

$$\frac{\mu}{\rho} = k t \qquad [2.98]$$

where k, the glass capillary viscometer constant, is defined as

$$k = \frac{g h \pi R^4}{8 L V} \qquad [2.99]$$

The value of k may be computed directly from Eq. [2.99] if an accurate physical description of the viscometer is provided. One problem with this method is that small variations in geometry, particularly variations in the radius due to wide manufacturing tolerances or film build up after repeated use, may significantly influence the numerical value of k. Hence, it is not surprising that the most common way to use Eq. [2.98] is to determine the properties of an unknown fluid from the known properties of a reference fluid. This experimental method may be implemented by noting that k is the same for both fluids, so

$$\frac{\mu_1}{\rho_1 t_1} = \frac{\mu_2}{\rho_2 t_2} \qquad [2.100]$$

or

$$\frac{\mu_1}{\mu_2} = \left(\frac{\rho_1}{\rho_2}\right)\left(\frac{t_1}{t_2}\right) \qquad [2.101]$$

where subscripts 1 and 2 refer to the unknown and known fluids, respectively. A common reference material is water but many commercially produced standards, mainly silicone oils, are also available. The above method of determining viscosity is usually within acceptable limits of accuracy but does not account for the various experimental errors discussed below.

A general working equation which incorporates errors associated with small variations in capillary radius, end effects, and kinetic energy may be written in terms of the kinematic viscosity ($\nu = \mu/\rho$) as (Kawata et al., 1991)

$$\nu = c_1 t - \frac{c_2}{t} \qquad [2.102]$$

where c_1 (with units of m^2/s^2) and c_2 (with units of m^2) are constants for a particular capillary. When the kinematic viscosities (ν_1, ν_2) and flow times (t_1, t_2) of two standard liquids are known, the instrument constants may be calculated:

$$c_1 = \frac{\nu_1 t_1 - \nu_2 t_2}{(t_1)^2 - (t_2)^2} \qquad [2.103]$$

and

$$c_2 = \frac{(\nu_1 t_1 - \nu_2 t_2) t_1 t_2}{(t_1)^2 - (t_2)^2} \qquad [2.104]$$

If the viscosity range of a glass capillary viscometer is increased by operating the instrument with applied external pressure, additional correction factors are needed (Kawata et al., 1991; Van Wazer et al., 1963).

2.10. Pipeline Design Calculations

The purpose of this section is to provide the practical information necessary to predict pressure drop and power requirements for homogeneous, non-time-dependent materials in fluid handling systems. Rheological properties have a strong influence on the calculations and this information is needed to select proper pumps and related equipment when designing large scale tube (pipe) viscometers or commercial fluid handling systems (Steffe and Morgan, 1986; Steffe and Garcia, 1987). Although rheological properties can only be evaluated from data taken in the laminar flow regime, the case of turbulent flow is also presented to provide a thorough analysis of pipeline design problems commonly encountered by food process engineers.

Mechanical Energy Balance. The mechanical energy balance for an incompressible fluid in a pipe may be written as

$$\left(\frac{(\bar{u}_2)^2-(\bar{u}_1)^2}{\alpha}\right)+g(z_2-z_1)+\frac{P_2-P_1}{\rho}+\sum F+W=0 \qquad [2.105]$$

where $\sum F$, the summation of all friction losses, is

$$\sum F=\sum\frac{2f(\bar{u})^2L}{D}+\sum\frac{k_f(\bar{u})^2}{2} \qquad [2.106]$$

and subscripts 1 and 2 refer to two specific locations in the system. The friction losses include those from pipes of different diameters and a contribution from each individual valve, fitting, and similar parts. W is the work output per unit mass and the power requirement of the system is found by calculating the product of W and the mass flow rate. A negative value of W indicates that work is being put into the system which is the normal function of a pump.

Rheological properties are required to evaluate the mechanical energy balance equation. Although there are many mathematical models available to describe flow behavior (Table 1.3), few can be considered practical for making pressure drop calculations involving pipe flow. Most pumping problems involving fluid foods can be solved using the Newtonian, power law or Bingham plastic models. Over simplification, however, can cause significant calculation errors (Steffe, 1984).

Fanning Friction Factor. The Fanning friction factor (f) is defined, from considerations in dimensional analysis, as the ratio of the wall shear stress in a pipe to the kinetic energy per unit volume:

$$f = \frac{2\sigma_w}{\rho(\bar{u})^2} \qquad [2.107]$$

Substituting the definition of the shear stress at the wall of a pipe (Eq. [2.2]) into Eq. [2.107] gives

$$f = \frac{(\delta P)R}{\rho L(\bar{u})^2} = \frac{(\delta P)D}{2\rho L(\bar{u})^2} \qquad [2.108]$$

where $\delta P = P_2 - P_1$. Hence, the energy loss per unit mass (needed in the mechanical energy balance) may be expressed in terms of f:

$$\frac{\delta P}{\rho} = \frac{f\,2L(\bar{u})^2}{D} \qquad [2.109]$$

Some engineers calculate the friction losses with the Darcy friction factor which is equal to four times the Fanning friction factor. Pressure drop calculations may be adjusted for this difference. Final results are the same using either friction factor. Calculations in this text deal exclusively with the Fanning friction factor.

In laminar flow, f values can be determined from the equations describing the relationship between pressure drop and flow rate for a particular fluid. Consider, for example, a Newtonian fluid ($\sigma = \mu\dot{\gamma}$). Using Eq. [2.28], the volumetric average velocity for this material, in laminar tube flow, may be expressed as:

$$\bar{u} = \frac{Q}{\pi R^2} = \frac{1}{\pi R^2}\left(\frac{\pi(\delta P)R^4}{8L\mu}\right) = \frac{(\delta P)D^2}{32L\mu} \qquad [2.110]$$

Simplification gives an expression for the pressure drop per unit length:

$$\frac{\delta P}{L} = \frac{32\bar{u}\mu}{D^2} \qquad [2.111]$$

Substituting Eq. [2.111] into Eq. [2.108] yields the friction factor:

$$f = \left[\frac{\delta P}{L}\right]\left(\frac{D}{2\rho(\bar{u})^2}\right) = \left[\frac{32(\bar{u})\mu}{D^2}\right]\left(\frac{D}{2\rho(\bar{u})^2}\right) = \frac{16}{N_{Re}} \qquad [2.112]$$

which is a common equation appropriate for predicting friction factors for Newtonian fluids when $N_{Re} < 2100$. Using the same approach, laminar flow friction factors for power law and Bingham plastic fluids may be calculated, respectively, from the following equations:

$$f = \frac{16}{N_{Re,PL}} \qquad [2.113]$$

and

$$f = \frac{16(6N_{Re,B} + N_{He})}{6N_{Re,B}^2} \qquad [2.114]$$

The above equations are appropriate when the laminar flow criteria, presented in Section 2.4, are satisfied. Eq. [2.114], plotted in Fig. 2.15, is an approximation for the Fanning friction factor based on the assumption that $(\sigma_o/\sigma_w)^4 \ll 1$ (Heywood, 1991a). This figure illustrates how the friction factor decreases with larger values of the Bingham Reynolds number, and increases with larger values of the Hedstrom number. A larger version of Fig. 2.15, more convenient for problem solving, is given in Appendix [6.17].

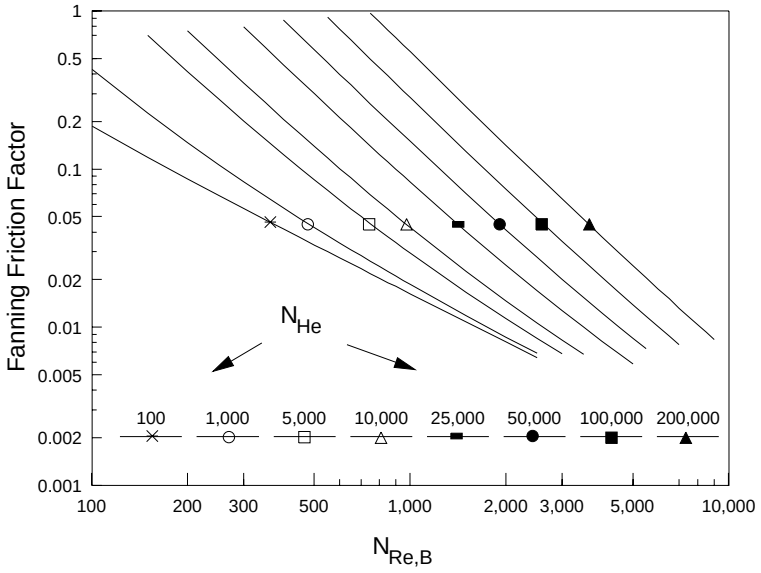

Figure 2.15. Fanning friction factors (from Eq. [2.114]) for Bingham plastic fluids in laminar flow at different values of the Hedstrom Number.

In turbulent flow, friction factors may be determined from empirical equations (Table 2.3) formulated from experimental data (Grovier and Aziz, 1972). The equations are only applicable to smooth pipes which include sanitary piping systems for food. It may be very difficult to accurately predict transition from laminar to turbulent flow in actual

Table 2.3. Fanning Friction Factor Equations for Turbulent Flow in Smooth Tubes

Fluid	Fanning Friction Factor
Newtonian $\sigma = \mu\dot{\gamma}$	$\frac{1}{\sqrt{f}} = 4.0\log_{10}(N_{Re}\sqrt{f}) - 0.4$ where: $N_{Re} = \frac{\rho D\bar{u}}{\mu}$
Power Law $\sigma = K(\dot{\gamma})^n$	$\frac{1}{\sqrt{f}} = \left(\frac{4}{n^{0.75}}\right)\log_{10}\left[(N_{Re,PL})f^{(1-(n/2))}\right] - \left(\frac{0.4}{n^{1.2}}\right)$ where: $N_{Re,PL} = \left(\frac{D^n(\bar{u})^{2-n}\rho}{8^{n-1}K}\right)\left(\frac{4n}{3n+1}\right)^n$
Bingham Plastic $\sigma = \mu_{pl}\dot{\gamma} + \sigma_o$	$\frac{1}{\sqrt{f}} = 4.53\log_{10}(1-c) + 4.53\log_{10}((N_{Re,B})\sqrt{f}) - 2.3$ where: $N_{Re,B} = \frac{D\bar{u}\rho}{\mu_{pl}}$ and $c = \frac{\sigma_o}{\sigma_w} = \frac{2\sigma_o}{f\rho(\bar{u})^2}$

processing systems and the equations given here are only intended for use in estimating the power requirements for pumping. Curves for power law fluids in turbulent flow are plotted in Fig. 2.16 (a larger version of the same plot is given in Appendix [6.18]). Newtonian fluids are represented by the curve with $n = 1.0$.

Kinetic Energy Evaluation. The kinetic energy term in the mechanical energy balance can be evaluated if the kinetic energy correction factor (α) is known. In turbulent flow of any fluid, $\alpha = 2$. Expressions to compute values for various fluids in laminar flow are summarized in Table 2.4. These equations may be given in terms of n, the flow behavior index, or c which is defined as the ratio of the yield stress (σ_o) to the shear stress at the wall (σ_w). Equations provided for the Bingham plastic and Herschel-Bulkley cases are approximations.

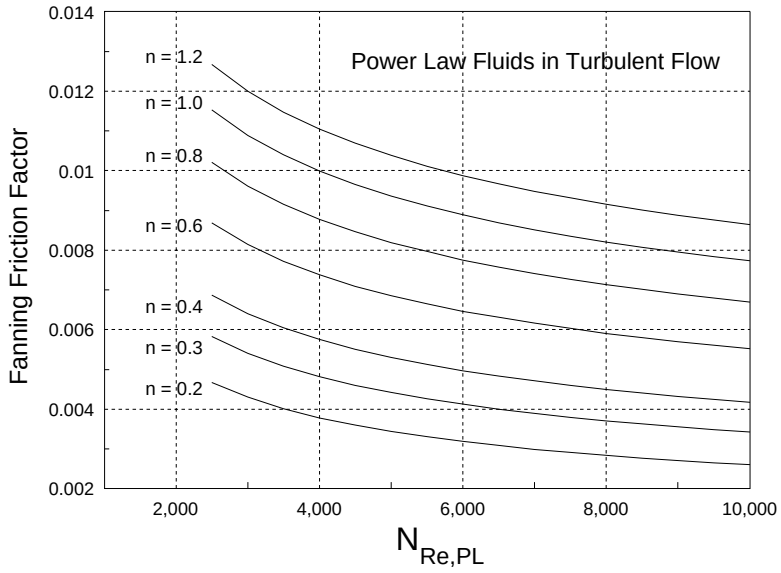

Figure 2.16. Fanning friction factors (equation given in Table 2.3) for power law fluids in turbulent flow at different values of the flow behavior index.

An exact, but cumbersome, mathematical equation for the kinetic energy correction factor of a Herschel-Bulkley fluid has been published by Osorio and Steffe (1984). Values of α, determined from this equation, are plotted in Fig. 2.17. This figure reveals some interesting features of the kinetic energy correction factor: α values go to 2 as the yield stress approaches the wall shear stress for all values of n; α values increase with decreasing values of n. Overall, the numerical value of α ranges from 0.74 to 2 for Herschel-Bulkley fluids (Osorio and Steffe, 1984). The minimum value of $\alpha = 0.74$ occurs at $c = 0$ as n approaches infinity. KE differences are usually small and often ignored in evaluating power requirements when selecting pumps.

Table 2.4. Kinetic Energy Correction Factors for Laminar Flow in Tubes

Fluid	α, dimensionless
Newtonian $\sigma = \mu\dot{\gamma}$	1.0
Power Law $\sigma = K(\dot{\gamma})^n$	$\alpha = \frac{2(2n+1)(5n+3)}{3(3n+1)^2}$
[+]Bingham Plastic $\sigma = \mu_{pl}\dot{\gamma} + \sigma_o$	$\alpha = \frac{2}{2-c}$
[+]Herschel-Bulkley $\sigma = K(\dot{\gamma})^n + \sigma_o$	$\alpha = \exp(0.168\,c - 1.062\,n\,c - 0.954\,n^{.5} - 0.115\,c^{.5} + 0.831)$ for $0.06 \le n \le 0.38$ and $\alpha = \exp(0.849\,c - 0.296\,n\,c - 0.600\,n^{.5} - 0.602\,c^{.5} + 0.733)$ for $0.38 < n \le 1.60$

[+] Solution for the Bingham plastic material is within 2.5% of the true solution (Metzner, 1956). Errors in using the Herschel-Bulkley solution are less than 3% for $0.1 \le c \le 1.0$ but as high as 14.2% for $0.0 \le c \le 0.1$ (Briggs and Steffe, 1995).

Friction Losses: Valves, Fittings, and Similar Parts. Friction loss coefficients (k_f) must be determined from experimental data. In general, published values are for the turbulent flow of water taken from Crane (1982). An adequate summary of these numbers may be found in Sakiadis (1984). Laminar flow data are much more limited. Some are available for various fluids: Newtonian (Kittredge and Rowley, 1957), shear-thinning (Banerjee et al., 1994; Lewicki and Skierkowski, 1988; Steffe et al., 1984) and shear-thickening (Griskey and Green, 1971). Overall, the quantity of engineering data required to predict pressure losses in valves and fittings for fluids, particularly non-Newtonian fluids, in laminar flow is insufficient.

Given this situation, a "rule of thumb" estimation procedure is needed. First some general observations should be made: a) The behavior of k_f values for Newtonian and non-Newtonian fluids is similar (Metzner, 1961; Skelland, 1967), b) k_f values decrease with increasing pipe diameter (Crane, 1982) -- they may drop as much as 30% in going from 3/4 to 4 inch (1.9 to 10.2 cm) pipe, c) k_f values sharply increase with

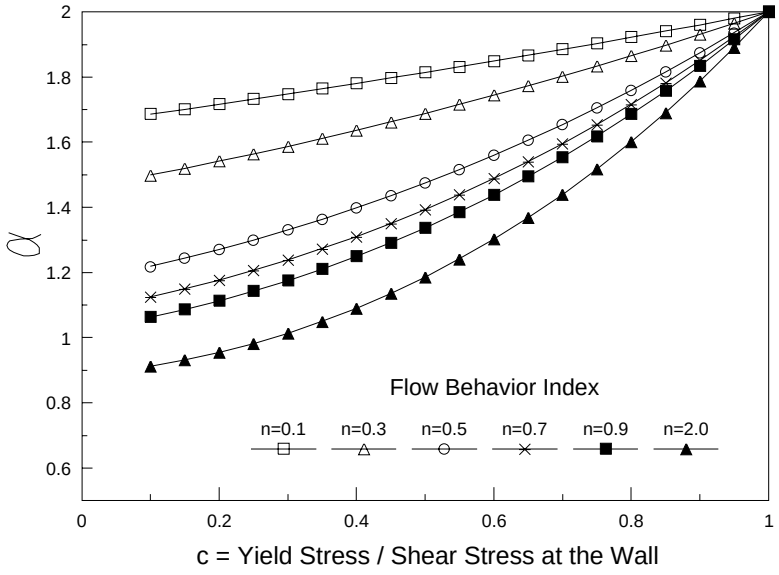

Figure 2.17. Kinetic energy correction factors for the laminar flow of Herschel-Bulkley fluids (from Osorio and Steffe, 1984).

decreasing Reynolds numbers (Cheng, 1970; Kittredge and Rowley, 1957; Lewicki and Skierkowski, 1988; Steffe et al., 1984) in the laminar flow regime but are constant in the turbulent flow regime (Sakiadis, 1984) and show little change above $N_{Re} = 500$ (Kittredge and Rowley, 1957), d) Entrance pressure losses for power law fluids in laminar flow decrease with smaller values of the flow behavior index (Collins and Schowalter, 1963), e) Entrance losses for Bingham plastic fluids decrease with increasing values of the yield stress when the wall shear stress ($\delta PR/(2L)$) is constant (Michiyosi et al., 1966), f) Resistance to flow of non-Newtonian fluids in laminar flow, through similar valves, can be expected to be up to 133 percent higher than that observed for Newtonian fluids (Ury, 1966).

Friction loss coefficients for many valves and fittings are summarized in Tables 2.5 and 2.6. k_f values for the sudden contraction, or expansion, of a Newtonian fluid in turbulent flow, may be found in Crane (1982). The loss coefficient for a sudden contraction is calculated in terms of the small and large pipe diameters:

Table 2.5. Friction Loss Coefficients (k_f Values) for the Laminar Flow of Newtonian Fluids through Valves and Fittings (from Sakiadis (1984) with Original Data from Kittredge and Rowley, 1957)

Type of Fitting or Valve	N_{Re}=1000	500	100
90-deg. elbow, short radius	0.9	1.0	7.5
Tee, standard, along run	0.4	0.5	2.5
Branch to line	1.5	1.8	4.9
Gate valve	1.2	1.7	9.9
Globe valve, composition disk	11	12	20
Plug	12	14	19
Angle valve	8	8.5	11
Check valve, swing	4	4.5	17

$$k_f = .5\left(1 - \left(\frac{D_{\text{small}}}{D_{\text{large}}}\right)^2\right) \qquad [2.115]$$

Losses for a sudden enlargement, or an exit, are determined as

$$k_f = \left(1 - \left(\frac{D_{\text{small}}}{D_{\text{large}}}\right)^2\right)^2 \qquad [2.116]$$

The largest velocity which is the mean velocity in the smallest diameter pipe, should be used for both contractions and expansions in calculating the friction loss term ($k_f \bar{u}^2/2$) found in Eq. [2.106].

After evaluating the available data for friction loss coefficients in laminar and turbulent flow, the following "rule-of-thumb" guidelines, conservative for shear-thinning fluids, are proposed for estimating k_f values:

1. For Newtonian fluids in laminar or turbulent flow use the data of Kittredge and Rowley (1957) or Sakiadis (1984), respectively (Tables 2.5 and 2.6).
2. For non-Newtonian fluids above a Reynolds number ($N_{Re,PL}$ or $N_{Re,B}$) of 500, use data for Newtonian fluids in turbulent flow (Table 2.6).
3. For non-Newtonian fluids in the Reynolds number range of $20 \le N \le 500$ use the following equation:

Table 2.6. Friction Loss Coefficients for the Turbulent Flow of Newtonian Fluids through Valves and Fittings (from Sakiadis, 1984)

Type of Fitting of Valve		k_f
45-deg. elbow, standard		0.35
45-deg. elbow, long radius		0.2
90-deg. elbow, standard		0.75
Long radius		0.45
Square or miter		1.3
180-deg. bend, close return		1.5
Tee, standard, along run, branch blanked off		0.4
Used as elbow, entering run		1.0
Used as elbow, entering branch		1.0
Branching flow		1.0
Coupling		0.04
Union		0.04
Gate valve, open		0.17
3/4 open		0.9
1/2 open		4.5
1/4 open		24.0
Diaphragm valve, open		2.3
3/4 open		2.6
1/2 open		4.3
1/4 open		21.0
Globe valve, bevel seat, open		6.0
1/2 open		9.5
Composition seat, open		6.0
1/2 open		8.5
Plug disk, open		9.0
3/4 open		13.0
1/2 open		36.0
1/4 open		112.0
Angle valve, open		2.0
Y or blowoff valve, open		3.0
Plug cock	θ=0° (fully open)	0.0
	θ=5°	0.05
	θ=10°	0.29
	θ=20°	1.56
	θ=40°	17.3
	θ=60°	206.0
Butterfly valve	θ=0° (fully open)	0.0
	θ=5°	0.24
	θ=10°	0.52
	θ=20°	1.54
	θ=40°	10.8
	θ=60°	118.0
Check valve, swing		2.0
Disk		10.0
Ball		70.0
Foot valve		15.0
Water meter, disk		7.0
Piston		15.0
Rotary (star-shaped disk)		10.0
Turbine-wheel		6.0

$$k_f = \frac{A}{N} \qquad [2.117]$$

where N is $N_{Re,PL}$ or $N_{Re,B}$ depending on the type of fluid in question. The constant, A, is found for a particular valve or fitting (or related items like contractions and expansions) by multiplying the turbulent flow friction loss coefficient by 500:

$$A = (k_f)_{\text{turbulent}}(500) \qquad [2.118]$$

Values of A for many standard items may be calculated from the k_f values provided in Table 2.6. The value of 20 was arbitrarily set as a lower limit of N in Eq. [2.117] because very low values of the Reynolds number in that equation will generate unreasonably high values of the friction loss coefficient. Values of $N \geq 20$ will cover most practical applications for fluid foods. Eq. [2.117] and [2.118] may also be used for Newtonian fluids when N_{Re} is used for N.

The above guidelines are offered with caution and should only be used in the absence of actual experimental data. Many factors, such as a high extensional viscosity, may significantly influence k_f values.

Generalized Pressure Drop Calculation. Metzner (1956) presents a generalized approach to relate flow rate and pressure drop for time-independent fluids in laminar flow. The governing equation is

$$\frac{(\delta P)R}{2L} = K'\left(\frac{4Q}{\pi R^3}\right)^{n'} \qquad [2.119]$$

where

$$n' = \frac{d\ln((\delta P)R/(2L))}{d\ln(4Q/(\pi R^3))} = \frac{d(\ln\sigma_w)}{d(\ln\Gamma)} \qquad [2.120]$$

K' and n' are easily determined from a plot of the experimental data.

There is a strong similarity with the above equation and those describing the flow of power law fluids in pipes. In fact, for a power law fluid,

$$n' = n \quad \text{and} \quad K' = K\left(\frac{3n+1}{4n}\right)^n \qquad [2.121]$$

With the general solution, n' may vary with the shear stress at the wall and must be evaluated at the particular value of σ_w in question.

Eq. [2.119] and [2.120] have practical value when considering direct scale-up from data taken with a small diameter tube or for cases where a well defined equation (power law, Bingham plastic or Herschel-Bulkley) is not applicable. A similar method is available for scale-up problems involving the turbulent flow of time-independent fluids (Lord et al., 1967).

Slip and time-dependent behavior may be a problem in predicting pressure loss in pipes. One solution is to incorporate these effects into the consistency coefficient. Houska et al. (1988) give an example of this technique for the transport of minced meat in pipes where K' incorporates the property changes due to the aging of the meat and wall slip as a function of pipe diameter. An exercise in pipeline design is presented in Example Problem 2.12.6.

2.11. Velocity Profiles In Turbulent Flow

Velocity profiles, critical in thermal processing systems (particularly in hold tubes), are strongly influenced by rheological properties. Accurately predicting velocity profiles for fluids in turbulent flow is difficult. Relationships for Newtonian fluids are reliable. Those for power law fluids are available but they have not received adequate experimental verification for fluid foods. Approximate mean, divided by maximum, velocities are summarized for some conditions in Table 2.7. A detailed discussion of laminar flow profiles is presented in Sec. 2.3.

Newtonian Fluids. Semi-theoretical prediction equations for the velocity profile of Newtonian fluids in turbulent flow are well established and presented in terms of three distinct regions of the pipe (Brodkey and Hershey, 1988):

for the viscous sublayer (called laminar sublayer in some literature)

$$u^+ = y^+ \qquad y^+ \le 5 \qquad [2.122]$$

for the transition zone where turbulent fluctuations are generated

$$u^+ = -3.05 + (11.513)\log_{10}(y^+) \qquad 5 < y^+ < 30 \qquad [2.123]$$

and for the turbulent core

Table 2.7. Approximate Average and Maximum Velocities for Newtonian and Power Law Fluids in Tube Flow

Newtonian Fluids

N_{Re}	< 2100	4000	10^4	10^5	10^6	10^7	10^8
$\bar{u}/u_{max}$	0.5	0.790	0.811	0.849	0.875	0.893	0.907

Power Law Fluids: Laminar Flow

$$\bar{u}/u_{max} = (n+1)/(3n+1)$$

n	0.0	0.3	0.4	0.5	1.0	2.0	∞
$\bar{u}/u_{max}$	1.00	0.68	0.64	0.60	0.50	0.43	0.33

Power Law Fluids: Turbulent Flow

n	0.2	0.2	0.2	0.5	0.5	0.5
$N_{Re,PL}$	10^4	10^5	10^6	10^4	10^5	10^6
$\bar{u}/u_{max}$	0.92	0.94	0.95	0.86	0.89	0.92

$$u^+ = 5.5 + (5.756)\log_{10}(y^+) \qquad 30 \le y^+ \qquad [2.124]$$

where

$$u^+ = \frac{u}{u^*} \qquad [2.125]$$

and

$$y^+ = \frac{y u^* \rho}{\mu} \qquad [2.126]$$

and

$$u^* = \sqrt{\frac{\sigma_w}{\rho}} = \bar{u}\sqrt{\frac{f}{2}} \qquad [2.127]$$

The distance from the pipe wall, y, is defined as

$$y = R - r \qquad [2.128]$$

Note that the origin of the coordinate system is (by convention) located at the wall, $r = R$. Therefore, the velocity is zero at $r = R$ where $y = 0$ and a maximum at the center of the pipe where $r = 0$ and $y = R$. The combined velocity equations constitute the universal velocity profile.

Once the maximum velocity has been determined, the 1/7 power law equation may be used to approximate $u/u_{\max}$ at other locations:

$$\frac{u}{u_{\max}} = \left(\frac{y}{R}\right)^{1/7} = \left(\frac{R-r}{R}\right)^{1/7} \qquad [2.129]$$

Eq. [2.129] does a reasonable job predicting velocity profiles in spite of the fact that it is not dependent on the Reynolds number. Grovier and Aziz (1972) note that this equation is most appropriate for $0.1 < y/R < 1.0$ and $3000 < N_{Re} < 100,000$. Also the exponent may vary from 1/6 at $N_{Re} = 4,000$ to 1/10 at $N_{Re} = 3,200,000$. Maximum velocity, of a turbulent Newtonian fluid in tube flow, is calculated in Example Problem 2.12.7.

Power Law Fluids. Dodge and Metzner (1959) derived equations to describe the velocity profile of power law fluids in tube flow. Small errors were corrected by Skelland (1967) and the final equations presented as

$$u^+ = (y^+)^{1/n} \qquad [2.130]$$

for the laminar sublayer and

$$u^+ = \frac{5.66}{n^{.75}}\log_{10}(y^+) - \frac{0.566}{n^{1.2}} + \frac{3.475}{n^{.75}}\left[1.960 + 0.815n - 1.628n\log_{10}\left(3 + \frac{1}{n}\right)\right] \qquad [2.131]$$

for the turbulent core, where y^+ incorporates the flow behavior index and the consistency coefficient needed for the consideration of power law fluids:

$$y^+ = y^n (u^*)^{2-n} \rho / K \qquad [2.132]$$

Constants were obtained from friction factor measurements so the thickness of the laminar sublayer was not obtained. These equations are applied in Example Problem 2.12.8.

An alternative equation for predicting velocity in the turbulent core for power law fluids was presented by Clapp (1961):

$$u^+ = \frac{2.78}{n} 2.303 \log_{10}(y^+) + \frac{3.80}{n} \qquad [2.133]$$

This equation correlated well with experimental data in which $0.698 < n < 0.813$ and $5,480 < N_{Re,PL} < 42,800$.

2.12. Example Problems

2.12.1. Conservation of Momentum Equations

Show that an equation describing the shear stress for a fluid in tube flow may be determined from the conservation of momentum principle. Compare the result to Eq. [2.2] which was derived directly from a force balance. This example problem is included to illustrate an alternative method of obtaining rheological relationships.

First a number of assumptions must be stated: flow is for an incompressible fluid under steady, laminar, isothermal conditions; there are no entrance and exit effects; and flow is parallel to the pipe wall, i.e., there is no radial or circumferential flow. Then, using cylindrical coordinates (Fig. 2.18),

$$u_r = u_\theta = 0 \qquad u_z = u_z(r) \qquad [2.134]$$

The continuity (conservation of mass) equation may be written as

$$\frac{\partial \rho}{\partial t} + \frac{1}{r}\frac{\partial}{\partial r}(\rho r u_r) + \frac{1}{r}\frac{\partial}{\partial \theta}(\rho u_\theta) + \frac{\partial}{\partial z}(\rho u_z) = 0 \qquad [2.135]$$

Under steady conditions with an incompressible fluid ($\partial\rho/\partial t = 0$) and, with the assumption that radial and circumferential velocities are zero, this equation reduces to

$$\frac{du_z}{dz} = 0 \qquad [2.136]$$

indicating that conservation of mass is satisfied and velocity is constant along the z (axial) direction. Considering the above assumptions the momentum equations (Fig. 2.18) collapse to the following:

r component: $$0 = -\frac{\partial P}{\partial r} \qquad [2.137]$$

θ component: $$0 = -\frac{1}{r}\frac{\partial P}{\partial \theta} \qquad [2.138]$$

z component: $$0 = -\frac{\partial P}{\partial z} + \frac{1}{r}\frac{\partial}{\partial r}(r\sigma_{rz}) \qquad [2.139]$$

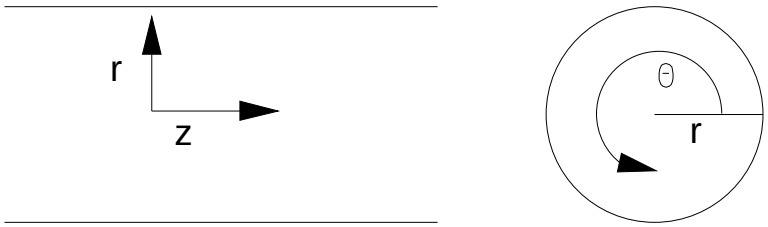

$$\rho\left(\frac{\partial u_r}{\partial t}+u_r\frac{\partial u_r}{\partial r}+\frac{u_\theta}{r}\frac{\partial u_r}{\partial \theta}-\frac{u_\theta^2}{r}+u_z\frac{\partial u_r}{\partial z}\right)=-\frac{\partial P}{\partial r}+\frac{1}{r}\frac{\partial}{\partial r}(r\sigma_{rr})+\frac{1}{r}\frac{\partial \sigma_{r\theta}}{\partial \theta}-\frac{\sigma_{\theta\theta}}{r}+\frac{\partial \sigma_{rz}}{\partial z}+\rho g_r$$

$$\rho\left(\frac{\partial u_\theta}{\partial t}+u_r\frac{\partial u_\theta}{\partial r}+\frac{u_\theta}{r}\frac{\partial u_\theta}{\partial \theta}+\frac{u_r u_\theta}{r}+u_z\frac{\partial u_\theta}{\partial z}\right)=-\frac{1}{r}\frac{\partial P}{\partial \theta}+\frac{1}{r^2}\frac{\partial}{\partial r}(r^2\sigma_{r\theta})+\frac{1}{r}\frac{\partial \sigma_{\theta\theta}}{\partial \theta}+\frac{\partial \sigma_{\theta z}}{\partial z}+\rho g_\theta$$

$$\rho\left(\frac{\partial u_z}{\partial t}+u_r\frac{\partial u_z}{\partial r}+\frac{u_\theta}{r}\frac{\partial u_z}{\partial \theta}+u_z\frac{\partial u_z}{\partial z}\right)=-\frac{\partial P}{\partial z}+\frac{1}{r}\frac{\partial}{\partial r}(r\sigma_{rz})+\frac{1}{r}\frac{\partial \sigma_{\theta z}}{\partial \theta}+\frac{\partial \sigma_{zz}}{\partial z}+\rho g_z$$

Figure 2.18. Momentum equations in cylindrical coordinates. [Note: P is an inclusive pressure term which ignores small variation in pressure due to variations in height (ρgh)].

The r and θ components would integrate to a constant indicating that P does not vary in those directions. It follows that P is a function of z only:

$$P = P(z) \qquad [2.140]$$

Then, we can replace $(1/r)\partial(r\sigma_{rz})/\partial r$ with $(1/r)d(r\sigma_{rz})/dr$, and $\partial P/\partial z$ with dP/dz to write the z component of the momentum equation, Eq. [2.139], as

$$\frac{1}{r}\frac{d}{dr}(r\sigma_{rz}) = \frac{dP}{dz} \qquad [2.141]$$

or

$$\frac{1}{r}\frac{d}{dr}(r\sigma_{rz}) = \frac{(-\delta P)}{L} \qquad [2.142]$$

where dP/dz is replaced by the constant term, $(-\delta P)/L$. This is allowed because the left hand side of Eq. [2.141] is a function of r only, and the

right hand side of the equation is a function of z only; hence, both sides are equal to a constant (the origin of the negative sign will be explained shortly). Integrating Eq. [2.142] yields

$$\int d(r\sigma_{rz}) = \int\left(\frac{(-\delta P)}{L} r\right) dr \qquad [2.143]$$

giving

$$\sigma_{rz} = \frac{(-\delta P)}{2L} r + \frac{C_1}{r} \qquad [2.144]$$

C_1 must be zero for the shear stress to be finite at the centerline of the pipe, therefore,

$$\sigma_{rz} = \frac{(-\delta P)r}{2L} \qquad [2.145]$$

which, written in one dimensional symbolism, is like Eq. [2.2] found from a simple force balance:

$$\sigma = \frac{(-\delta P)r}{2L} \qquad [2.146]$$

Eq. [2.146] and [2.2] are equivalent, but appear different, due to the presence of a negative sign in Eq. [2.146]. This reflects the sign convention adopted in developing the equations illustrated in Fig. 2.18 and utilized in various textbooks (Bird et al., 1960; Denn, 1980; Brodkey and Hershey, 1988). In those equations δP is negative so the negative sign is required to make the shear stress positive. In this book, however, δP was assumed to be a positive number in deriving our initial force balance (Eq. [2.1]) making a negative sign unnecessary.

2.12.2. Capillary Viscometry - Soy Dough

Data for a defatted soy flour dough from a capillary viscometer are summarized in Table 2.8. Determine the rheological properties of the material.

The first step in the analysis is to correct the measured pressure loss for entrance effects. Pressure losses are plotted (Fig. 2.19) at different values of L/D for constant apparent wall shear rates, $4Q/(\pi R^3)$. Regression analysis of these curves gives the required entrance loss correction values at $L/D = 0$. In this particular problem, entrance losses constitute a very high percentage, over 80% in many trials, of the total pressure drop across the capillary (Table 2.8).

Table 2.8. Capillary Viscometer (D=3.18mm) Data for Dough (34.7%) at Room Temperature Made from Defatted Soy Flour Treated to Cause Protein Denaturation (Data from Morgan, 1979)

$4Q/(\pi R^3)$ (1/s)	$Q/(\pi R^3)$ (1/s)	L/D (-)	$(\delta P)_m^*$ (MPa)	$(\delta P)_{en}^{**}$ (MPa)	$(\delta P)^{***}$ (MPa)	σ_w (kPa)	$\dot{\gamma}_w$ (1/s)
47.4	11.9	2	4.21	3.58	0.63	78.75	72.13
47.4	11.9	5	5.21	3.58	1.63	81.50	76.73
47.4	11.9	8	6.14	3.58	2.56	80.00	74.17
94.8	23.7	2	5.46	4.63	0.83	103.75	165.80
94.8	23.7	5	6.81	4.63	2.18	109.00	183.38
94.8	23.7	8	8.02	4.63	3.39	105.94	172.87
190.0	47.5	2	5.25	4.38	0.87	108.75	253.90
190.0	47.5	5	6.80	4.38	2.42	121.00	303.49
190.0	47.5	8	8.30	4.38	3.92	122.50	310.48
948.0	237.0	2	7.68	6.17	1.51	188.75	1457.45
948.0	237.0	5	10.12	6.17	3.95	197.50	1583.76
948.0	237.0	8	12.31	6.17	6.14	191.88	1500.96

* Measured pressure drop; ** Entrance loss pressure correction
*** Corrected pressure drop.

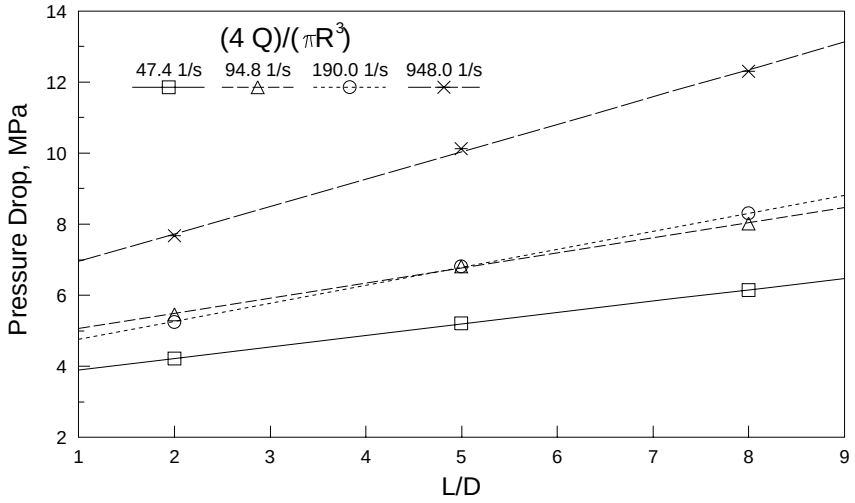

Figure 2.19. Measured pressure drop (including entrance loss) for capillary viscometer data from defatted soy flour.

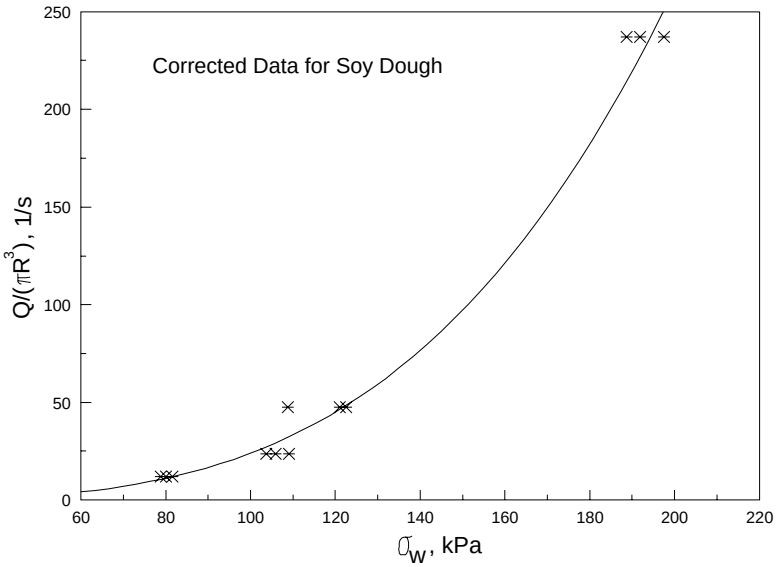

Figure 2.20. Capillary data for soy dough corrected for pressure loss.

To determine the shear rate, the Rabinowitsch-Mooney equation (Eq. [2.20]), must be evaluated:

$$\dot{\gamma}_w = f(\sigma_w) = \left(\frac{3Q}{\pi R^3}\right) + (\sigma_w)\left[\frac{d(Q/(\pi R^3))}{d\sigma_w}\right]$$

The relationship between $Q/(\pi R^3)$ and σ_w was plotted (Fig. 2.20) and determined (by curve fitting) as a power function:

$$\frac{Q}{\pi R^3} = 3.1(10^{-6})(\sigma_w)^{3.44}$$

The derivative of this equation is

$$\frac{d(Q/(\pi R^3))}{d\sigma_w} = 1.06(10^{-5})(\sigma_w)^{2.44}$$

which can be inserted into the Rabinowitsch-Mooney equation to determine the shear rate at the wall:

$$\dot{\gamma}_w = \left(\frac{3Q}{\pi R^3}\right) + \sigma_w[1.06(10^{-5})(\sigma_w)^{2.44}]$$

Results of this computation are summarized in Table 2.8. After making these calculations, the basic elements of the rheogram illustrating shear stress versus shear rate are available for plotting (Fig. 2.21). If the material is considered to be shear-thinning over the shear rate range considered, the following fluid parameters are calculated: K = 23.3 kPa s^n, n = 0.29.

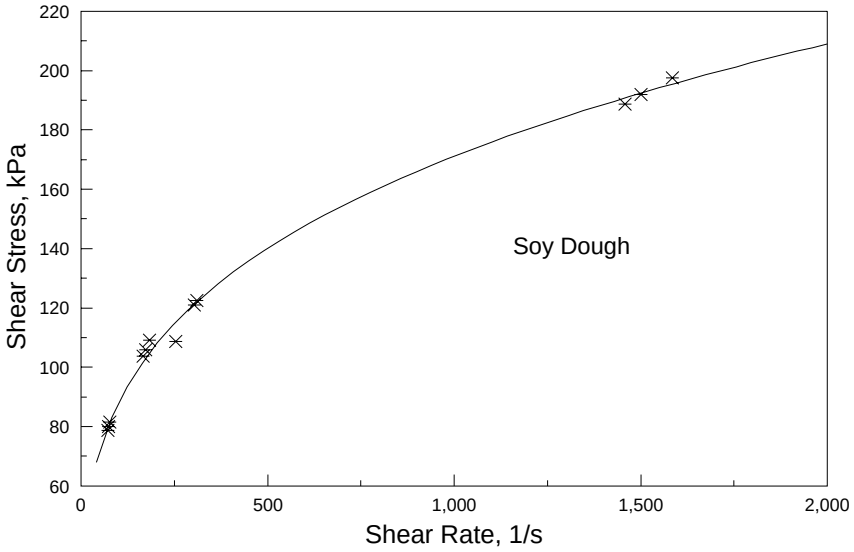

Figure 2.21. Rheogram for soy dough.

2.12.3. Tube Viscometry - 1.5% CMC

Data for a 1.5% aqueous solution of sodium carboxymethylcellulose (CMC) were collected at room temperature using a capillary tube viscometer (Table 2.9). Determine the rheological properties of this material. Since the minimum L/D is 248, entrance effects are assumed to be insignificant. Assume CMC density is equal to 1003 kg/m^3.

Regression analysis of $\ln(\sigma_w)$ versus $\ln(4Q/(\pi R^3))$ or $\ln(\Gamma)$ in the form of

Table 2.9. Rheological Data for a 1.5% Aqueous Solution of Sodium Carboxymethylcellulose (CMC; ρ=1003 kg/m³) Collected at Room Temperature (Data from Middleman, 1968)

D (m)	L (m)	δP (Pa)	Q (m^3/s)	σ_w (Pa)	$4Q/(\pi R^3)$ (1/s)	$\dot{\gamma}_w$ (1/s)
2.71E-03	0.944	1.379E+05	5.910E-07	98.97	302.47	409.50
2.71E-03	0.944	2.710E+05	2.950E-06	194.48	1509.78	2044.04
2.71E-03	0.944	4.103E+05	8.320E-06	294.43	4258.10	5764.89
2.71E-03	0.944	5.916E+05	2.100E-05	424.58	10747.61	14550.81
2.71E-03	0.674	1.034E+05	7.330E-07	103.96	375.14	507.89
2.71E-03	0.674	1.379E+05	1.260E-06	138.62	644.86	873.05
2.71E-03	0.674	2.724E+05	7.060E-06	273.77	3613.24	4891.84
2.71E-03	0.674	3.999E+05	1.760E-05	401.99	9007.52	12194.96
2.71E-03	0.674	5.482E+05	3.510E-05	551.00	17963.86	24320.64
1.82E-03	0.634	1.413E+05	1.920E-07	101.44	324.40	439.20
1.82E-03	0.634	1.931E+05	4.770E-07	138.55	805.94	1091.14
1.82E-03	0.634	2.586E+05	8.010E-07	185.56	1353.38	1832.29
1.82E-03	0.634	4.068E+05	2.580E-06	291.95	4359.19	5901.76
1.82E-03	0.634	5.482E+05	5.560E-06	393.39	9394.23	12718.51
1.82E-03	0.634	6.916E+05	9.340E-06	496.31	15780.95	21365.27
1.82E-03	0.452	6.206E+04	6.700E-08	62.47	113.20	156.26
1.82E-03	0.452	1.413E+05	3.500E-07	142.29	591.36	800.63
1.82E-03	0.452	2.137E+05	9.720E-07	215.16	1642.30	2223.45
1.82E-03	0.452	3.103E+05	2.720E-06	312.33	4595.74	6222.01
1.82E-03	0.452	4.103E+05	5.750E-06	412.98	9715.25	13153.14
1.82E-03	0.452	5.171E+05	9.840E-06	520.56	16625.76	22509.02

$$\ln(\sigma_w) = \ln(Constant) + n' \ln(\Gamma)$$

fits the data well (Fig. 2.22) and yields $n' = 0.414$ meaning that

$$n' = \frac{d(\ln(\sigma_w))}{d(\ln(\Gamma))} = 0.414$$

Note also (Fig. 2.22) that data for all tube sizes overlap verifying the assumption of a negligible entrance effect. Now, $\dot{\gamma}_w$ may be calculated using the Rabinowitsch-Mooney equation given in terms of Eq. [2.24] and [2.25]:

$$\dot{\gamma}_w = \left(\frac{3n'+1}{4n'} \right) \Gamma = \left(\frac{3(.414)+1}{4(.414)} \right) \Gamma = 1.35\,\Gamma$$

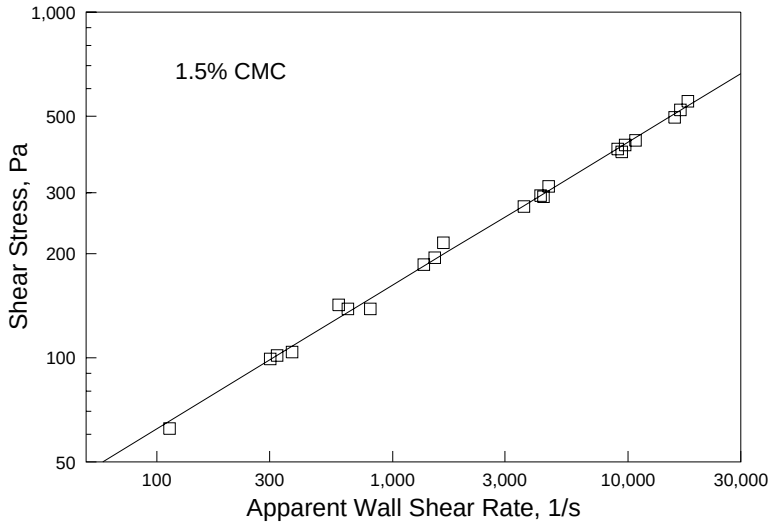

Figure 2.22. Shear stress versus apparent wall shear rate ($\Gamma = 4Q/(\pi R^3)$) *of 1.5% CMC at room temperature.*

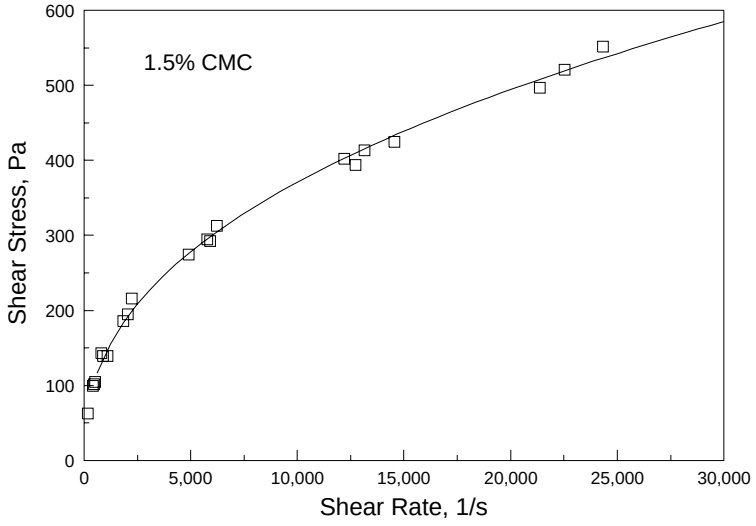

Figure 2.23. Rheogram for 1.5% CMC at room temperature.

Results are summarized in Table 2.9 and plotted in Fig. 2.23. The power law model was used to represent fluid behavior:

$$\sigma_w = 8.14(\dot{\gamma}_w)^{.414}$$

where K = 8.14 Pa s $^{.414}$ and n = 0.414. Note, with the power law model, $n = n'$, as expected.

$N_{Re,PL}$ should be checked, to be certain flow is laminar, using Eq. [2.51] or Eq. [2.53]. The "worst case," at D = 0.00271 m and $Q = 3.510(10^{-5})$ m^3/s, yields $\overline{u} = 6.09$ m/s and $N_{Re,PL} = 558$. With $n = 0.414$, $(N_{Re,PL})_{critical} = 2581$, when calculated using Eq. [2.53]. Since 558 < 2581, one may conclude that flow is laminar for all flow rates under consideration.

In this problem it was assumed the entrance effect was negligible. The actual entrance length can be estimated from Eq. [2.67]:

$$\frac{X_E}{DN_{Re,PL}} = (-.125n + .175)(8^{n-1})\left(\frac{3n+1}{4n}\right)^n$$

Taking the experimental values used in checking for laminar flow yields

$$X_E = .00271(558)(-.125(.414) + .175)(8^{.414-1})\left[\frac{3(.414)+1}{4(.414)}\right]^{.414} = .0625 \text{ m}$$

Meaning, for this particular case, the laminar flow velocity (as described by Eq. [2.40]) was 98% fully developed in the 0.271cm diameter tube at a distance of approximately 6.25cm (approximately 23 diameters) from the entrance. Since the minimum L/D of this system is 248, it is unlikely the entrance losses will significantly influence results.

2.12.4. Casson Model: Flow Rate Equation

Derive the relationship between volumetric flow rate and pressure drop for a Casson fluid in laminar tube flow.

The starting point in the solution is Eq. [2.15] giving the general flow rate relationship in tube flow:

$$\frac{Q}{\pi R^3} = \frac{1}{(\sigma_w)^3}\int_0^{\sigma_w} (\sigma)^2 f(\sigma)\, d\sigma$$

The Casson equation, given in Table 1.3, is

$$\sigma^{.5} = \sigma_o^{.5} + K_1(\dot{\gamma})^{.5} \qquad [2.147]$$

which can easily be solved for the shear rate:

$$\dot{\gamma} = f(\sigma) = \left[\frac{\sigma^{.5} - \sigma_o^{.5}}{K_1} \right]^2 \qquad [2.148]$$

Eq. [2.148] may be substituted into the flow rate equation: Recognizing that the presence of the yield stress makes the flow discontinuous gives

$$\frac{Q\sigma_w^3 K_1^2}{\pi R^3} = \int_0^{\sigma_o} \sigma^2 f(\sigma)\, d\sigma + \int_{\sigma_0}^{\sigma_w} \sigma^2 (\sigma^{.5} - \sigma_o^{.5})^2 d\sigma \qquad [2.149]$$

The first integral term in Eq. [2.149] is zero because $f(\sigma) = 0$ in the central plug region of the tube where $0 < \sigma < \sigma_o$; therefore,

$$\frac{Q\sigma_w^3 K_1^2}{\pi R^3} = \int_{\sigma_0}^{\sigma_w} \sigma^2 (\sigma^{.5} - \sigma_o^{.5})^2 d\sigma \qquad [2.150]$$

Expansion, integration, and algebraic manipulation yields the final solution:

$$Q = \frac{\pi R^3}{K_1^2} \left(\frac{\sigma_w}{4} - \frac{4\sigma_o^{.5}\sigma_w^{.5}}{7} + \frac{\sigma_o}{3} - \left(\frac{\sigma_o^4}{\sigma_w^4} \right) \left(\frac{1}{84} \right) \right) \qquad [2.151]$$

Since $\sigma_w = \delta P R/(2L)$, Eq. [2.151] provides the relationship between volumetric flow rate and pressure drop for a Casson fluid.

2.12.5. Slit Viscometry - Corn Syrup

Data (Table 2.10) for high fructose corn syrup were collected at 28°C using a slit viscometer. Determine the rheological properties of this material. Pressure drops were measured with flush mounted transducers in the region of the slit where flow was fully developed.

The apparent wall shear rate ($6Q/(wh^2)$) and shear stress ($\delta P h/(2L)$) were calculated (Table 2.10) and plotted (Fig. 2.24) to find $n' = 0.97$ from Eq. [2.89]:

$$n' = \frac{d \ln(\sigma_w)}{d \ln(\dot{\gamma}_w)} = 0.97$$

Table 2.10. Slit (Fig. 2.14: h=0.3375 cm, w= 8.89 cm, L= 33.02 cm) Flow Data of High Fructose Corn Syrup at 28°C

Q (m^3/s)	$6Q/(wh^2)$ (1/s)	$\delta P/L$ (Pa/m)	σ_w (kPa)	$\dot{\gamma}_w$ (1/s)
6.16 E-6	44.3	2.28	3.63	44.8
8.16 E-6	54.6	3.01	4.78	55.2
9.65 E-6	64.6	3.55	5.63	65.3
10.0 E-6	73.4	4.02	6.39	74.2
12.2 E-6	81.6	4.39	6.98	82.4
13.8 E-6	92.6	4.86	7.71	93.6
15.1 E-6	101.4	5.30	8.41	102.4
16.2 E-6	108.6	5.58	8.86	109.8

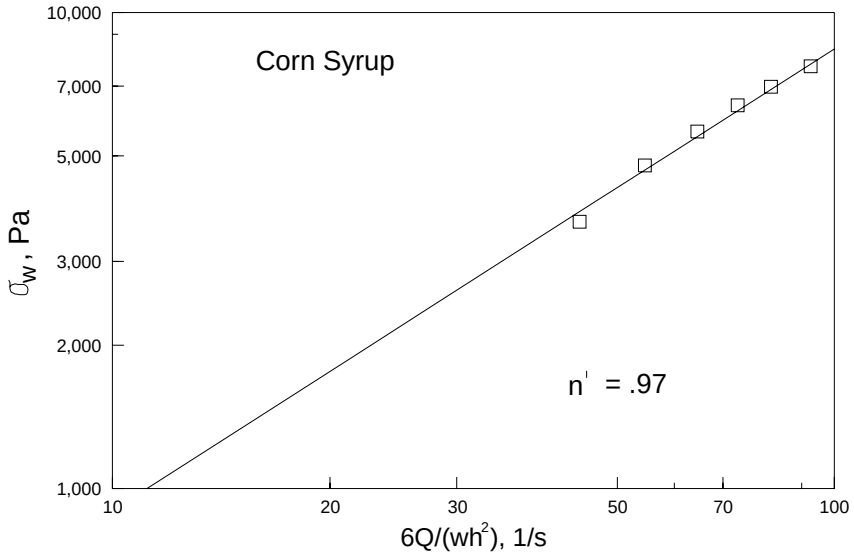

Figure 2.24. Shear stress versus apparent wall shear rate for slit flow data of high fructose corn syrup at 28°C.

A value of n' this close to 1.0 indicates the expected Newtonian behavior. Using Eq. [2.88], the shear rate was evaluated (Table 2.10). The rheogram was plotted (Fig. 2.25) and fit with a linear equation:

$$\sigma_w = 374.6 + 78.7\,\dot{\gamma}_w$$

Showing the viscosity of the sample is 78.7 Pa s. The intercept, 374.6 Pa, is a mathematical consequence of the statistical procedure and should not be interpreted as an absolute value of the yield stress.

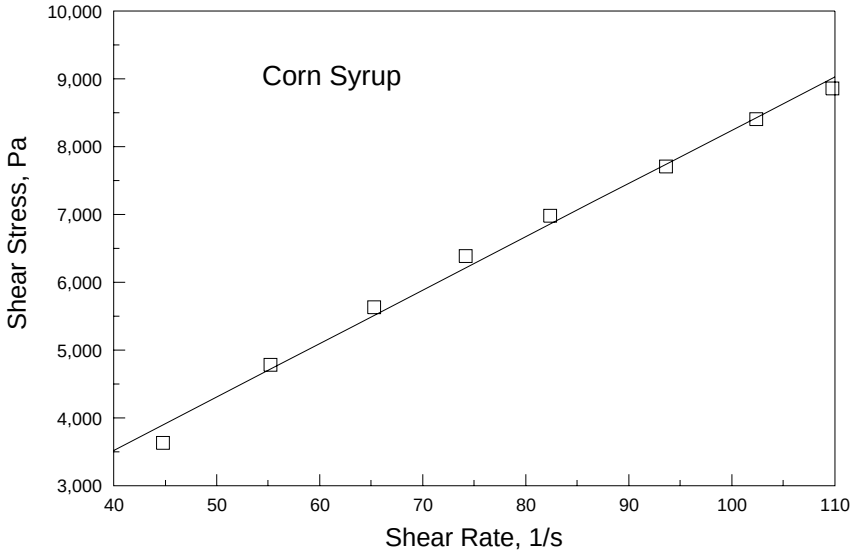

Figure 2.25. Rheogram for high fructose corn syrup at 28°C.

2.12.6. Friction Losses in Pumping

Consider the typical flow problem illustrated in Fig. 2.26. Assume the plug disk valve is open. The system has a 0.0348 m diameter pipe with a volumetric flow rate of 0.00157 m^3/s (1.97 kg/s) resulting in a volumetric average velocity of 1.66 m/s. The fluid density is equal to 1250 kg/m^3 and the pressure drop across the strainer is 100 kPa. Determine the friction losses in the system, and calculate the work input and pressure drop across the pump for the following two cases involving power law fluids: Case 1) Assume K = 5.2 Pa s^n and n = 0.45; Case 2) Assume K = 0.25 Pa s^n and n = 0.45.

Solving the mechanical energy balance equation, Eq. [2.105], for work output yields

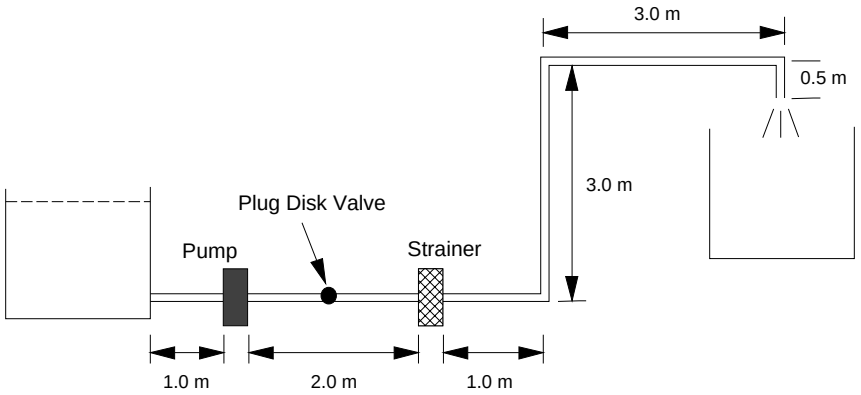

Figure 2.26. Pumping system for a power law fluid.

$$-W = \frac{(\bar{u}_2)^2}{\alpha_2} - \frac{(\bar{u}_1)^2}{\alpha_1} + g(z_2 - z_1) + \frac{P_2 - P_1}{\rho} + \sum F$$

Subscripts 1 and 2 refer to the fluid level in the input tank and the exit point of the system, respectively. The pressure at points 1 and 2 is equal to one atmosphere, therefore, $P_2 = P_1$. As a worst case for pumping, assume a near empty tank ($z_2 - z_1 = 2.5$). Also, assume a large diameter input tank making $\bar{u}_1 = 0$. These considerations simplify the above equation to

$$-W = g(z_2 - z_1) + \frac{(\bar{u}_2)^2}{\alpha_2} + \sum F = 9.81(2.5) + \frac{(1.66)^2}{\alpha_2} + \sum F$$

where ($-W$) represents the work input per unit mass. The summation term, given by Eq. [2.106], includes friction losses in straight pipe, fittings, and the strainer:

$$\sum F = \frac{2f(\bar{u})^2 L}{D} + \frac{(k_{f,entrance})(\bar{u})^2}{2} + \frac{(k_{f,valve})(\bar{u})^2}{2} + \frac{3(k_{f,elbow})(\bar{u})^2}{2} + \frac{100000}{1250}$$

or

$$\sum F = \frac{2f(\bar{u})^2 L}{D} + (k_{f,entrance} + k_{f,valve} + 3(k_{f,elbow}))\frac{(\bar{u})^2}{2} + 80.0$$

Pressure drop across the pump is

$$(\delta P)_p = (-W)\rho$$

The power requirement would be found by calculating the product of work input and mass flow rate.

Solution to Case 1: K **= 5.2 Pa s^n and** n **= 0.45.** Using Eq. [2.52], $N_{Re,PL}$ is calculated to be 323.9, a laminar flow value of $N_{Re,PL}$. Friction loss coefficients are determined from Eq. [2.115], Eq. [2.117], Eq. [2.118], and Table 2.6 yielding:

$$k_{f,entrance} = \frac{(.5)500}{323.9} = 0.77$$

$$k_{f,valve} = \frac{(9)\,(500)}{323.9} = 13.89$$

$$k_{f,elbow} = \frac{(.45)\,(500)}{323.9} = .69$$

and the friction factor is calculated from Eq. [2.113]:

$$f = \frac{16}{323.9} = .0494$$

Using the above values, the total friction loss is

$$\sum F = \frac{2(.0494)\,(1.66)^2\,(10.5)}{.0348} + (0.77 + 13.89 + 3(.69))\frac{(1.66)^2}{2} + 80.0 = 185.2 \text{ J/kg}$$

The kinetic energy correction factor is found from the laminar flow equation for power law fluids (Table 2.4):

$$\alpha = \frac{2(2n+1)\,(5n+3)}{3(3n+1)^2} = \frac{2(2(.45)+1)\,(5(.45)+3)}{3(3(.45)+1)^2} = 1.2$$

With this information, the calculations for work input and pressure drop can be completed:

$$-W = 9.81(2.5) + \frac{(1.66)^2}{1.2} + 185.2 = 212.0 \text{ J/kg}$$

and

$$(\delta P)_p = (212.0)\,(1250) = 265 \text{ kPa}$$

Solution to Case 2: K = 0.25 Pa s^n and n = 0.45. Using Eq. [2.52], $N_{Re,PL}$ is calculated as 6,737. The critical value of $N_{Re,PL}$, determined from Eq. [2.51], is

$$(N_{Re,PL})_{critical} = \frac{6464(.45)\,(2+.45)^{(2+.45)/(1+.45)}}{(1+3(.45))^2} = 2,394.$$

meaning the flow is turbulent since 6,737 > 2,394. Friction loss coefficients may be determined from Eq. [2.115], and Table 2.6: $k_{f,entrance} = 0.55$; $k_{f,valve} = 9$; $k_{f,elbow} = 0.45$. The friction factor is found by iteration of (equation from Table 2.4)

$$\frac{1}{\sqrt{f}} = \left(\frac{4}{(.45)^{0.75}}\right)\log_{10}[(6736.6)f^{(1-(.45/2))}] - \left(\frac{0.4}{(.45)^{1.2}}\right)$$

yielding f = 0.0052. Then,

$$\sum F = \frac{2(.0052)\,(1.66)^2\,(10.5)}{.0348} + (.5+9+3(.45))\frac{(1.66)^2}{2} + 80.0 = 103.6 \text{ J/kg}$$

In turbulent flow, the kinetic energy correction factor is equal to 2. Then, the work input and pressure drop are calculated as

$$-W = 9.81(2.5) + \frac{(1.66)^2}{2} + 103.6 = 129.5 \text{ J/kg}$$

and

$$(\delta P)_p = (129.5)\,(1250) = 162 \text{ kPa}$$

2.12.7. Turbulent Flow - Newtonian Fluid

A common problem facing food process engineers is to predict the maximum velocity found during flow in tubes. Determine, given the following data, the maximum velocity in the pipe: $\mu = 0.012$ Pa s; $D = 0.0348$ m; $\bar{u} = 1.66$ m/s; $\rho = 1250$ kg/m^3. Also, calculate the velocity at a point halfway between the center-line and the wall of the pipe.

The Reynolds number for a Newtonian fluid is calculated as

$$N_{Re} = \frac{\rho D\bar{u}}{\mu} = \frac{1250(.0348)1.66}{0.012} = 6017.5$$

which is sufficient to conclude that flow is in the turbulent regime. The friction factor equation for Newtonian fluids in turbulent flow (see Table 2.3) is:

$$\frac{1}{\sqrt{f}} = 4.0\log_{10}(N_{Re}\sqrt{f}) - 0.4 = 4.0\log_{10}((6017.5)\sqrt{f}) - 0.4$$

Solving for f gives

$$f = 0.0089$$

The velocity is maximum at the center-line where $r = 0$ and $y = R$. It must be calculated from the friction velocity, Eq. [2.127]:

$$u^* = \bar{u}\sqrt{\frac{f}{2}} = 1.66\sqrt{\frac{.0089}{2}} = .1107 \text{ m/s}$$

Calculations proceed using Eq. [2.126] and [2.124]:

$$y^+ = \frac{yu^*\rho}{\mu} = \frac{(.0348/2)(.1107)1250}{.012} = 200.64$$

and

$$u^+ = 5.5 + 5.756\log_{10}(y^+) = 5.5 + 5.756\log_{10}(200.64) = 18.753$$

The maximum velocity may be found from the definition (Eq. [2.125]) of the turbulent velocity, $u^+ = u/u^*$, as

$$u_{\max} = u^+u^* = (18.753).1107 = 2.075 \text{ m/s}$$

With this information, velocities at other locations can also be estimated. The 1/7 power law equation (Eq. [2.129]) may be used to approximate $u/u_{\max}$ at the velocity halfway between the center-line and the wall ($r = (.5)R$):

$$\frac{u}{u_{\max}} = \left(\frac{y}{R}\right)^{1/7} = \left(\frac{R-r}{R}\right)^{1/7} = (.5)^{1/7} = .906$$

giving

$$u = (2.075)(.906) = 1.879 \text{ m/s}$$

2.12.8. Turbulent Flow - Power Law Fluid

Determine the maximum velocity of a power law fluid in a pipe given the following information: $K = 0.25$ Pa s^n; $D = 0.0348$ m; $\bar{u} = 1.66$ m/s; $\rho = 1250$ kg/m^3; $n = 0.45$.

The Reynolds number (Eq. [2.52]) is

$$N_{Re,PL} = \left(\frac{D^n(\bar{u})^{2-n}\rho}{8^{n-1}K}\right)\left(\frac{4n}{3n+1}\right)^n = \left(\frac{.0348^{.45}(1.66)^{2-.45}1250}{8^{.45-1}(.25)}\right)\left(\frac{4(.45)}{3(.45)+1}\right)^{.45} = 6736.6$$

allowing f to be calculated (equation presented in Table 2.3) from:

$$\frac{1}{\sqrt{f}} = \left(\frac{4}{n^{0.75}}\right)\log_{10}[(N_{Re,PL})f^{(1-(n/2))}] - \left(\frac{0.4}{n^{1.2}}\right) = \left(\frac{4}{(.45)^{0.75}}\right)\log_{10}[(6736.6)f^{(1-(.45/2))}] - \left(\frac{0.4}{(.45)^{1.2}}\right)$$

yielding

$$f = 0.0052$$

Velocity is maximum at the center-line where $y = R$. The friction velocity (Eq. [2.127]) is

$$u^* = \bar{u}\sqrt{\frac{f}{2}} = 1.66\sqrt{\frac{.0052}{2}} = .0846 \text{ m/s}$$

y^+ is calculated using Eq. [2.132] as:

$$y^+ = y^n(u^*)^{2-n}\rho/K = (.0348/2)^{.45}(.0846)^{2-.45}(1250)/.25 = 17.6$$

Then, u^+ is determined from Eq. [2.131]:

$$u^+ = \frac{5.66}{(.45)^{.75}}\log_{10}(17.6) - \frac{0.566}{(.45)^{1.2}} + \frac{3.475}{(.45)^{.75}}\left[1.960 + 0.815(.45) - 1.628(.45)\log_{10}\left(3 + \frac{1}{(.45)}\right)\right] = 22.75$$

The maximum velocity is found from the definition (Eq. [2.125]) of the turbulent velocity ($u^+ = u/u^*$) as

$$u_{\max} = u^+u^* = (22.64).0846 = 1.92 \text{ m/s}$$

Chapter 3. Rotational Viscometry

3.1. Introduction

Traditional rotational viscometers include cone and plate, parallel plate, and concentric cylinder units operated under steady shear conditions Fig. 1.1). They may also be capable of operating in an oscillatory mode which will be considered in the discussion of viscoelasticity, Chapter 5. Cone and plate systems are sometimes capable of determining normal stress differences. Concentric cylinder systems have been used in research to evaluate these differences (Padden and DeWitt, 1954); however, commercial instruments of this type are not available. Mixer viscometry, a "less traditional" method in rotational viscometry, is also presented because it has excellent utility in solving many rheological problems found in the food industry.

3.2. Concentric Cylinder Viscometry

3.2.1. Derivation of the Basic Equation

The concentric cylinder viscometer is a very common instrument that will operate in a moderate shear rate range making it a good choice for collecting data used in many engineering calculations. A number of assumptions are made in developing the mathematical relationships describing instrument performance: flow is laminar and steady, end effects are negligible, test fluid is incompressible, properties are not a function of pressure, temperature is constant, there is no slip at the walls of the instrument, and radial and axial velocity components are zero. The derivation presented here is based on a physical setup known as the Searle system where the bob rotates and the cup is stationary: It is also applicable to a Couette-type system in which the cup rotates and the bob is stationary. Most concentric cylinder viscometers are Searle-type systems. Unfortunately, it is not uncommon for the word "Couette" to be used in referring to any concentric cylinder system.

When the bob rotates at a constant speed and the cup is stationary (Fig. 3.1), the instrument measures the torque (M) required to maintain a constant angular velocity of the bob (Ω). The opposing torque comes from the shear stress exerted on the bob by the fluid. A force balance yields

$$M = 2\pi r h r \sigma = 2\pi h r^2 \sigma \qquad [3.1]$$

where r is any location in the fluid, $R_b \le r \le R_c$. Solving Eq. [3.1] for the shear stress shows that σ decreases in moving from the bob to the cup:

$$\sigma = f(r) = \frac{M}{2\pi h r^2} \qquad [3.2]$$

Utilizing Eq. [3.2], the shear stress at the bob ($r = R_b$) can be defined as

$$\sigma_b = \frac{M}{2\pi h R_b^2} \qquad [3.3]$$

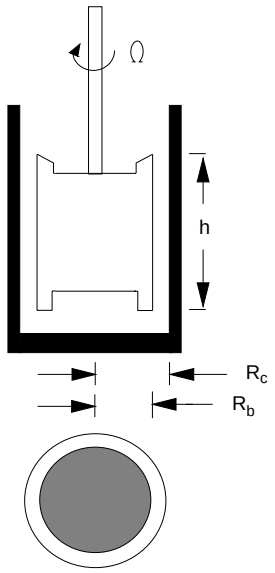

Figure 3.1. Typical concentric cylinder testing apparatus (based in DIN 53018) showing a bob with recessed top and bottom to minimize end effects.

To determine shear rate, consider the linear velocity at r in terms of the angular velocity (ω) at r:

$$u = r\omega \qquad [3.4]$$

The derivative of the velocity with respect to the radius is

$$\frac{du}{dr} = \frac{r\, d\omega}{dr} + \omega \qquad [3.5]$$

Since ω is related to the rotation of the entire body, it does not relate to internal shearing; therefore, Eq. [3.5] can be written as

$$\frac{du}{dr} = \frac{r\,d\omega}{dr} \qquad [3.6]$$

Using the definition of shear rate developed in Eq. [2.9], $\dot{\gamma}$ may be defined in terms of ω:

$$\dot{\gamma} = -\frac{du}{dr} = -\frac{r\,d\omega}{dr} \qquad [3.7]$$

To relate angular velocity to shear stress, note that torque is constant with steady flow so an expression for r may be determined from Eq. [3.2]:

$$r = \left(\frac{M}{2\pi h\sigma}\right)^{1/2} = \left(\frac{M}{2\pi h}\right)^{1/2}(\sigma)^{-1/2} \qquad [3.8]$$

Differentiating Eq. [3.8] with respect to the shear stress yields

$$\frac{dr}{d\sigma} = \left(\frac{M}{2\pi h}\right)^{1/2}\left(-\frac{1}{2}\right)(\sigma)^{-3/2} \qquad [3.9]$$

Substituting the value of torque defined by Eq. [3.1] into Eq. [3.9] gives

$$\frac{dr}{d\sigma} = \left(\frac{2\pi h r^2\sigma}{2\pi h}\right)^{1/2}\left(-\frac{1}{2}\right)(\sigma)^{-3/2} = \frac{-r}{2\sigma} \qquad [3.10]$$

or, with simplification,

$$\frac{dr}{r} = -\frac{d\sigma}{2\sigma} \qquad [3.11]$$

The shear rate is some function of the shear stress, hence,

$$\dot{\gamma} = -r\frac{d\omega}{dr} = f(\sigma) \qquad [3.12]$$

Solving Eq. [3.12] for the differential of the angular velocity yields

$$d\omega = -\frac{dr}{r}f(\sigma) \qquad [3.13]$$

which can be expressed in terms of $d\sigma$ by substituting Eq. [3.11] into Eq. [3.13]:

$$d\omega = \frac{1}{2}f(\sigma)\frac{d\sigma}{\sigma} \qquad [3.14]$$

Integrating Eq. [3.14] over the fluid present in the annulus results in a general expression for the angular velocity of the bob (Ω) as a function of the shear stress in the gap:

$$\int_{\omega=\Omega}^{\omega=0} d\omega = \frac{1}{2}\int_{\sigma_b}^{\sigma_c} f(\sigma)\frac{d\sigma}{\sigma} \qquad [3.15]$$

Note that the limits of integration are an expression of the no slip boundary condition assumed in the derivation: Angular velocity is zero at the cup (the stationary surface), and equal to Ω at the bob (the moving surface). The left hand side of Eq. [3.15] is easily integrated resulting in the following equation relating angular velocity to shear stress:

$$\Omega = -\frac{1}{2}\int_{\sigma_b}^{\sigma_c} f(\sigma)\frac{d\sigma}{\sigma} \qquad [3.16]$$

The solution of Eq. [3.16] depends on $f(\sigma)$ which is dictated by the behavior of the fluid in question. It can be solved directly if the functional relationship between shear stress and shear rate is known. Eq. [3.15] is used as the starting point in Example Problem 3.8.5 to find the velocity profile of a power law fluid in a concentric cylinder system.

Eq. [3.15] reflects a general solution for concentric cylinder viscometers because the limits of the integral could be easily changed to the case where the bob is stationary and the cup rotates (torque is equal in magnitude, but opposite in sign if measured on the cup) or even a situation where the bob and cup are both rotating. It is important to recognize the fact that Eq. [3.16] is analogous to the general solution (Eq. [2.15]) developed for tube viscometers. Both provide an overall starting point in developing mathematical relationships for specific types of fluids.

Application to Newtonian Fluids. The relationship between shear stress and shear rate for a Newtonian fluid is, by definition,

$$\dot{\gamma} = f(\sigma) = \frac{\sigma}{\mu} \qquad [3.17]$$

Substituting this into the general expression for Ω given by Eq. [3.16] yields

$$\Omega = -\frac{1}{2}\int_{\sigma_b}^{\sigma_c} f(\sigma)\frac{d\sigma}{\sigma} = -\frac{1}{2}\int_{\sigma_b}^{\sigma_c}\left(\frac{\sigma}{\mu}\right)\frac{d\sigma}{\sigma} = -\frac{1}{2\mu}\int_{\sigma_b}^{\sigma_c} d\sigma \qquad [3.18]$$

then,

$$\Omega = \frac{1}{2\mu}(\sigma_b - \sigma_c) \qquad [3.19]$$

Using Eq. [3.2] for shear stress allows Eq. [3.19] to be written in terms of the system geometry and the torque response of the instrument:

$$\Omega = \frac{1}{2\mu}\left[\frac{M}{2\pi h R_b^2} - \frac{M}{2\pi h R_c^2}\right] \qquad [3.20]$$

Rearrangement gives a simplified expression, called the Margules equation, describing the behavior of a Newtonian fluid in a concentric cylinder system:

$$\Omega = \frac{M}{4\pi\mu h}\left[\frac{1}{R_b^2} - \frac{1}{R_c^2}\right] \qquad [3.21]$$

This equation clearly indicates that experimental data for Newtonian fluids will show torque to be directly proportional to bob speed.

Application to Power Law Fluids. With a power law fluid, the relationship between shear stress and shear rate is

$$\dot{\gamma} = f(\sigma) = \left(\frac{\sigma}{K}\right)^{1/n} \qquad [3.22]$$

which can be substituted into Eq. [3.16] yielding

$$\Omega = -\frac{1}{2}\int_{\sigma_b}^{\sigma_c} f(\sigma)\frac{d\sigma}{\sigma} = -\frac{1}{2}\int_{\sigma_b}^{\sigma_c}\left(\frac{\sigma}{K}\right)^{1/n}\frac{d\sigma}{\sigma} \qquad [3.23]$$

or, after integration,

$$\Omega = \frac{n}{2K^{1/n}}[(\sigma_b)^{1/n} - (\sigma_c)^{1/n}] \qquad [3.24]$$

Using Eq. [3.2], an alternative expression for the power law fluid is obtained:

$$\Omega = \frac{n}{2K^{1/n}}\left[\left(\frac{M}{2\pi h R_b^2}\right)^{1/n} - \left(\frac{M}{2\pi h R_c^2}\right)^{1/n}\right] = \frac{n}{2K^{1/n}}\left(\frac{M}{2\pi h R_b^2}\right)^{1/n}\left[1 - \left(\frac{R_b}{R_c}\right)^{2/n}\right] \qquad [3.25]$$

Eq. [3.25] reveals that torque is not directly proportional to bob speed because it is strongly influenced by the flow behavior index.

Application to Bingham Plastic Fluids. A Bingham plastic fluid has the following relationship between shear stress and shear rate:

$$\dot{\gamma} = f(\sigma) = \frac{(\sigma - \sigma_o)}{\mu_{pl}} \qquad [3.26]$$

Substituting Eq. [3.26] into Eq. [3.16] yields

$$\Omega = -\frac{1}{2}\int_{\sigma_b}^{\sigma_c} f(\sigma)\frac{d\sigma}{\sigma} = -\frac{1}{2}\int_{\sigma_b}^{\sigma_c} \frac{(\sigma - \sigma_o)}{\mu_{pl}}\frac{d\sigma}{\sigma} \qquad [3.27]$$

Integration and substitution of Eq. [3.2] provides the general relationship (known as the Reiner-Riwlin equation) between the torque, angular velocity, and system geometry:

$$\Omega = \left[\frac{M}{4\pi h \mu_{pl}}\right]\left[\frac{1}{R_b^2} - \frac{1}{R_c^2}\right] - \frac{\sigma_o}{\mu_{pl}}\ln\left(\frac{R_c}{R_b}\right) \qquad [3.28]$$

This equation is valid only when the yield stress is exceeded at all points in the fluid meaning that the minimum shear stress must greater than the yield stress:

$$\sigma_{\min} = \frac{M_{\min}}{2\pi R_c^2 h} > \sigma_o \qquad [3.29]$$

$M_{\min}$ is the minimum torque required to overcome the yield stress. If evaluating fluid behavior near the limits described by Eq. [3.29], the yield stress should be determined before conducting standard tests in Searle-type concentric cylinder viscometers. This can be accomplished with various techniques, such as the vane method discussed in Sec. 3.7.3, With that data, one can calculate the minimum rotational speed of the bob required to insure shearing throughout the cylindrical gap (see Example Problem 3.8.1). In Couette systems, applying sufficient torque to rotate the cup assures shear flow in the entire annulus because the minimum shear stress occurs at R_c.

3.2.2. Shear Rate Calculations

Numerous methods of estimating shear rates in concentric cylinder viscometers have been proposed (Table 3.1) and many of those techniques are discussed in books by various authors: Whorlow (1992), Van Wazer et al. (1963), and Darby (1976). A few of the more practical approximation techniques are summarized in the current work.

Table 3.1. Some Mathematical Techniques for Analyzing Data from Concentric Cylinder Viscometers

Solution	Source
Shear rate calculation, multiple bobs.	Krieger, I.M. and S.H. Maron (1954)
Mean shear stress, small gaps.	Mooney, M. (1931)
Shear rate at the bob.	Krieger, I.M. and H. Elrod (1953)
Fluids following Ellis equation.	Van Wazer et al. (1963)
Fluids following Herschel-Bulkley equation.	Van Wazer et al. (1963)
Fluids following Eyring equation.	Van Wazer et al. (1963)
Fluids following Casson equation.	Murata, T. and S. Oka (1968)
Fluids following Vocadlo equation.	Parzonka, W. and J. Vocadlo (1968)

The error in using approximations can be calculated by evaluating the exact versus the approximate solution. Accuracy is improved as the approximation becomes more sophisticated. When studying fluid foods, the simple shear, Newtonian or power law approximations are often adequate.

Simple Shear Approximation. With a very narrow annulus ($R_c - R_b \ll R_b$), the curvature of the walls is negligible and the system approaches simple shear. Assuming a uniform shear rate across the gap gives

$$\dot{\gamma}_b = \frac{\Omega R_b}{R_c - R_b} = \frac{\Omega}{\alpha - 1} \qquad [3.30]$$

where $\alpha = R_c/R_b$. When calculating shear rates with Eq. [3.30] a corresponding average shear stress should be used:

$$\sigma_a = \frac{1}{2}(\sigma_c + \sigma_b) = \frac{1}{2}\left[\frac{M}{2\pi h R_c^2} + \frac{M}{2\pi h R_b^2} \right] = \frac{M(1+\alpha^2)}{4\pi h R_c^2} \qquad [3.31]$$

The error involved in using Eq. [3.30] for power law fluids is investigated in Example Problem 3.8.2.

Newtonian Approximation. The shear rate at the bob for a Newtonian fluid is determined from the definition of a Newtonian fluid as

$$\dot{\gamma}_b = (2\Omega)\left(\frac{\alpha^2}{\alpha^2 - 1} \right) \qquad [3.32]$$

Commercial viscometers frequently use this equation to approximate shear rate, often in the form of a representative (average) shear rate. The derivation of Eq. [3.32] is presented in Example Problem 3.8.3 and the representative shear rate concept, developed using this equation, is examined in Example Problem 3.8.4.

Power Law Approximation. Considering the definition of a power law fluid, an equation for the shear rate at the bob can be derived as

$$\dot{\gamma}_b = \left(\frac{2\Omega}{n}\right)\left[\frac{\alpha^{2/n}}{\alpha^{2/n}-1}\right] \qquad [3.33]$$

The complete development of Eq. [3.33] is given in Example Problem 3.8.5.

Using Eq. [3.33] requires a numerical value of the flow behavior index. It may be determined directly by considering the power law equation with Eq. [3.33] used as the expression for shear rate:

$$\sigma_b = K(\dot{\gamma}_b)^n = \Omega^n\left(K^{1/n}\left(\frac{2}{n}\right)\left[\frac{\alpha^{2/n}}{\alpha^{2/n}-1}\right]\right)^n \qquad [3.34]$$

Taking the logarithm of each side, Eq. [3.34] may be written as

$$\ln(\sigma_b) = n\,\ln(\Omega) + n\,\ln\left(\left(K^{1/n}\left(\frac{2}{n}\right)\left[\frac{\alpha^{2/n}}{\alpha^{2/n}-1}\right]\right)\right) \qquad [3.35]$$

which, by evaluating the derivative with respect to $\ln\Omega$, provides a simple expression for the flow behavior index:

$$n = \frac{d(\ln\sigma_b)}{d(\ln\Omega)} \qquad [3.36]$$

Since $\sigma_b = M/(2\pi h R_b^2)$, Eq. [3.36] may also be written as

$$n = \frac{d(\ln M)}{d(\ln\Omega)} \qquad [3.37]$$

Hence, for power law fluids, n is the slope (a straight line) of $\ln(M)$, or $\ln(\sigma_b)$, versus $\ln(\Omega)$. Once n is known, Eq. [3.33] can be easily evaluated.

Krieger Method. The general force balance on the bob gave the relationship between shear stress and shear rate as (Eq. [3.16])

$$\Omega = \frac{1}{2}\int_{\sigma_c}^{\sigma_b} f(\sigma)\frac{d\sigma}{\sigma}$$

Taking the derivative of this expression with respect to the shear stress at the bob yields (Krieger and Maron, 1952)

$$\frac{d\Omega}{d\sigma_b} = \frac{1}{2}\left[\frac{f(\sigma_b)}{\sigma_b} - \left(\frac{f(\sigma_c)}{\sigma_c} \right)\left(\frac{d\sigma_c}{d\sigma_b} \right)\right] \qquad [3.38]$$

From Eq. [3.1]

$$\frac{M}{2\pi h} = \sigma r^2 = \text{ constant} \qquad [3.39]$$

so

$$\sigma_c R_c^2 = \sigma_b R_b^2 \qquad [3.40]$$

and

$$\frac{d\sigma_c}{d\sigma_b} = \left(\frac{R_b}{R_c} \right)^2 = \frac{1}{\alpha^2} \qquad [3.41]$$

Substitution and simplification, using Eq. [3.40] and [3.41], transforms Eq. [3.38] into

$$\frac{d\Omega}{d\sigma_b} = \frac{1}{2\sigma_b}\left(f(\sigma_b) - \frac{f(\sigma_b)}{\alpha^2} \right) \qquad [3.42]$$

A solution (a suitable expression for shear rate at the bob) to equation Eq. [3.42] requires the evaluation of an infinite series. The best solutions are those which involve a series where a good approximation can be obtained by evaluating a small number of terms. An excellent solution to Eq. [3.42], one which truncates an infinite series after the first term, was developed by Krieger (1968) and recommended by Yang and Krieger (1978):

$$\dot{\gamma}_b = f(\sigma_b) = \left(\frac{2\Omega}{s} \right)\left[\frac{\alpha^{2/s}}{\alpha^{2/s} - 1} \right](1 + s^2 s' g) \qquad [3.43]$$

where:

$$1/s = \left(\frac{\sigma_b}{\Omega} \right)\frac{d\Omega}{d\sigma_b} = \frac{d(\ln\Omega)}{d(\ln\sigma_b)} = \frac{d(\ln\Omega)}{d(\ln M)} \qquad [3.44]$$

$$s' = \sigma_b \frac{d(1/s)}{d\sigma_b} = \frac{d(1/s)}{d(\ln\sigma_b)} = \frac{d(1/s)}{d(\ln M)} \qquad [3.45]$$

and

$$g = f(x) = \frac{x(e^x(x-2)+x+2)}{2(e^x-1)^2} \qquad [3.46]$$

with x, the argument of the function given by Eq. [3.46], defined as $2(\ln\alpha)/s$. In concentric cylinder viscometers, α is typically in the range of 1.01 to 1.40 with smaller values being more common. Eq. [3.43] is acceptable over this range of α, most accurate at small values of α, and good in many cases for α values up to 2.0 (Yang and Krieger, 1978).

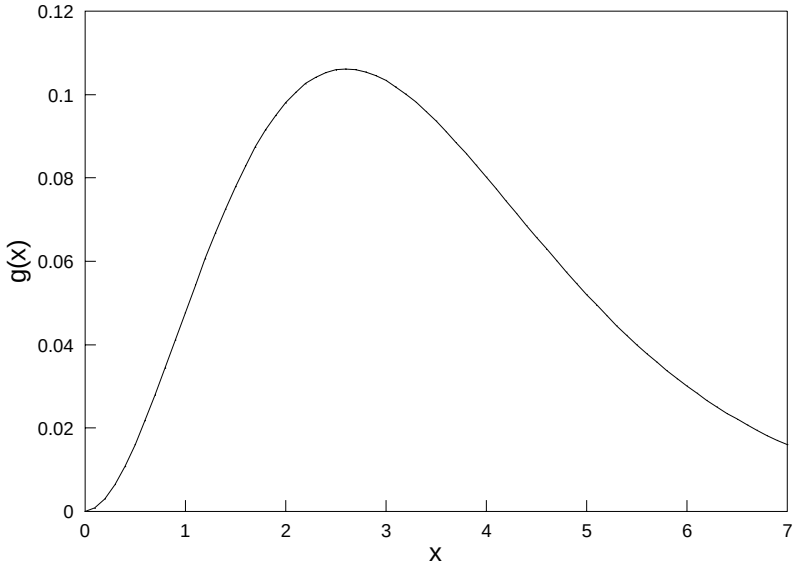

Figure 3.2. Plot of Eq. [3.46], $g(x)$, in Krieger (1968) solution for calculating shear rate at the bob of a concentric cylinder viscometer.

The Krieger solution (Eq. [3.43]) is very close to the power law approximation. In fact, with a power law fluid, $s = n$ and the Krieger equation becomes the power law solution given by Eq. [3.33]. It is also important to note that the maximum value of $g(x)$ is approximately 0.1 (Fig. 3.2) and, when calculating the correction factor in Eq. [3.43], this number is multiplied by other small numbers. Hence, the power law expression for shear rate, with s found at each value of σ_b, is an excellent approximation for the shear rate at the bob:

$$\dot{\gamma}_b = \left(\frac{2\Omega}{s}\right)\left[\frac{\alpha^{2/s}}{\alpha^{2/s}-1}\right] \qquad [3.47]$$

where s is defined by Eq. [3.44].

Other solutions to Eq. [3.42] have been summarized by Yang and Krieger (1978). Darby (1985) has discussed the problem of concentric cylinder viscometer data reduction for materials with a yield stress and found the power law approximation to give acceptable results in the majority of practical situations. Best results, however, are obtained with prior knowledge of the yield stress so complete shearing in the annulus can be assured (Nguyen and Boger, 1987). The utility of various shear rate approximation equations is illustrated in Example Problem 3.8.6. This example also presents the Krieger and Maron (1952) solution to Eq. [3.42] for calculating the shear rate at the bob in a concentric cylinder system.

3.2.3. Finite Bob in an Infinite Cup

When $R_c \gg R_b$, the case of a finite bob in an infinite cup, $1/\alpha$ is very small so Eq. [3.42] becomes

$$\frac{d\Omega}{d\sigma_b} = \frac{f(\sigma_b)}{2\sigma_b} \qquad [3.48]$$

Solving this expression for the shear rate at the bob and multiplying numerator and denominator by Ω, then simplifying, gives

$$f(\sigma_b) = \dot{\gamma}_b = (2\sigma_b)\frac{d\Omega}{d\sigma_b} = \left(\frac{2\Omega\sigma_b}{\Omega}\right)\frac{d\Omega}{d\sigma_b} = (2\Omega)\frac{d(\ln\Omega)}{d(\ln\sigma_b)} \qquad [3.49]$$

Eq. [3.49] provides an easy means of determining the shear rate at the bob in an infinite cup. The solution may be useful in tests involving very large beakers or industrial scale food vats. It is clearly valid for any time-independent material without a yield stress. Remarkably, it is also valid for fluids with a yield stress (the yield stress problem is discussed latter in this section).

Shear rate equations developed for concentric cylinder systems can also be used for the infinite cup case by making the appropriate allowance for geometry. This idea is illustrated for a power law fluid, tomato ketchup, in Example Problem 3.8.7. Errors involved in using the infinite cup approximation depend on geometry as well as fluid

properties (see Example Problem 3.8.8). A general problem illustrating the infinite cup calculation technique is given for salad dressing in Example Problem 3.8.9.

Eq. [3.49] may also be used to calculate an exact solution for the shear rate at the bob in concentric cylinder systems (Nguyen and Boger, 1987) when the fluid in the annulus is only partially sheared, i.e., when Eq. [3.29] is violated and the minimum shear stress is less than the yield stress. In this situation, the yield stress (σ_o) may be substituted for σ_c in Eq. [3.16], then differentiated to yield an expression similar to Eq. [3.38]:

$$\frac{d\Omega}{d\sigma_b} = \frac{1}{2}\left[\frac{f(\sigma_b)}{\sigma_b} - \left(\frac{f(\sigma_o)}{\sigma_o} \right)\left(\frac{d\sigma_o}{d\sigma_b} \right) \right] \qquad [3.50]$$

Since the second term within the brackets is zero, Eq. [3.50] becomes Eq. [3.48] which can be simplified to Eq. [3.49]. Therefore, the solution for a single cylinder rotating in an infinite medium and the solution for the case of a bob rotating in an annulus with partially sheared fluid are identical! This surprising result means that Eq. [3.49] can be used in a vat (or beaker) containing material with a yield stress if the bob is placed sufficiently far into the container so wall effects are not a source of error. The appropriate distance from the wall can be estimated from Eq. [3.2]. This idea is illustrated in Example Problem 3.8.10.

3.3. Cone and Plate Viscometry

Using a cone and plate apparatus (Fig. 3.3), the shear stress versus shear rate curve may usually be obtained directly so the calculations are quite simple. The instrument is a moderate shear rate device which is inappropriate for fluids with large particles because the cone angle (θ) is small, preferably less than 0.09 rad (5 degrees). In operating a cone and plate viscometer, the apex of the cone almost touches the plate and fluid fills the gap. The cone is rotated at a known angular velocity (Ω) and the resulting torque (M) is measured on the fixed plate or through the cone. Some instruments are designed with rotating plates and fixed cones.

Flow in a cone and plate viscometer can be very complex requiring a laborious solution of the fundamental equations of motion (Walters, 1975). However, when using a small cone angle (less than 5 degrees), sufficiently low rotational speeds, and with no errors due to surface

tension effects at the free fluid surface (surface should be spherical in shape with a radius of curvature equal to the cone radius), the shear rate at r may be calculated as

$$\dot{\gamma} = \frac{r\Omega}{r\tan\theta} = \frac{\Omega}{\tan\theta} \qquad [3.51]$$

indicating that the shear rate is constant throughout the gap. This is one of the main advantages of a cone and plate viscometer. With the small angles found in typical fixtures, $\tan\theta = \theta$.

To develop an expression for shear stress, consider the differential torque on an annular ring of thickness dr:

$$dM = (2\pi r\, dr)\sigma r \qquad [3.52]$$

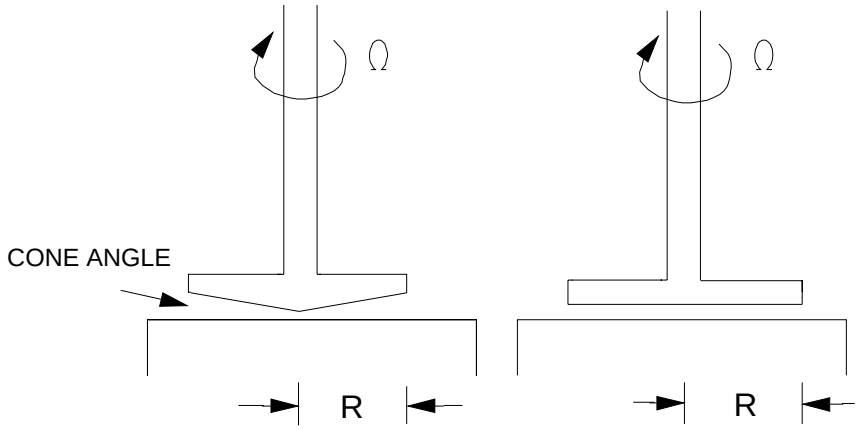

Figure 3.3. Cone and plate (left), and parallel plate (right) sensors.

Eq. [3.52] is integrated over the radius to find the total torque response:

$$\int_0^M dM = \int_0^R (2\pi r^2\sigma)\, dr \qquad [3.53]$$

Since the shear rate is constant in the gap, the shear stress is also constant in that area so $\sigma \neq f(r)$. Then, Eq. [3.53] can be simplified to

$$M = 2\pi\sigma \int_0^R r^2 dr \qquad [3.54]$$

hence,

$$\sigma = \frac{3M}{2\pi R^3} \qquad [3.55]$$

This result shows that σ, like $\dot{\gamma}$, is constant throughout the gap. Using Eq. [3.51] and [3.55], shear rate and shear stress can be easily calculated. By varying the angular velocity, cone angle and cone radius, a wide variety of conditions can be tested. If a specific model is selected, rheological properties can be calculated directly. The following equation, for example, would apply to power law fluids:

$$\frac{3M}{2\pi R^3} = K\left(\frac{\Omega}{\tan\theta}\right)^n \qquad [3.56]$$

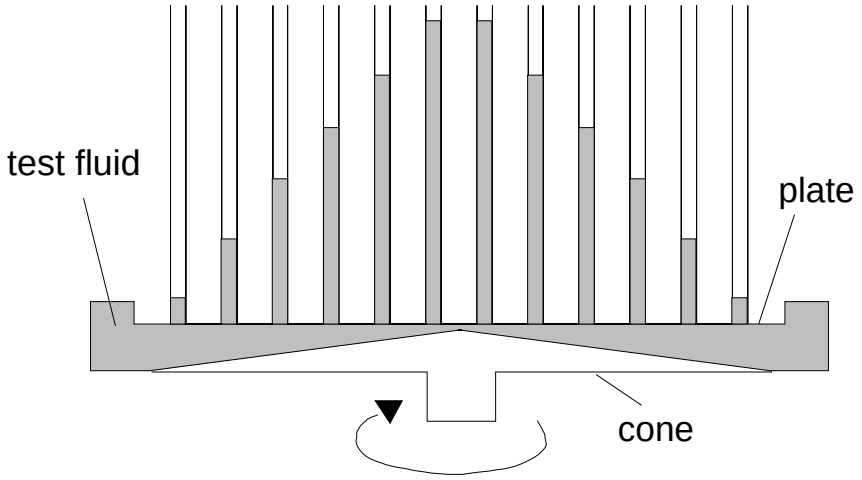

Figure 3.4. Cone and plate system showing pressure distribution on a plate for a viscoelastic fluid.

Fluids which have a significant elastic component will produce a measurable pressure distribution in the direction perpendicular to the shear field (Fig. 3.4). Some cone and plate viscometers allow measurement of the resulting normal (axial direction) force on the cone making it possible to calculate the first normal stress difference, noted in Eq. [1.23], as (Walters, 1995):

$$N_1 = (\sigma_{11} - \sigma_{22}) = \frac{2(F_{\text{normal}})}{\pi R^2} \qquad [3.57]$$

The normal force difference increases with the shear rate for viscoelastic fluids: It is equal to zero for Newtonian fluids. Expected torque response and data analyses for cone and plate systems are investigated in Example Problems 3.8.11 and 3.8.12, respectively.

3.4. Parallel Plate Viscometry (Torsional Flow)

Shear rate in a parallel plate apparatus (Fig. 3.3) is a function of r

$$\dot{\gamma} = f(r) = \frac{\Omega r}{h} \qquad [3.58]$$

so the shear rate at the rim of the plate ($\dot{\gamma}_R$) is

$$\dot{\gamma}_R = \frac{\Omega R}{h} \qquad [3.59]$$

Shear stress must be determined from the torque response of the instrument which is evaluated by constructing a force balance equation on the disk and integrating over the radius. The same procedure was followed in the previous section for the cone and plate viscometer.

With the cone and plate system, the shear stress was constant allowing Eq. [3.53] to be easily evaluated. In a parallel plate system, however, the shear stress is a function of the radius making the integration more complicated. Eq. [3.53] may be written in a simplified form as

$$\int_0^M dM = 2\pi \int_0^R (r^2\sigma)\, dr \qquad [3.60]$$

Using Eq. [3.58], the variable of integration may be changed from r to $\dot{\gamma}$. Making the appropriate substitutions ($r^2 = (\dot{\gamma}h/\Omega)^2$ and $dr = (h/\Omega)d\dot{\gamma}$), and evaluating the integral from 0 to $\dot{\gamma}_R$, yields

$$\int_0^M dM = 2\pi\left(\frac{h}{\Omega}\right)^3 \int_0^{\dot{\gamma}_R} (\dot{\gamma})^2\sigma\, d\dot{\gamma} \qquad [3.61]$$

Dividing each side of Eq. [3.61] by R^3 and simplifying the result gives

$$\frac{M}{2\pi R^3} = \frac{1}{(\dot{\gamma}_R)^3} \int_0^{\dot{\gamma}_R} (\dot{\gamma})^2\sigma\, d\dot{\gamma} \qquad [3.62]$$

or, since $\sigma = f(\dot{\gamma})$,

$$\frac{M}{2\pi R^3}(\dot{\gamma}_R)^3 = \int_0^{\dot{\gamma}_R} (\dot{\gamma})^2 f(\dot{\gamma})\, d\dot{\gamma} \qquad [3.63]$$

Differentiating Eq. [3.63] with respect to $\dot{\gamma}_R$, using Leibnitz' rule (Eq. [2.16] and [2.17]) on the right hand side, gives an independent term for $f(\dot{\gamma}_R)$:

$$(\dot{\gamma}_R)^3 \frac{d(M/(2\pi R^3))}{d\dot{\gamma}_R} + \left(\frac{M}{2\pi R^3}\right) 3(\dot{\gamma}_R)^2 = (\dot{\gamma}_R)^2 f(\dot{\gamma}_R) \qquad [3.64]$$

Simplification of Eq. [3.64] provides an expression for the shear stress at the rim of the plate (σ_R):

$$\sigma_R = f(\dot{\gamma}_R) = \frac{3M}{2\pi R^3} + \dot{\gamma}_R \frac{d(M/(2\pi R^3))}{d\dot{\gamma}_R} \qquad [3.65]$$

or

$$\sigma_R = f(\dot{\gamma}_R) = \frac{M}{2\pi R^3}\left[3 + \frac{d\ln(M)}{d\ln(\dot{\gamma}_R)}\right] \qquad [3.66]$$

where, recall, $\dot{\gamma}_R = \Omega R/h$. This expression is similar in form to the Rabinowitsch-Mooney equation, Eq. [2.20]. Application of Eq. [3.66] is demonstrated for a 3% hydroxypropyl methylcellulose solution in Example Problem 3.8.13.

The relationship between M and Ω can be evaluated directly for particular types of behavior. With a Newtonian fluid

$$\sigma = \mu\dot{\gamma} = \frac{\mu\Omega r}{h} \qquad [3.67]$$

which can be substituted into Eq. [3.60]:

$$\int_0^M dM = 2\pi \int_0^R \frac{r^3 \mu\Omega}{h}\, dr \qquad [3.68]$$

yielding, after integration and simplification,

$$\frac{2M}{\pi R^3} = \mu\frac{\Omega R}{h} \qquad [3.69]$$

When written in this form, it is clear that $\sigma_R = 2M/(\pi R^3)$ for Newtonian fluids. The same procedure can be followed for power law fluids giving

$$\frac{M(3+n)}{2\pi R^3} = K\left(\frac{\Omega R}{h}\right)^n \qquad [3.70]$$

showing that the shear stress at the rim for a power law fluid depends on the numerical value of the flow behavior index:

$$\sigma_R = \frac{M(3+n)}{2\pi R^3} \qquad [3.71]$$

Considering the above relationships, one can see that the derivative term in Eq. [3.66] is equal to one for Newtonian fluids and *n* for power law fluids.

Parallel plate systems, using axial thrust data, can be used to calculate the second normal stress difference (noted in Eq. [1.24]) provided the first normal stress difference has been determined from cone and plate measurements (Walters, 1975):

$$N_1 - N_2 = \left(\frac{2F_{\text{normal}}}{\pi R^2}\right)\left[1 + \left(\frac{1}{2}\right)\frac{d(\ln F_{\text{normal}})}{d(\ln \dot{\gamma}_R)}\right] \qquad [3.72]$$

If N_1 is known, this equation can be used to determine N_2. However, since N_2 is very small compared to N_1, it is often reasonable to assume that the normal stress determined from parallel plate data is a good approximation of N_1.

3.5. Corrections: Concentric Cylinder

End Correction. It is important to account for the influence of the bottom of the cylinder on the torque response of the system. This surface is in contact with the fluid but not taken into account in the force balance given by Eq. [3.1].

To determine the end correction, torque (or instrument scale division) is measured at a fixed rate of rotation when the annulus is filled to various heights (Fig. 3.5). Resulting data are plotted (Fig. 3.6) as torque versus the height of fluid in contact with the immersed length of the bob. The curve should be linear with the slope equal to the torque required to maintain the fixed rate of rotation per unit length of cylinder. Effective height (h_o) is determined from the intercept by extrapolating to a value of zero torque (Fig. 3.6). This technique is illustrated in Example Problem 3.8.14 for the tapered bob of a Hercules high-shear viscometer.

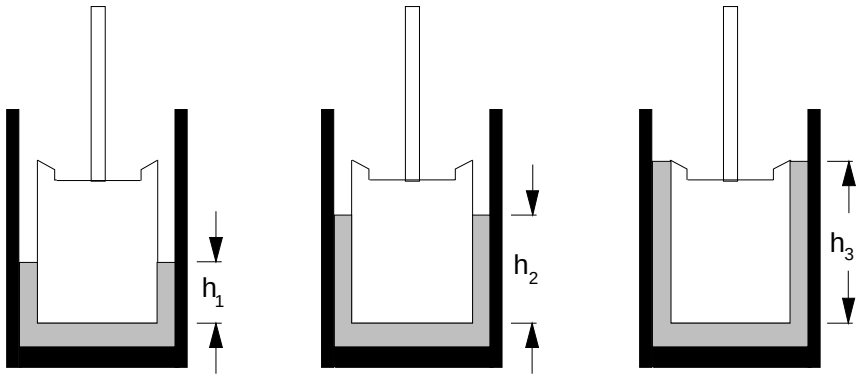

Figure 3.5. Illustration of h values used in determining end correction.

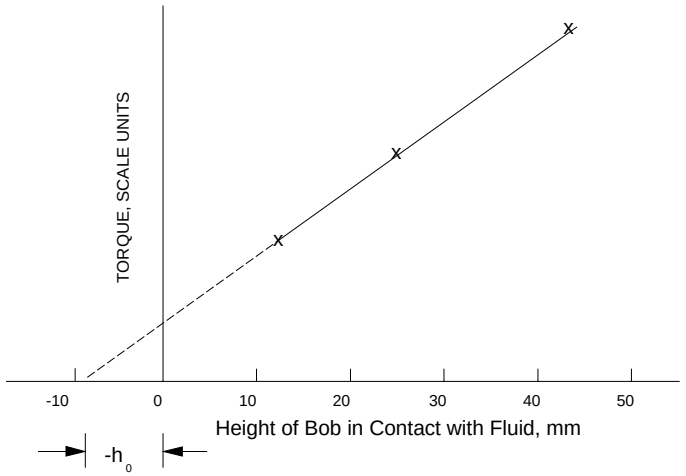

Figure 3.6. End correction for a concentric cylinder system using a graphical technique to determine h_o.

Effective height values are used in the previous equations developed for concentric cylinder systems. The Margules equation (Eq. [3.21]), for example, would be expressed as

$$\Omega = \frac{M}{4\pi\mu(h+h_o)}\left[\frac{1}{R_b^2}-\frac{1}{R_c^2}\right] \qquad [3.73]$$

The value of h given in Eq. [3.1] is replaced by $h+h_o$ which, together, may be thought of as the effective height of the bob. An end correction calculated for a particular bob with a standard Newtonian fluid provides a general approximation for h_o To obtain maximum accuracy, the end correction should be evaluated for each fluid and rotational speed under consideration. This procedure, however, is very laborious and not considered standard practice.

The end correction can also be evaluated in terms of an equivalent torque (M_e) generated by a fluid in contact with the bottom of the sensor. This idea is illustrated for three different speeds in Fig. 3.7. M_e can be plotted as a function of Ω to determine the relationship between the two parameters. The torque correction is subtracted from the measured torque in calculating the shear stress at the bob:

$$\sigma_b = \frac{M-M_e}{2\pi h R_b^2} \qquad [3.74]$$

Correcting for end effects with M_e or h_o should yield identical results.

Various bob designs have been developed to minimize end effects. Bobs can be made with a reservoir at the top and a recessed bottom. This bob design, shown in Fig. 3.1, is based on a German standard (DIN 53018) developed by the German Institute for Standardization (Deutsches Institut für Normung). End effect problems can also be reduced by designing the bottom with a slight angle (called a Mooney-Couette bob, Fig. 3.8) in an effort to make the shear rate at the bottom equivalent to the shear rate in the annulus. The proper angle (θ) can be calculated by equating the annular shear rate to the shear rate in the gap (see Example Problem 3.8.15). Problems with large particulates and sensor alignment limit the usefulness of Mooney-Couette systems. Other methods, such as using a mercury interface at the bottom of the bob (Princen, 1986), have also been proposed.

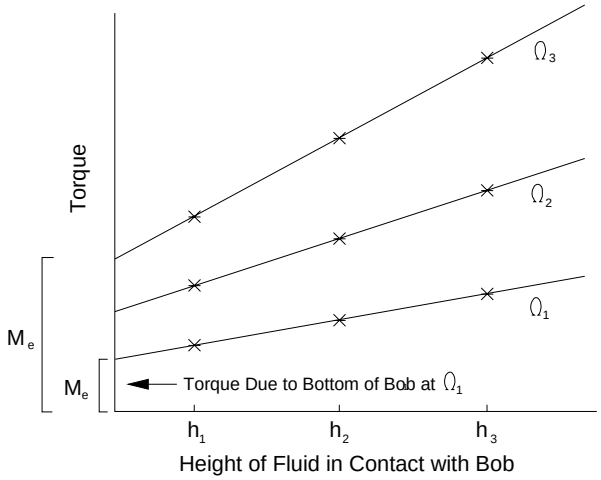

Figure 3.7. End correction for a concentric cylinder system using a graphical technique to determine a torque correction at different speeds.

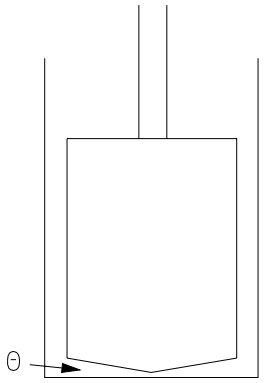

Figure 3.8. Mooney-Couette bob design.

Viscous Heating. Temperature increase in a fluid during rheological testing can be caused by the viscous generation of heat. It may be a serious problem in some experiments because rheological properties are strongly influenced by temperature. The purpose of this section is to provide a means of determining if a significant temperature increase

may occur during testing. If the problem is serious (it will always exist) appropriate action must be taken. Most viscometers are designed with effective temperature control systems that minimize viscous heating problems by rapidly removing the excess heat generated during testing.

To address viscous heating, the case of uniform shearing between parallel plates (Fig. 1.9) may be considered (Dealy, 1982). A concentric cylinder system can be approximated using this idea when the gap is narrow ($R_c - R_b \ll R_b$). This is a one dimensional problem where it is assumed that plates are separated by a distance s, with $x_2 = 0$ at the bottom plate and $x_2 = s$ at the top plate. Also, assume the fluid is Newtonian with a viscosity that does not vary with temperature. In this case the differential equation relating temperature and location, under steady state conditions, is

$$k\frac{d^2T}{dx_2^2} = -\mu(\dot{\gamma})^2 \qquad [3.75]$$

where k is the fluid thermal conductivity. $\mu(\dot{\gamma})^2$ is the viscous energy generated per unit time per unit volume expressed in units of J s^{-1} m^{-3}. Shear rate is considered to be uniform throughout the gap. The solution to Eq. [3.75] is

$$T = f(x_2) = -\frac{\mu(\dot{\gamma})^2}{2k}x_2^2 + C_1x_2 + C_2 \qquad [3.76]$$

where C_1 and C_2 are constants which depend on the boundary conditions of the problem being considered. Solutions for two different cases follow. The various scenarios should be visualized in terms of the propensity of heat to move through the cup and (or) the bob surfaces during shearing.

<u>Both surfaces are maintained at the same temperature</u> (T_o). In this situation the boundary conditions are $T = T_o$ at $x_2 = 0$, and $T = T_o$ at $x_2 = s$, which allow the constants in Eq. [3.76] to be determined: $C_2 = T_o$, $C_1 = \mu(\dot{\gamma})^2 s/(2k)$. Substituting these values back into Eq. [3.76] allows the temperature to be expressed as a function of position between the plates:

$$T = f(x_2) = T_o + \frac{\mu(\dot{\gamma})^2 x_2}{2k}(s - x_2) \qquad [3.77]$$

meaning temperature distribution is parabolic and the maximum temperature occurs at the midplane:

$$T_{\max} = f(s/2) = T_o + \frac{\mu(\dot{\gamma})^2 s^2}{8k} \qquad [3.78]$$

Hence, the temperature rise in the gap is equal to $\mu(\dot{\gamma})^2 s^2/(8k)$ indicating that minimizing the size of the gap $(R_c - R_b)$, analogous to having a smaller value of s, is beneficial in reducing viscous heating problems.

One surface is adiabatic and the other surface is maintained at T_o. In this case the boundary conditions are $T = T_o$ at $x_2 = 0$ and $dT/dx_2 = 0$ at $x_2 = s$ allowing determination of the constants: $C_2 = T_o$ and $C_1 = \mu(\dot{\gamma})^2 s/k$. Substitution of these values into Eq. [3.76] yields the temperature distribution function:

$$T = f(x_2) = T_o + \frac{\mu(\dot{\gamma})^2 x_2}{2k}(2s - x_2) \qquad [3.79]$$

The distribution is parabolic with the maximum temperature occurring at the adiabatic surface where $x_2 = s$:

$$T = f(s) = T_{\max} = T_o + \frac{\mu(\dot{\gamma})^2 s^2}{2k} \qquad [3.80]$$

Comparing this result to the case where both surfaces are maintained at T_o indicates the temperature variation in a sample may be four times greater when one surface is considered adiabatic. Eq. [3.80] has been applied to tomato ketchup in Example Problem 3.8.16.

Effect of temperature variation on viscosity. Problems associated with viscous heating will depend on the extent to which rheological properties are sensitive to temperature. Dealy (1982) gave an example in which viscosity was expressed as an exponential function of temperature:

$$\mu = f(T) = \mu_o\, e^{(-b(T - T_o)/T_o)} \qquad [3.81]$$

or

$$\ln\left(\frac{\mu_o}{\mu}\right) = b\left(\frac{T - T_o}{T_o}\right) \qquad [3.82]$$

where μ_o is the viscosity at T_o and b is a constant, numerically dependent on the fluid in question. Assuming T_o is the wall temperature, the ratio of the maximum to the minimum viscosity is

$$\ln\left(\frac{\mu_{max}}{\mu_{min}}\right) = b\left(\frac{T_{max} - T_o}{T_o}\right) \qquad [3.83]$$

Considering the case when both walls are maintained at T_o , Eq. [3.78] can be substituted into Eq. [3.83] yielding:

$$\ln\left(\frac{\mu_{max}}{\mu_{min}}\right) = b\left(\frac{T_o + \mu(\dot{\gamma})^2 s^2/(8k) - T_o}{T_o}\right) = \frac{b\mu(\dot{\gamma})^2 s^2}{8kT_o} \qquad [3.84]$$

Meaning, for example, if the variation in viscosity during testing is to be less than 10%, then

$$8(\ln(1.10)) = .76 \qquad [3.85]$$

making it necessary to maintain the following inequality:

$$\frac{b\mu(\dot{\gamma})^2 s^2}{kT_o} < .76 \qquad [3.86]$$

In the situation where one wall is maintained at T_o and the other wall is adiabatic, the viscosity ratio may be evaluated by combining Eq. [3.83] and [3.80]:

$$\ln\left(\frac{\mu_{max}}{\mu_{min}}\right) = \frac{b\mu(\dot{\gamma})^2 s^2}{2kT_o} \qquad [3.87]$$

To maintain a viscosity variation of less than 10%

$$\frac{b\mu(\dot{\gamma})^2 s^2}{kT_o} < 2(\ln(1.10)) = .19 \qquad [3.88]$$

Although the above calculations are not quantitatively exact for non-Newtonian fluids, they do illustrate the relative importance of different experimental variables. Analytical solutions for power law fluids in couette flow -where the consistency coefficient is expressed as a power series of temperature and the flow behavior index is assumed to be independent of temperature- are cumbersome, but available (Middleman, 1968).

Wall Effects (Slip). Wall effects due to separation in multiphase materials may cause errors in concentric cylinder systems similar to those discussed for tube viscometers in Sec. 2.5. Oldroyd (1956) suggested that slip may be considered in terms of the general expression for angular velocity (Eq. [3.16]) by adding a slip velocity (u_s) that is a function of wall shear stress at the bob and the cup:

$$\Omega = -\frac{1}{2}\int_{\sigma_b}^{\sigma_c} f(\sigma)\frac{d\sigma}{\sigma} \quad + \frac{(u_s)_{bob}}{R_b} + \frac{(u_s)_{cup}}{R_c} \qquad [3.89]$$

In the absence of slip, the slip velocity is zero and this equation reduces to Eq. [3.16]. Using the method of Mooney (1931), it is possible to correct for slip in concentric cylinder viscometers. The method requires numerous bobs because measurements are required at different values of R_c/R_b.

A simple slip evaluation method, requiring two series of measurements in two different measuring sets, that have different gap widths, has also been suggested (Kiljanski, 1989). Cheng and Parker (1976) presented a method of determining wall-slip based on the use of a smooth and a rough bob. They also urged caution in investigating slip because fluids exhibiting that phenomenon may have accompanying particulate behavior which may mask slip and complicate data treatment. A related procedure was proposed by Yoshimura and Prud'homme (1988). If slip is a serious problem, mixer viscometry should be evaluated as an alternate experimental method.

The Mooney technique was used by Qiu and Rao (1989) to evaluate slip in apple sauce, a typical food dispersion of solid particles in a liquid. This work represents one of the few thorough studies dealing with slip in a food product. The investigators found that the wall slip correction did not significantly influence the flow behavior index (the average value for applesauce was 0.253), but increased the consistency coefficient: An average consistency coefficient equal to 37.53 Pa s^n was found for typical applesauce and the slip correction caused this value to increase by an average of 5% to a value of 39.40 Pa s^n. Qui and Rao (1989) also made a very interesting observation when they said "Due to the fortuitous opposite effects of correction for non-Newtonian behavior (it increases the magnitudes of shear rates) and correction for slip effects (it decreases the magnitudes of shear rates), it appears that for food suspensions Newtonian shear rates uncorrected for slip may be closer to the shear

rates corrected for both non-Newtonian behavior and for wall slip." They cautioned that this conjecture should be verified before applying it to any particular product.

Secondary Flow. Equations developed for the analysis of rheological data assume that the streamlines are circular, i.e., flow is laminar. When an inner cylinder rotates in a concentric cylinder system, the fluid near the inner surface tries to move outward due to centrifugal forces. This movement may create non-streamline flow due to the presence of "Taylor vortices" (G.I. Taylor (1923. Phil. Trans. Roy. Soc. (London), Ser. A 223: 289). Such vortices may occur for Newtonian fluids when (Whorlow, 1992)

$$\frac{\Omega R_b(R_c - R_b)\rho}{\mu} > 41.3\sqrt{\frac{R_c}{R_c - R_b}} \qquad [3.90]$$

In a Couette type system where the outer surface (the cup) is rotated, the inertial forces have a stabilizing effect and flow is laminar at much higher shear rates. Consult Larson (1992) for a detailed analysis of flow instabilities in concentric cylinder systems. Application of Eq. [3.90] is presented in Example Problem 3.8.6 and 3.8.17.

Cavitation. The formation and collapse of vapor cavities, known as cavitation, may occur in a high shear environment when the radial pressure drop is sufficient to cause partial vaporization of the sample. By considering the Bernoulli equation in terms of the mechanical energy balance (Eq. [2.105]), one finds (Sakiadis, 1984) that cavitation will occur when $u > \sqrt{2(P_{atm} - P_{vap})/\rho}$ where u is the linear velocity of the bob or cup, whichever is greater. The left hand side of the equation (u) is related to the pressure drop (δP) across the gap: $u = (2\delta P/\rho)^{1/2}$. If present, cavitation may cause erroneous torque responses in a concentric cylinder viscometer. Cavitation is not a significant problem in food rheology because it is usually not present when laminar flow conditions are maintained. The cavitation problem is examined in Example Problem 3.8.17.

3.6. Corrections: Cone and Plate, and Parallel Plate

Sources of error in cone and plate, and parallel plate systems are similar and include the following (Dealy, 1982): viscous heating, secondary flow, shear rate nonuniformity due to large angles, edge effects, and non-ideal geometry (also a problem in concentric cylinder systems).

It is difficult, however, to numerically quantify these problems. Deviation from ideal geometry, involving eccentricity or incorrect angles, may be monitored by visual inspection. The temperature increase in cone and plate systems can be estimated in terms of the Brinkman number (Powell, 1988) defined as the rate of heat generated by viscous dissipation divided by the rate of heat conduction to the surface of the fluid containment system. Viscous heating is rarely a problem when testing biological materials in cone and plate, or parallel plate, systems.

Edge Effects. One type of edge effect, sample skin formation from dehydration, can be minimized by applying a thin coating of oil on the outer surface of the sample. Some rheometers come equipped with a solvent trap to reduce loss of volatiles and subsequent edge effects. A second edge effect, known as edge failure, may be observed with thick foods. Even at rather low shear rates, the sample may appear to be recessed at the center but flowing out on the top and bottom surfaces of the material. Typically, a sharp drop in torque is observed at the onset of edge failure. This problem may be the governing factor in establishing maximum shear rates in cone and plate, and parallel plate testing.

Slip. Slip correction methodology for parallel plate systems, based on a comparison of shear stress versus shear rate at different gap settings, has been presented by Yoshimura and Prud'homme (1988). This analysis is similar to that presented in Sec. 2.5 for evaluating a slip correction factor for capillary viscometers. In the absence of slip, plots of torque (M) versus the apparent shear rate at the rim ($\Omega R/h$), determined using a single plate (constant radius) but different gap heights, will yield identical curves. This fact is very useful in checking for slip because data sets can be collected, on the same sample, by running rate sweeps at successively smaller values of h.

Truncated Cones. Errors associated with truncated cones (Fig. 3.9) may be investigated as a deviation from ideal geometry. Fortunately, the maximum error introduced by the truncation can be easily estimated. Torque in the conical section is calculated from Eq. [3.54] using R_T, the radius of the truncated portion, as the lower limit of the integral:

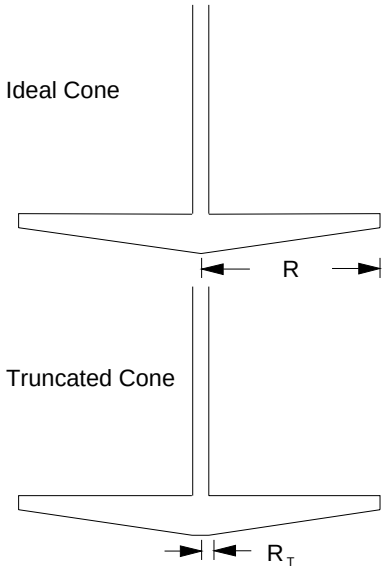

Figure 3.9. Ideal and truncated cone design.

$$M = 2\pi\sigma \int_{R_T}^{R} r^2 dr = (2/3)\pi(R^3 - R_T^3)\sigma \qquad [3.91]$$

The percent maximum error in torque in the conical section is

$$\%\ \text{Max. Error} = \left[1 - \frac{\text{approximate torque}}{\text{ideal torque}}\right]100 \qquad [3.92]$$

After substituting the appropriate expressions, Eq. [3.55] for the ideal torque and Eq. [3.91] for the approximate torque, Eq. [3.92] becomes

$$\%\ \text{Max. Error} = \left[1 - \frac{(2/3)\pi(R^3 - R_T^3)\sigma}{(2/3)\pi(R^3)\sigma}\right]100 \qquad [3.93]$$

or, with simplification,

$$\%\ \text{Max. Error} = \left[1 - \frac{R^3 - R_T^3}{R^3}\right]100 \qquad [3.94]$$

Using Eq. [3.94], the maximum error can be calculated. If, for example, R_T is $0.1R$ or $0.2R$, then the percent maximum error is 0.1 and 0.8, respectively. In actual operation, the true error is less than the predicted value because the truncated section of the cone also contributes some torque during measurement.

3.7. Mixer Viscometry

Extensive work has been conducted on mixer viscometry (Castell-Perez and Steffe, 1992). The technique has been used mostly for non-reacting biological materials but also applied in evaluating the workability of fresh concrete (Tattersall and Banfill, 1983), and to chemorheological studies involving starch gelatinization (Dolan and Steffe, 1990; Steffe et al., 1989). Mixer viscometry may be useful to the food engineer in evaluating difficult fluids like those exhibiting slip or time-dependent behavior, and those having large particles or particle settling problems. Some concepts, such as the matching viscosity method of determining the mixer viscometer constant, are also useful in developing models to simulate the shear history found in complex food processing equipment such as scrape-surface heat exchangers.

An unusual type of mixer viscometer, known as the helical screw rheometer, was proposed by Kraynik et al. (1984) and successfully used for tomato products (Tamura et al., 1989). The instrument consists of a helical screw in a tight fitting barrel and resembles a single screw extruder with a closed discharge. Screw rotation maintains particle suspension, and rheological properties are correlated to pressure drop over the length of the screw. The helical screw rheometer is not commercially available but has potential for future applications in on-line viscometry.

In past years, significant advances have been made in our understanding of commercial mixing and related processes (Harnby et al., 1985; Holland and Chapman, 1966; Nagata, 1975; Oldshue, 1983; Silvester, 1985; Skelland, 1983; Sweeney, 1978; Ulbrecht and Patterson, 1985; Uhl and Gary, 1986). Original ideas in mixer viscometry came from concepts developed to address industrial problems so a short review of commercial mixing is appropriate before examining mixer viscometry.

Commercial Mixing. The terms mixing, blending and dispersing are sometimes used interchangeably. Mixing can be defined as a unit operation which involves the intermingling of two or more dissimilar

materials to obtain a desired degree of uniformity. It is usually accomplished by mechanical agitation which creates motion in the material being processed.

In mixing, an agitator induces material flow by imparting inertial forces to the fluid which, if not significantly dampened by viscous forces, cause fluid motion at some distance away from the impeller. When materials are so thick that fluid cannot be convected away from the stirrer, mixing is accomplished by the bulk movement of material due to physical displacement by the agitator.

Mixer impellers for low viscosity fluids may be divided into axial and radial flow types. With axial flow impellers, such as the marine type and fixed blade turbines, top-to-bottom motion is promoted by placing blades at an angle of less than 90 degrees with the angle of rotation. Radial flow impellers, including flat and curved blade turbines, have blades which are mounted parallel to the vertical axis of the drive shaft. Anchor type agitators (Fig. 1.26) are commonly used for high viscosity materials. They may have a close-clearance between the impeller and the tank to enhance heat transfer. Extremely high viscosity materials including pastes, dough, and meat emulsions rely on helical ribbons, screws or kneaders for mixing.

Dimensional Analysis. Mixing is a complex process that does not lend itself to rigorous analytical treatment. Studies on the subject, and most practical results, have come from dimensional analysis and similarity theory (Gupta, 1984; Langharr, 1980; Murphy, 1950). The most common technique involves the Buckingham pi theorem discussed below.

If m physical variables influence a process, then the basic equation relating the variables may be written as

$$f_1(x_1, x_2, x_3, x_4, \ldots, x_m) = 0 \qquad [3.95]$$

The Buckingham pi theorem states that a relationship may be found between independent dimensionless groups of variables, called pi groups, which have fewer terms than the basic equations:

$$f_2(\Pi_1, \Pi_2, \Pi_3, \ldots, \Pi_i) = 0 \qquad [3.96]$$

where $i < m$ with i defined as

$$i = m - j \qquad [3.97]$$

The pi groups are

$$\Pi_1 = x_1^{a_1} x_2^{a_2} x_3^{a_3} \ldots x_m^{a_m} \quad [3.98]$$

$$\Pi_2 = x_1^{b_1} x_2^{b_2} x_3^{b_3} \ldots x_m^{b_m} \quad [3.99]$$

$$\Pi_3 = x_1^{c_1} x_2^{c_2} x_3^{c_3} \ldots x_m^{c_m} \quad [3.100]$$

where $a_1 \ldots a_m$, $b_1 \ldots b_m$, and $c_1 \ldots c_m$ are constants determined from the dimensions of the physical variables. In most cases, j is the number of fundamental dimensions (such as length, mass and time) involved in the problem. Eq. [3.96] is determined from experimental data. Reducing the number of variables by dimensional analysis has an obvious advantage of reducing the amount of data required to model mixing systems.

Power Consumption in Fluid Mixing. In fluid mixing, dimensional analysis shows that the power number is a function of many dimensionless variables:

$$N_{Po} = f(N_{Re,I}, N_{Fr}, N_{We}, N_{Wi}, \text{Geometric Dimensionless Numbers}) \quad [3.101]$$

where:

$$N_{Po} = \frac{P}{\rho \Omega^3 d^5} \quad [3.102]$$

$$N_{Re,I} = \frac{\rho \Omega d^2}{\mu} \quad [3.103]$$

$$N_{Fr} = \frac{\Omega^2 d}{g} \quad [3.104]$$

$$N_{We} = \frac{\Omega^2 d^3 \rho}{\sigma_{st}} \quad [3.105]$$

$$N_{Wi} = \left(\frac{\Psi_1}{\eta} \right) \Omega \quad [3.106]$$

The power is equal to the product of torque and angular velocity: $P = M\,\Omega$. η and Ψ_1 are the viscosity function (Eq. [1.22]) and the first normal stress coefficient (Eq. [1.23]), respectively. Numerous geometrical dimensionless numbers may be considered for a typical mixer (Fig. 3.10): d/D, $(Z_1 + Z_2 + h)/d$, Z_1/d, Z_2/d, h/d, W/d, width of baffle divided by the impeller diameter, number of impeller blades, impeller pitch, and number of

baffles. To be consistent with the previous work on rotational viscometry, the angular speed is given in units of rad/s instead of rev/s or revs/min which are frequently used in investigating commercial mixing.

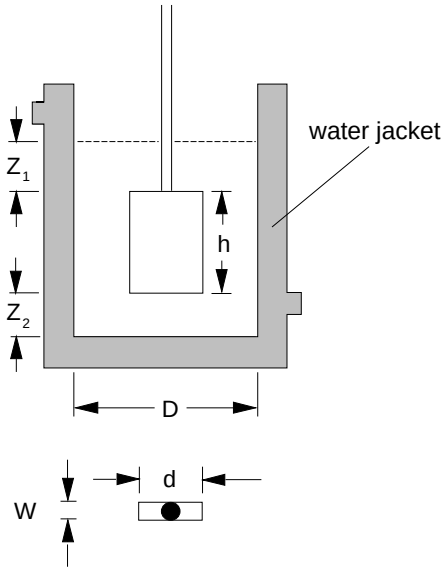

Figure 3.10. Typical mixer viscometer apparatus with paddle type impeller and water jacket for temperature control.

In geometrically similar systems, Eq. [3.101] may be simplified to

$$N_{Po} = f(N_{Re,I}, N_{Fr}, N_{We}, N_{Wi}) \qquad [3.107]$$

where the power number (N_{Po}) represents the ratio of the applied force to the opposing inertial force. The impeller Reynolds number ($N_{Re,I}$) represents the ratio of the inertial to the opposing viscous force in the mixing system and defines laminar, transitional, and turbulent flow in the mixing vessel. It is generally accepted that laminar flow exists for $N_{Re,I} < 63$ and turbulent flow is assured at $N_{Re,I} > 63,000$. [Note: if $N_{Re,I}$ is formulated with speed expressed as rev/s instead of rad/s, laminar and turbulent flows are found at $N_{Re,I} < 10$ and $N_{Re,I} > 10,000$, respectively. Different units, rev/s versus rad/s, cause the numbers to be different by

a factor or 2π.] The transition region is large and depends on the particular system in question. In some cases, turbulent flow may be present with an impeller Reynolds number as low as 1900.

The Froude number (N_{Fr}) reflects the ratio of inertial to gravitational forces and is used to account for the effect of vortexing on the power number. It may be important in unbaffled systems operating at high impeller Reynolds numbers but can be ignored at low speed, and in most baffled systems. The Weber number (N_{We}) represents the ratio of the inertial force to surface tension force. It should be considered in systems where interfacial effects are important such as those found in two phase dispersions. Viscoelastic behavior is characterized by the Weissenberg number (N_{Wi}) defined as the ratio of the primary normal stress coefficient (Eq. [1.23]) times the angular velocity, divided by the apparent viscosity function (Eq. [1.22]). The influence of liquid elasticity on power consumption is not clear but thought to be small (Ulbrecht and Carreau, 1985).

With a single phase fluid operating at low speed, or in a baffled system, the power number can be expressed with the impeller Reynolds number alone:

$$N_{Po} = f(N_{Re,I}) \qquad [3.108]$$

or

$$\frac{P}{\rho\Omega^3 d^5} = f\left(\frac{d^2\Omega\rho}{\mu}\right) \qquad [3.109]$$

The general functional relationship may be stated as

$$\frac{P}{\rho\Omega^3 d^5} = A\left(\frac{d^2\Omega\rho}{\mu}\right)^B \qquad [3.110]$$

where A and B depend on the geometry of the system and the flow regime present during mixing. $B = -1$ when $N_{Re,I} < 63$, and $B = 0$ when $N_{Re,I} > 63,000$. The values of A and B in the intermediate region will depend on the particular mixing system under consideration.

Holland and Chapman (1966) provide power versus Reynolds number solutions for a wide range of mixing systems. Relationships for some standard mixers are provided in Sakiadis (1984). Power curves are independent of scale and depend only on the geometry of the system. When the power curve is available for a particular configuration, it may

be used to calculate the power requirement given various agitator speeds, liquid viscosities, and densities. Other references (Ulbrecht and Carreau, 1985; Nagata, 1975) may also be consulted for power consumption information related to mixing with helical screws, ribbons, and draught tubes.

3.7.1. Mixer Viscometry: Power Law Fluids

Mixer viscometry, typically conducted using flag or pitched paddle impellers (Fig. 3.11), has been used extensively for power law fluids (Castell-Perez and Steffe, 1990; Castell-Perez and Steffe, 1992). Techniques have been developed for estimating power law fluid properties that are useful for quality control and engineering design applications. Shear rate estimation methods have been developed to allow fluid properties to be calculated over an appropriate shear rate range. They are also useful in determining the degree of mixing action present when evaluating process performance characteristics involving particle motion and gas dispersion.

Power Consumption and Average Shear Rate

Mixer viscometry is an important tool for investigating power law fluids. Working equations are developed by first considering a Newtonian fluid in laminar flow ($N_{Re,I} < 63$). When N_{We}, N_{Wi} and N_{Fr} may be neglected (surface tension, elastic, and vortexing effects are insignificant), the power consumption equation (Eq. [3.110]) may be written as

$$N_{Po} = \frac{A}{N_{Re,I}} \qquad [3.111]$$

or, incorporating Eq. [3.102] and [3.103], as

$$\frac{P}{d^5\Omega^3\rho} = \frac{A\mu}{d^2\Omega\rho} \qquad [3.112]$$

Eq. [3.112] may be used for power law fluids ($\sigma = K\dot{\gamma}^n$) if the Newtonian fluid viscosity (μ) is replaced by an apparent viscosity ($\eta = K(\dot{\gamma}_a)^{n-1}$) evaluated at an average shear rate ($\dot{\gamma}_a$) defined as

$$\dot{\gamma}_a = k'\Omega \qquad [3.113]$$

where k' is the mixer viscometer constant having units of 1/rad (units of 1/rev are found in some published works). k' is unique for any particular physical system and must be determined from experimental data.

In mixer viscometry, there are two primary techniques for determining k': the "slope method" and the "viscosity matching method." These methods are presented in the following discussion.

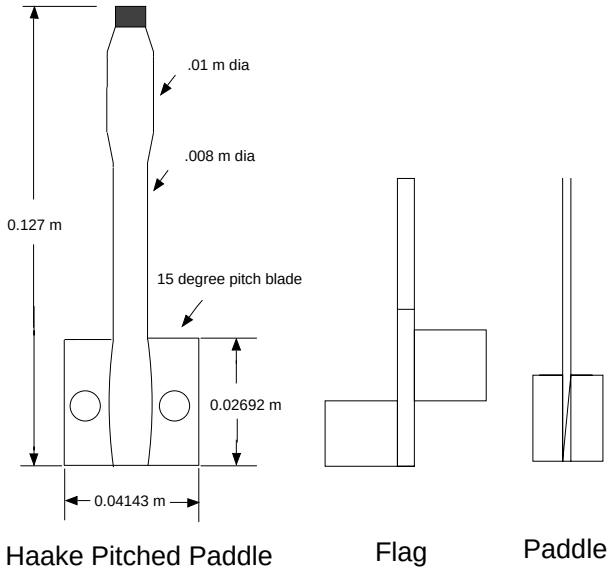

Figure 3.11. Typical impellers used in mixer viscometry.

Evaluation of k'

Slope Method. Substitution of Eq. [3.113], and the power law apparent viscosity for the Newtonian viscosity, into a simplified form of Eq. [3.112] gives

$$\frac{P}{d^3\Omega^2} = A\eta = AK(\dot{\gamma}_a)^{n-1} = AK(k'\Omega)^{n-1} \qquad [3.114]$$

or, after simplifying and taking logarithms,

$$\log_{10}\left(\frac{P}{K\Omega^{n+1}d^3}\right) = \log_{10}(A) - (1-n)\log_{10}(k') \qquad [3.115]$$

Using power law fluids with different known values of K and n, a plot of $\log_{10}(P/[K\Omega^{n+1}(d)^3])$ versus $(1-n)$ is used to determine k' from the slope of the line which is equal to $-\log_{10}(k')$. If the plot is a straight line, then the approximation proposed ($\dot{\gamma}_a = k'\Omega$) in Eq. [3.113] is valid.

One must exercise care in using the slope method for calculating the mixer viscometer constant. Small errors in determining the slope of the line will result in large errors in k' because of the logarithmic relationship between the two numbers. By convention, base 10 logarithms were used in Eq. [3.115]: Identical results would be obtained using base e. Determination of k' using the slope method is illustrated in Example Problem 3.8.18.

Matching Viscosity Method. This technique involves the comparison of power curves for Newtonian and non-Newtonian fluids using the idea of matching viscosities. The phrase "matching viscosities" refers to the assumption that the average shear rate for a non-Newtonian fluid is equal to the average shear rate for a Newtonian fluid when the Newtonian viscosity equals the apparent viscosity of the non-Newtonian fluid. The technique is excellent for determining the average shear rate in a mixer and is also useful to food process engineers in evaluating the performance of commercial equipment (e.g., a scraped-surface heat exchanger) having poorly defined shear fields.

Using Newtonian fluids such as silicone oil or corn syrup in the mixer viscometer, the constant A is determined from the slope of experimental data presented in the form of Eq. [3.111]. With a routine viscometer (like a concentric cylinder or cone and plate system) and traditional rheological techniques, the properties (K and n) of a power law fluid are determined. This "standard" (or reference) power law material is then placed in the mixer viscometer, and mixed at a constant speed. N_{Po} is determined and the resulting "average viscosity" calculated using the power number expression for the Newtonian fluids. This equation, found by combining Eq. [3.111] and [3.103], is

$$\mu = \frac{(d^2\Omega\rho)\,(N_{Po})}{A} \qquad [3.116]$$

Next, the matching viscosity assumption is applied and an average shear rate ($\dot{\gamma}_a$) calculated. First, assume,

$$\mu = \eta = K(\dot{\gamma}_a)^{n-1} \qquad [3.117]$$

then, substitute Eq. [3.117] into Eq. [3.116],

$$K(\dot{\gamma}_a)^{n-1} = \frac{(d^2\Omega\rho)\,(N_{Po})}{A} \qquad [3.118]$$

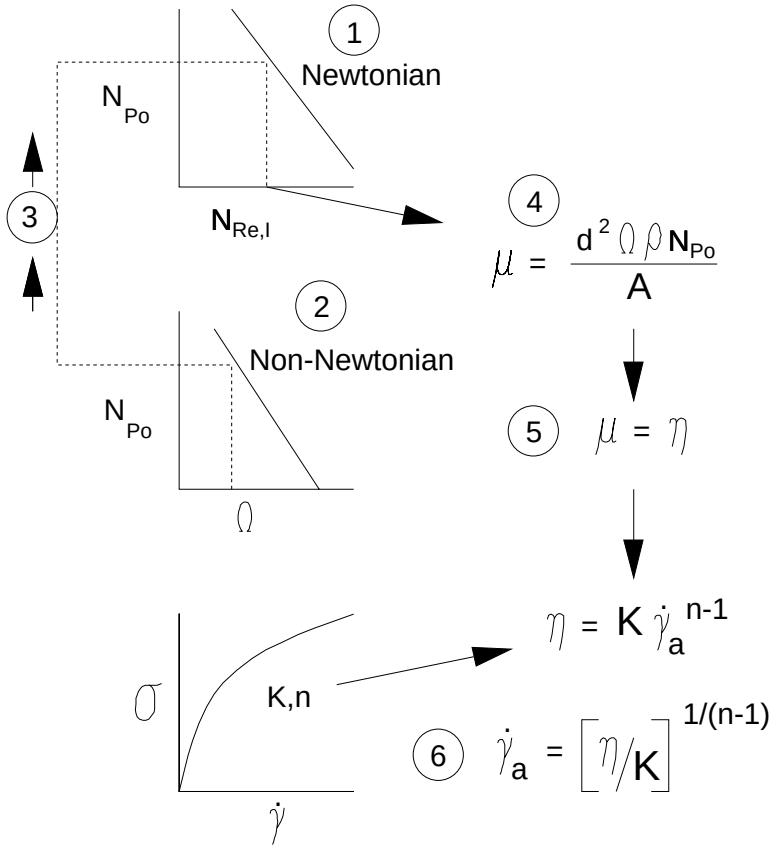

Figure 3.12. Matching viscosity method to calculate average shear rate.

and solve for the average shear rate:

$$\dot{\gamma}_a = \left[\frac{d^2 \Omega \rho (N_{Po})}{KA} \right]^{1/(n-1)} \qquad [3.119]$$

The matching viscosity procedure to evaluate the average shear rate is summarized in Fig. 3.12:

Step 1. Power number relationship is established for Newtonian fluids and the numerical value of *A* is determined using Eq. [3.111];

Step 2. At a steady impeller speed, the power number is measured for a non-Newtonian fluid;

Step 3. Newtonian and non-Newtonian power numbers are set equal and the corresponding impeller Reynolds number, from the Newtonian fluid data, is evaluated;

Step 4. "Viscosity" is calculated from the information generated in Step 3 using Eq. [3.116];

Step 5. Matching viscosity assumption is applied so the Newtonian and apparent viscosities are set equal as indicated in Eq. [3.117];

Step 6. Taking the apparent viscosity and power law fluid parameters, average shear rate is calculated using Eq. [3.119] written in terms of η where $\eta = d^2\Omega\rho N_{Po}/A$.

k' is calculated as $\dot{\gamma}_a/\Omega$. Steps 2-6 should be repeated at numerous impeller speeds to determine how k' may vary with Ω. An average value of k' may be taken to represent the constant required in Eq. [3.113].

Comparison of k' Calculation Methods. There are various advantages and disadvantages to consider before using the slope method (SM) or the matching viscosity method (MVM). SM and MVM both require power law fluid "standards" (reference fluids) to determine k' that, with an appropriate selection of fluids, will cover a suitable range of flow behavior indices. Fewer reference fluids may be needed using the MVM. The main advantage of the SM is the simplicity of the calculations; however, problems with accuracy may occur due to the high sensitivity of k' with the slope of a logarithmic plot. In comparison to SM, the MVM is somewhat laborious due to the larger amount of data handling. Results from the SM and MVM are similar. The effective shear rates of flag and star impellers were evaluated using both methods by Rao and Cooley (1984). Results from that work showed the two methods to be in good agreement. Briggs (1995) reached a similar conclusion working with flag impellers. MVM would be the method of choice for engineers attempting to evaluate average shear rates in complex processing equipment.

k' Values and Variables Influencing k'. Skelland (1983) has summarized values of mixer viscometer constants (k') and power curves for many commercial mixers. Using the average shear rate concept to calculate an apparent viscosity value, Nagata (1975) determined power correlations of Bingham plastic materials for turbine, anchor, and rib-

bon mixers. Bowen (1986) has presented an informative discussion related to the determination of average and maximum shear rates for radial flow turbine mixers. A mixer viscometer constant has been determined for the Brabender Viscograph by Wood and Goff (1973), and for a flag impeller rotated in a number 303 can by Rao (1975).

Using the slope method, Steffe and Ford (1985) found $k' = 4.47$ rad^{-1} for the Haake MV cup and pitched paddle impeller (Fig. 3.11). The pitched paddle impeller can be particularly useful in maintaining particle suspension in samples exhibiting sedimentation problems. Raw data, and analytical procedures for the determination of k', used by Steffe and Ford (1985) are presented in Example Problem 3.8.18.

Castell-Perez and Steffe (1990) studied shear rate evaluation using paddle impellers (Fig. 3.10) for power law fluids. The effects of numerous factors on the determination of k' were considered. Results showed that k' was higher with less shear-thinning fluids, k' increases with a decrease in rotational speed and reaches an almost constant value when operating at speeds greater that 0.33 rev/s (20 rev/min), and k' tends to decrease with an increase in the ratio of the impeller to cup diameter (d/D). The effort resulted in a number of recommendations for practical work in mixer viscometry involving paddle-type impellers: if possible, select a system with a small gap, $d/D > 0.709$; if the system to be used has a large gap, determine the effect of fluid properties on k'; and use a minimum impeller speed of 0.33 rev/s (20 rev/min).

Briggs (1995) found k' values for the flag impeller described in Fig. 3.13. Fluid samples were held in a Brookfield (Brookfield Engineering Laboratories, Stoughton, MA) small sample cup having a height of 6.48 cm, and an inside diameter of 1.90 cm making $d/D = 0.79$. Data were collected over speeds ranging from 0.5 to 100 rev/min (0.5 to 10.5 rad/s). Both the slope and matching viscosity methods were found to produce similar results for shear-thinning fluid foods. The slope analysis produced a constant value of the mixer viscometer constant: $k' = 2.92$ rad^{-1}. This value (and $A = 4.84$) is recommended for routine analysis. The small sample cup and flag impeller provide a simple, yet powerful, tool for the rheological investigation of fluid foods.

Determination of Non-Newtonian Fluid Properties

Evaluating $\log_{10}(M)$ versus $\log_{10}(\Omega)$. The relationship between power and angular velocity for a power law fluid was established in Eq. [3.114]:

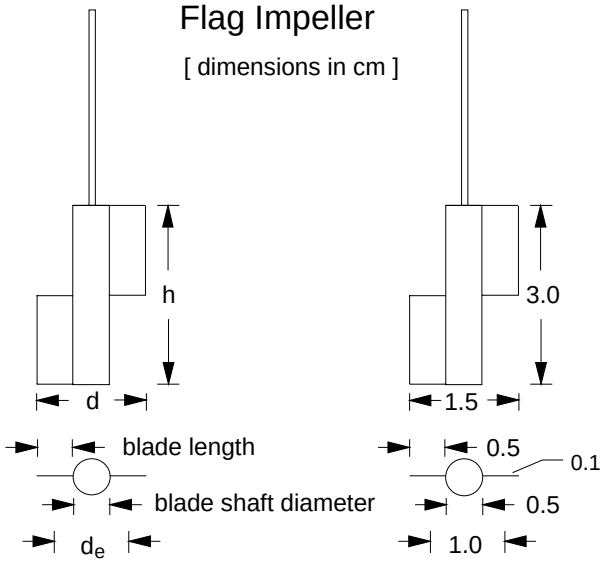

Figure 3.13. Flag impeller used by Castell-Perez et al. (1993) and Briggs (1995).

$$\frac{P}{d^3\Omega^2} = AK(k'\Omega)^{n-1}$$

Substituting $P = M\Omega$, and solving for the torque yields

$$M = d^3AK(k')^{n-1}\Omega^n \qquad [3.120]$$

or, in terms of logarithms,

$$\log_{10}(M) = \log_{10}(d^3AK(k')^{n-1}) + n\log_{10}(\Omega) \qquad [3.121]$$

The flow behavior index can be found as the slope of $\log_{10}(M)$ versus $\log_{10}(\Omega)$. The constant ($\log_{10}(d^3AK(k')^{n-1})$) is not required for the determination of n: It may be used to estimate K, if A and k' are known. The value of K, however, may be found without A by applying Eq. [3.120] to two fluids, one with unknown properties (fluid indicated with subscript x) and a reference fluid with known properties (fluid indicated with subscript y):

$$M_x = d^3AK_x(k')^{n_x-1}\Omega_x^{n_x} \qquad [3.122]$$

and

$$M_y = d^3 A K_y (k')^{n_y - 1} \Omega_y^{n_y} \qquad [3.123]$$

Dividing M_x by M_y, Eq. [3.122] by Eq. [3.123], gives

$$\frac{M_x}{M_y} = \frac{K_x \Omega_x^{n_x} (k')^{n_x}}{K_y \Omega_y^{n_y} (k')^{n_y}} \qquad [3.124]$$

which may be solved for K_x:

$$K_x = K_y \left(\frac{M_x}{M_y} \right) \left(\frac{\Omega_y^{n_y} (k')^{n_y}}{\Omega_x^{n_x} (k')^{n_x}} \right) \qquad [3.125]$$

The properties of the known fluid (K_y and n_y) are determined using conventional rheological methods. n_x is found as the slope of Eq. [3.121] and k' is determined using the slope or matching viscosity method. Under some conditions the calculation of K_x may be greatly simplified: If $\Omega_y = \Omega_x$ and n_y is close to n_x, then K_x is approximately $K_y M_x/M_y$. Mixer viscometry techniques discussed above are used to determine power law fluid properties in Example Problem 3.8.18.

Applying the Matching Viscosity Assumption. Power law fluid properties may also be estimated using the matching viscosity assumption. An average apparent viscosity is calculated using Eq. [3.116] at an average shear rate defined by Eq. [3.113], $\dot{\gamma}_a = k'\Omega$. Then, fluid properties are found by regression analysis of $\eta = K(\dot{\gamma}_a)^{n-1}$ with an appropriate set of experimental data. This technique is illustrated in Example Problem 3.8.18.

One advantage of using the matching viscosity assumption is that it easily allows the investigation of a wide array of non-Newtonian behavior. Although the average shear rate determined using power law fluids can be considered "exact" for these materials, it may also be considered a shear rate approximation for other types of fluids. This is analogous to the way in which Eq. [3.32], the Newtonian approximation, may be used to estimate the shear rate of a non-Newtonian fluid in a concentric cylinder apparatus.

Using the Concentric Cylinder Analogy. Fluid properties may be determined from shear stress and shear rate approximations developed from a concentric cylinder analogy. Mixing systems (identical to the one illustrated in Fig. 3.10) using different cylindrical cups and paddle impellers were considered by Castell-Perez et al. (1991) in developing rheograms for power law fluids. The research assumed that mixers were analogous to concentric cylinder systems. This work showed that the average shear stress and average shear rate could be estimated from geometrical parameters and the flow behavior index using the following equations:

$$\sigma_a = \left[\frac{\pi d^3}{2} \left[\frac{h}{d} + \frac{1}{3} \right] \right]^{-1} M \qquad [3.126]$$

and

$$\dot{\gamma}_a = 2\Omega \left[\frac{(D/d)^{(2-n)/n}}{(D/d)^{2n} - 1} \right] \left(\frac{d}{h} \right)^{n/2} \qquad [3.127]$$

for $d/D \geq 0.709$ and $0.36 < d/h < 1.80$ with $1.0\,cm \geq h \geq 5.0\,cm$ and $0.5 \geq n \geq 0.9$. The flow behavior index is found as the slope of Eq. [3.121].

Castell-Perez et al. (1993) determined shear stress and shear rate estimates for power law fluids using a flag impeller (Fig. 3.13):

$$\sigma_a = \frac{2M}{\pi d_e^2 h} \qquad [3.128]$$

and

$$\dot{\gamma}_a = 2\Omega \left(\frac{D}{d} \right)^{n/2} \qquad [3.129]$$

where d_e, the equivalent diameter, is equal to the length of the impeller blade plus the diameter of the blade shaft. Dimensions of the impeller used in the Castell-Perez et al. (1993) study are given in Fig. 3.13: The equivalent diameter for that geometry is equal to 1.0 cm. Blade thickness was 0.1 cm. Values of d/D were limited to the range of 0.27 to 0.59; however, the influence of diameter was minimal in that range making it acceptable to assume $d/D = 1$ in Eq. [3.129]. With this assumption, it is possible to obtain a reasonable estimate of the average

shear rate without knowing the flow behavior index. The greatest level of accuracy, however, is obtained using the flow behavior index calculated from the relationship given in Eq. [3.121].

3.7.2. Mixer Viscometry: Bingham Plastic Fluids

Power law fluids have been studied extensively using mixer viscometry, but little work has been done with materials exhibiting a yield stress (Castell-Perez and Steffe, 1992). Nagata (1975) investigated power consumption in mixing Bingham plastics and some success has been reported using mixer viscometry methods on fresh concrete showing Bingham plastic behavior (Tattersall and Banfill, 1983).

Determination of Fluid Properties. Using the Newtonian relationship between N_{Po} and $N_{Re,I}$, assuming $\dot{\gamma}_a = k'\Omega$, and using the definition of apparent viscosity for a Bingham plastic fluid ($\eta = \sigma_o/\dot{\gamma} + \mu_{pl}$), yields

$$N_{Po} = \frac{A}{N_{Re,I}} = \frac{A\mu}{d^2\Omega\rho} = \frac{A\eta}{d^2\Omega\rho} = \frac{A(\sigma_o/\dot{\gamma}_a + \mu_{pl})}{d^2\Omega\rho} = \frac{A(\sigma_o/(k'\Omega) + \mu_{pl})}{d^2\Omega\rho} \qquad [3.130]$$

Substituting the definition of N_{Po} (Eq. [3.102]) into Eq. [3.130], recognizing that $P = M\Omega$, then simplifying the resulting equation gives an expression relating torque and speed in a mixer viscometer:

$$\frac{M\Omega}{d^5\Omega^3\rho} = A\left(\frac{\sigma_o}{k'd^2\Omega^2\rho} + \frac{\mu_{pl}}{d^2\Omega\rho}\right) \qquad [3.131]$$

which, after additional manipulation, becomes

$$M = \frac{Ad^3\sigma_o}{k'} + Ad^3\mu_{pl}\Omega \qquad [3.132]$$

Collecting mixer viscometer data of torque versus angular velocity for a Bingham plastic and plotting the result will provide a slope ($Ad^3\mu_{pl}$) and an intercept ($Ad^3\sigma_o/k'$) that reflect the rheological properties of the fluid. If A and k' are known, plastic viscosity and the yield stress can be calculated.

Evaluation of k'. Theoretically, k' can be determined with the same matching viscosity technique discussed for power law fluids. Using the relationship for Newtonian fluids, Eq. [3.111], A is determined from data involving standard Newtonian materials. Taking data with a tradi-

tional instrument, such as a concentric cylinder viscometer, the properties of a "standard" (or reference) Bingham plastic fluid are evaluated. This material is placed in a mixer viscometer and mixed at constant speed (Ω) allowing determination of N_{Po}. Using that information, the "viscosity" is calculated from Eq. [3.116]:

$$\mu = \frac{d^2 \Omega \rho N_{Po}}{A} \qquad [3.133]$$

The matching viscosity assumption ($\mu = \eta$) is applied:

$$\eta = \sigma_o / \dot{\gamma}_a + \mu_{pl} = \frac{d^2 \Omega \rho N_{Po}}{A} \qquad [3.134]$$

and the average shear rate determined:

$$\dot{\gamma}_a = \sigma_o \left(\frac{d^2 \Omega \rho N_{Po}}{A} - \mu_{pl} \right)^{-1} \qquad [3.135]$$

Using Eq. [3.113], k' is found as $\dot{\gamma}_a / \Omega$. If the behavior of different reference fluids is evaluated, the influence of angular velocity and fluid properties on k' can be investigated.

The presence of a yield stress in a mixer means there will be areas in the system where $\sigma < \sigma_o$. This creates plug flow and "dead spots" that may adversely influence results. Work by Nagata et al. (1970) indicates that k' may be a function of the yield stress.

3.7.3. Yield Stress Calculation: Vane Method

Yield stress can be determined using the same basic equipment required in mixer viscometry. In the vane method, the stress to initiate flow from a vane immersed in test material is measured (Nguyen and Boger, 1985). Vane and vessel dimensions (Fig. 3.14) should stay within specified limits (Steffe, 1992): $1.5 \leq h/d \leq 4.0$; $Z_2/d \geq 0.5$; $Z_1 = 0.0$ or $Z_1/d \geq 1.0$ if the vane is completely immersed in the sample; $D/d \geq 2.0$ where D is the diameter of the container if circular, or the minimum crossectional dimension if some other shape is used. Vanes with 4 (Nguyen and Boger, 1985), 6 and 8 blades (Qiu and Rao, 1988) have been used. All produce similar results.

If you assume the test material yields along a cylindrical surface (shaft excluded), then the total torque (M_o) to overcome the yield stress of the fluid is

$$M_o = (\pi d h)\left(\frac{d}{2}\right)\sigma_o + 2\int_0^{d/2} 2\pi r^2 \sigma_e \, dr \qquad [3.136]$$

where σ_e is the shear stress on the end surfaces (top and bottom). Simplification of Eq. [3.136] yields

$$M_o = \frac{\pi h d^2}{2}\sigma_o + 4\pi\int_0^{d/2} r^2 \sigma_e \, dr \qquad [3.137]$$

Assume σ_e varies with the radius according to a power relationship:

$$\sigma_e = f(r) = \left(\frac{2r}{d}\right)^m \sigma_o \qquad [3.138]$$

where *m* is a constant. This assumption is somewhat arbitrary, but reasonable. Substituting Eq. [3.138] into [3.137] yields

$$M_o = \frac{\pi h d^2}{2}\sigma_o + 4\pi\int_0^{d/2} r^2\left(\frac{2r}{d}\right)^m \sigma_o \, dr \qquad [3.139]$$

which, with simplification, gives

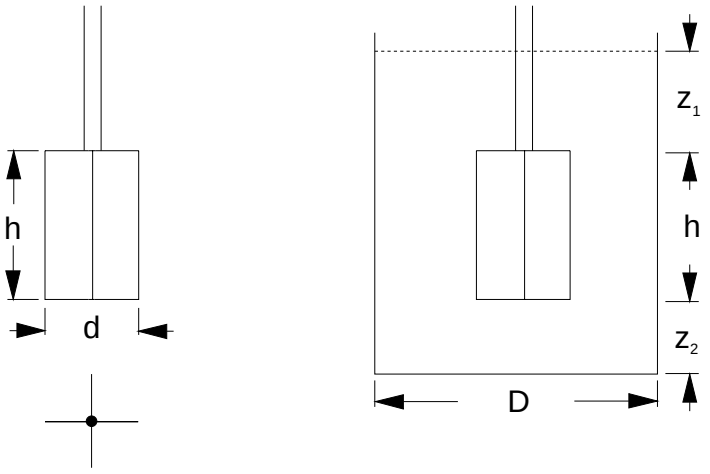

Figure 3.14. Vane, with 4 blades, and vessel for yield stress determination.

$$M_o = \frac{\pi d^3}{2}\left(\frac{h}{d} + \frac{1}{m+3}\right)\sigma_o \qquad [3.140]$$

or, if solved for the yield stress:

$$\sigma_o = \frac{2M_o}{\pi d^3}\left(\frac{h}{d} + \frac{1}{m+3}\right)^{-1} \qquad [3.141]$$

Errors in using Eq. [3.141] for $m > 1$ decrease with larger values of h/d. If $m = 1$, errors less than or equal to 3.7 percent may be obtained when $h/d > 2$ (Steffe, 1992). The assumption that $m = 0$ is usually satisfactory. It is certainly acceptable when making a quality control comparison between products or when simple, quick solutions are needed. To eliminate error due to the upper end effect, the top surface of the vane may be placed even with the fluid ($Z_1 = 0.0$, Fig. 3.14) giving (assuming $m = 0$) the following torque equation at the yield point:

$$M_o = \frac{\pi d^3}{2}\left(\frac{h}{d} + \frac{1}{6}\right)\sigma_o \qquad [3.142]$$

This expression was used by Yoshimura et al. (1987) to evaluate the yield stresses of various non-food emulsions.

Error associated with the stress distribution over the ends can be avoided if Eq. [3.137] is used to determine the yield stress: A plot of M_o versus h is made using data collected from vanes having the same diameter but different lengths. The yield stress is calculated from the slope of the resulting line which is equal to $\pi\sigma_o d^2/2$. This procedure should be used if there is any doubt regarding the validity of the assumption that $m = 0$ or when more precise values of the yield stress are needed.

When measuring the static yield stress (discussed in Sec. 1.6), vanes should be carefully placed in the sample to minimize disruption to surrounding material. In quality control work, it may be possible to use the food container itself as the test vessel to minimize sample disruption. When measuring the dynamic yield stress, sample disruption is not a problem because the weak structure is already destroyed from prior handling operations such as mixing or pumping. This assumption would be invalid if the material was able to rapidly rebuild internal structure. Rapid redevelopment of structure is unusual in food products.

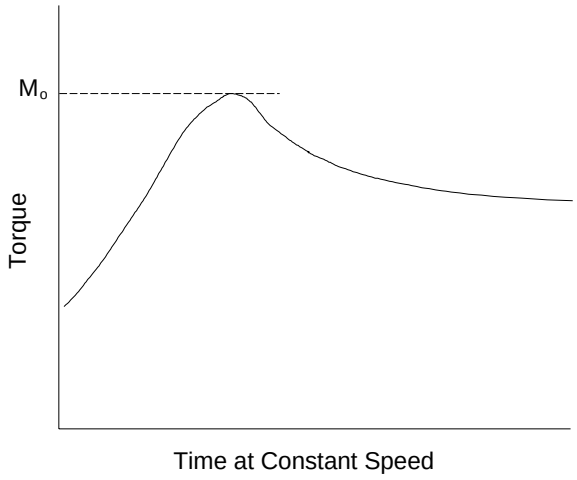

Figure 3.15. Typical torque time response when operating the vane in the controlled rate mode.

Modes of Operation. The vane may be operated in two modes when collecting experimental data: controlled rate or controlled stress. A typical curve for testing in the controlled rate mode (Fig. 3.15) shows a steady increase in torque up to a peak value (M_o) followed by a gradual decline until reaching an equilibrium level. In a sample completely broken down prior to testing, the peak torque would represent the dynamic yield stress. In an undisturbed sample taken from storage, the peak torque would represent the static yield stress; however, in this type of controlled rate test, some weak structural bonds may be disrupted before the peak torque is reached perhaps causing the measured value to be lower than that found in a controlled stress experiment.

In the controlled rate mode, various speeds of operation have been considered. Speeds as low as possible should be used, preferably no higher than 1.0 rpm (Steffe, 1992). Velocities of greater magnitude will alter results for many products. The angle of rotation at which yield occurs, needed to determine the strain at failure, depends on many factors: type of material being tested, size of the vane, angular velocity of the vane, and the wind-up characteristics of the viscometer. Calculating yield stress using the vane method in the controlled rate mode is

investigated in Example Problems 3.8.19 and 3.8.20. Wind-up characteristics of rotational viscometers are discussed latter in this section.

Vanes can also be operated in the controlled stress mode. In experimentation, the torque (or stress) is increased until flow is observed. Data may show the angle of rotation (related to strain) as a function of time with stepped increases in torque. When the yield stress is exceeded, the strain will increase rapidly with time. In a typical plot, the torque at yield (M_o) is between torque levels M4 and M5 (Fig. 3.16).

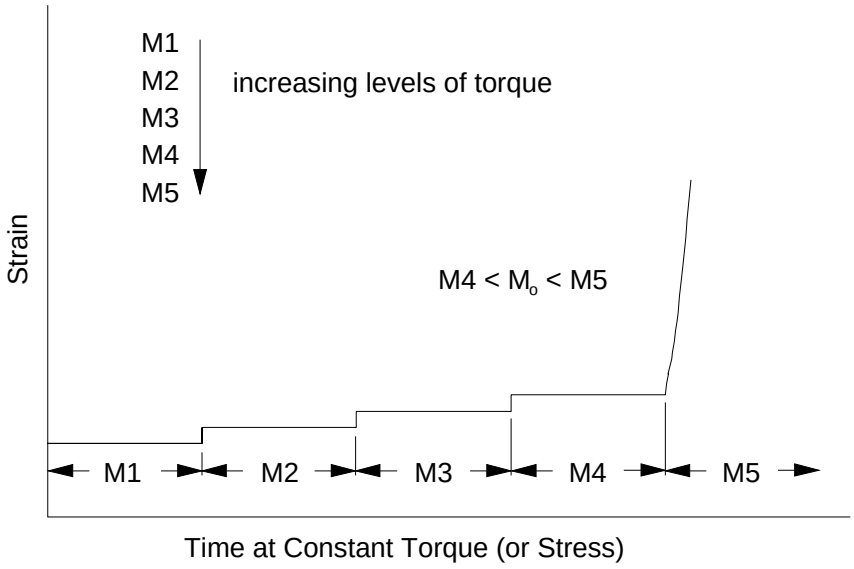

Figure 3.16. Typical response curve when operating the vane in the controlled stress mode.

Testing in the controlled stress mode has the implicit assumption (which is easily tested experimentally) that results are not time-dependent so the amount of time spent at each stress level has no influence on the outcome. Fig. 3.16 shows changes in strain increasing slightly (but remaining constant) with each stepped increase in torque below the failure torque. In a time-dependent material the plot may exhibit a gradual increase in strain, in addition to the step increase, during the holding period at torque levels M1 through M4 (Fig. 3.16).

Controlled stress rheometers may allow the application of a ramped (linear) increase in stress. This will produce a strain response that is unique for the material being tested. Results may be plotted to show changes in strain over time, or the corresponding changes in strain with torque or stress (Fig. 3.17). Behavior is very different depending on whether or not the material is demonstrating solid or fluid-like behavior. There would be a linear relationship between stress and strain with Hookean behavior. When the yield stress is exceeded, the onset of flow causes a dramatic change in strain. If the strain response (Fig. 3.17) is considered in terms of two curves, one for the case where $\sigma \leq \sigma_o$ and the other for $\sigma > \sigma_o$, the point of intersection may be defined as the peak torque (M_o) required in the yield stress calculation. The actual yield stress would be found at the intersection point if stress, instead of torque, is plotted. When a break point is evident, this is a convenient method of determining the yield stress from controlled stress data. Logarithmic plots may be useful in amplifying differences.

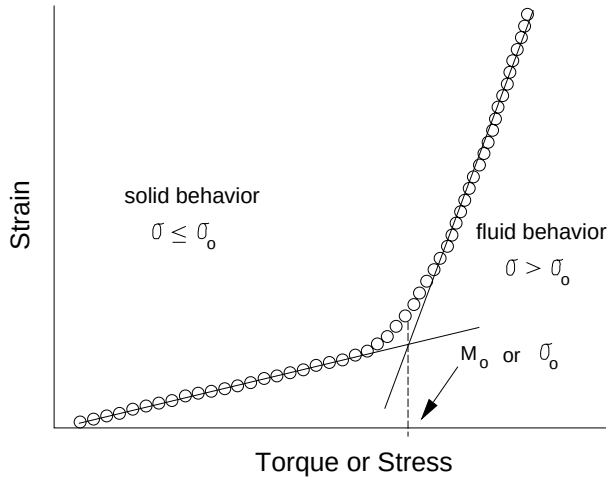

Figure 3.17. Strain-stress curve showing the location of the yield stress when a linear increase in stress is applied to the sample.

The idea of investigating the relationship between strain and stress to determine a yield stress can be applied to samples held within fixtures other than vanes: concentric cylinder, cone and plate, and parallel plate. Data for Colgate Toothpaste Gel, collected at room temperature using a cone and plate apparatus, are presented in Fig. 3.18. The information was obtained by subjecting the sample to a linear change in shear stress, from 1 Pa to 5 Pa, over a period of 500 s. Strain is held near zero until the applied stress exceeds the yield stress (approximately 2.1 Pa) where a substantial increase in strain is observed (Fig. 3.18). Many samples do not produce such clearly defined differences. Data in the early portion of the strain - stress curve (Fig. 3.17) can also be used to calculate a shear modulus.

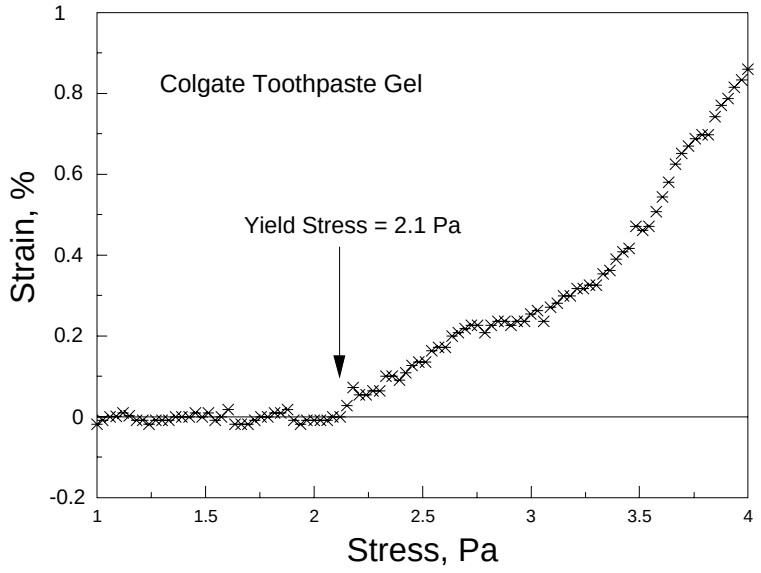

Figure 3.18. Strain-stress data for presheared Colgate Toothpaste Gel, at 25°C, collected on a cone (60mm diameter, 4°) and plate rheometer.

Numerous means of evaluating the yield stress are noted in Table 1.4. Most cannot measure a static yield stress because sample structure is broken down during testing. Also, the experimental difficulties of many approaches make them unattractive. Overall, the vane method has much to offer someone in need of a yield stress measurement: The

technique involves a simple theory that can produce quick, reproducible results. Operating the vane in the controlled rate, versus controlled stress, mode offers some advantages because it produces unequivocal results (M_o is precisely defined in the controlled rate mode) which are the most sensitive to differences between static and dynamic yield stresses (Yoo et al., 1995). In addition, controlled rate instruments are generally less expensive and more durable than controlled stress units.

Wind-up Characteristics of Rotational Viscometers. It is important to understand the physical characteristics of the torque sensor when considering yield stress measurements using a rotational viscometer. Two typical torque measuring concepts, used in controlled rate instruments, are illustrated in Fig. 3.19. In one system, force is transferred through the sample from the bottom plate causing the deflection of a coiled spring. Spring deformation is measured and correlated to torque. Full scale wind-up (how much the upper plate must rotate before the full scale torque is measured) is high for this type of system, often reaching as much as 80 degrees.

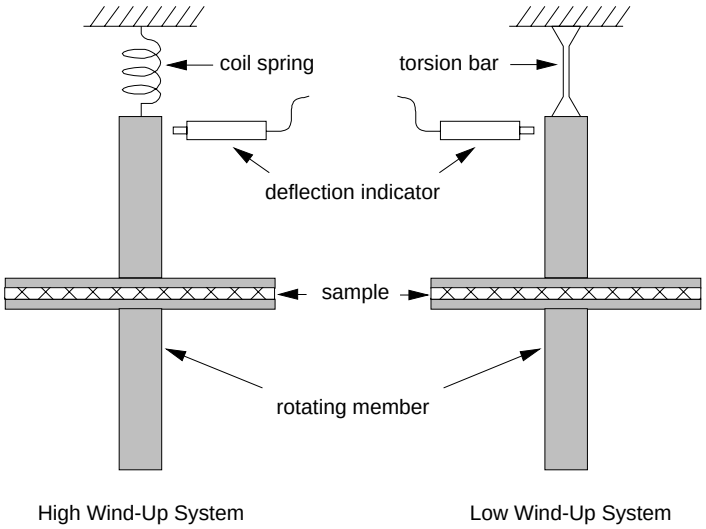

Figure 3.19. Rotational viscometers with coil spring (high wind-up) and torsion bar (low wind-up) torque sensing elements.

A system with low wind-up is also illustrated in Fig. 3.19. In this system the deflection of a torsion bar is correlated to torque. Full scale deflection is achieved with very low wind-up values often in the range of 1 to 2 degrees. The wind-up characteristics of two viscometers, one with a spring type system and the other with a torsion bar, are considered in Example Problem 3.8.21.

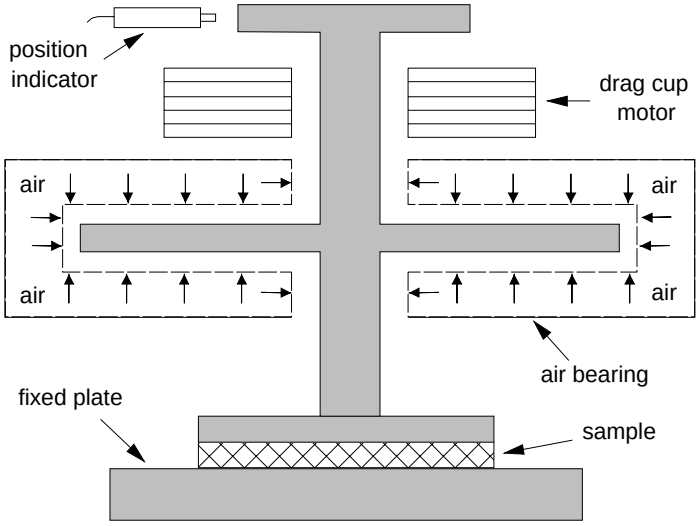

Figure 3.20. Parallel plate viscometer with air bearing sensor support.

Controlled stress instruments use an air bearing to provide "frictionless" movement of the upper fixture (Fig. 3.20) and a drag cup motor to generate controlled torque on the shaft. A position indicator is used to measure displacement. Wind-up in controlled stress systems is essentially zero.

3.7.4. Investigating Rheomalaxis

Mixer viscometry can be a useful, and simple, method of subjectively quantifying rheomalaxis (irreversible structural breakdown) because damage is minimized during loading. The impeller of a mixer viscometer is placed in an undisturbed sample and torque decay data are collected at various speeds (at least three). A new, undisturbed, sample is required for each test. Raw data are plotted as shown in Fig. 3.21. A cross plot of the data is made: first, one finds torque at time zero (start

of test) and equilibrium time (after the curve becomes horizontal) for each angular velocity, then torque (M) versus angular velocity (Ω) is plotted. The area between the resulting initial and equilibrium time curves reflects the degree of rheomalaxis in the sample. If the initial and equilibrium torque curves are modeled as functions $f_1(\Omega)$ and $f_2(\Omega)$, respectively, the area (Δ) between the curves may be calculated as

$$\Delta = \int_{\Omega_1}^{\Omega_3} (f_1(\Omega) - f_2(\Omega)) d\Omega \qquad [3.143]$$

Δ has the units of power, N m s^{-1}. If Δ is large, the power required to mix an undisturbed sample is high compared to that required for a fully broken down sample. If the material is not time-dependent, $\Delta = 0$. Since this is an empirical testing method, identical equipment and testing procedures must be followed to compare different samples. The above concept is illustrated for strained apricots in Example Problem 3.8.22.

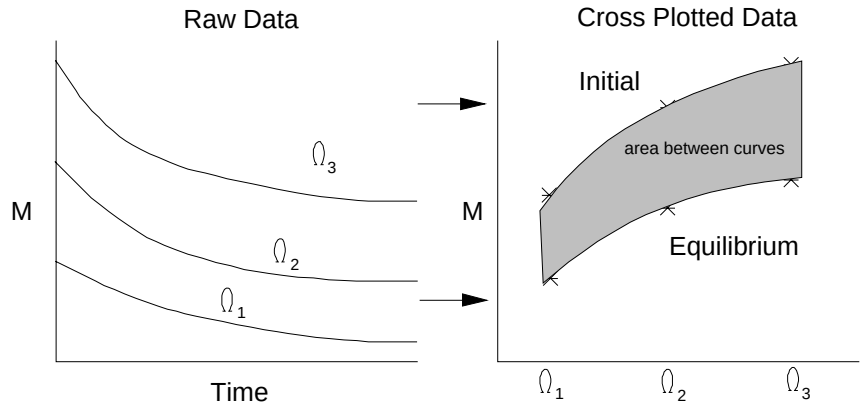

Figure 3.21. Raw and cross plotted data to quantify rheomalatic behavior.

Torque decay data can provide a useful quality control parameter for comparing the structure of different food products by considering energy levels required for mixing. Power ($M\Omega$) versus time, at a constant value of Ω, is plotted so the area under the resulting curve represents the mechanical energy input to the sample. Samples requiring low energy levels for mixing reflect structural breakdown in the material when compared to similar, but non-time-dependent, fluids. One can

investigate recovery of sample structure by introducing a rest period, then repeating the test procedure. To make meaningful comparisons, the volume of sample subjected to agitation during testing must be constant. This energy analysis concept is examined in Example Problem 3.8.22.

Mixer viscometry data can also be used to evaluate a structural parameter for rheomalatic materials, such as λ defined by Eq. [1.37] (Ford and Steffe, 1986), or to model torque decay with a simple exponential equation (Steffe and Ford, 1985).

3.7.5. Defining An Effective Viscosity

A simple approach can be used to characterize non-time-dependent fluids for the purpose of quality control. In this case absolute rheological properties are not needed or difficult to obtain: Only a representative flow curve, which can be compared to a reference flow curve, is required. The reference flow curve is determined from products considered to be acceptable for the intended market.

An effective viscosity may be defined in terms of mixing parameters:

$$\eta_{effective} = \frac{M}{\Omega d^3} \qquad [3.144]$$

where d is equal to the diameter of the impeller. Since effective viscosity is a relative value, other parameters, such as the volume of the mixing vessel or the sample volume swept through by the impeller, could be used in place of d^3. Equipment, sample volume and impeller orientation should be constant for all tests. Eq. [3.144] is similar to Eq. [3.116] with the assumption that $A = 1.0$ and the recognition that $N_{Po} = M/(d^5\Omega^2\rho)$.

One can assume that effective viscosity is directly proportional to apparent viscosity, and angular velocity is directly proportional to shear rate. These values can be plotted to determine effective rheological properties to characterize samples. Suitable quality control criteria can be developed using this concept. The effective viscosity idea is applied to strained apricots in Example Problem 3.8.18.

3.8. Example Problems

3.8.1. Bob Speed for a Bingham Plastic Fluid

Consider testing a Bingham plastic fluid (yield stress = 13 Pa ; plastic viscosity = 1.7 Pa s) in a Searle-type (the bob rotates and the cup is

stationary) concentric cylinder viscometer with α values ($\alpha = R_c/R_b$) of 1.1, 1.3, and 1.5. In each case, estimate the minimum angular velocity of the bob required to achieve flow at the wall of the cup, thus, assuring complete flow in the annulus.

Eq. [3.29] states that

$$\frac{M_{\min}}{2\pi R_c^2 h} > \sigma_o$$

Therefore, the minimum value of torque to achieve flow at R_c is

$$M_{\min} = 2\pi R_c^2 h \sigma_o \qquad [3.145]$$

The equation relating torque to angular velocity in this system, assuming flow throughout the annulus, is given by Eq. [3.28]:

$$\Omega = \left[\frac{M}{4\pi h \eta_{pl}}\right]\left[\frac{1}{R_b^2} - \frac{1}{R_c^2}\right] - \frac{\sigma_o}{\eta_{pl}} \ln\left(\frac{R_c}{R_b}\right)$$

Using Eq. [3.145], the minimum torque expression, the minimum angular velocity may be calculated:

$$\Omega_{\min} = \left[\frac{M_{\min}}{4\pi h \eta_{pl}}\right]\left[\frac{1}{R_b^2} - \frac{1}{R_c^2}\right] - \frac{\sigma_o}{\eta_{pl}} \ln\left(\frac{R_c}{R_b}\right) \qquad [3.146]$$

or, given the above expression for minimum torque,

$$\Omega_{\min} = \left[\frac{2\pi R_c^2 h \sigma_o}{4\pi h \eta_{pl}}\right]\left[\frac{1}{R_b^2} - \frac{1}{R_c^2}\right] - \frac{\sigma_o}{\eta_{pl}} \ln\left(\frac{R_c}{R_b}\right) \qquad [3.147]$$

Simplification, and substitution of $\alpha = R_c/R_b$, yields a general expression for the minimum angular velocity of the bob:

$$\Omega_{\min} = \frac{\sigma_o}{2\eta_{pl}}[\alpha^2 - 1 - 2\ln\alpha] \qquad [3.148]$$

This equation indicates the critical importance of gap size in determining minimum angular velocity. Using the specified yield stress and the plastic viscosity gives

$$\Omega_{\min} = \frac{13}{2(1.7)}[\alpha^2 - 1 - 2\ln\alpha] \qquad [3.149]$$

Substituting the specified values of α into Eq. [3.149] produces the following results:

$\alpha = R_c/R_b$	Ω_{min}, rad/s
1.1	0.074 (0.71 rpm)
1.3	0.63 (6.04 rpm)
1.5	1.67 (15.95 rpm)
2.0	6.16 (58.82 rpm)

The minimum bob speed to maintain flow of a Bingham plastic fluid in the annulus increases rapidly as the size of the gap increases. Therefore, small gaps, appropriate for given particle size limitations, are preferred to large gaps.

3.8.2. Simple Shear in Power Law Fluids

Determine the error involved in using the simple shear approximation for power law fluids at different values of $\alpha = R_c/R_b$.

To solve this problem, both the approximate (Eq. [3.30]) and actual (Eq. [3.33]) solutions must be considered:

$$(\dot{\gamma}_b)_{approximate} = \frac{\Omega}{\alpha - 1} \qquad [3.150]$$

$$(\dot{\gamma}_b)_{actual} = \left(\frac{2\Omega}{n}\right)\left[\frac{\alpha^{2/n}}{\alpha^{2/n} - 1}\right] \qquad [3.151]$$

The "% Error" may be calculated as

$$\%\ \text{Error} = \left[1 - \frac{(\dot{\gamma}_b)_{approximate}}{(\dot{\gamma}_b)_{actual}}\right]100 \qquad [3.152]$$

Substituting Eq. [3.150] and Eq. [3.151] into Eq. [3.152] yields

$$\%\ \text{Error} = \left[1 - \frac{n}{2(\alpha - 1)}\left(\frac{\alpha^{2/n} - 1}{\alpha^{2/n}}\right)\right]100 \qquad [3.153]$$

which describes the error expected for different values of n and α. Results are best seen in graphical form (Fig. 3.22). To keep error to a minimum, smaller gaps (reflected in smaller values of α) are needed for

lower values of the flow behavior index. If $n = 0.4$ and $1.0 < \alpha < 1.02$, error involved in using the simple shear approximation will be less than 6%: At $n = 0.2$ and $\alpha > 1.02$, the error will exceed 10%.

3.8.3. Newtonian Fluid in a Concentric Cylinder

Determine an expression for the shear rate as a function of the radius for a Newtonian fluid in the annulus of a concentric cylinder viscometer. Using this expression, determine the shear rate at the bob and cup.

A Newtonian fluid is defined (Eq. [1.25]) as

$$\dot{\gamma} = \frac{\sigma}{\mu}$$

and the equation giving the shear stress in the annulus (Eq. [3.2]) is

$$\sigma = f(r) = \frac{M}{2\pi h r^2}$$

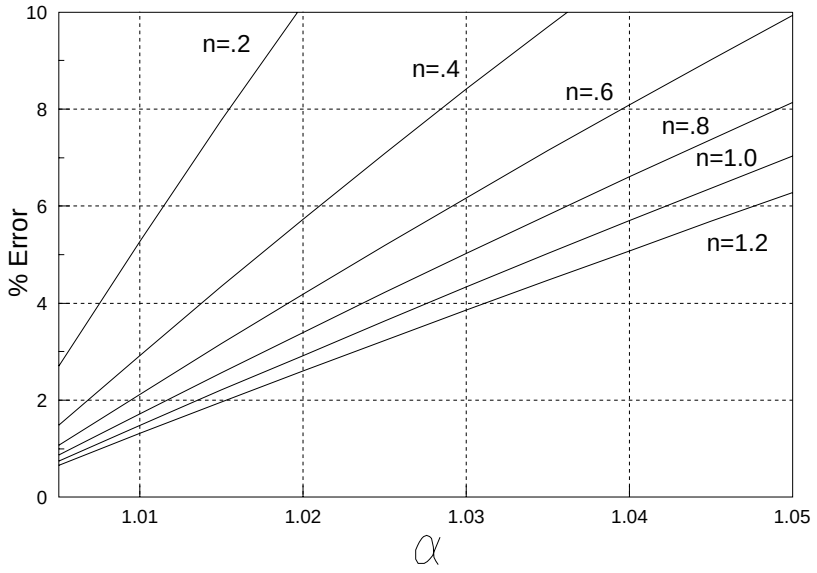

Figure 3.22. Error (Eq [3.153]) in shear rate calculation when using the simple shear approximation for a power law fluid in a concentric cylinder system ($\alpha = R_c/R_b$).

for $R_b \le r \le R_c$. Combining the above equations, the shear rate may be written as

$$\dot{\gamma} = f(r) = \frac{M}{2\pi h r^2 \mu} \qquad [3.154]$$

Eq. [3.21] states that

$$\Omega = \frac{M}{4\pi\mu h}\left[\frac{1}{R_b^2} - \frac{1}{R_c^2}\right]$$

which can be solved for torque as

$$M = \frac{4\Omega\pi h \mu R_c^2}{\alpha^2 - 1} \qquad [3.155]$$

where, recall, $\alpha = R_c/R_b$. Substituting Eq. [3.155] into Eq. [3.154] gives the shear rate as a function of the radius for any constant value of the angular velocity:

$$\dot{\gamma} = f(r) = \frac{M}{2\pi h r^2 \mu} = \left[\frac{1}{2\pi h r^2 \mu}\right]\left[\frac{4\Omega\pi h \mu R_c^2}{\alpha^2 - 1}\right] = 2\Omega\left(\frac{R_c^2/r^2}{\alpha^2 - 1}\right) \qquad [3.156]$$

where $R_b \le r \le R_c$. The expressions for the shear rate at the bob ($\dot{\gamma}_b$, given previously as Eq. [3.32]) and cup ($\dot{\gamma}_c$) can be easily calculated from Eq. [3.156]:

$$\dot{\gamma}_b = f(R_b) = 2\Omega\left(\frac{\alpha^2}{\alpha^2 - 1}\right)$$

$$\dot{\gamma}_c = f(R_c) = 2\Omega\left(\frac{1}{\alpha^2 - 1}\right) \qquad [3.157]$$

3.8.4. Representative (Average) Shear Rate

Fig. 3.23 shows a popular bob design based on a German standard (DIN 53019) developed by the German Institute for Standardization, Deutsches Institut für Normung, known by the DIN acronym. The following restrictions are given for dimensional considerations: $\alpha = R_c / R_b \le 1.1$; $h/R_b \ge 3$; $h'/R_b \ge 1$; $R_s/R_b \le 0.3$; $90° \le \theta \le 150°$. Preferred dimensions are also stated: $\alpha = 1.0847; h/R_b = 3; h'/R_b = 1; h''/R_b = 1; \theta = 120°$. No preferred dimension is given for R_s/R_b. Note that θ is the apex angle of the cone at the bottom of the inner cylinder, and the summation of h values ($h'' + h + h'$) is equal to the fluid level in the cup.

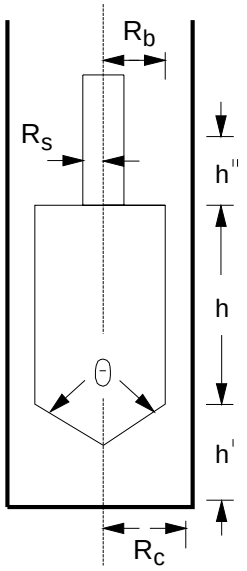

Figure 3.23. Bob and cup design based on German standard, DIN 53018.

DIN 53019 states that the bob and cup combination illustrated in Fig. 3.23 can be used in conjunction with representative values (average values) of the shear stress and the shear rate in determining rheological behavior of Newtonian and non-Newtonian fluids. The representative shear stress, defined as the average shear stress between the bob and the cup, was presented in Eq. [3.31]:

$$\sigma_a = \frac{M(1+\alpha^2)}{4\pi(h+h_o)R_c^2}$$

where h_o has been added to account for both the top and bottom end effects. The DIN standard states that $h_o = 0.1h$ for the preferred geometrical relations allowing the working equation for average shear stress to be written as

$$\sigma_a = \frac{M(1+\alpha^2)}{4\pi(h+.1h)R_c^2} = \frac{M(1+\alpha^2)}{(4.4)\,\pi h R_c^2} \qquad [3.158]$$

Question: Taking the Newtonian approximation for shear rate (Eq. [3.32]), determine the representative shear rate that would be appropriate in evaluating the rheogram.

The representative shear rate is the average shear rate ($\dot{\gamma}_a$) between the bob and the cup:

$$\dot{\gamma}_a = \frac{\dot{\gamma}_b + \dot{\gamma}_c}{2} \qquad [3.159]$$

Using the values of $\dot{\gamma}_b$ and $\dot{\gamma}_c$ (Eq. [3.32] and Eq. [3.157]) given in Example Problem 3.8.3, Eq. [3.159] can be written as

$$\dot{\gamma}_a = \left[2\Omega\left(\frac{\alpha^2}{\alpha^2 - 1} \right) + 2\Omega\left(\frac{1}{\alpha^2 - 1} \right) \right] / 2 \qquad [3.160]$$

Manipulation yields a simple equation to calculate the representative shear rate:

$$\dot{\gamma}_a = \frac{\Omega(\alpha^2 + 1)}{\alpha^2 - 1} \qquad [3.161]$$

A rheogram can be developed from representative values of shear stress and shear rate. These equations are often used in the computer software calculations found in commercially available concentric cylinder viscometers. This idea is applicable to most concentric cylinder systems with narrow gaps ($R_c/R_b \leq 1.1$). When using the average shear rate equation for bobs having an end geometry different than that illustrated in Fig. 3.23, the average shear stress equation would need to be adjusted for different values of h_o. If applied to the bob shown in Fig. 3.1, for example, the value of h_o would be smaller than the value of $0.1h$ specified by the DIN standard. Theoretical justification for using representative shear stress and shear rate values may be found in Giesekus and Langer (1977).

3.8.5. Concentric Cylinder Viscometer: Power Law Fluid

Develop an expression for the shear rate at the bob for a power law fluid in a concentric cylinder viscometer. Also derive an equation describing the fluid velocity profile found in this system. Assume the viscometer is a Searle system where the bob rotates and the cup is stationary.

This problem can be solved using the same approach taken in Example Problem 3.8.3. By considering the definition of a power law fluid ($\sigma = K\dot{\gamma}^n$) and the force balance on a bob (Eq. [3.2]), the following expression for the shear rate in the annulus is obtained:

$$\dot{\gamma} = f(r) = \left(\frac{M}{2\pi h r^2 K} \right)^{1/n} \qquad [3.162]$$

Then, the shear rate at the bob is

$$\dot{\gamma}_b = f(R_b) = \left(\frac{M}{2\pi h R_b^2 K} \right)^{1/n} \qquad [3.163]$$

However, from Eq. [3.25],

$$\Omega = \frac{n}{2K^{1/n}} \left(1 - \left(\frac{R_b}{R_c} \right)^{2/n} \right) \left[\frac{M}{2\pi h R_b^2} \right]^{1/n}$$

Solving this equation for M and substituting the result into the above expression for $\dot{\gamma}_b$ yields

$$\dot{\gamma}_b = \frac{2\Omega}{n} \left(\frac{R_c^{2/n}}{R_c^{2/n} - R_b^{2/n}} \right) \qquad [3.164]$$

or, using $\alpha = R_c/R_b$, Eq. [3.164] becomes

$$\dot{\gamma}_b = \frac{2\Omega}{n} \left(\frac{\alpha^{2/n}}{\alpha^{2/n} - 1} \right)$$

which provides the final solution given earlier as Eq. [3.33].

To derive an equation for the velocity profile of a power law fluid in a concentric cylinder viscometer, start with Eq. [3.15]:

$$\int_{\omega=\Omega}^{\omega=0} d\omega = \frac{1}{2} \int_{\sigma_b}^{\sigma_c} f(\sigma) \frac{d\sigma}{\sigma}$$

Changing the limits of integration, and substituting $f(\sigma) = (\sigma/K)^{1/n}$, yields

$$\int_{\omega}^{0} d\omega = \frac{1}{2} \int_{\sigma}^{\sigma_c} \left(\frac{\sigma}{K} \right)^{1/n} \frac{d\sigma}{\sigma} \qquad [3.165]$$

or, after integration,

$$\omega = f(\sigma) = \frac{n}{2K^{1/n}}[\sigma^{1/n} - \sigma_c^{1/n}] \qquad [3.166]$$

Using Eq. [3.2], Eq. [3.166] can be written as a function of the radius:

$$\omega = f(r) = \frac{n}{2K^{1/n}}\left[\left(\frac{M}{2\pi h r^2}\right)^{1/n} - \left(\frac{M}{2\pi h R_c^2}\right)^{1/n}\right] \qquad [3.167]$$

Simplification gives

$$\omega = f(r) = \frac{n}{2K^{1/n}}\left(\frac{M}{2\pi h R_c^2}\right)^{1/n}\left[\left(\frac{R_c}{r}\right)^{2/n} - 1\right] \qquad [3.168]$$

which can be used to generate an expression for a dimensionless velocity profile in the gap:

$$\frac{\omega}{\Omega} = \frac{f(r)}{f(R_b)} = \frac{\left[(1/r^2)^{1/n} - (1/R_c^2)^{1/n}\right]}{\left[(1/R_b^2)^{1/n} - (1/R_c^2)^{1/n}\right]} = \frac{[(R_c/r)^{2/n} - 1]}{[(R_c/R_b)^{2/n} - 1]} \qquad [3.169]$$

where $R_b \le r \le R_c$. As expected, $\omega = \Omega$ at $r = R_b$, and $\omega = 0$ at $r = R_c$.

3.8.6. Concentric Cylinder Data - Tomato Ketchup

Given raw data for tomato ketchup (Table 3.2), determine the rheological properties of the fluid. Use the power law approximation for shear rate presented in Eq. [3.33]:

$$\dot{\gamma}_b = \left(\frac{2\Omega}{n}\right)\left[\frac{\alpha^{2/n}}{\alpha^{2/n} - 1}\right]$$

Also evaluate the alternative equation for $\dot{\gamma}_b$ given by Heywood (1991b).

The first step in finding the shear rate at the bob is to calculate the flow behavior index. Regression analysis of $\ln(M)$ versus $\ln(\Omega)$ yields

$$\ln(M) = (.307)\ln(\Omega) - 5.0529$$

meaning, from Eq. [3.37], that

$$n = \frac{d\ln(M)}{d\ln(\Omega)} = 0.307$$

With this result and the equation for $\dot{\gamma}_b$, the shear rate at each value of Ω may be calculated. Shear stress at the bob is determined from Eq. [3.3]:

Table 3.2. Data and Results for a Rheological Test for Tomato Ketchup at 25°C Conducted using a Concentric Cylinder Viscometer: h=60.00 mm; R_c=21.00 mm; R_b=20.04 mm; ρ=1050 kg/m^3.

RPM	Ω (rad/s)	ln(Ω)	*M* (N m)	ln(*M*)	σ_b (Pa)	$\dot{\gamma}_b$ (1/s)
1	0.105	-2.256	0.00346	-5.666	22.85	2.60
2	0.209	-1.563	0.00398	-5.526	26.29	5.19
4	0.419	-0.870	0.00484	-5.331	31.97	10.39
8	0.838	-0.177	0.00606	-5.106	40.03	20.77
16	1.676	0.516	0.00709	-4.949	46.83	41.55
32	3.351	1.209	0.00848	-4.770	56.01	83.10
64	6.702	1.902	0.01060	-4.547	70.01	166.20
128	13.404	2.596	0.01460	-4.227	96.43	332.39
256	26.808	3.289	0.01970	-3.927	130.12	664.78

$$\sigma_b = \frac{M}{2\pi h R_b^2}$$

Results of these calculations are presented in Table 3.2.

Assuming a power law model to represent the rheogram of this material gives an excellent representation of the data and a value for the consistency coefficient (*K*) equal to 15.73 Pa s^n. Since this material exhibits power law behavior, the results are almost identical to those found using the Krieger approximation (Eq. [3.47]) because 1/*s* is essentially equal to 1/*n*. In addition, one can observe that simple and Newtonian shear rate equations (Eq. [3.30] and [3.32]) give, at best, gross approximations. Considering the shear rate at 256 rpm (26.808 rad/s) for both cases gives

$$(\dot{\gamma}_b)_{\text{simple shear}} = \frac{\Omega}{\alpha - 1} = \frac{26.808}{1.048 - 1} = 558.5\ s^{-1}$$

and

$$(\dot{\gamma}_b)_{\text{Newtonian}} = (2\Omega)\left[\frac{\alpha^2}{\alpha^2 - 1}\right] = 2(26.808)\left[\frac{(1.048)^2}{(1.048)^2 - 1}\right] = 599.0\ s^{-1}$$

Although, these values are the same order of magnitude as the power law approximation of 664.78 s^{-1}, the error would be unacceptable in most cases.

To check for potential problems due to secondary flow Eq. [3.90] must be evaluated:

$$\frac{\Omega R_b (R_c - R_b)\rho}{\mu} > 41.3\sqrt{\frac{R_c}{R_c - R_b}}$$

Recall that Taylor vortices may be expected when this inequality is satisfied. Although the equation was established for Newtonian fluids, a reasonable assessment of the current problem can be obtained by substituting the apparent viscosity ($\sigma_b / \dot{\gamma}_b$) for μ. Taking the worst case (highest speed) the calculation can be made as

$$\frac{(26.81)(.02004)(.02100 - .02004)(1050)}{(130.12/664.78)} = 2.77$$

which is clearly much less than

$$41.3\sqrt{\frac{.02100}{.02100 - .02004}} = 193.16$$

meaning errors due to the presence of secondary flow are negligible.

Heywood (1991b) offered the following equation to determine the shear rate at the bob in a concentric cylinder system:

$$\dot{\gamma}_b = \frac{\Omega}{\ln\alpha}\left[1 + \frac{\ln\alpha}{a'} + \frac{1}{3}\left(\frac{\ln\alpha}{a'}\right)^2 (1 - a'') + \ldots.\right] \qquad [3.170]$$

where

$$a' = \frac{d(\ln M)}{d(\ln\Omega)} \qquad [3.171]$$

and

$$a'' = \frac{d(a')}{d(\ln\Omega)} \qquad [3.172]$$

Eq. [3.170] is a simplified form of an infinite series solution of Eq [3.42] given by Krieger and Maron (1952). To evaluate Eq. [3.170] for the special case of a power law fluid one must recognize, by observing Eq. [3.37], that $a' = n$ and $a'' = 0$. Making these substitutions, Eq. [3.170] becomes

$$\dot{\gamma}_b = \frac{\Omega}{\ln\alpha}\left[1 + \frac{\ln\alpha}{n} + \frac{1}{3}\left(\frac{\ln\alpha}{n}\right)^2\right] \qquad [3.173]$$

In the case of tomato ketchup, $n = 0.307$ and $\alpha = 21.00/20.04 = 1.048$. Substituting these values into the Krieger and Maron solution yields

$$\dot{\gamma}_b = \frac{\Omega}{\ln(1.048)}\left[1 + \frac{\ln(1.048)}{.307} + \frac{1}{3}\left(\frac{\ln(1.048)}{.307}\right)^2\right] = 24.75\Omega$$

The exact power law solution is

$$\dot{\gamma}_b = \left(\frac{2\Omega}{.307}\right)\left[\frac{1.048^{2/.307}}{1.048^{2/.307} - 1}\right] = 24.75\Omega$$

meaning the above equations to calculate shear rate are equivalent to the second decimal place.

3.8.7. Infinite Cup - Single Point Test

A viscometer with a single bob, and no cup, is to be used in developing a single point quality control test for tomato ketchup (at 25°C) when held in a large vat. If the instrument is run at 50 rpm, what apparent viscosity would be expected?

Previous work (Example Problem 3.8.6) with a concentric cylinder instrument yielded power law parameters for the fluid: K = 15.73 Pa s^n and n = 0.307 . The shear rate at the bob for this material in a concentric cylinder system (Eq. [3.33]) is

$$\dot{\gamma}_b = \left(\frac{2\Omega}{n}\right)\left[\frac{\alpha^{2/n}}{\alpha^{2/n} - 1}\right]$$

In a vat, α which equals R_c/R_b is large so the term in brackets is effectively one. Therefore, the shear rate may be expressed as

$$\dot{\gamma}_b = \frac{2\Omega}{n}$$

allowing the shear rate at 50 rpm to be calculated:

$$\dot{\gamma}_b = \frac{2(50)(2\pi)}{(.307)60} = 34.11\ s^{-1}$$

With this value of the shear rate, the expected apparent viscosity may be determined:

$$\eta = K(\dot{\gamma}_b)^{n-1} = 15.73(34.11)^{.307-1} = 1.36\ Pa\ s$$

3.8.8. Infinite Cup Approximation - Power Law Fluid

Determine the error involved in using the infinite cup approximation for power law fluids at different values of $\alpha = R_c/R_b$.

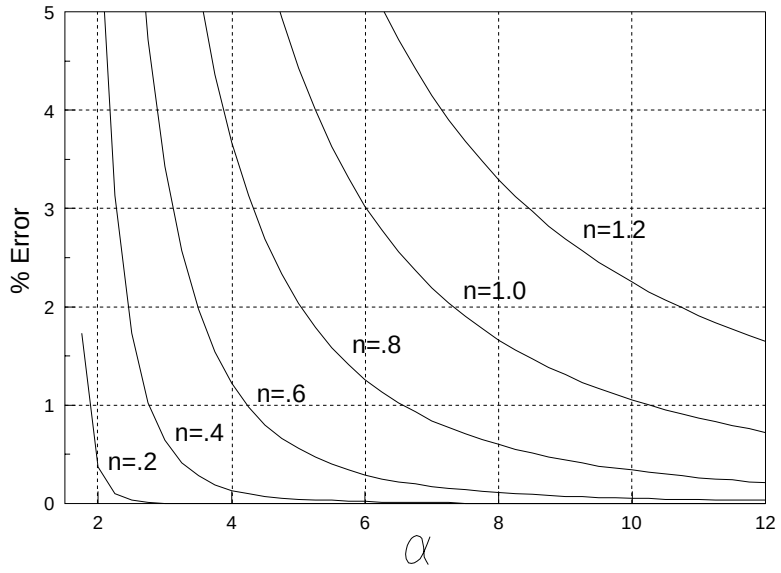

Figure 3.24. Error (Eq. [3.177]) in using the infinite cup solution for power law fluids in a concentric cylinder system ($\alpha = R_c/R_b$).

The approximate solution is found from Eq. [3.49] by noting (Eq. [3.36]) that $d(\ln\Omega)/d(\ln\sigma_b) = 1/n$ for a power law fluid:

$$(\dot{\gamma}_b)_{approximate} = \frac{2\Omega}{n} \qquad [3.174]$$

The actual solution, provided Eq. [3.33], is

$$(\dot{\gamma}_b)_{actual} = \left(\frac{2\Omega}{n}\right)\left[\frac{\alpha^{2/n}}{\alpha^{2/n}-1}\right] \qquad [3.175]$$

The "% Error" may be calculated as

$$\%\ \text{Error} = \left[1 - \frac{(\dot{\gamma}_b)_{approximate}}{(\dot{\gamma}_b)_{actual}}\right]100 \qquad [3.176]$$

Substituting Eq. [3.174] and Eq. [3.175] into Eq. [3.176] yields

$$\%\ \text{Error} = \left[1 - \left(\frac{\alpha^{2/n}-1}{\alpha^{2/n}}\right)\right]100 \qquad [3.177]$$

which gives the error expected for different values of n and α. Plotting the results (Fig. 3.24) makes it clear that larger containers are required (larger α) to keep error to acceptable levels as the flow behavior index increases. With $n = 0.6$, α must be greater than 3 to keep the error below 5%. The technique of error determination used above (and in Example Problem 3.8.2) can be very helpful in evaluating the assumptions made in the "automatic" calculations of commercial instruments.

3.8.9. Infinite Cup - Salad Dressing

Rheological data (Table 3.3) for Kraft French salad dressing were collected using a concentric cylinder geometry with the following dimensions: bob radius = 20.04 mm; cup radius = 73.00 mm; bob height = 60.00 mm. The bob has a recessed top and bottom like the one illustrated in Fig. 3.1 so we will assume end effects are negligible. Using the infinite cup assumption, determine the rheological properties of this time-independent material.

Table 3.3. Rheological Data for Kraft French Salad Dressing at 22°C [Concentric Cylinder System: R_b=20.04 mm, R_c=73.00 mm, h=60.00 mm]

Ω (rad/s)	M (N m)	σ_b (Pa)	$\dot{\gamma}_b$ (1/s)
0.146	0.000609	4.02	0.79
0.512	0.000998	6.59	2.77
1.036	0.001264	8.35	5.60
2.087	0.001623	10.72	11.28
4.163	0.002033	13.43	22.50
6.276	0.002430	16.05	33.92
8.359	0.002708	17.89	45.18
10.490	0.002970	19.62	56.70
12.590	0.003149	20.80	68.05
14.680	0.003335	22.03	79.35
16.770	0.003509	23.18	90.65

Shear stress at the bob is calculated from Eq. [3.3] as

$$\sigma_b = \frac{M}{2\pi h R_b^2}$$

The shear rate may be determined from Eq. [3.49] as

$$\dot{\gamma}_b = (2\Omega)\frac{d(\ln\Omega)}{d(\ln\sigma_b)}$$

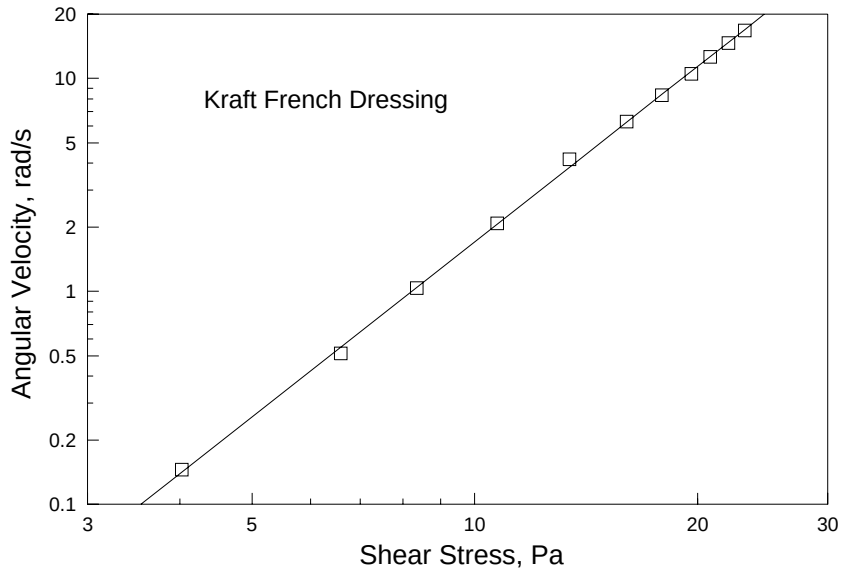

Figure 3.25. Logarithmic plot of angular velocity versus shear stress for Kraft French salad dressing.

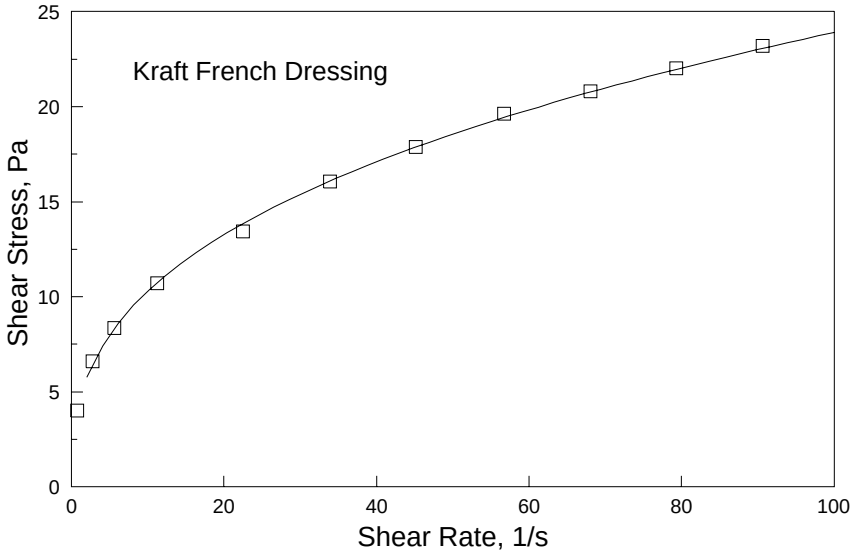

Figure 3.26. Rheogram for Kraft French salad dressing at 22°C.

Regression of the data indicates a good fit of the logarithmic plot (Fig. 3.25) with a slope of 2.73:

$$\frac{d(\ln \Omega)}{d(\ln \sigma_b)} = 2.73$$

Knowing the slope, the shear rate can be calculated as

$$\dot{\gamma}_b = (2\Omega)2.73$$

With the shear stress and shear rate data computed (Table 3.3), the rheogram may be plotted (Fig. 3.26), power law constants determined (more regression analysis) and the final model presented:

$$\sigma = 4.43(\dot{\gamma})^{.37}$$

Note, the slope of the logarithmic plot is the reciprocal of the flow behavior index ($1/n = 1/0.37 \approx 2.7$) because, as stated in the previous example problem, the infinite cup solution for a power law fluid is

$$\dot{\gamma}_b = \frac{2\Omega}{n}$$

Also, in consulting Fig. 3.24, one can see the error in using the infinite cup approximation for $\alpha = 73.00/20.04 = 3.64$ and $n = 0.37$ should be less than 0.5%.

3.8.10. Infinite Cup - Yield Stress Materials

Under what conditions could Eq. [3.49], an expression to determine the shear rate at the bob in an infinite cup, be used for a vat containing a material with a yield stress?

Knowing the yield stress, the critical radius (R_o) can be calculated by considering Eq. [3.2]:

$$R_o = \sqrt{\frac{M_{\max}}{2\pi h \sigma_o}} \qquad [3.178]$$

where $M_{\max}$ is the maximum torque generated by the instrument during testing. R_o defines the sheared area of the sample in the vat when fluid motion is due only to bob rotation.

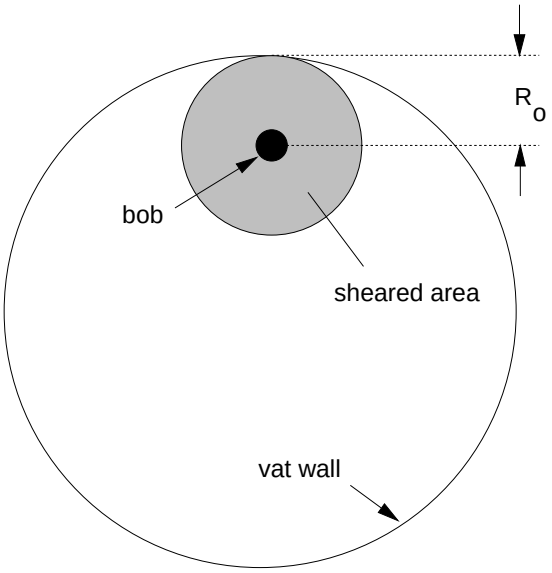

Figure 3.27. Bob placement, showing sheared area, in a vat full of fluid having a yield stress.

The instrument should be positioned (Fig. 3.27) so the center of the bob is, at a minimum, a distance equal to R_o from the wall of the vat. Under these conditions, the physical situation in the vat is analogous to having a concentric cylinder system, with a partially sheared annulus; hence, Eq. [3.49] should give satisfactory results.

3.8.11. Cone and Plate - Speed and Torque Range

Assume tomato ketchup will be tested in a cone and plate viscometer so the results can be compared with those found in the concentric cylinder tests. Using a cone with an angle of 0.0524 rad (3 degrees) and a diameter of 5.0 cm, what speed and torque response would be needed to cover an experimental shear rate range of 1 to 100 s^{-1}?

In a cone and plate system, the relationship between angular velocity and shear rate is given by rearranging Eq. [3.51]:

$$\Omega = \dot{\gamma}(\tan\theta)$$

Using this expression, the minimum and maximum velocities may be calculated as

$$\Omega_{min} = 1(\tan(0.0524)) = 0.0524\, rad/s\,(0.50\, rpm)$$

and

$$\Omega_{max} = 100(\tan(0.0524)) = 0.524\, rad/s\,(5.00\, rpm)$$

To cover the shear rate range of 1 to 100 s^{-1} the instrument should have a minimum speed range of 0.5 to 50 rpm. The required torque capability of the instrument may be considered from Eq. [3.55]:

$$\sigma = \frac{3M}{2\pi R^3}$$

Rearranging this expression, and incorporating the definition of the shear stress for a power law fluid yields

$$M = \frac{2\pi R^3 \sigma}{3} = \frac{2\pi R^3 K(\dot{\gamma})^n}{3}$$

Substituting the appropriate numbers (from Example 3.8.6: $K = 15.73$ Pa s^n, $n = 0.307$) and calculating the results gives

$$M_{min} = \frac{2\pi(.05/2)^3 (15.73)(1)^{.307}}{3} = 0.000515\, N\, m = 5,150.0\, dyne\, cm$$

and

$$M_{max} = \frac{2\pi(.05/2)^3 (15.73)(100)^{.307}}{3} = 0.00212\, N\, m = 21,000\, dyne\, cm$$

To test samples over the shear rate range of 1 to 100 s^{-1} the instrument torque response must include the range from 5,150 to 21,2000 dyne cm.

3.8.12. Cone and Plate - Salad Dressing

Rheological data (Table 3.4) were collected for Kraft French salad dressing using a cone and plate system. Determine if a power law model will adequately describe the behavior of this material.

Using Eq. [3.51] and [3.55], the shear rate and shear stress can be calculated directly from the raw data:

$$\dot{\gamma} = \frac{\Omega}{\tan\theta}$$

and

$$\sigma = \frac{3M}{2\pi R^3}$$

Table 3.4. Cone and Plate Data (R=25mm; θ=0.02 rad) for Kraft French Salad Dressing at 22 °C

Ω rad/s	*M* N m	$\dot{\gamma}$ 1/s	σ Pa
0.002	1.34E-4	0.10	4.09
0.005	1.65E-4	0.25	5.04
0.013	2.16E-4	0.63	6.60
0.025	2.59E-4	1.25	7.91
0.040	2.98E-4	1.99	9.11
0.063	3.42E-4	3.16	10.45
0.100	3.97E-4	5.01	12.13
0.159	4.58E-4	7.94	14.00
0.252	5.28E-4	12.59	16.13
0.399	6.24E-4	19.95	19.07
0.632	7.33E-4	31.62	22.40
1.002	8.70E-4	50.11	26.59

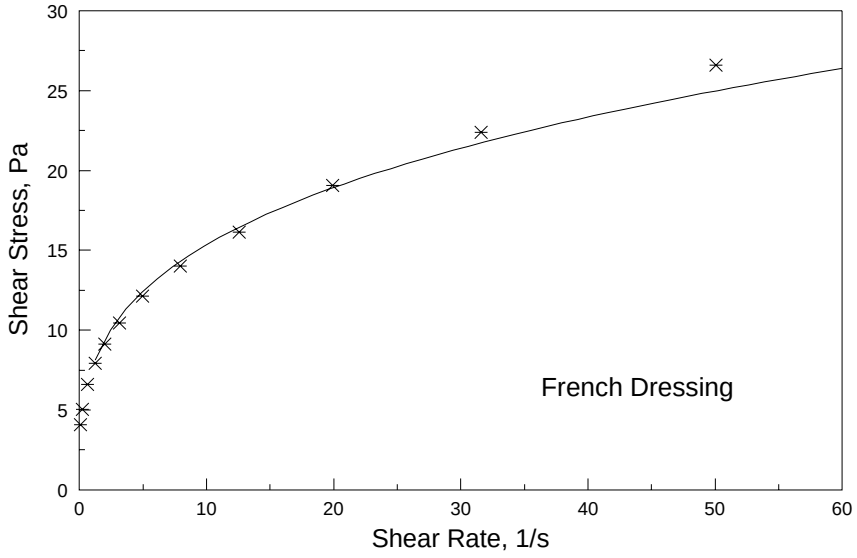

Figure 3.28. Rheogram for Kraft French salad dressing (22 °C) determined from cone and plate data.

Regression analysis of the results (Table 3.4 and Fig. 3.28) yields a statistically acceptable fit to the experimental data as

$$\sigma = 7.64(\dot{\gamma})^{.303}$$

where K = 7.64 Pa s^n and n = 0.303. These results are different than those found in Example Problem 3.8.9 when evaluating Kraft French salad dressing using the infinite cup assumption with a concentric cylinder viscometer. Differences may be due to various factors such as analytical assumptions, natural biological variability, and differences in shear rate coverage. More experimental data would be required to resolve these issues.

3.8.13. Parallel Plate - Methylcellulose Solution

Data for a 3% hydroxypropyl methylcellulose solution have been collected using a parallel plate viscometer (Table 3.5). Generate a rheogram for this material.

Table 3.5. Parallel Plate Data (R=25mm; h=0.70mm) for a 3% Aqueous Solution of Hydroxypropyl Methylcellulose (Methocel K4M, Dow Chemical Co.) at 24.2 °C

M N m	$\dot{\gamma}_R$ 1/s	ln M	ln $\dot{\gamma}_R$	σ_R Pa
0.116E-4	0.0127	-11.36	-4.37	0.5
0.211E-4	0.0198	-10.77	-3.92	0.8
0.334E-4	0.0317	-10.31	-3.45	1.3
0.442E-4	0.0503	-10.03	-2.99	1.7
0.807E-4	0.0797	-9.42	-2.53	3.2
1.259E-4	0.1262	-8.98	-2.07	4.9
2.029E-4	0.1999	-8.50	-1.61	7.9
2.979E-4	0.3166	-8.12	-1.15	11.7
4.536E-4	0.5016	-7.70	-0.69	17.8
6.687E-4	0.7945	-7.31	-0.23	26.2
9.343E-4	1.258	-6.98	0.23	36.6
12.900E-4	1.994	-6.65	0.69	50.5
17.270E-4	3.158	-6.36	1.15	67.6
22.700E-4	5.003	-6.09	1.61	88.8
29.260E-4	7.925	-5.83	2.07	114.5
37.320E-4	12.55	-5.59	2.53	146.0

The shear rate at the rim of the plate was determined, by considering angular velocity and geometry, from Eq. [3.59] as

$$\dot{\gamma}_R = \frac{\Omega R}{h}$$

and shear stress was calculated with Eq. [3.66]:

$$\sigma_R = f(\dot{\gamma}_R) = \frac{M}{2\pi R^3}\left[3 + \frac{d\ln(M)}{d\ln(\dot{\gamma}_R)}\right]$$

Using linear regression, the following relationship was determined from the torque and shear rate data (Fig. 3.29):

$$\ln(M) = -7.12 + .934\ln(\dot{\gamma}_R)$$

which identifies the slope term as

$$\frac{d\ln(M)}{d\ln(\dot{\gamma}_R)} = .934$$

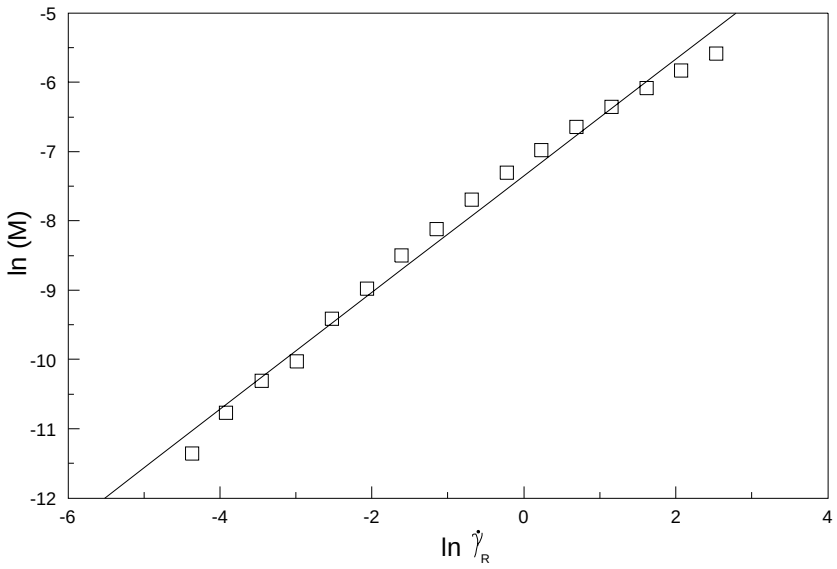

Figure 3.29. Torque versus shear rate for 3% aqueous solution of hydroxypropyl methylcellulose at 24.2 °C.

This result can be used to evaluate the shear stress at the rim for each torque value:

$$\sigma_R = \frac{M}{2\pi R^3}[3 + .934]$$

Shear stress values calculated from this equation are presented in Table 3.5 and plotted in Fig. 3.30. Using the power law model, values of the consistency coefficient and the flow behavior index were determined: K = 25.3 Pa s^n and n = 0.83.

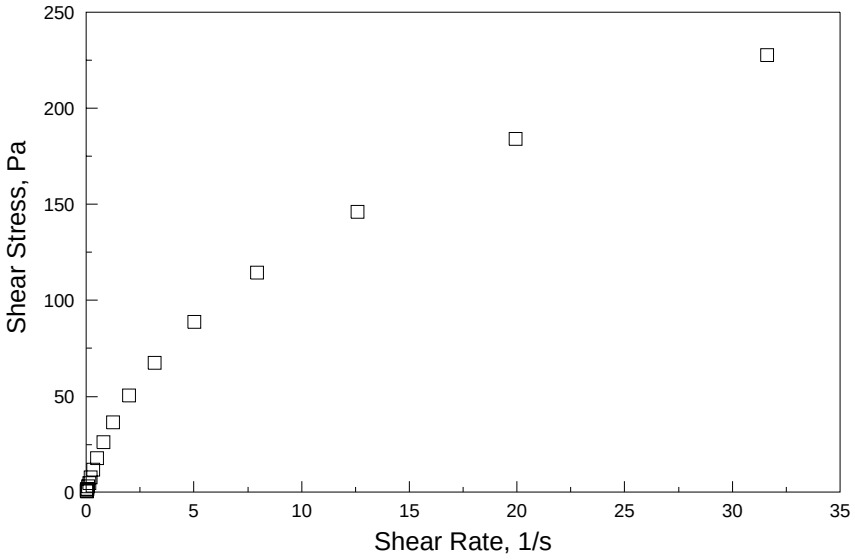

Figure 3.30. Flow behavior of a 3% aqueous solution of hydroxypropyl methyl-cellulose (Methocel K4M, Dow Chemical Co.) at 24.2 °C.

3.8.14. End Effect Calculation for a Cylindrical Bob

Determine the bottom end effect (h_o) for the bob (R_b = 1.95 cm) and cup (R_c = 2.00 cm) combination illustrated in Fig. 3.31.

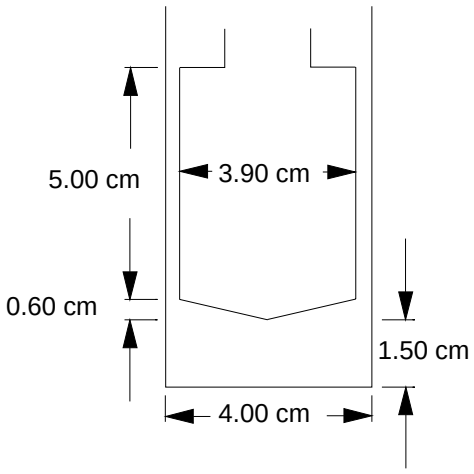

Figure 3.31. Bob and cup combination tested for end effect correction.

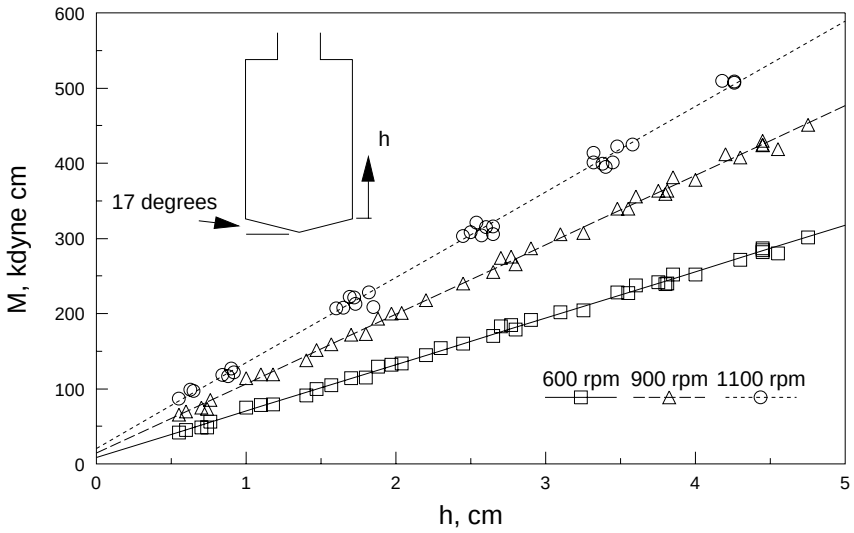

Figure 3.32. End effect data for the "A-bob" of the Hercules high-shear viscometer.

The end correction for the bottom of the bob was evaluated from torque data taken at three fixed bob speeds with different values of h (Fig. 3.32) using the technique presented in Sec. 3.5. Note that h is measured from the top of the cone shaped projection of the bob. All tests were run at room temperature with a Dow Corning 200 fluid which is a dimethyl-silicone material having the following characteristics at 25°C: Newtonian behavior with μ = 95.63 cP , and ρ = 0.965 g cm^{-3}.

Torque data were plotted (Fig. 3.32) as $M = ah + b$ at three speeds: 600 rpm, 900 rpm, and 1100 rpm. h_o values were determined (Table 3.6) from linear regression coefficients: at $M = 0$, $h_o = -b/a$. Correlation coefficients were 0.99 for each curve. Results showed the magnitude of the end effect increasing with increasing speed going from 0.141 cm at 600 rpm to 0.182 cm at 1100 rpm. An average value of h_o = 0.158 cm is recommended for making practical end effect corrections over the rpm range considered.

Table 3.6. Linear Regression Parameters ($M = ah + b$) Relating Torque (M) and Length (h) of Bob Immersed in Fluid to Evaluate End Effect Correction (h_o)

	600 rpm	900 rpm	1100 rpm
a, dyne	61.74	92.48	113.72
b, dyne cm	8.68	14.04	20.67
h_o, cm	0.141	0.152	0.182

3.8.15. Bob Angle for a Mooney-Couette Viscometer

The Mooney-Couette viscometer is a concentric cylinder system constructed so the bob has a conical bottom which almost touches the bottom surface of the cup (Fig. 3.8). If the system is designed so the shear rate in the bottom gap is equal to the shear rate in the annulus, the end effect can be significantly reduced. Determine the bottom angle required to

redesign a concentric cylinder bob so the shear rate in the conical and annular gaps are equal. Also explain how the end effect can be incorporated into the shear stress calculation. Assume the bob under consideration has the following dimensions: $R_c = 21.00$ mm, $R_b = 20.04$ mm, $h = 60.00$ mm.

The Newtonian approximation (Eq. [3.32]) can provide a reasonable estimate of the shear rate in the gap:

$$\dot{\gamma}_b = 2\Omega\left(\frac{\alpha^2}{\alpha^2 - 1}\right)$$

where:

$$\alpha = \frac{R_c}{R_b} = \frac{21.00}{20.04} = 1.048$$

One can solve for the required cone angle by equating the shear rates in the conical section, given by Eq. [3.51], to the shear rate in the gap:

$$\frac{\Omega}{\tan(\theta)} = 2\Omega\left(\frac{\alpha^2}{\alpha^2 - 1}\right)$$

Solving for $\tan(\theta)$ yields

$$\tan(\theta) = \frac{1}{2}\left(\frac{\alpha^2 - 1}{\alpha^2}\right) = \frac{1}{2}\left(\frac{1.048^2 - 1}{1.048^2}\right) = 0.0447$$

so

$$\theta = .0447 \text{ radians } = .0447\left(\frac{360}{2\pi}\right) = 2.56 \text{ degrees}$$

Therefore, making a bob with a bottom angle (Fig. 3.8) of 2.56 degrees will result in an apparatus where the shear rate in the annulus and bottom gap are approximately equal. If the simple shear approximation (Eq. [3.30]) is used in the determination, a slightly larger angle of 2.75 degrees is calculated.

The end effect can be incorporated into the calculation of the shear stress at the bob by finding a numerical value for h_o. When ignoring the end effect, shear stress at bob is given by Eq. [3.3]:

$$\sigma_b = \frac{M}{2\pi h R_b^2}$$

and the shear stress in the conical section is taken from Eq. [3.55] as

$$\sigma = \frac{3M}{2\pi R^3}$$

With the Mooney-Couette sensor the radius of the cone and the bob are equal, $R = R_b$, so the above equation may be written as

$$\sigma = \frac{3M}{2\pi R_b^3} \qquad [3.179]$$

Assuming the shear stress contribution in the conical section can be calculated in terms of h_o, the shear stresses for the bob and the cup can be equated:

$$\frac{M}{2\pi h_o R_b^2} = \frac{3M}{2\pi R_b^3} \qquad [3.180]$$

Solving for the effective height yields

$$h_o = \frac{R_b}{3} \qquad [3.181]$$

Using Eq.]3.181], the overall shear stress in the Mooney-Couette system can be calculated in terms of the effective height:

$$\sigma_b = \frac{M}{2\pi(h + h_o)R_b^2} = \frac{M}{2\pi(h + R_b/3)R_b^2} \qquad [3.182]$$

3.8.16. Viscous Heating

Considering a previous problem (Example Problem 3.8.6) dealing with concentric cylinder data for tomato ketchup, estimate the extent of viscous heating that may occur during data collection.

To consider the worst case, take the highest shear rate given, 664.78 s^{-1}. Also, assume the bob surface is adiabatic and the cup wall is maintained at a constant temperature equal to T_o. Then, the maximum temperature difference found at the surface of the bob may be estimated as (Eq. [3.80])

$$T_{\max} - T_o = \frac{\mu(\dot{\gamma})^2 s^2}{2k}$$

This expression can be evaluated after substituting an apparent viscosity function for the Newtonian viscosity and the size of the annulus for s:

$$T_{\max} - T_o = \frac{K(\dot{\gamma})^{n-1}(\dot{\gamma})^2 (R_c - R_b)^2}{2k}$$

Assuming a thermal conductivity of 0.516 W/(m K) and, using rheological properties determined in Example Problem 3.8.6 (K = 15.73 Pa s^n and n = 0.307), yields

$$T_{\max} - T_o = \frac{15.73(664.78)^{.307-1}(664.78)^2 (.02100 - .02004)^2}{2(.516)} = .069\ ^\circ C$$

A temperature increase of this magnitude will usually have a negligible influence on experimental results.

3.8.17. Cavitation in Concentric Cylinder Systems

Given a concentric cylinder system like the one illustrated in Fig. 3.31 ($R_b = 1.95$ cm, $R_c = 2.00$ cm, $h = 5.00$ cm), what bob speed is required to produce cavitation in 40°C water?

At atmospheric pressure (101.35 kPa), water at 40°C has the following properties: P_{vap} = 7.38 kPa, ρ = 992.2 kg m^{-3}, μ = 0.6529 cP. Considering the cavitation criterion given in Sec 3.5 yields

$$u > \sqrt{\frac{2(P_{atm} - P_{vap})}{\rho}} = \sqrt{\frac{2(101.35 - 7.38)(1000)}{992.2}} = 13.76 \text{ m/s}$$

When u > 13.76 m/s, bob speed is 6738 rpm and cavitation may be present.

In checking the thermodynamic properties of water, one finds that the vapor pressure of water varies from 1.4 kPa at 12°C to 19.9 kPa at 60°C. Therefore, the speed required to achieve cavitation in water is higher at lower temperatures. Minimum speeds required to produce cavitation can be increased in pressurized systems: They will decrease in systems held under a vacuum.

It is interesting to compare the speed required for cavitation and the formation of Taylor vortices. Vortex formation is expected when the inequality expressed by Eq. [3.90] is satisfied:

$$\frac{\Omega R_b (R_c - R_b)\rho}{\mu} > 41.3\sqrt{\frac{R_c}{R_c - R_b}}$$

or

$$\frac{\Omega(.0195)\,(.02-.0195)992.2}{.0006529} > 41.3\sqrt{\frac{.02}{.02-.0195}}$$

$$\Omega > 17.63 \text{ rad/s or } 168.3 \text{ rpm}$$

Meaning that Taylor vortices can be expected when bob speeds exceed 168.3 rpm. In this example, the minimum bob speed required for vortex formation is much lower than the minimum speed needed for the onset of cavitation. It would be unusual to develop cavitation problems when testing food products. In general, the laminar flow assumption would be violated before the onset of cavitation.

3.8.18. Mixer Viscometry

A mixer viscometer was used to determine the rheological properties of a starch-thickened baby food product, strained apricots at 25°C. The material was mixed sufficiently to remove time-dependent effects. Mixer viscometer data were collected using a rotational viscometer equipped with a cup (inside radius = 0.021 m), and Haake pitched-paddle impeller (blade diameter = 0.04143 m, blade height = 0.02692 m) illustrated in Fig. 3.11. Rheological properties (K and n) stated in Table 3.7 were determined using concentric cylinder data, with Eq. [3.3] to calculate shear stress, the Krieger method to calculate shear rate (Eq. [3.47]), and standard statistical methods to evaluate the rheogram.

Questions: Part a. Taking the raw data for corn syrup and various aqueous solutions found in Table 3.7, determine the mixer viscometer constant (k') using the slope method. **Part b.** Using the data for strained apricots given in Table 3.8, calculate the flow behavior index and the consistency coefficient of the product. Compare different methods of evaluation. **Part c.** Using the data for strained apricots (Table 3.8), determine an effective viscosity flow curve for this material which may be used for quality control purposes.

Part a. First, the raw data are manipulated into the appropriate form (Table 3.7) and plotted (Fig. 3.33). Regression analysis of $\log_{10}(P/(K\Omega^{n+1}d^3))$ versus $(1-n)$ as specified in Eq. [3.115],

Table 3.7. Raw (first three columns) and Manipulated Data used to Determine the Mixer Viscometer Constant. [$\Omega = 60$ rpm $= 6.283$ rad/s] Data from: Steffe and Ford (1985)

Fluid	K (Pa s^n)	n (-)	$P = M\Omega$ (N m / s)	$1-n$ (-)	$\frac{P}{K\Omega^{n+1}d^3}$	$\log_{10}\left(\frac{P}{K\Omega^{n+1}d^3}\right)$
2.5%	16.55	0.513	0.0585	0.487	3.0882	0.4897
Hydroxypropyl	15.56	0.520	0.0573	0.480	3.1762	0.5019
Methylcellulose	16.61	0.505	0.0577	0.495	3.0799	0.4885
	15.90	0.513	0.0562	0.487	3.0881	0.4897
2.0%	7.29	0.574	0.0300	0.426	3.2141	0.5071
Hydroxypropyl	6.94	0.586	0.0311	0.414	3.4236	0.5345
Methylcellulose	6.72	0.588	0.0306	0.412	3.4661	0.5398
	7.06	0.576	0.0308	0.424	3.3948	0.5308
1.5%	2.10	0.676	0.0129	0.324	3.9776	0.5996
Hydroxypropyl	2.16	0.672	0.0127	0.328	3.8352	0.5838
Methylcellulose	2.16	0.675	0.0130	0.325	3.9042	0.5915
	2.10	0.680	0.0129	0.320	3.9484	0.5964
1.0%	1.84	0.560	0.0072	0.440	3.1532	0.4988
Hydroxypropyl	1.26	0.605	0.0058	0.395	3.4136	0.5332
Methylcellulose	0.85	0.683	0.0054	0.317	4.0685	0.6094
	1.83	0.504	0.0063	0.496	3.0385	0.4827
Corn Syrup	2.70	1.000	0.0488	0.000	6.4520	0.8097
	2.84	0.992	0.0474	0.008	6.0462	0.7815
	2.64	1.000	0.0482	0.000	6.5175	0.8141
1.5% Guar Gum	30.98	0.158	0.0328	0.842	1.7762	0.2495
	31.65	0.159	0.0339	0.841	1.7936	0.2537
	27.39	0.169	0.0316	0.831	1.8968	0.2780
1.0% Guar Gum	7.28	0.275	0.0113	0.725	2.1002	0.3223
	4.93	0.292	0.0083	0.708	2.2159	0.3455
	7.99	0.266	0.0121	0.734	2.0832	0.3187
	8.62	0.237	0.0123	0.763	2.0704	0.3160
	10.76	0.224	0.0143	0.776	1.9749	0.2955

$$\log_{10}\left(\frac{P}{K\Omega^{n+1}d^3}\right) = \log_{10}(A) - (1-n)\log_{10}(k')$$

gives a good straight line fit ($r^2 = 0.99$) with $\log_{10}A = 0.803$, and a slope equal to -0.6503 meaning that

$$-\log_{10}(k') = -0.6503$$

so

$$k' = 4.47\ rad^{-1}$$

Also since $\log_{10} = 0.803$, $A = 6.35$ rad^{-1}.

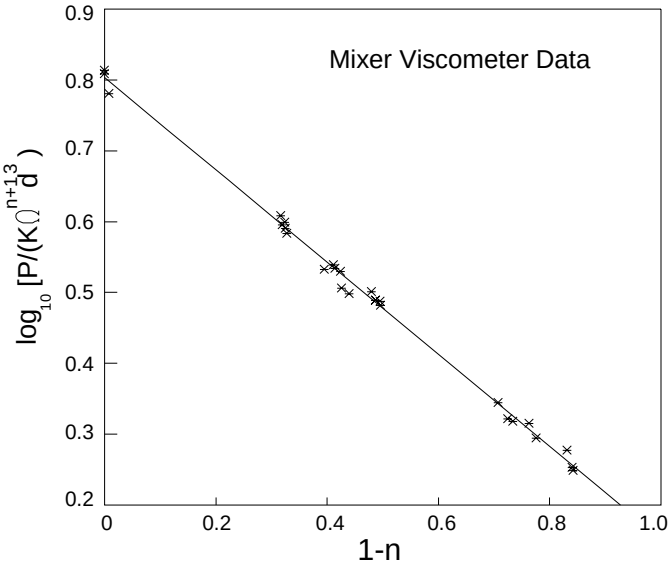

Figure 3.33. Plot of data needed to determine the mixer viscometer constant (k′) using the slope method.

Part b. Raw data are manipulated into the appropriate form (Table 3.8). Evaluation of Eq. [3.121],

$$\log_{10}(M) = \log_{10}(d^3AK(k')^{n-1}) + n\log_{10}(\Omega)$$

using linear regression analysis yields $\log_{10}[d^3AK(k')^{n-1}] = -2.597$ and $n = 0.378$ with $r^2 = 0.99$. K may be found without using the numerical value of A, as K_x, from Eq. [3.125],

$$K_x = K_y\left(\frac{M_x}{M_y}\right)\left(\frac{\Omega_y^{n_y}(k')^{n_y}}{\Omega_x^{n_x}(k')^{n_x}}\right)$$

Taking data at 60 rpm (mid-range value) and the average values of the 1% hydroxypropyl methylcellulose as the known fluid gives: $M_x = 0.00533$

Table 3.8. Raw (first two columns) and Manipulated Mixer Viscometer Data for Strained Apricots at 25°C

Speed (rpm)	Ω (rad/s)	M (N m)	$\log_{10}\Omega$	$\log_{10}M$	η (Pa s)	$\dot{\gamma}_a$ (1/s)	$M\Omega^{-1}d^{-3}$ (Pa s)
20	2.094	0.00332	0.321	-2.479	3.511	9.36	22.30
40	4.189	0.00429	0.622	-2.368	2.268	18.72	14.40
60	6.283	0.00533	0.798	-2.273	1.879	28.09	11.93
80	8.378	0.00556	0.923	-2.255	1.470	37.45	9.33
100	10.47	0.00607	1.020	-2.217	1.284	46.81	8.15
120	12.57	0.00655	1.099	-2.184	1.154	56.17	7.33

N m; $\Omega_x = \Omega_y$ = 6.283 rad/s; n_x = 0.378; k' = 4.47 rad^{-1}; n_y = 0.588; M_y = 0.000984 N m; K_y = 1.45 Pa s^n. Substituting these values into the above equation yields

$$K_x = \frac{(.00533)(1.45)(6.28)^{.588}(4.47)^{.588}}{(.000984)(6.28)^{.378}(4.47)^{.378}} = 15.77 \text{ Pa s}^n$$

Each "standard" or reference fluid used in determining k' gives a slightly different value of K_x. Variations of 5 to 10% have been observed with this method of calculation (Steffe and Ford, 1985).

The consistency coefficient may also be found using the known value of A and the intercept determined from our evaluation of Eq. [3.121]:

$$\log_{10}[d^3AK(k')^{n-1}] = -2.597$$

Substituting known values gives

$$\log_{10}[(.04143)^3(6.35)K(4.47)^{.378-1}] = -2.597$$

which can be solved for the consistency coefficient:

$$K = 14.22 \text{ Pa s}^n$$

This compares reasonably well with the value of 15.77 Pa s^n found previously, and probably gives a more accurate indication of sample behavior.

With a known value of k', power law fluid properties can also be determined by applying the matching viscosity assumption to the raw data. An average apparent viscosity may be found using Eq. [3.116] written as

$$\eta = \frac{d^2\Omega\rho}{A}(N_{Po}) = \frac{d^2\Omega\rho}{A}\left(\frac{M\Omega}{d^5\Omega^3\rho}\right) = \frac{M}{Ad^3\Omega}$$

Since A was found to be 6.35 rad^{-1} and the diameter was given (d = 0.04143 m), apparent viscosity can be directly calculated from the torque:

$$\eta = \frac{M}{6.35(.04143)^3\Omega}$$

The mixer viscometer constant was determined to be 4.47 rad^{-1} so the average shear rate is

$$\dot{\gamma}_a = k'\Omega = 4.47\Omega$$

η and $\dot{\gamma}_a$, evaluated using the above equations, are given in Table 3.8. Assuming power law fluid behavior, these terms are related as

$$\eta = K(\dot{\gamma}_a)^{n-1}$$

or

$$\ln\eta = \ln K + (n-1)\ln\dot{\gamma}_a$$

Regression analysis of the data, using this relationship, yields $n = 0.378$ and $K = 14.22$ Pa s^n. Since η and $\dot{\gamma}_a$ are directly proportional to M and Ω, respectively, results are the same as those found previously. Note that average shear stress could also be calculated as $\eta/\dot{\gamma}_a$, and regression analysis could be preformed on σ_a versus $\dot{\gamma}_a$.

Part c. An effective viscosity can be calculated on the basis of Eq. [3.144]:

$$\eta_{effective} = \frac{M}{\Omega d^3}$$

Numerical values of this term are given in Table 3.8 and plotted as a function of angular velocity in Fig. 3.34. Assuming effective viscosity is directly proportional to apparent viscosity and angular velocity is directly proportional to shear rate, the viscosity may be modeled as a power law function:

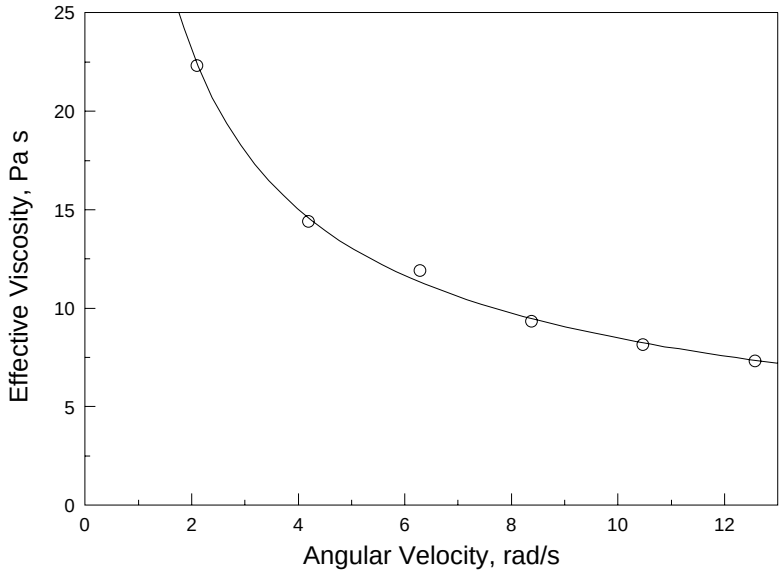

Figure 3.34. Effective viscosity of strained apricots at 25°C determined from mixer viscometry data.

$$\eta_{effective} = K'(\Omega)^{n'-1} \qquad [3.183]$$

where K' may be defined as an effective consistency coefficient (Pa $s^{n'}$) and n' as an effective flow behavior index (dimensionless). Performing a regression analysis on the data gave

$$\eta_{effective} = 35.59(\Omega)^{-.623}$$

meaning K' = 35.59 Pa $s^{n'}$ and n' = 0.378. This expression is plotted as the line displayed in Fig. 3.34. Due to the definition of effective viscosity, the value of K' is unique to the fluid in question with respect to the experimental equipment employed; n', however, is numerically the same as the value of the flow behavior index found in Part b. These results could be compared to those from a reference fluid (product found acceptable in the market place) and used in making quality control decisions in a commercial food processing operation.

3.8.19. Vane Method - Sizing the Viscometer

The vane method will be used to investigate various food products that have yield stresses ranging from 10 to 150 Pa. Vane speed is 0.1 rpm (or as low as possible) and the dimensions of the vane are d = 26.15 mm and h/d = 1.92. It is proposed that one of the following Brookfield viscometers be used for this task (Note, 1 N m = 10^7 dyne cm):

Instrument Model	Full Scale Torque Range (dyne cm)
LV Series	673.7
RV Series	7,187
HAT Series	14,374
HBT Series	57,496

Part a. Determine the feasibility of using one of the above viscometers for the proposed yield stress measurement. **Part b.** Design an appropriate sample container for yield stress measurement and specify the minimum sample size required for conducting each experiment.

Part a. The torque range required to determine the specified yield stresses must be evaluated. Assuming the vane is fully immersed in the sample, and $m = 0$, the peak torque is evaluated from Eq. [3.141] as

$$M_o = \sigma_o\left[\left(\frac{\pi d^3}{2}\right)\left(\frac{h}{d}+\frac{1}{3}\right)\right] = \sigma_o\left[\left(\frac{\pi(.02615)^3}{2}\right)\left(1.92+\frac{1}{3}\right)\right] = 6.329(10^{-5})\sigma_o$$

Therefore the range of maximum torque response will be

$$6.329(10^{-5})\,(10) < M_o < 6.329(10^{-5})\,(150)$$

or

$$6.329(10^{-4})\text{ N m} < M_o < 9.494(10^{-3})\text{ N m}$$

or

$$6,329\text{ dyne cm} < M_o < 94,940\text{ dyne cm}$$

According to the torque capabilities of the instruments, none are sufficient to handle the job. The HBT, which has the maximum torque capacity, can measure a yield stress with the following maximum value:

$$\sigma_o = \left(\frac{57496}{6.329(10^{-5})}\right)10^{-7} = 90.85\text{ Pa}$$

One solution to this problem is to work with Brookfield to "special order" an instrument with a larger spring constant. Alternatively, a smaller vane could be utilized to reduce the torque requirements of the instrument.

Part b. Typical container dimensions, suggested in Sec. [3.7.3] and illustrated in Fig. 3.14, may be calculated from the size of the vane. If $d = 0.02615$ m and $h/d = 1.92$, then $h = 0.05021$ m. The minimum container size can be calculated from this information:

$$D/d \geq 2.0 \text{ so } D \geq 2.0(d) = 0.0523 \text{ m}$$

$$Z_1/d \geq 1.0 \text{ so } Z_1 \geq 1.0(d) = 0.02615 \text{ m}$$

$$Z_2/d \geq 0.5 \text{ so } Z_1 \geq 0.5(d) = 0.01308 \text{ m}$$

With these results, the minimum sample volume may be determined:

$$\text{min. sample } = \pi\left(\frac{D}{2}\right)^2 (z_1 + h + z_2)$$

$$\text{min. sample } = \pi\left(\frac{0.0523}{2}\right)^2 (0.02615 + 0.05021 + 0.01308) = 1.921(10^{-4})\, m^3 = 192.1\, cm^3$$

A minimum sample volume of 192.1 cm^3 is needed to perform the test.

3.8.20. Vane Method to Find Yield Stresses

Calculate the static and dynamic yield stresses, using both the single point and slope methods, with the data for tomato ketchup found in Table 3.9. Data for calculating static yield stresses were collected using undisturbed samples. Dynamic stress data were taken from stirred samples where gentle agitation eliminated the time-dependent structure of the material. Vanes were completely immersed in the sample following the guidelines for vane and vessel dimensions given in Sec. 3.3.7 and summarized in the previous example problem.

Eq. [3.141] is needed to calculate the yield stress using the single point method:

Table 3.9. Raw Data, and Yield Stresses, for Tomato Ketchup at 21 °C Taken with a Brookfield Viscometer Having a Full Scale Torque of 0.00575 N m Using a Vane with 4 Blades having a Diameter of 2.5 cm.

Stress	Torque (% total)	Torque (N m)	Vane Height (cm)	Yield Stress[1] (Pa)
Static	30.00	0.00173	5.0	30.12
Static	29.25	0.00168	5.0	29.37
Static	27.50	0.00158	5.0	27.61
Static	26.00	0.00150	5.0	26.11
Static	34.00	0.00196	6.6	26.79
Static	37.25	0.00214	6.6	29.35
Static	38.00	0.00219	6.6	29.94
Static	47.50	0.00273	9.0	28.29
Static	48.00	0.00276	9.0	28.59
Static	48.75	0.00280	9.0	29.04
			Average	28.52
			SDEV	1.33
Dynamic	22.50	0.00129	5.0	22.59
Dynamic	22.50	0.00129	5.0	22.59
Dynamic	21.00	0.00121	5.0	21.08
Dynamic	20.00	0.00115	5.0	20.08
Dynamic	25.33	0.00146	6.6	19.96
Dynamic	26.50	0.00152	6.6	20.87
Dynamic	27.50	0.00158	6.6	21.67
Dynamic	37.00	0.00213	9.0	22.04
Dynamic	35.00	0.00201	9.0	20.85
Dynamic	36.00	0.00207	9.0	21.44
Dynamic	34.75	0.00200	9.0	20.70
			Average	21.26
			SDEV	0.90

[1] Yield Stress calculated by the single point method, Eq. [3.141].

$$\sigma_o = \frac{2M_o}{\pi d^3}\left(\frac{h}{d} + \frac{1}{m+3}\right)^{-1}$$

Assuming $m = 0$, this expression can be reduced to

$$\sigma_o = \frac{6M_o}{\pi d^2(3h + d)}$$

A typical calculation can be used to illustrate the method. If, for example (see first data line, Table 3.9), $M_o = 0.3(0.00575) = 0.00173\,N\,m$, $d = 0.025\,m$, and $h = 0.050\,m$, then $\sigma_o = 30.12\,Pa$. Results for each trial, as well as average values, are given in Table 3.9.

Eq. [3.137] is required to calculate the yield stress using the slope method:

$$M_o = \frac{\pi h d^2}{2}\sigma_o + 4\pi \int_0^{d/2} r^2 \sigma_e \, dr$$

Noting that the integral term is constant, M_o versus h may be plotted as

$$M_o = a\,h + constant \qquad [3.184]$$

The slope (a) of the best fitting line through the data points will include the yield stress:

$$a = \frac{\pi d^2 \sigma_o}{2} \qquad [3.185]$$

therefore,

$$\sigma_o = \frac{2a}{\pi d^2} \qquad [3.186]$$

This technique must be performed separately for static and dynamic data sets. Data are plotted (Fig. 3.35), and slopes are found from a standard linear regression program, allowing the static and dynamic yield stresses to be calculated from Eq. [3.186]:

$$(\sigma_o)_{\text{static}} = \frac{2a}{\pi d^2} = \frac{2(0.0285)}{\pi(0.025)^2} = 29.03\,Pa$$

and

$$(\sigma_o)_{\text{dynamic}} = \frac{2a}{\pi d^2} = \frac{2(0.0205)}{\pi(0.025)^2} = 20.88\,Pa$$

Reasonably good agreement was found between yield stresses calculated using the slope and single point methods (Table 3.10). Single point yield stresses are averaged values taken from Table 3.9.

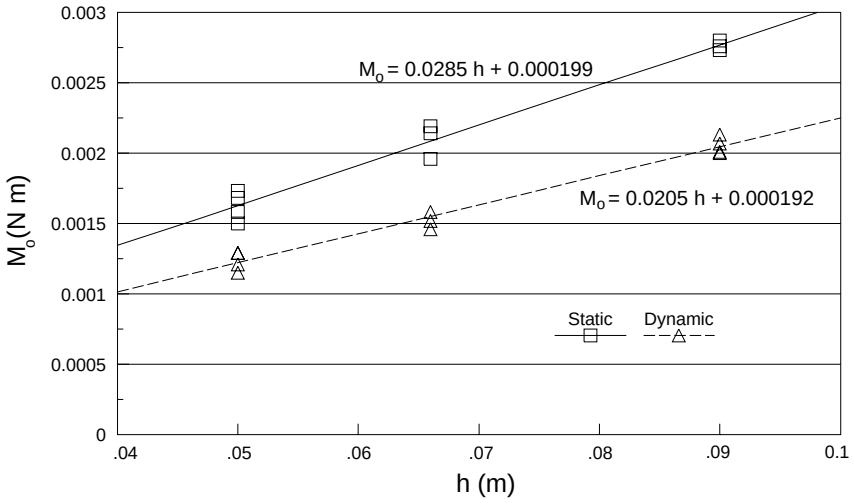

Figure 3.35. Plot of the raw data needed to determine the yield stress using the slope method.

Table 3.10. Comparison of Yield Stresses Calculated for Tomato Ketchup at 21 °C.

Method	Static Yield Stress (Pa)	Dynamic Yield Stress (Pa)
Single Point	28.52	21.26
Slope	29.03	20.88

3.8.21. Vane Rotation in Yield Stress Calculation

Typical data, for undisturbed tomato ketchup at 23°C, collected to determine the yield stress using the vane method, are illustrated in Fig. 3.36 and 3.37. The data in each figure are taken with two instruments having different wind-up characteristics: the Brookfield uses a coiled spring and the Haake instrument uses a torsion bar type system (Fig. 3.19). Both systems have rotating vanes and stationary sample holders. Given the characteristics of each instrument (Table 3.11), determine the amount of vane rotation (Fig. 3.38) which has occurred between the start of the test and the time the peak torque value (M_o) is observed.

Also, compare yield stresses calculated from each curve (Fig. 3.36 and Fig. 3.37) using the single point method.

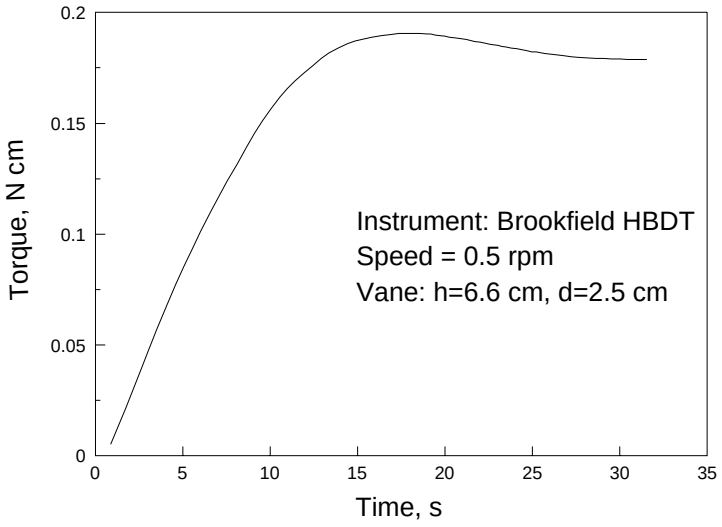

Figure 3.36. Torque response for 23°C ketchup obtained using the Brookfield HBDT viscometer and a vane with 4 blades.

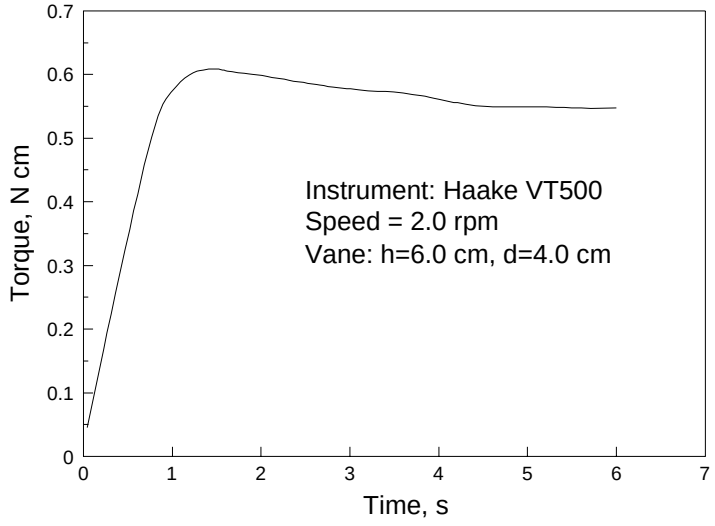

Figure 3.37. Torque response for 23°C ketchup obtained using the Haake VT500 viscometer and a vane with 4 blades.

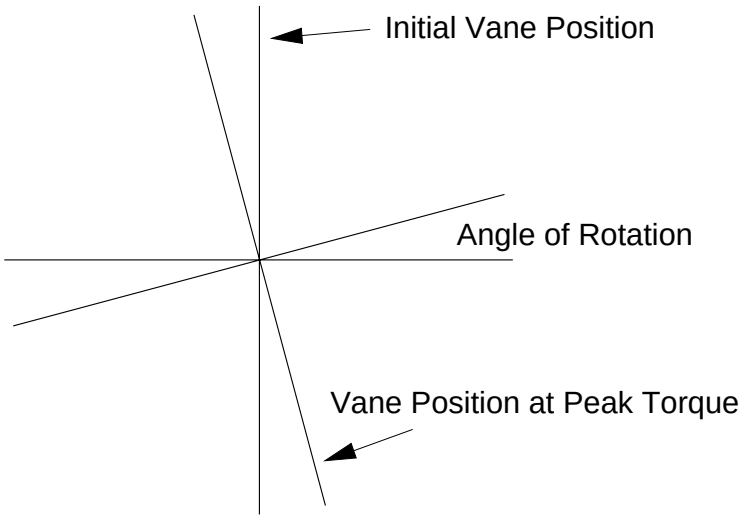

Figure 3.38. Movement of a 4-bladed vane during yield stress testing.

Table 3.11. Vane Rotation Data and Instrument Characteristics for Two Viscometers.

	Haake VT500	Brookfield HBDT
Vane height (h), cm	6.0	6.6
Vane diameter (d), cm	4.0	2.5
Full Scale Torque, N cm	2.0	0.575
Full Scale Wind-up, degree	1.0	80
Time to Peak Torque, s	1.3	18
Peak Torque (M_o), N cm	0.605	0.184
Test Speed, rev/min (degree/sec)	2 (12)	0.5 (3.0)
Zero-Load Rotation at Peak Torque, degree	15.6	54.0
Wind-up at Peak Torque, degree	0.3	25.6
Actual Rotation at Peak Torque, degree	15.3	28.4
Yield Stress (σ_o) from Eq. [3.141], Pa	32.8	28.4

The maximum torque measured in the VT500 test was 0.605 N cm. Since the full scale torque of this instrument is 2 N cm and the full scale wind-up is 1 degree, the wind-up in this experiment was approximately 0.605 (1) / 2 = 0.3 degrees. The test was run with an impeller speed of 2 rpm or 12 degrees /s. Taking the time to achieve peak torque as 1.3 s means that an unrestricted impeller would travel 1.3 (12) = 15.6 degrees. This is referred to as the zero-load rotation. After accounting for wind-up, the actual VT500 vane rotation can be calculated as 15.6-0.3 = 15.3 degrees. The comparable value for the Brookfield is 28.4 degrees (Table 3.11).

Static yield stresses were calculated using Eq. [3.141] with the assumption that $m = 0$. The value measured with the Brookfield (σ_o = 25.1 Pa) is lower than the value measured by the VT500 (σ_o = 32.8 Pa). This is due, in part, to the different wind-up characteristics of each viscometer: At full scale torque, the VT500 wind-up is 1 degree and the Brookfield wind-up is approximately 80 degrees. The combination of vane speed and wind-up caused a greater amount of vane rotation in the Brookfield during testing. This produced greater fluid motion which subsequently reduced peak torque values. Differences in the wind-up characteristics of rotational viscometers should always be taken into consideration when evaluating yield stresses determined using the vane method. These differences may be particularly important when the yield stresses under consideration exhibit strong time-dependent behavior.

3.8.22. Rheomalaxis from Mixer Viscometer Data

Torque decay data for starch thickened strained apricots were collected at various angular velocities (Table 3.12, Fig. 3.39). The material was rheomalactic, i.e., no structural recovery was evident in a reasonable period of time (three hours). Evaluate the relative degree of irreversible thixotropy in this material by calculating the area between the initial and equilibrium torque curves. Also determine the energy input to the sample when the impeller is rotated at 3.14 rad/s for approximately 10 minutes. (Note: data in Table 3.12 could also be used to evaluate the parameters in the thixotropy model given by Eq. [1.36].)

Initial and equilibrium torque values, obtained from the raw data, are plotted on Fig. 3.40 and summarized in Table 3.13. Fitting these curves to a power equation (any equation which adequately fits the data would be acceptable) yields:

Table 3.12. Torque Decay Data for Starch Thickened, Strained Apricots at 22°C Collected with a Rotational Viscometer using a Cup (R_c=21.00 mm) and Pitched Paddle Impeller (Fig. 3.11)

	Torque, N m				
Time (min.)	1.05 rad/s	1.57 rad/s	2.09 rad/s	2.62 rad/s	3.14 rad/s
0.42	0.00301	0.00324	0.00369	0.00404	0.00424
1.223	0.00259	0.00292	0.00324	0.00348	0.00369
2.023	0.00240	0.00280	0.00310	0.00330	0.00354
2.821	0.00238	0.00272	0.00299	0.00322	0.00340
3.623	0.00230	0.00266	0.00293	0.00312	0.00332
4.421	0.00224	0.00260	0.00287	0.00306	0.00326
5.223	0.00219	0.00255	0.00284	0.00303	0.00321
6.023	0.00214	0.00251	0.00279	0.00298	0.00315
6.821	0.00210	0.00245	0.00273	0.00294	0.00311
7.623	0.00205	0.00242	0.00270	0.00292	0.00309
8.421	0.00201	0.00238	0.00267	0.00287	0.00304
9.223	0.00198	0.00237	0.00265	0.00286	0.00301
10.02	0.00194	0.00234	0.00262	0.00282	0.00298
10.83	0.00192	0.00230	0.00260	0.00280	0.00297
11.63	0.00190	0.00228	0.00258	0.00277	0.00295
12.43	0.00188	0.00227	0.00255	0.00275	0.00293
13.23	0.00186	0.00224	0.00254	0.00273	0.00289
14.03	0.00184	0.00223	0.00253	0.00270	0.00288
14.83	0.00182	0.00220	0.00250	0.00269	0.00286
15.63	0.00180	0.00218	0.00248	0.00267	0.00286

$$M_{initial} = .00290(\Omega)^{.33}$$

and

$$M_{equilibrium} = .00179(\Omega)^{.42}$$

The area between the two curves is found from Eq. [3.143]:

$$\Delta = \int_{\Omega_{low}}^{\Omega_{high}} [M_{initial} - M_{equlibrium}] d\Omega$$

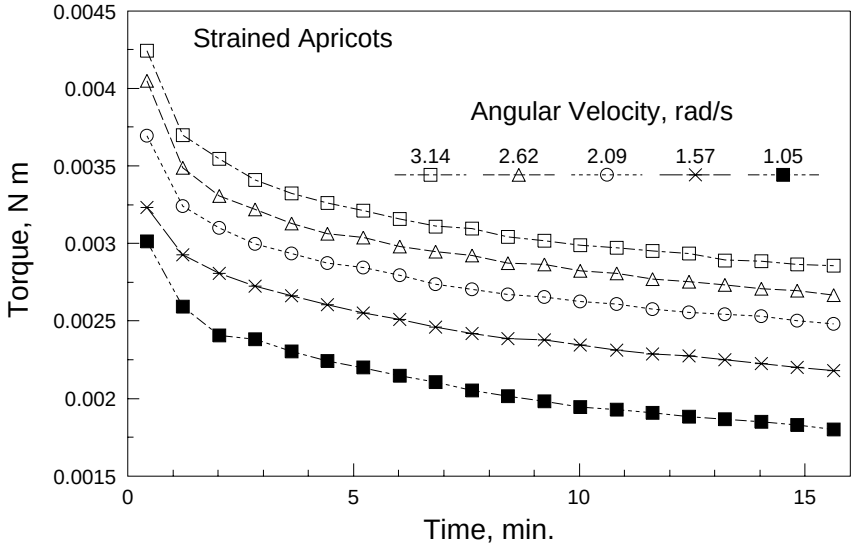

Figure 3.39. Torque decay data for strained apricots at 22 °C.

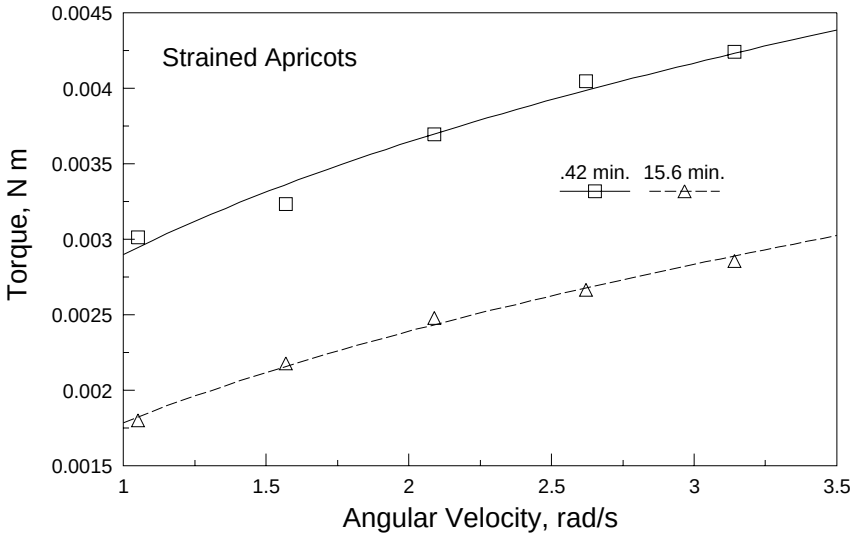

Figure 3.40. "Initial" and "equilibrium" torque curves for apricots at 22 °C.

Evaluating the integral with the appropriate torque curves and limits yields

$$\Delta = \int_{\Omega=1.05}^{\Omega=3.14} (.00290(\Omega)^{.33} - .00179(\Omega)^{.42}) d\Omega = .00261\ N\ m\ s^{-1}$$

Δ is a relative measure of thixotropy; when none is present $\Delta = 0$.

Table 3.13. "Initial" and "Equilibrium" Torque values, for Strained Apricots, at Different Angular Velocities

	Torque, N m	
Ω (rad/s)	"Initial" (after 0.42 min.)	"Equilibrium" (after 15.6 min.)
1.05	.00301	.00180
1.57	.00324	.00218
2.09	.00369	.00248
2.62	.00404	.00267
3.14	.00424	.00286

Torque decay curves also provide a practical way of evaluating thixotropy by considering the energy input to the sample. Data (Table 3.12) taken at an impeller angular velocity of 3.14 rad/s may be replotted in terms of power ($P = M\Omega$) versus time. The area under the resulting power decay curve (Fig. 3.41) represents the mechanical energy input to the sample.

The power decay data were fit to a simple mathematical model yielding

$$P = .0186(t)^{-.108}$$

which is the line plotted on Fig. 3.41. The exponent in this equation is an index of thixotropy: More negative values indicate a rapid rate of structural breakdown, and a value of zero means the sample is not time-dependent. Using the above equation, the energy input over the period of time (Table 3.12) under consideration (t = 0.42 min = 25.2 s to t = 10.02 min = 601.2 s) is easily calculated:

$$\text{Energy Input} = \int_{t=25.2}^{t=601.2} .0186(t)^{-.108} dt = 5.91\ \text{N m}$$

In contrast, if there was no thixotropy, the energy required to maintain Ω = 3.14 rad/s over the same time would be approximately 0.00424(3.14)(601.2 - 25.2) = 7.67 N m. This calculation assumes the power level is constant and equal to the initial value when no time-dependent behavior is present.

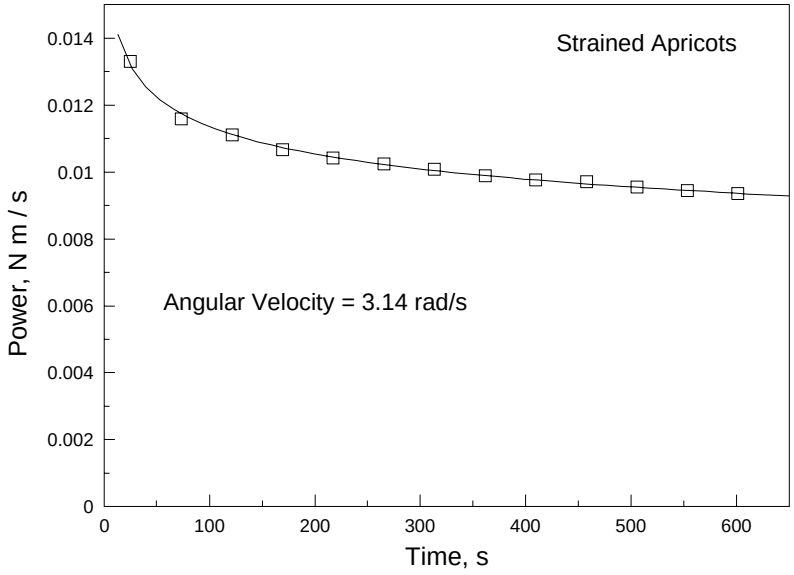

Figure 3.41. Power decay curves obtained for strained apricots at 22°C with a constant impeller velocity of 3.14 rad/s.

Torque or power decay data curves can provide a useful measure of thixotropy. Results depend on the particular mixing system and sample volume used in the study. These factors must be kept constant to make meaningful sample to sample comparisons. Temperature is also a significant factor which should be carefully controlled during testing.

Chapter 4. Extensional Flow

4.1. Introduction

A basic knowledge of extensional viscosity is essential for understanding many flow situations found in the food industry. The three basic types of extensional flow - uniaxial, biaxial, and planar - along with numerous applications of extensional deformation are described in Section 1.7. Experimental methods to determine extensional viscosity are discussed in this chapter. Techniques involving tension (stretching or pulling), squeezing flow (flow between parallel plates being pushed together), converging flow into a die, flow into opposing jets, spinning, and the tubeless siphon phenomenon (Fano flow) are presented. In addition, alternative interpretations of squeezing flow data are considered because of the relative ease with which this experiment can be conducted in a laboratory. Biaxial extension, produced by lubricated squeezing flow, is considered in terms of steady shear properties (Sec. 4.8.1). Similar considerations are made in the case of non-lubricated squeezing flow (Sec. 4.8.2) which generates a combined shear and extensional deformation.

4.2. Uniaxial Extension

Consider the uniaxial extension (Fig. 1.24) of a material where one end is stationary and the other end is moving at some velocity, u_1. This can be accomplished experimentally if one end is fixed (by gluing or clamping) and the other end is pulled by a moving clamp, wrapping it around a rod, or pulling it between rotating gears. The differential Hencky strain (Eq. [1.2]: $\varepsilon_h = \ln(L/L_o)$) describing displacement is

$$d\varepsilon_h = \frac{dL}{L} \qquad [4.1]$$

and the strain rate is

$$\dot{\varepsilon}_h = \frac{d\varepsilon_h}{dt} = \frac{1}{L}\frac{dL}{dt} \qquad [4.2]$$

Since dL/dt is the velocity at the end of the sample, the strain rate can be expressed as

$$\dot{\varepsilon}_h = \frac{u_1}{L} \qquad [4.3]$$

If the velocity is held constant ($u_1 = u_o$) during experimentation, then the strain rate would continually decrease during elongation due to increasing values of L. At very low speeds, a constant velocity test may approximate a constant strain rate; however, to maintain a truly constant value of the strain rate, the velocity of the moving end of the sample must be increased during testing.

Integrating Eq. [4.2] for a constant strain rate ($\dot{\varepsilon}_{ho}$), using L_o as the initial sample length, gives

$$\int_0^t \dot{\varepsilon}_{ho} dt = \int_{L_o}^{L} \frac{dL}{L} \qquad [4.4]$$

resulting in the following expression for L as a function of time:

$$L = f(t) = L_o \exp(\dot{\varepsilon}_{ho} t) \qquad [4.5]$$

To produce a constant strain rate, Eq. [4.3] shows that $L = u_1/\dot{\varepsilon}_{ho}$. Combining this expression and Eq. [4.5] demonstrates that the velocity at the moving end of the sample must exponentially increase over time to maintain a constant strain rate:

$$u_1 = f(t) = \dot{\varepsilon}_{ho} L_o \exp(\dot{\varepsilon}_{ho} t) \qquad [4.6]$$

Assuming the material is incompressible, the volume is constant so

$$AL = A_o L_o \qquad [4.7]$$

where A_o is the initial crossectional area. Combining Eq. [4.5] and [4.7] shows the crossectional area of the sample must decrease exponentially during testing as a consequence of the exponential change in length:

$$A = f(t) = A_o \exp(-\dot{\varepsilon}_{ho} t) \qquad [4.8]$$

The normal stress difference over the material defines the net tensile stress:

$$\sigma_E = \sigma_{11} - \sigma_{22} = \frac{F}{A} \qquad [4.9]$$

F is the force required to stretch the sample. Using Eq. [4.7], the stretching stress can be expressed as

$$\sigma_E = \frac{FL}{A_o L_o} \qquad [4.10]$$

In an ideal stretching experiment the strain is increased to a constant value (ε_{ho}) instantaneously:

$$\dot{\varepsilon}_h = \dot{\varepsilon}_{ho} \quad \text{for} \quad t \geq 0 \qquad [4.11]$$

which establishes the velocity function described by Eq. [4.6]. The force ($F(t)$) required to maintain $\dot{\varepsilon}_{ho}$ is experimentally determined during testing. Results may be presented in terms of the tensile growth function defined by combining Eq. [4.5] and [4.10]:

$$\eta_E^+ = f(\dot{\varepsilon}_{ho}, t) = \frac{\sigma_E}{\dot{\varepsilon}_{ho}} = \frac{FL}{A_o L_o \dot{\varepsilon}_{ho}} = \frac{F \exp(\dot{\varepsilon}_{ho} t)}{A_o \dot{\varepsilon}_{ho}} \qquad [4.12]$$

The stress growth function becomes equal to the tensile viscosity as time goes to infinity and a constant value of the stress (σ_E) is obtained:

$$\eta_E = \lim_{t \to \infty} \eta_E^+ \qquad [4.13]$$

where $\eta_E = f(\dot{\varepsilon}_{ho})$ and $\eta_E^+ = f(\dot{\varepsilon}_{ho}, t)$. Bagley and Christianson (1988) have noted that this limit may not be observed over experimentally practical time periods.

Meissner (1972) devised a method of achieving a constant strain rate in polymer melts using a device (Fig. 4.1) consisting of two sets of counter rotating gears moving at constant speeds. The strain rate is related to the constant sample velocities, in opposite directions (u_a and u_b), located a constant distance (L_o) apart:

$$\dot{\varepsilon}_{ho} = \frac{u_a + u_b}{L_o} \qquad [4.14]$$

Constant velocities can be used because the sample length is constant. The tensile force, required to maintain a constant strain rate, is measured during testing and used to calculate the stretching stress. Extensional viscosity is determined from Eq. [4.12]. In the original device (Meissner, 1972), samples were supported in a silicone oil bath. Rheometrics, Inc. (Piscataway, NJ), introduced a commercial version of this instrument, intended for polymer melts, which uses an inert gas to support the sample.

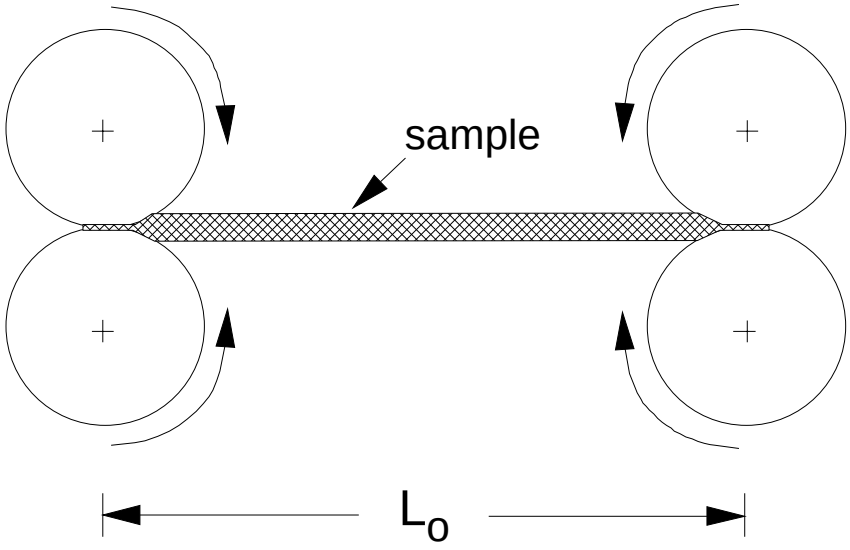

Figure 4.1. Counter rotating clamps, based on the design of Meissner (1972), to achieve a constant strain rate in uniaxial extension.

4.3. Biaxial Extension

Biaxial extension can be achieved in a lubricated squeezing flow between parallel plates. Fig. 4.2 illustrates the normal case where the lower plate is fixed and the upper plate moves vertically downward. During squeezing, the cylindrical shape is maintained while the area in contact with the plate increases as the height of the sample decreases. Test samples are lubricated with a lower viscosity liquid.

The importance of proper lubrication cannot be underestimated. Unlubricated samples require more force to achieve deformation than that required for lubricated samples (Christianson et al., 1985). This is even true in food materials, such as butter (Fig. 4.3), that have a high fat content and may appear to be self-lubricating. The extra force is needed to overcome the friction introduced by the shear deformation that occurs in unlubricated testing. Perfectly lubricated samples experience only extensional deformation.

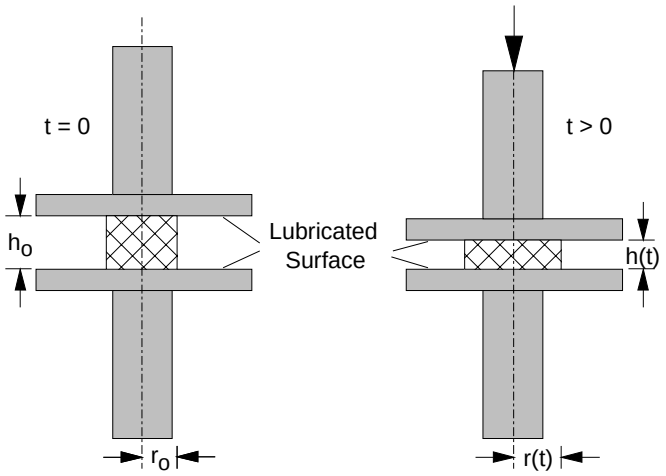

Figure 4.2. Flow between lubricated parallel plates to create sample deformation in biaxial extension.

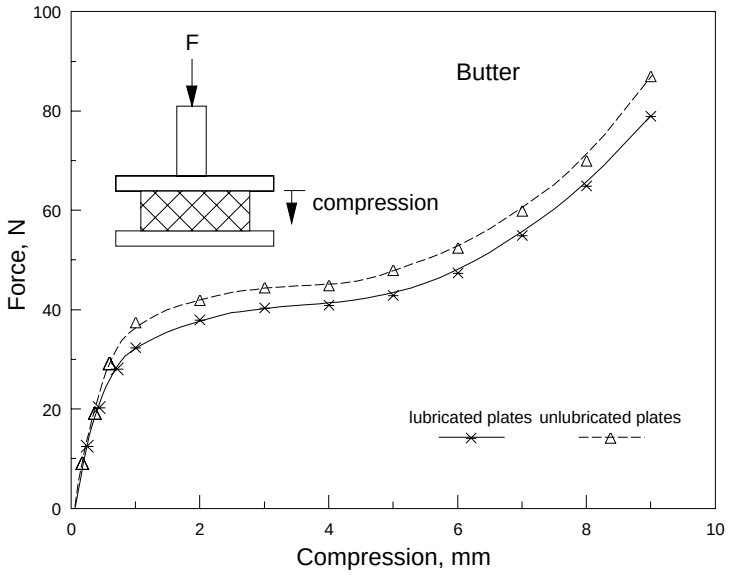

Figure 4.3. Force versus compression for lubricated and unlubricated squeezing flow of butter at 15°C: h_o = 15 mm, R_o = 14mm, u_z = 100 mm/min. (Data from Rohm, 1993))

The velocity distribution in biaxial extension can be expressed in terms of Hencky strain as

$$u_z = -2\dot{\varepsilon}_B z = -\dot{\varepsilon}_h z \qquad [4.15]$$

$$u_r = \dot{\varepsilon}_B r = \frac{\dot{\varepsilon}_h r}{2} \qquad [4.16]$$

$$u_\theta = 0 \qquad [4.17]$$

where $\dot{\varepsilon}_B = \dot{\varepsilon}_h/2$. These equations are a slightly modified version of Eq. [1.67], [1.68] and [1.69]. Compressive strain in the vertical direction is

$$d\varepsilon_h = -\frac{dh}{h} \qquad [4.18]$$

where $h = f(t)$, the height separating the plates. The strain rate is

$$\dot{\varepsilon}_h = \frac{d\varepsilon_h}{dt} = \left(-\frac{1}{h}\right)\frac{dh}{dt} \qquad [4.19]$$

To produce a constant strain rate during experimentation, the velocity of the moving plate must decrease as the plates approach each other. Following the same procedure given for uniaxial extension, the strain rate equation describing vertical motion (Eq. [4.19]) can be integrated to give

$$\int_0^t -\dot{\varepsilon}_{ho}\,dt = \int_{h_o}^{h} \frac{dh}{h} \qquad [4.20]$$

or

$$h = f(t) = h_o \exp(-\dot{\varepsilon}_{ho} t) \qquad [4.21]$$

where h_o is the initial sample thickness. Eq. [4.21] shows that the distance separating the plates must exponentially decrease over time. Assuming the material is incompressible and the volume is constant yields:

$$Ah = A_o h_o \qquad [4.22]$$

where A_o is the initial area of the sample in contact with one plate.

Biaxial strain is instantaneously increased to a constant value ($\dot{\varepsilon}_{Bo}$) in an ideal experiment:

$$\dot{\varepsilon}_B = \dot{\varepsilon}_{Bo} \quad \text{for} \quad t \geq 0 \qquad [4.23]$$

which determines the plate spacing requirements specified by Eq. [4.21]. Biaxial stress (radial net stretching stress) is determined from the squeezing force ($F = f(t)$) which is measured during testing:

$$\sigma_B = \sigma_{rr} - \sigma_{zz} = \frac{F}{A} = \frac{Fh}{A_o h_o} \qquad [4.24]$$

A biaxial extensional growth function is defined by combining Eq. [4.21] and Eq. [4.24]

$$\eta_B^+ = f(\dot{\varepsilon}_{Bo}, t) = \frac{\sigma_B}{\dot{\varepsilon}_{Bo}} = \frac{2F \exp(-\dot{\varepsilon}_{ho} t)}{A_o \dot{\varepsilon}_{ho}} = \frac{F \exp(-2\dot{\varepsilon}_{Bo} t)}{A_o \dot{\varepsilon}_{Bo}} \qquad [4.25]$$

The stress growth function becomes equal to the biaxial extensional viscosity as time goes to infinity and a constant value of the net stretching stress (σ_B) is obtained:

$$\eta_B = \lim_{t \to \infty} \eta_B^+ \qquad [4.26]$$

where $\eta_B = f(\dot{\varepsilon}_{Bo})$ and $\eta_B^+ = f(\dot{\varepsilon}_{Bo}, t)$. Obtaining steady-state conditions during experimentation may be difficult. Comparing growth functions (Eq. [4.25]) alone may be sufficient to distinguish food samples.

If the lubricated squeezing flow experiment is operated so the downward velocity of the upper plate is constant and the bottom plate is fixed (the common mode of operation in testing equipment such as the Instron Universal Testing Machine), then sample height decreases linearly:

$$h = f(t) = h_o - u_z t \qquad [4.27]$$

The biaxial extensional strain rate (also called the radial extension rate) is equal to one-half the vertical Hencky strain rate:

$$\dot{\varepsilon}_B = \left(\frac{1}{2}\right)\dot{\varepsilon}_h = \left(-\frac{1}{2h}\right)\frac{dh}{dt} = \frac{u_z}{2(h_o - u_z t)} \qquad [4.28]$$

Extensional viscosity is calculated from the net stretching stress and the strain rate:

$$\eta_B = f(t) = \frac{\sigma_B}{\dot{\varepsilon}_B} = \frac{\sigma_B 2(h_o - u_z t)}{u_z} \qquad [4.29]$$

σ_B is obtained from one of the following equations depending on the degree of fill between the plates during testing:

$$\sigma_B = \frac{F}{\pi r^2} \qquad \text{(partially full gap where } r \le R\text{)} \qquad [4.30]$$

or

$$\sigma_B = \frac{F}{\pi R^2} \qquad \text{(full gap)} \qquad [4.31]$$

where r is the radius of the sample, R is the radius of the plate, and F is the experimentally determined force pushing down on the upper plate. When the gap is filling with an incompressible material, the sample volume is constant making $\pi R_o^2 h_o = \pi r^2 h$. This expression can be solved for πr^2 allowing Eq. [4.30] to be calculated in terms of h:

$$\sigma_B = \frac{Fh}{\pi R_o^2 h_o} \quad \text{for } r \le R \qquad \text{(partially full gap)} \qquad [4.32]$$

where R_o is the initial radius of the sample.

High levels of strain can result in loss of lubrication between plates, and subsequent introduction of shear flow into the experiment. The maximum strain can be calculated as

$$(\varepsilon_B)_{\max} = -\frac{1}{2}\ln\left(\frac{h}{h_o}\right) \qquad [4.33]$$

According to Macosko (1994), loss of lubrication is typical when the maximum strain is near 1.0. Macosko (1994) also notes that the decrease in lubricant thickness (δ) is approximately equal to the square of root of the gap:

$$\frac{\delta}{\delta_o} = \sqrt{\frac{h}{h_o}} \qquad [4.34]$$

where δ_o is the initial thickness of the lubricant. Furthermore, he recommends (based on Secor, 1988) the following criterion for lubrication:

$$\frac{2\delta}{h} < \frac{\mu_L R^2}{\mu \delta^2} < 20 \qquad [4.35]$$

where μ_L and μ are the Newtonian shear viscosities of the lubricant and test sample, respectively. These results give us valuable insight into the lubrication problem. Unfortunately, they are not directly applicable to the biaxial extension of non-Newtonian foods. Experimental conditions used in lubricated squeezing flow of some food materials are summarized in Table 4.1.

Typical data analysis of biaxial extensional flow, for the case where the bottom plate is fixed and the upper plate moves downward at a constant velocity, is discussed in Example Problems 4.9.1. Results show a typical change (sharp increase followed by a gradual decrease) in extensional viscosity with strain rate. Example Problem 4.9.2 illustrates how results from individual tests, such as the one given in Example 4.9.1, can be combined to examine the tension-thinning (or tension-thickening) characteristics of a sample.

Table 4.1. Product, Initial Sample Size, Lubricant, and Test Conditions used to Determine Biaxial Extensional Viscosity in Lubricated Squeezing Flow

Product	h_o (cm)	R_o (cm)	lubricant	u_z (cm/min)	Reference
butter	1.5	2.80	paraffin oil[1]	0.1,1.0,10	Rohm, 1993
butter	1.0	3.67	cooking oil[2]	0.05	Shukla et al., 1995
starch gels	1.2-4.0	3.85	paraffin oil[3]	0.5	Christianson et al., 1985
cheese	2.0-4.0	2.85	paraffin oil[3]	0.5 - 5.0	Casiraghi et al., 1985
cheese		3.18	silicone oil[4]	1.0	Campanella et al., 1987
wheat dough	2.0	3.1	paraffin oil[3]	0.2 - 5.0	Bagley and Christianson, 1986
wheat dough	0.54-1.92	5.72-8.0	Super Lube[5]	constant stress	Huang and Kokini, 1993

[1] Merck 7174; $\mu \leq 70$ mPa s at 20°C; [2] PAM, American Home Foods; [3] USP/TCC white, light. Fisher Scientific Co.; [4] Dow Corning 500; [5] Super Lube, Inc., Bohemia, NY

4.4. Flow Through a Converging Die

Flow into a convergence involves an energy loss due to shear and an additional loss due to the extension (stretching) of fluid streamlines. Converging flow is sometimes called uncontrolled flow because fluid streamlines are a function of fluid properties. It is also not pure extensional flow because it involves a combination of both shear and extensional deformation. Analyses described here are based on separating the entrance pressure drop into two components: one due to shear and the other due to extension. An alternative method, called the sink flow analysis based on the work of Metzner and Metzner (1970), assumes

pure (no shear) extensional flow. This method requires knowledge of an angle of convergence typically found from flow visualization. Another technique, involving energy principles, has been developed by Binding (1988).

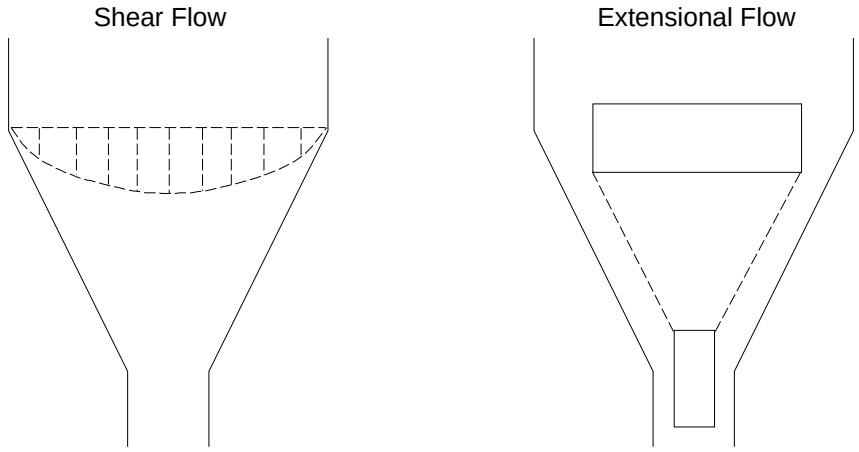

Figure 4.4. Shear (showing velocity profile) and extensional flow components causing pressure drop in a convergence.

4.4.1. Cogswell's Equations

Cogswell (1972) assumed the entry pressure drop over an area of converging flow, from a circular barrel into a capillary die, was made up of two components, one related to shear flow and one related to extensional flow (Fig. 4.4):

$$\delta P_{en} = \delta P_{en,S} + \delta P_{en,E} \qquad [4.36]$$

This flow situation could be referred to as unlubricated, constrained convergence (Cogswell, 1978). It is assumed that no slip occurs at the wall.

The pressure drop due to shear can be derived by considering the differential pressure drop (based on the power law form of the flow rate equation, Eq. [2.31]) over the length *dl* at radius *r* (Fig. 4.5):

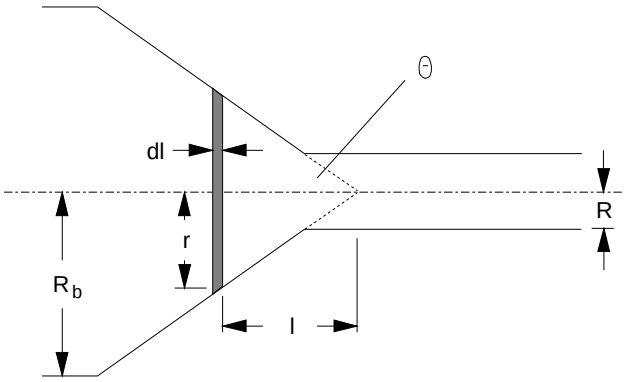

Figure 4.5. Geometry for converging flow from a barrel of radius R_b into a capillary die of radius R.

$$d(\delta P_{en,S}) = \frac{Q^n}{r^{3n+1}}\left(\frac{3n+1}{\pi n}\right)^n 2K\,dl \qquad [4.37]$$

Since $r/l = \tan\theta$, $dl = dr/\tan\theta$. Substituting this equation into Eq. [4.37] yields

$$d(\delta P_{en,S}) = \frac{Q^n}{r^{3n+1}}\left(\frac{3n+1}{\pi n}\right)^n \frac{2K}{\tan\theta}\,dr \qquad [4.38]$$

which must be integrated between the die and the barrel:

$$\int_0^{\delta P_{en,S}} d(\delta P_{en,S}) = \int_R^{R_b} \frac{Q^n}{r^{3n+1}}\left(\frac{3n+1}{\pi n}\right)^n \frac{2K}{\tan\theta}\,dr \qquad [4.39]$$

Evaluating the integral and simplifying the result yields the component of the pressure drop in the convergence due to shear flow:

$$\delta P_{en,S} = \Gamma^n\left(\frac{3n+1}{4n}\right)^n \frac{2K}{3n\tan\theta}\left(1-\left(\frac{R}{R_b}\right)^{3n}\right) \qquad [4.40]$$

where $\Gamma = 4Q/(\pi R^3)$, the apparent wall shear rate in the die.

The volumetric average velocity at any particular crossection of the die is

$$\bar{u} = \frac{Q}{\pi r^2} = \frac{Q}{\pi l^2 \tan^2 \theta} \qquad [4.41]$$

Eq. [4.41] may be differentiated to give the average extensional strain rate at each crossection:

$$\dot{\varepsilon}_E = -\left(\frac{d\bar{u}}{dl} \right) = \frac{-(-2Q)}{\pi l^3 \tan^2 \theta} = \frac{2Q \tan \theta}{\pi r^3} \qquad [4.42]$$

Unlike the shear rate, this expression does not depend on the form of the velocity profile. The differential pressure drop, due to the dissipation of extensional energy, may be written in terms of an average extensional stress acting on an annulus:

$$(d\delta P_{en,E})\pi r^2 = \sigma_E(\pi(r + dr)^2 - \pi r^2) \qquad [4.43]$$

or, recognizing that $(dr)^2$ is negligible, Eq. [4.43] is simply

$$d(\delta P_{en,E}) = 2\sigma_E \frac{dr}{r} \qquad [4.44]$$

Assuming a power law relationship between the average stress and the average strain rate,

$$\sigma_E = K_E(\dot{\varepsilon}_E)^m \qquad [4.45]$$

allows Eq. [4.44] to be rewritten as

$$d(\delta P_{en,E}) = 2K_E(\dot{\varepsilon}_E)^m \frac{dr}{r} \qquad [4.46]$$

Substituting Eq. [4.42], for the average strain rate, into Eq. [4.46] yields

$$d(\delta P_{en,E}) = 2K_E\left(\frac{2Q \tan \theta}{\pi r^3} \right)^m \frac{dr}{r} \qquad [4.47]$$

Eq. [4.47] must be integrated between the radius of the capillary (R) and the radius of the barrel (R_b) to determine the component of the entrance pressure loss due to extensional flow:

$$\int_0^{\delta P_{en,E}} d(\delta P_{en,E}) = \int_R^{R_b} 2K_E\left(\frac{2Q \tan \theta}{\pi r^3} \right)^m \frac{dr}{r} \qquad [4.48]$$

Evaluating the integrals and simplifying the result gives

$$\delta P_{en,E} = \Gamma^m \left(\frac{2K_E}{3m} \right)\left(\frac{\tan \theta}{2} \right)^m \left(1 - \left(\frac{R}{R_b} \right)^{3m} \right) \qquad [4.49]$$

Taking the logarithm of this equation yields

$$\ln(\delta P_{en,E}) = m \ln \Gamma + \ln\left[\left(\frac{2K_E}{3m}\right)\left(\frac{\tan\theta}{2}\right)^m\left(1-\left(\frac{R}{R_b}\right)^{3m}\right)\right] \qquad [4.50]$$

which can be used in regression analysis to calculate m from the slope of the line, and K_E from the intercept. Values of K_E and m may be used to calculate the average extensional viscosity:

$$\eta_E = K_E(\dot{\varepsilon}_{E,R})^{m-1} \qquad [4.51]$$

where $\dot{\varepsilon}_{E,R}$ is the average extensional strain rate at the die (where $r = R$) computed from Eq. [4.42] as

$$\dot{\varepsilon}_{E,R} = \frac{\Gamma \tan\theta}{2} \qquad [4.52]$$

Using the above equations, the following procedure can be utilized to calculate extensional viscosity from die entry pressure data:

1. Determine the total entrance pressure loss (δP_{en}) using the Bagley procedure discussed in Sec. 2.5. Also, determine the shear flow rheological parameters (K, n) using standard methods in capillary viscometry presented in Chapter 2. Although it may be convenient to find shear properties from capillary data, any standard rheological technique could be used to determine K and n.
2. Using Eq. [4.40], find the pressure drop in the convergence due to shear flow, $\delta P_{en,S}$.
3. Subtract this from δP_{en}, found in Step 1, to yield the component of the pressure drop in the entrance due to extensional flow, $\delta P_{en,E}$.
4. Use Eq. [4.50] in a regression analysis procedure to evaluate m and K_E. Calculate the strain rate and the extensional viscosity from Eq. [4.52] and [4.51], respectively.

The preceding equations describe behavior acceptably up to die angles of approximately 45 degrees (Gibson, 1988). When $\theta < 10°$, shear flow is dominant; when $\theta > 45°$, materials may form their own convergence pattern (Cogswell, 1981) resulting in an unknown entry angle. Formation of a product convergence pattern will be a function of the

rheological properties. It may be a particularly significant problem with foods having a high yield stress. Cogswell's equations are used to investigate soy dough in Example Problem 4.9.3.

Cogswell (1972) formulated expressions for the net average extensional stress and net average extensional strain for flat entry dies (Fig. 4.5 with $\theta = 90°$) as

$$\sigma_E = \frac{3}{8}(n+1)\,\delta P_{en} \qquad [4.53]$$

and

$$\dot{\varepsilon}_E = \frac{4\eta\Gamma^2}{3(n+1)\,\delta P_{en}} \qquad [4.54]$$

where η is the apparent shear viscosity based on a power law relationship: $\eta = K(\Gamma)^{n-1}$. The average extensional viscosity is easily calculated from Eq. [4.53] and [4.54]:

$$\eta_E = \frac{\sigma_E}{\dot{\varepsilon}_E} = \frac{9(n+1)^2(\delta P_{en})^2}{32\eta\Gamma^2} \qquad [4.55]$$

Eq. [4.55] is very convenient for making a rapid comparison between fluids.

An alternative analysis for converging flow has been proposed by Binding (1988) and used to evaluate corn meal dough (Padmanabhan and Bhattacharya, 1993) and polymer melts (Padmanabhan and Bhattacharya, 1994). The technique involves axis-symmetric flow but emphasizes planar contraction which involves the convergence from a rectangular channel into a rectangular orifice. Also, a refined version of Cogswell's method has been proposed, and successfully used for molten polymers, by Bersted (1993). This analysis does not require a constant extensional viscosity in the convergence, but an iterative procedure is needed to find a solution to the pressure drop equations.

4.4.2. Gibson's Equations

Using spherical coordinates, Gibson (1988) developed a method of determining extensional viscosity for the full range of die angles up to 90 degrees. The analysis included a power law model (Eq. [4.45]) relating average extensional stress and strain. Components of the pressure drop due to shear flow and extensional flow were found to be

$$\delta P_{en,S} = \frac{2K(\sin^{3n}\theta)}{3n\theta^{1+3n}}\left(\frac{1+3n}{4n}\right)^{n}\Gamma^{n}\left(1-\left(\frac{R}{R_b}\right)^{3n}\right) \qquad [4.56]$$

where θ is expressed in radians and

$$\delta P_{en,E} = K_E\Gamma^{m}\left[\frac{2}{3m}\left(\frac{(\sin\theta)(1+\cos\theta)}{4}\right)^{m}\left(1-\left(\frac{R}{R_b}\right)^{3m}+\frac{\Phi}{4^m}\right)\right] \qquad [4.57]$$

respectively. The die exit effect integral(Φ) was given as a function of *m* and the angle of convergence:

$$\Phi = f(m,\theta) = \int_0^{\theta}(\sin^{m+1}\beta)(1+\cos\beta)^{m-1}d\beta \qquad [4.58]$$

Φ can be integrated directly at $m = 1$ but a numerical solution is required at other values of *m*. Solutions to Eq. [4.58] covering most practical situations are given in Table 4.2 and Fig. 4.6. Interpolation between different values of *m* and die entry angles (Table 4.2) does not introduce a significant level of error. Equations given in Fig. 4.6 were generated from linear regression analyses of the information provided in Table 4.2.

The average die exit elongational strain rate is

$$\dot{\varepsilon}_{E,R} = \frac{\Gamma(\sin\theta)(1+\cos\theta)}{4} \qquad [4.59]$$

Procedures for finding $\delta P_{en,E}$, *K*, and *n* are the same as those outlined, in the preceding section, for Cogswell's method. Values of K_E and *m* are determined from raw data of $\delta P_{en,E}$ versus Γ. Taking the logarithm of Eq. [4.57] yields

$$\ln(\delta P_{en,E}) = m\ln(\Gamma) + \ln\left[K_E\left[\frac{2}{3m}\left(\frac{(\sin\theta)(1+\cos\theta)}{4}\right)^{m}\left(1-\left(\frac{R}{R_b}\right)^{3m}+\frac{\Phi}{4^m}\right)\right]\right] \qquad [4.60]$$

showing that *m* is the slope of the resulting line. The numerical value of K_E is determined from the intercept. Extensional viscosity is calculated from Eq. [4.51] with $\dot{\varepsilon}_{E,R}$ defined by Eq. [4.59]. The last term in Eq. [4.60] (equal to $\Phi/4^m$) is small and often negligible for die angles less than 45 degrees. This analysis, like that of Cogswell, may be complicated by the tendency of foods with a high yield stress to form a natural angle of convergence. Gibson's equations are used to investigate soy dough in Example Problem 4.9.4.

Table 4.2. Numerical Solutions of the Die Exit Effect Integral (from Gibson, 1988):

$$\Phi = f(m,\theta) = \int_0^{\theta} (\sin^{m+1}\beta)\,(1+\cos\beta)^{m-1} d\beta$$

m	$\theta = 30°$	$\theta = 45°$	$\theta = 60°$	$\theta = 75°$	$\theta = 90°$
0.1	0.0660	0.1558	0.2882	0.4677	0.7003
0.2	0.0629	0.1535	0.2892	0.4730	0.7080
0.3	0.0601	0.1515	0.2904	0.4787	0.7162
0.4	0.0575	0.1497	0.2920	0.4848	0.7249
0.5	0.0550	0.1481	0.2939	0.4913	0.7339
0.6	0.0528	0.1467	0.2961	0.4983	0.7434
0.7	0.0507	0.1455	0.2985	0.5055	0.7533
0.8	0.0488	0.1444	0.3011	0.5132	0.7636
0.9	0.0470	0.1435	0.3040	0.5212	0.7743
1.0	0.0453	0.1427	0.3071	0.5295	0.7854
1.2	0.0422	0.1414	0.3139	0.5472	0.8087
1.4	0.0394	0.1406	0.3215	0.5662	0.8334
1.6	0.0370	0.1401	0.3299	0.5865	0.8597
1.8	0.0348	0.1399	0.3391	0.6082	0.8874
2.0	0.0328	0.1399	0.3490	0.6313	0.9167

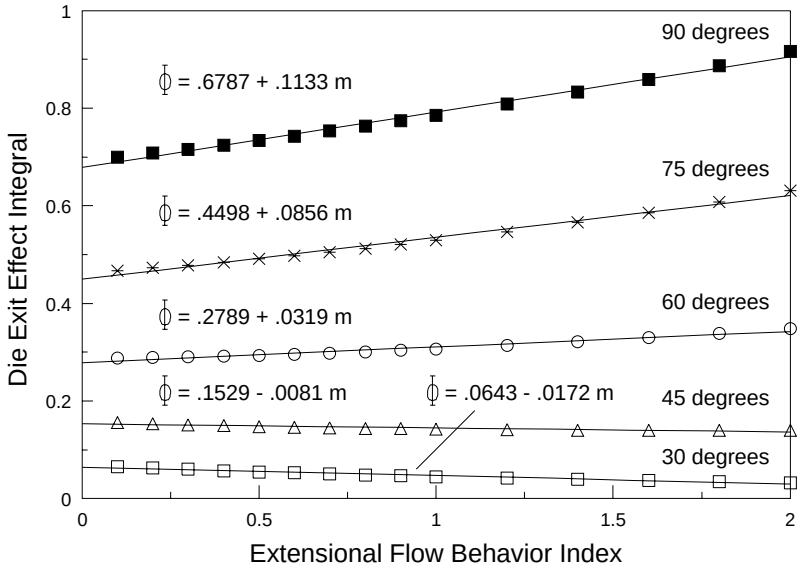

Figure 4.6. Numerical solutions of the die exit effect integral for different values of the extensional flow behavior index (m) and die entry angles.

4.4.3. Empirical Method

Extensional viscosity may be estimated using a standard material. Assuming $m = 1$ making (from Eq. [4.51]) $\eta_E = K_E$, and that the shear contribution to the pressure loss is small, then Eq. [4.49] shows that an average extensional viscosity is proportional to the entrance pressure drop divided by the apparent wall shear rate in the die:

$$\eta_E = C\frac{\delta P_{en}}{\Gamma} \qquad [4.61]$$

where C is a dimensionless constant assumed to be a function of the system geometry, not strain rate or the rheological properties of the sample. The numerical value of C could be estimated using a standard Newtonian material with a known value of η_E.

Eq. [4.61] can also be used with a zero length die where it is assumed the entire pressure drop is the entrance loss. This idea is illustrated in Fig. 4.7 where a plunger, moving downward at a constant velocity (u_z), is forcing material through an orifice with a 90 degree entry angle. The entrance pressure loss is calculated from the force on the plunger and the crossectional area of the barrel: $\delta P_{en} = F/(\pi R_b^2)$. Assuming the test material is incompressible, the volumetric flow through the orifice is a function of the plunger velocity ($Q = u_z \pi R_b^2$). Given Eq. [4.61] and the above definitions, extensional viscosity may be estimated as

$$\eta_E = C\frac{\delta P_{en}}{\Gamma} = \left(\frac{C}{4\pi}\right)\left(\frac{FR^3}{u_z R_b^4}\right) \qquad [4.62]$$

Eq. [4.62] can be used, for both tapered or flat entry dies, as the basis of a quality control test if making a relative comparison between the extensional viscosities of similar foods. A commercially manufactured on-line system (Rheometrics, Inc., Piscatawa, NJ), based on this principle, is available to the food industry. The unit has been used successfully with cookie and cracker dough. It should be noted that C could be a function of the strain rate and the rheological properties of the test substance. This may be particularly important for high yield stress materials tested in instruments constructed with large entry angles. Menjivar et al. (1992) used data from a zero length die to calculate Trouton ratios which correlated well with the extrudate swell behavior of wheat flour doughs.

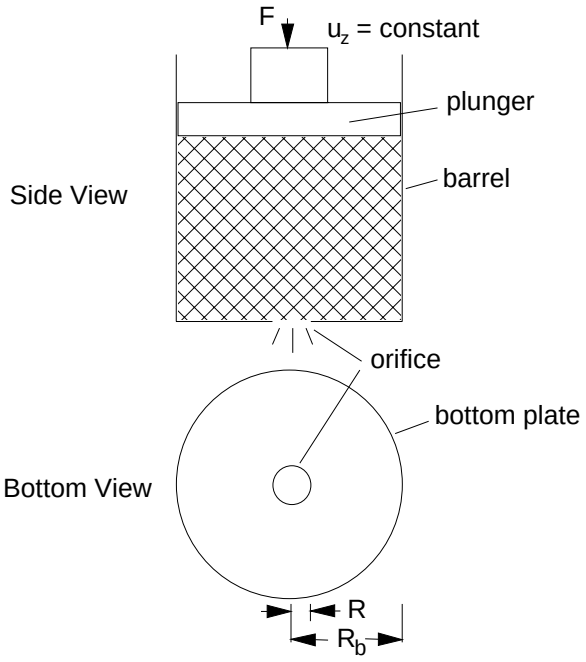

Figure 4.7. Flow through an orifice (zero-length die) controlled by the constant downward velocity of the plunger.

4.5. Opposing Jets

In the method of opposing jets, opposing nozzles are completely immersed in a test fluid (Fig. 4.8). Using a vacuum, fluid is sucked into the nozzles creating uniaxial extensional flow in the region between them. This flow causes a tensile stress which, if unrestrained, would cause the nozzles to approach each other. In experimentation, one nozzle is fixed and the other nozzle is restrained from movement but allowed to transmit a resultant force to an appropriate transducer. A momentum balance indicates that pressure and momentum forces cancel, so the force (F) measured at the transducer represents the tensile stress (Fuller et al., 1987). An opposing jet device could also be used to create uniaxial compressive flow if fluid was forced to move out of the nozzles instead of being sucked into them.

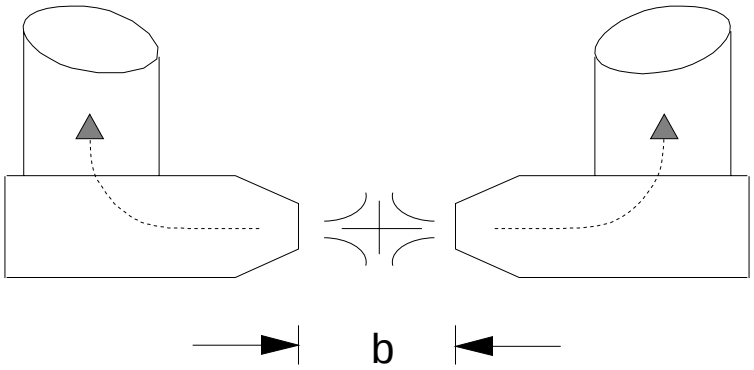

Figure 4.8. Opposing jets configuration to achieve uniaxial extensional flow by sucking fluid into the nozzles.

The average extensional strain rate may be taken as the mean velocity at the nozzle divided by one-half the distance separating the nozzles:

$$\dot{\varepsilon}_E = \left(\frac{Q}{A}\right)\left(\frac{1}{b/2}\right) = \frac{2Q}{Ab} \qquad [4.63]$$

where b is the distance separating the nozzles, Q is the total volumetric flow rate into both nozzles, and A is the cross-sectional flow area of the nozzle. Extensional viscosity is calculated by dividing the mean tensile stress (F/A) by the strain rate:

$$\eta_E = \frac{\sigma_{11} - \sigma_{22}}{\dot{\varepsilon}_E} = \frac{F/A}{2Q/(Ab)} = \frac{Fb}{2Q} \qquad [4.64]$$

Since the strain rate is an average value and the residence time of fluid elements entering the orifice is non-uniform, the value calculated using Eq. [4.64] should be considered an average extensional viscosity.

Using the opposing jet method, Fuller et al. (1987) were able to obtain good results (approximately correct Trouton ratios) for Newtonian fluids consisting of glycerin-water mixtures. Only qualitative differences, however, were observed for non-Newtonian fluids made from polymers (Xanthan gum and polyacrylamide) dissolved in mixtures of glycerin and water. In the Fuller et al. (1987) experiments, a nozzle diameter of 1mm was used and, in most testing, the separation distance between

nozzles was 1mm. A commercial instrument based on the opposing jet principle is available (Rheometrics, Inc., Piscatawa, NJ). This method of measurement may yield valuable results for numerous fluid food systems such as pancake syrup where stringiness (formation of thin threads) is an important factor in evaluating quality. Similar considerations may be associated with thickened drinks and oral drugs using a fluid carrier (cough syrup, pain drugs, and antibiotics).

4.6. Spinning

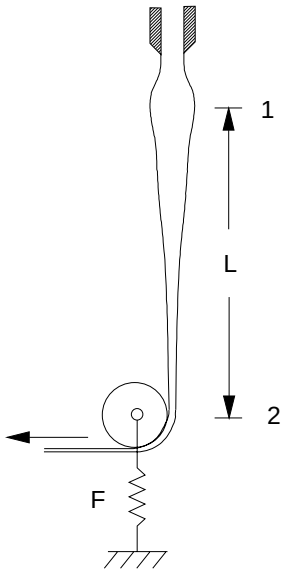

Figure 4.9. Spinning apparatus to evaluate extensional viscosity.

Spinning is a method of evaluating extensional viscosity of moderate viscosity fluids by subjecting the sample to a uniaxial elongation. Extrudate drawing, melt spinning, and fiber spinning are synonyms for the procedure. The test is conducted by extruding a sample from a small diameter tube on to a rotating drum or wheel (Fig. 4.9). Extension rates experienced by the material may be varied by changing the wind-up speed of the drum. Stress on the sample is determined from the force measured on the drum.

Experimental data from a spinning test is ordinarily evaluated using a simplified analysis producing average values. Assuming the extension rate is constant over the length of the sample, the average rate of extension may be calculated as

$$\dot{\varepsilon}_E = \frac{u_2 - u_1}{L} \qquad [4.65]$$

where u_1 and u_2 are the mean velocities at points 1 and 2 separated by a distance equal to L (Fig. 4.9). Taking Q as the volumetric flow rate through the extrusion tube, Eq. [4.65] may be written as

$$\dot{\varepsilon}_E = \frac{1}{L}\left(\frac{Q}{\pi R_2^2} - \frac{Q}{\pi R_1^2}\right) = \frac{Q}{\pi L}\left(\frac{1}{R_2^2} - \frac{1}{R_1^2}\right) \qquad [4.66]$$

where R_1 and R_2 are the radii at points 1 and 2, respectively. These radii are usually determined by photographic methods. Strain imposed on the sample during testing is calculated as

$$\varepsilon_E = \ln\left(\frac{u_2}{u_1}\right) = \ln\left(\frac{R_1^2}{R_2^2}\right) \qquad [4.67]$$

An average extensional stress is determined from the tensile force on the sample:

$$\sigma_E = \frac{F}{\pi R^2} \qquad [4.68]$$

where R is taken as the average radius over the length of the sample: $R = (R_1 + R_2)/2$. Using Eq. [4.66] and [4.68], an average extensional viscosity may be calculated:

$$\eta_E = \frac{\sigma_E}{\dot{\varepsilon}_E} = \frac{FL}{R^2 Q}\left(\frac{R_2^2}{1 - \left(\frac{R_2}{R_1}\right)^2}\right) \qquad [4.69]$$

Spinning tests have commonly been conducted on polymer melts and solutions. The method has also been used as a means of evaluating the stretchability of Mozzarella cheese (Cavella et al., 1992). This research showed that cheese reached a maximum stretchability over a well defined temperature range. Experimentation also allowed an accurate evaluation of maximum elongation and sample strength. Information of this type may be very useful in comparing and screening different Mozzarella cheeses for use with pizza and pasta products.

4.7. Tubeless Siphon (Fano Flow)

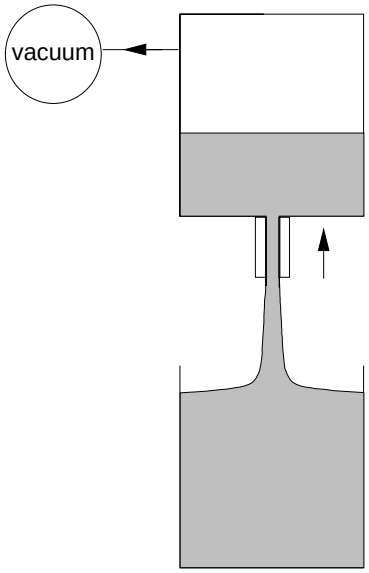

Figure 4.10. Apparatus to evaluate extensional viscosity using the tubeless siphon phenomenon.

Data collected employing the tubeless siphon phenomenon (also called open siphon or Fano flow) are useful in evaluating extensional behavior. Testing is carried out using a low pressure reservoir with a protruding capillary tube (Fig. 4.10). The upper container is lowered until the tube touches the fluid contained in the bottom vessel. Then, the vacuum is applied and the tube is slowly raised allowing a free standing column of fluid to be formed. An advantage of this method, over the spinning technique, is that the sample receives less severe treatment prior to testing. Strain rates and extensional viscosities can be calculated using the same considerations discussed for spinning. Comparative data can be easily collected merely by determining the maximum column height that can be obtained with a constant vacuum.

4.8. Steady Shear Properties from Squeezing Flow Data

Biaxial extensional viscosity can be determined from squeezing flow data (Sec. 4.3). Alternative interpretations of these data are presented in this section. Power law fluid properties, for example, can also be

estimated from squeezing flow data. In addition, parallel plate equipment can be used to produce a combined shear and extensional flow when the interface between the plate and the fluid is not lubricated so the sample adheres firmly to the plate. In this case, Newtonian and power law fluid properties as well as yield stresses may be calculated. Squeezing flow data may also provide empirical information that can form the basis of a useful quality control test.

4.8.1. Lubricated Squeezing Flow

Squeezing flow between parallel plates can be achieved in many food rheology laboratories. When this deformation is executed between lubricated plates, biaxial extensional flow is achieved and an extensional viscosity can be calculated. Data from lubricated squeezing flow may also be evaluated in a manner that produces steady shear fluid parameters. This is advantageous in some cases. Food materials, for example, that have a high fat content (raw meat emulsions, butter, margarine, soft cheese, etc.) may violate the no slip boundary condition required in a traditional viscometer. True slip, however, is a necessary condition in lubricated squeezing flow. Campanella and Peleg (1987c) have taken advantage of this idea in evaluating the power law flow behavior of peanut butter. Squeezing flow can also be useful for very thick fluids which are difficult to load into conventional viscometers.

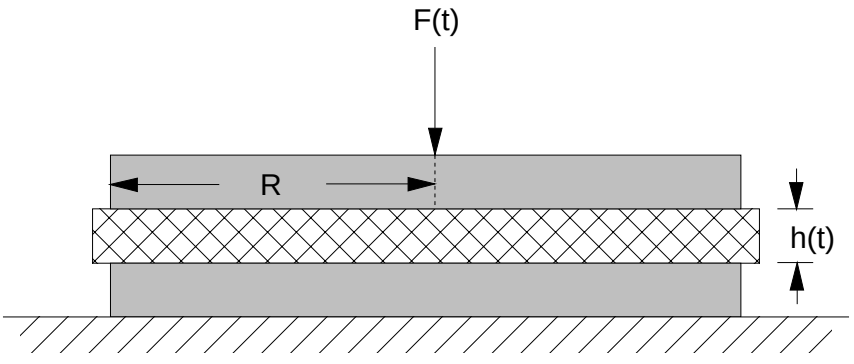

Figure 4.11. Lubricated squeezing flow with sample completely filling the gap between two parallel plates.

In lubricated squeezing flow of a power law fluid with a system having a fixed bottom plate, and constant sample area in contact with the plates (meaning the gap between the plates is completely full during testing, Fig. 4.11), the force (F) required to maintain a constant downward velocity (u_z) of the upper plate is (Campanella and Peleg, 1987c), for a power law fluid,

$$F = \frac{3^{(n+1)/2} R^2 \pi K u_z^n}{h^n} \qquad [4.70]$$

where $h = f(t) = h_o - u_z t$. Taking the logarithm of each side yields

$$\ln(F) = C_1 + n \ln\left(\frac{1}{h}\right) \qquad [4.71]$$

where:

$$C_1 = \ln(3^{(n+1)/2} R^2 \pi K u_z^n) \qquad [4.72]$$

Power law fluid parameters (K, n) may be determined from linear regression of experimental data using Eq. [4.71]. Early data points should be neglected: Only the linear portion of the curve, where steady flow is present, should be used in the analysis. This technique is demonstrated to evaluate the behavior of peanut butter in Example Problem 4.9.5.

The squeezing flow solution for a power law fluid in the case of flow under a constant force, producing a constant stress when the gap is completely full (Fig. 4.11) during testing, is (Campanella and Peleg, 1987c)

$$\ln\left(\frac{h}{h_o}\right) = -C_2 t \qquad [4.73]$$

where:

$$C_2 = \left(\frac{W}{3^{(n+1)/2} R^2 \pi K}\right)^{1/n} \qquad [4.74]$$

and W is a constant force applied to the sample through the upper plate. Since C_2 contains both unknown properties, multiple experiments with at least two different loads are required to determine the numerical values of K and n.

The potential error introduced by the existence of a yield stress during lubricated squeezing flow should not be overlooked. Fortunately, this problem is not serious regardless of whether or not a yield stress is present: In constant deformation experiments flow will occur irrespective of the yield stress, and in constant stress experiments, applied stresses must exceed the yield stress for flow to occur (Campanella and Peleg, 1987a).

It is instructive to consider the theoretical relationship between the power law fluid parameters determined by the above procedures and extensional viscosity. Consider, for example, data obtained in the constant displacement mode. Eq. [4.70], involving steady shear parameters for power law fluids ($\sigma = K(\dot{\gamma})^n$), may be rewritten as

$$\frac{F}{\pi R^2} = 3^{(n+1)/2} K \left(\frac{u_z}{h} \right)^n \qquad [4.75]$$

which, by considering Eq. [4.28] and [4.31], is equivalent to

$$\sigma_B = 3^{(n+1)/2} K (\dot{\varepsilon}_h)^n \qquad [4.76]$$

Since $\dot{\varepsilon}_h = 2\dot{\varepsilon}_B$, Eq. [4.76] can be expressed as

$$\sigma_B = 3^{(n+1)/2} 2^n K (\dot{\varepsilon}_B)^n \qquad [4.77]$$

or, in terms of biaxial extensional viscosity as,

$$\eta_B = \frac{\sigma_B}{\dot{\varepsilon}_B} = 3^{(n+1)/2} 2^n K (\dot{\varepsilon}_B)^{n-1} \qquad [4.78]$$

A comparable expression for tensile extensional viscosity was given earlier as Eq. [4.51]. For the special case of a Newtonian fluid ($n = 1$ and $\mu = K$), Eq. [4.78] shows the extensional viscosity to be six times the shear viscosity as predicted by Eq. [1.79].

4.8.2. Nonlubricated Squeezing Flow

Nonlubricated squeezing flow produces a barreling effect (Fig. 4.12) due to shear flow caused by adhesion of the sample to the plates. The resulting complex flow is not purely viscometric or extensional, but some combination of each. Equations relating the force required to move the plates and plate separation distance can be derived by assuming specific constitutive relationships. The device originally made to produce nonlubricated squeezing flow was called a parallel plate plastometer

(Dienes and Klemm, 1946). That terminology is still common today, but the published literature contains numerous synonyms for the parallel plate plastometer (Bird and Leider, 1974): parallel plate viscometer, compression plastometer, transverse flow viscometer, and parallel-plate plastimeter. More recently (Covey and Stanmore, 1981), it has been called the squeeze film viscometer.

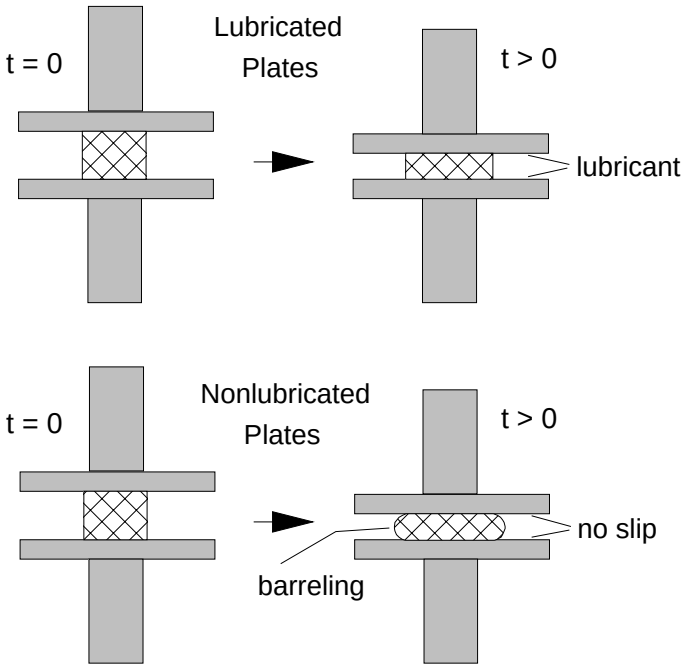

Figure 4.12. Flow between lubricated and nonlubricated parallel plates.

It is important to remember that the equations presented in this section are based on the no-slip premise which may be enhanced when testing with metal fixtures by using various methods such as pitted plates, an adhesive like cyanoacrylate ester (Superglue), emery paper attached with double adhesive tape (Rhom and Weidinger, 1993), or by coating the plates with spray lacquer and ordinary sand (Nolan et al., 1989; Navackis and Bagley, 1983). Unless otherwise noted, the solutions presented in this section are for the case of a fully loaded gap. Initial sample size is important: A sufficient amount of material to produce a

value of $R > 10h_o$, where R equals the radius of the plate and h_o is the initial height of the sample (also the initial distance between the plates), is recommended (Dienes and Klemm, 1946). Development of the following equations also ignores elastic effects which could be significant at high squeezing rates.

Newtonian Fluids. Derivations and solutions for Newtonian fluids and power law fluids are given in Bird et al. (1987) and Leider and Bird (1974). The nonlubricated squeezing flow of a Newtonian fluid, in an experimental system using an immobile bottom plate with a fully loaded gap, is (Winther et al., 1991)

$$F = \frac{3\pi R^4 u_z \mu}{2h^3} \qquad [4.79]$$

where $h = f(t) = h_o - u_z t$ and $F = f(t)$, the force required to maintain a constant downward velocity of the upper plate. Eq. [4.79] is known as the Stefan equation. The viscosity can be calculated as the slope of F versus $1/h^3$ determined from regression analysis.

The shear rate, evaluated from the velocity profile in the gap, is (Winther et al., 1991; Churchill, 1988)

$$\dot{\gamma} = f(r,z) = \frac{6rzu_z}{h^3} \qquad [4.80]$$

where r is the distance from the center line and z is the vertical distance from the horizontal midplane of the sample. A maximum shear rate is found at $r = R$ and $z = h/2$:

$$\dot{\gamma}_{\max} = \frac{3Ru_z}{h^2} \qquad [4.81]$$

The average shear rate is equal to 2/3 of the maximum shear rate.

The case for squeezing flow of a Newtonian fluid with a constant force, full gap, can be determined by integrating the Stefan equation. First, it must be recognized that $u_z = -dh/dt$, so Eq. [4.79] may be written as

$$-h^{-3}dh = \frac{2W}{3\pi R^4 \mu}dt \qquad [4.82]$$

where W is the constant force applied to the sample. This equation is easily integrated to give

$$\frac{1}{2h^2} = \frac{2Wt}{3\pi R^4 \mu} + C \qquad [4.83]$$

The constant of integration is evaluated from the initial condition that $h = h_o$ at $t = 0$ making $C = 1/(2h_o^2)$. Substituting this into Eq. [4.83], and simplifying the result, produces the final solution:

$$\left(\frac{h_o}{h}\right)^2 = \frac{4Wh_o^2 t}{3\pi R^4 \mu} + 1 \qquad [4.84]$$

Viscosity can be calculated from the slope of $(h_o/h)^2$ versus t. Also, if the viscosity was known, $h = f(t)$ could be determined by solving for h.

Power Law Fluids. The nonlubricated squeezing flow of a power law fluid, in an experimental system using an immobile bottom plate with a full gap, is (Winther et al., 1991)

$$F = \left(\frac{2n+1}{n}\right)^n \left(\frac{2\pi K R^{n+3}}{n+3}\right)\left(\frac{u_z^n}{h^{2n+1}}\right) \qquad [4.85]$$

where $h = f(t) = h_o - u_z t$. Eq. [4.85] is known as the Scott equation and it reduces to the Stefan equation when $n = 1$. Winther et al. (1991) suggest evaluating Eq. [4.85] by multiplying both sides by h giving

$$Fh = \left(\frac{2n+1}{n}\right)^n \left(\frac{2\pi K R^{n+3}}{n+3}\right)\left(\frac{u_z}{h^2}\right)^n \qquad [4.86]$$

then, taking the logarithm of each side of the equation, to get

$$\ln(Fh) = \ln\left[\left(\frac{2n+1}{n}\right)^n \left(\frac{2\pi K R^{n+3}}{n+3}\right)\right] + n \ln\left(\frac{u_z}{h^2}\right) \qquad [4.87]$$

Using Eq. [4.87], n may be found from the slope of $\ln(Fh)$ versus $\ln(u_z/h^2)$. The value of K is determined from the intercept. Since the inertia terms in the equations of motion are neglected in developing Eq. [4.87], the earliest data points may not lie on the line and should be neglected. The average shear rate for a power law fluid in nonlubricated squeezing flow is (Winther et al., 1991)

$$\dot{\gamma}_{\text{average}} = \left(\frac{2(2n+1)}{3n} \right) \left(\frac{u_z R}{h^2} \right) \qquad [4.88]$$

Integrating Eq. [4.85] can produce a solution for describing the case where a constant weight is used to deform a power law fluid. This problem has been solved by Leider and Bird (1974).

Yield Stress Evaluation. Nonlubricated squeezing flow has been used to evaluate the behavior of Bingham plastic and Herschel-Bulkley fluids (Covey and Stanmore, 1981). General solutions are somewhat cumbersome but the work verified a simple procedure to determine the yield stress of semi-solid materials. In testing, a constant force (W) is placed on samples which completely fill the gap between parallel plates. The yield stress is calculated on the basis of the asymptotic or residual thickness (h_a) of the sample:

$$\sigma_o = \frac{3Wh_a}{2\pi R^3} \qquad [4.89]$$

The technique works reasonably well when the materials tested have a high yield stress and the rate of deformation produced by the constant force is small. Campanella and Peleg (1987a) used this method to evaluate the yield stresses of tomato ketchup, mustard, and mayonnaise. Also, values of the yield stress, for a TiO_2/treacle paste, determined with Eq. [4.89] compared well to those found by extrapolation of a rheogram to zero shear rate (Covey and Stanmore, 1981).

4.9. Example Problems

4.9.1. Biaxial Extension of Processed Cheese Spread

Given the data in Table 4.3, determine the biaxial extensional strain rate and the extensional viscosity of processed cheese spread. Also calculate the maximum strain found during testing. Data are for the lubricated squeezing flow between parallel plates where the gap is filling during experimentation (Fig. 4.12). The lower plate is fixed and the upper plate is moving downward with a constant velocity. Paraffin oil was used as the lubricant.

Table 4.3. Data for the Lubricated Squeezing Flow (h_o = 0.04 m, R_o = 0.057 m, u_z = 0.0005 m/min) of Processed Cheese Spread at 7°C (Data from Casiraghi et al., 1985)

F (N)	compression (m)	h (m)	$\dot{\varepsilon}_B$ (1/s)	$\dot{\varepsilon}_h$ (1/s)	η_B (MPa s)
5.1	0.0014	0.0386	0.000108	0.000216	4.5
13.8	0.0027	0.0373	0.000112	0.000227	11.3
22.9	0.0048	0.0352	0.000118	0.000236	16.7
29.6	0.0067	0.0333	0.000125	0.000250	19.3
39.1	0.0094	0.0306	0.000136	0.000272	21.5
50.0	0.0120	0.0279	0.000149	0.000298	22.9
59.5	0.0141	0.0258	0.000161	0.000322	23.3
69.7	0.0160	0.0240	0.000174	0.000348	23.5
80.8	0.0180	0.0220	0.000189	0.000378	23.0
91.5	0.0200	0.0199	0.000209	0.000418	21.3
106.3	0.0227	0.0173	0.000241	0.000482	18.7
137.1	0.0260	0.0140	0.000298	0.000596	15.8
192.3	0.0294	0.0106	0.000392	0.000784	12.7

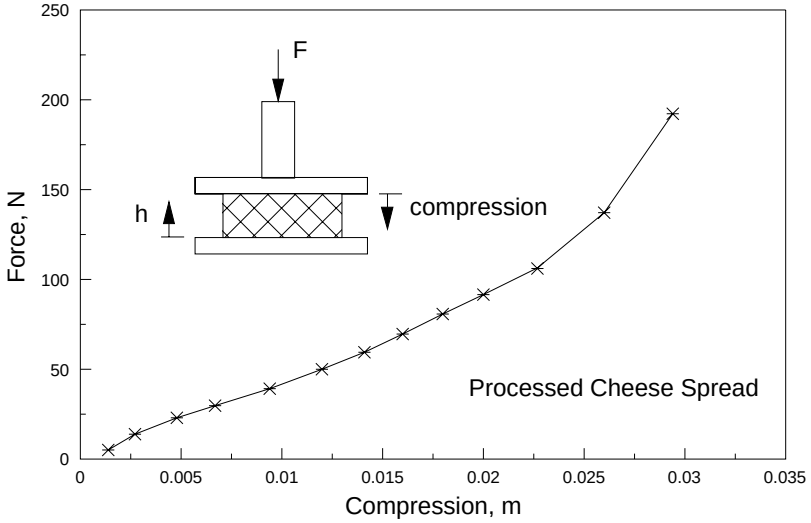

Figure 4.13. Raw data of force versus compression for the lubricated squeezing flow of processed cheese spread at 7°C.

Plotting the raw data (Fig. 4.13) clearly illustrates the change in force during compression. Results are summarized in Table 4.3 and the following equations show the computations needed to generate the first row of information:

$$h = h_o \text{ - compression} = 0.0400 - 0.0014 = 0.0386 \text{ m}$$

$$\dot{\varepsilon}_B = 0.5\left(\frac{u_z}{h}\right) = 0.5\left(\frac{.0005}{(60).0386}\right) = 0.000108\ s^{-1}$$

$$\dot{\varepsilon}_h = 2\,\dot{\varepsilon}_B = 2(0.000108) = 0.000216\ s^{-1}$$

$$\eta_B = \frac{Fh}{\pi R_o^2 h_o \dot{\varepsilon}_B} = \frac{5.14(.0386)}{\pi(.057)^2(.040)(.000108)} = 4.5(10)^6 \text{ Pa s} = 4.5 \text{ MPa s}$$

Biaxial extensional viscosity, plotted in terms of the Hencky strain rate, is illustrated in Fig. 4.14. The maximum strain found during testing is calculated from Eq. [4.33]:

$$(\varepsilon_B)_{\max} = -\frac{1}{2}\ln\left(\frac{h}{h_o}\right) = -\frac{1}{2}\ln\left(\frac{.0106}{.04}\right) = 0.66$$

Since this value is less than 1.0, it is unlikely that experimental errors associated with lubricant loss occurred during testing.

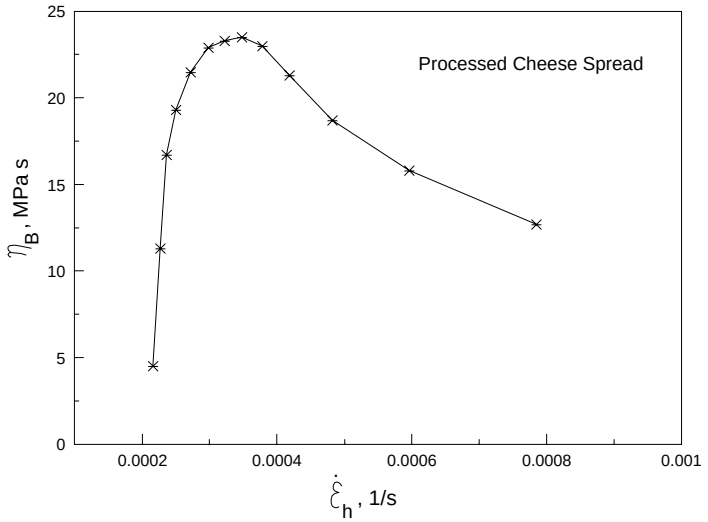

Figure 4.14. Biaxial extensional viscosity of processed cheese spread at 7°C.

4.9.2. Biaxial Extension of Butter

Biaxial extension data are available for butter at 15°C and 20°C (Fig. 4.15). These tests were conducted using parallel plates with a fixed lower plate. The upper plate was lowered at different downward velocities indicated by the crosshead speeds. All samples had an initial diameter of 28 mm and an initial height of 15 mm. Evaluate the behavior of this material.

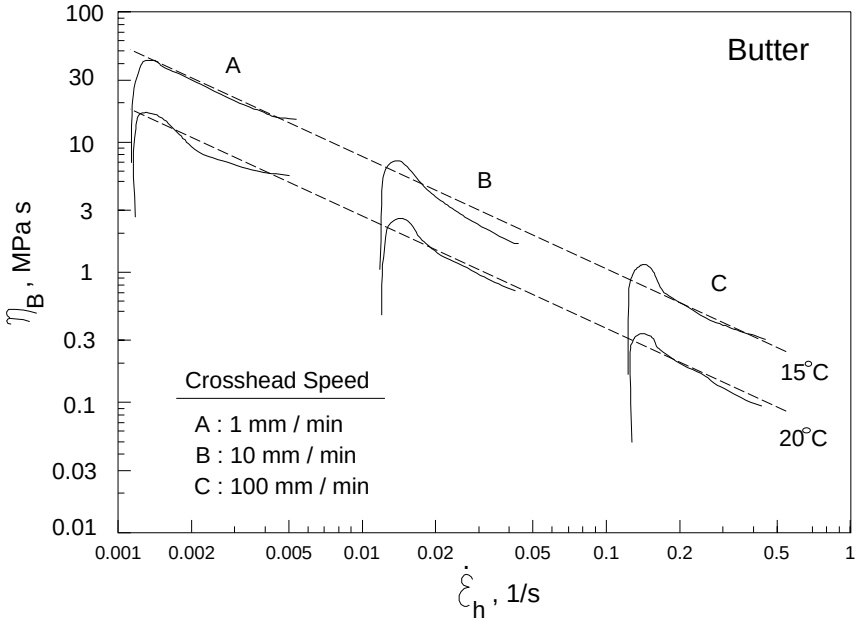

Figure 4.15. Biaxial extensional viscosity of butter at 15°C and 20°C (Data from Rohm, 1993).

Higher crosshead speeds produced larger strain rates. In each test, a sharp initial increase was followed by a gradual decline, similar to the results found for processed cheese spread (Fig. 4.14) in the previous example. Plotting a line through the downward slope of each data set (dashed line, Fig. 4.15) suggest a power law relationship between viscosity and strain rate. Fitting the line through representative points yields

$$\eta_B = 9.55(10^4)(\dot{\varepsilon}_h)^{.08-1} \qquad \text{at } 15°C$$

and

$$\eta_B = 3.55(10^4)(\dot{\varepsilon}_h)^{.10-1} \qquad \text{at } 20°C$$

The slope terms given above are analogous to $n-1$ used to express the relationship (Eq. [1.28]) between apparent viscosity and shear rate in a standard power law fluid. Hence, the results could be interpreted as extensional-thinning behavior. Similar results have been observed for processed cheese spread. Other materials, such as mozzarella cheese, show a leveling off of extensional viscosity after the initial sharp increase (Casiraghi et al., 1985) making the interpretation of data much more difficult.

4.9.3. 45° Converging Die, Cogswell's Method

Taking the capillary viscometer data for soy dough presented in Example 2.12.2, estimate the extensional viscosity assuming that the entrance pressure loss can be divided into two separate components: one related to shear and one related to extensional flow. Data from Table 2.8 are summarized in Table 4.4. Assume the material forms a natural convergence angle of $\theta = \pi/4 \text{ rad} = 45°$ in the die. Solve the problem using Cogswell's equations presented in Sec. 4.4.1.

Analysis of the data conducted in Example 2.12.2 generated values of the flow behavior index and the consistency coefficient: n = 0.29, K = 23,300 Pa s^n. Eq. [4.40] must be evaluated to determine the component of the entrance pressure drop due to shear:

$$\delta P_{en,S} = (\Gamma)^n \left(\frac{3n+1}{4n}\right)^n \frac{2K}{3n\tan\theta}\left(1-\left(\frac{R}{R_b}\right)^{3n}\right)$$

Given, R = 0.00159 m and R_b = 0.0075 m, the equation may be simplified:

$$\delta P_{en,S} = (\Gamma)^{.29}\left(\frac{3(.29)+1}{4(.29)}\right)^{.29} \frac{2(23,300)}{3(.29)\tan(\pi/4)}\left(1-\left(\frac{.00159}{.0075}\right)^{3(.29)}\right) = (\Gamma)^{.29}(45,560)$$

Calculating $\delta P_{en,S}$ for each value of Γ shows that the pressure drop, due to shear flow, is a small portion of the total pressure drop at the entrance (Table 4.4). The component of the entrance pressure drop due to extensional flow is found from Eq. [4.36]:

$$\delta P_{en,E} = \delta P_{en} - \delta P_{en,S}$$

Results are summarized in Table 4.4.

Extensional flow parameters may be estimated from regression of Eq. [4.50]:

$$\ln(\delta P_{en,E}) = m \ln\Gamma + \ln\left[\left(\frac{2K_E}{3m}\right)\left(\frac{\tan\theta}{2}\right)^m\left(1-\left(\frac{R}{R_b}\right)^{3m}\right)\right]$$

yielding the slope,

$$m = \frac{d(\ln \delta P_{en})}{d(\ln\Gamma)} = 0.159$$

and intercept,

$$\ln\left[\left(\frac{2K_E}{3m}\right)\left(\frac{\tan\theta}{2}\right)^m\left(1-\left(\frac{R}{R_b}\right)^{3m}\right)\right] = 14.479$$

Substituting appropriate values into the intercept equation gives

$$K_E\left(\frac{2}{3(.159)}\right)\left(\frac{\tan(\pi/4)}{2}\right)^{(.159)}\left(1-\left(\frac{.00159}{.0075}\right)^{3(.159)}\right) = K_E(1.96) = \exp(14.479)$$

which can be solved for the extensional consistency coefficient:

$$K_E = 991{,}000 \text{ Pa s}^m$$

Average extensional viscosity is determined from Eq. [4.51]:

$$\eta_E = K_E(\dot{\varepsilon}_{E,R})^{m-1} = 991{,}000(\dot{\varepsilon}_{E,R})^{.159-1}$$

with the average extensional strain rate at the die evaluated from Eq. [4.52]:

$$\dot{\varepsilon}_{E,R} = \frac{\Gamma\tan(\pi/4)}{2} = \Gamma(.5)$$

The Trouton number (η_E/η) is calculated from Eq. [1.82] where η is evaluated, as uniaxial extension, at a shear rate numerically equal to $\sqrt{3}\dot{\varepsilon}_{E,R}$:

$$\eta = K(\sqrt{3}\dot{\varepsilon}_{E,R})^{n-1} = 23{,}300(\sqrt{3}\dot{\varepsilon}_{E,R})^{.29-1}$$

Results are summarized in Table 4.4.

Table 4.4. Capillary Viscometer Data for Defatted Soy Flour Dough (34.7%) at Room Temperature (Data from Morgan, 1979)

Γ (1/s)	$(\delta P)_{en}$ (MPa)	$(\delta P)_{en,S}$ (k Pa)	$(\delta P)_{en,E}$ (MPa)	$\dot{\varepsilon}_{E,R}$ (1/s)	η_E (kPa s^m)	η (kPa s^n)	N_{Tr} (-)
47.4	3.58	139.5	3.58	23.7	65.1	1.65	39
47.4	3.58	139.5	3.58	23.7	65.1	1.65	39
47.4	3.58	139.5	3.58	23.7	65.1	1.65	39
94.8	4.63	170.6	4.63	47.4	38.2	1.01	38
94.8	4.63	170.6	4.63	47.4	38.2	1.01	38
94.8	4.63	170.6	4.63	47.4	38.2	1.01	38
190.0	4.38	208.7	4.38	95.0	21.2	0.614	35
190.0	4.38	208.7	4.38	95.0	21.2	0.614	35
190.0	4.38	208.7	4.38	95.0	21.2	0.614	35
948.0	6.17	332.6	6.17	474	5.44	0.196	28
948.0	6.17	332.6	6.17	474	5.44	0.196	28
948.0	6.17	332.6	6.17	474	5.44	0.196	28

4.9.4. 45° Converging Die, Gibson's Method

Reexamine the soy dough data given in the previous example problem using Gibson's equations (Sec. 4.4.2) to separate the pressure drop into the shear and extensional components. Assume the natural angle of convergence (θ) produced by the material is $\pi/4$ radians or 45 degrees.

Analysis of the data conducted in Example 2.12.2 gave values of the flow behavior index and the consistency coefficient: $n = 0.29$, $K = 23{,}300$ Pa s^n. Eq. [4.56] must be evaluated to determine the component of the entrance pressure drop due to shear:

$$\delta P_{en,S} = \frac{2K(\sin^{3n}\theta)}{3n\theta^{1+3n}}\left(\frac{1+3n}{4n}\right)^n \Gamma^n \left(1-\left(\frac{R}{R_b}\right)^{3n}\right)$$

Given, $R = 0.00159$ m and $R_b = 0.0075$ m, the equation may be simplified:

$$\delta P_{en,S} = \frac{2(23,300)(\sin^{3(.29)}(\pi/4))}{3(.29)(\pi/4)^{1+3(.29)}}\left(\frac{1+3(.29)}{4(.29)}\right)^{.29} \Gamma^{.29}\left(1-\left(\frac{.00159}{.0075}\right)^{3(.29)}\right) = 52,995(\Gamma)^{.29}$$

Entrance pressure loss due to extensional flow is found, from Eq. [4.36], as

$$\delta P_{en,E} = \delta P_{en} - \delta P_{en,S}$$

Results of the pressure loss calculations are summarized in Table 4.5. Using these data, extensional flow parameters are estimated from regression of Eq. [4.60]:

Table 4.5. Capillary Viscometer Data for Defatted Soy Flour Dough (34.7%) at Room Temperature (Data from Morgan, 1979)

Γ (1/s)	$(\delta P)_{en}$ (MPa)	$(\delta P)_{en,S}$ (k Pa)	$(\delta P)_{en,E}$ (MPa)	$\dot{\varepsilon}_{E,R}$ (1/s)	η_E (kPa s^m)	η (kPa s^n)	N_{Tr} (-)
47.4	3.58	162.3	3.42	14.3	92.1	2.38	39
47.4	3.58	162.3	3.42	14.3	92.1	2.38	39
47.4	3.58	162.3	3.42	14.3	92.1	2.38	39
94.8	4.63	198.4	4.43	28.6	51.4	1.46	35
94.8	4.63	198.4	4.43	28.6	51.4	1.46	35
94.8	4.63	198.4	4.43	28.6	51.4	1.46	35
190.0	4.38	242.7	4.14	57.4	28.6	0.889	32
190.0	4.38	242.7	4.14	57.4	28.6	0.889	32
190.0	4.38	242.7	4.14	57.4	28.6	0.889	32
948.0	6.17	386.8	5.78	286	7.40	0.284	26
948.0	6.17	386.8	5.78	286	7.40	0.284	26
948.0	6.17	386.8	5.78	286	7.40	0.284	26

$$\ln(\delta P_{en,E}) = m\ln(\Gamma) + \ln\left[K_E\left[\frac{2}{3m}\left(\frac{(\sin\theta)(1+\cos\theta)}{4}\right)^m\left(1-\left(\frac{R}{R_b}\right)^{3m}+\frac{\Phi}{4^m}\right)\right]\right]$$

yielding the slope,

$$m = \frac{d(\ln\delta P_{en,E})}{d(\ln\Gamma)} = 0.158$$

and intercept,

$$\ln\left[K_E\left[\frac{2}{3m}\left(\frac{(\sin\theta)(1+\cos\theta)}{4}\right)^m\left(1-\left(\frac{R}{R_b}\right)^{3m}+\frac{\Phi}{4^m}\right)\right]\right] = 14.478$$

Substituting known values into the intercept equation gives

$$K_E\left[\frac{2}{3(.156)}\left(\frac{(\sin(\pi/4))(1+\cos(\pi/4))}{4}\right)^{.156}\left(1-\left(\frac{.00159}{.0075}\right)^{3(.156)}+\frac{.1516}{4^{.156}}\right)\right] = K_E(2.24) = \exp(14.478)$$

which can be solved for the extensional consistency coefficient:

$$K_E = 865,467 \text{ Pa s}^m$$

Hence, the average extensional viscosity can be expressed as

$$\eta_E = K_E(\dot{\varepsilon}_{E,R})^{m-1} = 865,467(\dot{\varepsilon}_{E,R})^{.158-1}$$

where the average extensional strain rate at the die is determined from Eq. [4.59]:

$$\dot{\varepsilon}_{E,R} = \frac{\Gamma(\sin\theta)(1+\cos\theta)}{4} = \frac{\Gamma(\sin(\pi/4))(1+\cos(\pi/4))}{4} = \Gamma(.302)$$

The Trouton number (η_E/η) is calculated from Eq. [1.82] where η is evaluated at a shear rate of $\sqrt{3}\dot{\varepsilon}_{E,R}$:

$$\eta = K(\sqrt{3}\dot{\varepsilon}_{E,R})^{n-1} = 23,300(\sqrt{3}\dot{\varepsilon}_{E,R})^{.29-1}$$

Results are given in Table 4.5.

Comparing solutions from the Cogswell (Table 4.4) and Gibson (Table 4.5) methods shows practically identical Trouton Numbers. Values of the extensional and steady shear viscosities are the same order of magnitude but significantly different. Since fluid motion in a convergence has both shear and extensional components, it is not considered pure flow making it difficult to say that one method is quantitatively superior to the other. Both are reasonable and provide a good basis for investigating extensional flow of food in a convergence.

4.9.5. Lubricated Squeezing Flow of Peanut Butter

Data for the lubricated squeezing flow of peanut butter were collected for the case of constant displacement and constant area (Fig. 4.11, Table 4.6). Assume power law fluid behavior, and determine the steady shear rheological properties (K and n) of the material. Also, compute the biaxial extensional strain rate and the comparable shear rate.

Using the linear portion of the curve (Fig. 4.16: $1/h(t) > 200\ 1/m$) where steady flow has been achieved, regression of Eq. [4.71],

$$\ln(F) = C_1 + n\ln\left(\frac{1}{h}\right)$$

where, from Eq. [4.72],

$$C_1 = \ln(3^{(n+1)/2}R^2\pi K u_z^n)$$

yields n = 0.79 and C_1 = -2.118. Solving for K gives

$$-2.118 = \ln[3^{(.79+1)/2}(.0318)^2\pi K\left(\frac{.05}{(100)(60)}\right)^{.79}]$$

$$K = 146\ \text{kPa s}^n$$

The biaxial extensional strain rate is

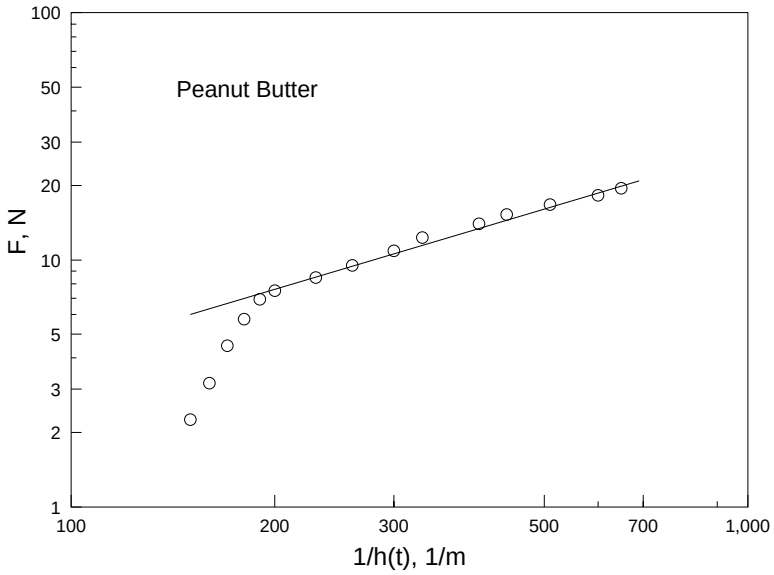

Figure 4.16. Raw data of force versus reciprocal height for the lubricated squeezing flow of peanut butter at 23°C.

$$\dot{\varepsilon}_B = \frac{u_z}{2(h_o - u_z t)} = \frac{u_z}{2}\left(\frac{1}{h}\right)$$

and a comparable shear rate, based on our consideration of the Trouton number (Eq. [1.84]), is

$$\dot{\gamma} = \sqrt{12}\,\dot{\varepsilon}_B$$

Sample calculations for the first data point ($1/h$ = 230 m^{-1}) included in the straight line relationship between F and $1/h$, are

$$\dot{\varepsilon}_B = \frac{u_z}{2}\left(\frac{1}{h}\right) = \frac{.05(230)}{2(60)(100)} = 9.58(10)^{-4}\ s^{-1}$$

and

$$\dot{\gamma} = \sqrt{12}\,\dot{\varepsilon}_B = \sqrt{12}\,(9.58)\,(10)^{-4} = 3.32(10)^{-3}\ s^{-1}$$

Results are summarized in Table 4.6. The approximate shear rate range covered in determining K and n was 0.00332 to 0.00938 s^{-1}.

Table 4.6. Lubricated Squeezing Flow (h_o= 7.14 mm, R = 0.0318 m, u_z = 0.05 cm/min) Data for Peanut Butter at 23°C (Data from Campanella and Peleg, 1987c)

F	h(t)	1 / h(t)	ln (F)	ln(1 / h(t))	$\dot{\varepsilon}_B$	$\dot{\gamma}=\sqrt{12}\dot{\varepsilon}_B$
N	mm	1 / m			1 / s	1 / s
2.25	6.67	150	0.811	5.012	-	-
3.16	6.25	160	1.151	5.075	-	-
4.50	5.88	170	1.504	5.136	-	-
5.75	5.56	180	1.749	5.193	-	-
6.90	5.26	190	1.932	5.247	-	-
7.50	5.00	200	2.015	5.298	-	-
8.50	4.44	230	2.140	5.438	9.58E-4	3.32E-3
9.50	3.85	260	2.251	5.561	1.08E-3	3.75E-3
10.9	3.33	300	2.389	5.704	1.25E-3	4.33E-3
12.3	3.03	330	2.509	5.799	1.38E-3	4.76E-3
14.0	2.50	400	2.639	5.991	1.67E-3	5.77E-3
15.3	2.27	440	2.728	6.087	1.83E-3	6.35E-3
16.7	1.96	510	2.815	6.234	2.13E-3	7.36E-3
18.2	1.67	600	2.901	6.397	2.50E-3	8.66E-3
19.5	1.54	650	2.970	6.477	2.71E-3	9.38E-3

Chapter 5. Viscoelasticity

5.1. Introduction

Rheology is the science of the deformation and flow of matter. There are three ways to deform a substance: shear, extension, and bulk compression. Shear and extensional deformation have been thoroughly discussed in earlier chapters. Bulk compression, where a uniform change in external pressure produces a volumetric change in the material, was briefly discussed in defining the bulk modulus (Sec. 1.4). It is possible to conduct tests in all three modes of deformation, under steady state or dynamic conditions, and compare the resulting moduli and compliances (Ferry, 1980). This chapter will focus on viscoelastic material functions determined from shear and extensional deformation data. Bulk compression testing is not considered here because technology in the area is not well developed. Future research may show the concept to be valuable in defining a pressure dependent viscosity function to examine high pressure processes such as food extrusion.

Viscoelastic Material Functions. In Chapters 2 (Tube Viscometry) and 3 (Rotational Viscometry) the emphasis was on measurement methods to determine flow curves for non-Newtonian materials under steady shear conditions. All foods have unique flow curves and this information is very useful in a large number of industrial applications. Clearly, from an engineering standpoint, the steady flow curve is the most valuable way to characterize the rheological behavior of fluid foods. Steady shear viscosity is a property of all fluids regardless of whether or not they exhibit elastic behavior; however, many phenomena cannot be described by the viscosity function alone and elastic behavior must be taken into consideration. This chapter will investigate experimental methods to generate data that reflect the combined viscous and elastic character of materials.

In steady shear, viscoelastic fluids exhibit normal stresses and measuring them provides one way of characterizing elasticity. Normal stress differences (Eq. [1.23] and Eq. [1.24]) can be measured on rotational rheometers produced by various instrument companies. Computations (Eq. [3.57]) require an evaluation of axial force under steady shear conditions. Unsteady state shear measurements provide a dynamic means of evaluating viscoelasticity. The two major categories of unsteady shear testing are transient and oscillatory.

Table 5.1. Material Functions Determined in Transient Shear Flow Experiments

Start-up flow: Material at rest is suddenly subjected to a constant shear rate.
- Shear stress growth function
- First normal stress growth function
- Second normal stress growth function

Cessation of steady shear flow: Material undergoing steady state shear flow is suddenly brought to rest.
- Shear stress decay function
- First normal stress decay function
- Second normal stress decay function

Step strain: Material at rest is given a sudden step increase in strain.
- Shear stress relaxation function
- First normal stress relaxation function
- Second normal stress relaxation function

Creep: Material at rest is given a sudden step increase in stress.
- Shear creep compliance
- Steady-state compliance

Recoil: Stress, in a fluid in steady state shear flow, is suddenly brought to zero. Material is constrained in one direction and recoil (the degree of retraction) is measured in the second direction.
- Recoil function
- Ultimate recoil function

Transient shear testing (Table 5.1) is a category that includes numerous measurement concepts: start-up flow, cessation of steady shear flow, step strain, creep, and recoil. Data generated using these methods may lead to numerous material functions (Table 5.1) such as the shear stress growth function, shear stress decay function, shear stress relaxation function, shear creep compliance, and the recoil function. In oscillatory testing, a sample is subjected to harmonically varying (usually sinusoidal) small amplitude deformations in a simple shear field. Various companies make instruments to accomplish oscillatory tests which have proved their usefulness in addressing numerous food industry problems. Many functions (Table 5.2) can be generated from oscillatory experiments. A comprehensive list of viscoelastic material functions and coefficients is available in Dealy (1994).

Extensional flow was investigated in Chapter 4. What has been discussed above, relative to shear flow, is also true for extensional flow. The extensional viscosity function is determined in steady-state extensional flow, but transient experiments generate data which reflect

the viscoelastic character of the material. The following tests, for example, could be conducted in tensile extension: tensile start-up, cessation of steady tensile extension, tensile step strain, tensile creep, and tensile recoil. This type of experimental testing leads to numerous viscoelastic material functions (Table 5.3). Similar functions could be generated for experiments involving biaxial or planar extensional flow.

Table 5.2. Material Functions Determined in Oscillatory Shear Testing (Harmonically Varying Simple Shear) Experiments

- Complex viscosity
- Dynamic viscosity
- Out-of-phase component of the complex viscosity
- Complex shear modulus
- Shear storage modulus
- Shear loss modulus
- Complex shear compliance
- Shear storage compliance
- Shear loss compliance

Linear Versus Non-linear Viscoelasticity. In process engineering, data on viscoelasticity may be very helpful in understanding various problems. Shear creep data, for example, are useful in examining gravity driven phenomena such as coating and sagging. This information can also be an invaluable tool in product development. Means of evaluating linear viscoelastic behavior are the primary foci of this chapter. When materials are tested in the linear range, material functions do not depend on the magnitude of the stress, the magnitude of the deforming strain, or the rate of application of the strain. If linear, an applied stress will produce a proportional strain response. Doubling the stress, for example, will double the strain response. The linear range of testing is determined from experimental data. Testing can easily enter the non-linear range by applying excessive strain (usually greater than 1%) or high deformation rates to a sample.

The importance of large deformation (non-linear) behavior in food rheology should not be overlooked. Many processes, such as mastication and swallowing, are only accomplished with very large deformations. Collecting viscoelastic data relevant to this type of problem involves

testing in the non-linear range of behavior. These data may be useful in attacking practical problems; however, from a fundamental standpoint, they can only be used for comparative purposes because the theoretical complexity of non-linear viscoelasticity makes it impractical for most applications. More research is needed in this area.

Table 5.3. Experimental Tests and Material functions Determined in Transient Tensile Extension

Tensile start-up: Material at rest is suddenly subjected to a constant extensional strain rate.
• Tensile stress growth function
Cessation of steady tensile extension: Material subjected to a steady state extensional strain rate is suddenly brought to rest.
• Tensile stress decay coefficient
Tensile step strain: Material at rest is given a sudden step increase in strain.
• Tensile relaxation modulus
Tensile creep: Material at rest is given a sudden step increase in tensile stress.
• Tensile creep compliance
• Tensile creep rate decay function
Tensile recoil: Material subject to steady state stress and strain has the stress suddenly reduced to zero.
• Tensile recoil function
• Ultimate tensile recoil function

5.2. Transient Tests for Viscoelasticity

In this section, three typical transient tests of viscoelasticity are presented: step strain (stress relaxation), creep, and start-up flow. These tests involve small strains and can be conducted with commercially available or easily constructed instruments. Although there are numerous potential experimental methods (Table 5.1 and 5.3) to elucidate viscoelasticity, many are difficult to perform and questionable for use on food products. Practical rheology is application driven so the most appropriate test for a particular material depends on the problem under consideration. Tests described in this section have all been conducted on food, and produced useful results.

5.2.1. Mechanical Analogues

Massless mechanical models, composed of springs and dashpots, are useful in conceptualizing rheological behavior. The spring is considered an ideal solid element obeying Hooke's law:

$$\sigma = G\gamma \qquad [5.1]$$

and the dashpot is considered an ideal fluid element obeying Newton's law:

$$\sigma = \mu\dot{\gamma} \qquad [5.2]$$

Springs and dashpots can be connected in various ways to portray the behavior of viscoelastic materials; however, a particular combination of elements is not unique because many different combinations can be used to model the same set of experimental data. The most common mechanical analogs of rheological behavior are the Maxwell and Kelvin (sometimes called Kelvin-Voigt) models depicted in Fig. 5.1.

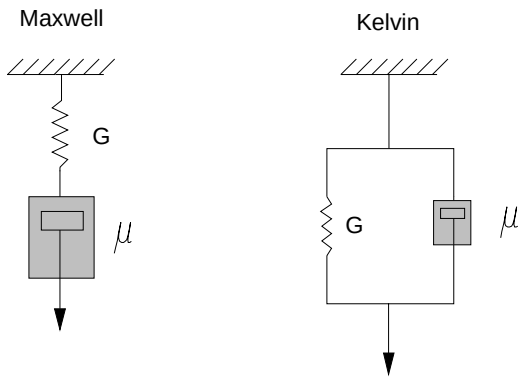

Figure 5.1. Maxwell and Kelvin models.

Mechanical analogues provide a useful means of investigating creep and step strain data. These data may also be presented in terms of various compliance and modulus distribution functions (or spectra) as well as electrical models (Mohsenin, 1986; Polakowski and Ripling, 1966; Sherman, 1970; Barnes et al., 1989; Whorlow, 1992; Ferry, 1980). In addition, step strain and creep curves can be normalized and presented in linear form (Peleg, 1980). This technique can be quite useful in biological materials where it is often difficult to achieve equilibrium conditions.

5.2.2. Step Strain (Stress Relaxation)

In a step strain test the sample is given an instantaneous strain and the stress required to maintain the deformation is observed as a function of time. This experiment is commonly known as a "stress relaxation" test and it may be conducted in shear, uniaxial tension, or uniaxial compression. Stress relaxation data may also be obtained by subjecting a fluid to a constant rate of strain (in, for example, a concentric cylinder viscometer), then suddenly stopping the deformation and observing the change in stress over time.

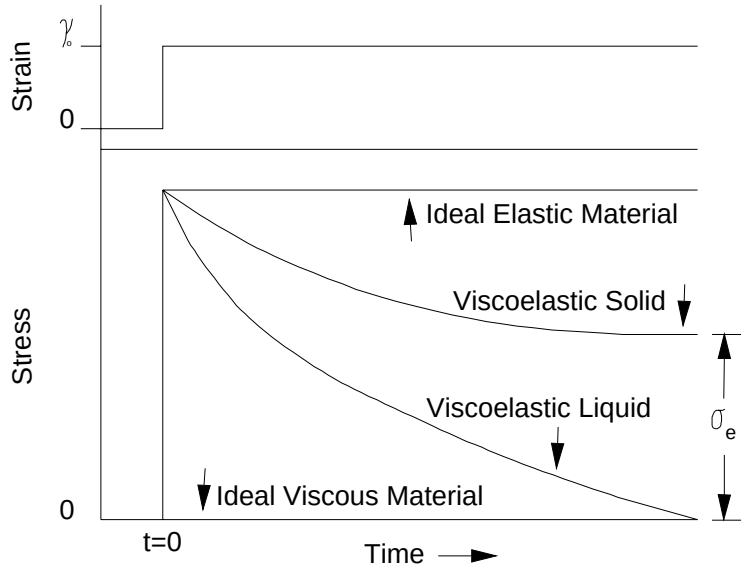

Figure 5.2. Stress relaxation curves.

A wide range of behavior may be observed in stress relaxation tests (Fig. 5.2). No relaxation would be observed in ideal elastic materials while ideal viscous substances would relax instantaneously. Viscoelastic materials would relax gradually with the end point depending on the molecular structure of the material being tested: stress in viscoelastic solids would decay to an equilibrium stress ($\sigma_e > 0$), but the residual stress in viscoelastic liquids would be zero.

Stress relaxation data are commonly presented in terms of a stress relaxation modulus:

$$G = f(t) = \frac{\sigma}{\gamma_{constant}} \qquad [5.3]$$

If a material is perfectly elastic, the relaxation modulus is equal to the shear modulus defined by Eq. [1.10]: $G = \sigma/\gamma$. $G(t)$ is a similar, but time-dependent, quantity determined from experimental data. Curves of the stress relaxation modulus versus time, generated at different levels of strain, overlap if data are collected in the linear viscoelastic region of material behavior. Related functions (Ferry, 1980) can be found in tension ($E(t)$) and bulk compression ($K(t)$).

The Maxwell model, one which contains a Hookean spring in series with a Newtonian dashpot, has frequently been used to interpret stress relaxation data for viscoelastic liquids, particularly polymeric liquids. The total shear strain in a Maxwell fluid element (Fig. 5.1) is equal to the sum of the strain in the spring and the dashpot:

$$\gamma = (\gamma)_{spring} + (\gamma)_{dashpot} \qquad [5.4]$$

Differentiating Eq. [5.4] with respect to time, and using the definitions provided by Eq. [5.1] and [5.2], yields

$$\frac{d\gamma}{dt} = \dot{\gamma} = \frac{1}{G}\left(\frac{d\sigma}{dt}\right) + \frac{\sigma}{\mu} \qquad [5.5]$$

or

$$\sigma + \lambda_{rel}\left(\frac{d\sigma}{dt}\right) = \mu\dot{\gamma} \qquad [5.6]$$

where the relaxation time (also called the characteristic time of a Maxwell fluid) is defined as

$$\lambda_{rel} = \frac{\mu}{G} \qquad [5.7]$$

Although an exact definition of λ_{rel} is difficult, it can be thought of as the time it takes a macromolecule to be stretched out when deformed. Relaxation times for common fluids vary a great deal as shown by the information in Table 5.4. The above equations are presented in terms of shear deformation. If testing is conducted in uniaxial tension or compression, then the relaxation time can be thought of in terms of an extensional viscosity (η_E) and Young's modulus (E).

Table 5.4. Relaxation Time and Limiting Viscosity at Zero Shear for various Viscoelastic Fluids (Source: Tanner, 1985).

Fluid	T (°C)	λ_{rel} (s)	η_o (Pa s)
Water	20	1E-12	0.001
Mineral oil	30	7E-10	0.5
Poly-dimethylsiloxane	30	1E-6	0.3
	125	1.7E-4	100
Low-density polyethylene	115	10	2E5
	240	0.1	3000
High-density polyethylene	180	0.07	2000
	220	0.05	1000
High-impact polystyrene	170	7	2E5
	210	3	1E5
0.5% Hydroxyethyl-cellulose in water	27	0.1	1.3
Glass	27	> 1E5	> 1E18

The Maxwell model is useful in understanding stress relaxation data. Consider a step strain (stress relaxation) experiment where there is a sudden application of a constant shear strain, γ_o . When the strain is constant, the shear rate is equal to zero ($\dot{\gamma} = 0.0$) and Eq. [5.6] becomes

$$\sigma + \lambda_{rel}\left(\frac{d\sigma}{dt}\right) = 0 \qquad [5.8]$$

This equation may be integrated using the initial condition that $\sigma = \sigma_o$ at $t = 0$:

$$\int_{\sigma_o}^{\sigma} \frac{d\sigma}{\sigma} = \int_0^t -\frac{dt}{\lambda_{rel}} \qquad [5.9]$$

or, after evaluating the integral,

$$\sigma = f(t) = \sigma_o \exp\left(\frac{-t}{\lambda_{rel}}\right) \qquad [5.10]$$

Eq. [5.10] describes the gradual relaxation of stress (from σ_o to zero) after the application of a sudden strain. The relationship provides a means of determining the relaxation time: λ_{rel} is the time it takes for the stress to decay to 1/e (approximately 36.8%) of its initial value.

Experimental data show that the Maxwell model does not account for the stress relaxation behavior of many viscoelastic materials because it does not include an equilibrium stress (σ_e). This problem may be addressed for numerous foods by constructing a model which has a single Maxwell element connected in parallel with a spring. The stress relaxation equation described by this mechanical model (Fig. 5.3a) is

$$\sigma = f(t) = \sigma_e + (\sigma_o - \sigma_e)\exp\left(\frac{-t}{\lambda_{rel}}\right) \qquad [5.11]$$

with the free spring (where $\sigma_e = \gamma_o G_0$) accounting for the equilibrium stress (Fig. 5.4). The relaxation time is defined in terms of the standard Maxwell portion of the model: $\lambda_{rel} = \mu_1/G_1$. Application of Eq. [5.11] is illustrated in Example Problem 5.8.1.

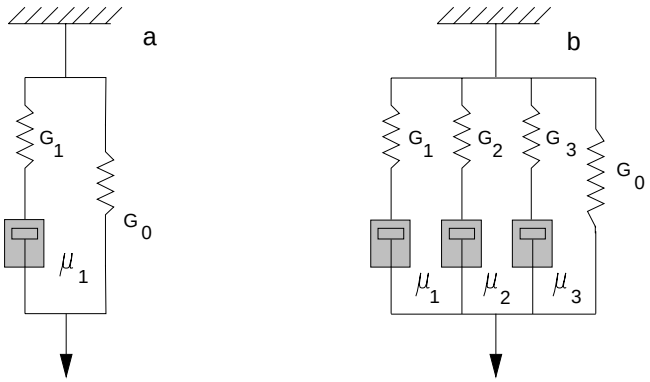

Figure 5.3. Maxwell elements in parallel with a spring: a) one Maxwell element and a free spring, b) three Maxwell elements and a free spring.

Added complexity can be obtained by constructing a more generalized Maxwell model consisting of several Maxwell elements in parallel with an independent spring. If the system is subjected to a constant strain, the total stress is the sum of the individual stresses in each element. In a four element model, a model containing three Maxwell elements and a spring (Fig. 5.3b), the solution for stress as a function of time is

$$\sigma = f(t) = A_1\exp\left(\frac{-tG_1}{\mu_1}\right) + A_2\exp\left(\frac{-tG_2}{\mu_2}\right) + A_3\exp\left(\frac{-tG_3}{\mu_3}\right) + \gamma_o G_0 \qquad [5.12]$$

or

$$\sigma = f(t) = A_1 \exp\left(\frac{-t}{(\lambda_{rel})_1}\right) + A_2 \exp\left(\frac{-t}{(\lambda_{rel})_2}\right) + A_3 \exp\left(\frac{-t}{(\lambda_{rel})_3}\right) + \sigma_e \qquad [5.13]$$

where the subscripts refer to different mechanical elements in the system. Each Maxwell element may have a different relaxation time. This concept can be generalized to determine a relaxation spectra for a viscoelastic material (Ferry, 1980). Eq. [5.10], [5.11], [5.12], and [5.13] can be expressed in terms of the relaxation modulus, defined by Eq. [5.3], by dividing each equation by the applied strain.

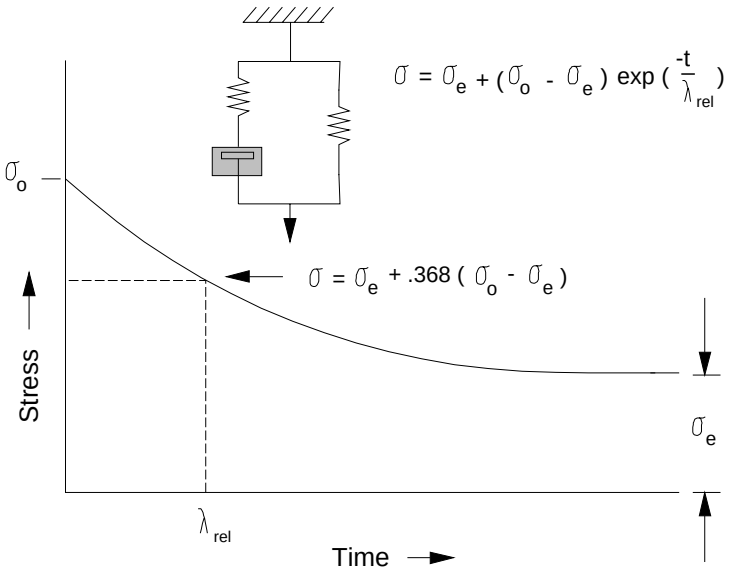

Figure 5.4. Typical stress relaxation curve modeled with Eq. [5.11] describing a single Maxwell element in parallel with a spring.

Peleg and Normand (1983) noted two major problems in collecting stress relaxation data for foods: 1) When subjected to large deformation they usually exhibit non-linear viscoelastic behavior; 2) Natural instability or biological activity make it difficult to determine equilibrium mechanical parameters. To overcome these difficulties, they

suggest stress relaxation data be calculated as a normalized stress (a normalized force term is also acceptable) and fit to the following linear equation:

$$\frac{\sigma_o t}{\sigma_o - \sigma} = k_1 + k_2 t \qquad [5.14]$$

where σ_o is the initial stress, σ is the decreasing stress at time t, and k_1 and k_2 are constants. The reciprocal of k_1 depicts the initial decay rate and k_2 is a hypothetical value of the asymptotic normalized force. Fitting experimental data to Eq. [5.14] is a quick and effective way to handle stress relaxation data for many foods. Typical values of k_1 and k_2 are summarized in Table 5.5. Also, the technique is illustrated for apple tissue in Example Problem 5.8.2.

Table 5.5. Stress Relaxation Parameters of Eq. [5.14] for Various Biological Materials (Source: Peleg and Normand, 1983)

Material	k_1 (s or min)	k_2 -
Cheddar Cheese	3.23 min	1.11
Corn Grains	10.9 min	5.18
Low Methoxyl Pectin Gel (No.31)	68.2 s	1.21
Pea Beans	2.41 s	2.26
Potato Flesh	4.40 s	1.56

5.2.3. Creep and Recovery

In a creep test, an instantaneous stress is applied to the sample and the change in strain (called the creep) is observed over time. When the stress is released, some recovery may be observed as the material attempts a return to the original shape. Increased availability of controlled stress rheometers has greatly improved our ability to conduct shear creep and recovery experiments on a wide variety of materials. These tests can be particularly useful in studying the behavior existing in constant stress environments such as those found in leveling, sedimentation, and coating applications where gravity is the driving force.

Creep experiments can also be conducted in uniaxial tension or compression. The analytical methods presented in this section have been used to study typical fluid foods like salad dressing (Paredes et al., 1989), and very complex bodies such as whole oranges (Chuma et al., 1978).

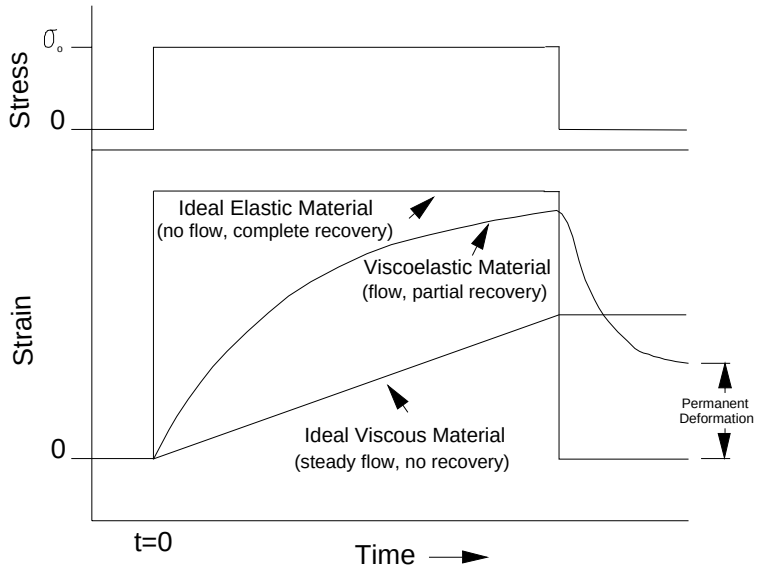

Figure 5.5. Creep and recovery curves.

Idealized creep and recovery curves are illustrated in Fig. 5.5. Subjected to a constant stress, strain in an ideal elastic material would be constant due to the lack of flow, and the material would return to the original shape upon removal of stress. An ideal viscous material would show steady flow, producing a linear response to stress with the inability to recover any of the imposed deformation. Viscoelastic materials (e.g., bread dough) would exhibit a nonlinear response to strain and, due to their ability to recover some structure by storing energy, show a permanent deformation less than the total deformation applied to the sample. This strain recovery, or creep recovery, is also called recoil and may be investigated in terms of a recoil function (Dealy, 1994).

Creep data may be described in terms of a creep compliance function:

$$J = f(t) = \frac{\gamma}{\sigma_{\text{constant}}} \qquad [5.15]$$

Compliance curves generated at different stress levels overlap when data are collected in the range of linear viscoelastic behavior. With a perfectly elastic solid, $J = 1/G$, the reciprocal of the shear modulus; however, different time patterns in experimental testing mean that $J(t) \neq 1/G(t)$. Eq. [5.15] is presented in terms of shear deformation. Similar material functions (Ferry, 1980) can be determined from creep data generated in tension ($D(t)$) and bulk compression ($B(t)$) studies.

To develop a mechanical analog describing creep behavior, the starting point is the Kelvin model (Fig. 5.1) which contains a spring connected in parallel with a dashpot. When this system is subjected to shear strain, the spring and dashpot are strained equally:

$$\gamma = (\gamma)_{\text{spring}} = (\gamma)_{\text{dashpot}} \qquad [5.16]$$

The total shear stress (σ) caused by the deformation is the sum of the individual shear stresses which, using Eq. [5.1] and Eq. [5.2], can be written as

$$\sigma = G\gamma + \mu\dot{\gamma} \qquad [5.17]$$

Differentiating Eq. [5.17] with respect to time yields

$$\frac{1}{G}\frac{d\sigma}{dt} = \dot{\gamma} + (\lambda_{\text{ret}})\frac{d\dot{\gamma}}{dt} \qquad [5.18]$$

where the retardation time ($\lambda_{\text{ret}} = \mu/G$) is unique for any substance. If a material was a Hookean solid, the retardation time would be zero and the maximum strain would be obtained immediately with the application of stress: Time to achieve maximum strain in viscoelastic materials is delayed (or retarded). The retardation time can be thought of in terms of extensional viscosity (η_E) and Young's modulus (E) if testing is conducted in uniaxial tension or compression.

In creep, where the material is allowed to flow after being subjected to a constant shear stress (σ_o), the change in stress with time is zero ($d\sigma/dt = 0$) and the solution to Eq. [5.18] is

$$\gamma = f(t) = \frac{\sigma_o}{G}\left(1 - \exp\left(\frac{-t}{\lambda_{\text{ret}}}\right)\right) \qquad [5.19]$$

showing that the initial strain is zero ($\gamma = 0$ at $t = 0$). Eq. [5.19] predicts a strain that asymptotically approaches the maximum strain (σ_o/G) associated with the spring. λ_{ret} is the time taken for the delayed strain to reach approximately 63.2% (1-1/e) of the final value. Materials with a large retardation time reach full deformation slowly.

The Kelvin model (Fig. 5.1) shows excellent elastic retardation but is not general enough to model creep in many biological materials. The solution to this problem is to use a Burgers model (Fig. 5.6) which is a Kelvin and a Maxwell model placed in series. Data following this mechanical analog show an initial elastic response due to the free spring, retarded elastic behavior related to the parallel spring-dashpot combination, and Newtonian type flow after long periods of time due to the free dashpot (Fig. 5.7):

$$\gamma = f(t) = \frac{\sigma_o}{G_0} + \frac{\sigma_o}{G_1}\left(1 - \exp\left(\frac{-t}{\lambda_{ret}}\right)\right) + \frac{\sigma_o t}{\mu_0} \qquad [5.20]$$

where $\lambda_{ret} = \mu_1/G_1$, the retardation time of the Kelvin portion of the model.

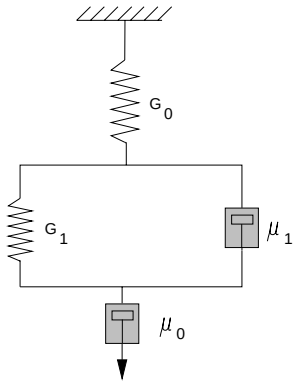

Figure 5.6. Four element Burgers model.

The Burgers model can also be expressed in terms of creep compliance by dividing Eq. [5.20] by the constant stress:

$$\frac{\gamma}{\sigma_o} = f(t) = \frac{1}{G_0} + \frac{1}{G_1}\left(1 - \exp\left(\frac{-t}{\lambda_{ret}}\right)\right) + \frac{t}{\mu_0} \qquad [5.21]$$

Writing the result as a creep compliance function (Eq. [5.15]) yields

$$J = f(t) = J_0 + J_1\left(1 - \exp\left(\frac{-t}{\lambda_{ret}}\right)\right) + \frac{t}{\mu_0} \qquad [5.22]$$

where J_0 is the instantaneous compliance, J_1 is the retarded compliance, λ_{ret} is the retardation time (μ_1/G_1) of the Kelvin component, and μ_0 is the Newtonian viscosity of the free dashpot. The sum of J_o and J_1 is called the steady state compliance. Using the same procedure, Eq. [5.19] could also be expressed in term of the creep compliance function. The Burgers model (Fig. 5.6), less the free spring (G_o), is sometimes called the Jeffreys model. Eq. [5.22] is applied to skim milk curd in Example Problem 5.8.3. Parameters of Eq. [5.22], for creamy salad dressing, are given in Appendix 6.19.

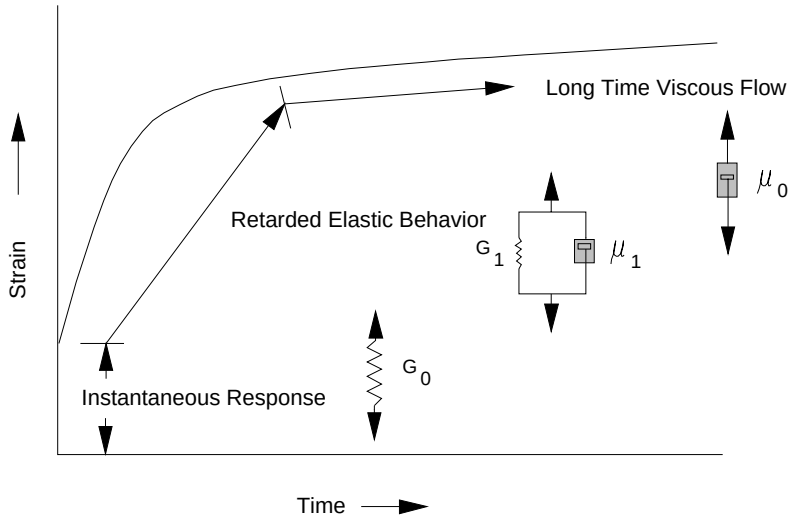

Figure 5.7. Typical creep curve showing where various elements of the Burgers model (Fig. 5.6 and Eq. [5.20]) describe flow behavior.

When conducting creep experiments, controlled stress rheometers allow one to measure the strain recovered when the constant stress is removed. The complete creep and recovery curve may be expressed using the Burgers model (Fig. 5.6). When calculated as compliance, the creep is given by Eq. [5.22] for $0 < t < t_1$ where t_1 is the time when the constant stress is removed. At the beginning of creep, there is an

instantaneous change in compliance (J_0) due to the spring in the Maxwell portion of the model (Fig. 5.8). Then, the Kelvin component produces an exponential change in compliance related to the retardation time. After sufficient time has passed, the independent dashpot (Fig. 5.6) generates a purely viscous response. Data from the linear portion of the creep curve (Fig. 5.8) are related to two parameters: the slope is equal to $1/\mu_0$; and the intercept, sometimes called the steady state compliance, is equal to $J_0 + J_1$.

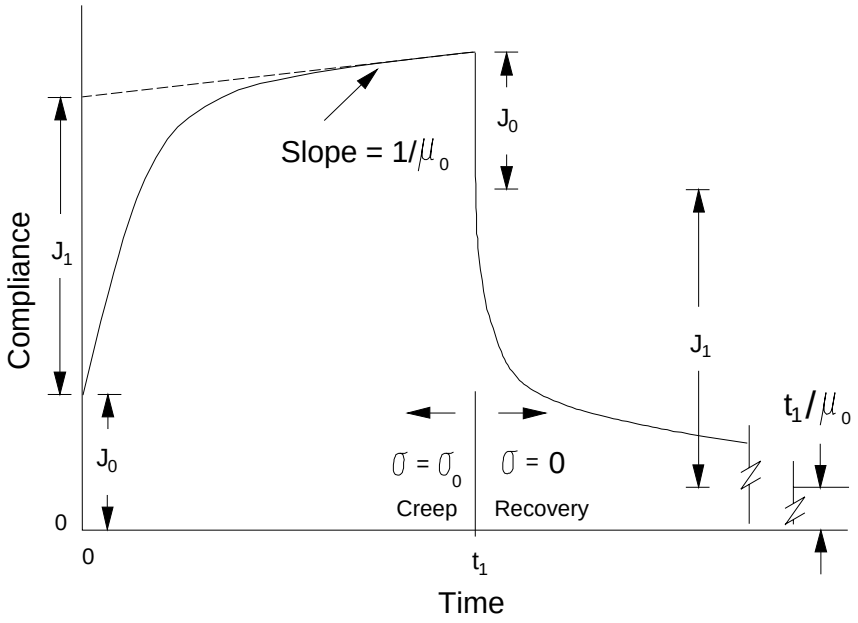

Figure 5.8. Compliance and recovery (or recoil) curves showing compliance parameters for the Burgers model (Fig. 5.6 and Eq. [5.22]).

At $t = t_1$, the stress is removed ($\sigma = 0$) and there is an instantaneous change in compliance (Fig. 5.8) equal to J_0. The free dashpot causes permanent deformation in the material related to a compliance of t_1/μ_0. This factor is directly related to the non-recoverable sample strain of $\sigma_0 t_1/\mu_0$. If a substance obeying the Burgers model is tested in the linear

viscoelastic region of material behavior, then the values of J_0 and J_1 determined from the creep curve will be equal to the values of J_0 and J_1 determined from the recovery curve.

If necessary, additional Kelvin elements can be added to the Burgers model to better represent experimental data. Mathematically, this idea can be described with the following equation:

$$J = f(t) = J_0 + \sum_{i=1}^{m}\left[J_i\left(1 - \exp\left(\frac{-t}{(\lambda_{ret})_i} \right)\right)\right] + \frac{t}{\mu_0} \qquad [5.23]$$

where m is the total number of Kelvin elements in the model, each having a unique retarded compliance and retardation time. A system with two Kelvin elements ($m = 2$) was used by Halim and Shoemaker (1990) to model skim milk curd. This model is explored in Example Problem 5.8.3. The same equation worked well for Purkayastha et al. (1985) in evaluating the compressive creep behavior of potato flesh and cheddar cheese. Balaban et al. (1988) presented systematic procedures to determine the constants involved in Eq. [5.23]. Some advanced rheometers provide computer software to generate appropriate constants. A simple linearized model (presented in Example Problem 5.8.3), similar to Eq. [5.14], has been suggested by Peleg (1980) to characterize the creep of biological materials.

5.2.4. Start-Up Flow (Stress Overshoot)

During start-up flow, a shear rate is suddenly imposed on a viscoelastic fluid held previously at rest. Shear stress produced by this transient deformation displays an initial overshoot before reaching a steady-state value; hence, the phenomenon is commonly referred to as stress overshoot. Results can be used to produce a shear stress growth function. The general behavior can be modeled using an empirical equation developed by Leider and Bird (1974) which includes rheological properties related to the first normal stress difference, and the shear rate. This equation, usually called the Bird-Leider equation, is expressed as a function of time and the applied shear rate:

$$\sigma_{21}^{+} = f(\dot{\gamma}, t) = K(\dot{\gamma})^n \left(1 + (b\dot{\gamma}t - 1)\exp\left(\frac{-t}{an\lambda} \right)\right) \qquad [5.24]$$

where:

$$\lambda = \left(\frac{K'}{2K} \right)^{1/(n'-n)} \qquad [5.25]$$

$$\sigma_{21} = K(\dot{\gamma})^n \qquad [5.26]$$

$$\sigma_{11} - \sigma_{22} == K'(\dot{\gamma})^{n'} \qquad [5.27]$$

λ is the time constant while *a* and *b* are adjustable parameters. Over short periods of time, the equation models the elastic response (sudden overshoot) of the material. Once the peak torque is reached, exponential decay is simulated. After long periods of time, the Bird-Leider equation collapses to the standard power law equation:

$$\sigma^+_{21\infty} = f(\dot{\gamma}, t = \infty) = K(\dot{\gamma})^n \qquad [5.28]$$

Typical curves of Eq. [5.24], modeling the behavior of mayonnaise, are illustrated in Fig. 5.9. The information is plotted in terms of a dimensionless shear stress:

$$\frac{\sigma^+_{21}}{\sigma^+_{21\infty}} = 1 + (b\dot{\gamma}t - 1)\exp\left(\frac{-t}{an\lambda}\right) \qquad [5.29]$$

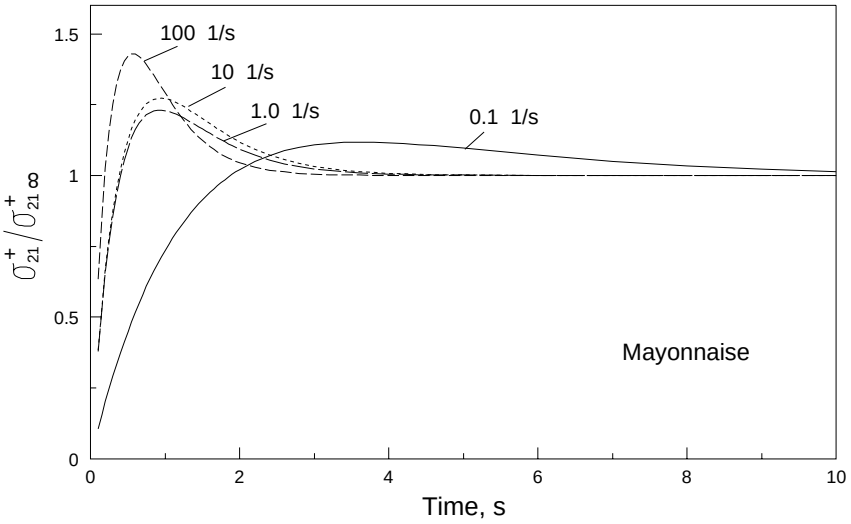

Figure 5.9. Typical stress overshoot curves at various shear rates for mayonnaise at 25°C (based on data from Kokini and Dickie, 1981).

The Bird-Leider equation was used by Kokini and Dickie (1981) and Dickie and Kokini (1982) to evaluate stress overshoot data for various foods including ketchup, mustard, mayonnaise, apple butter, butter, margarine, and canned frosting. The authors concluded that the relationship provided a moderately good prediction of peak shear stress and peak times but gave only a crude prediction of stress decay. Campanella and Peleg (1987b) were able to get a better fit of stress growth data for mayonnaise using a more complex model proposed by Larson (1985). The Bird-Leider equation, in strictly empirical form (K, n, K', n' not required) has also been used to interpret stress overshoot behavior in cream (Prentice, 1992). Stress overshoot data were found useful in modeling the human perception of fluid thickness in the mouth (Dickie and Kokini, 1983).

5.3. Oscillatory Testing

In oscillatory instruments, samples are subjected to harmonically varying stress or strain. This testing procedure is the most common dynamic method for studying the viscoelastic behavior of food. Results are very sensitive to chemical composition and physical structure so they are useful in a variety of applications including gel strength evaluation, monitoring starch gelatinization, studying the glass transition phenomenon, observing protein coagulation or denaturation, evaluating curd formation in dairy products, cheese melting, texture development in bakery and meat products, shelf-life testing, and correlation of rheological properties to human sensory perception. Food scientists have found oscillatory testing instruments to be particularly valuable tools for product development work.

Oscillatory testing may be conducted in tension, bulk compression, or shear. Typical commercial instruments operate in the shear deformation mode and this is the predominant testing method used for food. Shear strain may be generated using parallel plate, cone and plate, or concentric cylinder fixtures. Dynamic testing instruments may be divided into two general categories: controlled rate instruments where the deformation (strain) is fixed and stress is measured, and controlled stress instruments where the stress amplitude is fixed and the deformation is measured. Both produce similar results. The emphasis in this section is on fluid and semi-solid foods. Dynamic testing of solid foods has been reviewed by Rao and Skinner (1986).

Application of Stress and Strain. A number of assumptions are made in developing the mathematical equations to describe oscillatory testing: strain is the same at all points in the sample, sample inertia may be neglected, and the material behaves as a linear viscoelastic substance. When these assumptions are violated, more complex analytical considerations enter the problem (Whorlow, 1992).

In oscillatory tests, materials are subjected to deformation (in controlled rate instruments) or stress (in controlled stress instruments) which varies harmonically with time. Sinusoidial, simple shear is typical. To illustrate the concept, consider two rectangular plates oriented parallel to each other (Fig. 5.10). The lower plate is fixed and the upper plate is allowed to move back and forth in a horizontal direction. Assume the sample being tested is located between the plates of a controlled rate device. Suppose the strain in the material between the plates is a function of time defined as

$$\gamma = \gamma_o \sin(\omega t) \qquad [5.30]$$

where γ_o is the amplitude of the strain equal to L/h when the motion of the upper plate is $L \sin(\omega t)$. ω is the frequency expressed in rad/s which is equivalent to $\omega/(2\pi)$ hertz. The period of time required to complete one cycle is equal to $2\pi/\omega$. If the two plates (Fig. 5.10) were separated by a distance of 1.5 mm and the upper moved 0.3 mm from the center line, then the maximum strain amplitude may be calculated as 0.2 or 20%: $\gamma_o = L/h = 0.3/1.5 = 0.2$. A 10% strain could be achieved by maintaining $h = 1.5$ mm and moving the plate 0.15 mm.

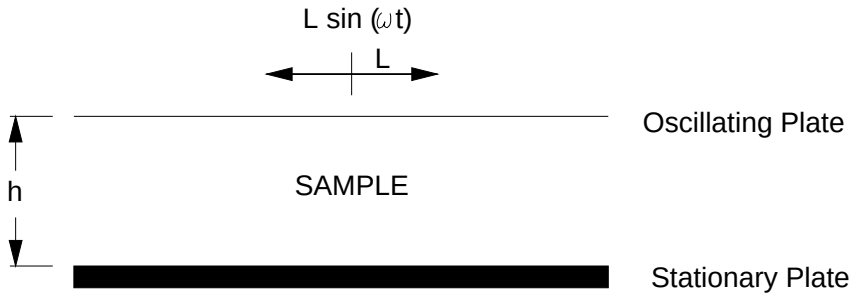

Figure 5.10. Oscillatory strain between rectangular plates.

Effects of changing the amplitude and frequency on the input strain function are illustrated in Fig. 5.11. Doubling the amplitude from 0.1 (Curve 2) to 0.2 (Curve 1 or Curve 3) doubles the height of the curve. Doubling the frequency from 1 rad/s (Curve 1) to 2 rad/s (Curve 2 or Curve 3) cuts, by one-half, the time between peaks of the two curves.

Using a sine wave for strain input results in a periodic shear rate found by taking the derivative of Eq. [5.30]:

$$\frac{d\gamma}{dt} = \dot{\gamma} = \frac{d(\gamma_o \sin(\omega t))}{dt} \qquad [5.31]$$

which can be evaluated as

$$\dot{\gamma} = \gamma_o \omega \cos(\omega t) \qquad [5.32]$$

With a small strain amplitude (so the material will behave in a linear viscoelastic manner), the following shear stress is produced by the strain input:

$$\sigma = \sigma_o \sin(\omega t + \delta) \qquad [5.33]$$

where σ_o is the amplitude of the shear stress (not to be confused with the yield stress symbolized by σ_o in earlier chapters) and δ is the phase lag or phase shift (also called the mechanical loss angle) relative to the strain. The time period associated with the phase lag is equal to δ/ω. σ_o can be thought of as the peak force per unit area received by the stationary plate (Fig. 5.10). Dividing both sides of Eq. [5.33] by γ_o yields

$$\frac{\sigma}{\gamma_o} = \left(\frac{\sigma_o}{\gamma_o}\right) \sin(\omega t + \delta) \qquad [5.34]$$

The complete results of small amplitude oscillatory tests can be described by plots of the amplitude ratio (σ_o/γ_o) and the phase shift (δ) as frequency dependent functions. These parameters alone, however, are not commonly used to describe results and other material functions (which may all be written in terms of σ_o/γ_o and δ) have been defined.

The shear stress output produced by a sinusoidal strain input may be written as

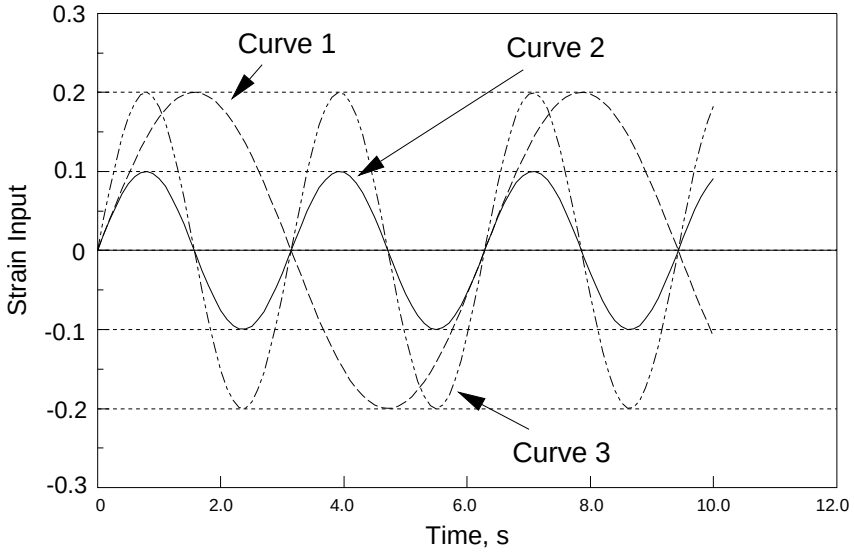

Figure 5.11. Strain input functions showing variations in frequency and strain amplitude: Curve 1) $\gamma_o = 0.2$, $\omega = 1$ rad/s*; Curve 2)* $\gamma_o = 0.1$, $\omega = 2$ rad/s*; Curve 3)* $\gamma_o = 0.2$, $\omega = 2$ rad/s.

$$\sigma = G'\gamma + (G''/\omega)\dot{\gamma} \qquad [5.35]$$

G' (called the shear storage modulus) and G'' (called the shear loss modulus) are both functions of frequency and can be expressed in terms of the amplitude ratio and the phase shift:

$$G' = \left(\frac{\sigma_o}{\gamma_o}\right)\cos(\delta) \qquad [5.36]$$

and

$$G'' = \left(\frac{\sigma_o}{\gamma_o}\right)\sin(\delta) \qquad [5.37]$$

$G'\gamma_o$ may be interpreted as the component of the stress in phase with the strain: $G''\gamma_o$ may be interpreted as the component of the stress 90° out of phase with the strain. Additional frequency dependent material functions (Table 5.2) include the complex modulus (G^*), complex vis-

cosity (η^*), dynamic viscosity (η'), out of phase component of the complex viscosity (η''), complex compliance (J^*), storage compliance (J'), and the loss compliance (J''):

$$G^* = \frac{\sigma_o}{\gamma_o} = \sqrt{(G')^2 + (G'')^2} \qquad [5.38]$$

$$\eta^* = \frac{G^*}{\omega} = \sqrt{(\eta')^2 + (\eta'')^2} \qquad [5.39]$$

$$\eta' = \frac{G''}{\omega} \qquad [5.40]$$

$$\eta'' = \frac{G'}{\omega} \qquad [5.41]$$

$$J^* = \frac{1}{G^*} \qquad [5.42]$$

$$J' = \frac{G'}{(G')^2 + (G'')^2} \qquad [5.43]$$

$$J'' = \frac{G''}{(G')^2 + (G'')^2} \qquad [5.44]$$

Although $J^* = 1/G^*$, it is important to note that $J' \neq 1/G'$ and $J'' \neq 1/G''$. Oscillatory data for various food products may be found in Appendices [6.20], [6.21], and [6.22].

Using Eq. [5.40], Eq. [5.35] can be expressed as

$$\sigma = G'\gamma + \eta'\dot{\gamma} \qquad [5.45]$$

which is an excellent equation to represent material behavior because it clearly indicates the elastic ($G'\gamma$) and viscous ($\eta'\dot{\gamma}$) nature of a substance. This idea is expanded in Sec. 5.5 to explain the behavior of "silly putty" using the Deborah number concept.

Another popular material function used to describe viscoelastic behavior is the tangent of the phase shift or phase angle (called tan delta) which is also a function of frequency:

$$\tan(\delta) = \frac{G''}{G'} \qquad [5.46]$$

This parameter is directly related to the energy lost per cycle divided by the energy stored per cycle. Since $0 \leq \delta \leq \pi/2$, $\tan\delta$ can vary from zero to infinity. Observations of polymer systems give the following numerical ranges for $\tan\delta$: very high for dilute solutions, 0.2 to 0.3 for

amorphous polymers, low (near 0.01) for glassy crystalline polymers and gels. Values of $\tan\delta$ for typical food systems (dilute solution, concentrated solution, and gel) are considered in Sec. 5.4.

To better understand the viscoelastic parameters defined above, it is helpful to look at behavior which is solely Hookean or solely Newtonian. If a material is a Hookean solid, the stress and strain are in phase and $\delta = 0$. Hence, G'' and η' are also equal to 0 because there is no viscous dissipation of energy. In this case, G' is a constant equal to the shear modulus (G). If a material behaves as a Newtonian fluid, the stress (Eq. [5.33]) and strain (Eq. [5.30]) are 90 degrees out of phase ($\delta = \pi/2$); hence, the shear rate (Eq. [5.32]) is also 90 degrees out of phase with the shear stress. In this case, G' and η'' are zero because the material does not store energy. Then, η' is constant and equal to the Newtonian viscosity (μ). Similar behavior is often observed for non-Newtonian fluids as the frequency approaches zero.

Further assessment of the phase lag concept can help clarify the meaning of σ_o given as part of the amplitude ratio in Eq. [5.34]. As the phase lag approaches zero, force is transmitted through the sample (Fig. 5.10) quickly and the changes in stress are observed at nearly the same time as the applied deformation produces strain. In solids, rapid force transmission is due to the crystalline nature of the material. The amount of force transmitted for a given strain depends on the material modulus. In a Hookean solid the maximum force per unit area transmitted through the sample (σ_o) is equal to the shear modulus times the maximum strain ($G\gamma_o$). Viscous heating absorbs some energy in viscoelastic materials resulting in smaller values of σ_o.

The phase lag approaches the maximum value of $\pi/2$ with fluids exhibiting a high degree of Newtonian behavior. The maximum force per unit area (σ_o) transmitted through a Newtonian fluid depends on the maximum shear rate induced during deformation. Considering Eq. [5.32], the maximum shear rate is frequency dependent and may be calculated as $\gamma_o\,\omega$. Consequently, σ_o is equal to the maximum shear rate times the viscosity ($\gamma_o\,\omega\mu$) for a Newtonian fluid. σ_o is larger in viscoelastic materials that have less tendency to flow: In these substances, greater force is transmitted through the sample because the viscous dissipation of energy is smaller.

The Maxwell fluid model (Fig. 5.1) is often used to interpret data from dynamic testing of polymeric liquids. If the strain input is harmonic, $\gamma = \gamma_o \sin(\omega t)$, then $\dot{\gamma} = \gamma_o \omega \cos(\omega t)$. This relationship (Eq. [5.32]) can be substituted into Eq. [5.6] and the resulting differential equation solved to produce a number of frequency dependent rheological functions for Maxwell fluids:

$$G' = \frac{G\omega^2\lambda_{rel}^2}{1+\omega^2\lambda_{rel}^2} \qquad [5.47]$$

$$G'' = \frac{G\omega\lambda_{rel}}{1+\omega^2\lambda_{rel}^2} \qquad [5.48]$$

$$\eta' = \frac{\eta}{1+\omega^2\lambda_{rel}^2} \qquad [5.49]$$

$$\tan\delta = \frac{G''}{G'} = \frac{1}{\omega\lambda_{rel}} \qquad [5.50]$$

where λ_{rel}, the relaxation time of a Maxwell fluid, is equal to μ/G. Looking at experimental data may allow material constants of the Maxwell model to be evaluated from the asymptotes: as ω goes to zero, η' goes to η; and as ω goes to infinity, G' goes to G. These ideas are used in Sec. 5.5 to examine the behavior of "silly putty."

Comparison of Moduli and Compliances. The mathematical relationships presented in this section are for shear deformation. Analogous moduli and compliances can be defined for the tension (or compression) and bulk compression modes of deformation (Table 5.6). These functions are generally more difficult to measure than shear functions and few data are available in the published literature. Analogues for the relaxation modulus and creep compliance are also presented in Table 5.6.

Typical Operating Modes of an Oscillatory Testing Instrument. Commercially available oscillatory instruments will operate in numerous modes. A strain or stress sweep, conducted by varying the amplitude of the input signal at a constant frequency (Fig. 5.12), is used to determine the limits of linear viscoelastic behavior by identifying a critical value of the sweep parameter. In the linear region (Fig. 5.13), rheological properties are not strain or stress dependent. Storage and

loss moduli versus the sweep parameter are plotted in Fig. 5.13. Some experimenters prefer to plot combined material functions such as the complex modulus or the complex viscosity.

Table 5.6. Comparison of Moduli and Compliances Determined in Oscillatory Testing Using Three Modes of Deformation: Shear, Bulk Compression, and Tension (Ferry, 1980).

	Shear	Bulk Compression	Tension
Complex Modulus	$G^*(\omega)$	$K^*(\omega)$	$E^*(\omega)$
Storage Modulus	$G'(\omega)$	$K'(\omega)$	$E'(\omega)$
Loss Modulus	$G''(\omega)$	$K''(\omega)$	$E''(\omega)$
Complex Compliance	$J^*(\omega)$	$B^*(\omega)$	$D^*(\omega)$
Storage Compliance	$J'(\omega)$	$B'(\omega)$	$D'(\omega)$
Loss Compliance	$J''(\omega)$	$B''(\omega)$	$D''(\omega)$
Relaxation Modulus	$G(t)$	$K(t)$	$E(t)$
Creep Compliance	$J(t)$	$B(t)$	$D(t)$

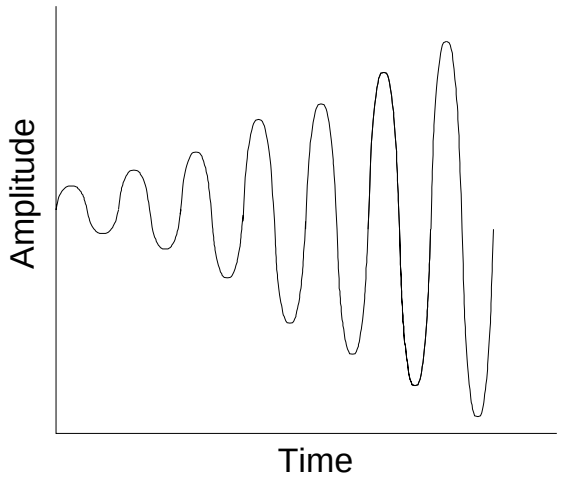

Figure 5.12. Strain or stress sweep mode in oscillatory testing.

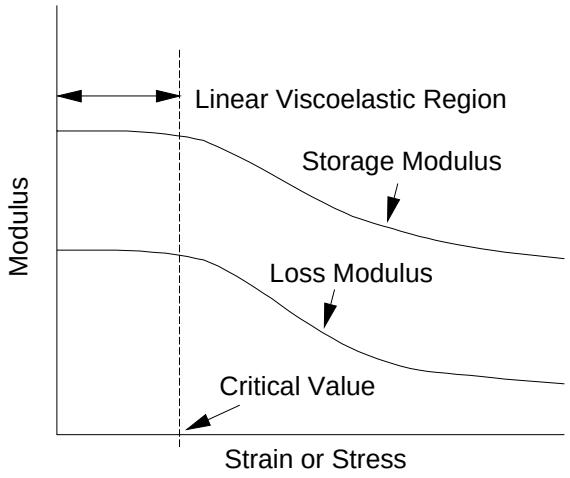

Figure 5.13. Typical response to a strain or stress sweep showing the linear viscoelastic region defined by the critical value of the sweep parameter.

Strain and stress sweeps are conducted on controlled rate and controlled stress instruments, respectively. It has been suggested that stress sweeps produce superior results (Holland, 1994); however, both strain and stress sweeps are known to provide an excellent basis for comparing the viscoelastic nature food products. In addition to establishing the linear viscoelastic range of the sweep parameter, strain and stress sweeps have been used to differentiate weak and strong gels: Strong gels may remain in the linear viscoelastic region over greater strains than weak gels.

The frequency sweep is probably the most common mode of oscillatory testing because it shows how the viscous and elastic behavior of the material changes with the rate of application of strain or stress. In this test the frequency is increased while the amplitude of the input signal (stress or strain) is held constant (Fig. 5.14). Frequency sweeps are very useful in comparing, sometimes called "finger printing," different food products or in comparing the effects of various ingredients and processing treatments on viscoelasticity. Materials usually exhibit more solid like characteristics at higher frequencies.

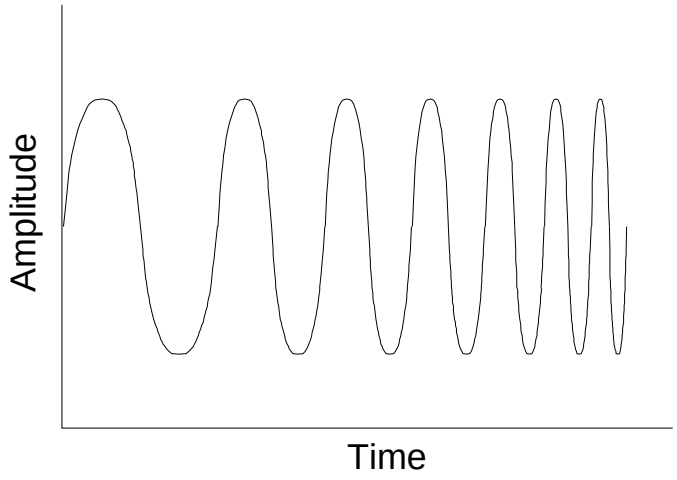

Figure 5.14. Frequency sweep mode in oscillatory testing.

An isothermal time sweep, where frequency and amplitude are constant over time, can indicate time-dependent structural changes such as those associated with firming of cheese curd or yogurt. A time sweep (Fig. 5.15) may be conducted in conjunction with a controlled change in temperature (Fig. 5.16). This type of testing is very useful in studying problems that involve temperature induced changes in rheological behavior. Typical examples associated with heating would include the softening of chocolate or cheese due to the melting of fat, gelation to form pectin gels, thickening of solutions from starch gelatinization, and firming of meat or egg products caused by protein denaturation. The study of time-dependent flow behavior resulting from chemical reactions such as these is called chemorheology.

Strain in Rotational-Type Fixtures. Parallel plate, cone and plate, and concentric cylinder fixtures are the preferred geometries for subjecting fluid and semi-solid foods to an oscillatory strain. In a parallel plate apparatus, such as that used in a traditional parallel plate viscometer (Fig. 5.17), the shear strain is a function of the radius. It varies from zero at the center of the sample ($r = 0$) to a maximum at the outer edge of the plate ($r = R$). Maximum strain (γ_o) is calculated as the distance traveled at the rim of the upper plate (δr) divided by the distance between the plates (h):

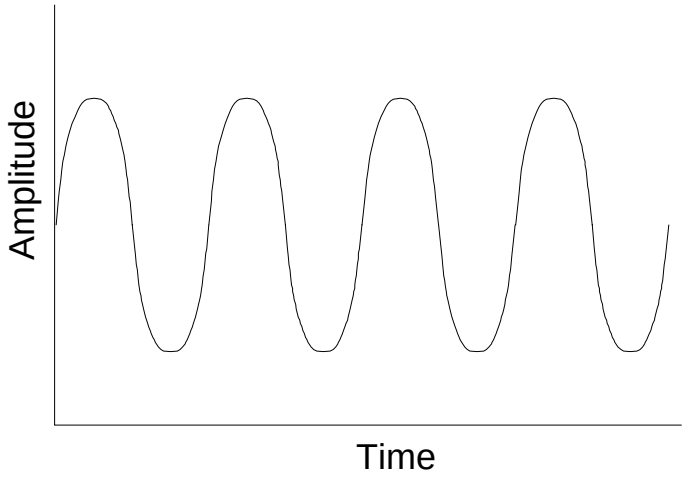

Figure 5.15. Time sweep mode in oscillatory testing.

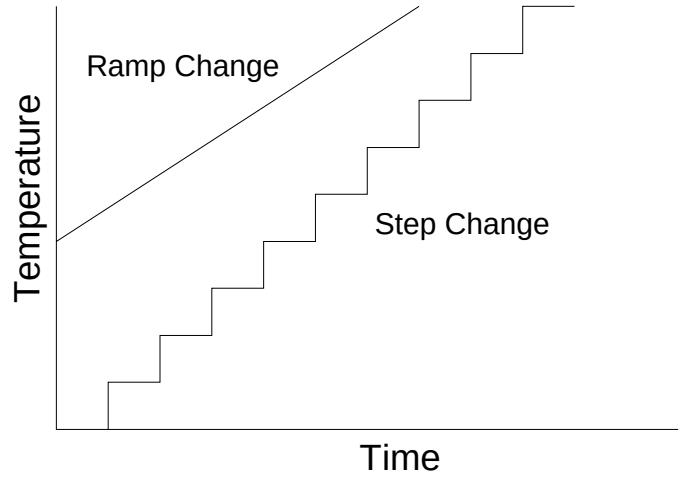

Figure 5.16. Controlled temperature changes in oscillatory testing.

$$\gamma_o = \gamma_R = \frac{\delta r}{h} = 2\pi R\left(\frac{\Psi}{2\pi}\right)\left(\frac{1}{h}\right) = \frac{R\Psi}{h} \qquad [5.51]$$

Assume experimentation starts with the system at rest, then the sample is subjected to a sine wave strain function described by Eq. [5.30]. The plate will move through a positive sweep angle ($+\Psi$), then pass through the starting position while rotating to a negative value of the sweep angle ($-\Psi$). Ψ(in radians) is the amount of angular travel of the upper plate from the starting position to the point of maximum rotation. At this point the maximum strain is induced in the sample. To achieve, for example, a 10% maximum strain in a parallel plate apparatus with 50 mm diameter plates separated by a distance of 2.0 mm will require the following sweep angle:

$$\Psi = \frac{(\gamma_o)h}{R} = \frac{.1(2)}{50/2} = 0.008 \text{ rad or } 0.458 \text{ degrees} \qquad [5.52]$$

A sweep angle resulting in a strain of 10% or less is usually required to stay in the region of linear viscoelastic material behavior.

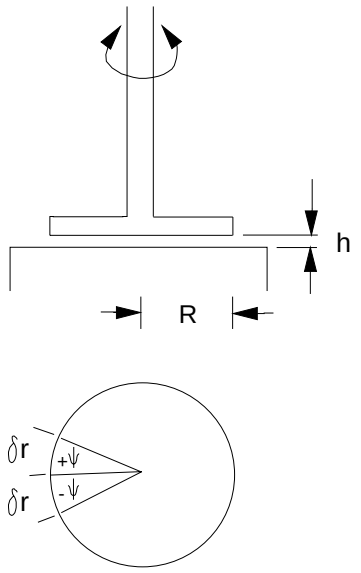

Figure 5.17. Sweep angle in a parallel plate apparatus.

Shear strain in a cone and plate fixture (Fig. 3.3) is uniform throughout the gap and equal to the sweep angle divided by the tangent of the cone angle:

$$\gamma_o = \frac{\Psi}{\tan\theta} \qquad [5.53]$$

Recall that $\tan\theta = \theta$ for the preferred cone angles, $\theta \leq 0.07$ rad (4 degrees).

Shear strain in a concentric cylinder fixture (Fig. 3.1) is a function of the radius. In the case where the bob rotates and the cup is fixed, the maximum strain occurs at the bob:

$$\gamma_o = \gamma_{bob} = 2\Psi\left(\frac{\alpha^2}{\alpha^2 - 1}\right) \qquad [5.54]$$

where, recall, $\alpha = R_c/R_b$. When the bob is fixed and the cup rotates, the maximum strain occurs at the cup:

$$\gamma_o = \gamma_{cup} = 2\Psi\left(\frac{1}{\alpha^2 - 1}\right) \qquad [5.55]$$

Shear stresses for parallel plate, cone and plate, and concentric cylinder fixtures are calculated using the appropriate expressions developed in Chapter 3: Eq. [3.71] with $n = 1$, Eq. [3.55], and Eq. [3.3], respectively.

5.4. Typical Oscillatory Data

Single Frequency Tests. Typical input and output for a dilute solution showing Newtonian type behavior is illustrated in Fig. 5.18 with accompanying data in Table 5.7. In this case, an input strain amplitude of 10% ($\gamma_o = 0.1$) with a constant frequency of 10 rad/s gives an input strain function of $\gamma = 0.1\sin(10t)$. The output stress function is shifted by 1.48 rad (85°) and shows an amplitude ratio of 0.1 ($G^* = \sigma_o/\gamma_o = 0.1$):

$$\sigma = G^*\gamma_o \sin(\omega t + \delta) = .01\sin(10t + 1.48) \qquad [5.56]$$

Typical output data for a gel showing very elastic (solid like) behavior and a concentrated solution showing viscoelastic behavior are seen in Fig. 5.19 with companion data in Table 5.7. The input strain function is the same as that shown in Fig. 5.18: $\gamma = 0.1\sin(10t)$.

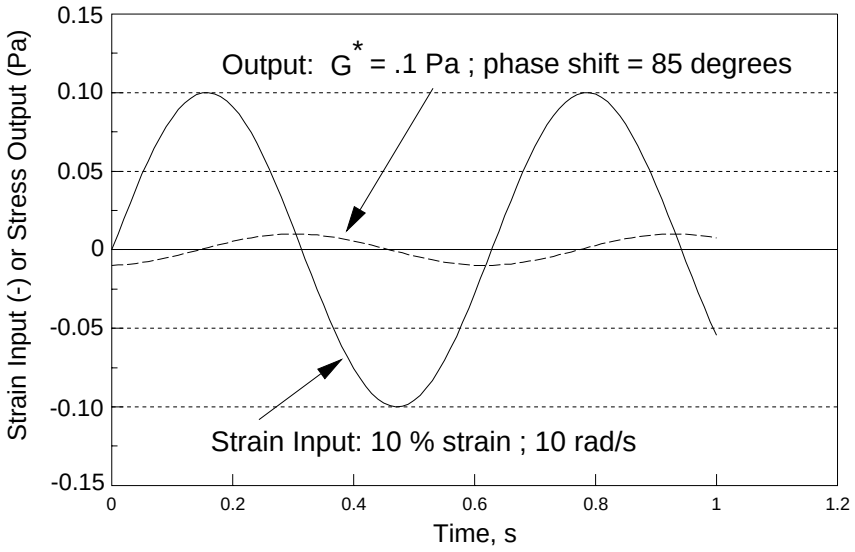

Figure 5.18. Typical input and output for a dilute solution showing Newtonian like behavior at a constant frequency of 10 rad/s.

Table 5.7. Typical Output for a Dilute Solution (Newtonian Behavior), Gel (Elastic Behavior) and a Concentrated Solution (Viscoelastic Behavior) from a Strain Input Function having a Frequency of 10 rad/s and a Strain Amplitude of 10 Percent: $\gamma = 0.1\sin(10t)$

	Dilute Solution	Gel	Concentrated Solution
δ, rad (degrees)	1.48 (85°)	0.0698 (4°)	0.873 (50°)
$\sigma_o/\gamma_o = G^*$, Pa	0.100	5200	200
$G' = G^*\cos\delta$, Pa	0.00907	5187	129
$G'' = G^*\sin\delta$, Pa	0.0996	363	153
$\eta' = G''/\omega$, Pa s	0.00996	36.3	0.140
$\eta'' = G'/\omega$, Pa s	0.000907	518.7	12.9
$\eta^* = G^*/\omega$, Pa s	0.010	520.0	20.0
$\tan\delta = G''/G'$	10.9	0.0699	1.19

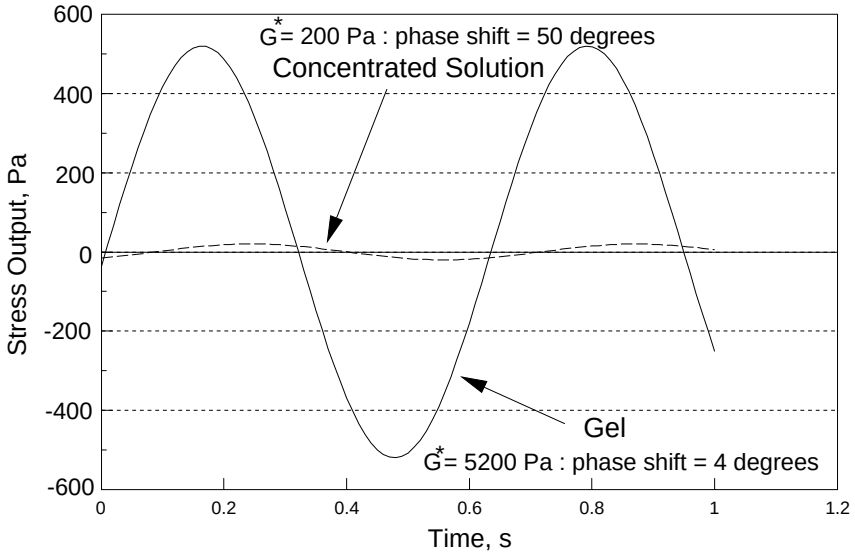

Figure 5.19. Typical output (Input: $\gamma = 0.1\sin(10t)$) for a gel showing elastic type behavior and a concentrated solution showing viscoelastic behavior.

Output stress for the gel (Fig. 5.19) has a small phase shift, $\delta = 0.0698$ rad (4°), but a large amplitude ratio ($G^* = \sigma_o/\gamma_o = 5213$ Pa) producing the following shear stress function:

$$\sigma = G^*\gamma_o \sin(\omega t + \delta) = 521.3\sin(10t + 0.0698) \qquad [5.57]$$

The output stress for the concentrated solution has a greater phase shift, $\delta = 0.873$ rad (50°), and an amplitude ratio between the dilute solution and the gel ($G^* = 200$ Pa):

$$\sigma = G^*\gamma_o \sin(\omega t + \delta) = 20\sin(10t + 0.873) \qquad [5.58]$$

Normalized Strain and Stress. Input and output at a particular frequency may also be visualized in terms of a normalized strain,

$$\gamma^* = \frac{\gamma}{\gamma_o} \qquad [5.59]$$

and a normalized stress,

$$\sigma^* = \frac{\sigma}{\sigma_o} \qquad [5.60]$$

Values of γ^* and σ^* range from -1.0 to 1.0.

The normalized strain input function is the same for the three materials currently under consideration:

$$\gamma^* = \frac{\gamma}{\gamma_o} = 0.1\sin(10\,t)/0.1 \qquad [5.61]$$

Normalized stress output functions are

$$\sigma^* = \frac{\sigma}{\sigma_o} = 0.01\sin(10\,t + 1.148)/0.01 \qquad [5.62]$$

for the dilute solution,

$$\sigma^* = \frac{\sigma}{\sigma_o} = 20\sin(10\,t + 0.873)/20 \qquad [5.63]$$

for the concentrated solution, and

$$\sigma^* = \frac{\sigma}{\sigma_o} = 521.3\sin(10\,t + 0.0698)/521.3 \qquad [5.64]$$

for the gel. Eq. [5.61] through [5.64] are plotted in Fig. 5.20. Phase shifts for the dilute solution (1.48 rad) and the concentrated solution (0.873 rad) are indicated on the figure. The phase shift for the gel (0.0698 rad) is small but still visible. Advanced rheometers may provide a continuously updated display of these (or equivalent) waveforms during oscillatory testing. This information can be very useful in determining whether or not the material being tested is displaying viscoelastic behavior. It can also be used to detect distorted waveforms that may produce misleading results.

Further consideration of Fig. 5.20 can provide added physical meaning to the phase lag phenomenon. Frequency of the strain input is 10 rad/s so the frequency of the output signals for each material (dilute solution, concentrated solution, and gel) is also 10 rad/s. The period of time required to complete a sine wave strain cycle is $2\pi/\omega$. In this experiment, the period is equal to $2\pi/10$ or 0.628 s. The maximum phase lag (δ) which can occur is $\pi/2$ meaning the stress signal, corresponding to a particular strain input, could be observed at a maximum of $\pi/(2\omega) = \pi/(2)\,(10) = 0.157$ s after the strain is applied. Stress is observed 1.48/10 = 0.148 s after the strain in the dilute solution because δ is 1.48 rad. This is close to maximum phase lag expected for a Newtonian fluid at the 10 rad/s test frequency. A δ value of 0.0698 rad (the minimum possible value of δ is zero) for the gel means the stress signal is 0.0698/10 = 0.00698 s behind the strain input. This Hookean-like behavior is not

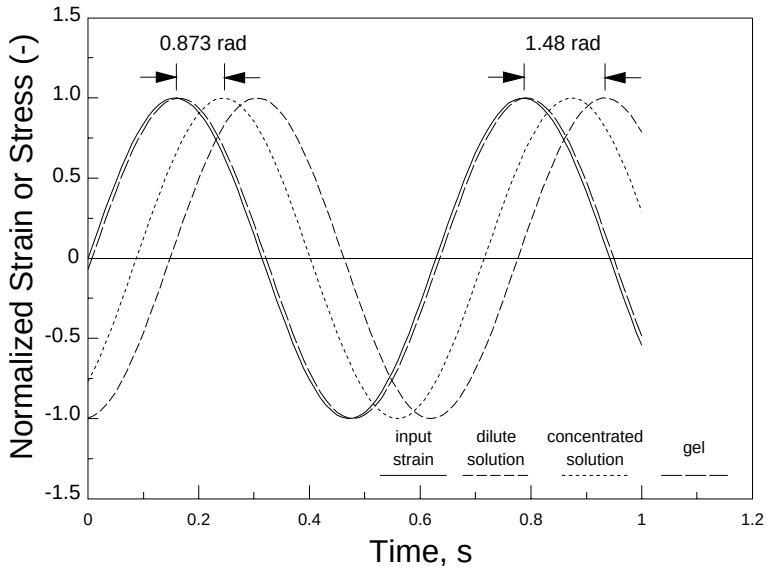

Figure 5.20. Normalized curves for input strain (γ/γ_o) and output stresses (σ/σ_o) showing the phase shift for a dilute solution (1.48 rad or 85°) and a concentrated solution (0.873 rad or 50°).

unusual due to the high level of molecular structure present in a gel. The lag period of 0.0873 s found for the concentrated solution represents a signal transmission time between the dilute solution and the gel. Clearly, the concentrated solution has more structure than the dilute solution but significantly less than the gel.

Frequency Sweeps. Fig. 5.18, 5.19, 5.20 illustrate rheological behavior at a single frequency of 10 rad/s. To effectively characterize the rheological behavior of these substances, material functions should be determined over a wide range of frequencies using the frequency sweep testing concept illustrated in Fig. 5.14. Data may be plotted with the frequency given as radians per second or hertz by recognizing that 1 hz = 1 cycle/s = 2π rad/s. The choice is essentially a matter of individual preference.

A dilute solution, a concentrated solution, and a gel show distinctive behavior (Fig. 5.21, 5.22 and 5.23) when subjected to a frequency sweep. With a dilute solution (Fig. 5.21), G'' is larger than G' over the entire frequency range but approach each other at higher frequencies. G'' and G' curves intersect at the middle of the frequency range for the concentrated solution (Fig. 5.22) showing a clear tendency for more solid-like behavior at higher frequencies. The crossover frequency is sometimes a useful criterion for product evaluation. It occurs when $G' = G''$, the point where the phase lag (δ) equals $\pi/4$. G' is significantly higher than G'' throughout the frequency range for the gel (Fig. 5.23). It is meaningful to observe that moduli are a strong function of frequency in the dilute and concentrated solutions, but practically constant with the gel. Alternate ways of plotting oscillatory data are discussed in Example Problem 5.8.4.

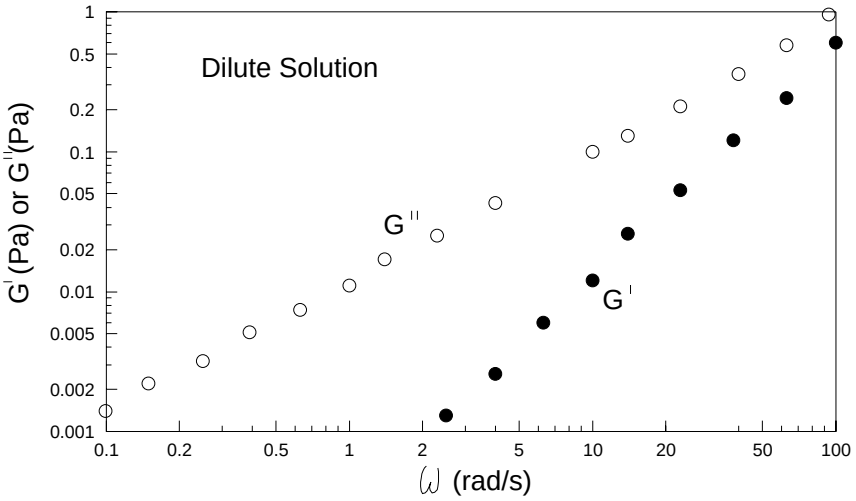

Figure 5.21. Mechanical spectra for a dilute solution made from 5% dextrin (Data from Ross-Murphy, 1988).

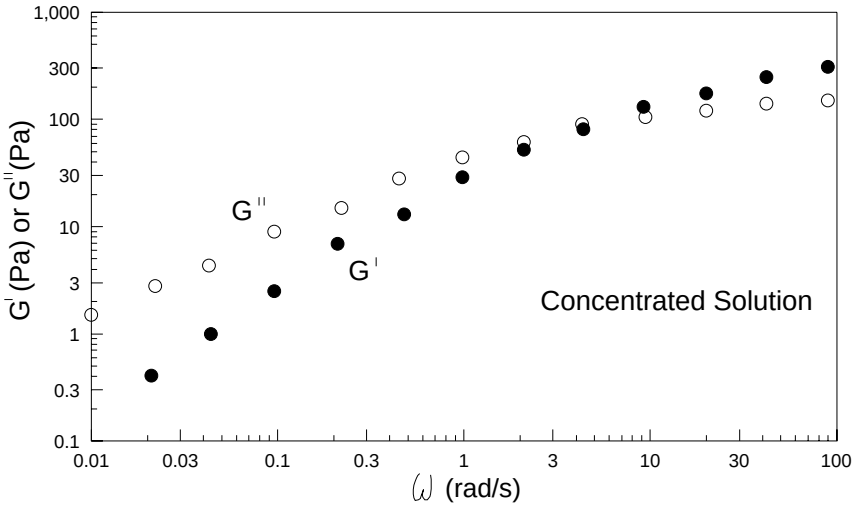

Figure 5.22. Mechanical spectra for a concentrated solution made from 5% lambda carrageenan (Data from Ross-Murphy, 1988).

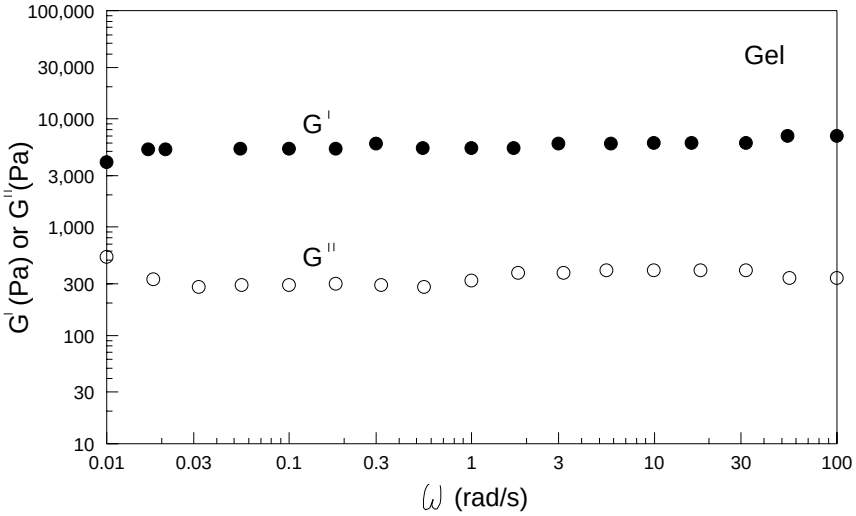

Figure 5.23. Mechanical spectra for a gel made from 1% agar (Data from Ross-Murphy, 1988).

Analysis of the Phase Lag (δ). The tendency of the dilute solution and the concentrated solution to exhibit more fluid or solid-like behavior with increasing frequency can be examined in more detail by considering the frequency dependence of the phase lag. First, the data shown in Fig. 5.21, 5.22, and 5.23 are summarized in the form of power law equations (Table 5.8). Using this information the phase lag may be calculated from the loss and storage moduli: $\delta = arctan(G''/G')$. Results are illustrated in Fig. 5.24. The maximum phase lag which can be observed is $\pi/2$ found with a Newtonian fluid: The minimum value is zero found with a Hookean solid. High values of δ at low frequencies indicate a tendency toward more fluid-like behavior for both the dilute and concentrated solutions at low deformation rates. More solid-like behavior is observed for these solutions at the high deformation rates associated with high frequencies. The phase lag for the gel (Fig. 5.24) is practically constant indicating consistent solid-like behavior over the entire frequency range.

Table 5.8. Values of the storage modulus ($G' = a\omega^b$) and the loss modulus ($G'' = c\omega^d$) for typical materials: dilute solution (Fig. 5.21), concentrated solution (Fig. 5.22), and gel (Fig. 5.23).

Material	*a* (Pa s^b)	*b* (-)	*c* (Pa s^d)	*d* (-)	ω (rad/s)
Dilute Solution	.00028	1.66	.01186	.934	.1 - 100
Concentrated Solution	16.26	.840	27.78	.520	.01 - 100
Gel	5626	.0371	344.7	.0145	.01 - 100

Time to Complete an Oscillatory Test. Oscillatory data for a particular frequency must be collected over one complete sine wave cycle, and two or three cycles may be needed to obtain equilibrium values. It is important to consider the time required to complete low frequency tests when selecting a frequency range for the experimentation. If, for example, a test was conducted at a low frequency of $\omega = 0.01$ rad s^{-1}, then the time required to complete one cycle can be calculated $(2\pi/(.01)(60))$ as 10.5 minutes. Therefore, it would take at least 31.5 minutes to obtain a single pair of G' and G'' values if three cycles were needed! It is usually unnecessary to collect dynamic data at frequencies

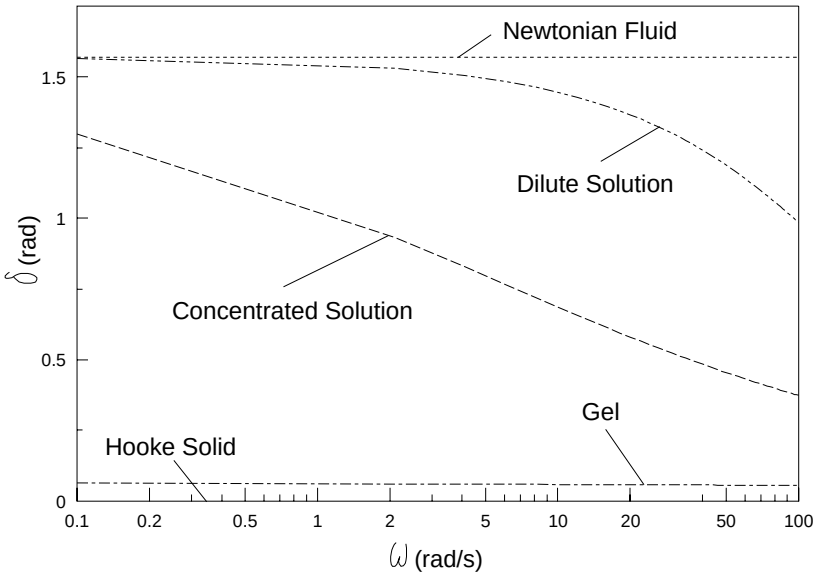

Figure 5.24. Variation of the phase lag (δ) with frequency (ω) for typical materials. The upper limit is represented by a Newtonian fluid ($\delta = \pi/2$) and the lower limit by a Hooke solid ($\delta = 0$).

less than 0.01 rad s^{-1} and a lower limit of $\omega = 0.1$ rad s^{-1} is often adequate. In contrast, the time required to complete one cycle at a frequency of 100 rad s^{-1}, a suitable upper limit for many experiments, is 0.063 s meaning that a three cycle test could be completed in less than 0.19 s.

5.5. Deborah Number

Marcus Reiner (Reiner, 1964) proposed the Deborah number as a means of distinguishing between solids and liquids. The number, named after the prophetess Deborah, is based on his interpretation of a biblical passage found in Judges 5:5. He stated that Deborah's song, given after the victory over the Philistines, could be translated as "The mountains flowed before the Lord." His point was that mountains could flow before God, not before man, because the time of observation for God is infinite. (A similar argument could be made from Psalm 97:5: "The mountains melt like wax before the Lord.") Thus, Prof. Reiner recognized the need to consider the time of the process as a factor when characterizing a

substance as a solid or a liquid. This idea has not been extensively applied to food products but still provides a very useful means for understanding the behavior of viscoelastic materials.

The Deborah number is defined as

$$N_{De} = \frac{t_{material}}{t_{process}} \qquad [5.65]$$

where $t_{material}$ is the characteristic time of the material and $t_{process}$ is the characteristic time of the process. $\lambda_{rel} = t_{material}$ for a Maxwell fluid and $\lambda_{ret} = t_{material}$ for a Kelvin solid (Fig. 5.1). Giving a precise definition of $t_{process}$ is more difficult. It is related to the time scale of the deformation and is roughly equal to the length scale in the flow direction divided by the mean velocity. It might be the reciprocal of frequency for an oscillating surface, or the time for a particle to pass through a converging die and experience the subsequent increase in velocity. Any process must be investigated individually but Deborah numbers tend to be high for processes such as fiber spinning and plastic moulding but low for extrusion.

All the viscometric flow situations described in Chapters 2, 3 and 4 involve low values of the Deborah Number. Creep and stress relaxation discussed in this chapter also involve low Deborah Number values. The other main topic of this chapter, oscillatory testing, involves both low and moderate values of the Deborah Number. Changes in the phase lag with increasing frequency for the dilute and concentrated solutions illustrated in Fig. 5.24 demonstrate the concept. Although the characteristic time of the material is unaffected by oscillatory testing, the characteristic time of the process is inversely proportional to the frequency; therefore, as the frequency increases, the Deborah Number increases causing the solutions to exhibit the more solid-like characteristics associated with lower values of the phase lag (Fig. 5.24).

It is important to remember that all materials are viscoelastic, but the viscous or the elastic character may dominate in certain situations. Pipkin (1986), suggests that the characteristic time of a material may be provisionally considered as an order-of-magnitude estimate for how long it takes the substance to complete a stress relaxation process. If a material is an ideal elastic solid, $t_{material} = \infty$, and no relaxation occurs. With an ideal viscous material, $t_{material} = 0$, meaning relaxation is imme-

diate. The characteristic time of water is on the order of 10^{-12} s and the characteristic time for window glass (a super cooled liquid at room temperature) is greater than 10^5 s. Hence, when water is deformed, elastic effects are difficult to observe because the material relaxes so quickly. Conversely, the viscous behavior of glass is not easily observed because the response to the deforming force (gravity) on a vertical pane is very slow; consequently, decades are needed for observable changes to occur. The characteristic time of the material and the process must be examined together to determine if viscous or elastic type behavior will dominate a particular flow problem. Materials exhibit pronounced viscoelastic behavior when these times are similar in magnitude.

The previous discussion provides insight concerning how the numerical value of N_{De} can be used as a measure of the degree of viscoelasticity. If $N_{De} \ll 1$, the stress is proportional to the viscosity times the shear rate and the material behaves as a viscous liquid. On the other hand, if $N_{De} \gg 1$, then stress is proportional to the modulus of rigidity times the strain and the material behaves like an elastic solid. If the N_{De} is on the order of one, materials will show viscoelastic behavior. When N_{De} is very high, the model for a Hookean solid may best describe material behavior. The Newtonian model may be the best choice when very small N_{De} are present.

To further expand the concept of the Deborah number, consider data from a common silicone polymer known as "bouncing putty" or "silly putty". This substance, sold as a toy for children, is interesting because it has a relaxation time well within the limits of human perception. If the material is assumed to behave as a Maxwell fluid, constants may be determined from the asymptotes found in Fig. 5.25. Taking the limit (as ω goes to infinity) of Eq. [5.47] shows that $G' = G = 260{,}000$ Pa and taking the limit (as ω goes to zero) of Eq. [5.49] indicates that $\eta' = \eta = 80{,}000$ Pa s. Using these values, the relaxation time can be calculated: $\lambda_{rel} = \eta/G = 0.31$ s.

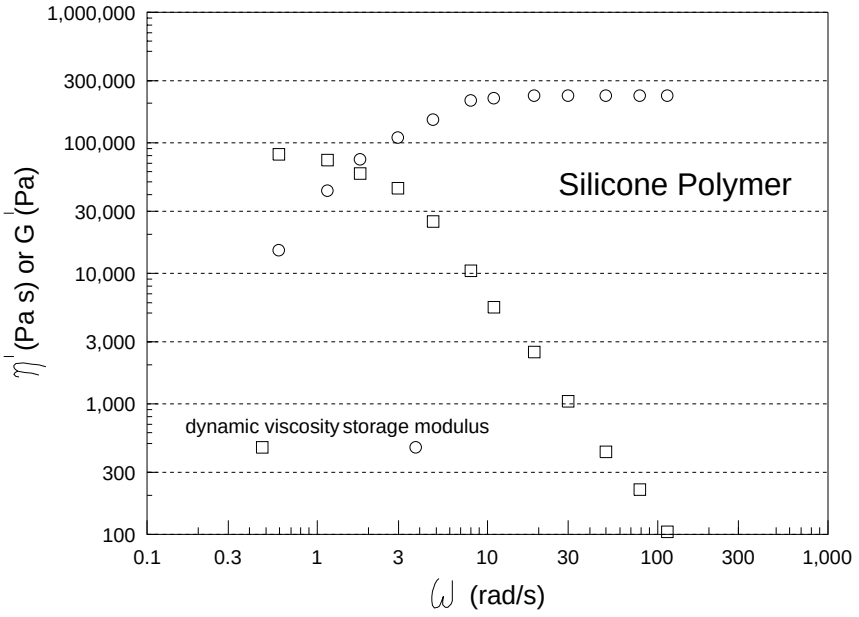

Figure 5.25. Oscillatory shear measurements on a silicone polymer (Data from Denn, 1980).

Continued analysis of silly putty shows that $G' = 260,000$ Pa and $\eta' = 100$ Pa s at $\omega = 100$ rad/s. Expressing this in terms of the shear stress given by Eq. [5.45] yields

$$\sigma = G'\gamma + \eta'\dot{\gamma} = 260,000\,\gamma + 100\,\dot{\gamma} \qquad [5.66]$$

Clearly, the elastic portion of the equation $(260,000\,\gamma)$ dominates the mathematical relationship. Assuming $\gamma_o = 0.1$, the Deborah number for this case can be is approximated as

$$N_{\mathrm{De}} = \frac{\lambda_{\mathrm{rel}}}{t_{\mathrm{process}}} = \frac{\lambda_{\mathrm{rel}}}{(\gamma_o \omega)^{-1}} = 0.31(.1)\,(100) = 3.1 \qquad [5.67]$$

which is a numerical value of sufficient magnitude to indicate that significant elastic effects would be present. The characteristic time of the process would be much lower, causing the Deborah number to be much higher, in situations where silly putty bounces when dropped and shows brittle fracture when pulled quickly.

Viewing the problem at a low frequency ($\omega = 0.1$ rad/s), $G' = 200$ Pa and $\eta' = 80,000$ Pa s, gives a shear stress equation (Eq. [5.45]) of

$$\sigma = G'\gamma + \eta'\dot{\gamma} = 200\,\gamma + 80,000\,\dot{\gamma} \qquad [5.68]$$

Testing under these conditions result in a low value of the Deborah number:

$$N_{De} = \frac{\lambda_{rel}}{t_{process}} = \frac{\lambda_{rel}}{(\gamma_o \omega)^{-1}} = 0.31(.1)(.1) = 0.003 \qquad [5.69]$$

At low frequency (long characteristic time of the process), the Deborah number is very small and the viscous component ($80,000\,\dot{\gamma}$) dominates material behavior explaining why the substance flows, as a liquid, when pulled slowly. Given the above discussion, one can conclude that advertising silly putty as the "real solid-liquid" is technically acceptable.

5.6. Experimental Difficulties in Oscillatory Testing of Food

There are various sources of error which may be particularly problematic when testing food products using oscillatory methods. Many foods may not exhibit a well defined strain or stress range where the principle of linear viscoelasticity applies. This may be due to non-homogeneous samples, the presence of wall slip, or time-dependent material behavior. Preshearing with steady rotation, before conducting oscillatory tests, can be useful in controlling (or eliminating) thixotropy in some materials. Serrated or roughened surfaces may be effective in dealing with wall slip. Special surfaces have been used, for example, in testing cracker and cookie doughs (Menjivar, 1994), and cheddar cheese (Rosenberg et al., 1995).

The presence of a yield stress may also cause serious difficulties in oscillatory testing of food. This problem was observed many years ago by Elliot and Ganz (1971, 1977) in studies involving mayonnaise, salad dressing, and margarine. If the applied strain causes the resulting stress to exceed the yield stress, then the output sin wave will be truncated due to partial flow of the material. This deviant behavior is illustrated in Fig. 5.26 where the peak values of the normalized stress are equal to 0.7: $\sigma^* = \sigma/\sigma_o \leq 0.7$. Since the yield stress is equal to 70% of the maximum shear stress (σ_o), σ^* cannot exceed 0.7.

The transition from solid-like to fluid-like behavior may be thought of in terms of a critical strain or stress, below which the material behaves as an elastic solid. Applied stresses which exceed the yield stress cause a deviation from solid-like behavior resulting in a non-sinusoidal output wave; consequently, measured values of the storage and loss moduli do not fall within the scope of linear viscoelasticity. These moduli, although quite useful in comparing different food products, will be a function of both the strain (or stress) amplitude and frequency (Yoshimura and Purd'homme, 1987). The problem can be further complicated by the fact that the yield stress itself may be a time-dependent parameter for many food products (Steffe, 1992).

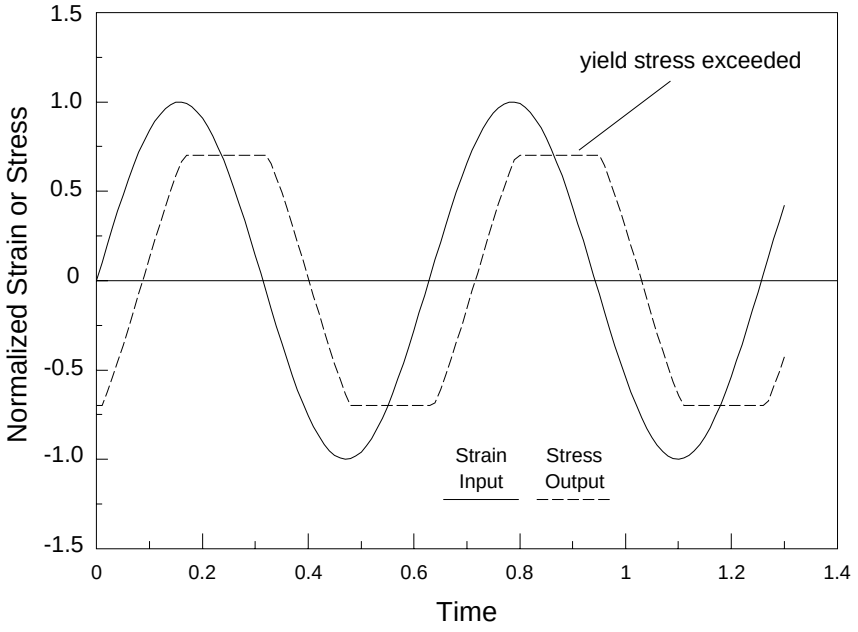

Figure 5.26. Stress output when the applied strain takes the material outside the regime where the material exhibits solid-like behavior.

The above explanation of the yield stress issue in oscillatory testing illustrates the dilemma, but may oversimplify the problem. An alternative approach is to assume that the yield stress does not exist and everything flows. This means that even materials appearing to have a very solid-like nature would, given sufficient time, flow. Barnes et al.

(1987) mention growing evidence showing that concentrated systems (e.g., gels, margarine, ice cream, and stiff pastes) flow at very low stresses. They explain that the hypothesis of a yield stress, and the subsequent observation that a material does not flow, could be interpreted to mean that the material has a very high zero shear viscosity. Normal window glass, for example, has a zero shear viscosity greater than 10^{18} Pa s. This material appears to be solid but given sufficient time (decades) shows observable changes due to flow. Latter work (Barnes, 1992) has acknowledged scientific evidence suggesting the presence of a yield stress in non-interacting and flocculated suspensions. Regardless of the explanation for deviant behavior, oscillatory information is of limited usefulness if data are not collected within the linear viscoelastic range of the material behavior.

5.7. Viscometric and Linear Viscoelastic Functions

Normal stress functions arise from the viscoelastic nature of materials; therefore, it is reasonable to expect linear viscoelastic material functions determined from oscillatory testing to be related to steady shear behavior. Exact relationships can be determined in the lower limits of shear rate and frequency (Walters, 1975):

$$\eta'|_{\omega\to 0} = \eta|_{\dot\gamma\to 0} \qquad [5.70]$$

and

$$\left.\frac{G'}{\omega^2}\right|_{\omega\to 0} = \left.\frac{\Psi_1}{2}\right|_{\dot\gamma\to 0} \qquad [5.71]$$

where, recall (Eq. [1.23]), $\Psi_1 = f(\dot\gamma) = (\sigma_{11} - \sigma_{22})/(\dot\gamma)^2$. Although their usefullness is limited because they only apply at low frequencies and shear rates, the above equations have proven to be valid for numerous polymer melts and solutions.

Cox and Merz (1958) observed that the complex viscosity is nearly equal to the steady shear viscosity when the shear rate and frequency are equal:

$$\eta^* = \eta|_{\omega=\dot\gamma} \qquad [5.72]$$

This empirical relationship, now referred to as the "Cox-Merz rule," may be useful for materials that are more easily tested under oscillatory instead of steady shear conditions. The rule may, for example, apply to

polymeric fluids that have a large normal stress difference, leading to a Weissenberg effect (rod climbing), that complicates steady shear testing.

The Cox-Merz rule seems to work well with many synthetic and biopolymer dispersions (da Silva and Rao, 1992). Rao and Cooley (1992) found that Eq. [5.72] could be applied to tomato paste by introducing a simple shift factor into the computation: Complex viscosity was evaluated at a frequency of $\alpha\omega$ where α, the shift factor, was equal to approximately 0.0074. Bistany and Kokini (1983) found the Cox-Merz rule to be inapplicable to various foods. In the same work, however, the following relationships were able to effectively relate steady shear and dynamic rheological properties:

$$\frac{G'}{\omega^2} = C(\Psi_1)^{\alpha}\,|_{\omega=\dot{\gamma}} \qquad [5.73]$$

and

$$\eta^* = C'(\eta)^{\alpha'}\,|_{\omega=\dot{\gamma}} \qquad [5.74]$$

where C, α, C', and α' are empirical constants determined from experimental data. Values of these constants for various foods are given in Table 5.9. The corresponding normal stress differences and power law fluid properties (needed to calculate apparent viscosity) for the foods listed in Table 5.9 are given in Appendix [6.6].

Doraiswamy et al. (1991) proposed an extended Cox-Merz rule relating the complex viscosity to the steady shear viscosity. They found that a plot of the complex viscosity versus $\gamma_o\,\omega$ was equivalent to a plot of the apparent viscosity versus shear rate. $\gamma_o\,\omega$ was defined as the "effective shear rate" where γ_o is the strain amplitude given in Eq. [5.30]. The equivalence of complex and steady shear viscosities was found to be valid over a wide range of parameters involving concentrated suspensions having yield stresses.

Table 5.9. Empirical Constants for Eq. [5.73] and [5.74] (Source: Kokini, 1992)*

Food	C	α	C'	α'
Whipped cream cheese	93.21	0.750	13.87	1.146
Cool Whip	50.13	1.400	6.16	1.098
Stick Butter	49.64	0.986	0.79	1.204
Whipped butter	43.26	0.948	33.42	1.255
Stick margarine	35.48	0.934	1.28	1.140
Ketchup	13.97	0.940	14.45	1.069
Peanut butter	13.18	1.266	1.66	1.124
Squeeze margarine	11.12	1.084	52.48	1.022
Canned frosting	4.40	1.208	4.89	1.098
Marshmallow fluff	3.53	0.988	1.26	0.810

* Data collected at room temperature over a shear rate and frequency range of 0.1 to 100 s^{-1}. Units of $\omega, \dot{\gamma}, G', \Psi_1, \eta^*$ and η used in Eq. [5.73] and [5.74] are rad s^{-1}, s^{-1}, Pa, Pa s^2, Pa s and Pa s, respectively.

Table 5.10. Stress Relaxation Data from Compression Testing of Apple Tissue at Room Temperature (Cylindrical Sample: Length = 2 cm, Diameter = 2 cm)

t (s)	σ (Pa)	$\frac{\sigma_o t}{\sigma_o - \sigma}$ (s)
0.0	754	
0.6	601	3.0
1.2	572	5.0
1.8	562	7.1
2.4	549	8.8
3.0	536	10.4
3.6	526	11.9
6.0	504	18.1
9.0	484	25.1
12.0	468	31.6
15.0	461	38.6
18.0	452	44.9
24.0	435	56.7
30.0	426	69.0
42.0	409	91.8
54.0	406	117.0

5.8. Example Problems

5.8.1. Generalized Maxwell Model of Stress Relaxation

Using the generalized Maxwell model (Eq. [5.11]), estimate the relaxation time (λ_{rel}) of the apple tissue described by the data presented in Table 5.10.

Recall Eq. [5.11], with σ referring to the stress in compression:

$$\sigma = f(t) = \sigma_e + (\sigma_o - \sigma_e)\exp\left(\frac{-t}{\lambda_{rel}}\right)$$

Assume the material has reached equilibrium at the completion of the test so σ_e = 406 Pa. Then, regression of the data (Fig. 5.27) using the logarithmic transformation of Eq. [5.11],

$$\ln(\sigma - 406) = \ln(\sigma_o - \sigma_e) - t/\lambda_{rel}$$

yields $-1/\lambda_{rel} = -0.0906$ s^{-1} or $\lambda_{rel} = 11.04$ s, and $\sigma_o - 406 = 200.75$ Pa making $\sigma_o = 606.75$ Pa. Note that the value of σ_o, determined from the regression parameter, is lower than the experimental value of 754 Pa given for the initial stress in Table 5.10.

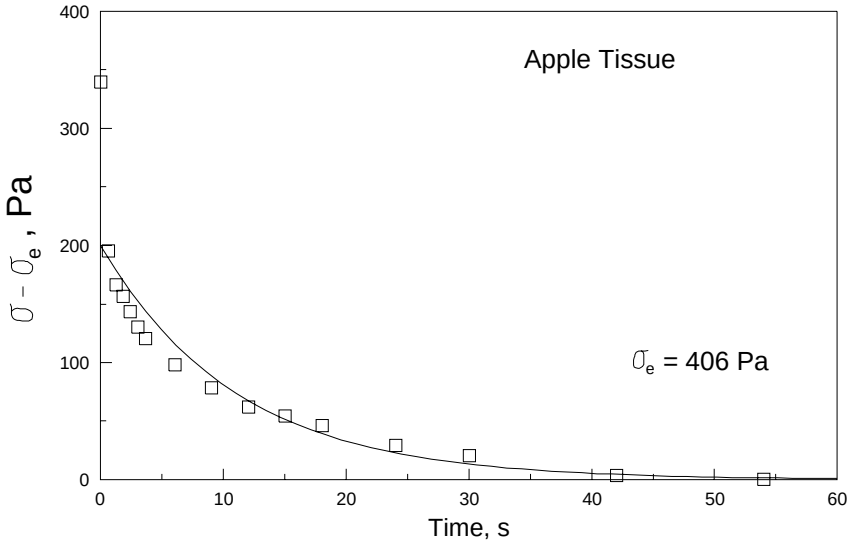

Figure 5.27. Stress relaxation data for apple tissue modeled using Eq. [5.11].

5.8.2. Linearized Stress Relaxation

Stress relaxation data for apple tissue are given in Table 5.10 with the raw data plotted in Fig. 5.28. Determine the coefficients for the normalized stress equation proposed by Peleg and Normand (1983), Eq. [5.14]:

$$\frac{\sigma_o\, t}{\sigma_o - \sigma} = k_1 + k_2\, t$$

where the value of σ_o is taken from Table 5.10 as 754 Pa.

Linear regression of this equation (an excellent fit) yields the following: k_1 = 4.52 s, k_2 = 2.12. Linearized data are plotted in Fig. 5.29. Results are comparable to those reported for potato flesh (Table 5.5: k_1 = 4.40 s, k_2 = 1.56).

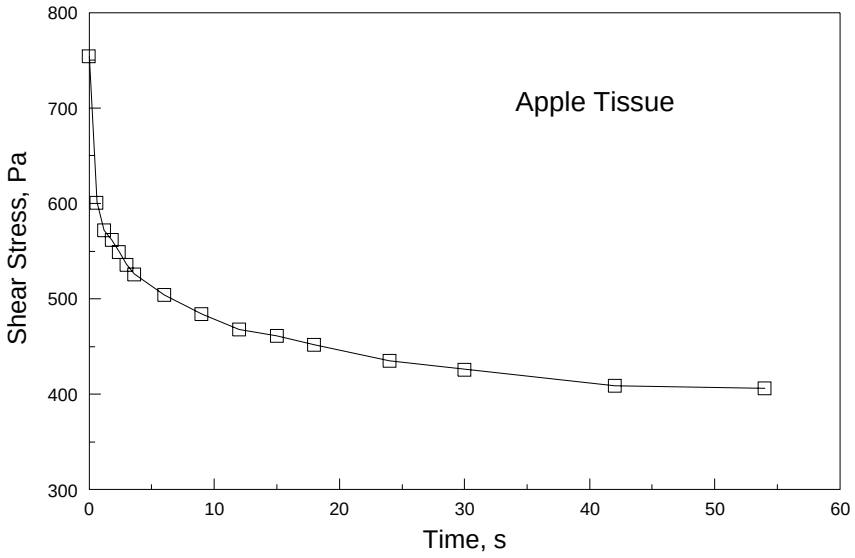

Figure 5.28. Stress relaxation data for apple tissue at room temperature.

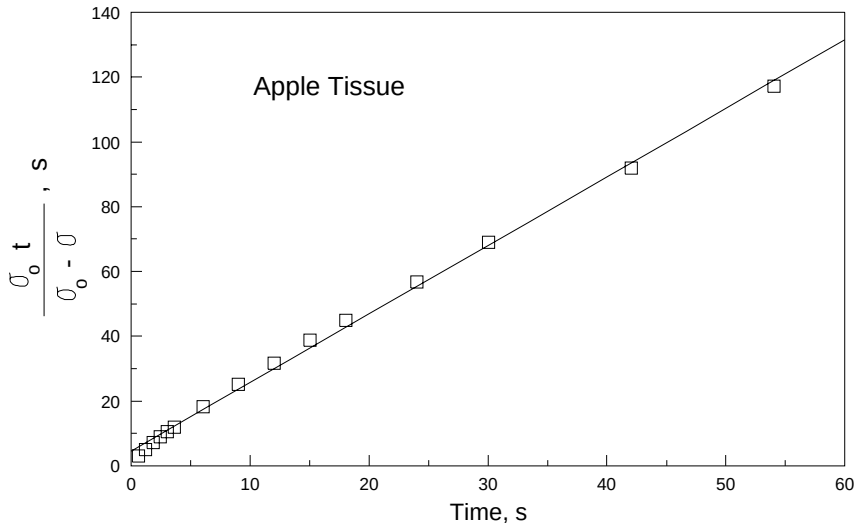

Figure 5.29. Normalized stress relaxation data for apple tissue.

5.8.3. Analysis of Creep Compliance Data

Estimate the parameters of the four parameter Burgers model (Fig. 5.6) to represent the shear creep compliance data given in Table 5.11. Compare the resulting curve to the 6 parameter model (Fig. 5.30) formulated by adding an additional Kelvin element to the Burgers model. Also, determine the parameters for the simple linearized creep compliance model suggested by Peleg (1980).

The Burgers model, expressed in terms of the creep compliance function, is described by Eq. [5.22]:

$$J = f(t) = J_0 + J_1\left(1 - \exp\left(\frac{-t}{\lambda_{ret}}\right)\right) + \frac{t}{\mu_0}$$

Model parameters may be estimated using the following procedure:

1. The instantaneous compliance, J_0, is determined from the original data (Curve 1 on Fig. 5.31 or Table 5.11) at $t = 0$ as 0.00220 cm^2/dyne.

Table 5.11. Shear Creep Compliance of Skim Milk Curd Fortified with α-casein (Data from Halim and Shoemaker, 1990)

Data Point	Time (s)	J^a (cm^2/dyne)	J^b (cm^2/dyne)	J^c (cm^2/dyne)	t/J^d (s dyne/cm^2)
1	0	0.00220	0.00220	0.00220	0
2	0.89	0.00249	0.00237	0.00241	357
3	2.01	0.00264	0.00257	0.00262	761
4	3.79	0.00293	0.00284	0.00287	1,293
5	8.93	0.00331	0.00337	0.00328	2,698
6	14.06	0.00355	0.00369	0.00352	3,961
7	18.97	0.00372	0.00389	0.00369	5,099
8	23.44	0.00386	0.00401	0.00382	6,073
9	28.71	0.00398	0.00411	0.00395	7,241
10	34.02	0.00408	0.00419	0.00406	8,338
11	39.06	0.00418	0.00426	0.00416	9,344
12	44.20	0.00426	0.00432	0.00424	10,376
13	48.88	0.00434	0.00437	0.00432	11,263
14	58.48	0.00447	0.00447	0.00445	13,083
15	68.97	0.00458	0.00458	0.00458	15,059
16	78.57	0.00469	0.00468	0.00469	16,752
17	93.75	0.00485	0.00484	0.00485	19,330
18	109.25	0.00499	0.00500	0.00502	21,894
19	118.97	0.00509	0.00509	0.00512	23,373

[a] raw data; [b] predicted using 4 parameter Burgers model; [c] predicted using 6 parameter model; [d] calculated from raw data

2. Subtract J_0 from Curve 1 to generate Curve 2 (Fig. 5.31). Using the straight portion of the curve (the last six data points, $t \geq 58.48$), linear regression analysis yields J_1 and μ_0 from the intercept and slope of

$$(J - J_0) = J_1 + \frac{t}{\mu_0} \qquad [5.75]$$

as J_1 = 0.00168 cm^2/dyne and μ_0 = 97,847 P. Note that J_1 reflects the fully extended (equlibrated) Kelvin element making the exponential term in the original equation equal to zero.

3. Using the exponential portion of the data (the first 8 data points, $t \leq 28.71$s), the retardation time is determined from linear regression analysis (including a logarithmic transformation of the data) over $J < J_1 + J_0$ of

$$\ln\left(1 - \frac{J - J_0}{J_1}\right) = \frac{-t}{\lambda_{ret}} \qquad [5.76]$$

as λ_{ret} = 8.635 s.

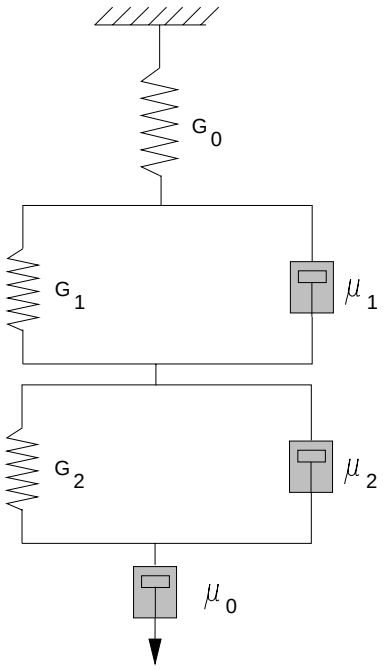

Figure 5.30. Six parameter model for creep compliance.

Substituting the constants found above, the complete Burgers model may be expressed as

$$J = 0.0022 + 0.00168\left(1 - \exp\left(\frac{-t}{8.635}\right)\right) + \frac{t}{97847}$$

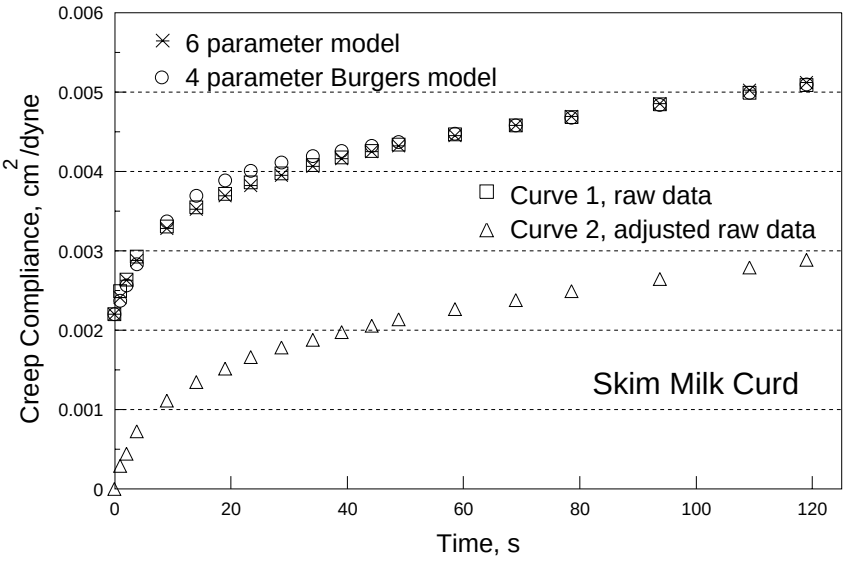

Figure 5.31. Shear creep compliance of skim milk curd fortified with α-casein.

A comparison of the curve predicted with the above equation and actual data reveals (Fig. 5.31, Table 5.11) that the Burgers model adequately represents the data; however, better accuracy is obtained using a more complex 6 parameter model (Fig. 5.30) described by Eq. [5.23], with $m = 2$, as

$$J = f(t) = J_0 + J_1\left(1 - \exp\left(\frac{-t}{(\lambda_{ret})_1}\right)\right) + J_2\left(1 - \exp\left(\frac{-t}{(\lambda_{ret})_2}\right)\right) + \frac{t}{\mu_0} \qquad [5.77]$$

where:

$$(\lambda_{ret})_1 = \frac{\mu_1}{G_1} \qquad [5.78]$$

and

$$(\lambda_{ret})_2 = \frac{\mu_2}{G_2} \qquad [5.79]$$

The constants in Eq. [5.77] (for the same α-casein fortified skin milk curd under consideration) were determined by Halim and Shoemaker (1990), using nonlinear curve fitting procedures, with the following result:

$$J = 0.0022 + 0.00064\left(1 - \exp\left(\frac{-t}{3.14}\right)\right) + 0.001068\left(1 - \exp\left(\frac{-t}{19.5}\right)\right) + \frac{t}{97707}$$

Comparing this prediction equation to the raw data shows that it does an excellent job modeling the shear creep compliance (Fig. 5.31, Table 5.11).

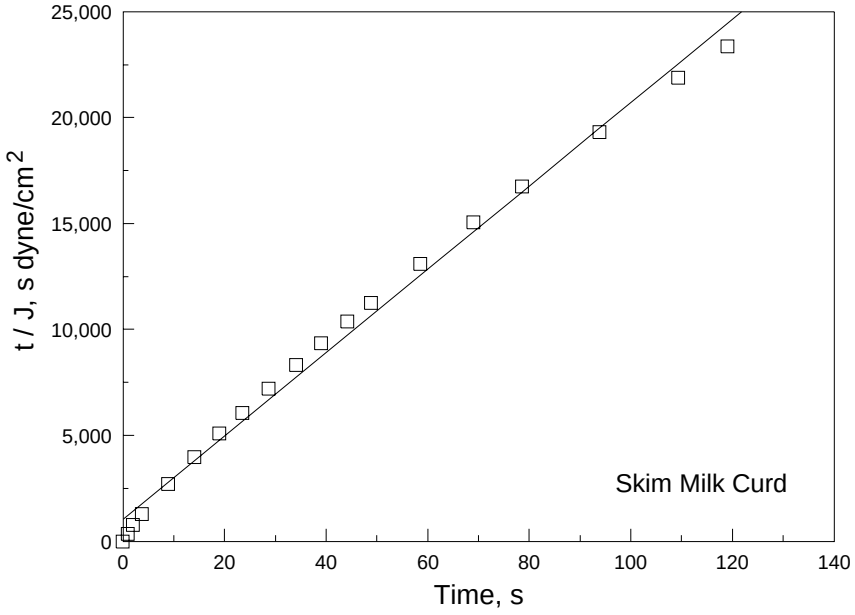

Figure 5.32. Linearized shear creep compliance of skim milk curd fortified with α-casein.

Peleg (1980) suggested that creep data could be modeled with the following linear equation:

$$\frac{t}{J} = k_1 + k_2 t \qquad [5.80]$$

Regression analysis of the data, using Eq. [5.80], yielded $k_1 = 1050.8$ dyne cm^{-2} s and $k_2 = 196.6$ dyne cm^{-2} with $r^2 = 0.99$. Raw data and the resulting curve are plotted in Fig. 5.32. The 6 parameter model involves complex curve fitting, but gives a very accurate representation of experimental data. The simple linear equation is less precise, but often adequate for investigating practical creep problems involving biological materials.

5.8.4. Plotting Oscillatory Data

Develop alternative plots showing the dynamic behavior of the concentrated solution (5% lambda carrageenan solution) illustrated in Fig. 5.21.

The data given in Fig. 5.22 were fit to a power law model resulting in the following equations (Table 5.8):

$$G' = 16.26(\omega)^{.84}$$

and

$$G'' = 27.78(\omega)^{.52}$$

Using these equations other rheological parameters can be easily calculated:

$$\eta' = \frac{G''}{\omega} = 27.78(\omega)^{-.48}$$

$$\eta'' = \frac{G'}{\omega} = 16.26(\omega)^{-.16}$$

$$\tan\delta = \frac{G''}{G'} = 1.71(\omega)^{-.32}$$

$$G^* = \sqrt{(G')^2 + (G'')^2} = \sqrt{(16.26(\omega)^{.84})^2 + (27.78(\omega)^{.52})^2}$$

$$\eta^* = \sqrt{(\eta')^2 + (\eta'')^2} = \sqrt{(27.78(\omega)^{-.48})^2 + (16.26(\omega)^{-.16})^2}$$

Results are presented in Fig. 5.33.

Two very useful methods of representing mechanical spectra are to plot the storage modulus and the loss modulus, or the storage modulus and the dynamic viscosity. Crossover points (Fig. 5.33), such as the one provided by the intersection of G' and G'', may provide useful benchmarks for comparing products or treatments. In this case the crossover occurs at a frequency of 5.61 rad/s. Since $G' = G''$ at that point, it is also the frequency where the tangent of the phase angle ($\tan\delta$) is equal to 1

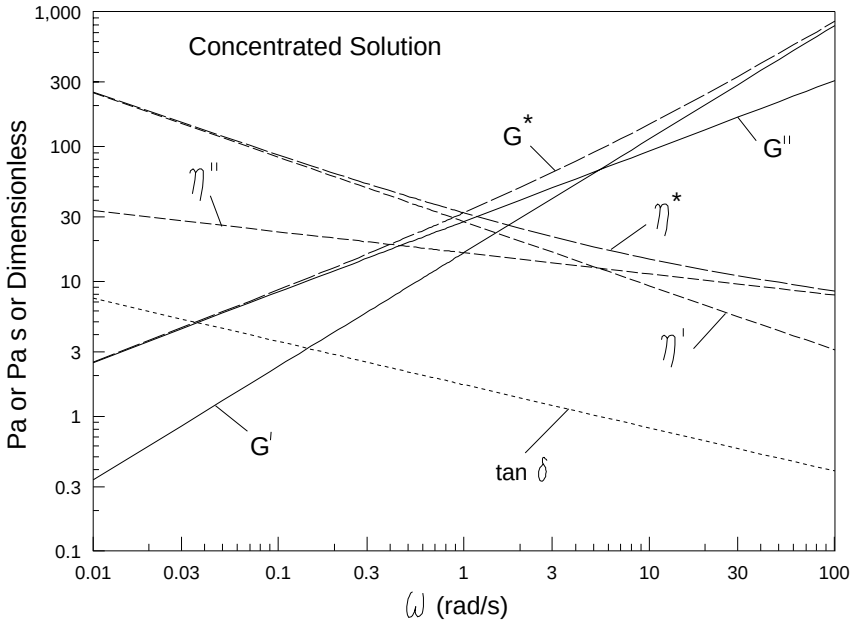

Figure 5.33. Oscillatory testing results for a 5% lambda carrageenan solution.

because $\delta = \pi/4$. Observing changes in $\tan\delta$ is a useful means of evaluating the transition from liquid-like to solid-like behavior: tan delta decreases with more solid-like behavior. Combined parameters, η^* and G^*, are also useful in looking at overall rheological behavior. A popular combination is to plot the variation of η^*, G', and G'' with frequency. In some cases, single point measurements are useful: η^*, measured at 50 rad/s, correlates well with the human perception of thickness or viscosity (Hill, 1991; Hill et al., 1995).

6. Appendices

6.1. Conversion Factors and SI Prefixes

Density

1 g cm^{-3} = 1000 kg m^{-3} = 62.428 lbm ft^{-3} = 0.0361 lbm in^{-3}

1 lbm ft^{-3} = 16.0185 kg m^{-3}

Force

1 N = 1 kg m s^{-2} = 10^5 dyne = 0.22481 lbf = 0.102 kgf

1 lbf = 4.448 N = 0.4536 kgf

1 dyne = 1 g cm s^{-2} = 10^{-5} N

Length

1 m = 100 cm = 1000 mm = 10^6 μm = 3.2808 ft = 39.37 in = 1.0936 yd

1 in = 2.54 cm = 25.40 mm = 0.0254 m = 0.0833 ft = 0.02778 yd

Power

1 hp = 550 ft lbf s^{-1} = 745.70 W = 0.7457 kW = 0.7068 Btu s^{-1}

1 Btu hr^{-1} = 0.2931 W = 0.2931 J s^{-1}

Pressure and Stress

1 bar = 10^5 N m^{-2} = 10^5 Pa = 14.5038 lbf in^{-2} = 0.987 atm = 10.2 m H_2O at 4°C

1 Pa = 1 N m^{-2} = 10 dyne cm^{-2} = 9.8692 (10^{-6}) atm = 0.1020 kgf m^{-2}

1 lbf in^{-2} = 6895 Pa = 6.804 (10^{-2})atm = 6.895 kPa = 2.307 ft H_2O at 4°C

1 dyne cm^{-2} = 0.10 Pa = 10 $^{-6}$ bar = 0.987 (10^{-6}) atm

1 atm = 1.01325 (10^5) N m^{-2} = 101.325 kPa = 14.696 psi = 1.013 bar = 760 torr

1 atm = 760 mm Hg at 0°C = 33.90 ft H_2O at 4°C = 1.013 (10^6) dyne cm^{-2}

Revolution and Rotational Speed

1 rev = 1 cycle = 2 π rad

1 Hz = 1 cycle/s = 1 rev/s = 2 π rad/s = 6.283 rad/s

1 rev/min = 0.1047 rad/s

Temperature

$T_{Kelvin} = T_{Celsius} + 273.15$

$T_{Kelvin} = (T_{Fahrenheit} + 459.67) / 1.8$

$T_{Fahrenheit} = 1.8\ T_{Celsius} + 32$

$T_{Celsius} = (T_{Fahrenheit} - 32) / 1.8$

Torque, Energy, and Work

1 N m = 100 N cm = 1 J = 1 kg m^2 s^{-2} = 10^7 dyne cm = 8.85 in lbf

1 dyne cm = 10^{-7} N m = 10^{-5} N cm

Viscosity (Absolute or Dynamic, followed by Kinematic)

1 P = 1 dyne s cm^{-2} = 0.1 Pa s = 100 cP = 100 mPa s

1 Pa s = 1000 cP = 10 P = 1 kg m^{-1} s^{-1} = 1 N s m^{-2} = 0.67197 lbm ft^{-1} s^{-1}

1 cP = 1 mPa s = 0.001 Pa s = 0.01 P

1 lbm ft^{-1} s^{-1} = 1.4882 kg $m^{-1}s^{-1}$ = 1488.2 cP = 2.0885 (10^{-2}) lbf s ft^{-2}

kinematic viscosity (cSt) = absolute viscosity (cP) / density (g cm^{-3})

1 cSt = 0.000001 m^2 s^{-1} = 1 mm^2 s^{-1} = 5.58001 in^2 hr^{-1} = 0.00155 in^2 s^{-1}

1 St = 100 cSt = 0.0001 m^2 s^{-1}

1 m^2 s^{-1} = 10^{-5} cSt = 10.7639 ft^2 s^{-1}

Volume

1 m^3 = 10^6 cm^3 = 10^3 L (liter) = 264.17 gal (US) = 35.315 ft^3 = 219.97 gal (UK)

1 ft^3 = 0.028317 m^3 = 7.481 gal (US) = 28.317 L = 6.2288 gal(UK)

1 gal (US) = 4 qt = 3.7854 L = 3785.4 cm^3 = 0.8327 gal (UK) = 0.003785 m^3

SI Prefixes

Factor	Prefix	Symbol	Factor	Prefix	Symbol
10^{18}	exa	E	10^{-1}	deci	d
10^{15}	peta	P	10^{-2}	centi	c
10^{12}	tera	T	10^{-3}	milli	m
10^{9}	giga	G	10^{-6}	micro	μ
10^{6}	mega	M	10^{-9}	nano	n
10^{3}	kilo	k	10^{-12}	pico	p
10^{2}	hecto	h	10^{-15}	femto	f
10^{1}	deka	da	10^{-18}	atto	a

6.2. Greek Alphabet

Α α	Alpha	Ν ν	Nu
Β β	Beta	Ξ ξ	Xi
Γ γ	Gamma	Ο ο	Omicron
Δ δ	Delta	Π π	Pi
Ε ε	Epsilon	Ρ ρ	Rho
Ζ ζ	Zeta	Σ σ	Sigma
Η η	Eta	Τ τ	Tau
Θ θ	Theta	Υ υ	Upsilon
Ι ι	Iota	Φ φ	Phi
Κ κ	Kappa	Χ χ	Chi
Λ λ	Lambda	Ψ ψ	Psi
Μ μ	Mu	Ω ω	Omega

6.3. Mathematics: Roots, Powers, and Logarithms

Roots and Powers*

$a^n = a\ a\ a\ a\ \ldots$ to n factors $\qquad a^{-n} = \dfrac{1}{a^n}$

$a^m\, a^n = a^{m+n}$ $\qquad \dfrac{a^m}{a^n} = a^{m-n}$

$(ab)^n = a^n b^n$ $\qquad \left(\dfrac{a}{b}\right)^n = \dfrac{a^n}{b^n}$

$(a^m)^n = (a^n)^m = a^{mn}$ $\qquad (\sqrt[n]{a}\,)^n = a$

$a^{\frac{1}{n}} = \sqrt[n]{a}$ $\qquad a^{\frac{m}{n}} = \sqrt[n]{a^m}$

$\sqrt[n]{ab} = (\sqrt[n]{a}\,)(\sqrt[n]{b}\,)$ $\qquad \sqrt[n]{\dfrac{a}{b}} = \dfrac{\sqrt[n]{a}}{\sqrt[n]{b}}$

Logarithms*

If $\log_b N = x$, then x is the logarithm of N to the base b where b is a finite positive number other than 1. Also, if $b^x = N$ then $\log_b N = x$. In this text, values of b equal to 10 and e are used meaning

$$\log_{10} N = x \quad \text{or} \quad 10^x = N$$

and

$$\log_e N = \ln N = x \quad \text{or} \quad e^x = \exp(x) = N$$

The following properties of logarithms, expressed in terms of base e, are true for any base:

$\ln(MN) = \ln(M) + \ln(N)$ $\qquad \ln\left(\dfrac{M}{N}\right) = \ln(M) - \ln(N)$

$\ln(M^a) = a\,\ln(M)$ $\qquad \ln\left(\sqrt[a]{M^c}\right) = \dfrac{c}{a}\ln(M)$

* Based on a summary given in Hudson, R.G. 1939. The Engineers' Manual (second edition, 25th printing). John Wiley & Sons, NY.

6.4. Linear Regression Analysis of Two Variables

Linear regression is a statistical method of fitting two variables to a linear equation:

$$y = a + b\,x$$

The constants, a (the intercept) and b (the slope), are calculated with the following formulas:

$$b = \frac{n \sum_{i=1}^{n} x_i y_i - \sum_{i=1}^{n} x_i \sum_{i=1}^{n} y_i}{n \sum_{i=1}^{n} (x_i)^2 - \left(\sum_{i=1}^{n} x_i \right)^2}$$

$$a = \bar{y} - b\bar{x}$$

where:

n = number of observations in the sample

$\bar{x}$ = mean of x values

$\bar{y}$ = mean of y values

The method of least squares minimizes the sum of the squared error between the actual and estimated values: a and b are found using a procedure which minimizes

$$n \sum_{i=1}^{n} (y_i - \bar{y}_x)^2$$

where y_i is the value to be estimated and $\bar{y}_x$ is the corresponding estimate of y at x. Computations are easily done using computer spread-sheet programs or hand calculators.

A measure of correlation between two variables can be defined in terms of the sample correlation coefficient (r) which can take on values between -1 and 1. A correlation value of zero means there is no association. A value of -1 means there is a perfect negative correlation and a value of +1 means there is a perfect positive correlation (Fig. 6.1). Correlation may also be expressed in terms of the coefficient of determination, r^2. When $r^2 = 1$, all points fall on the predicted line. If $r^2 = 0$, there is as much variation in the estimate of y as there is in the y variable meaning that any observed fluctuations are due to random variations in y.

The standard error of the estimate can also be a useful measure of how well the regression line fits the data. This parameter is calculated as

$$s_{y,x} = \sqrt{\frac{\sum_{i=1}^{n} (y_i - \bar{y}_x)^2}{n-2}}$$

where:

$s_{y,x}$ = the standard error of the estimate of y on x

Properties of the standard error of the estimate are analogous to those of standard deviation. Assuming a sufficiently large sample, pairs of lines constructed parallel to the regression line of y on x, at vertical distances of $s_{y,x}$, $2s_{y,x}$ and $3s_{y,x}$, should include 68%, 95% and 99.7% (respectively) of the sample data points.

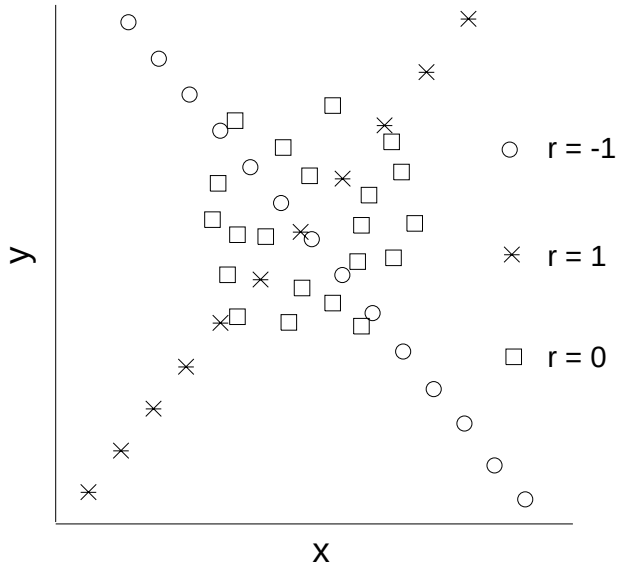

Figure 6.1. Relationship between y and x for a perfect positive correlation (r = 1), a perfect negative correlation (r = -1), and no correlation (r = 0).

Example Problem. Determine the power law, Bingham plastic, Casson, and Herschel-Bulkley model parameters from the data for the carrageenan gum solution given in Table 6.1.

Linear regression can only be performed on a linear equation of the form $y = a + bx$. The Bingham plastic model already exists in this form; however, the other models may require a transformation of the data before they can be presented in a linear form. A summary

Table 6.1. Raw and Transformed Data of a 1% aqueous solution of carrageenan gum at 25°C (Data from Prentice and Huber, 1983)

σ	$\dot{\gamma}$	$\ln\sigma$	$\ln\dot{\gamma}$	$(\sigma)^{.5}$	$(\dot{\gamma})^{.5}$	$\ln(\sigma - 1.1)$
2.61	9.88	0.96	2.29	1.62	3.14	0.412
2.97	11.4	1.09	2.43	1.72	3.38	0.626
2.81	12.9	1.03	2.56	1.68	3.59	0.536
3.44	14.1	1.24	2.65	1.85	3.75	0.850
3.80	17.6	1.34	2.87	1.95	4.20	0.993
4.85	26.3	1.58	3.27	2.20	5.13	1.322
6.61	42.0	1.89	3.74	2.57	6.48	1.707
6.19	48.6	1.82	3.88	2.49	6.97	1.627
5.89	49.3	1.77	3.90	2.43	7.02	1.567
7.22	55.5	1.98	4.02	2.69	7.45	1.812
8.20	58.8	2.10	4.07	2.86	7.67	1.960
9.08	75.4	2.21	4.32	3.01	8.68	2.076
11.63	104.1	2.45	4.65	3.41	10.20	2.354
10.65	110.4	2.37	4.70	3.26	10.51	2.257
12.75	120.5	2.55	4.79	3.57	10.98	2.455
13.10	136.5	2.57	4.92	3.62	11.68	2.484
14.90	145.8	2.70	4.98	3.86	12.07	2.624
15.85	187.1	2.76	5.23	3.98	13.68	2.691
12.70	210.2	2.54	5.35	3.56	14.50	2.451
20.50	270.0	3.02	5.60	4.53	16.43	2.965

of this transformation, and regression results, are given in Table 6.2. Note that the yield stress for the Herschel-Bulkley model must be estimated before linear regression can proceed. Estimating σ_o, K, and n simultaneously would require a nonlinear estimation procedure.

Information presented in Table 6.2 can be presented in terms of the models under investigation:

Bingham, $\sigma = \mu_{pl}(\dot{\gamma}) + \sigma_o$:

$\sigma_o = 3.20$ Pa, $\mu_{pl} = 0.066$ Pa s

Herschel-Bulkley, $\sigma = K(\dot{\gamma})^n + \sigma_o$:

$\sigma_o = 1.10$ Pa, $K = 0.306$ Pa s^n, $n = 0.74$

Casson, $(\sigma)^{.5} = K_1(\dot{\gamma})^{.5} + (\sigma_o)^{.5}$:

$\sigma_o = 1.16$ Pa, $K_1 = 0.211$ $Pa^{.5}$ $s^{.5}$

Power Law, $\sigma = K(\dot{\gamma})^n$:

$K = 0.66$ Pa s^n, $n = 0.60$

Coefficients of determination (Table 6.2) indicate that the power law and Herschel-Bulkley equations provide the best model of the experimental data.

Table 6.2. Linear regression parameters for different rheological models.

Model	y	x	a	b	r^2	$s_{y,x}$
Bingham	σ	$\dot{\gamma}$	$\sigma_o = 3.20$	$\mu_{pl} = 0.066$	0.92	1.44
Power Law	$\ln\sigma$	$\ln\dot{\gamma}$	$\ln K = -0.411$	$n = 0.60$	0.98	0.094
Casson	$(\sigma)^{.5}$	$(\dot{\gamma})^{.5}$	$(\sigma_o)^{.5} = 1.078$	$K_1 = 0.211$	0.96	0.179
*Herschel-Bulkley	$\ln(\sigma - \sigma_o)$	$\ln\dot{\gamma}$	$\ln K = -1.185$	$n = 0.74$	0.98	0.119

*$\sigma_o = 1.1$ Pa was determined from a graphical analysis of the data.

6.5. Hookean Properties

Material	E ($N\ m^{-2}$)	Material	E ($N\ m^{-2}$)
Soft foam rubber	10^2	Carrots	$(2\text{-}4) \times 10^7$
Rubber	8×10^5	Pears	$(1.2\text{-}3) \times 10^7$
Dry Spaghetti	0.3×10^{10}	Potatoes	$(0.6\text{-}1.4) \times 10^7$
Lead	1.0×10^{10}	Apples raw	$(0.6\text{-}1.4) \times 10^7$
Concrete	1.7×10^{10}	Gelatin (gel)	0.02×10^7
Glass	7×10^{10}	Peach	$(0.2\text{-}2) \times 10^7$
Iron	8×10^{10}	Banana	$(0.08\text{-}0.3) \times 10^7$
Steel	25×10^{10}		

Material	ν (-)	Material	ν (-)
Cheddar cheese	0.50	Copper	0.33
Potato tissue	0.49	Steel	0.30
Rubber	0.49	Glass	0.24
Apple tissue	0.37	Bread-crumbs	0.00
Apple	0.21-0.34	Cork	0.00

Material	K ($N\ m^{-2}$)	Material	K ($N\ m^{-2}$)
Dough	1.4×10^6	Silver	10^{11}
Rubber	1.9×10^7	Steel	1.6×10^{11}
Granite	3×10^{10}	Glass	3.9×10^{10}

Source: Lewis, 1987.

6.6. Steady Shear and Normal Stress Difference

Product*	K ($Pa\ s^n$)	n (-)	K' ($Pa\ s^{n'}$)	n' (-)
Apple butter	222.90	0.145	156.03	0.566
Canned frosting	355.84	0.117	816.11	0.244
Honey	15.39	0.989	-	-
Ketchup	29.10	0.136	39.47	0.258
Marshmallow cream	563.10	0.379	185.45	0.127
Mayonnaise	100.13	0.131	256.40	-0.048
Mustard	35.05	0.196	65.69	0.136
Peanut butter	501.13	0.065	3785.00	0.175
Stick butter	199.29	0.085	3403.00	0.393
Stick margarine	297.58	0.074	3010.13	0.299
Squeeze margarine	8.68	0.124	15.70	0.168
Tub margarine	106.68	0.077	177.20	0.358
Whipped butter	312.30	0.057	110.76	0.476
Whipped cream cheese	422.30	0.058	363.70	0.418
Whipped desert topping	35.98	0.120	138.00	0.309

* Data were collected over a shear rate of 0.1 to 100 s^{-1} at 30.5 °C

$$\sigma = K(\dot{\gamma})^n$$

$$N_1 = \sigma_{11} - \sigma_{22} = K'(\dot{\gamma})^{n'}$$

Source: Dickie and Kokini, 1983.

6.7. Yield Stress of Fluid Foods

Product	σ_o (Pa)	Measurement Method	Source
Ketchup	22.8	extrapolation	Ofoli et al. (1987)
Mustard	34.0	extrapolation	Ofoli et al. (1987)
Miracle Whip	54.3	extrapolation	Ofoli et al. (1987)
Apricot Puree	17.4	extrapolation	Ofoli et al. (1987)
Milk Chocolate	10.9	extrapolation	Ofoli et al. (1987)
Minced Fish Paste	1600-2300	extrapolation	Nakayama et al.(1980)
Mayonnaise	24.8-26.9	stress to initiate flow	De Kee et al.(1980)
Ketchup	15.4-16.0	stress to initiate flow	De Kee et al.(1980)
Tomato Paste	83.9-84.9	stress to initiate flow	De Kee et al.(1980)
Raw Meat Batter	17.9	extrapolation	Toledo et al.(1977)
Tomato Puree	23.0	stress decay	Charm(1962)
Applesauce	58.6	stress decay	Charm(1962)
Tomato Paste	107-135	squeezing flow	Campanella and Peleg(1987)
Ketchup	18-30	squeezing flow	Campanella and Peleg(1987)
Mustard	52-78	squeezing flow	Campanella and Peleg(1987)
Mayonnaise	81-91	squeezing flow	Campanella and Peleg(1987)
Applesauce	45-87	squeezing flow	Campanella and Peleg(1987)
Applesauce	46-82	vane method	Qiu and Rao(1988)
Ketchup	26-30	vane method	Missaire et al. (1990)
Spaghetti Sauce	24-28	vane method	Missaire et al. (1990)
Tomato Puree	25-34	vane method	Missaire et al. (1990)
Pumpkin Filling	20	vane method	Missaire et al. (1990)
Applesauce	38-46	vane method	Missaire et al. (1990)
Baby food, pears	49	vane method	Missaire et al. (1990)
Baby food, peaches	25	vane method	Missaire et al. (1990)
Baby food, carrots	71	vane method	Missaire et al. (1990)

Static and Dynamic Yield Stresses of Food Products

Product*	Static Yield Stress (Pa)	Dynamic Yield Stress (Pa)
Tomato puree, Brand A	34.4 ± 3.7	28.1 ± 4.2
Tomato puree, Brand B	30.0 ± 4.2	27.6 ± 3.4
Apple sauce, Brand A	77.3 ± 0.0	48.2 ± 4.7
Apple sauce, Brand B	48.2 ± 4.7	38.0 ± 4.7
Tomato ketchup, Brand A	51.3 ± 5.0	40.6 ± 4.5
Tomato ketchup, Brand A	43.2 ± 3.4	39.6 ± 3.4
Spaghetti sauce, Brand A	26.3 ± 4.5	18.3 ± 0.0
Spaghetti sauce, Brand B	24.8 ± 3.4	21.9 ± 0.0
Baby food, pears	31.8 ± 5.0	24.8 ± 4.0
Baby food, carrots	64.0 ± 4.0	35.7 ± 5.0
Baby food, peaches	22.9 ± 3.4	20.1 ± 3.4
Mayonnaise, Brand A	204.4 ± 5.0	112.6 ± 4.0
Mayonnaise, Brand B	163.8 ± 4.2	99.4 ± 4.0
Mustard, Brand A	82.5 ± 5.0	53.1 ± 5.3
Mustard, Brand B	103.8 ± 5.0	53.4 ± 5.0

* Data were collected at 25°C by using the vane method operating in the controlled rate mode. Source: Yoo et al., 1995.

Briggs and Steffe (1996) determined the yield stress of frozen ice cream using the vane method. Results were summarized with the following equations:

$$\sigma_o = 22.33 \exp(-.37T) \qquad \text{for chocolate ice cream}$$

$$\sigma_o = 39.32 \exp(-.33T) \qquad \text{for vanilla ice cream}$$

where σ_o is the yield stress in Pa, and T is the temperature in $°C$. These equations are valid over the range of temperatures typically maintained for hand-dipped ice cream: -12°*C* to -16°*C*. Yield stresses, ranging from 2.5 to 8.0 kPa, decreased with reductions in temperature. Chocolate had sightly higher values than vanilla.

6.8. Newtonian Fluids

Product	T (°C)	μ (cP)
Acetic acid	15	1.31
	18	1.30
	25.2	1.155
	30	1.04
	41	1.00
	59	0.70
	70	0.60
	100	0.43
Acetone	-42.5	0.695
	-30.0	0.575
	-20.9	0.510
	-13.0	0.470
	-10.0	0.450
	0	0.399
	15	0.337
	25	0.316
	30	0.295
	41	0.280
Ethanol	-32.01	3.84
	-17.59	2.68
	-0.30	1.80
	0	1.773
	10	1.466
	20	1.200
	30	1.003
	40	0.834
	50	0.702
	60	0.592
	70	0.504
Glycol	20	19.9
	40	9.13
	60	4.95
	80	3.02
	100	1.99
Glycerin	-42	6.71E6
	-36	2.05E6
	-25	2.62E5
	-20	1.34E5
	-15.4	6.65E4
	-10.8	3.55E4
	-4.2	1.49E4

	0	1.21E4
	6	6260
	15	2330
	20	1490
	25	954
	30	629
Mercury	-20	1.855
	-10	1.764
	0	1.685
	10	1.615
	20	1.554
	30	1.499
	40	1.450
	50	1.407
	60	1.367
	70	1.331
	80	1.298
	90	1.268
	100	1.240
	150	1.300
	200	1.052
	250	0.995
	300	0.950
	340	0.921
Water	0	1.787
	5	1.519
	10	1.307
	15	1.139
	20	1.002
	25	0.8904
	30	0.7975
	35	0.7194
	40	0.6529
	45	0.5960
	50	0.5468
	55	0.5040
	60	0.4665
	65	0.4335
	70	0.4042
	75	0.3781
	80	0.3547
	85	0.3337
	90	0.3147
	95	0.2975
	100	0.2818

Source: Weast et al., 1984.

Viscosity Prediction Equations for Various Liquids

Equation 1 $$\log(\mu) = A + (B/T)$$

Equation 2 $$\mu = AT^{B}$$

Equation 3 $$\log(\mu) = A + B/(C - T)$$

where μ is in units of Pa s and T in degrees Kelvin.

Material	Eq. #	*A*	*B*	*C*	T range(K)
Acetic Acid	2	1.2106×10^{6}	-3.6612		270-390
Corn Oil	3	-3.5581	-263.32	183.60	290-340
Corn Syrup: DE=100, 20% dry substance	3	-4.4500	-234.80	159.91	280-360
Corn Syrup: DE=42.9, 20% dry substance	3	-4.0137	-129.07	201.23	280-360
Corn Syrup: DE=35.4, 20% dry substance	1	-5.5478	868.35		280-360
Corn Syrup: DE=35.4, 50% dry substance	3	-3.8025	-258.10	186.88	280-360
Corn Syrup: DE=42.9, 50% dry substance	3	-3.9975	-267.36	182.96	280-360
Corn Syrup: DE=75.4, 20% dry substance	1	-5.8508	924.84	201.23	280-360
Ethanol	3	-5.5972	-846.95	-24.124	210-350
Ethylene Glycol	3	-4.5448	-417.05	146.53	280-420
Groundnut Oil	3	-3.9621	-407.46	151.23	290-340
Rapseed Oil	3	-4.4802	-597.20	1119.99	290-340
Soybean Oil	3	-4.4977	-581.28	115.71	290-340
Sunflower Oil	3	-3.6505	-304.27	168.98	290-340
Water	3	-4.5318	-220.57	149.39	270-380

Source: Viswanath and Natarajan, 1989.

Viscosity (centipoise) of Sucrose Solutions

	% sucrose by weight		
T (°C)	20	40	60
0	3.818	14.82	-
5	3.166	11.60	-
10	2.662	9.830	113.90
15	2.275	7.496	74.90
20	1.967	6.223	56.70
25	1.710	5.206	44.02
35	1.336	3.776	26.62
40	1.197	3.261	21.30
45	1.074	2.858	17.24
50	0.974	2.506	14.06
55	0.887	2.227	11.71
60	0.811	1.989	9.87
65	0.745	1.785	8.37
70	0.688	1.614	7.18
80	0.592	1.339	5.42
85	0.552	1.226	4.75
90	-	1.127	4.17
95	-	1.041	3.73

Source: International Critical Tables 5:23 (1917).

Viscosity (centipoise) of Ethanol-Water Mixtures

	Concentration of ethanol, % by weight									
T (°C)	10	20	30	40	50	60	70	80	90	100
0	3.311	5.32	6.94	7.14	6.58	5.75	4.76	3.69	2.73	1.77
5	2.58	4.06	5.29	5.59	5.26	4.63	3.91	3.12	2.31	1.62
10	2.18	3.16	4.05	4.39	4.18	3.77	3.27	2.71	2.10	1.47
15	1.79	2.62	3.26	3.53	3.44	3.14	2.77	2.31	1.80	1.33
20	1.54	2.18	2.71	2.91	2.87	2.67	2.37	2.01	1.61	1.20
25	1.32	1.82	2.18	2.35	2.40	2.24	2.04	1.75	1.42	1.10
30	1.16	1.55	1.87	2.02	2.02	1.93	1.77	1.53	1.28	1.00
35	1.01	1.33	1.58	1.72	1.72	1.66	1.53	1.36	1.15	0.91
60	0.91	1.16	1.37	1.48	1.50	1.45	1.34	1.20	1.04	0.83

Source: Matz, 1962.

Viscosity (centipoise) of Corn Syrup

[1]DS	T (°F)	[2]DE=35.4	DE=42.9	DE=53.7	DE=75.4	DE=92.4
85	60		0	0	457000	-
	80	7080000	1410000	537000	83200	-
	100	1000000	227000	85200	17000	-
	120	188000	50100	20000	4270	-
	140	44900	13000	6310	1660	-
	160	13000	5190	2290	589	-
	180	4420	1760	944	275	-
80	60		266000	89100	24000	-
	80	126000	59600	17800	4570	-
	100	29900	15000	5010	1550	-
	120	9810	4840	1800	603	-
	140	3350	1860	785	282	-
	160	1410	851	367	141	-
	180	687	386	196	75.9	-
75	60	39800	18200	7590	6030	-
	80	10000	5390	2140	741	501
	100	3020	1880	807	331	211
	120	1260	817	372	159	106
	140	620	389	191	83.2	56.2
	160	325	197	103	47.9	32.4
	180	180	110	62	28.8	19.5
65	60	1060	560	389	178	-
	80	398	237	159	77.6	56.2
	100	182	119	83.2	45.7	30.7
	120	108	69.2	47.3	26.3	18.6
	140	67.9	43.4	29.0	16.2	12.2
	160	43.2	26.6	18.6	10.7	8.41
	180	29.0	17.8	12.6	7.76	5.96
50	60	54.6	34.0	33.5	18.6	-
	80	30.0	19.5	18.4	11.8	9.66
	100	18.5	12.0	11.6	7.94	6.31
	120	12.9	8.51	7.71	5.50	4.39
	140	9.44	6.31	5.43	3.24	3.20
	160	6.92	4.49	4.03	3.02	2.50
	180	5.27	3.55	3.16	2.19	1.97
35	60	9.16	7.16	7.5	5.13	-
	80	6.31	4.75	4.95	3.22	3.35
	100	4.52	3.29	3.35	2.74	2.41
	120	3.35	2.51	2.51	2.07	1.78
	140	2.66	1.99	1.88	1.57	1.41
	160	2.20	1.59	1.56	1.27	1.12
	180	1.68	1.33	1.26	1.00	0.944
20	60	2.90	2.82	2.63	2.26	-
	80	2.24	2.04	1.94	1.70	1.72
	100	1.78	1.45	1.45	1.33	1.27
	120	1.35	1.14	1.12	1.06	1.00
	140	1.12	0.922	0.908	0.832	0.804
	160	1.00	0.759	0.794	0.692	0.689
	180	0.773	0.673	0.668	0.562	0.576

[1]DS = Percent Dry Substance; [2]DE = Dextrose Equivalent
Source: Erickson et al., 1966.

6.9. Dairy, Fish and Meat Products

Product	T (°C)	*n* (-)	*K* (Pa s^n)	σ_o (Pa)	$\dot{\gamma}$ (s^{-1})
Cream, 10% fat	40	1.0	.00148	-	-
	60	1.0	.00107	-	-
	80	1.0	.00083	-	-
Cream, 20% fat	40	1.0	.00238	-	-
	60	1.0	.00171	-	-
	80	1.0	.00129	-	-
Cream, 30% fat	40	1.0	.00395	-	-
	60	1.0	.00289	-	-
	80	1.0	.00220	-	-
Cream, 40% fat	40	1.0	.00690	-	-
	60	1.0	.00510	-	-
	80	1.0	.00395	-	-
Minced fish paste	3-6	.91	8.55	1600.0	67-238
Raw, Meat Batters					
15[1] 13[2] 68.8[3]	15	.156	639.3	1.53	300-500
18.7 12.9 65.9	15	.104	858.0	.28	300-500
22.5 12.1 63.2	15	.209	429.5	0	300-500
30.0 10.4 57.5	15	.341	160.2	27.8	300-500
33.8 9.5 54.5	15	.390	103.3	17.9	300-500
45.0 6.9 45.9	15	.723	14.0	2.3	300-500
45.0 6.9 45.9	15	.685	17.9	27.6	300-500
67.3 28.9 1.8	15	.205	306.8	0	300-500
Milk, homogenized	20	1.0	.002000	-	-
	30	1.0	.001500	-	-
	40	1.0	.001100	-	-
	50	1.0	.000950	-	-
	60	1.0	.000775	-	-
	70	1.0	.00070	-	-
	80	1.0	.00060	-	-
Milk, raw	0	1.0	.00344	-	-
	5	1.0	.00305	-	-
	10	1.0	.00264	-	-
	20	1.0	.00199	-	-
	25	1.0	.00170	-	-
	30	1.0	.00149	-	-
	35	1.0	.00134	-	-
	40	1.0	.00123	-	-

[1] %Fat; [2] %Protein; [3] %MC
Source: Steffe et al., 1986.

6.10. Oils and Miscellaneous Products

Product	% Total Solids	T (°C)	*n* (-)	*K* (Pa s^n)	σ_o (Pa)	$\dot{\gamma}$ (s^{-1})
Chocolate, melted	-	46.1	.574	.57	1.16	-
Honey					-	-
Buckwheat	18.6	24.8	1.0	3.86	-	-
Golden Rod	19.4	24.3	1.0	2.93	-	-
Sage	18.6	25.9	1.0	8.88	-	-
Sweet Clover	17.0	24.7	1.0	7.20	-	-
White Clover	18.2	25.2	1.0	4.80	-	-
Mayonnaise	-	25	.55	6.4	-	30-1300
	-	25	.60	4.2	-	40-1100
Mustard	-	25	.39	18.5	-	30-1300
	-	25	.34	27.0	-	40-1100
Oils						
Castor	-	10	1.0	2.42	-	-
	-	30	1.0	.451	-	-
	-	40	1.0	.231	-	-
	-	100	1.0	.0169	-	-
Corn	-	38	1.0	.0317	-	-
	-	25	1.0	.0565	-	-
Cottonseed	-	20	1.0	.0704	-	-
	-	38	1.0	.0306	-	-
Linseed	-	50	1.0	.0176	-	-
	-	90	1.0	.0071	-	-
Olive	-	10	1.0	.1380	-	-
	-	40	1.0	.0363	-	-
	-	70	1.0	.0124	-	-
Peanut	-	25.5	1.0	.0656	-	-
	-	38.0	1.0	.0251	-	-
	-	21.1	1.0	.0647	-	.32-64
	-	37.8	1.0	.0387	-	.32-64
	-	54.4	1.0	.0268	-	.32-64
Rapeseed	-	0.0	1.0	2.530	-	-
	-	20.0	1.0	.163	-	-
	-	30.0	1.0	.096	-	-
Safflower	-	38.0	1.0	.0286	-	-
	-	25.0	1.0	.0522	-	-
Sesame	-	38.0	1.0	.0324	-	-
Soybean	-	30.0	1.0	.0406	-	-
	-	50.0	1.0	.0206	-	-
	-	90.0	1.0	.0078	-	-
Sunflower	-	38.0	1.0	.0311	-	-

Source: Steffe et al., 1986.

6.11. Fruit and Vegetable Products

Product	% Total Solids	T (°C)	*n* (-)	*K* (Pa s^n)	$\dot{\gamma}$ (s^{-1})
Apple					
Pulp	-	25.0	.084	65.03	-
Sauce	11.6	27	.28	12.7	160-340
	11.0	30	.30	11.6	5-50
	11.0	82.2	.30	9.0	5-50
Sauce	10.5	26	.45	7.32	.78-1260
	9.6	26	.45	5.63	.78-1260
	8.5	26	.44	4.18	.78-1260
Apricots					
Puree	17.7	26.6	.29	5.4	-
	23.4	26.6	.35	11.2	-
	41.4	26.6	.35	54.0	-
	44.3	26.6	.37	56.0	.5-80
	51.4	26.6	.36	108.0	.5-80
	55.2	26.6	.34	152.0	.5-80
	59.3	26.6	.32	300.0	.5-80
Reliable,					
Conc., green	27.0	4.4	.25	170.0	3.3-137
	27.0	25	.22	141.0	3.3-137
" ripe	24.1	4.4	.25	67.0	3.3-137
	24.1	25	.22	54.0	3.3-137
" ripened	25.6	4.4	.24	85.0	3.3-137
	25.6	25	.26	71.0	3.3-137
" overripe	26.0	4.4	.27	90.0	3.3-137
	26.0	25	.30	67.0	3.3-137
Banana					
Puree A	-	23.8	.458	6.5	-
Puree B	-	23.8	.333	10.7	-
Puree (17.7 Brix)	-	22	.283	107.3	28-200
Blueberry					
Pie Filling	-	20	.426	6.08	3.3-530
Carrot					
Puree	-	25	.228	24.16	-
Green Bean					
Puree	-	25	.246	16.91	-
Guava					
Puree (10.3 Brix)	-	23.4	.494	39.98	15-400
Mango					
Puree (9.3 Brix)	-	24.2	.334	20.58	15-1000

Orange Juice Concentrate					
Hamlin, early	-	25	.585	4.121	0-500
42-5 Brix	-	15	.602	5.973	0-500
	-	0	.676	9.157	0-500
	-	-10	.705	14.25	0-500
Hamlin, late	-	25	.725	1.930	0.500
41.1 Brix	-	15	.560	8.118	0.500
	-	0	.620	1.754	0-500
	-	-10	.708	13.87	0-500
Pineapple, early	-	25	.643	2.613	0-500
40.3 Brix	-	15	.587	5.887	0-500
	-	0	.681	8.938	0-500
	-	-10	.713	12.18	0-500
Pineapple, late	-	25	.532	8.564	0-500
41.8 Brix	-	15	.538	13.43	0-500
	-	0	.636	18.58	0-500
	-	-10	.629	36.41	0-500
Valencia, early	-	25	.583	5.059	0-500
43.0 Brix	-	15	.609	6.714	0-500
	-	-10	.619	27.16	0-500
Valencia, late	-	25	.538	8.417	0-500
	-	15	.568	11.80	0-500
41.9 Brix	-	0	.644	18.75	0-500
	-	-10	.628	41.41	0-500
Naval					
65.1 Brix	-	-18.5	.71	29.2	-
	-	-14.1	.76	14.6	-
	-	-9.3	.74	10.8	-
	-	-5.0	.72	7.9	-
	-	-0.7	.71	5.9	-
	-	10.1	.73	2.7	-
	-	19.9	.72	1.6	-
	-	29.5	.74	.9	-
Papaya					
Puree (7.3 Brix)	-	26.0	.528	9.09	20-450
Peach					
Pie Filling	-	20.0	.46	20.22	1.-140
Puree	10.9	26.6	.44	.94	-
	17.0	26.6	.55	1.38	-
	21.9	26.6	.55	2.11	-
	26.0	26.6	.40	13.4	80-1000
	29.6	26.6	.40	18.0	80-1000
	37.5	26.6	.38	44.0	-
	40.1	26.6	.35	58.5	2-300
	49.8	26.6	.34	85.5	2-300
	58.4	26.6	.34	440.0	-
Puree	11.7	30.0	.28	7.2	5-50

	11.7	82.2	.27	5.8	5-50
	10.0	27.0	.34	4.5	160-3200
Pear					
Puree	15.2	26.6	.35	4.25	-
	24.3	26.6	.39	5.75	-
	33.4	26.6	.38	38.5	80-1000
	37.6	26.6	.38	49.7	-
	39.5	26.6	.38	64.8	2-300
	47.6	26.6	.33	120.0	.5-1000
	49.3	26.6	.34	170.0	-
	51.3	26.6	.34	205.0	-
	45.8	32.2	.479	35.5	-
	45.8	48.8	.477	26.0	-
	45.8	65.5	.484	20.0	-
	45.8	82.2	.481	16.0	-
	14.0	30.0	.35	5.6	5-50
	14.0	82.2	.35	4.6	5-50
Plum					
Puree	14.0	30.0	.34	2.2	5-50
	14.0	82.2	.34	2.0	5-50
Squash					
Puree A	-	25	.149	20.65	-
Puree B	-	25	.281	11.42	-
Tomato					
Juice Conc.	5.8	32.2	.59	.223	500-800
	5.8	38.8	.54	.27	500-800
	5.8	65.5	.47	.37	500-800
	12.8	32.2	.43	2.0	500-800
	12.8	48.8	.43	2.28	500-800
	12.8	65.5	.34	2.28	500-800
	12.8	82.2	.35	2.12	500-800
	16.0	32.2	.45	3.16	500-800
	16.0	48.8	.45	2.77	500-800
	16.0	65.5	.40	3.18	500-800
	16.0	82.2	.38	3.27	500-800
	25.0	32.2	.41	12.9	500-800
	25.0	48.8	.42	10.5	500-800
	25.0	65.5	.43	8.0	500-800
	25.0	82.2	.43	6.1	500-800
	30.0	32.2	.40	18.7	500-800
	30.0	48.8	.42	15.1	500-800
	30.0	65.5	.43	11.7	500-800
	30.0	82.2	.45	7.9	500-800

Source: Steffe et al., 1986.

6.12. Polymer Melts

Polymer	T (°C)	n (-)	K (Pa s^n)	η_o (Pa s^n)	$\dot{\gamma}$ (s^{-1})
High impact polystyrene	170	0.20	7.58×10^4	2.1×10^5	100-7000
	190	0.21	4.57×10^4	1.48×10^5	100-7000
	210	0.19	3.61×10^4	1.05×10^5	100-7000
Polystyrene	190	0.22	4.47×10^4	1.4×10^4	100-4500
	210	0.25	2.38×10^4	9.2×10^3	100-4000
	225	0.28	1.56×10^4	6.6×10^3	100-5000
Styrene Acrylonitril	190	0.21	9.0×10^4	2.2×10^4	100-9000
	220	0.27	3.22×10^4	9.0×10^3	100-8000
	250	0.35	1.11×10^4	4.2×10^3	100-8000
Thermoplastic olefin	200	0.27	2.75×10^4	3.6×10^4	100-5000
	220	0.30	1.83×10^4	2.15×10^4	100-4000
	240	0.28	1.99×10^4	1.35×10^4	100-3000
Acrylonitrile butadiene styrene	170	0.25	1.19×10^5	7.95×10^4	100-5500
	190	0.25	6.29×10^4	4.4×10^4	100-6000
	210	0.25	3.93×10^4	2.6×10^4	100-7000
Polypropylene	180	0.37	6.79×10^3	4.21×10^3	100-4000
	190	0.41	4.89×10^3	3.02×10^3	100-3500
	200	0.41	4.35×10^3	205×10^3	100-4000
Ethylene ethyl acrylate	170	0.38	1.21×10^4	5.4×10^3	100-6000
	190	0.43	6.91×10^3	3.5×10^3	100-4000
	210	0.48	3.77×10^3	2.3×10^3	100-6000
High density polyethylene	180	0.56	6.19×10^3	2.1×10^3	100-1000
	200	0.59	4.68×10^3	1.52×10^3	100-1000
	220	0.61	3.73×10^3	1.17×10^3	100-1000
Low density polyethylene	160	0.41	9.36×10^3	6.3×10^3	100-4000
	180	0.46	5.21×10^3	3.2×10^3	100-6500
	200	0.47	4.31×10^3	1.7×10^3	100-6000
Nylon	220	0.63	2.62×10^3	1.6×10^3	100-2500
	230	0.66	1.95×10^3	1.3×10^3	100-2000
	235	0.66	1.81×10^3	1.1×10^3	100-2300
Polymethylmethacrylate	220	0.19	8.83×10^4	1.3×10^3	100-6000
	240	0.25	4.27×10^4	6.0×10^3	100-6000
	260	0.27	2.62×10^4	2.9×10^3	100-7000
Polycarbonate	280	0.64	8.39×10^3	1.54×10^3	100-1000
	300	0.67	4.31×10^3	8.0×10^2	100-1000
	320	0.80	1.08×10^3	4.2×10^2	100-1000

Source: Tadmor, Z. and C.G. Gogos. 1979.

6.13. Cosmetic and Toiletry Products

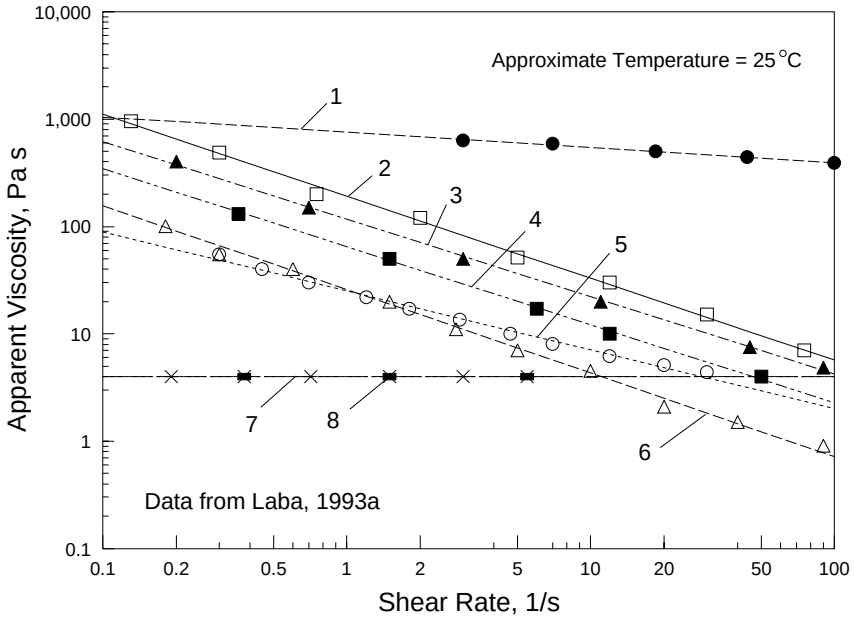

Approximate parameters, at 25°C, for the apparent viscosity function based on the power law form of the model: $\eta = K(\dot{\gamma})^{n-1}$

(Curve #): Product	*n* (-)	*K* (Pa s)	$\dot{\gamma}$ (1/s)
1: Shine On Lasting Color Nail Enamel*	0.86	754	3.0 - 99
2: Cover Girl Marathon Mascara*	0.24	191	0.1 - 75
3: Muppets Toothpaste, Bubble Gum Gel	0.28	117	0.1 - 90
4: Johnson's Baby Sunblock Lotion*	0.28	75	0.1 - 50
5: Pond's Cold Cream*	0.45	25	0.3 - 90
6: Oil of Olay Beauty Fluid	0.22	26	0.1 - 90
7: Head & Shoulders Shampoo	1.0	4	0.1 - 6
8: Jergens Lotion Enriched Liquid Soap	1.0	4	0.1 - 6

* Average values, original data indicate some time-dependent behavior.

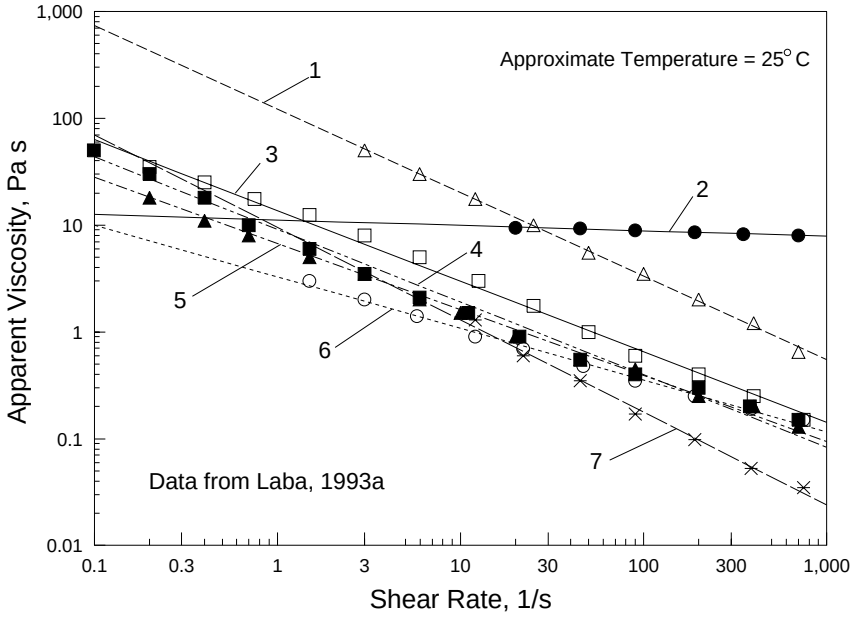

Approximate parameters, at 25°C, for the apparent viscosity function based on the power law form of the model: $\eta = K(\dot{\gamma})^{n-1}$

(Curve #): Product	n (-)	K (Pa s)	$\dot{\gamma}$ (1/s)
1: Colgate Toothpaste*	0.22	121.7	3.0 - 700
2: Suave Balsam & Protein Shampoo	0.95	11.1	20.0 - 700
3: Vaseline Intensive Care Lotion	0.34	13.7	0.09 - 750
4: Moisturizing Sunblock Lotion*	0.32	9.1	0.05 - 700
5: Baby Magic Baby Lotion*	0.38	6.7	0.02 - 700
6: BAN Antiperspirant/Deodorant Roll-on	0.52	3.3	1.5 - 750
7: Dry Idea Dry Roll-on Deodorant	0.13	9.5	12.0 750

* Average values, original data indicate some time-dependent behavior.

6.14. Energy of Activation for Flow for Fluid Foods

Fluid food	Concentration	n (-)	E_a (kcal/g mol)	η at 50°C [1] (mPa s^n)
Depectinized apple	75° Brix	1.0	14.2	150.0
juice [a]	50° Brix	1.0	8.4	4.0
	30° Brix	1.0	6.3	1.6
	15° Brix	1.0	5.3	0.7
Cloudy apple juice [a]	40° Brix	1.0	5.8	4.9
	30° Brix	1.0	5.1	2.0
Concord grape juice [a]	50° Brix	1.0	6.9	15.0
	30° Brix	1.0	6.2	1.8
Cloudy apple juice [a]	65.5° Brix	0.65	9.1	258.5
	50.0° Brix	0.85	6.1	25.0
Apple sauce [a]	11.0° Brix	0.30	1.2	730.0
Peach puree [a]	11.7° Brix	0.30	1.7	190.0
Pear puree [a]	16.0° Brix	0.30	1.9	375.0
Filtered orange juice [b]	18.0° Brix	1.0	5.8	1.5
	10° Brix	1.0	5.3	0.8
Whole egg [c]	75 Wt.% water	1.0	5.9	3.7
Stabilized egg white [c]	88 Wt.% water	1.0	5.9	1.9
Plain yolk [c]	55 Wt.% water	1.0	6.4	48.2
Salted yolk [c]	10 Wt.% salt	1.0	8.3	153.0
Sugared yolk [c]	10 Wt.% sugar	1.0	6.9	32.1

[1] η = apparent viscosity at 100 1/s.

Source: [a] Rao (1986); [b] Saravacos (1970); [c] Scalzo et al. (1970)

6.15. Extensional Viscosities of Newtonian Fluids

Liquid	η_E (Pa s)	$\dot{\varepsilon}_h$ (s^{-1})	Trouton Ratio (-)
Silicone Oil	102.5	0.5-10	2.4-3.6
Polybutene	24	1.6-5	2.7-3.3
Polybutene	23	2-10	2.6-3.8
Corn Syrup	25	-	4
Oil	750	0.08-0.14	3.1-3.5
Maltose Sryup	104	2-5	5
Glycerol-water	0.357	4000-9000	1.7-3.4
Glycerol-water	0.4-1.7	40-180	2.7-3.3
Glycerol-water	0.12-0.25	200-4000	2.4-3.9
Viscasil	30	1-30	2.4-3.9

Source: Gupta and Sridhar, 1987.

6.16. Extensional Viscosities of Non-Newtonian Fluids

Solute	Solvent	Conc. (%)	$\dot{\varepsilon}_h$ (s^{-1})	η_E (*Pa s*)	Trouton Ratio (-)
PAA	Glycerol	1.5	0.1-10	2-8E3	-
PAA	Water	1.0	8-230	2.4-250	-
PAA	Glycerol	1.0	1-10	-	0.1-6.0
PAA	Glycerol	0.175-0.5	0.17-1.4	-	20-1000
PAA	Glycerol	0.5	0.1-0.2	1-5E4	-
PAA	Maltose	0.1	0.5-5.0	-	70
PAA	Water	0.1	100-750	-	3000
PAA	Water	0.1	40-80	-	250-400
PAA	Water	0.01-0.5	33-19000	-	500-29000
PAA	Corn Syrup	0.05	-	-	300
PAA	Glycerol	0.01-0.03	4-17	30-100	-
PAA	Glycerol	0.005-0.05	50-1400	1-100	-
PAA	Water	0.0051	50-800	0.5-25	-
PEO	Sucrose	3.0	1-20	20-500	-
PEO	Glycerol	3.0	0.4-2.0	0.4-7.0E6	-
PEO	Water	0.1	100-750	8-11.4	-
PEO	Water	0.1	40-80	-	1500-2400
PIB	Decalin	6.4-11.6	2-100	0.5-7	-
PIB	Kerosene	3.0-4.0	3-100	-	1.2-40
PIB	Polybutene	0.18	0.4-3.0	-	3-30
XG	Glycerol	0.03-0.05	20-40	1-10	-
XG	Glycerol	0.005-0.01	50-1400	1-8	-
HPC	Water	2.0	0.1-1.0	-	2.0-5.0
HPC	Acetic Acid	40.0	0.01-10.0	-	10
HC	Jet Fuel	0.4-1.0	3-40	-	80-2000
PU	DMF	18-30	-	8-30	-

PAA, polyacrylamide; PEO, polyethylene oxide; PIB, poly-isobutylene; XG, xanthan gum; HPC, hydroxy-propylcellulose; HC, hydrocarbon; PU, polyurethane; DMF, dimethylformamide.

Source: Gupta and Sridhar, 1987.

6.17. Fanning Friction Factors: Bingham Plastics

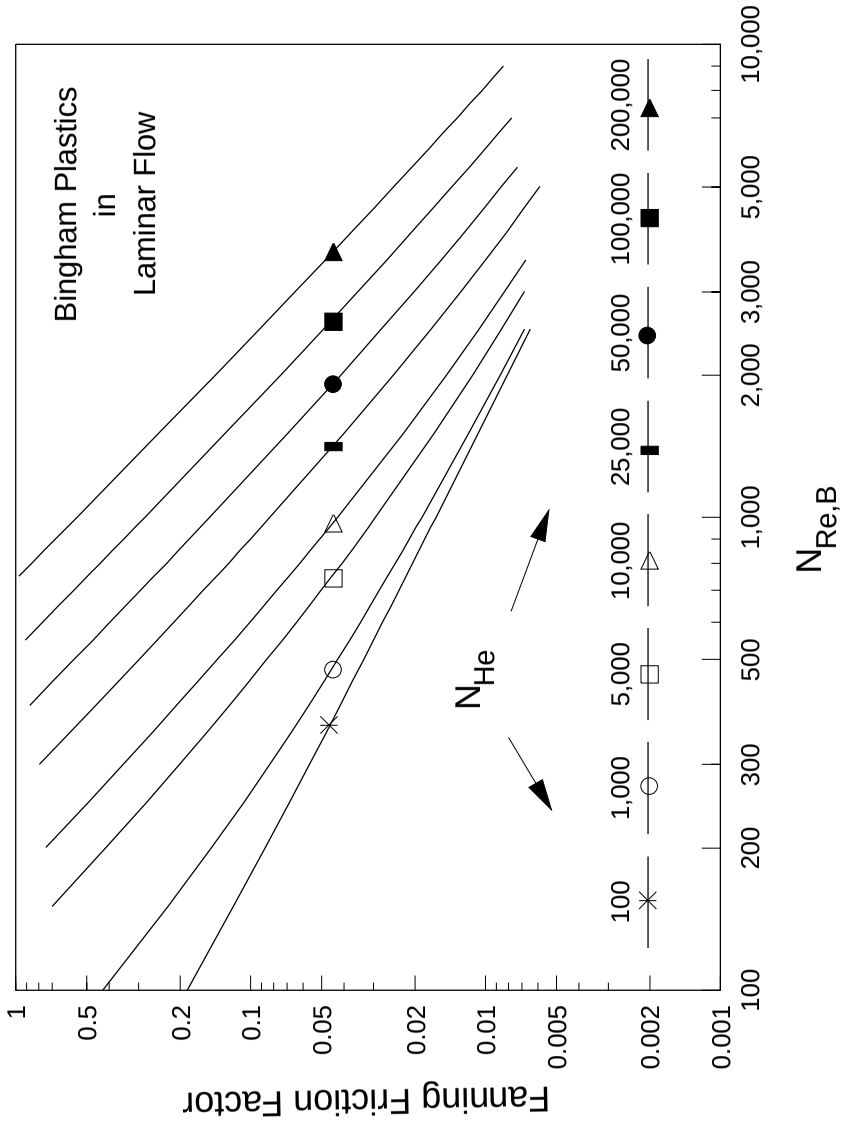

6.18. Fanning Friction Factors: Power Law Fluids

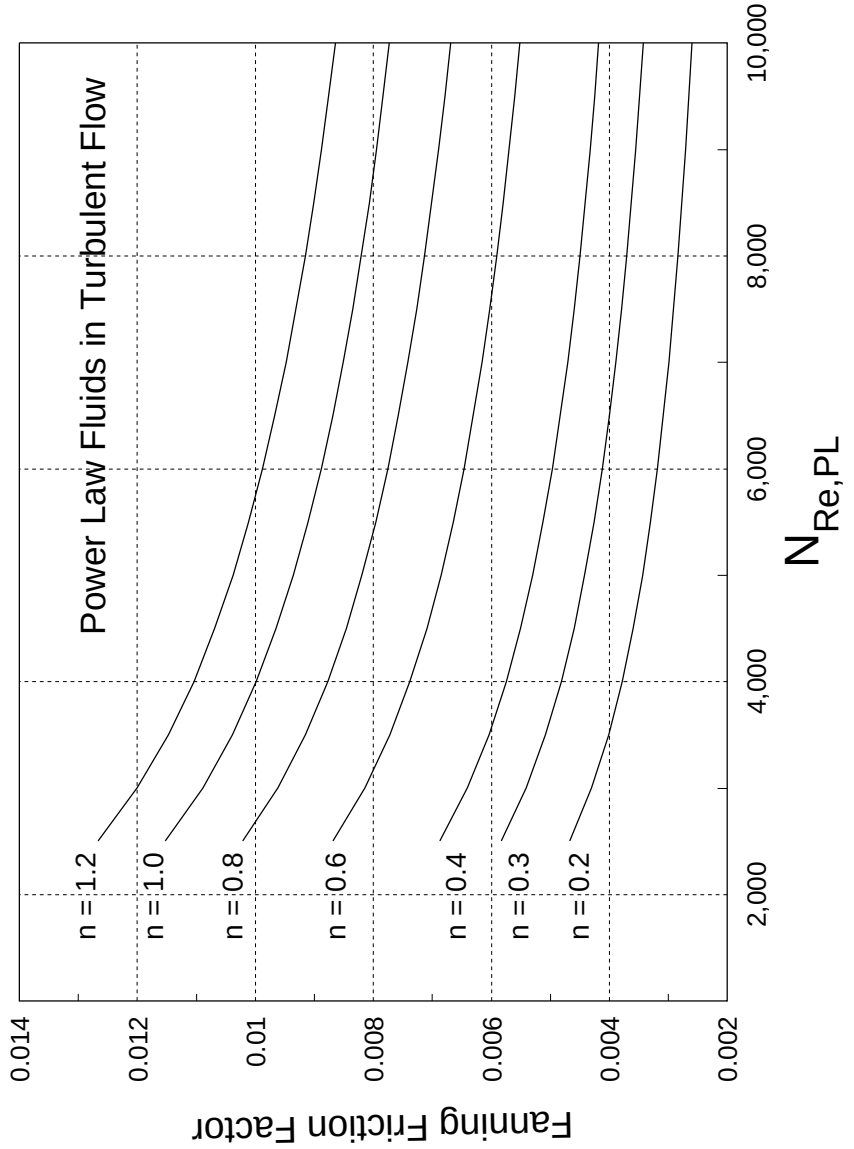

6.19. Creep (Burgers Model) of Salad Dressing

Creamy-style Salad Dressing at 2.8°C	J_o (cm^2 $dyne^{-1}$)	J_1 (cm^2 $dyne^{-1}$)	λ_{ret} (s)	μ_o (P)
Regular, bottled[1]	0.000704	0.00100	16.2	79800
Reduced Calorie, bottled[1]	0.00182	0.00192	43.2	148800
Regular, bottled[1]	0.000490	0.000481	18.5	587400
Reduced Calorie, bottled[1]	0.000870	0.00370	26.1	672000
Regular, dry mix[2]	0.00161	0.000980	8.92	19800
Regular, dry mix[2]	0.00164	0.00208	2.42	3600

[1] Constant Applied Shear Stress: σ_o = 55.2 dyne cm^2
[2] Constant Applied Shear Stress: σ_o = 22.8 dyne cm^2
Source: Paredes et al., 1989

The above constants were determined for the Bugers model (Eq. [5.22]) written in terms of the shear creep compliance function:

$$J = f(t) = J_0 + J_1\left(1 - \exp\left(\frac{-t}{\lambda_{ret}}\right)\right) + \frac{t}{\mu_0}$$

Results are typical of creamy-style salad dressing purchased in a bottle or made from dry mix. Creep testing may be useful in considering the stability of salad dressing.

6.20. Oscillatory Data for Butter

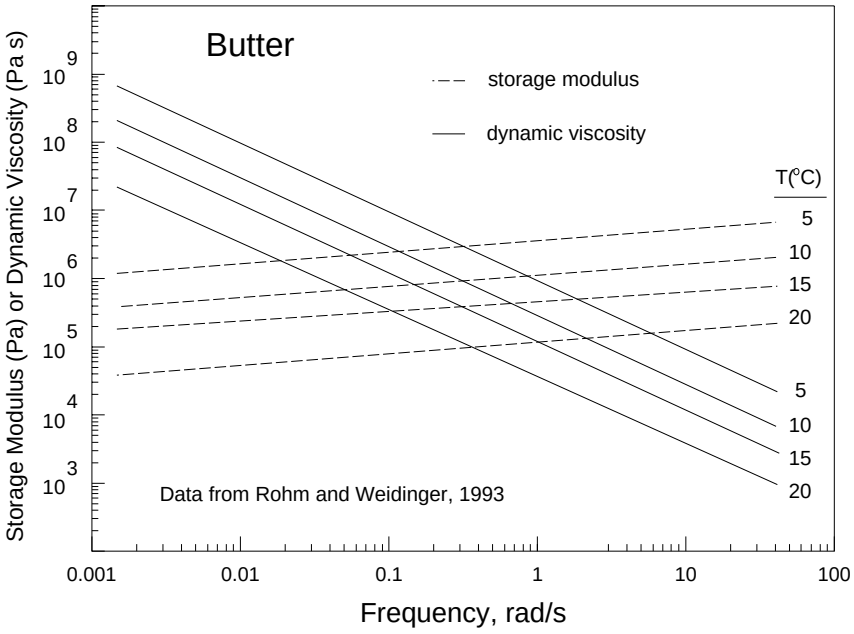

Approximate mathematical parameters describing the above curves: $\eta' = a(\omega)^b$ and $G' = c(\omega)^d$

T (°C)	*a* (Pa s^{1+b})	*b* (-)	*c* (Pa s^d)	*d* (-)
5	1,073,300	-1.0	4,395,900	0.18
10	350,100	-1.0	1,339,500	0.16
15	140,400	-1.0	561,400	0.16
20	35,000	-1.0	151,700	0.17

6.21. Oscillatory Data Iota-Carrageenan Gel

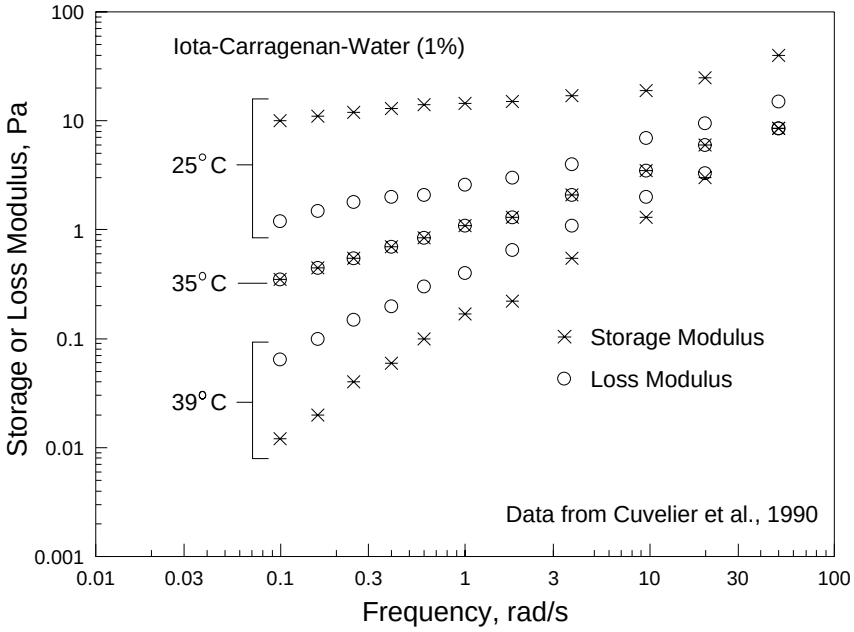

This figure illustrates the effect of temperature in transforming a gel into a solution. Iota-carrageenan (1%) was prepared by dispersing the gum in cold water and heating for 15 min. The frequency sweep was conducted at a strain amplitude of 8% using a coaxial cylinder geometry ($R_b/R_c = 0.96$). A structured gel is observed at 25°C where the storage modulus is only slightly dependent on frequency. The storage modulus and the loss modulus are almost the same at 35°C. Behavior typical of a macromolecular solution (the storage modulus is less than the loss modulus) is observed at 39°C.

6.22. Storage and Loss Moduli of Fluid Foods

$$G' = a\omega^b \qquad G'' = c\omega^d$$

Product	T (°C)	a (Pa s^b)	b (-)	c (Pa s^d)	d (-)	ω (rad / s)
Mustard[1]						
fine	25	800.6	0.120	149.5	0.177	0.01 - 100
standard	25	897.5	0.130	185.9	0.171	0.01 - 100
course	25	1160.0	0.135	265.0	0.139	0.01 - 100
Tomato Paste[2]	40	8434.0	0.117	2101.0	0.153	5.0 - 55.0
Blueberry Pie Filling[3]	40	278.3	0.17	64.2	0.26	1 - 100
	85	237.9	0.13	45.5	0.26	1-100
Cookie Dough[4]	RT*	4.66E7	1.49	1.20E7	1.30	0.01-100
Cracker Dough[4]	RT*	6.50E6	1.24	2.10E6	1.12	0.01-100
Mozzarella Cheese[5]						
natural	70	22,700	0.17	10,300	0.19	0.01 - 100
with 1% Ca caseinate	70	59,200	0.20	19,800	0.14	0.01 - 100
with 2% Ca caseinate	70	15,900	0.21	19,800	0.16	0.01 - 100

*RT = Room Temperature
[1] from Aguilar et al., 1991.
[2] from Rao and Cooley, 1992.
[3] from Steffe et al., 1989.
[4] from Menjivar and Faridi, 1994.
[5] from Nolan et al., 1989.

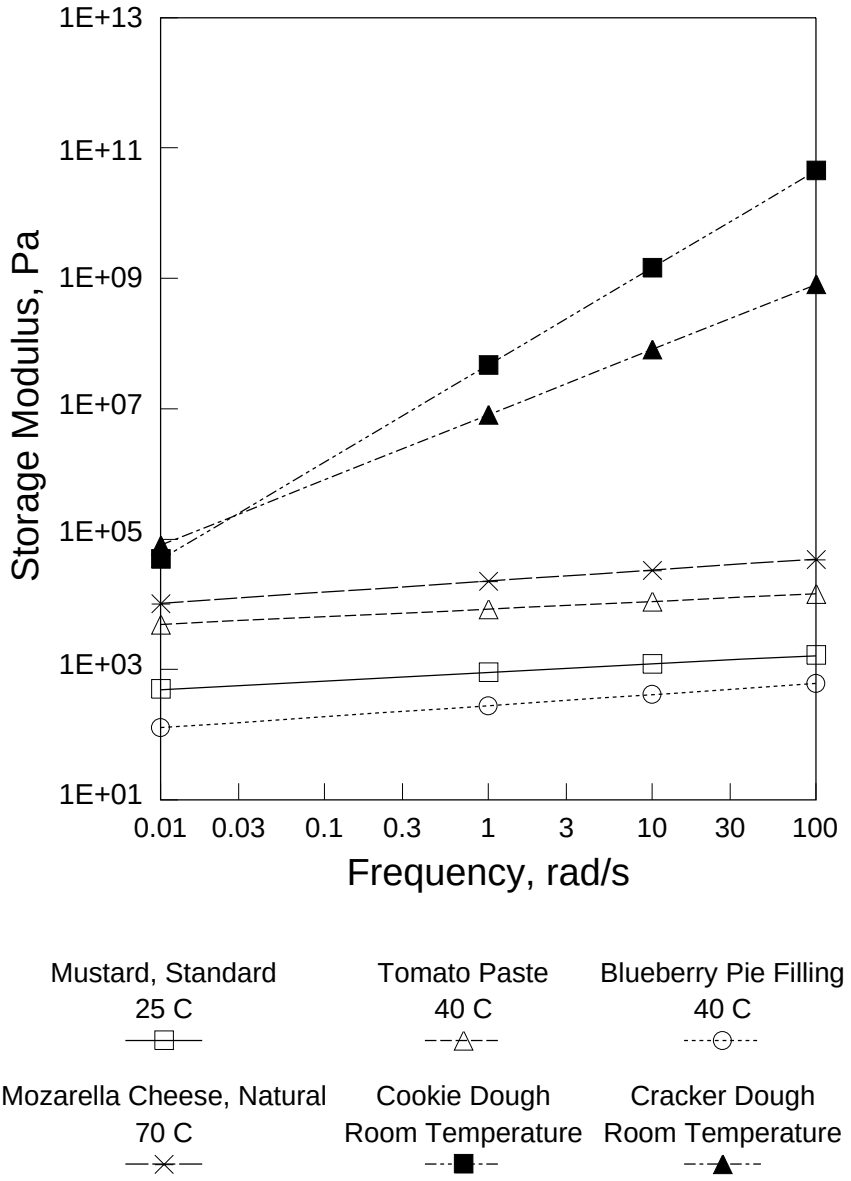
1E+13
1E+11
1E+09
1E+07
1E+05
1E+03
1E+01
Storage Modulus, Pa
0.01
0.03
0.1
0.3
1
3
10
30
100
Frequency, rad/s
Mustard, Standard
25 C
Tomato Paste
40 C
Blueberry Pie Filling
40 C
Mozarella Cheese, Natural
70 C
Cookie Dough
Room Temperature
Cracker Dough
Room Temperature

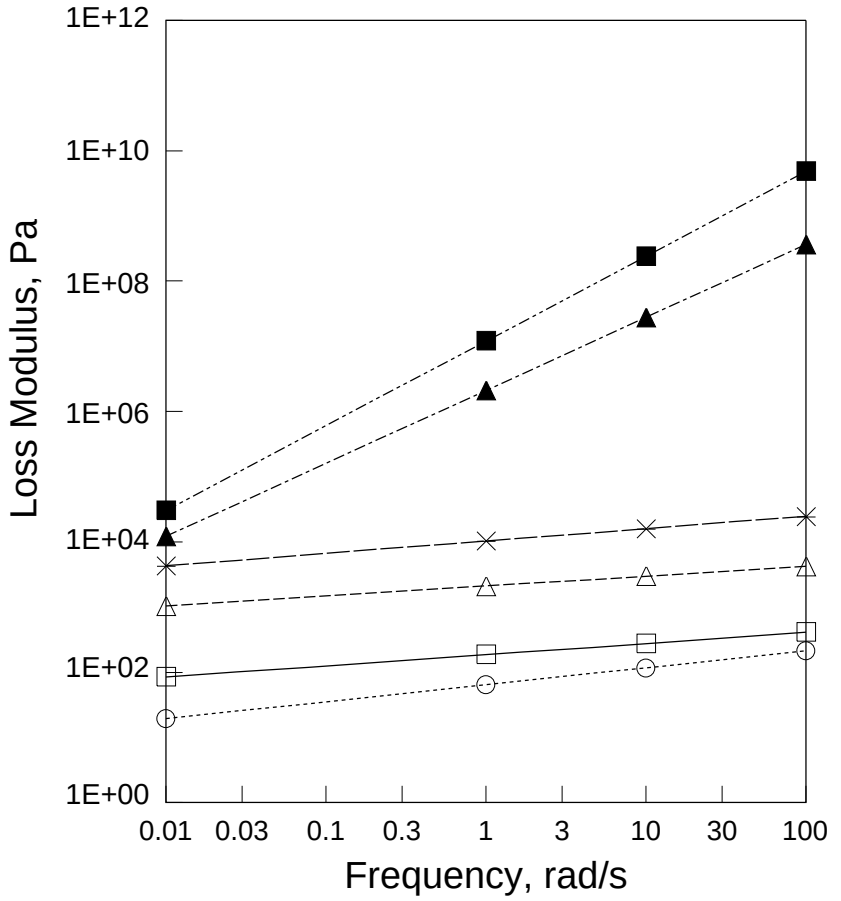
1E+12
1E+10
1E+08
1E+06
1E+04
1E+02
1E+00
Loss Modulus, Pa
0.01
0.03
0.1
0.3
1
3
10
30
100
Frequency, rad/s
Mustard, Standard
25 C
Tomato Paste
40 C
Blueberry Pie Filling
40 C
Mozarella Cheese, Natural
70 C
Cookie Dough
Room Temperature
Cracker Dough
Room Temperature

Nomenclature

a_T	shift factor, dimensionless
A	area, m^2
A_o	initial sample area, m^2
b	height of mixer blade, m
B	bulk compression creep compliance, Pa^{-1}
B^*	bulk compression complex compliance, Pa^{-1}
B'	bulk compression storage compliance, Pa^{-1}
B''	bulk compression loss compliance, Pa^{-1}
c	σ_o/σ_w , dimensionless
c_p	specific heat, J kg^{-1} K^{-1}
C	mass concentration, g/dl or g/100 ml
d	impeller blade or vane diameter, m
d_e	equivalent diameter, m
D	diameter, m
D	tensile creep compliance, Pa^{-1}
D^*	tensile complex compliance, Pa^{-1}
D'	tensile storage compliance, Pa^{-1}
D''	tensile loss compliance, Pa^{-1}
D_e	diameter of extrudate, m
E	Young's modulus or modulus of elasticity, Pa
E	tensile relaxation modulus, Pa
E_a	energy of activation for flow, cal/g mole
E^*	tensile complex modulus, Pa
E'	tensile storage modulus, Pa
E''	tensile loss modulus, Pa
f	Fanning friction factor, dimensionless
F	force, N
g	acceleration due to gravity, 9.81 m s^{-2}
G	shear modulus, Pa
G	shear relaxation modulus, Pa
G^*	shear complex modulus, Pa

G'	shear storage modulus, Pa
G''	shear loss modulus, Pa
h	height, m
h_a	asympotic or residual thickness, m
h_o	effective height, m
h_o	initial sample height, m
J	shear creep compliance, Pa^{-1}
J_0	instantaneous compliance, Pa^{-1}
J_1	retarded compliance, Pa^{-1}
J^*	shear complex compliance, Pa^{-1}
J'	shear storage compliance, Pa^{-1}
J''	shear loss compliance, Pa^{-1}
k	falling ball viscometer constant $[2R^2g/(9L)]$, $m^2\ s^{-2}$
k	glass capillary viscometer constant $[gh\pi R^4/(8LV)]$, $m^2\ s^{-2}$
k	thermal conductivity, $W\ m^{-1}\ K^{-1}$
k_f	friction loss coefficient, dimensionless
k'	mixer viscometer constant, rad^{-1}
K	bulk modulus, Pa
K	consistency coefficient, $Pa\ s^n$
K	bulk compression relaxation modulus, Pa
K^*	bulk compression complex modulus, Pa
K'	bulk compression storage modulus, Pa
K''	bulk compression loss modulus, Pa
K_E	extensional consistency coefficient, $Pa\ s^m$
K_T	temperature dependent constant
$K_{T,C}$	temperature and concentration dependent constant
$K_{\dot{\gamma},T,C}$	shear rate, temperature and conc. dependent constant
l	variable length, m
L	length, m
L_o	initial length or length of undeformed sample, m
m	extensional flow behavior index, dimensionless
M	torque, N m

M_o	torque to overcome yield stress, N m
M_e	end effect torque on a bob, N m
n	flow behavior index, dimensionless
$\overline{n}$	average flow behavior index, dimensionless
N_1	first normal stress difference $[\sigma_{11} - \sigma_{22}]$, Pa
N_2	second normal stress difference $[\sigma_{22} - \sigma_{33}]$, Pa
N_{Bo}	Boussinesq number, dimensionless
N_{De}	Deborah number, dimensionless
N_{Fr}	Froude number $[\Omega^2 d/g]$, dimensionless
N_{He}	Hedstrom number $[D^2\sigma_o\rho/(\mu_{pl})^2]$, dimensionless
N_{Po}	power number $[P/(d^5\Omega^3\rho)]$, dimensionless
N_{Re}	Newtonian fluid Reynolds number $[D\overline{u}\rho/\mu]$, dimensionless
$N_{Re,B}$	Bingham fluid Reynolds number $[D\overline{u}\rho/\mu_{pl}]$, dimensionless
$N_{Re,I}$	impeller Reynolds number $[d^2\Omega\rho/\mu]$, dimensionless
$N_{Re,PL}$	Power law fluid Reynolds number, dimensionless
N_{Tr}	Trouton ratio, dimensionless
N_{We}	Weber number $[\rho N^2 d^3/\sigma_{st}]$, dimensionless
N_{Wi}	Weissenberg number $[\Psi_1\Omega/\eta]$, dimensionless
P	power input to a mixer $[M\Omega]$, N m s^{-1}
P	pressure, Pa
P_{atm}	static pressure (absolute) in the undisturbed flow, Pa
P_{ex}	exit pressure (absolute) of a slit viscometer, Pa
P_{ex}	exit pressure of a slit viscometer, Pa
P_{vap}	liquid vapor pressure (absolute), Pa
Q	volumetric flow rate in a pipe, m^3 s^{-1}
Q_m	measured volumetric flow rate, m^3 s^{-1}
Q_{ws}	volumetric flow rate without slip, m^3 s^{-1}
r	radial coordinate, m
R	universal gas constant, 1.987 cal/(g-mole K)
R	radius, m

R_b	bob radius, m
R_b	radius of barrel in converging die, m
R_c	cup radius, m
R_o	radius of undeformed cylinder, m
R_o	initial radius of sample, m
R_o	critical radius, m
R_s	radius of shaft, m
R_T	radius of truncated portion of cone, m
t	time, s
T	temperature, K or °C
T_r	reference temperature, K or °C
u	velocity, m s^{-1}
u^+	turbulent velocity $[u/u^*]$, dimensionless
u^*	friction velocity $[\sqrt{\sigma_w/\rho} = \bar{u}\sqrt{f/2}]$, m s^{-1}
u_1, u_2, u_3	velocity in the x_1, x_2 and x_3 directions, m s^{-1}
u_r, u_z, u_θ	velocity in the r, z and θ directions, m s^{-1}
u_s	effective slip velocity, m s^{-1}
u_t	terminal velocity, m s^{-1}
$\bar{u}$	volumetric average velocity $[Q/(\pi R^2)]$, m s^{-1}
V	volume of mixing vessel, m^3
V	volume of a glass capillary viscometer bulb, m^3
w	width of slit or blade, m
W	work output per unit mass, J kg^{-1}
W	constant force, N
x_1, x_2, x_3	Cartesian coordinates, m
X_E	pipe length required for fully developed flow, m
y	distance from pipe wall into fluid $[R - r]$, m
y^+	distance from the tube wall $[u^*\rho y/\mu]$, dimensionless
z	height above a reference plane, m
z	distance between two points (mixer viscometer), m
z	axial coordinate, m

α	R_c/R_b , dimensionless
α	d/D , dimensionless
α	kinetic energy correction factor, dimensionless
β	effective slip coefficient [u_s/σ_w], m Pa^{-1} s^{-1}
β_c	corrected slip coefficient [βR], m^2 Pa^{-1} s^{-1}
γ	angle of shear, rad
γ	shear strain, dimensionless
γ_o	amplitude of strain function [$\gamma = \gamma_o \sin(\omega t)$], dimensionless
γ_o	constant shear strain, dimensionless
γ_R	strain at the rim of a parallel plate, dimensionless
γ^*	normalized shear strain (γ/γ_o), dimensionless
$\dot{\gamma}$	shear rate, s^{-1}
$\dot{\gamma}_a$	average shear rate, s^{-1}
$\dot{\gamma}_b$	shear rate at the bob, s^{-1}
$\dot{\gamma}_R$	shear rate at the rim of a parallel plate, s^{-1}
$\dot{\gamma}_w$	shear rate at the wall, s^{-1}
Γ	apparent wall shear rate [$4Q/(\pi R^3)$], s^{-1}
δ	phase shift or phase angle, rad
δh	change in height, m
δL	linear displacement, Pa
δP	pressure drop, Pa
δP_{en}	entrance pressure loss, Pa
$\delta P_{en,E}$	entrance pressure loss due to extensional flow, Pa
$\delta P_{en,S}$	entrance pressure loss due to shear flow, Pa
δR	radial displacement, Pa
δt	change in time, s
ε_c	Cauchy strain [$(L - L_o)/L_o$], dimensionless
ε_h	Hencky strain [$\ln(L/L_o)$], dimensionless
$\dot{\varepsilon}_h$	Hencky strain rate, s^{-1}
$\dot{\varepsilon}_{ho}$	constant Hencky strain rate, s^{-1}
$\dot{\varepsilon}_B$	biaxial extensional strain rate, s^{-1}

$\dot{\varepsilon}_{Bo}$	constant biaxial extensional strain rate, s^{-1}
$\dot{\varepsilon}_{E}$	average extensional strain rate in converging flow, s^{-1}
$\dot{\varepsilon}_{E,R}$	average extensional strain rate at the die, s^{-1}
η	apparent viscosity, Pa s
η_B	biaxial extensional viscosity, Pa s
η_B^+	biaxial growth function, Pa s
η_e	equilibrium apparent viscosity, Pa s
η_E	tensile extensional viscosity, Pa s
η_E^+	tensile growth function, Pa s
η_{inh}	inherent viscosity, dl g^{-1}
η_{int}	intrinsic viscosity, dl g^{-1}
η_o	limiting viscosity at zero shear rate, Pa s
η_P	planar extensional viscosity, Pa s
η_r	reference apparent viscosity, Pa s
η_{red}	reduced viscosity, dl g^{-1}
η_{rel}	relative viscosity, dimensionless
η_{sp}	specific viscosity, dimensionless
η_∞	limiting viscosity at infinite shear rate, Pa s
η^*	complex viscosity, Pa s
η'	dynamic viscosity, Pa s
η''	out of phase component of η^*, Pa s
θ	angle, rad
θ	apex angle of cone at bottom of bob, degrees
θ	half angle of converging die, degrees or rad
θ	circumferential coordinate, rad
λ	structural parameter, dimensionless
λ	time constant in Bird-Leider equation, dimensionless
λ_e	equilibrium value of structural parameter, λ, dimensionless
λ_{rel}	relaxation time, s
λ_{ret}	retardation time, s
μ	Newtonian viscosity, Pa s

μ_c	corrected viscosity, Pa s
μ_{pl}	plastic viscosity of a Bingham fluid, Pa s
μ_r	reference Newtonian viscosity, Pa s
ν	kinematic viscosity (μ/ρ), $m^2\ s^{-1}$
ν	Poisson's ratio, dimensionless
ρ	density, kg m^{-3}
ρ_l	liquid density, kg m^{-3}
ρ_s	sphere density, kg m^{-3}
σ	shear stress, Pa
σ_a	average shear stress, Pa
σ_b	shear stress at bob, Pa
σ_B	biaxial (radial) stretching stress, Pa
σ_c	shear stress at cup, Pa
σ_e	shear stress on ends of vane, Pa
σ_e	equilibrium shear stress, Pa
σ_E	tensile stretching stress, Pa
σ_{Eo}	constant tensile stretching stress, Pa
σ_{ij}	stress on plane perpendicular to i in the direction of j, Pa
σ_o	yield stress, Pa
σ_o	initial shear stress, Pa
σ_o	constant shear stress, Pa
σ_o	amplitude of the stress function [$\sigma = \sigma_o \sin(\omega t - \delta)$], Pa
σ_R	shear stress at the rim of a parallel plate, Pa
σ_{st}	surface tension, N m^{-1}
σ_w	shear stress at the wall of tube or slit, Pa
σ^*	normalized shear stress (σ/σ_o), dimensionless
σ_{21}^+	shear stress growth function, Pa
Φ	die exit effect integral, dimensionless
Ψ	sweep angle, rad
Ψ_1	first normal stress coefficient, Pa s^2
Ψ_2	second normal stress coefficient, Pa s^2

ω	angular velocity at r, rad s^{-1}
Ω	angular velocity [2π(rpm)/60], rad s^{-1}

Bibliography

Aguilar, C., S.S.H. Rizva, J.F. Ramirez and A. Inda. 1991. Rheological behavior of processed mustard. I: effect of milling treatment. J. Texture Stud. 22: 59-84.

Ak, M.M. and S. Gunasekaran. 1995. Measuring elongational properties of Mozzarella cheese. J. Texture Stud. 26: 147-160.

Altomare, R.E., M. Anelich and R. Rakos. 1992. An experimental investigation of the rheology of rice flour dough with an extruder-coupled slit die rheometer. In: Kokini, J.L., C-T. Ho and M.V. Karwe (editors). Food Extrusion Science and Technology. Marcel Dekker, Inc., New York. pg. 233-254.

Bagley, E.B. 1957. End corrections in the capillary flow of polyethylene. J. Appl. Phys. 28: 624-627.

Bagley, E.B. and D.D. Christianson. 1986. Response of chemically leavened dough to uniaxial compression. In: Faridi, H. and J.M. Faubion (editors). Fundamentals of Dough Rheology. Amer. Assoc. of Cereal Chemists, St. Paul, MN.

Bagley, E.B. and D.D. Christianson. 1988. Behavior of foods in large deformations. In: Blanshard, J.M.V. and J.R. Mitchel (editors). Food Structure - Its Creation and Evaluation. Butterworths, London. pg 401-416.

Bagley, E.B., D.D. Christianson and W.J. Wolf. 1985. Frictional effects in compressional deformation of gelatin and starch gels and comparison of material response in simple shear, torsion, and lubricated compression. J. Rheol. 29: 103-108.

Balaban, M., A.R. Carrillo and J.L. Kokini. 1988. A computerized method to analyze the creep behavior of viscoelastic foods. J. Texture Stud. 19: 171-183.

Banerjee, T.K., D. Manas and S.K. Das. 1994. Non-Newtonian liquid flow through globe and gate valves. Can. J. Chem. Engn. 72: 207-211.

Barbosa Canovas, G.V. and M. Peleg. 1983. Flow parameters of selected commercial semi-liquid food products. J. Texture Stud. 14: 213-234.

Barnes, H.A. 1992. 'The yield stress myth?' revisited. In: Moldenaers, P. and R. Keunings (editors). Theoretical and Applied Rheology, Volume 2. Proc. XIth Int. Congr. on Rheology, Brussels, Belgium, Aug. 17-21, 1992. Elsevier Science Publishers, New York. pg. 576-578.

Barnes, H.A., J.F. Hutton and K. Walters. 1989. An Introduction to Rheology. Elsevier Science Publishing Company Inc., New York.

Barnes, H.A. and K. Walters. 1985. The yield stress myth. Rheol. Acta 24: 323-326.

Bersted, B.H. 1993. Refinement of the converging flow method of measuring extensional viscosity in polymers. Polymer Engn. Sci. 33(16): 1079-1083.

Bhattacharya, M. 1993. Slit rheometer studies of wheat flour dough. J. Texture Stud. 24:391-409.

Bhattacharya, M., and M. Padmanabhan. 1992. On-line rheological measurements of food dough during extrusion cooking. In: Kokini, J.L., C-T. Ho and M.V. Karwe (editors). Food Extrusion Science and Technology. Marcel Dekker, Inc., New York. pg. 213-232.

Bhattacharya, M., M. Padmanabhan and K. Seethamraju. 1994. Uniaxial extensional viscosity during extrusion cooking from entrance pressure drop method. J. Food Sci. 59: 221-226, 230.

Binding, D.M. 1988. A approximate analysis for contraction and converging flows. J. Non-Newtonian Fluid Mech. 27: 173-189.

Bird, R.B., R.C. Armstrong and O. Hassager. 1987. Dynamics of Polymeric Liquids, Volume 1. John Wiley and Sons, New York.

Bird, R.B., W.E. Stewart and E.N. Lightfoot. 1960. Transport Phenomena. John Wiley and Sons, Inc., New York.

Bistany, K.L. and J.L. Kokini. 1983. Comparison of steady shear rheological properties and small amplitude dynamic viscoelastic properties of fluid food materials. J. Texture Stud. 14: 113-124.

Block, H. and J.P. Kelly. 1986. Electro-rheology. J. Phys. D: Appl. Phys. 21: 1661-1677.

Boger, D.V. 1982. Circular entry flows of inelastic and viscoelastic fluids. In: Mujumdar, A.S. and R.A. Mashelkar (editors). Advances in Transport Processes, Vol. II. Halsted Press. John Wiley and Sons, New York. pg. 43-104.

Boger, D.V. and K. Walters. 1993. Rheological Phenomena in Focus. Elsevier Science Publishers, New York.

Bogue, D.C. and J.L. White. 1970. Engineering Analysis of Non-Newtonian Fluids. AGARDograph No. 144. North Atlantic Treaty Organization. Advisor Group for Aerospace Research & Development. Etat Major Forces Aériennes, Caserne Prince Baudouin, Place Dailly, Bruxelles, 3, Belgium.

Bourne, M.C. 1968. Texture profile of ripening pears. J. Food Sci. 33: 223-226.

Bourne, M.C. 1974. Texture changes in ripening peaches. J. Can Inst. Food Sci. Technol. 7: 11-15.

Bourne, M.C. 1978. Texture profile analysis. Food Technol. 32(7): 62-66, 72.

Bourne, M.C. 1982. Food Texture and Viscosity: Concept and Measurement. Academic Press, New York.

Bourne, M.C., J.F. Kenny and J. Barnard. 1978. Computer-assisted readout of data from texture profile analysis curves. J. Texture Studies 9: 481-494.

Bowen, R.L. 1986. Unraveling the mysteries of shear-sensitive mixing systems. Chem. Engn. June 9: 55-63.

Brennan, J.G. 1980. Food texture measurement. In: King, R.D. (editor). Developments in Food Analysis Techniques - 2. Applied Sci. Pub. Ltd., London. pg. 1-78.

Briggs, J.L. 1995. Methods to Characterize Power Fluids Using a Brookfield Viscometer. MS Thesis. Dept. of Agricultural Engineering. Michigan State University.

Briggs, J.L. and J.F. Steffe. 1995. Kinetic energy correction factor of a Herschel-Bulkley fluid. J. Food Proc. Engn. 18: 115-118.

Briggs, J.L. and J.F. Steffe. 1996. Vane method to evaluate the yield stress of frozen ice cream. J. Dairy Sci. 79: 527-531.

Butler, F. and P. McNulty. 1995. Time-dependent rheological characterization of buttermilk at 5°C. J. Food Proc. Engn. 25: 569-580.

Brodkey, R.S. and H.C. Hershey. 1988. Transport Phenomena. McGraw-Hill Book Company. New York.

Callister, W.D. 1991. Material Science and Engineering (Second Edition). John Wiley & Sons, Inc., New York.

Campanella, O.H. and M. Peleg. 1987a. Determination of the yield stress of semi-liquid foods from squeezing flow data. J. Food Sci. 52: 214-217.

Campanella, O.H. and M. Peleg. 1987b. Analysis of transient flow of mayonnaise in a coaxial cylinder viscometer. J. Rheol. 31: 439-452.

Campanella, O.H. and M. Peleg. 1987c. Squeezing flow viscosimetry of peanut butter. J. Food Sci. 52: 180-184.

Campanella, O.H., L.M. Popplewell, J.R. Rosenau and M. Peleg. 1987. Elongational viscosity measurements of melting American process cheese. J. Food Sci. 52: 1249-1251.

Campos, D.T., J.F. Steffe and R.Y. Ofoli. 1994. Statistical method to evaluate the critical Reynolds number for pseudoplastic fluids in tubes. J. Food Engn. 23: 21-32.

Carreau, P.J. 1968. Ph.D. Dissertation. Dept. of Chemical Engineering, University of Wisconsin, Madison.

Casiraghi, E.M., E.B. Bagley and D.D. Christianson. 1985. Behavior of Mozzarella, Cheddar and process cheese spread in lubricated and bonded uniaxial compression. J. Texture Stud. 16: 281-301.

Casson, N. 1959. A flow equation for pigmented-oil suspension of the printing ink type. In: Mill, C.C. (editor). Rheology of Dispersed Systems. Pergamon Press, New York. pg. 84-104.

Castaldo, D., L. Palmieri, A. Lo Voi and P. Costabile. 1990. Flow properties of Babaco (Carica Pentagona) purees and concentrates. J. Texture Stud. 21: 253-264.

Castell-Perez, M.E., R.G. Moreira and J.F. Steffe. 1993. Método simplificado para caracterizar fluidos que siguen la ley de potencia con un viscosímetro de mezcla tipo bandera. Revista Española de Ciencia y Tecnología de Alimentos 33: 529-547.

Castell-Perez, M.E. and J.F. Steffe. 1990. Evaluating shear rates for power law fluids in mixer viscometry. J. Texture Stud. 21: 439-453.

Castell-Perez, E.M. and J.F. Steffe. 1992. Using mixing to evaluate rheological properties. In: Rao, A.M. and J.F. Steffe (editors). Viscoelastic Properties of Food. Elsevier Applied Sci. Pub., Ltd., Barking, England. pg. 247-284.

Castell-Perez, M.E., J.F. Steffe and R.G. Moreira. 1991. Simple determination of power law flow curves using a paddle type mixer viscometer. J. Texture Stud. 22: 303-316.

Cavella, S., S. Chemin and P. Masi. 1992. Objective measurement of the stretchability of Mozzarella cheese. J. Texture Stud. 23: 185-194.

Charm, S.E. 1962. Determination of shear stress shear rate behavior in foods in the presence of a yield stress. J. Food Sci. 28: 107-113.

Chatraei, SH., C.W. Macosko. 1981. Lubricated squeezing flow: a new biaxial extensional rheometer. J. Rheol. 25: 433-443.

Cheng, D.C-H. 1970. A design procedure for pipeline flow of non-Newtonian dispersed systems. Proceedings of the First International Conference in the Hydraulic Transport of Solids in Pipes (Hydrotransport I), Sept. 1-4. British Hydromechanics Research Association, Cranfield, Bedford, England. pg. J5-77 to J5-95.

Cheng, D.C-H. 1973. A differential form of constitutive relation for thixotropy. Rheol. Acta 12: 228-233.

Cheng, D.C-H. 1986. Yield stress: a time-dependent property and how to measure it. Rheol. Acta 25: 542-554.

Cheng, D.C-H. and B.R. Parker. 1976. The determination of wall-slip velocity in the coaxial cylinder viscometer. Proceedings of the Seventh International Congress on Rheology. Gotenberg, Sweden. pg. 518-519.

Chhabra, R.P. 1992. Bubbles, Drops and Particles in Non-Newtonian Fluids. CRC Press, Boca Raton, FL.

Christensen, C.M. 1987. Perception of solution viscosity. In: Moskowitz, H.R. (editor). Food Texture. Marcel Dekker, New York.

Christianson, D.D., Casiraghi, E.M. and E.B. Bagley. 1985. Uniaxial compression of bonded and lubricated gels. J. Rheol. 29: 671-684.

Chuma, Y., T. Shiga and M. Iwamoto. 1978. Mechanical properties of Satsuma orange as related to the design of a container for bulk shipment. J. Texture Stud. 9: 461-479.

Churchill, S.W. 1988. Viscous Flows: The Practical Use of Theory. Butterworths, Boston.

Clapp, R.M. 1961. Turbulent heat transfer in pseudoplastic non-Newtonian fluids. International Development in Heat transfer. ASME, Part III, Sec. A., pg. 652-661.

Cogswell, F.N. 1972. Converging flow of polymer melts in extrusion dies. Poly. Engn. and Sci. 12(1): 64-73.

Cogswell, F.N. 1978. Converging flow and stretching flow: a compilation. J. Non-Newtonian Fluid Mech. 4: 23-38.

Cogswell, F.N. 1981. Polymer Melt Rheology. Halsted Press, New York.

Collins, M. and W.R. Schowalter. 1963. Behavior of non-Newtonian fluids in the entry region of a pipe. AIChE J. 9: 804-809.

Covey, G.H. and B.R. Stanmore. 1981. Use of the parallel plate plastometer for the characterization of viscous fluids with a yield stress. J. Non-Newtonian Fluid Mech. 8: 249-260.

Cox, W.P. and E.H. Merz. 1958. Correlation of dynamic and steady flow viscosities. J. Polymer Sci. 28: 619-622.

Crane Co. 1982. Flow of fluids through valves, fittings and pipe. Technical Paper No. 410M, twenty-first printing. Crane Co. 300 Park Ave., New York.

Cristescu, N. 1989. Rock Rheology. Kluwer Academic Pub., Boston.

Cross, M.M. 1965. Rheology of non-Newtonian flow: equation for pseudoplastic systems. J. Colloid Sci. 20: 417-437.

Cuvelier, G., C. Peigney-Noury and B. Lunay. 1990. Viscoelastic properties of physical gels: critical behavior at the gel point. In: Phillips, G.O., P.A. Williams and D.J. Wedlock (editors). Gums and Stabilizers for the Food Industry 5, IRL Press, New York.

Dail, R.V. and J.F. Steffe. 1990a. Rheological characterization of crosslinked waxy maize starch solutions under low acid aseptic processing conditions using tube viscometry techniques. J. Food Sci. 53: 1660-1665.

Dail, R.V. and J.F. Steffe. 1990b. Dilatancy in starch solutions under low acid aseptic processing conditions. J. Food Sci. 53: 1764-1765.

Dally, J.W. and W.F. Riley. 1965. Experimental Stress Analysis. McGraw-Hill Book Company, New York.

D'Appolonia, B.L. and W.H. Kunerth (editors). 1984. The Farinograph Handbook, Third Edition. The American Association of Cereal Chemists, St. Paul, MN.

Darby, R. 1976. Viscoelastic Fluids: An Introduction to Properties and Behavior. Marcel Dekker, New York.

Darby, R. 1985. Couette viscometer data reduction for materials with a yield stress. J. Rheol. 29: 369-378.

da Silva, J.A.L., M.P. Gonçalves and M.A. Rao. 1994. Influence of temperature on the dynamic and steady-shear rheology of pectin dispersions. Carbohydrate Polymers 23: 77-87.

da Silva, J.A.L. and M.A. Rao. 1992. Viscoelastic properties of food hydrocolloid dispersions. In: Rao, A.M. and J.F. Steffe (editors). Viscoelastic Properties of Food. Elsevier Applied Sci. Pub., Ltd., Barking, England. pg. 247-284.

Daubert, C.R. and J.F. Steffe. 1995. Electrorheology of milk chocolate. J. Texture Stud. 27: 93-108.

Dealy, J.M. 1982. Rheometers for Molten Plastics. Van Nostrand Reinhold Company. New York.

Dealy, J.M. 1994. Official nomenclature for material functions describing the response to a viscoelastic fluid to various shearing and extensional deformations. J. Rheol. 38: 179-191.

Dealy, J.D. and A.J. Giacomin. 1988. Sliding plate and sliding cylinder rheometers. In: Collyer, A.A. and D.W. Clegg (editors). Rheological Measurements. Elsevier Applied Science, New York. pg. 383-404.

Dealy, J.M. and K.F. Wissburn. 1990. Melt Rheology and its Role in Plastics Processing. Van Nostrand Reinhold, New York.

de Bruijne, D.W., J. de Looff and A. van Eulem. 1990. The rheological properties of bread dough and their relation to baking. In: Carter, R.E. (editor). Rheology of Food, Pharmaceutical and Biological Materials with General Rheology. Elsevier Applied Science, New York.

De Kee, D., G. Turcotte and K. Fildey. 1980. New method for the determination of yield stress. J. Texture Stud. 10: 281-288.

Denn, M.M. 1980. Process Fluid Mechanics. Prentice-Hall, Inc., Englewood Cliffs, NJ.

Dervisoglu, M. and J.L. Kokini. 1986. Steady shear rheology and fluid mechanics of four semi-solid foods. J. Food Sci. 51: 541-545, 625.

Dickie, A.M. and J.L. Kokini. 1982. Use of the Bird-Leider equation in food rheology. J. Food Proc. Engn. 5: 157-174.

Dickie, A.M. and J.L Kokini. 1983. An improved model for food thickness from non-Newtonian fluid mechanics in the mouth. J. Food Sci. 48: 57-61, 65.

Dienes, G.J. and H.F. Klemm. 1946. Theory and application of parallel plate plastometer. J. Appl. Phys. 17: 458-471.

Dintenfass, L. 1985. Blood Viscosity, Hyperviscosity & Hyperviscosaemia. MTP Press Limited. Boston, MA.

Dodge, D.W. and A.B. Metzner. 1959. Turbulent flow of non-Newtonian systems. AIChE J. 5: 189-204.

Dolan, K.D. and J.F. Steffe. 1990. Modeling the rheological behavior of gelatinizing starch solutions using mixer viscometry data. J. Texture Stud. 21: 265-294.

Dolan, K.D., J.F. Steffe and R.G. Morgan. 1989. Back extrusion and simulation of viscosity development during starch gelatinization. J. Food Proc. Engn. 11: 79-101.

Doraiswamy, D., A.N. Mujumdar, I. Tsao, A.N. Beris, S.C. Danforth and A.B. Metzner. 1991. The Cox-Mertz rule extended: A rheological model for concentrated suspensions and other materials with a yield stress. J. Rheol. 35: 647-685.

Drake, B. 1987. Food psychorheology. In: Moskowitz, H.R. (editor). Food Texture. Marcel Dekker, New York.

Durgueil, E.J. 1987. Determination of the consistency of non-Newtonian fluids using a Brookfield HBT viscometer. Proc. South African Sugar Technol. Assoc., June: 32-39.

Edwards, D.A., H. Brenner and D.T. Wasan. 1991. Interfacial Transport Processes and Rheology. Butterworth-Heinemam, Stonheam, MA.

Elliott, J.H. and A.J. Ganz. 1971. Modification of food characteristics with cellulose hydrocolloids, I. Rheological characterization of an organoleptic property. J. Text. Stud. 2: 220-229.

Elliott, J.H. and A.J. Ganz. 1977. Salad Dressings - preliminary rheological characterization. J. Text. Stud. 8: 359-371.

Ellis, S.B. 1927. Thesis, Lafayette College, Pa. Cited in: Whorlow, R.W. 1980. Rheological Techniques. Halsted Press (Div. of John Wiley & Sons), New York.

Erickson, E.R., R.A. Berntsen and M.A. Eliason. 1966. Viscosity of corn syrup. J. of Chem. and Engn. Data 11: 485-488.

Faridi, H. and V.F. Rasper. 1987. The Alveograph Handbook. Amer. Assoc. of Cereal Chemists. St. Paul, MN.

Ferguson, J. and Z. Kemblowski. 1991. Applied Fluid Rheology. Elsevier Applied Science, New York.

Ferry, J.D. 1977. Oscillation viscometry - effects of shear rate and frequency. Measurement & Control, September - October: 89-91.

Ferry, J.D. 1980. Viscoelastic Properties of Polymers (Third Edition). John Wiley and Sons, New York.

Ford, E.W. and J.F. Steffe. 1986. Quantifying thixotropy in starch-thickened, strained apricots using mixer viscometry techniques. J. Texture Stud. 17: 75-85.

Friedman, H.H., J.E. Whitney and A.S. Szczesnaik. 1963. The Texturometer - a new instrument for texture measurement. J. Food Sci. 28: 390-396.

Fuller, G.G., C.A. Cathey, B. Hubbard and B.E. Zebrowski. 1987. Extensional viscosity measurement for low-viscosity fluids. J. Rheol. 31: 235-249.

Garcia, E.J. and J.F. Steffe. 1986. Optimum economic pipe diameter for pumping Herschel-Bulkley fluids in laminar flow. J. Food Proc. Engn. 8: 117-136.

Garcia, E.J. and J.F. Steffe. 1987. Comparison of friction factor equations for non-Newtonian fluids in tube flow. J. Food Proc. Engn. 9: 93-120.

Gibson, A.G. 1988. Converging dies. In: Collyer, A.A. and D.W. Clegg (editors). Rheological Measurements. Elsevier Applied Science, New York. pg. 49-92.

Giesekus, H. and G. Langer. 1977. Die Bestimmung der wahren Fließkurven nicht-newtonscher Flüssigkeiten und plastischer Stoffe mit der Methode der repräsentativen Viskosität. Rheol. Acta 16: 1-22.

Gogos, C.G. and S. Bhakuni. 1992. An on-line slit rheometer for measurement of the rheological properties of doughs. In: Kokini, J.L., C-T. Ho and M.V. Karwe (editors). Food Extrusion Science and Technology. Marcel Dekker, Inc., New York. pg. 255-262.

Goodrich, K., A. Yoshimura and R.K. Prud'homme. 1989. Measurement of the modulus and yield strength of soft gels: experiments and numerical simulation. J. Rheol. 33: 317-327.

Griskey, R.G. and R.G. Green. 1971. Flow of dilatant (shear-thickening) fluids. AIChE J. 17: 725-728.

Grovier, G.W. and K. Aziz. 1972. The Flow of Complex Mixtures in Pipes. R.E. Krieger Publishing Co., Malabar, Florida.

Grulke, E.A. 1994. Polymer Process Engineering. PTR Prentice Hall, Englewood Cliffs, NJ.

Gupta, B.P. 1984. Dimensional analysis. In: Hill, H.E. and J.W. Prane (editors). Applied Statistical Techniques for Selected Industries. John Wiley and Sons, New York. pg. 551-581.

Gupta, R.K. and T. Sridhar. 1988. Elongational rheometers. In: Collyer, A.A. and D.W. Clegg (editors). Rheological Measurements. Elsevier Applied Science, New York. pg. 211-246.

Haghighi, K., A.K. Srivastava and J.F. Steffe. 1987. The rheological approach to soil modeling. Trans. ASAE 30: 1661-1672.

Haighton, A.J. 1959. The measurement of hardness of margarine and fats with cone penetrometers. J. Amer. Oil Chem. Soc. 36: 345-348.

Halim, H.K. and C.F. Shoemaker. 1990. Effect of addition of α-, β-, and κ-casein, and Na-caseinate on viscoelastic properties of skim milk curd. J. Texture Stud. 21: 323-337.

Halliday, P.J. and A.C. Smith. 1995. Estimation of the wall slip velocity in the capillary flow of potato granule pastes. J. Rheol. 39: 139-149.

Halmos, A.L. and C. Tiu. 1981. Liquid foodstuffs exhibiting yield stress and shear-degradability. J. Texture Stud. 12: 39-46.

Hamann, D.D. 1983. Structural failure in solid foods. In: Peleg, M. and E.B. Bagley (editors). Physical Properties of Foods. AVI Publishing Co., Westport, CT. pg. 351-384.

Hamann, D.D. and T.C. Lanier. 1987. Instrumental methods for predicting seafood sensory texture quality. In: Kramer, D.E. and J. Liston (editors). Seafood Quality Determination. Elsevier Applied Sci. Publishers, Barking, Essex, England. pg. 123-136.

Han, C.D. 1988. Slit rheometry. In: Collyer, A.A. and D.W. Clegg (editors). Rheological Measurements. Elsevier Applied Science, New York. pg. 25-48.

Hanks, R.W. 1963. Laminar-turbulent transition of fluids with a yield stress. AIChE J. 9: 306-309.

Harnby, N., M.F. Edwards and A.W. Nienow (editors). 1985. Mixing in the Process Industries. Butterworth, Boston.

Harper, J.C. and A.F. El Sahrigi. 1965. Viscometric behavior of tomato concentrates. J. Food Sci. 30: 470-476.

Hartnett, J.P. and R.Y.Z. Hu. 1989. The yield stress-an engineering reality. J. Rheol. 33: 671-679.

Hayashi, N., I. Hayakawa and Y. Fujio. 1991. Entrance effect correction on the flow of moisturized soy protein isolate melt in an extrusion rheometer. Int. J. Food Sci. Technol. 26: 567-574.

Heywood, N. 1991a. Pipeline design for non-settling slurries. In: Brown, N.P. and N.I. Heywood (editors). Slurry Handling: Design of Solid Liquid Systems. Elsevier Applied Science, New York. pg. 125-165.

Heywood, N.I. 1991b. Rheological characterization of non-settling slurries. In: Brown, N.P. and N.I. Heywood (editors). Slurry Handling: Design of Solid-Liquid Systems. Elsevier Applied Science, New York.

Hill, M.A. 1991. Dynamic rheology: application to the formulation of a real food product. Food Sci. Technol. Today 5(1): 29-31.

Hill, M.A., J.R. Mitchel and P.A. Sherman. 1995. The relationship between the rheological and sensory properties of lemon pie filling. J. Texture Stud. 26: 457-470.

Holdsworth, S.D. 1993. Rheological models used for the prediction of the flow properties of food products: a literature review. Trans. I. Chem. E. 71 (Part C): 139-179.

Holland, D. 1994. Letter to the editor: which is more critical - the stress or the strain. J. Rheol. 38: 1941-1943.

Holland, F.A. and F.S. Chapman. 1966. Liquid Mixing and Processing in Stirred Tanks. Reinholt Publishing Corp., New York.

Houska, M., J. Sesrák, J. Jeschke, M. Adam and J. Pridal. 1988. In: H. Giesekus (editor). Progress and Trends in Rheology II. Proceedings of the Second Conference of European Rheologists, Prague, June 17-20, 1986. Springer-Verlag, New York. pg 460-463.

Huang, H. and J.L. Kokini. 1993. Measurement of biaxial extensional viscosity of wheat flour doughs. J. Rheol. 37: 879-891.

James, A.E., D.J.A. Williams and P.R. Williams. 1987. Direct measurement of static yield properties of cohesive suspensions. Rheol. Acta 26: 437-446.

James, D.F. and K. Walters. 1993. A critical appraisal of available methods for the measurement of extensional properties of mobile systems. In: Collyer, A.A. (editor). Techniques in Rheological Measurement. Chapman & Hall, New York.

Jastrzebski, Z.D. 1967. Entrance effects and wall effects in an extrusion rheometer during the flow of concentrated suspensions. Ind. Engn. Chem. Fund. 6: 445-454.

Jones, D.M., K. Walters and P.R. Williams. 1987. On the extensional viscosity of mobile polymer systems. Rheol. Acta 26: 20-30.

Kaletunc-Gencer, G. and M. Peleg. 1984. Digitizer aided determination of yield stress in semi-liquid foods. J. Food Sci. 49: 1620-1621.

Kawanari, M., D.D. Hamann, K.R. Swartzel and A.P. Hansen. 1981. Rheological and texture studies of butter. J. Texture Stud. 12: 483-505.

Kawata, M.K. Kurase, A. Nagashima and K.Yoshida. 1991. Capillary viscometers. In: Wakeham, W.A., A. Nagashima and J.V. Sengers (editors). Measurement of the Transport Properties of Liquids, Vol. III. Blackwell Scientific, London.

Keentok, H. 1982. The measurement of yield stress of liquids. Rheol. Acta 21: 325-332.

Kiljanski, T. 1989. A method for the correction of wall-slip effect in a Couette rheometer. Rheol. Acta 28: 61-64.

Kittredge, C.P. and D.S. Rowley. 1957. Resistance coefficients for laminar and turbulent flow through one-half inch valves and fittings. Trans. ASME 79: 1759-1766.

Kokini, J.L. 1992. Rheological properties of food. In: Heldman, D.R. and D.B. Lund (editors). Handbook of Food Engineering. Marcel Dekker, New York. pg. 1-38.

Kokini, J.L. and E.L. Cussler. 1987. The psychophysics of fluid texture. In: Moskowitz, H.R. (editor). Food Texture. Marcel Dekker, New York.

Kokini, J.L. and A. Dickie. 1981. An attempt to identify and model transient viscoelastic flow in foods. J. Texture Stud. 12: 539-557.

Kokini, J.L. and G.L. Plutchok. 1987. Viscoelastic properties of semisolid foods and their biopolymeric components. Food Technol. 41: 89-95.

Koutsakos, E. and A.W. Nienow. 1990. Effects of rheological properties of simulated fermentation broths on flow in stirred bioreactors: a laser

anemometry study. In: R.E. Carter (editor). Rheology of Food, Pharmaceutical and Biological Materials with General Rheology. Elsevier Applied Science, New York. pg. 284-303.

Kraynik, A.M., J.H. Aubert, R.N. Chapman and D.C. Gyure. 1984. The helical screw rheometer: a new concept in rotational rheometry. Proc. Ann. Tech. Conf. Soc. Plastics Engrs. pg. 405-408.

Krieger, I.M. 1968. Shear rate in couette viscometer. Trans. Soc. Rheol. 12: 5-11.

Krieger, I.M. and H. Elrod. 1953. Direct determination of the flow curves of non-Newtonian Fluids. II. Shear rate in the concentric cylinder viscometer. J. Appl. Physics. 24: 134-136.

Krieger, I.M. and S.H. Maron. 1952. Direct determination of the flow curves of non-Newtonian fluids. J. Appl. Physics 23: 147-149.

Krieger, I.M. and S.H. Maron. 1954. Direct determination of the flow curves of non-Newtonian Fluids. III. Standardized treatment of viscometric data. J. Appl. Physics. 25: 72-75.

Laba, D. 1993a. Rheological profiles. In: Laba, D. (editor). 1993. Rheological Properties of Cosmetics and Toiletries. Marcel Dekker, Inc. New York. pg. 403-420

Laba, D. (editor). 1993b. Rheological Properties of Cosmetics and Toiletries. Marcel Dekker, Inc. New York.

Lang, E.R. and C. Rha. 1981. Determination of yield stresses of hydrocolloid dispersions. J. Texture Stud. 12: 47-62.

Langhaar, H.L. 1980. Dimensional Analysis and Theory of Models. Robert E. Krieger Publishing Company, Huntington, New York.

Larson, R.G. 1985. Constitutive relationships for polymeric materials with power-law of relaxation times. Rheol. Acta 24: 327-334.

Larson, R.G. 1992. Instabilities in viscoelastic flows. Rheol. Acta 31: 213-263.

Launay, B. and J. Buré. 1977. Use of the Chopin Alveographe as a rheological tool. II. Dough properties in biaxial extension. Cereal Chem. 54: 1152-1158.

Leider, P.L. and R.B. Bird. 1974. Squeezing flow between parallel plates. I. Theoretical analysis. Ind. Engn. Chem. Fundam. 13: 336-341.

Leighton, A., A. Leviton and O.E. Williams. 1934. The apparent viscosity of ice cream. J. Dairy Sci. 17: 639-650.

Lewicki, P.P. and K. Skierkowski. 1988. Flow of fruit and vegetable purees through pipelines. In: H. Giesekus (editor). Progress and Trends in Rheology II. Proceedings of the Second Conference of European Rheologists, Prague, June 17-20, 1986. Springer-Verlag, New York. pg 443-445.

Lewis, M.J. 1987. Physical Properties of Foods and Food Processing Systems. Ellis Horwood. Chichester, England.

Lodge, A.S. 1988. Normal stress differences from hole pressure measurements. In: Collyer, A.A. and D.W. Clegg (editors). Rheological Measurements. Elsevier Applied Science, New York. pg. 345-382.

Lord, D.L., B.W. Hulsey and L.L. Melton. 1967. General turbulent pipe flow scale-up correlation for rheologically complex fluids. Soc. Petrol. Engrs. J. 7: 252-258.

Mackey, K.L., R.Y. Ofoli, R.G. Morgan and J.F. Steffe. 1989. Rheological modeling of potato flour during extrusion cooking. J. Food Proc. Engn. 12: 1-11.

Macosko, C. W. 1994. Rheology: Principles, Measurements and Applications. VCH Publishers. New York.

Matz, S.A. 1962. Food Texture. AVI Publishing Co., Inc., Westport, Connecticut.

McCarthy, K.L. and J.D. Seymour. 1994. Gravity current analysis of the Bostwick Consistometer for power law fluids. J. Text. Stud. 25: 207-220.

Meissner, J. 1972. Development of a universal extensional rheometer for the uniaxial extension of polymer melts. Trans. Soc. Rheol. 16: 405-420.

Menjivar, J.A., C.N. Chang and L. Maceil. 1992. Extrudate swell behavior of wheat flour doughs. In: P. Moldenaers and R. Keunings (editors). Theoretical and Applied Rheology, Volume 2. Proceedings of the XIth International Congress on Rheology. Brussels, Belgium, Aug. 17-21, 1992. Elsevier Science Publishers, New York. pg. 714-716.

Menjivar, J.A. and H. Faridi. 1994. Rheological properties of cookie and cracker doughs. In: Faridi, H. (editor). The Science of Cookie and Cracker Production. Chapman & Hall, New York. pg. 283-322.

Metzner, A.B. 1956. Non-Newtonian technology: fluid mechanics, mixing, heat transfer. In: Drew, T.B. and J.W. Hoopes (editors). Advances in Chemical Engineering, Vol. 1. Academic Press, Inc., New York. pg. 77-153.

Metzner, A.B. 1961. Flow of non-Newtonian fluids. In: Handbook of Fluid Dynamics, Section 7, McGraw-Hill Book Co., Inc. pg. 7-1 to 7-30.

Metzner, A.B. and A.P. Metzner. 1970. Stress levels in rapid extensional flows of polymeric fluids. Rheol. Acta 9: 174-181.

Mewis, J. 1979. Thixotropy - a general review. J. Non-Newtonian Fluid Mech. 6: 1-20.

Michiyosi, L., K. Mizuno and Y. Hoshiai. 1966. Studies on the flow of slurries through pipe. I. Entrance Region of laminar flow. Int. Chem. Engn. 6: 373-381

Middleman, S. 1968. The Flow of High Polymers. Interscience Publishers, New York.

Middleman, S. 1977. Fundamentals of Polymer Processing. McGraw-Hill Book Co., New York.

Missaire, F., C-G. Qiu and M.A. Rao. 1990. Yield stress of structured and unstructured food suspensions. J. Texture Stud. 21: 479-490.

Mitschka, P. 1982. Simple conversion of Brookfield R.V.T. readings into viscosity functions. Rheol. Acta 21: 207-209.

Mizrahi, S. and Z. Berk. 1972. Flow behavior of concentrated orange juice: mathematical treatment. J. Texture Stud. 3: 69-79.

Mohsenin, H. 1986. Physical Properties of Plant and Animal Materials, Vol. 1 (Second Edition). Gordon and Breach Science Publishers, New York.

Montejano, J.G., D.D. Hamann and T.C. Lanier. 1985. Comparison of two instrumental methods with sensory texture of protein gels. J. Texture Stud. 16: 403-424.

Mooney, M. 1931. Explicit formulas for slip and fluidity. J. Rheol. 30: 337-357.

Morgan, R.G. 1979. Modeling the effects of temperature-time history, temperature, shear rate and moisture on the viscosity of defatted soy flour. Ph.D. Dissertation. Texas A&M University, College Station, TX.

Morgan, R.G., J.F. Steffe and R.Y. Ofoli. 1989. A generalized rheological model for extrusion of protein doughs. J. Food Proc. Engn. 11: 55-78.

Morton-Jones, D.H. 1989. Polymer Processing. Chapman and Hall. New York.

Muñoz, A.M., A.S. Szczesnaik, M.A. Einstein and N.O. Schwartz, 1992. The texture profile. In: Hootman, R.C. (editor). Manual on Descriptive Analysis Testing for Sensory Evaluation. ASTM Manual Series: MNL 13. Amer. Soc. for Testing and Materials, 1916 Race Street, Philadelphia, PA.

Murata, T. and S. Oka. 1968. Determination of parameters of a material obeying Casson's equation by some rheometers. Biorheology 5: 95-102.

Murphy, C.E. 1950. Similitude in Engineering. The Ronald Press Company, New York.

Nagata, S. 1975. Mixing: Principles and Applications. John Wiley and Sons, New York.

Nagata, S., N. Masabuma, T. Hisayuki, H. Hirabayashi and S. Gotoh. 1970. Power consumption of mixing impellers in Bingham plastic liquids. J. Chem. Engn. of Japan 3: 237-243.

Nakayama, T., E. Niwa and I. Hamada. 1980. Pipe transportation of minced fish paste. J. Food Sci. 45: 844-847.

Navickis, L.L. and E.B. Bagley. 1983. Yield stresses in concentrated dispersions of closely packed, deformable gel particles. J. Rheol. 27: 519-536.

Nielsen, L.E. and R.F. Landel. 1994. Mechanical Properties of Polymers and Composites (Second Edition). Marcel Dekker, Inc. New York.

Nguyen, Q.D. and D.V. Boger. 1985. Direct yield stress measurement with the vane method. J. Rheol. 29: 335-347.

Nguyen, Q.D. and D.V. Boger. 1987. Characterization of yield stress with concentric cylinder viscometers. Rheol. Acta 26: 508-515.

Nolan, E.J., V.H. Holsinger and J.J. Shieh. 1989. Dynamic rheological properties of natural and imitation mozzarella cheese. J. Texture Stud. 20: 179-189.

Ofoli, R.Y., R.G. Morgan and J.F. Steffe. 1987. A generalized rheological model for inelastic fluid foods. J. Texture Stud. 18: 213-230.

Ofoli, R.Y. and J.F. Steffe. 1992. Some observations on the use of slit rheometry for characterizing the primary normal stress difference of extrudates. J. Food Engn. 18: 145-157.

Oldroyd, J.G. 1956. Non-Newtonian flow of solids and liquids. In: Eirich, F.R. (editor). Rheology: Theory and Applications, Vol. 1. Academic Press Inc., New York. pg 653-682.

Oldshue, J.Y. 1983 Fluid Mixing Technology. Chemical Engineering, McGraw-Hill Publications Co., New York

Osorio, F.A. and J.F. Steffe. 1984. Kinetic energy calculations for non-Newtonian fluids in circular tubes. J. Food Sci. 49: 1295-1296, 1315.

Osorio, F.A. and J.F. Steffe. 1986. Back extrusion of power law fluids. J. Texture Stud. 18: 43-63

Padden, F.J. and T.W. Dewitt. 1954. Some rheological properties of concentrated polyisobutylene solutions. J. Appl. Physics 28: 1086-1091.

Padmanabhan, M. and M. Bhattacharya. 1993. Planar extensional viscosity of corn meal dough. J. Food Engn. 18: 389-411.

Padmanabhan, M. and M. Bhattacharya. 1994. In-line measurements of rheological properties of polymer melts. Rheol. Acta 33: 71-87.

Paredes, M.D.C., M.A. Rao and M.C. Bourne. 1989. Rheological characteristics of salad dressings 2: effect of storage. J. Texture Stud. 20: 235-250.

Parzonka, W. and J. Vocadlo. 1968. Méthode de la caractéristique du comportement rhéologique des substances viscoplastiques d'après les mesures au viscosimètre de Couette (modèle nouveau à trois paramèters). Rheol. Acta. 7: 260-265.

Patton, T.C. 1964. Paint Flow and Pigment Dispersion. Interscience Publishers, New York.

Peleg, M. 1980. Linearization of relaxation and creep curves of solid biological materials. J. Rheol. 24: 451-463.

Peleg, M. and M.D. Normand. 1983. Comparison of two methods for stress relaxation data presentation of solid foods. Rheol. Acta 22: 108-113.

Peleg, M. and M.D. Normand. 1995. Stiffness assessment from jagged force-deformation relationships. J. Texture Stud. 26: 353-370.

Petrie, C.J.S. 1979. Extensional Flows. Pittman, London.

Philippoff, W. 1935. Kolloid-Zeit. 71:1-16. Cited in: Brodkey, R.S. 1967. The Phenomena of Fluid Motions. Addison-Wesley Publishing Co., Menlo Park, California.

Pipkin, A.C. 1986. Lectures on Viscoelasticity Theory (Second Edition). Springer-Verlag, New York.

Pokorny, J., J. Davidek, S. Dobiasova, P. Stern and J. Cmolik. 1984. Comparison of sensory analysis and rotational rheometry in the texture evaluation of margarines. J. Texture Stud. 15: 395-406.

Polakowski, N.H. and E.J. Ripling. 1966. Strength and Structure of Engineering Materials. Prentice-Hall, Inc., Englewood Cliffs, NJ

Powell, R.E. and H.J. Eyring. 1944. Mechanisms for the relaxation theory of viscosity. Nature 154: 427-428.

Powell, R.L. 1988. Rotational viscometry. In: Collyer, A.A. and D.W. Clegg (editors). Rheological Measurements. Elsevier Applied Science, New York. pg. 247-296.

Prentice, J.H. 1992. Dairy Rheology: A Concise Guide. VCH Publishers, Inc., New York.

Prentice, J.H. and D. Huber. 1983. Results of a collaborative study on measuring rheological properties of foodstuffs. In: Jowitt R., F. Escher, B. Hallström, H.F.Th. Meffert, W.E.L. Spies and G. Vos (editors). Physical Properties of Foods. Applied Science Publishers. pg. 123-184.

Princen, H.M. 1986. A novel design to eliminate end effects in a concentric cylinder viscometer. J. Rheol. 30: 271-283.

Progelhof, R.C. and J.L. Throne. 1993. Polymer Engineering Principles. Hansen Publishers, New York.

Purkayastha, S., M. Peleg, E.A. Johnson and M.D. Normand. 1985. A computer aided characterization of the compressive creep behavior of potato and cheddar cheese. J. Food Sci. 50: 45-50, 55.

Qiu, C-G. and M.A. Rao. 1988. Role of pulp content and particle size in yield stress of apple sauce. J. Food Sci. 53: 1165-1170.

Qiu, C-G. and M.A. Rao. 1989. Effect of dispersed phase on the slip coefficient of applesauce in a concentric cylinder viscometer. J. Texture Stud. 20: 57-70.

Rao, M.A. 1975. Measurement of flow of a food suspension with a mixer. J. Texture Stud. 6: 533-539.

Rao, M.A. 1986. Rheological properties of fluid foods. In: Rao, M.A. and S.S.H. Rizvi (editors). Engineering Properties of Foods. Marcel Dekker, Inc., New York. pg. 1-48.

Rao, M.A. and H.J. Cooley. 1984. Determination of effective shear rates in rotational viscometers with complex geometries. J. Texture Stud. 15: 327-335.

Rao, M.A. and H.J. Cooley. 1992. Rheological behavior of tomato pastes in steady and dynamic shear. J. Texture Stud. 23: 415-425.

Rao, M.A. and J.F. Steffe (editors). 1992. Viscoelastic Properties of Foods. Elsevier Applied Science, New York.

Rao, V.N.M. and G.E. Skinner. 1986. Rheological properties of solid foods. In: Rao, M.A. and S.S.H. Rizvi (editors). Engineering Properties of Foods. Marcel Dekker, Inc., New York. pg. 215-254.

Rasper, V.F. and K.R. Preston (editors). 1991. The Extensigraph Handbook. The American Association of Cereal Chemists, St. Paul, MN.

Reiner, M. 1964. The Deborah Number. Physics Today. January: 62.

Rha, C. and P. Pradipasena. 1986. Viscosity of proteins. In: Mitchell, J.R. and D.A. Leward (editors). Functional Properties of Food Macromolecules. Elsevier Science Publishing Co., Inc., New York.

Rodriguez, F. 1982. Principles of Polymer Systems (Second Edition). Hemisphere Publishing Corp., New York.

Rohm, H. 1993. Rheological behaviour of butter at large deformations. J. Texture Stud. 24: 139-155.

Rohm, H. and K.-H. Weidinger. 1993. Rheological behaviour of butter at small deformations. J. Texture Stud. 24: 157-172.

Roos, Y.H. 1992. Phase transitions in food systems. In: Heldman, D.R. and D.B. Lund (editors). Handbook of Food Engineering. Marcel Dekker, Inc., New York.

Roos, Y.H. 1995. Glass transition - related chemical changes in foods. Food Technol. 49: 97-102.

Rosenberg, M., Z. Wang, S.L. Chuang and C.F. Shoemaker. 1995. Viscoelastic property changes in Cheddar cheese during ripening. J. Food Sci. 60: 640-644.

Ross-Murphy, S.B. 1988. Small deformation measurements. In: Blanshard, J.M.V. and J.R. Mitchel (editors). Food Structure - Its Creation and Evaluation. Butterworths, London. pg 387-400.

Ryan, N.W. and M.M. Johnson. 1959. Transition from laminar to turbulent flow in pipes. AIChE J. 5: 433-435.

Sakiadis, B.C. 1984. Fluid and particle mechanics. In: Perry, R.H., D.W. Green and J.O. Maloney (editors). Perry's Chemical Engineers' Handbook (Sixth Edition), Section 5. McGraw-Hill Book Company, New York. pg. 5-4 to 5-68.

Saravacos, G.D. 1970. Effect of temperature on viscosity of fruit juices and purees. J. Food Sci. 35: 122-125.

Saunders, S.R., D.D. Hamann and D.R. Lineback. 1992. A systems approach to food material adhesion. Lebensm.-Wiss. u.-Technol. 25: 309-315.

Scalzo, A.M., R.W. Dickerson, J.T. Peeler and R.B. Read. 1970. The viscosity of egg products. Food Tech. 24 (Nov.): 113-119.

Secor, R.B. 1988. Operability of Extensional Rheometry by Stagnation, Squeezing, and Fiber Drawing Flows: Computer-Aided-Analysis, Viscoelastic Characterization, and Experimental Analysis. Ph.D. Dissertation. Univ. of Minnesota.

Seethamraju, K. and M. Bhattacharya. 1994. Effect of ingredients on the rheological properties of extruded corn meal. J. Rheol. 38: 1029-1044.

Senouci, A. and A.C. Smith. 1988a. An experimental study of food melt rheology I. Shear viscosity using a slit die viscometer and a capillary rheometer. Rheol. Acta 27: 546-554.

Senouci, A. and A.C. Smith. 1988b. An experimental study of food melt rheology II. End pressure effects. Rheol. Acta 27: 649-655.

Severs. E.T. 1962. Rheology of Polymers. Reinhold Publishing Company, New York.

Sharma, S.K., A.R. Hill, H.D. Goff and R. Yada. 1989. Measurement of coagulation time and curd firmness of renneted milk using a Nameter viscometer. Milchwissenschaft 44: 682-685.

Sherman, P. 1970. Industrial Rheology. Academic Press. New York.

Sherman, P. 1988. The sensory - rheology interface. In: Blanshard, J.M.V. and J.R. Mitchel (editors). Food Structure - Its Creation and Evaluation. Butterworths, London. pg 417-432.

Shuey, W.C. and K.H. Tipples (editors). 1980. The Amylograph Handbook. The American Association of Cereal Chemists, St. Paul, MN.

Shukla, A. and S.S.H. Rizvi. 1995. Measurements of flowability of butter by capillary rheometry. J Texture Stud. 26: 299-311.

Shukla, A., S.S.H. Rizvi and J.A. Bartsch. 1995. Rheological characterization of butter using lubricated squeezing flow. J Texture Stud. 26: 313-323.

Silvester, R.S. 1985. Mixing of Non-Newtonian Media, A Technical Review. (British Hyrdomechanics Research Association. Fluid Engineering. Fluid Engineering Series; Vol. 12.) BHRA, Cranfield, Bedford, England

Skalak, R. and S. Chien (editors). 1987. Handbook of Bioengineering. McGraw-Hill Book Company, New York.

Skelland, A.P.H. 1967. Non-Newtonian Flow and Heat Transfer. John Wiley and Sons, Inc. New York.

Skelland, A.P.H. 1983. Mixing and agitation of non-Newtonian fluids. In: Cheremisinoff, N.P. and R. Gupta (editors). Handbook of Fluids in Motion. Ann Arbor Science Publishers, Ann Arbor, Michigan. pg. 179-209.

Sone, T. 1972. Consistency of Foodstuffs. D. Reidel Publishing Co., Dordrecht, Holland.

Steffe, J.F. 1984. Problems in using apparent viscosity to select pumps for pseudoplastic fluids. Trans. ASAE 27: 629-634.

Steffe, J.F. 1992. Yield stress: phenomena and measurement. In: Singh, R.P. and A. Wirakartakusumah (editors). Advances in Food Engineering. CRC Press, Boca Raton, FL. pg. 363-376.

Steffe, J.F., E.M. Castell-Perez, K.J. Rose and M.E. Zabik. 1989. Rapid testing method for characterizing the rheological behavior of gelatinizing corn starch slurries. Cereal Chem. 66: 65-68.

Steffe, J.F. and E.W. Ford. 1985. Rheological techniques to evaluate the shelf-stability of starch-thickened, strained apricots. J. Texture Stud. 16: 179-192.

Steffe, J.F., I.O. Mohamed and E.W. Ford. 1986. Rheological properties of fluid foods: data compilation. In: Okos, M.R. (editor). Physical and Chemical Properties of Foods. ASAE. St. Joseph, Michigan. pg. 1-13.

Steffe, J.F., I.O. Mohamed and E.W. Ford. 1984. Pressure drop across valves and fittings for pseudoplastic fluids in laminar flow. Trans. ASAE 27: 616-619.

Steffe, J.F. and R.G. Morgan. 1986. Pipeline design and pump selection for non-Newtonian fluid foods. Food Technol. 40: 78-85. [Addendum: Food Technol. 41: 32].

Steffe, J.F. and F.A. Osorio. 1987. Back extrusion of non-Newtonian fluids. Food Technol. 41: 72-77.

Steffe, J.F., F.A. Osorio and R.Y. Ofoli. 1989. Dynamic and steady rheological properties of starch based pie filling. In: Ang, H.G. (edi-

tor). Trends in Food Science. Part Six, Rheological Studies," pg. 128-130. The Singapore Inst. Food Sci. and Technol., Republic of Singapore.

Sweeney, E.T. 1978. An Introduction and Literature Guide to Mixing. - (British Hyrdomechanics Research Association. Fluid Engineering. Fluid Engineering Series; Vol. 5.) BHRA, Cranfield, Bedford, England

Szczesnaik, A.S. 1995. Texture profile analysis-methodology interpretation clarified. J. Food Sci. (Letters) 60: vii.

Szczesnaik, A.S., M.A. Brandt and H.H. Friedman. 1963. Development of standard rating scales for mechanical parameters of texture and correlation between the objective and sensory methods of texture evaluation.. J. Food Sci. 28: 397-403.

Tadmor, Z. and C.G. Gogos. 1979. Principles of Polymer Processing. John Wiley and Sons, New York.

Tamura, M.S., J.M. Henderson, R.L. Powell and C.F. Shoemaker. 1989. Evaluation of the helical screw rheometer as an on-line viscometer. J. Food Sci. 54: 483-484.

Tanaka, M., J.M. De Man and P.W. Voisey. 1971. Measurement of textural properties of foods with constant speed cone penetrometer. J. Texture Stud. 2: 306-315.

Tanner, R.I. 1985. Engineering Rheology. Oxford University Press, Oxford.

Tanner, R.I. 1988. Recoverable elastic strain and swelling ratio. In: Collyer, A.A. and D.W. Clegg (editors). Rheological Measurements. Elsevier Applied Science, New York. pg. 93-118.

Tattersall, G.H. and P.F.G. Banfill. 1983. The Rheology of Fresh Concrete. Pitman Publishing Inc., Boston.

Tirtaatmadja, V. and T. Sridhar. 1993. A filament stretching device for measurement of extensional viscosity. J. Rheol. 37: 1081-1102.

Tiu, C. and D.V. Boger. 1974. Complete rheological characterization of time-dependent food products. J. Texture Stud. 5: 329-338.

Toledo, R., J. Cabot and D. Brown. 1977. Relationship between composition, stability and rheological properties of raw comminuted meat batters. J. Food Sci. 42: 725-727.

Toms, B.A. 1958. Fundamental techniques: fluids. In: Eirich, F.R. (editor). Rheology: Theory and Applications, Volume II. Academic Press, New York. pg. 475-500.

Trouton, F.T. 1906. On the coefficient of viscous traction and its relation to that of viscosity. Proceedings of the Royal Society of London. Series A, Vol. LXXVII: 426-440.

Uhl, V.W. and J.B. Gray (editors). 1986. Mixing, Theory and Practice, Vol. III. Academic Press, Inc., New York.

Ulbrecht, J.J. and P. Carreau. 1985. Mixing of viscous non-Newtonian liquids. In: Ulbrecht, J.J. and G.K. Patterson (editors). Mixing of Liquids by Mechanical Agitation. Gordon and Breach Science Publishers, New York. pg. 93-138.

Ulbrecht, J.J. and G.K. Patterson (editors). 1985. Mixing of Liquids by Mechanical Agitation. Gordon and Breach Science Publishers, New York.

Ulbricht, D. M.D. Normand and M. Peleg. 1995. Creating typical jagged force-deformation relationships from the irregular and irreproducible compression data of crunchy foods. J. Sci. Food Agric. 67: 453-459.

Ury, J.F. 1966. Resistance to steady laminar flow of pseudoplastic fluids through pipes and valves. J. Mech. Engn. Sci. 8: 226-233.

Van Wazer, J.R. 1963. Viscosity and Flow Measurement. Interscience Publishers, New York.

Vercruysse, M.C.M. and J.F. Steffe. 1989. On-line viscometry for pureed baby food: correlation of Bostwick Consistometer readings and apparent viscosity data. J. Food Proc. Engn. 11: 193-202.

Vocadlo, J.J. and M.E. Charles. 1971. Measurement of yield stress of fluid-like viscoplastic substances. Canadian J. Chem. Engn. 49: 576-582.

Viswanath, D.S. and G. Natarajan. 1989. Data Book on the Viscosity of Liquids. Hemisphere Publishing Corp., New York.

Vitali, A.A. and M.A. Rao. 1984. Flow properties of low pulp concentrated orange juice: effect of temperature and concentration. J. Food Sci. 49: 882-888.

Vyalov, S.S. 1986. Rheological Fundamentals of Soil Mechanics. Elsevier Science Publishers, New York.

Walters, K. 1975. Rheometry. Chapman and Hall, London.

Warren, R.C. 1988. Viscous heating. In: Collyer, A.A. and D.W. Clegg (editors). Rheological Measurements. Elsevier Applied Science, New York. pg. 119-150.

Weast, R.C., M.J. Astle and W.H. Beyer. 1985. CRC Handbook of Chemistry and Physics. CRC Press, Inc.. Boca Raton, FL

Weipert, D., H.-D. Tscheuschner and E. Windhab (editors). 1993. Rheologie der Lebensmittel. B. Behr's Verlag GmbH & Co., Hamberg, Germany.

Whorlow, R.W. 1992. Rheological Techniques (Second Edition). Ellis Horwood, New York.

Wikström, K., L. Bohlin and A. Eliasson. 1994. Biaxial extension of wheat flour doughs. Rheology 94, 4: 192-197.

Williams, M.L., R.F. Landel and J.D. Ferry. 1955. The temperature dependence of relaxation mechanisms in amorphous polymers and other glass forming liquids. J. Am. Chem Soc. 77: 3701-3707.

Williams, R.W. 1979. Determination of viscometric data from the Brookfield R.V.T. viscometer. Rheol. Acta 18: 345-359.

Winther, G., K. Almdal and O. Kramer. 1991. Determination of the polymer melt viscosity by squeezing flow with constant plate viscosity. J. Non-Newtonian Fluid Mech. 39: 119-136.

Wood, F.W. and T.C. Goff. 1973. The determination of the effective shear rate in the Brabender Viscograph and in other systems of complex geometry. Die Starke 25: 89-91.

Yang, T.M.T. and I.M. Krieger. 1978. Comparison of methods for calculating shear rates in coaxial viscometers. J. Rheol. 22: 413-421.

Yanovsky, Y.G. 1993. Polymer Rheology: Theory and Practice. Chapman and Hall, New York.

Yoo, B., M.A. Rao and J.F. Steffe. 1995. Yield stress of food dispersions with the vane method at controlled shear rate and shear stress. J. Texture Stud. 26: 1-10.

Yoshimura, A.S. and R.K. Prud'homme. 1987. Response of and elastic Bingham fluid to oscillatory shear. Rheol. Acta 26: 428-436.

Yoshimura, A.S. and R.K. Prud'homme. 1988. Wall slip corrections for couette and parallel disk viscometers. J. Rheol. 32: 53-67.

Yoshimura, A.S. R.K. Prud'homme, H.M. Princen and A.D. Kiss. 1987. A comparison of techniques for measuring yield stress. J. Rheol. 31: 699-710.

Zukoski, C.F. 1993. Material properties and the electrorheological response. Annu. Rev. Mater. Sci. 23: 45-78.

Index